Pt Nanophase supported catalysts and electrode systems for water electrolysis

Leslie Felicia Petrik

A thesis submitted in fulfilment of the requirements for the degree of

Doctorate in Chemistry

in the

Department of Chemistry,
University of the Western Cape.

Supervisor: Professor Emmanuel I. Iwuoha May 2008

KEYWORDS

Mesoporous support

Catalyst dispersion

Nanophase electro catalyst

Cathode

Anode

Electrolysis

Proton conductivity

Membrane Electrode Assembly

Hydrogen production

Solid Polymer Electrolyte Electrolyzer

ABSTRACT

Pt Nanophase supported catalysts and electrode systems for water electrolysis

L.F. Petrik

PhD Thesis

Department of Chemistry

University of the Western Cape

In this study novel composite electrodes were developed, in which the catalytic components were deposited in nanoparticulate form. The efficiency of the nanophase catalysts and membrane electrodes were tested in an important electrocatalytic process, namely hydrogen production by water electrolysis, for renewable energy systems. The activity of electrocatalytic nanostructured electrodes for hydrogen production by water electrolysis were compared with that of more conventional electrodes. Development of the methodology of preparing nanophase materials in a rapid, efficient and simple manner was investigated for potential application at industrial scale. Comparisons with industry standards were performed and electrodes with incorporated nanophases were characterized and evaluated for activity and durability.

A CVD technique using LPG as a carbon source, pyrolized upon a mesoporous Si matrix, HMS, produced nanostructured ordered mesoporous carbon (OMC) with graphitic character after removing the Si matrix. This OMC is useful as a conductive three dimensional porous support for catalytic nanophase Pt metals. Processes to incorporate active nanophase Pt metal electro catalysts into microporous FAU, and mesoporous HMS or MCM-41 supports were developed. The influence of the nature and porosity of the catalyst support upon activity for hydrogen production by water electrolysis was demonstrated with Pt FAU< PtHMS=PtMCM-41.

Methods for preparing active nanophase Pt electro catalysts on CNT or CNT paper substrates were developed. Deposition of Pt on CNT paper by a simple galvanic displacement technique formed a new, highly conductive and active Pt containing gas diffusion electrode, eliminating the extensive processing required to prepare composite gas diffusion electrodes (GDE). It was found that the reduction potential of the sacrificial anode (Al, Fe, Pb foils) did not correlate with Pt deposition rate but bimetallic systems were controlled by deposition time. The new electro catalysts were compared to an industry standard commercial Pt catalyst stabilized on Vulcan carbon black for electro activity and the overpotential of hydrogen evolution occurred at similar or lower overpotential than the commercial electrocatalyst.

The sequential deposition method was developed to incorporate 3-dimensional supported nanophase catalytic materials, Pt-FAU, Au–HMS, Pt- HMS and Pt MCM-41 into composite GDE, and it was shown that such electrodes could achieve current densities of ~650mA cm^{-2} at 60 °C and an applied potential of -2 V in an alkaline electrolyzer and electrodes were durable. It was found that nanophase Sb/SnO, a non noble metal oxide nano particulate could also be applied as electrocatalyst for hydrogen production.

Optimization of the catalyst-containing ink formulation and ink deposition by screenprinting produced homogeneous and well dispersed layers of 0.001 - 0.0015 g cm^{-2} of electrocatalyst per unit area of substrate. The morphology of the screenprinted film was strongly affected by the ink formulation. Reversible viscoelastic behaviour of inks correlated with good print quality, which also was affected by the polarity and viscosity of the solvent, the printed layer thickness, and the nature as well as the surface energy of the substrate. Hence, no matter how active the electrocatalyst, if the catalyst containing film on the GDE substrate is substandard, resistance will be high and electroactivity low.

A paper substrate method was developed to evaluate the electronic characteristics of catalyst containing films separately from the GDL substrate using Variable Field Hall

measurements. It was found that improving the film morphology reduced the positive Sheet Hall Coefficient significantly and promoted n-type rather than p-type carriers. On the contrary, n-type carrier CNT paper with low resistance and high carrier density switched to a p-type carrier upon deposition of Pt by galvanic displacement.

Technological improvement of membrane electrode assemblies applicable in a solid polymer electrolyte electrolyzer showed that Bekinit Titanium fibre substrate was the most promising anodic GDL catalyst support, and hydrophilic Lydall carbon cloth (6100-300 and 6100-200) was suitable as cathode GDL. A cathode loading of 1 mg cm^{-2} Pt/C and anode loading of 6 mg cm^{-2} IrO_2 was found to be the optimum catalyst loading using commercial catalysts. The Nafion®115 membrane proved to be the best ionomer membrane. High output (current density of 1.33 A cm^{-2} at 97 ^{o}C and -1.7 V) was realized when system parameters such as operational temperature, water flow rate, moisturization time, current collector clamping pressure, insulation and low resistance electrical leads were optimized.

May, 2008

DECLARATION

" I declare that "*Pt Nanophase supported catalysts and electrode systems for water electrolysis"* is my own work, that it has not been submitted for any degree or examination in any other university and that all the sources I have used or quoted have been indicated and acknowledged by means of complete references".

Full name _____ Date _____

Signed: _____

ACKNOWLEDGEMENTS

My deepest gratitude goes to God for carrying me through this time and to my family for supporting me in my studies. I would like to thank the NRF and ESKOM for financial support and for promoting this research direction. I would like to sincerely thank my supervisor, Prof. E.I Iwuoha, for his assistance and guidance of my research as well as the SensorLab post docs and students, especially Tesfayo Taddesse Waryo and Amir Al-Ahmed. I would like to thank Prof. Margit Härting, Prof. David Britton and Girma Goro Gonfa of the Physics Department at the University of Cape Town for their useful advice on electrode materials and Hall measurements; Dr Veruscha Fester of the Flow Process Centre at CPUT for advice in Rheological measurements; Prof Dirk Knoesen, Basil Julies and Adrian Josephs of the Physics Department at University of the Western Cape for advice and assistance with EDS, HRTEM and SEM micrographs; Miranda Waldron and Mohammed Jafta at UCT for assistance with TEM micrographs; Dr Remi Bucher at the XRD facilities and Dr Carlos Pineda for assistance with PIXE analysis at iThembaLABS. My heartfelt thanks particularly to Thotyelwa Zondani, Japhet Ali, Ziboneni Godongwane, Tankiso Thamahane, Mario Williams and Qiling Ying for the assistance they gave me with many different tasks in the laboratory. Many thanks also to Dr Alexander Nechaev for his advice and support. I gratefully acknowledge the Chemistry Department at the University of the Western Cape for their support during my PhD programme and the technical staff of the Chemistry Department who assisted with instrumental analysis, especially to Timmy Lesch for technical expertise and Andile Mantyi for assisting with providing necessary equipment and supplies. I acknowledge the South African Institute for Advanced Materials Chemistry for support and Cedric Achilles, Vincent Starkey and the secondary works technical and electronic workshop staff for their assistance in manufacturing various reactors, devices and repairing instruments.

TABLE OF CONTENTS

LIST OF TABLES

LIST OF FIGURES

LIST OF ABBREVIATIONS

ABB	ABB company, Switzerland Ltd. High Power Rectifiers
AMTS	Advanced Materials Technology Strategy
BET	Brunauer-Emmett-Teller
BJH	Barrett-Joyner-Halenda
BSE	Back scattered electrons
CA	Carbon Analogue
CNF	nanofibers (s)
CNM	Carbon nanostructured materials
CNT	carbon nanotubes (s)
CV	Cyclic Voltammetry
Cute	Clean Urban Transport for Europe
DMFC	Direct Methanol Fuel Cell
DOE	Department of Energy (USA)
DSA	Dimensionally stable anodes
DST	Department of Science and Technology
DTI	Department of Trade and Industry
ESB	Electron Spectral Beam
ESKOM	Electricity supply commission (SA)
EBSD	Electon Back Scattered Diffraction
EDS	Energy dispersive spectroscopy
FP6	Framework Programme 6, European Union
Fed-Ex	Federal express courier services

FTIR	Fourier Transform Infrared spectroscopy
G	Conductance
GDE	Gas Diffusion Electrode
GDL	Gas Diffusion Layer
GM	General Motors
HER	Hydrogen Evolution Reaction
HMS	Hexagonal Mesoporous Silica
HPPS	High-Performance Particle Sizing
HOPG	Highly Oriented Pyrolytic Graphite
HRSEM	High-Resolution Scanning Electron Microscopy
H_{UPD}	Hydrogen Underpotential Deposition
I	Current
IJP	Inkjet printing
IPHE	International Partnership for the Hydrogen Economy
JM Pt/C	Commercial Johnson Matthey™ Carbon Black-Supported Nanophase Platinum
LPG	Liquid Petroleum Gas
LPI	Lines-per-inch
LSV	Linear-Sweep Voltammetry
micro-PIXE	Micro-particle induced x-ray emission spectroscopy
MOR	Methanol Oxidation Reaction
MEA	Membrane electrode assembly
MSI	Metal-support interactions
MSE	Mercury Sulphate Electrode
MW	Molecular weight

NACI	National Advisory Council on Innovation
NASA	National Aeronautics and Space Agency (USA)
NH	Carrier concentration
NIBS	Non-Invasive Beam Scattering
NMP	Nuclear microprobe
OER	Oxygen Evolution Reaction
OMC	Ordered mesoporous carbon
ORR	Oxygen Reduction Reaction
PIXE	Proton-Induced X-ray Emission Spectroscopy
PEMFC	Polymer electrolyte fuel cell
PGM's	Platinum group metals
PSA	Pressure swing adsorption
PTFE	Polytetrafluoroethylene
Pt/C	Carbon Black-Supported Nanophase Platinum
Pt/CNT	Carbon Nanotube-Supported Nanophase Platinum
PtRu/C	Carbon Black-Supported Nanophase Platinum-Ruthenium
R	Resistance (Ω)
RDE	Rotating-Disk Electrode
RRDE	Rotating Ring Disc Electrode
SAED	Selected-Area Electron Diffraction
Sb/SnO	Antimony tin oxide
SCE	Saturated Calomel Electrode
SECM	Scanning Electrochemical Microscopy
SEM	Scanning Electron Microscopy

SHE	Standard Hydrogen Electrode
SOFC	Solid Oxide Fuel Cell
SPE	Solid polymer electrolyte
SPE-electrolyser	Solid-Polymer Electrolyte Electrolyser
SOT	Solar thermal energy conversion systems
STPP	Solar thermal power plants
STEM	Scanning Transmission Electron Microscopy
TEM	Transmission Electron Microscopy
TGA	Thermogravimetric Analysis
TPR	Temperature-Programmed Reduction
UME	Ultra-Micro Electrode
URFC	Unitized regenerative fuel cell (s)
UPS	United Postal Services
V	Voltage (Volts)
WE-NET	World Energy Network
XRD	X-ray Diffractometry

LIST OF SYMBOLS

C	Charge
B	Magnetic field
d	Sample thickness
ΔG	Change in Gibbs free energy
E	potential
E_0	Standard potential for the half cell reaction
E_{anode}	Half cell potential for anode reaction
$E_{catthode}$	Half cell potential for cathode reaction
F	Faraday constant
ρH	Hall resistivity
I	current
j	current density
n	Number of mole gas produced
n	flow behaviour index
ne	number of electrons used per molecule gas
P	Pressure
ρH	Hall resistivity
Q	thermodynamic reaction quotient
R	Gas constant
s	second
τ_y	yield stress
T	Temperature
V	Volume
d_{hkl}	Inter-planar Spacing
a_0	Lattice Parameter
$SA_{Pt/C}$	Platinum Metal Surface Area
V_H	Hall voltage
i_{PA}	Anodic Peak Current

i_{PC}	Cathodic Peak Current
j_{PA}	Anodic Peak Current Density
j_{PC}	Cathodic Peak Current Density
E_{PA}	Anodic Peak Potential
E_{PC}	Cathodic Peak Potential
ΔE_P	Peak Separation
$E^{0'}$	Formal Potential
Q_{H+}	Charge Associated with a Hydride Monolayer
q	Elementary charge (1.602×10^{-19} C)
n	Bulk carrier density
μ	Hall Mobility
n_s	Sheet carrier density
R_S	Film resistance

CHAPTER 1

1. Introduction and overview

The dissertation addresses supported nanophase electrocatalysts and electrode systems for the process of water electrolysis. South Africa, the main supplier of PGM metal, stands to benefit from diversification of Pt containing materials and developed capabilities in the emerging hydrogen economy. When hydrogen production cost can be reduced and the output increased, a viable hydrogen economy may be realized. The purpose of this study was the development of nanophase PGM electrocatalysts based on high surface area supports and their application in composite gas diffusion electrodes, for improving the efficiency of hydrogen generation by water electrolysis through reduction of the overvoltage of electrolyzer systems.

This chapter introduces the dissertation topic and specifies the main perspective, from which the topic was researched, and the rationale and motivation of the study. The main research questions and problem statements are set out and the research framework and the refinement of research are presented. The research approach and design and the methodology that was used is then described. The scope and delimitations of the research are presented. The dissertation outline is finally given in this chapter with an overview of the structure of the dissertation showing how the dissertation will unfold and describing the main topics of each chapter of the dissertation. The citations list presented in Chapter 8 gives details of the publications resulting from this study.

1.1. DISSERTATION TOPIC AND MAIN PERSPECTIVE

Global energy consumption is expected to increase very significantly in the next decades, driven by rising standards of living and a growing population worldwide. The increased need for energy will require vast growth in energy generation capacity, secure and diversified energy sources, and a successful strategy to reduce greenhouse

gas emissions. Various alternative energy strategies are being considered, and building an energy infrastructure that uses hydrogen - the third most abundant element on the earth's surface - as the primary carrier may enable a secure and clean energy future (WE-NET report, 1998).

Hydrogen is an attractive energy carrier for its high energy/weight ratio. Hydrogen can be produced from most energy sources such as thermo chemical processing of primary energy sources such as coal, natural gas or oil; from renewables such as methanol or biomass; or by generation via water electrolysis. Electricity can also be derived from renewable sources such as wind power, or photovoltaic systems, or by using off peak electricity. Hydrogen as fuel promotes diversification of energy supply thus ensuring energy security, sustainability, flexibility and efficiency. Energy supply systems of the future could combine the production of electricity, heat and hydrogen as a transport fuel with high efficiency. Such systems should be robust, affordable and environmentally benign (Parfit, 2005).

When hydrogen is generated using renewable energy sources and then used as fuel in a fuel cell, the energy released during the oxidation of hydrogen can be captured in the form of electrical energy. Since water is the only reaction product in a fuel cell, the environmental impact of the energy generating device using hydrogen as fuel is minimal. This approach to generating electricity, which is part of the hydrogen economy, is already accepted as a key element in the future demand for electrical energy, and will be essential for many countries that need to increase or maintain economic growth but simultaneously need to minimize environmental pollution (Sørenson et al., 2004).

Water electrolysis as an approach to generating hydrogen for power forms the topic of this dissertation. Hydrogen production using water electrolysis is still expensive compared to the other routes mentioned, but as the oil price rises and research progressively increases the output and reduces the cost of hydrogen production, the realization of an economically feasible hydrogen economy may be within reach. The

ultimate aim is a hydrogen-based economy driven by renewable and carbon-neutral energy sources.

However, cost effective hydrogen production from water remains difficult and technologies for generating hydrogen from biomass, such as enzymatic decomposition of sugars, steam-reforming of bio-oils and gasification, suffer from low hydrogen production rates or complex processing requirements as well as engender significant environmental costs (Nordstrom, 2002). For instance, in a recent press release (Stoltenberg, 2008), it was revealed that Secunda, the largest H_2 producer via coal gasification in South Africa, is also the largest single point source CO_2 emitter in the southern hemisphere.

In order for South Africa to be internationally competitive in the energy arena, it needs to be in touch with the emerging technology of the developed countries. For South Africa to participate as a partner in the new US and worldwide hydrogen economy development and not become an economic hostage, capability is essential in the following aspects of a hydrogen economy: hydrogen production; purification and storage; control systems; infrastructure and delivery; conversion of hydrogen into useful energy; end use applications; codes and standards; manpower development and scarce skills; environmental compliance etc..

The topic of the dissertation is focussed exclusively upon hydrogen production by water electrolysis. The other aspects of the hydrogen economy as mentioned above, fall outside the scope of this study. This dissertation specifically addresses the optimization of hydrogen production by water electrolysis using nanophase materials, as one approach to reduce the cost of hydrogen. The emphasis of the dissertation is on preparing and incorporating nanophase materials into electrodes for electrolyzer systems applied in hydrogen production.

1.2. RATIONALE AND MOTIVATION

CHAPTER 1

Despite significant advancements and commitment of resources by technology providers, end-users and international governments, projections are that extensive use of hydrogen as fuel for fuel cell vehicles is ten years away at best. Hydrogen is a high cost fuel and the price should be reduced for successful commercialization to be achieved. Most major countries have investment and commercialization strategies aimed at enabling the development of relevant technologies that will advance the move to a hydrogen economy.

In the light of huge international R & D spending in the hydrogen economy and also nanotechnology, the Department of Science and Technology (DST) of South Africa has recently investigated the necessity of strategic planning and funding in these areas. The author of this dissertation was closely involved with and co-authored the development of appropriate strategies for South Africa in these key areas and in preparing the government commissioned baseline studies (Benson et al., 2005).

It is in this regard that this topic is addressed in the dissertation. The goal of this effort is a contribution to catalyze the development of South Africa's capabilities and roles in this emerging hydrogen economy. Reducing our dependency on imported hydrocarbon fuels by moving to a fuel such as hydrogen may be of significant advantage to the South African economy, if hydrogen is prepared from water.

In relation to the key areas specified above, the dissertation specifically addresses the issue of the development, or application and integration of nanophase electrocatalysts in electrochemical systems for the production of hydrogen via water electrolysis.

Nanotechnology can be used to reduce noble metal content and thus capital costs, and also improve efficiency of hydrogen generation systems such as alkaline flow cells as well as solid state polymer electrolyte membrane (PEM) electrolyzers. This is possible by, for instance, the development of novel nanophase containing electrode materials that replace the existing commercially available electrodes or electrocatalysts which are required for such hydrogen production systems. In the case

where noble metals and non-noble metal oxides are used as electrocatalysts for cathodes and anodes, the development of efficient nanosized catalysts are of great industrial interest. However, many challenges remain before nanomaterials are fully integrated into viable applications and processes. The relevant fundamental chemistry for their synthesis and manipulation is still limiting in order to develop technically feasible materials and devices.

Although nanostructured catalytic materials have received attention from both theoretical and experimental standpoints, the greatest challenge at present is to find effective low cost synthesis procedures for specific applications. Simple and reliable methods for exploration and characterization of the physical-chemical, mechanical and electrical properties of nanosized particles are required and dependable evaluation methods of their application in catalysis and zero-emission technologies. It is important to gain an understanding of the influence of size and microstructure on the physical, chemical and mechanical properties of nanoparticulates so that new types of nanosized materials can be developed that will possess enhanced properties. Furthermore design of the working laboratory modules incorporating nanomaterials that can be scaled up to industrial applications is necessary. Considering diverse aspects of assembly for integration into workable units is essential so that it becomes possible to evaluate requirements for large-scale applications. Comparison with existing technologies is important for viable applications of nanophase materials in energy generation, and fuel production. Currently the challenge is to develop hydrogen generation systems that overcome current price constraints, due to low cell efficiencies and high cost of components.

All these different aspects should be explored prior to expecting successful commercialization, and the dissertation addressed aspects of these challenges.

1.3. RESEARCH APPROACH

Electrochemical hydrogen generation systems include aqueous alkaline flow cells as well as solid state electrolyzers that are based on reverse fuel cell systems called Proton Exchange Membrane (PEM) electrolysis units (otherwise known as solid polymer electrolyte (SPE) electrolyzers), making possible clean hydrogen production by low conductivity water electrolysis. The main requirements in efficient hydrogen generation on a large scale are the supporting electrolyte, low cost, stable, large surface area electrodes, high current densities and product separation from the electrolyte.

The electrical cost involved in the hydrogen production process is mainly a function of the cell potential. It is therefore important that research should be focused on minimization of the required cell potential. This is mainly determined by the electrode material and the current density. The cell resistance (R) depends on cell design and on the temperature, type and concentration of the electrolyte. For a conventional alkaline electrolysis cell the optimum (=minimum) resistance is 0.2 to 0.4 Ohm and cannot be decreased any further unless a solid electrolyte system is adopted. Electrode development for such systems should optimize the charge transfer resistance of both anode and cathode which could be achieved by application of advanced nanophase materials. The electrodes must eventually be integrated with the nanophase electrocatalyst in such a system. The catalyst may be located on the electrodes where it is exposed to the electrolyte containing environment or presented as modified composite nanostructured electrodes in solid polymer electrolyte (SPE) systems.

In recent years electro membrane reactors such as solid polymer electrolyte (SPE) based electrolyzer technologies have been developed where composite membranes are used as supports for nanophase catalytic electrodes. In these reactors the membrane plays several parts, namely being an electrode, a dosing device and a separation device. The membrane electrodes possess significant advantages compared

to conventional electrosynthesis systems namely higher catalytic activity thus lower overpotential and improved selectivity. However, SPE based electrolyzer technologies suffer from the high cost of the electrocatalysts and membranes and non-SPE based electrolyzer technologies have the problem of low efficiency and disposal of alkaline electrolytes that could cause health hazards. Moreover, the cost involved in the maintenance and handling of such technologies is considered to be higher than the SPE-based electrolyzer technologies.

Composite electrodes with multiple layers of different electrolyte materials may aggravate issues such as high resistivity, insulating interphases, suppression of interphase reactivity, as each new material introduced into such a composite may introduce its own set of interface problems. However, use of nano-phase composite catalytic electrodes in SPE systems may circumvent such disadvantages. Moreover, novel high surface area nano structured catalytic electrodes may find application for electrosynthesis. Issues such as the cell design and electrochemical reactions, catalyst lifetime, reaction kinetics, mass transfer processes, and heat transfer are important in order to optimize cell performance.

Basic research that leads to innovative design of electrode materials and process optimization is the only way to overcome the challenges to achieve the hydrogen economy.

1.4. SCOPE OF STUDY

In this study novel composite electrodes were developed, in which the catalytic components was deposited in nanoparticulate form. The efficiency of the nanophase catalysts and membrane electrodes were tested in an important electrocatalytic process such as hydrogen production by water electrolysis for renewable energy systems. The activity of electrocatalytic nanostructured electrodes for hydrogen production by water electrolysis were compared with that of more conventional electrodes. Development of the methodology of preparing nanophase materials in a

rapid, efficient and simple manner was investigated for potential future application at industrial scale. Comparisons with industry standards were performed and electrodes with incorporated nanophases were evaluated for activity and durability.

The overall aim was the production according to commercially viable techniques of electrodes incorporating supported nano materials capable of high current densities with high hydrogen production capacity in comparison to existing technology, with optimized process applications in suitable reactors.

The scope of the dissertation was thus to develop new routes to prepare nanophase electrocatalysts and apply nanophase electrocatalysts in composite electrode materials for electrolyzer systems to achieve high energy efficiency combined with a high production capacity at a low loading of noble metal catalyst. Methods were investigated for preparation nanophase electrocatalysts that can be easily upgraded to industrial conditions for electrocatalytic processes. Nanophase materials were then incorporated by various means into composite electrodes which were evaluated in hydrogen production by water electrolysis for stability and durability. Both aqueous and solid polymer electrolyte environments were evaluated, to obtain an understanding of the relative contribution of each variable upon the functionality of the system.

1.5. DELIMITATION OF STUDY

The study was limited to the following activities: Develop and characterize nanophase electrocatalysts; Improve catalytic ink formulations and methods for their deposition; Improve and characterize composite catalytic electrodes incorporating such nanophase electrocatalysts; Demonstrate stability of nanophase composite electrodes; Apply improved electrodes in electrosynthesis using hydrogen production as probe reaction; Optimize operational conditions for hydrogen production. Subsidiary activities aimed to: Improve the three phase interface between catalyst,

proton conductor and electron conductor; Improve gas diffusion layers; Improve membrane electrode assemblies.

1.6. RESEARCH DESIGN AND REFINEMENT OF APPROACH

The detailed approach in this study was to:

(1) Develop or apply primary nanophase electrocatalytic materials for the H_2 evolution cathode and the O_2 evolution anode used in water electrolysis based upon: (a) nanophase noble metals, (b) nanophase metal oxides.

(2) Find supporting methods to stabilize such nanophases by use of: (a) micro and mesoporous materials (b) colloidal dispersions (c) physical admixtures with conductive binders. Various supports suitable as substrates for stabilizing nanoparticles were explored, including zeolites, conductive mesoporous carbons, carbon nanotubes, and Vulcan carbon black.

(3) Explore methods for incorporating such nanophase materials into composite membrane electrodes, including (a) incorporation into catalytic inks (b) incorporation into gas diffusion layers or onto proton conducting membranes. Different ink compositions incorporating various nanophase materials, proton and electron conductive phases, binders and solvents were investigated for suitability for composite formation on a variety of conductive substrates. Printing technologies such as screen printing were applied for achieving homogeneous and highly dispersed nanophases in stable thin films.

(4) Develop composite nanophase electrodes that are (a) active in aqueous or solid polymer electrolyte systems; (b) that are durable and easily scaled up to industrial conditions (c) screen materials for activity and durability in high electrolyte systems.

(5) Apply materials containing nanophases in membrane electrode assemblies that are (a) suitable for operation in prototype electrolyzers at bench scale installations; that will be tested for (b) for hydrogen production by water electrolysis.

(6) Develop replacement gas diffusion layers applicable to membrane electrode assemblies.

(7) Optimize operational parameters in a solid polymer electrolyte (SPE) electrolyzer or reverse fuel cell.

Outputs envisaged included: developed novel nanostructured electrocatalytic materials and procedures for their manufacture; characterization of fabricated materials; optimized processing conditions when such materials are applied in high efficiency nanophase composite membrane electrodes; optimized electrocatalytic process conditions for hydrogen production.

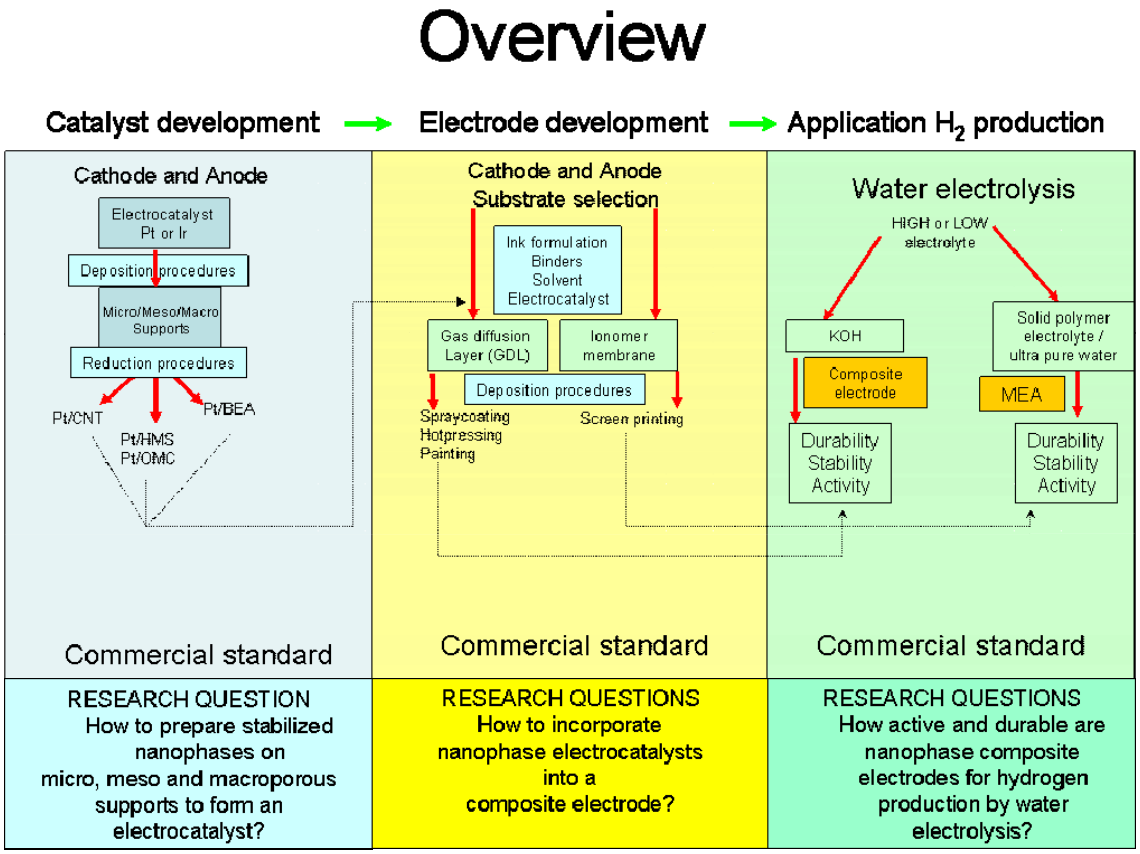

Figure 1.1 Schematic overview of scope of dissertation

1.7. RESEARCH HYPOTHESIS

High dispersal of nanophase Pt metals in three dimensional substrates will enhance the process of water electrolysis. Nanoscale highly dispersed active components will reduce the overvoltage of electrocatalytic reactions. Composite gas diffusion electrode surfaces containing nanophases will result in high activity for hydrogen production. Nanophase electrocatalytic materials can be incorporated into composite gas diffusion electrodes and maintain high catalytic activity for hydrogen production and high electro- and proton conductivity.

Research questions included:

i) Can nanophase electrocatalytic Pt particulates be stabilized on micro, meso and macroporous supports?

ii) Does the porous or high surface area support substrate improve the dispersion of Pt nanophase electrocatalytic particulates?

iii) Can nanostructured electrocatalytic materials be prepared using simple synthesis methods?

iv) Which are the most suitable matrices to be used as supports for nanostructured electrocatalytic materials?

v) Can the nanophase electrocatalysts be processed into composite electrodes without agglomeration and with high dispersion?

vi) Can nanophase catalysts be processed into the form of catalytic membranes and membrane electrodes?

vii) Can the characteristics of the electrocatalysts and the composite electrodes be determined in terms of their activity?

viii) How should the electrocatalytic membrane reactor be operated in order to achieve optimum performance of nanostructured catalytic electrodes?

ix) Which analytical methods can be used for evaluation of characteristics of nanostructured catalysts and electrodes?

x) How will nanostructured catalysts in electrodes perform in electrosynthesis reactions, and particularly for hydrogen production?

1.8. MAIN PERSPECTIVE FROM WHICH THE TOPIC WAS RESEARCHED

Nanofabrication methods, which are simple and have high potential for upscaling to industrial volume output were selected for preparation of high surface area nanophase electrodes. These materials should be applicable in:

1) Nanophase composite electrode materials for alkaline electrolyzers
2) Nanophase composite electrode materials for SPE electrolyzers

The goal was to optimize the following properties iteratively: (1) High catalytic activity due to high dispersion of the active components as nanophases; (2) Increased activity due to tailor made porous matrices impregnated with catalytic nanoclusters; (3) Low overpotential because nanoscale dispersed active components may reduce the overpotential of electrocatalytic reactions resulting in overall increase in energy efficiency of the process; (4) Intensification of external kinetics. The specially designed geometry of the electrode surface should result in enhanced transport of reagents and products. (5) Commercially viable procedures for materials preparation. The newly developed composite, nanophase electrocatalytic materials were tested in small prototype electrolyzers for hydrogen production. Thus the development of electrocatalysts, properties of electrodes containing the electrocatalysts and their application as electrodes for hydrogen evolution was investigated in this study.

1.9. METHODOLOGY

Micro and mesoporous support materials were characterized to determine the phases present, the phase purity, the composition, the pore volume and the morphology. Supported catalytic nanoparticles were prepared on these substrates and characterized, then incorporated in composite electrodes. Fabricated electrodes containing nanophases were characterized in terms of homogeneity, dispersion of the

active metal and activity, and were tested in electrolysis of water. Each of these aspects is presented in different chapters.

Various techniques are useful for the characterization/identification of nanophase materials as well as prepared composite membranes which may include the following methods (Petrik 2002; Williams et al. 2008). The methods used for characterization are described in Section 3.3.5 and in each specific chapter as necessary. Particle size, particle size distribution, metal surface area, and metal dispersion/agglomeration can be established by scanning and transmission electron microscopy (SEM/TEM). Surface micro- and macrostructure, and degree of agglomeration can be determined by High-Resolution Scanning Electron Microscopy (HRSEM). Fourier transform Infra red (FTIR) gives information of structural configuration. X-ray diffractometry (XRD) gives information about crystal/atomic structure and phase identity and purity. Qualitative crystallinity and crystal symmetry can be determined by Selected Area Electron Diffraction (SAED). Volatile and template content as well as thermal stability is determined with Thermogravimetry (TGA) and surface oxidized or reducible species (metal chemical state) can be analyzed using Temperature-Programmed Reduction (TPR). Composition can be quantitatively determined by elemental analysis using atomic adsorption spectroscopy (AAS), Ion Coupled Plasma (ICP), X-ray Fluorescence spectroscopy (XRF) or qualitatively by using energy dispersive analysis (EDS). Aggregate size and aggregate size distribution can be determined by Non-Invasive Beam Scattering (NIBS). Total surface area, pore size distribution and porosity can be determined by N_2 adsorption/desorption at -196 ºC (77 K) (N_2BET). Electrochemical properties can be determined using cyclic voltammetry or square wave voltammetry using a potentiostat/galvanostat. Elemental mapping was determined by proton Induced X-ray emission (PIXE). Electrical characteristics of samples were determined by Hall measurements, which will be fully described in Chapter 6.

1.10. STRUCTURE OF THESIS

Each chapter opens with an overview of the literature related to the specific topic covered in that chapter, followed by an experimental section, results and discussion section and a concluding section. The unfolding sequence of the dissertation in separate chapters hereafter is as follows: Background overview of the hydrogen economy; Catalyst support types (micro- and mesoporous silica vs carbon substrates); Preparation of nanophase electrocatalysts; Methods for fabrication of composite electrodes; Optimization of electrodes including finding suitable gas diffusion layers (GDL) and stability testing; Screenprinitng and testing of catalytic layers on substrates; Optimizing membrane electrode assemblies (MEA) and an SPE electrolyzer cell.

CHAPTER 1

This Chapter has introduced the dissertation topic.

CHAPTER 2

In Chapter 2 an overview of the hydrogen economy and background information is presented.

CHAPTER 3

In Chapter 3 after an overview of the substrate support types, the preparation and characterization of nanostructured porous template matrices that were used as supports or sacrificial templates with precise parameters is described. The details of preparation and characterization of micro, meso and macro porous supports are then described. High silica micro and mesoporous matrixes were used as supports or as sacrificial templates for preparation of carbon analogues. This included preparation of zeolites and mesoporous materials with angstrom or nanosized pores respectively as supports for electrocatalysts. Deposition of carbon into the pore volume of such sacrificial matrixes was followed by pyrolysis of the carbonaceous materials and subsequent dissolution of the silica matrix resulting in an ordered mesoporous carbon

(OMC) analogue. Alternatively the carbonization of the electrocatalyst could be achieved by sputter coating or pyrolysis of LPG.

CHAPTER 4

Chapter 4 details the stabilization of nanophases of Pt on macroporous supports (CNT). A review of various approaches is firstly presented. Various routes of Pt deposition on CNT and CNT paper including a galvanic displacement technique using Al, Pb and Fe foils are developed. Characterization of the electrochemical activity of the most promising CNT supported nanophase electrocatalysts was performed with cyclic voltammetry. A state of the art, highly active, commercial carbon black supported Pt catalyst with a 40% loading of Pt, that was purchased from a well-known company was characterized and used in subsequent chapters as baseline comparison.

CHAPTER 5

In Chapter 5 the development, characterization and application of noble metal nanophase electrocatalysts supported on microporous (FAU), mesoporous (HMS, MCM-41) is described. Various nanoparticle fabrication techniques for nanometal deposition and reduction on these Si based porous supports are developed. The catalysts are processed into composite nanophase containing electrode materials suitable to aqueous alkaline electrolyzer systems. A review of the methods used to prepare such electrodes is presented. The characteristics of composite electrodes manufactured via brush coating, casting, hot pressing, and spray coating are evaluated for durability and stability in an aqueous alkaline environment.

CHAPTER 6

In Chapter 6 ink formulations containing the benchmark commercial electrocatalyst were developed and used to prepare composite electrodes suitable for SPE electrolyzers. The characteristics of the catalyst containing film or layer on composite electrodes manufactured via screen printing are evaluated. Homogeneity and reproducibility are key issues in preparing larger scale composite electrodes

supporting a catalytic layer, and various preparation techniques may produce materials with different surface dispersion that may have an effect upon properties such as stability, lifetime and activity. Characterization of composite nanophase materials was performed by Scanning Electrochemical Microscopy and Proton induced X-Ray emission spectroscopy (PIXE) for elemental mapping to ascertain the ability to obtain the required composition, dispersion, homogeneity, and also the details such as defects, concentration gradients, etc, in composite materials. Resistivity, IV characteristics, Hall sheet carrier density, Hall mobility of electrodes was performed using a Hall measurement system.

CHAPTER 7

Chapter 7 describes the optimization of a Membrane Electrode Assembly (MEA) for the SPE system using benchmark commercial Pt and Ir electrocatalysts. A review of components and conditions of assembly for these systems is presented. Optimization included selection of the most suitable prototype designs, electrodes, diaphragms or membrane materials, catalysts, backing layers for cathode and anode, MEA assembly conditions and bench scale prototype development. The MEA with the most successful performance (Pt-C cathode and IrO_2 anode) was reproduced and subjected to long term polarization tests whereby the output current was a measure of the electrode stability. Many variables that may influence the observed activity for hydrogen production were optimized.

CHAPTER 8

Finally, in Chapter 8, the overall conclusions are presented and the recommendations for future studies are made. The citations list of the outputs from this study appears in Chapter 8. The last chapter is followed by all the references for each Chapter that have been consolidated into one alphabetical list.

CHAPTER 2

2. LITERATURE REVIEW

The literature review presented in this chapter informed and defined the thesis topic and main perspective, rationale and motivation, research approach and scope of study as well as the delimitation of the study, as was presented in Chapter 1. The research design and refinement of approach and research hypothesis as well as the delimitations of the research and the main perspective from which the topic was researched were also developed from the perspective gained from the literature review.

2.1 BACKGROUND

Worldwide, large investments are being made into the hydrogen economy because of the likelihood that the world oil supply will decline within the next 10 to 15 years, and that a gap will develop between the demand and supply, which will lead to cost increases and possible shortages of oil. The energy security of oil importing countries that are increasingly dependent on imports is becoming an issue. Fluctuating fossil fuel prices may further compound the issue of energy security. South Africa currently imports about 65 % of its liquid fuel needs and the United States of America about 55 %. These figures are likely to increase. There is also growing concern about air pollution in especially the highly populated cities of the world, and about the effect of greenhouse gas emissions on global warming. Policies such as the Kyoto protocol are being implemented widely. South Africa is a signatory and will in future have to abide by these regulations to mitigate global warming. Depletion of natural resources is a further concern. Moreover it is difficult to store energy from renewable resources. Hydrogen together with fuel cell technology are one of only a few comprehensive long-term, sustainable solutions to the reduction of the greenhouse gas emissions and pollution from the transportation and fossil fuel based industrial sector. There are significant economic benefits for countries and companies that succeed in the field of hydrogen and fuel cell technology. Currently there is already a market demand for high end users and niche applications such as

space and military applications of hydrogen as fuel. Hydrogen as fuel source can contribute to solving the potable water crises as hydrogen production requires less water than is used in the production of hydrocarbon based fuels, resulting in significantly fewer negative environmental impacts on water systems, and its use as fuel to drive a polymer electrolyte membrane (PEM) fuel cell system for energy production produces clean water as a product (Benson et al., 2004).

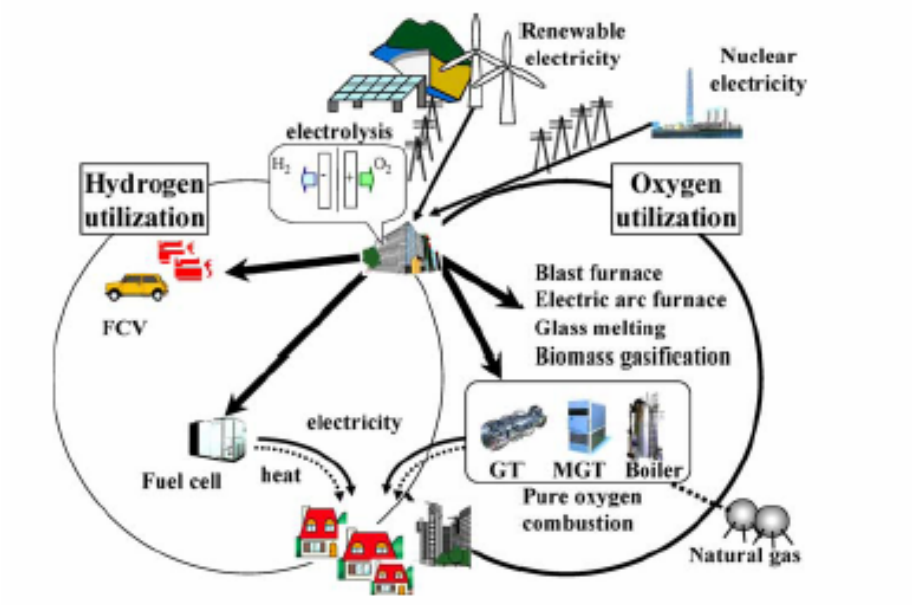

Figure 2.1 Schematic of Hydrogen Economy infrastructure (Kato et al., 2005).

The potential market for fuel cells and their related products is enormous with the global demand projected to reach $46 billion by 2011 and the potential for 2021 could exceed $2.6 trillion. In the hydrogen economy fitness of fuel cell technology and the supporting / peripheral (balance of plant) technologies will require development of innovative systems for competitiveness. Chief amongst these are innovation in fuel cells, hydrogen production and storage. Future product development would require techno-economic studies, techno-transfer, scale up, pilot studies and other issues such as venture capital and commercial partnerships. All these different aspects should be explored prior to expecting successful commercialization of hydrogen driven fuel cells (Benson et al., 2004).

It should be kept in mind that hydrogen is not truly a source of energy because it is mainly bonded in the form of water and requires more energy to liberate than it provides. Therefore to be non-polluting, the energy used to liberate or produce hydrogen should not be carbon based, thus should be derived from renewable sources such as wind or solar energy (Parfit, 2005).

2.2 GLOBAL PERSPECTIVE

It is estimated that the world currently uses 320 billion kilowatt-hours of energy a day and with development and growth this figure is projected to rise three-fold within the next century. Maturing global efforts for a wholesale conversion to hydrogen as fuel reflect a growing awareness of the many efficient, environmentally sound, and lower cost methods available today to produce and store hydrogen. Hydrogen is seen worldwide as the clean fuel of the future. Most of the major countries of the world have initiated coordinated investment and commercialisation strategies in the field of hydrogen and fuel cells, e.g. The United States of America, Canada, Japan, The European Union and Australia (Parfit, 2005).

In a July 8, 2005 memo entitled, "FY 2007" of the USA Administration Research and Development Budget Priorities Office of Science and Technology, from Policy Director, John Marburger and Office of Management and Budget Director, Joshua Bolten provided six pages of guidance to the heads of executive departments and agencies describing six "Interagency R&D Priorities"; and also "General R&D Program Guidance" and "R&D Investment Criteria." (Marburger et al., 2007). The following extract is noteworthy:

"In support of the President's Hydrogen Fuel Initiative, agency efforts should address the critical technology barriers of on-board hydrogen storage density, hydrogen production cost, and fuel cell cost, as well as distributed production and delivery systems. R&D should focus on novel materials for fuel cells and hydrogen storage (including nanostructured materials), durable and inexpensive catalysts, and hydrogen production from renewable energy, …and electrochemical processes…"

In addition to nationally coordinated plans, the United States of America has taken the lead to organize and implement international collaboration by forming the International Partnership for the Hydrogen Economy (IPHE). The terms of reference of the IPHE was signed by senior representatives of 16 countries on 20 November 2003. These countries are: The United States of America, Australia, Brazil, Canada, China, the European Commission, France, Germany, Iceland, India, Italy, Japan, Norway, Korea, the Russian Federation and the United Kingdom.

Internationally, the hydrogen economy, together with fuel cell technology, is receiving significant support and global investments are estimated to be in the region of US$3 billion per year. For instance, government funding in Japan totals about US$400 million, in the USA about US$500 million, in the EU about US$800 million, in Brazil a part of US$200 million, in Canada about US$50 million and in South Korea about US$50 million. In addition to this, there are substantial private sector investments. In the EU a consortium of 30 participants is working on the Cute (Clean Urban Transport for Europe) demonstration project to put into service a fleet of 27 clean and silent hydrogen buses on public transport networks in nine EU cities. Test buses are already operating in Porto, Madrid, Stockholm, Stuttgart and London. It is envisaged that eventually decentralized hydrogen production would make possible the fuelling of a car before it leaves the garage of a residential unit. Hycom projects, supported by the FP6, aimed at the development of a number of "hydrogen villages" demonstrating the concept are being planned. Moreover, two electrolysis pilot plants supplied by wind power are currently at the testing stage, in Greece and the Canary Islands, as part of an European project to demonstrate a reliable capacity for hydrogen production (HyWeb Gazette, 2008).

Recently, hydrogen production technologies have seen important improvements (Manitoba Hydrogen Steering Committee and Working Group, 2003). International research has mainly focused upon replacement technology for petroleum and the internal combustion engine in motor vehicles. Hydrogen fed fuel cells were already

used in the 1960`s in the Gemini aerospace program of NASA (United States). Although hydrogen fed fuel cells were used since the 1960`s for aerospace and military applications, the cost was a strong impediment for broader applications. With advances in the field, there are now several hydrogen vehicles in production, including those manufactured by the Hydrogen Car Company and Stuart Energy, and automobile manufacturers such as Mercedes, BMW, GM, and Ford. Moreover, fleet owners in the USA, are currently test driving hydrogen fuel cell vehicles and plan to replace some medium-duty vehicles in the short term and their entire fleets by 2014 (Benson et al., 2004).

It is important to identify the most promising hydrogen production methods that incorporate other forms of renewable energy. The USA DOE Hydrogen Program FY 2005 in its progress report on a low-cost, high-pressure hydrogen generator had as a target the development of a 1,500 kg per day hydrogen refueling station by 2010. Their intent was to develop and demonstrate a low-cost, high-pressure water electrolyzer system for hydrogen production and eliminate the need for mechanical hydrogen compression while increasing electrolyzer hydrogen discharge pressure to 5,000 psig. The goal of the DOE project was to reduce the cost of the stack and system to provide a cost-efficient reliable system for generating high-pressure hydrogen. To increase the hydrogen production pressure alternative materials and designs were evaluated for end-plates, internal cell components that support the membrane, and cell frames that provide sealing. To reduce cost, replacements for the expensive cell supports/current collectors were developed. Advances in materials and fabrication allowed the parts in electrolyzer cells to be decreased. Improving electrolyzer electrochemical performance reduced costs by decreasing the number of cells required to produce a given quantity of hydrogen, while maintaining efficiency. Performance was improved through use of thinner, less resistive membranes and advanced lower-cost catalysts and electrode structures. The operating life of thin membranes was a concern, particularly at the high differential pressures of operation but it was found that Nafion 115 membrane performance was stable over 2280 h. The

DOE project did not focus specifically upon the development of nanophase electrodes for achieving higher efficiencies (Norman and Schmitt, 2004).

Internationally, the recent escalation of gas prices and global instability has had the result that support of an alternative energy source such as hydrogen has increased, even though that may cost more initially. Europe and Asia have been pursuing environmentally friendly energy alternatives for years, whereas the USA has consistently moved toward higher energy consumption, for instance, by preferring larger vehicles that have high fuel consumption. The dependence of the United States on imported oil is today much higher than in the late 1970s (about 53% vs. 45%). The growing dependence on imported oil of the USA, has a direct effect on the economic stability of the rest of the world. This trend may finally be changing as negative aspects such as dependency on foreign oil, global warming, urban pollution, and acid rain become more apparent (Benson et al., 2004).

2.3 SOUTH AFRICAN PERSPECTIVE

In South Africa there is a strong need for distributed (off-grid) power supply and for load levelling and energy storage of excess off peak electricity. Moving electricity for long distances in South Africa requires balancing the energy system and there is a loss of energy when supplied over long distances. Energy levels have to be modulated according to use and it is necessary to create a range of options for supplying electricity to any one point of use. South Africa's high altitude, heat and tendency for lightening and fires provide further challenges. It is costly, wasteful and technically problematic to keep the system at full capacity constantly because demand for electricity fluctuates during the course of the day and over the seasons of the year. Different types of generation are necessary such as a base load, a mid-range that is provided at certain times and then short-lived spikes of high demand. Base load demand has risen significantly over the last few years in South Africa and peak demand capacity is lacking. Diversification of energy sources is necessary in future in order to make the necessary contribution to the reduction of greenhouse gases,

increasing costs. The current low price of electricity in South Africa and the low price increases up to date were due to past investment and are now at an end. Cost should be carried within the electricity system as it is in effect an investment in its future effectiveness (Erwin, 2006).

Internationally there is no strong research development of stand alone power generation for off grid electricity supply, since power supply to remote locations is very much a problem for developing nations such as South Africa that do not yet have installed capacity for all regions. This problem could be addressed in the medium term by on site solar or wind powered generation and use of hydrogen as fuel for fuel cells powering mini- grids, neighbourhoods or households (Benson et al., 2004).

SA representative Tony Surridge of the Department of Minerals and Energy (DME) was invited as observer to the International Partnership for the Hydrogen Economy (IPHE) that was launched at an USA- EU summit and it was recommended that South Africa join the IPHE. As a result of these and other networking interactions a stakeholder group was formed in SA called the South African Fuel Cell Initiative (SAFCI) which developed a hydrogen economy strategy that was published in 2006 by the Department of Science and Technology (DST) in order to position South Africa as a player in the field. The hydrogen economy as such is not currently part of the SA integrated energy plan. It would however fit in under the drive towards renewable energy sources (Benson et al., 2004). The access to a cheap and clean fuel such as hydrogen is essential for a country that needs to increase or maintain economic growth but simultaneously needs to minimize environmental pollution.

Currently, South African direct investment into the local hydrogen economy and fuel cell technology developments amounts to only about R5 million per year (only about 0.03% of the global investment) but this is growing. For South Africa to participate as a partner in the new US and worldwide H_2 economy development and not become an economic hostage, capability is essential in the following key areas: H_2 production

and storage, Pt/PGM beneficiation and application as nanophase catalysts in systems such as fuel cells and solid state electrolyzers, novel inorganic proton conductors based on nanophase metal oxides, manpower and scarce skills development, environmental compliance, regulatory requirements, infrastructural developments and governmental support in all these areas. Future product development requires techno-economic studies, techno-transfer, scale up, pilot studies and other issues such as venture capital and commercial partnerships (Benson et al, 2004).

SA industry has a continuous need to stay competitive by reducing costs, increasing market share and developing new products. Especially in the area of high technology, international competition is strong. Should SA companies license international technology it comes at a high price. South Africa's rich platinum reserves could assist to make it a key player in future energy technologies. Anglo Platinum, South Africa's largest platinum producer, has plans to start investing in the development of hydrogen technology, and has significant holdings in Johnson Matthey (UK), one of the leading researchers in the platinum market and international suppliers of electrocatalysts (Bruce, 1996).

South Africa's main supplier of electricity, the parastatal ESKOM, has expressed its commitment to embracing renewable energy sources such as wind turbines, fuel cells and photo-voltaics as a part of its complete energy generation portfolio. There is also a direct need for hydrogen within ESKOM as cooling gas for the generators/ reactors of the power stations. Besides using hydrogen as cooling gas ESKOM should be in a position to take an active role in the energy supply of the future, locally and internationally. Moreover, ESKOM has a significant need for distributed (off-grid) power supply and for load leveling and energy storage, which can be addressed by the production of hydrogen as fuel. Therefore ESKOM has an interest in the hydrogen economy including hydrogen generation, distribution, storage, conversion to energy using fuel cells, and applications of energy devices fueled by hydrogen. It is the direct availability of hydrogen for energy storage that will affect the decision of companies at which stage to switch their power requirements to fuel cell sources and

ESKOM would benefit immensely from offering a complete approach to renewable energy generation and distribution (G.Gericke, Eskom representative, personal communication).

Many inhabitants of South Africa do not have direct access to electrical power. One of the priorities of the Department of Trade and Industry (DTI) is to drastically reduce this number. ESKOM has indicated that small scale, local generation of electrical energy is the only answer to this commitment of the DTI. The technology competing with fuel cells in this segment of the market are solar cells and wind mills/turbines. Even though these alternative energy generation devices are low maintenance solutions, energy storage using conventional lead acid batteries is a weak link. The production of hydrogen using excess energy that cannot otherwise be stored can be used to ensure continued power supply and will eventually be a more economic solution (Yumurtaci & Bilgen, 2004).

It should be noted that if hydrogen production is much cheaper when alternative routes such as nuclear power is used or if the steam reforming process is widely adopted then those processes will be used for hydrogen production. However, for some situations the economic picture of the production of hydrogen is different. First of all, electrolysis of water is a much simpler technology than steam reforming (or nuclear power) which makes water electrolysis more competitive on the small scale. Secondly, renewable energy sources like wind and solar energy are available almost everywhere in South Africa unlike natural gas or coal. Harnessing these resources for small communities' power needs would make a big difference to the quality of life of many people in this country. Thirdly, electrolysis can be strongly recommended as an integrated technology in existing power stations for hydrogen production during off peak hours, when electricity is cheap (Barbir, 2005).

2.4 THE HYDROGEN ECONOMY

CHAPTER 2

Hydrogen is one of the most important feed stock gases with an annual global demand of more than 1,6 trillion m^3 (SHEC-labs press release, 2006). Hydrogen is considered as an industrial commodity in the energy using sectors. It is widely consumed by industries involved in ammonia production, refining and petrochemicals production, methanol synthesis, chemical production, paper, textiles and steel manufacturing, fat and oil hydration units, manufacturing of vegetable oils, float glass producers, electronics, and metal treatments. Apart from the conventional uses, hydrogen as a fuel can be utilized as liquid hydrogen at fuelling stations for vehicles or as compressed hydrogen for onboard storage in vehicles. Hybrid electric vehicles where hydrogen is injected along with the conventional fuels to the internal combustion engines is seen as a relatively immediate route to diminishing emissions and an intermediate option prior to fully integrated hydrogen powered vehicles. Moreover, hydrogen as fuel would be suitable for distributed power applications for producing power on demand, or uninterrupted power supplies. It is also possible to utilize hydrogen as fuel for fuel cell energy for mobile applications replacing lap top batteries, mobile phone batteries and other battery powered electronic devices. Hydrogen has already been used as fuel for a variety of military applications (Benson et al, 2004).

The amount of energy released during the reaction of hydrogen on a mass basis is approximately 2.5 times the heat of combustion of hydrocarbon fuels. Hydrogen is also an attractive energy carrier for its high energy/weight ratio. The energy produced by hydrogen per unit weight of fuel is approximately three times the amount of energy contained in the equivalent weight of hydrocarbon based fuel. The advantages of hydrogen in the pure form make hydrogen a potential alternative fuel with higher efficiency than that of known fuels (Frost and Sullivan, 2003; 2004).

Its further value as an energy carrier, rather than as a direct fuel, is because excess energy can be stored in the form of hydrogen. Subsequently the stored energy is released during the oxidation of hydrogen in the form of electrical energy by using hydrogen as fuel for a fuel cell. A fuel cell is an electrochemical system, which

converts chemical energy to electrical energy. A fuel cell differs from a battery in that fuels are continuously supplied and also the products, mainly water, are continuously removed. Hydrogen will be a major factor in successful fuel cell commercialization. The high efficiency of fuel cells makes hydrogen a cost effective, energy efficient, and environmentally friendly alternative to current fuels when considering the full lifecycle (Thomas et al., 1998).

The benefit of the hydrogen production- storage- transport chain forms the basis of the hydrogen economy. The pure "hydrogen economy" is the ideal situation. Barriers to implementing the hydrogen economy include the need to improve the performance of hydrogen and hydrogen related technologies in order to advance an economically viable hydrogen economy (Thomas et al., 1998).

Hydrogen is looked upon as one of the best alternatives to fossil fuels. Burning hydrogen as a fuel in vehicles will reduce nitrogen oxide emissions. The combustion of hydrogen does not produce pollutants such as particulate matter or sulfur emissions. When burnt as a fuel or converted to electricity, the only by product is water. If hydrogen is produced using non-fossil fuels, then it is possible to reduce carbon dioxide and carbon monoxide emissions in the transportation sector. With no CO_2, CO, NOx or SOx emissions from hydrogen fueled devices there will be a much lower release of greenhouse gases, thus there would be a negligible impact on global warming. Studies of the impact of hydrogen use would have on air pollution and the climate showed that if vehicles were powered entirely by hydrogen fuel cell technology, anthropogenic emissions of the ozone precursors nitrogen oxide and carbon monoxide could be reduced by up to 50%, but this would depend on the technology used to generate the hydrogen (Frost and Sullivan, 2003; 2004). Thus, the concept of a hydrogen-based energy and transportation system offers energy resource flexibility and the potential for energy independence, as well as the elimination of net carbon dioxide emissions. Use of hydrogen as a fuel offers the opportunity to shift the energy requirements for, for instance transportation, from imported oil to diverse, domestically available resources. Hydrogen powered fuel cell vehicles are an

attractive alternative to gasoline and diesel powered automobiles as they emit only water with essentially no criteria pollutants.

However, progress in implementation is hampered until a system of hydrogen production, storage, distribution and utilization is put into place with appropriate standards and the correct legislative environment. Despite significant advances and commitment of resources by technology providers, end-users and international governments, experts project that extensive use of hydrogen as fuel for fuel cell vehicles is at least ten years away. This problem could be addressed in the medium term by on site solar or wind-powered generation and use of hydrogen as fuel for fuel cells powering mini- grids, neighbourhoods or households (Benson et al, 2004). Barriers to the hydrogen economy include the lack of infrastructure for distribution and storage of hydrogen (Nielsen et al., 2004). Moreover there are significant challenges in meeting the present price of conventional fuels because of the cost and inefficiencies of current hydrogen production and storage technologies. A further issue is the matter of consumer perception relating to safety risks. Codes of practice and the correct legislation as well as standardization and government policies would need to be considered as well.

Hydrogen could be generated by water electrolysis using renewable energy and the generated hydrogen stored and later used as an input for fuel cells to generate electricity. Hydrogen and electricity would be generated as long as it is required by the applications. Large-scale stationary fuel cells fed by hydrogen would be able to meet the demand of delocalized industrial, agricultural, tertiary or residential users. Other scenarios that have been envisaged for the implementation of hydrogen as fuel for fuel cells include a home hydrogen refueling unit that consists of a small-scale electrolyzer powered by mains electricity that converts water from the domestic supply into a slow stream of hydrogen (Ivy, 2004). The only local emission is oxygen. The technology offers the prospect of car users parking at the end of the day and connecting their vehicles to home refueling units for a hydrogen refill overnight. Shell Hydrogen is exploring the potential of home hydrogen refueling as part of a

global hydrogen refueling infrastructure, and is participating in demonstration projects of hydrogen refueling stations, for instance, in Reykjavik, Iceland. Jeremy Bentham, chief executive officer of Shell Hydrogen said that ultimately customers would decide how they wanted to receive hydrogen. He noted that for widespread acceptance, refueling infrastructure should resemble existing infrastructure and foresaw that new and innovative solutions, such as home refueling, may prove successful with consumers. His opinion was that home refueling may be a solution for remote locations or regions with limited hydrogen demand. Technical problems such as hydrogen storage should still however, be resolved (Bentham, 2005).

Hydrogen is a high cost fuel and the price should be reduced for successful commercialization to be achieved. Options of generating hydrogen that are being explored include hydrocarbon based onboard reformers for use with fuel cells, but because of associated costs this is not yet feasible. However, the requirement to reduce green house emissions in automobiles would in future prevent hydrogen generation using reforming technologies. Hydrogen gas may be formed by water electrolysis and this process may ultimately be used as the cleanest way of supplying or generating fuel in a fuel processor for fuel cell utilization, provided that the electricity used is generated from renewable sources such as wind and solar (Sørensen et al., 2004). Water electrolysis as means of hydrogen production is a suitable alternative for the existing reforming technologies because of its environmental friendliness, and because of fluctuations in the price of natural gas or other conventional hydrocarbons.

Emission during electrolysis when renewable energy is used to split water to hydrogen is virtually zero. Hydrogen is produced via electrolysis by passing electricity through two electrodes in water. The water molecule is split and produces oxygen at the anode and hydrogen at the cathode. The only requirement is that hydrogen should be produced in a controlled environment to minimize hazards and then can be used anywhere as fuel without leaving a trace of pollution (Janssen et al., 2004).

CHAPTER 2

Price and performance determine the market success of hydrogen. In order for hydrogen from water electrolysis to achieve significant market penetration and widespread acceptance, it must be more efficient, equally convenient, and cheaper than other routes to prepare hydrogen, or cheaper than other sources of fuel such as petroleum, or have significant environmental or logistical benefits. Off peak electricity prices are one way by which electrolytic hydrogen production can become more economical. This approach is especially important for large territory developing countries, like South Africa (Benson et al., 2004).

Hydrogen as fuel does however, present significant challenges to commercial production, storage and transportation. Although hydrogen has the highest energy density of known fuel, it should be stored as a compressed gas or as cryogenic liquid if not generated on site and used directly. Compressors have to be deployed in order to step up the pressure of hydrogen as hydrogen is produced at low pressure. Storing hydrogen in compressed gas or cryogenic liquid form requires special handling techniques and high safety standards. Hydrogen must be liquefied at -253 º C in order to store a useful amount of hydrogen particularly for vehicles, but liquefaction is time-consuming and energy-intensive. Using current compression or liquefaction technology, about 30 % to 40 % of the energy content in the hydrogen could be lost in the process. Compressed hydrogen would require huge tanks for storage, which create space problems for onboard storage and require adequate safety standards. It is estimated that a hydrogen gas tank would be 3000 times bigger than a conventional fuel tank, to store the same energy equivalents (Frost and Sullivan, 2004).

Hydrogen generation is fundamentally important for renewable power generation applications. Grid stability and intermittency issues limit the market for use of renewables such as wind and solar in the electricity market, according to US DOE's National Renewable Energy Laboratory; but the addition of hydrogen could help. The combination of renewable technologies with hydrogen production and storage, would enable intermittent renewables such as wind and solar to contribute to a larger share

of the power production market without major upgrades to the existing grid. Because most sources of renewable energy are intermittent in nature (i.e. when the sun does not shine, or the wind does not blow, electricity from solar panels and wind turbines, respectively, cannot be generated), their practical use is limited unless the user is also connected to the electricity grid or installs large, heavy and relatively expensive battery backup systems. For non- grid-connected electricity supply, renewables such as wind and solar generation cannot produce electricity in response to demand. These technologies only produce when the source of energy (wind or solar) is available. This increases the system costs, as extra storage is necessary if renewables are the only source of energy (Sørensen et al., 2004).

The use of water electrolysis for hydrogen generation addresses this limitation by enabling the production and storage of hydrogen to occur during times of excess electricity generation and allowing for the later generation of electricity. The hydrogen produced can be utilized at any given moment in a fuel cell to generate electrical energy or as a fuel for heating or cooking appliances. According to the IEA Renewable Energy paper (2002), renewable sources of power that can be applied as energy source for hydrogen production include hydro, geothermal, solar thermal, solar photovoltaics, tide, wind, renewable municipal solid waste, solid biomass and gases from biomass. Key issues are reliability and durability of hydrogen production systems and their integration with subsequent storage systems and delivery to power generation units such as fuel cells.

Renewable energy sources by themselves do supply energy without being coupled to hydrogen generation systems, but have various drawbacks. Wind energy generation in good wind areas, is comparable to fossil fuels when economic or environmental costs are factored in, but is still not entirely satisfactory because of the unsightliness and large footprint of wind arrays for bulk power generation as well as the unreliability and intermittent nature of wind. Wind generators can be immobile for days or suddenly produce an excess of power. Wind energy which, in fact, is also solar energy in the form of the movement of sun- warmed air, is becoming more

competitive. In the EU the equivalent of 35 large coal power plants of installed wind generator capacity already provides about 35000 megawatts of power. Wind and solar systems require a way to store excess capacity and this is where hydrogen generation fits in. Conversion of wind energy to hydrogen demonstrates the value of hydrogen as an energy storage medium for excess wind power, and is a feasible example of what is possible in future (Parfit, 2005).

Renewable energy from the sun can be captured using photo-voltaics in for instance, thin film solar cells. According to the IEA Renewable Energy paper (2000) the costs of solar based energy systems including photo-voltaics have decreased very significantly over the years and are now considered cost competitive for a number of grid-connected, building-integrated uses as well as for off-grid applications. The drawback is energy storage requirements, since the peak electricity demand is not usually during the daytime in summer. Moreover, many areas of the world do not receive significant solar flux during certain seasons. Solar photovoltaic arrays demand a large area of land which cannot always be accommodated economically. Solar thermal technologies are being installed widely for heating and hot water for residential, commercial and industrial end uses and are relatively competitive. Large scale solar thermal systems are not yet economically competitive for providing heat to produce steam for power generation.

Renewable energy from the sun can be captured by using solar thermal (SOT) energy conversion systems. SOT collects direct solar radiation via parabolic trough mirrors which are then focussed on heat exchanger systems allowing the heat to be transferred to steam which is passed though a turbine to generate electricity. At this stage of development however, the costs are still considerably higher than fossil fuel based energy (Parfit, 2005). Geothermal systems are used for power generation and space heating applications where hot water or steam resources are available at a high temperature and near the earth's surface. Ocean energy systems based upon tidal forces, ocean currents, wave power or thermal gradients are being explored to produce electricity. Hydrogen, generated from excess capacity derived from

renewable power, is seen as a major potential contributor to the sustainability of the energy sector. In the longer term, if costs can be dramatically reduced, hydrogen can act as the crucial storage medium and carrier of energy produced from renewables (IEA Renewable Energy paper, 2000).

2.5 NANOTECHNOLOGY

Material properties change dramatically when constructed from particles that are less than 100nm in size, that is, when materials are structured at the nanoscale. Large, highly active catalyst surface areas with the minimal catalyst expenditure are obtainable using such nanophase materials. In recent years, nanostructured electrode materials suitable for energy devices have attracted great interests since they show better rate capabilities than conventional electrodes composed of the same materials. The high specific surface area of these materials also has significant implications with respect to energy storage devices based on electrochemically active sites (batteries, supercapacitors) and energy conversion devices (fuel cells and thermoelectric devices). In electrolyzer technologies significant improvements are possible using nanophase materials as the cost of the currently used bulk phase Pt containing electrocatalysts are very high(Li, et al., 2000 a&b; Spahr et al., 1999; Shen et al., 2003; Zhou et al., 2003).

Nanotechnology has been identified as a lead project in the National Advanced Manufacturing and Logistics Technology Strategy developed by the National Advisory Council on Innovation (NACI) as well as in the Advanced Materials Technology Strategy (AMTS) for the Department of Science and Technology (DST) in South Africa. In the light of huge international R & D spending in the Hydrogen Economy and also in Nanotechnology development, the DST has recently investigated the necessity of strategic planning and funding in the area of both nanotechnology and the hydrogen economy. The author of this thesis was closely involved with the development of appropriate government commissioned strategies for South Africa in Nanotechnology (Scriba et al., 2003) and the hydrogen economy

(Benson et al., 2004) and in the associated commissioned baseline studies and the thesis is designed specifically to address some of the components relating to integration of Nanotechnology in the hydrogen economy.

Nanotechnology will be an integral part of manufactured goods relating to energy systems in future and SA will have to be a player. Already South Africa has to pay substantial annual technology licence fees to manufacture goods, pharmaceuticals, chemicals and many other products and services. Unless South Africa develops applications of nanotechnology in appropriate processes and products, specifically relating to the energy sector, future technological benefits in this field could only be enjoyed at great cost to our nation. Furthermore nanotechnology is an emerging technology and real industrial applications might only be commercialised in SA in a few years time, giving South Africa a window of opportunity to become a player. Additionally, the natural resource base of platinum (Pt) and platinum group metals (PGMs) such as ruthenium, palladium, and iridium, which might give South Africa a strategic advantage relating to energy production, are currently being exported without full beneficiation. South Africa's known reserve base of PGMs represented 87,7 per cent of the world total (Kendal, 2006). Other countries are importing bulk PGM's, precisely for beneficiation by development into electrocatalysts applicable in energy systems such as fuel cells. Development of PGM containing electrocatalysts for energy systems such as fuel cells and PEM electrolyzers is a key area where South Africa has a significant strategic advantage if beneficiation is done locally (Scriba et al., 2003).

There is a major potential for the generation of new knowledge and successful commercial products in the application of nanotechnology in energy systems, which will impact upon the strategic advantage of South Africa. Advances in fabrication and processing of nano-sized materials have the potential to reduce the costs and increase the efficiency of existing energy generation technology such as water electrolyzers and fuel cells. The renewable power generation sector in particular stands to benefit from appropriate implementation of novel nanoscale materials in integrated energy

generation systems. The economic windfall for the applications of nanotechnology based research in energy generation is expected to have a huge commercial potential. Moreover, expertise in integration of nanotechnology in energy systems should be developed and a product base established in South Africa in this fast developing technology focus area. The development of home grown technology based on nanotechnology will benefit South Africa in the long run by assisting to prevent marginalization, and saving foreign currency and will contribute to the bridging of the technological divide in line with national strategy (Scriba et al., 2003).

Nanotechnology can be used to reduce noble metal content of electrodes and thus capital costs, and also improve efficiency of hydrogen generation systems such as alkaline flow cells as well as solid state PEM electrolyzers. This is possible by, for instance, the development of novel nanophase electrode materials that replace the existing electrodes or electrocatalysts respectively required, for such hydrogen production systems. In the case where noble metals and non-noble metal oxides are used as electrocatalysts for cathodes and anodes, development of efficient nanosized catalysts is of great industrial interest. Large, highly active catalyst surface areas with the minimal catalyst expenditure are obtainable using such nano structured materials. In recent years, nanostructured electrode materials have attracted great interests since the nanostructured electrodes show better rate capabilities than conventional electrodes composed of the same materials. The surface area of the nanostructured electrode is much larger. The high specific surface area of these materials also has significant implications with respect to energy storage devices based on electrochemically active sites (batteries, supercapacitors) and energy conversion devices depending on catalytic site of defect structure (fuel cells and thermoelectric devices) (Li, et al., 2000 a&b; Spahr et al., 1999; Shen et al., 2003; Zhou et al., 2003).

In the surface coverage of a substrate with catalysts, the relatively low amount of active sites obtainable per unit area in a two dimensional plane has to date not resulted in sufficiently high catalytic activity for overcoming the barrier to producing cost competitive catalytic electrodes for hydrogen production or fuel cell

applications. The potential application of three dimensional catalytic supports for maximum dispersion of nanophase electrocatalysts for hydrogen production in a solid state electrolyzer is being explored in this thesis. In this approach, the highest number of active sites per unit volume may be obtainable in close contact with the solid electrolyte, Nafion®.

2.6 HYDROGEN PRODUCTION

A range of renewable and non-renewable hydrogen production options and technologies exist and include ethanol reformation and partial oxidation, nuclear, biomass fermentation and photosynthesis, electrolysis via wind, hydro, solar, thermochemical cycles, biomass and coal gasification and sequestration. Production, storage and transport of hydrogen is, however, still problematic and costly. Specifically, hydrogen production technologies that reduce environmental impacts are required for an energy system that will in future be based on renewable and carbon-neutral hydrogen production. This approach should also promote economic development and energy independence and security for countries such as South Africa (Nordstrom, 2002).

Hydrogen is conventionally produced by three methods, namely thermochemically, by electrolysis, and by photochemical reactions, depending on the feedstock used to generate hydrogen. Competing fuels are biofuels, methanol and natural gas. It is estimated that 48% of hydrogen is produced from natural gas, 30 % from oil, 18 % from coal, and the remaining 4% through water electrolysis. Thermochemical technologies for hydrogen production use heat and chemical reactions to convert hydrocarbon feedstocks to hydrogen. Some of the thermochemical processes used for producing hydrogen are steam methane reforming, partial oxidation of methane, and biomass gasification. A reformer is used to separate the hydrogen from methanol, natural gas, or other light hydrocarbons. In the steam reforming process, hydrogen is produced by mixing either natural gas, liquid petroleum gas (LPG) or naptha with steam. The reformer has to extract as much hydrogen as possible with low emission

of pollutants such as carbon monoxide. The hydrocarbon feedstock is reacted with water vapour to liberate hydrogen and carbon monoxide. The water vapour reacts with carbon monoxide to form carbon dioxide and hydrogen. Crude hydrogen is generated when this mixture is heated in the presence of a catalyst. The crude hydrogen is then purified up to 99.99 % by using pressure swing adsorption (PSA).

Electrolysis is a proven and easy method to generate hydrogen on a large scale for conventional industrial markets. In electrolysis, electrical energy is used to break the bond between the hydrogen and oxygen in water. Hydrogen and oxygen are liberated as elemental gases in the electrolysis process.

Other possible routes for hydrogen production are for instance, by photo electrochemical methods, biological methods, and biomass reforming. Apart from direct solar electrolysis, biomass fermentation is a further method for producing hydrogen. These methods still have to overcome challenges such as efficiency (for instance, to convert sunlight, via bacterial interaction to hydrogen), and the availability of the resources for the generation of hydrogen. Biomass reforming, using enzymatic decomposition of sugars, or steam-reforming of bio-oils and gasification, suffers from low hydrogen production rates, impure effluent streams causing complex processing requirements as well as significant environmental costs. Such technologies may generally suitable for large-scale production but are associated with costly purification operations (Frost & Sullivan, 2004).

Dissociation of water is a reaction that is not favoured thermodynamically, requiring extremely high temperatures (> 2200 ºC) for obtaining a significant degree of dissociation. However, solar thermal power plants (STPP) may be a viable option to fulfil the world's enormous expectation of clean electrical energy. The World Bank expects very significant investment in STPPs over the next 20 to 30 years. It is widely accepted that electricity produced by such solar thermal concentrating systems is the cheapest solar generated electricity available today (Goswami, 1998).

CHAPTER 2

Thermal splitting of water by high temperature solar energy is possible using metal/oxide cycles, based on materials that can act as effective redox catalysts via two-step water splitting process at lower temperatures. A metal oxide is reduced delivering some of its lattice oxygen; during the second step the reduced catalyst is oxidized by taking oxygen from water and producing hydrogen. The synthesis of oxide-based redox catalysts with high defect concentration and their incorporation upon ceramic thin-wall multichannelled monolithic honeycomb reactors as supports where the catalyst particles are coated upon the inner walls of the honeycomb structure, act as collectors of solar heat and achieve temperatures in excess of 1100ºC, due to their high absorbance and thermal conductivity. A 10 MW solar thermal power plant was scheduled to produce electricity in 2002 in Spain and plans for additional plants are in progress (Frost and Sullivan, 2003; 2004).

Another method to produce hydrogen using solar energy is by using photo catalytic cells in series. Solar power is used to break the water molecule in the electrolyte over a thin film of photo catalyst for direct conversion of solar energy and can convert more than 8 per cent of solar energy to hydrogen fuel. The catalyst comprises nano crystalline metal oxide films for the absorption of solar energy. This system is marketed by Hydrogen Solar Ltd and was developed in collaboration with Ecole Polytechnique Federale de Lausanne (EPFL), Switzerland and the University of Geneva (Frost and Sullivan, 2004).

A high-temperature solar reactor has been developed by Laboratoire Procédés, Matériaux, et Energie Solaire (Processes, Materials, and Solar Energy Laboratory), France that can be used to produce hydrogen, based on natural gas de-carbonization. The solar reactor co-produces hydrogen-rich gas and high-grade carbon black (CB) from concentrated solar energy via a single-step thermal pyrolysis of methane without using catalysts. The maximum chemical conversion of methane to hydrogen and CB was found to be 95 % and the typical conversion was in the range of 30 % to 90 % (Frost and Sullivan, 2004).

US Patent 6,726,893 by Lee et al., (2004) describes a method for hydrogen production by high-temperature water splitting using electron-conducting membranes. In the photoelectrochemical method of hydrogen production, the development of novel photo anode materials, which utilizes maximum solar energy is essential. The hydrogen storage material should have 6.5 wt % of reversible hydrogen storage capacity which are limitations.

Millennium Cell, Inc. (MCEL) Hydrogen on Demand (HOD™) produces a system that generates pure hydrogen from environment friendly raw materials. The hydrogen is stored at ambient conditions in an aqueous solution of sodium borohydride ($NaBH_4$).

Microbes allow the production of hydrogen from carbohydrates for instance by using naturally occurring, hardy and non-recombinant *Thermotoga neapolitana* organisms. 14 L of culture can produce at least 8 L of hydrogen at STP. This process does not require sunlight or open ponds and produces very little sulfur dioxide so there is no danger of poisoning the fuel cell. The process was developed by National Energy Technology Laboratory and Brookhaven National Laboratory. The Institute of Chemistry, Chinese Academy of Sciences, Beijing, generated hydrogen with anaerobic mixed bacteria on a large scale using residues containing sucrose. 99 % of the product gas is composed of hydrogen and carbon dioxide without methane. Generally it has been found necessary to increase the bioactivity of hydrogen-producing bacteria for these processes (Frost and Sullivan, 2004).

US Patent 6,737,184 by Rusta-Sellehy and Frank (2004) describes a chemical hydride hydrogen generation system as a way to produce hydrogen by using sodium borohydride which is reacted with steam in the gas phase to liberate hydrogen and claims that under certain conditions the reaction can liberate essentially 100 % of the hydrogen from the hydrides using steam.

CHAPTER 2

Hydrogen production is possible by water electrolysis. Hydrogen can be produced via electrolysis using zero emission technologies to produce carbon-dioxide –free energy. However, this would require a vast expansion of renewable energy capability to allow sufficient capacity for hydrogen to be a contender to fossil fuel derived energy.

2.7 WATER ELECTROLYSIS

Hydrogen can be produced either at small or large scale at any location by implementation of water electrolysis. Hydrogen production by electrolysis and subsequent storage is one option for conversion and storage of energy. This process is fundamentally important for renewable power generation applications. Renewable sources of energy such as hydropower, ocean thermal energy conversion, tidal power, solar, wind, geothermal or biomass can be used as energy source for driving electrolysis systems for hydrogen production but only small decentralized electrolysis systems can be coupled to these renewable energy sources without need for significant additional infrastructure (R.Wurster and J. Schindler in Vielstich et al., 2003: 64). Systems should be compatible with the fluctuating power supply that is typical for renewable energy supplies.

In hydrogen production by electrolysis of water it is important to consider the geographical location of energy generation, availability of water resources and requirements for transport of energy in relation to the energy user. Electricity provided to an electrolysis system should be available according to the system requirements of power and voltage, thus usually needing rectifiers and inverters. Other issues are requirements for small-scale versus large scale generators. Furthermore, the benefits of distributed versus centralized production, requirements for purification, and conversion technologies for liquefaction of hydrogen or gas compression and storage should also be kept in mind. It will also be important to evaluate the technical and economic feasibility of obtaining hydrogen from scattered renewable sources within any particular region and transporting it to market. Life-

cycle costs must be established to supply hydrogen to the end user via various options such as either liquid or gas form; transportation with pipeline or tanker truck; storage in metal hydrides or ethanol, etc. High-pressure electrolysis is feasible for distributed, on-site hydrogen production without the need for additional compression (usually to 5000 psi) and production of hydrogen by electrolysis would become much more competitive by eliminating the need for a compression step. High pressure generation would not only improve efficiency but also reduce the cost and maintenance of compressors. High pressure electrolysis would make hydrogen storage and transport in pipelines more feasible. Moreover, the use of hydrogen as fuel in fuel cells to provide heat, power and cooling in homes, businesses and other institutions is envisaged to become a practical option (Nordstrom, 2002).

Hydrogen generation by electrolysis include alkaline flow cells as well as solid state electrolyzers that are based on reverse fuel cell systems called Proton Exchange Membrane (PEM) electrolysis units (Ivy, 2004). Two types of electrolyzers are used, based on the electrolyte, namely electrolyzers that typically use caustic electrolytes (KOH or NaOH), and PEM based electolyzers that use solid polymer electrolytes (SPE) and thus are also known as SPE electrolyzers. In electrolyzers it is possible to separately generate the H_2 in high purity but at relatively low pressures. The electricity passed through the electrolyte solution splits water in to hydrogen and oxygen. These gases are generated separately in chambers separated by a gas impermeable membrane. Various other types of electrolytes can also be applied such as acidic electrolytes to optimize conductivity. After purification from residual oxygen the hydrogen can be compressed for storage. Unfortunately compression is expensive. Companies that produce such systems are Norsk Hydro, Norway and Stuart Energy, Canada, Shell etc. High pressure electrolyzers have been developed for producing smaller volumes of hydrogen in the range of 10 to 65 $Nm^3\ h^{-1}$. The electrolyzer discharges the hydrogen at a pressure of 15 bar, which eliminates the need for compressors. Atmospheric electrolyzers can produce hydrogen volumes from 60 $Nm^3\ h^{-1}$ or more (Barbir, 2005).

PEM electrolyzers typically use a solid polymer electrolyte membrane such as Nafion in the place of a fluid alkaline or acidic electrolyte. The electrolyzers have the ability to electrochemically generate hydrogen at pressures of more than 2000 psi, eliminating the need for mechanical compression. The benefits of PEM vs alkaline electrolyzers are that the solid electrolyte should last for the lifetime of the electrolyzer whereas the alkali electrolyte requires replenishing and disposal of corrosive wastes. Moreover, the purity of H_2 is significantly greater in a PEM system and the hazards of explosive gas mixtures are eliminated. PEM electrolyzer technologies have been commercially developed for hydrogen generation by companies such as Ballard Power Systems or Hydrogenics Corporation, Canada and Proton Energy Systems, United States. Automobile companies such as General Motors are also involved to produce onboard systems. In vehicles, the liberated hydrogen fuel prepared in an onboard system is stored in a metal hydride storage module, prior to being fed to a fuel cell to produce electricity (Turner, 2004).

PEM electrolyzers can also be used in a format called a regenerative fuel cell system, which uses renewable electricity to produce hydrogen by electrolysis and then by reversing the process uses the hydrogen in turn, to produce electricity for power applications. This system is suited for back up power systems that could be powered by grid, renewable energy sources or hydroelectric sources (Lee et al., 2004).

Electrolyzers are available as pressurized units typically between 1 and 3 MPa. Various types of industrial electrolysis units are commercialy produced. Some involve an aqueous electrolyte solution of potassium hydroxide (usually 30 % v/v KOH), which is used because of its high conductivity, and these units are referred to as alkaline electrolyzers. These units can be either unipolar or bipolar (Ivy, 2004). The unipolar electrolyzer resembles a tank and has electrodes connected in parallel. A membrane is placed between the cathode and anode, which separates the hydrogen and oxygen gases that are produced, but allows the transfer of ions. The bipolar design resembles a filter press. Electrolysis cells are connected in series, and hydrogen is produced on one side of the cell, oxygen on the other. Again, a

membrane separates the electrodes. SPE or PEM electrolyzers may be applicable for the home or as small neighbourhood systems (Ivy, 2004).

The high capital costs of SPE or PEM units limit their current viability in the large hydrogen production market, while alkaline units, with their lower capital costs, can produce hydrogen across a range of capacities. In the SPE unit the electrolyte is a solid ion conducting membrane as opposed to the aqueous solution in the alkaline electrolyzers. The membrane allows the H^+ ion to transfer from the anode side of the membrane to the cathode side, where it forms hydrogen. The SPE membrane also serves to separate the hydrogen and oxygen gases, as oxygen is produced at the anode on one side of the membrane and hydrogen is produced on the opposite side of the membrane, at the cathode (Ivy, 2004).

The electrochemical dissociation of water includes:

Reduction of water : $4H_2O + 4e^- \rightarrow H_2 + 2OH^-$
Oxidation of water : $2H_2O - 4e^- \rightarrow O_2 + 4H^+ + 4e^-$

The cathodic evolution of hydrogen from acidic solutions is due to a discharge of hydroxonium ions:
$H_3O^+ + e = ½H_2 + H_2O$.

In alkaline and neutral solutions, hydrogen evolution is associated with a discharge (ionization) of water molecules:

$H_2O + e = ½H_2 + OH^-$

The cathodic evolution of hydrogen occurs at potentials that are more negative than that of the equilibrium hydrogen electrode. A shift in the potential under the action of an electric current, φ_i, from its equilibrium value, φ_τ, which is necessary to initiate the

cathodic evolution of hydrogen on a given electrode at a given rate of j is termed as the overvoltage of hydrogen evolution, η_{H2}.

The magnitude of the hydrogen overvoltage is a measure of the irreversibility of the cathodic evolution process of hydrogen, and it is dependent upon the current density, j, as well as the type of electrode, temperature, and electrolyte composition. Depending on these factors, η_{H2} might vary from a few millivolts to 1.5 V and more.

In the case of moderate or high values of the hydrogen overvoltage, its dependence versus the current density is described by the Tafels equation (Tafel, 1905):

$$\eta_{H2} = a + b \lg j, \qquad (2.1)$$

where a and b are coefficients, which may be determined according to a linear sector of the semi-logarithmic dependence $\eta_{H2} - \lg j$, or $\varphi_j - \lg j$.

An analysis of both coefficients of the Tafels equation and the dependencies reached provides a means to study the mechanism, the kinetics and the limiting stage of the cathodic evolution of hydrogen. This dependence makes it possible also to obtain the value of the exchange current density, $\lg j_o$, which characterizes the exchange kinetics of the charged species between the electrode and solution at the equilibrium potential φ_τ.

In a SPE system the reactions at the electrodes are:

Hydrogen Production at the Cathode: $2\ H^+ + 2e^- \longrightarrow H_2$

Oxygen Production at the Anode: $H_2O \rightarrow ½\ O_2 + 2\ H^+ + 2e^-$

In an alkaline system the reaction at each electrode is:

Alkaline Hydrogen Production at the Cathode: $2\ H_2O + 2e^- \rightarrow H_2 + 2OH^-$

Alkaline Oxygen Production at the Anode: $2OH^- \rightarrow ½\ O_2 + 2\ H_2O + 2e^-$

The conversion efficiency of water to hydrogen is high, ranging from 80-95%. Energy efficiency is defined as the higher heating value of hydrogen divided by the energy consumed by the electrolysis system per kilogram of hydrogen produced. The amount of energy currently needed to create hydrogen from water using electrolysis is 39 kWh/kg. In order to determine the efficiency of the electrolysis process, the theoretical amount of energy needed, 39 kWh/kg of hydrogen, needs to be divided by the actual amount of energy used by the electrolysis unit to create hydrogen. The energy efficiency of the electrolysis process ranges from 56-73% based upon the higher heating value (HHV) of hydrogen. The PEM process currently has the lowest efficiency at 56 % and bipolar alkaline efficiencies are the highest at 73 % (Ivy, 2004).

An electrolyzer producing 1 kg H_2 working at a cell potential of 2 V uses 54 kWh. At current electrolyzer efficiencies, in order to produce hydrogen at lower than $3.00 per kg, electricity costs must be lower than 4 and 5.5 cents per kWh. For an ideal system operating at 100 % efficiency, electricity costs must be less than 7.5 cents per kWh to produce hydrogen at lower than $3.00 per kg (Ivy, 2004). Ivy (2004) determined that for a small neighbourhood case (~20 kg H_2/day), the capital costs become the major cost factor, but electricity costs are still significant. This analysis demonstrated that for all systems electricity price is a major contributor to hydrogen price.

The main requirements in efficient hydrogen generation on a large scale by water electrolysis are the supporting electrolyte, low-cost, stable, large surface area electrodes, high current densities and product separation from the electrolyte. For low cost hydrogen production by water electrolysis, low cost high efficiency electrode materials need to be developed.

CHAPTER 2

Water electrolysis with a solid polymer electrolyte (SPE)-cell possesses certain advantages compared with the classical alkaline process such as increased energy efficiency and specific production capacity and a simple system with a solid electrolyte at a low temperature. The development of processes for catalyst production and application on electrode membrane assemblies (MEAs) for solid polymer electrolyte (SPE)-cells is of significance. The first electrolyzers using polymer membranes as electrolyte were developed by General Electric Co. in 1966 for space applications. Extensive research and development on SPE electrolyzers has been performed within the Japanese World Energy Network (WE-NET) program. A cell voltage of 1.68 V at 1 A cm^{-2} was obtained on a single cell of 50 cm^2 at 80 °C. Kondoh et al. (2000) tested two cell stacks of 0.25 m^2 X 10 for 2500 h at 1 A cm^{-2} with an average cell voltage of 1.74 V at 1 A cm^{-2} and 1.9 V at 2 A cm^{-2}, respectively. The Swiss company ABB developed the commercial MEMBREL™ process membrane electrolyzer in the period 1976/1989. Two units of 100 kW were tested over the longer term with an average voltage 1.75 V at 1 A cm^{-2} and 80 °C. The oxygen electrode is the main source of overpotential in this system. In contact with the acidic Nafion membrane non-noble catalytic metals like Ni and Co will corrode and Pt will be covered by a low conducting oxide film.

Conducting oxide materials have attracted considerable interest as activated cathodes for electrocatalysis of H_2 evolution (Patil et al., 2003). The oxygen electrode is the main source of overpotential in the SPE electrolyzer system and IrO_2 is one of several oxides chosen as the active catalyst for the electrocatalytic process. The performance of IrO_2 as anode electrocatalyst has been found to be much superior to that of pure platinum for oxygen evolution. (Blouion et al, 1997). The various methods used for preparing Ir-oxide films include anodic oxidation (Beni et al., 1982), reactive sputtering (Hackwood et al., 1982), electrodeposition (Yamanaka et al., 1989), sol–gel (Takasu et al., 1994) and spray pyrolysis techniques (SPT) with variable thickness (Patil et al., 2003). On the hydrogen evolution side (cathode) of an electrolyzer metallic Pt is commonly used (Millet et al., 1993; Ioroi et al., 2000), but dissolves on the anode side (Tafel, 1905). Pt can also be co-deposited on an oxide such as TiO_2

(Sato et al., 1980). Nanocrystalline electrodeposited Ni–Mo–C cathodes have recently been developed for hydrogen production (Hashimoto et al., 2004)

Nanostructured materials can be applied as electroconductive and catalytic membrane electrodes. Promising composite electrodes and nanophase electrocatalysts are much more active for hydrogen generation than current commercial materials applied in alkaline systems. Cost effective methods to prepare catalytically active, nanophase inorganic membrane electrodes show significant promise to overcome current obstacles to implementing large scale use of such materials. The incorporation of nanophases into composite electrodes as electrocatalysts involve developing catalytic inks, membrane electrode assemblies, gas diffusion layers, and cell design with prototyping. Process development and optimization of electrochemical catalytic systems are required for demonstration and cost evaluation of such systems.

The rate of the cathodic evolution of hydrogen depends upon the overvoltage, ηH_2, which depends in turn upon the nature of the electrode potential, its surface state, and the conditions under which the electrolysis process is carried out. These conditions are as follows: both concentration and temperature of the electrolyte solution, stirring of the electrolyte solution, density of the polarizing current, and other factors that may be difficult to control, need be taken into account, for example, the presence of a reducing agent in a solution etc. To make a rational choice of electrode based upon prediction of its performance, it is necessary to establish interdependence between the ηH_2 value of the metal of choice and any other relevant property. As has been established for a number of metals (Petrii and Tsirlina, 1994), the exchange current density, j_0, (inversely dependent upon ηH_2) increases as the energy of the metal/hydrogen bond, GM-H, rises. This has been explained by the fact that an increase in the bond energy results in a decrease of the activation energy of the discharge stage of H_3O^+ ions or water molecules and an increase in activation energy of the recombination process of atomic hydrogen.

CHAPTER 2

Use of the quantum-mechanical theory of electrode reactions adopted by Prisyazhyi et al., (2000) to explain the reaction of hydrogen evolution on metals elucidates the experimentally observed dependence of the exchange current density, j_0, versus adsorption of hydrogen atoms for different metallic electrodes. This characteristic feature holds true for most metals. Therefore, the lowest values in the overvoltage of hydrogen evolution are characteristic for those metals having the highest energy values for the metal/hydrogen bond. The same metals possess a high degree of adsorptivity of atomic hydrogen, show a trend to form hydrides, and are distinguished by low desorption of hydrogen from their surfaces. Depending on the overvoltage value of hydrogen evolution, the metals used to prepare cathodes are subdivided into two main groups (Prisyazhyi et al., 2000) : those showing a low overvoltage, such as Pt, Pd, Au, Rh, Re, Ir, Ni, Co, and Fe (here the high GM-H and j_0 values are characteristic), and those showing a high overvoltage, namely Sn, Bi, Zn, Pb, Ti, Ln, Hg etc. (here the aforementioned values are low). As seen from this list, the first group of metals mainly consists of precious metals - an essential drawback of which is their high cost. Ni, Fe and Co belong to this group but as cathodic materials, the widest use is made of Ni and Fe.

The activity of the cathodic catalyst depends not only upon the nature of the metal but also upon its structure formed during the electrode molding process. Of the non-platinum catalysts applied for hydrogen electrodes in alkaline solutions, skeletal catalysts, mainly nickel based (Yusti, et al., 1962), are assumed to be the most promising. Except for nickel, such skeletal catalysts may comprise other metals of variable valence. A number of authors have revealed that the addition of such elements as cobalt (Kudryashov et al., 1970a; Kudryashov et al., 1970b), tungsten, chromium, titanium, zirconium etc. (Jaksis 1984) into the composition mixture increased the activity of the catalysts. Electrodes with a current supply made of stainless steel are of practical interest. The active coating might be applied onto an iron support by plasma spraying of powders available for industrial use. As Sklyarov et al., (1991) have shown, mixtures of the powdered alloyed stainless steel with powdered aluminium and the nickel/aluminium alloy powder are promising as

material for an active cathode coating. The stainless steel may contain between 6 to 10% of Co, Mo, Cr, Ni, and W in a mixture with aluminium powder. This may be followed by leaching of the nickel skeletal catalyst, i.e., an alloy of nickel with aluminium and other additives. Thermal treatment of the above mixtures provided a means to obtain cathodes characterized by a low overvoltage (300 mV in 30wt % KOH solution at a current density of 0.4 A cm^{-2} and a temperature of 90ºC). Such cathodes were found to be stable with respect to contamination by iron and maintained their characteristics during long-term operation. Various patents make claims for Ni, Co and Fe or alloy electrodes as summarized in Table 2.1.

CHAPTER 2

Table 2.1 Summary of patents

No	Patent No	year	Coating method	Substrate	Electrolyte	Temp	Over potential (mV)	Curr.dens. (mA/cm^2)	Time (h)	Cell potential (V) / (A/cm2)
1	5,084,154	1990	Ni-Ti-Zr, plasma spray power	Ni	45% NaOH	100	170 195	400 400	1 800 (cathode)	
2	4,839,015		Ni-Cr-Ti							
3	4,605,484		Ni-Cr							
4	4,586,998	1986	Pt electroplated	Ni	35% NaOH		80 100	300 300	1 3000 cathode	
5	4,567,374	1985	Co-Ni cosputteriing + post treatment	Ni, Co or alloys	17% NaOH	80	288 310 360 295 340 410	100 200 500 100 200 500	1 1 1 4600 4600 4600 (anode)	
6	4,498,962		Co-Ni surface enlarged + Rh Ir: melt coating	Ni, Co or alloys	15% KOH	110	250	70	1.91 Cell potential	
7	4,447,302		Ni-Ti: hot pressed	Ni	35% KOH	80	75 >260	150 200	(Cathode) 1000h (Anode)	
8	4,363,707	1982	NiS electroplated plasma blown	Ni enlarged surfacwe	33% KOH	160 160		1000 1000 1000 1000	1 (cell) 200 (cell) 1 (cell) 200 (cell)	1.8 / 1000 1.85 / 1000 1.68 / 1000 1.7 / 1000
9	4,361,602	1982	Ni-Rh electroless plating	Surface enlarged Ni	40% KOH	100		200 500		1.6 /200 1.8 /500
10	4,251,344		Porous Ni sintering Mild Fe	Fe	12% NaOH + 16% NaCl	96	1.11 1.12 1.13 1.35	70 145 290 155	Cathode potentials Cathode potentials	
11	4,100,049		Pd + Zr	Ni, Co, Fe						

CHAPTER 2

So far, only Pt or Pt alloys can efficiency keep the stability of the oxygen-electrode catalyst activity in fuel cells. Previously pure Pt black was used as catalyst and the dosage was 4mg cm^{-2}. In recent years, the dosage of carbon-supported black Pt catalyst is 0.5mg cm^{-2}. Using relative larger surface area supported material is an effective method in which it is possible to achieve highly dispersed Pt crystallite and reduce the ratio of catalyst applied. The requirements of a support for an active electrocatalyst are that it must provide a structural, conductive, and durable support for the active metal particles. By far the most common support materials used in PEMFCs are carbon blacks. As expected, increasing the surface area of the carbon leads to greater Pt dispersion at a given loading. Uchida et al. (1996) showed that Pt crystallite size decreased from 3.7 to 1.0 nm when the carbon surface area increased from 58 to 1500 m^2 g^{-1} for a series of 23 to 24nm wt% Pt catalysts. Similarly, Tokumisu et al. (1999) reported that increasing the carbon surface from 60 m^2 g^{-1} to over 1300 m^2 g^{-1} leads to a reduction in Pt particle size from 2.5 to 1.5nm for 10 wt% catalyst. However, despite the increase in Pt surface area achieved by higher-area carbon support, both these studies showed little effect of carbon support on activity. It was suggested that both the Pt particle size effect and the interaction of the ionomer with the carbon support played important roles in determining activity.

In conclusion, the literature review presented in Chapter 2 was used to develop the thesis topic and the main perspective, rationale and motivation, research approach and scope of study as well as the delimitation of the study, as was presented in Chapter 1. The research design, refinement of approach and research hypothesis as well as the delimitations of the research and the main perspective from which the topic was researched were also developed from the perspective gained from the literature review and were set out in Chapter 1. More detailed and specific review of the applicable literature will be presented in the introductory sections presented in Chapters 3-7.

CHAPTER 3

3 NANOPHASE SUBSTRATES AND SUPPORTS FOR ELECTRO-CATALYSTS

3.1 INTRODUCTION

The approach in this aspect of the study was to explore the use of three dimensional porous substrates as supports for high dispersion of active nanophase Pt electrocatalysts for hydrogen production in a solid state electrolyzer. Because two dimensional electrode surfaces do not provide sufficiently high catalytic activity for hydrogen production or fuel cell applications, the highest number of active sites per unit volume may be obtainable using three dimensional materials as supports for the electrocatalysts. New routes to form nanophase electrocatalysts on such supports are necessary because current techniques are costly, laborious, and require sophisticated fabrication facilities, thus are not industrially or economically viable in the local South African environment.

This section will focus on microporous, and mesoporous support substrates and their characteristics. Methods to achieve dispersion of the metal nanophase upon these supports will be detailed in Chapters 4 and 5.

3.2 OVERVIEW OF SUPPORT SUBSTRATES

Various support substrates have previously been considered for preparation of three dimensional porous substrates as supports for high dispersion of active nanophase Pt electrocatalysts. Typically in gas phase catalysis of hydrocarbons, Pt supported zeolites (Ho et al., 1998) are used as bifunctional heterogeneous catalysts. More recent efforts have included the use of mesoporous materials and high surface area carbon substrates such as carbon black, carbon nanotubes and mesoporous carbons,

the purpose being to form a three dimensional array of pores with interconnected channels, so that metal catalysts can be highly dispersed without agglomeration and that the two way flow of liquid reactants and gaseous products may not be impeded (Xie et al., 2008).

3.2.1 Microporous supports: Zeolites

Zeolites are crystalline aluminosilicate materials with regular uniform, Angstrom sized pore systems. Zeolites have the following unique properties (Moscou, 1991; Maxwell and Stork, 2001): Microporous character with uniform pore dimensions; Ion-exchange properties; Ability to possess acidity; High thermal and hydrothermal stability. The framework oxide structures are associated with certain unique features, among which the strictly uniform two – or three dimensional pores of characteristic diameters and widths, give rise to a pronounced "sieving action", on the molecular scale (Meier, 1968). According to the IUPAC classification, micropores have a diameter (dp) smaller than 20 Å (Weitkamp, 2000). Hence zeolites are structured nanophase materials.

Zeolites offer extremely large specific surface areas because of their high micro porosity with pores typically in the Ångstrom range. The surface areas of fully crystalline zeolites are typically in the order of 400-600 m^2g^{-1}, of which approximately 66-85 % is internal, in the microporous channel. Zeolites are stable to well over 1000 °C, allowing thermal regeneration of these catalysts, and are resistant to attrition posing few handling problems. Surface properties can be either hydrophilic or hydrophobic based on the desired degree of incorporation of Al into the lattice framework. A highly siliceous zeolite repels water. On the other hand Al rich zeolites attract water. The relative affinity of various hydrocarbon compounds for the zeolite surface and the zeolite pore size may allow separations of mixtures of

hydrocarbons. There are more than 200 unique zeolitic structures that have been identified in nature or synthesized (Szostak, 1992)

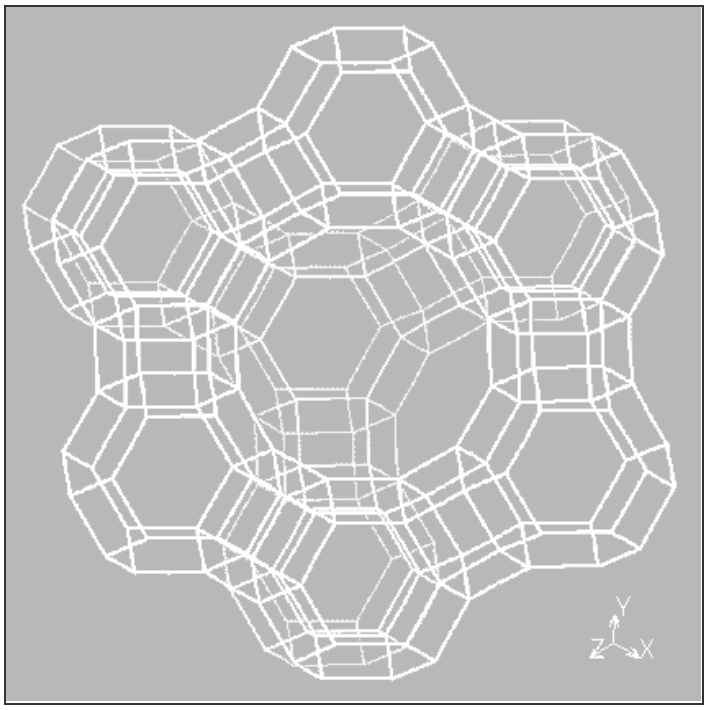

Figure 3.1 Schematic of unit cell structure of zeolite FAU (IZA_online, 2008).

Unit cell formulae differ for each unique zeolite structure, depending on the configuration of the framework and its composition. The empirical unit cell formula of a zeolite is of the type: $M_{2/n}O \bullet Al_2O_3 \bullet xSiO_2 \bullet yH_2O$, where M is any alkali or alkaline earth atom, n is the charge on that atom, x is a number from 2 to 10, and y is a number from 2 to 7. For example, for FAU (alternatively known as zeolite Y or faujasite) the formula is $(Na_{58})(Al_{58}Si_{134}O_{384})\bullet 240H_2O$. Atoms within the second set of parentheses are structural atoms, because with oxygen they make up the rigid lattice framework of the structure. Those within the first set of parentheses are known as exchangeable ions, because they can be replaced (exchanged) more or less easily with other cations in aqueous solution, without affecting the aluminosilicate framework (Szostak, 1992; Feijen et al., in Ertl and Knozinger, 1997).

CHAPTER 3

Natural zeolite mineral phases may originate from volcanic ash. The chemical reaction of glassy volcanic ash (source of aluminosilicate) with pervading pore water changes the glass fraction into various crystalline mineral zeolite phases over geological time scales under certain conditions. Many pure zeolite types can also be prepared more rapidly via various hydrothermal synthetic routes (Ginter 1989; Petrik et al., 1995; Petrik et al., 2008). The hydrothermal synthesis of aluminosilicate zeolites corresponds to the conversion of a mixture of silicon and aluminium compounds, alkali metal cations, organic molecules in some cases and water via an alkaline supersaturated solution into a microporous crystalline aluminosilicate. Synthetic zeolites play a major role on industrial scale, in terms of catalysis, molecular sieving and environmental protection (Ertl and Knozinger, 1997).

The negative charge of the zeolite lattice framework is caused by the substitution of Si^{4+} with Al^{3+}. The residing excess negative charge requires the introduction of charge compensating cations to stabilize the structure. These charge compensating cations are not incorporated into the lattice framework or covalently bound to the zeolite structure, but have considerable freedom of movement and can readily be substituted with a host of other cations. The charge balancing cation associated with the framework acid site is usually a Group I element such as Na or K (Barrer, 1981; 1982). Group II elements such as Mg and Ca are also used to change pore diameters, exchange- or catalytic properties. For acid catalysis the charge balancing cation is exchanged with NH_4^+ and then calcined at 500 °C to activate and generate the acidic, H-form of the zeolite catalyst (Ertl and Knozinger, 1997). Various other metals such as Pt and Pd can also be exchanged into the zeolite, to form bi-functional catalysts.

The Si/Al ratio usually determines the amount of exchangeable cations that may be present within the pores of a zeolite and this, as well as the relative accessibility of the cation, will define to what extent the cations may be exchanged. The lowest Si/Al ratio is 1:1, due to the next nearest neighbour (NNN) exclusion principle, thus T-O-T linkages may not accommodate two adjacent Al atoms. The highest Si/Al ratio is

unlimited, but depends on whether a completely siliceous composition is stable for a particular structure (Breck, 1973).

Among the active sites on the zeolite surface, some have a fixed charge and thus represent the effective negative charge of the zeolite; as such they may be referred to as permanently active charged sites or Brönsted acid sites. Thus, the bridged ≡Al-O-Si≡ functional groups represent Brönsted acid sites which can be used for potential ion exchange, acid catalysis or complex formation (Ikhsan et al., 1999; Tamura, 2004). Catalytic activity is determined by the relative amount of bridging hydroxyl groups and this in turn is typically determined by the amount of Al incorporated in the framework.

The strength of the acid site is a function of its isolation. Typically weak acid sites occur in material with a Si/Al ratio of <12, in other words Al rich materials, and strong acid sites above this ratio (Ginter et al., 1989). A basic catalyst is prepared by substituting a metal such as Titanium for the Al in the lattice framework. In many cases it is necessary to incorporate a metal centre in the zeolite to prepare a bifunctional and active catalyst and this is the case in the preparation of electrocatalysts as is envisaged in this study. As zeolites are well known to stabilize metal centres, these materials were considered to be suitable to prepare electrocatalysts and were found to provide a stable, constraining environment for dispersion of the nanophase metal (Rolison et al.,1992; Bessel et al., 1992; Petrik, 2002)

3.2.2 Mesoporous materials

Mesoporous materials are defined as having pores with diameters between 2 – 50 nm. Ordered mesoporous materials are used extensively in separation science, catalysis, and various ‘host-guest’ chemistry applications (Langley and Hulliger, 1999; Hartmann, 2005; Li et al., 2008). Initially these materials consisted of various

inorganic materials either silica or alumina based (Pauly and Pinnavaia, 2001; Tanev and Pinnavaia, 1995). More recently a range of other elements have been incorporated into these materials (Shan et al., 2002; Liu et al., 2006; Li et al., 2007). With the advent of carbon based mesoporous materials (Kim et al.,2003; Lee et al., 2006; Fuertes et al., 2003), the range of potential applications for mesoporous materials has been extended to include separation science, catalysis, non-hydrocarbon based energy systems, and biomedical applications.

Carbon nanostructured materials (CNM) have gathered research momentum in recent years. The various forms of CNMs include, but is not limited too, ordered mesoporous carbon (OMC) materials (Lee et al., 2006; Kim et al., 2003; Fuertes et al., 2003), carbon nanotubes (CNTs) (Baughman et al., 2002; Popov, 2004) and nanofibers (CNFs) (De Jong et al., 2000; Che et al., 1998), carbon nanoballs (Liu et al., 2002), and carbon nanowalls (Wu et al., 2002). When examining the volume of literature available on the different CNMs, in terms of potential applications OMCs, CNTs, and CNFs have proven to be the most practical forms of carbon nanostructured materials.

CNTs can be defined as mesoporous materials since they have pores in this range (Lee et al., 2006). Typical sizes for CNT's are an inner diameter of 1-3 nm and an outer diameter of approximately 10 nm. Their length can vary considerably depending on the method of preparation. Extensive research in synthesis methods are reported online and in the scientific literature since early reports were made of this new material (W. Krätschmer 1990; Benning, 1993; Iijima, 1991; 1993). The most common methods for preparing CNT's include arc discharge, chemical vapour deposition (CVD) and laser ablation (Nanotube Synthesis, 2008). Laser ablation produces a small amount of clean nanotubes whereas arc discharge methods generally produce impure materials. CVD synthesis is achieved by subjecting a gas phase carbon source such as methane, carbon monoxide, benzene and acetylene to pyrolysis by thermal energy at about 700 °C. The gaseous carbon source is brought into contact with a catalyst such as Ni, Fe or Co where it will bind to form the CNT. A method to

prepare CNTs using nebulized spray pyrolysis and other vapour phase techniques have recently been reported (Vivekchand et al., 2004; Govindaraj 2007). It is proposed that CNT mechanism of growth involves a nucleation process where growth of the CNT occurs on the catalyst surface through atoms of the gas phase carbon source being captured. Purifying CNTs using acid treatments can cause loss of structure and disorders the walls (Strong et al., 2003). It has been reported that Pt can be deposited electrochemically upon the exterior walls of CNTs (Adora, 2004) or by in situ deposition (Wang et al., 2006). CNTs can form bundles of tubules, which are organized structures held together by weak van der Waals' forces (Popov, 2004).

In contrast, OMC are an intricately connected network of covalently bonded carbon material with periodic pores in the mesoporous size regime in the nanometer range (Lee et al., 2006; Kim et al., 2003; Fuertes et al., 2003; Li et al., 2008). The desired mesoporous ordering can be derived from a silica based mesoporous precursor that provides control over the final OMC. One of the most facile methods for the synthesis of OMCs is the template method. The choice of template determines the pore size, arrangement of the pores and thus the overall structure of the resulting OMC. In order to synthesize OMCs, silica templates with an ordered and interconnected pore structure need to be used to produce a structurally stable OMC. Such ordered mesoporous silica templates can be synthesized with the desired mesoporous ordering, which in turn provides control over the final OMC. In general, OMCs can be synthesized by first impregnating the Si template with a suitable carbon precursor, followed by a separate carbonization step. Alternatively, the carbon precursor can impregnate the template and undergo decomposition to carbon at the same time using a chemical vapour deposition (CVD) process. In both methods the silica based mesoporous template has to be removed in a separate step (Lee et al., 2006; Kim et al., 2003; Fuertes et al., 2003; Langley and Hulliger, 1999; Hartmann, 2005).

CVD is a relatively easy method to implement and the added simplicity of infiltration and decomposition in one continuous process is a key reason this method was explored to produce the OMC materials.

3.3 EXPERIMENTAL

3.3.1 Preparation of the microporous zeolite support

Commercial FAU zeolite was obtained from Zeolyst company and characterized prior to using this material as support for metals. The specifications for Zeolite H-FAU (CBV780 Lot. No 78001N00257; Zeolyst International) is a dealuminated faujasite with a given analysis of: Si/Al 80; wt% Na 0.03; BET surface area of 780 $m^2 g^{-1}$.

3.3.2 Preparation of the Mesoporous Silica Template

The HMS silica based mesoporous precursor was synthesized by adapting methods from Zhang et al., (1997). Initially 4.0 g of the surfactant 1-hexadecylamine (Aldrich) was added to 350.0 mL of an ethanol/water mixture (35/70, v/v). The mixture was stirred in an open vessel for 24 h. 50.0 mL of tetraethoxysilane (TEOS, Aldrich) was then added drop-wise to the mixture (1-hexadecylamine in ethanol/water) whilst continuously stirring the solution. After adding the TEOS, the mixture was left to stir under ambient conditions for 24 h. For HMS assembly where water:ethanol ratio was 25/10, the molar compositions of the reaction mixture was 16 TEOS: 0.066 surfactant: 10 EtOH: 25 H_2O. The solid product was then filtered (Whatman, 545 grade filter paper) and washed with distilled water. 150.0 mL of 100.0 % ethanol (Kimix, South Africa) was mixed with the solid product and then refluxed under air at 120 °C for 2.0 h. The resulting suspension was then filtered and dried at 100 °C in a muffle furnace. Calcination of the dry solid product was done in a muffle furnace using a heating rate of 1 °C min^{-1}, a final temperature of 550 °C, and holding the

furnace at 550 °C for 8.0 h. The final yield of the HMS silica template was approximately 2.0 g when using the specified amounts of starting materials.

MCM-41 was synthesized at room temperature. Cetytrimethylammonium bromide (CTAB) was used as template in order to control the pore size of the resulting mesoporous silica. A typical preparation was as follow: CTAB (4.0 g) was dissolved in 250 mL of HCl solution. The mixture was stirred at room temperature for 1 h, then TEOS (20 mL) was added to the above solution. The mixture was vigorously stirred in a sealed flask under ambient conditions for 20 h. The resulting white precipitate was filtered, washed by water and dried at room temperature. Template removal was achieved either by calcination at 550 °C for 4 h.

3.3.3 Preparation of the ordered mesoporous carbon (OMC)

1.0 g of HMS was loaded in to a ceramic sample boat; this was then placed inside a quartz tube located in a horizontally aligned tube furnace. Once appropriately sealed, an LPG flow was initiated at 50.0 mL min^{-1}, and the furnace was ramped to temperatures between 600-800 °C using a heating rate of 1.67 °C min^{-1}. After 90 min, the LPG flow was terminated and the furnace was cooled to ambient. The resulting mesoporous silica/carbon composite was refluxed with 50.0 mL of 1.0 M NaOH (Kimix, South Africa) at 75 °C for 3.0 h, and the mixture was continuously stirred to aid in dissolving the silica template. The product was rinsed with ultra pure water over a nylon membrane filter (0.45 μm pores, Whatman), until the pH was between 7 and 8 as determined by pH paper. Finally the product was dried at 100 °C in an oven for 60 minutes.

3.3.4 Preparation of the Carbon Nanotubes

CNTs were prepared according to Vivekchand et al., (2003) by pyrolysis of a ferrocene-toluene (20.00 g L^{-1}) solution which mixture was fed into a quartz tube reactor at 900 ºC in the form of a fine nebulised spray generated by ultrasound. Ar was used as the carrier gas at a flow of 500 cm^{-3} min^{-1}. The nebuliser frequency was 1.6 MHz and the total reaction time was 45 min (Pinault et al, 2005). A further sample of CNT was synthesized under the same conditions, by the nebulised spray pyrolysis of a solution of ferrocene in benzene. The prepared CNTs were collected and about 0.2 g of CNTs were weighed out and placed into a round bottomed flask fitted with a thermostat and thermometer, where after 100 mL mixture of a sulphuric acid-nitric acid (2:3 ratio by volume of concentrated sulphuric acid (98 %) and concentrated nitric acid (55 %), was carefully added into the flask. The CNTs were heated under reflux for three hours in this solution, where after the mixture was cooled down and filtered using a Buchner apparatus. Acid treatment of CNTs was used to break up bundles, to reduce their length and remove metal impurities present from the catalyst used during synthesis. The CNTs were recovered upon a filter paper, washed until the rinse water had a pH of between 6 and 7 as determined by indicator paper and then dried at 100 °C overnight.

3.3.5 Characterization

The methods described below provide a fairly comprehensive overview of the analyses and measurements that were undertaken during this study. However, it should be noted that not all measurements and analyses were done on every sample. Many experiments were undertaken to investigate the effect of an altered parameter on only one or two variables (e.g. crystallinity, activity, etc.). Full analysis of all samples would therefore be unnecessary and costly. The various analytical techniques and are described in more detail in each chapter where applicable. Crystal/atomic structure and metal particle size was determined by X-ray Diffractometry (XRD, Bruker AXS D8 Advance, Cu Kα (λ = 1.5418), 0.05 degrees min^{-1}). Qualitative crystallinity and crystal symmetry was determined by Selected Area Electron Diffraction (SAED, Hitachi H-800 EM, 200 kV, 20 μA). Surface micro- and

macrostructure, and degree of agglomeration were determined by High-Resolution Scanning Electron Microscopy (HRSEM, Zeiss Ultra 55 Field Emission – In-lens detection, 30 kV, 80 μA). Aggregate particle size and distribution was determined by Non-Invasive Beam Scattering (NIBS, Malvern HPPS, ethanol/water dispersant, 0.1 mg L^{-1}, 25 °C). Metal particle size, particle size distribution, metal surface area, and metal dispersion/agglomeration were established by Transmission Electron Microscopy (TEM, Hitachi H-800 EM, 200 kV, 20 μA) and total surface area and porosity by N_2-adsorption at -196 ºC (77 K) (Micromeritics ASAP 2010, 20 mg sample). Topography and surface elemental distribution of electrocatalyst cast-films was studied using Particle-Induced X-ray Emission Spectroscopy (micro-PIXE, Oxford, 3 MeV). Topography and surface activity of electrocatalyst cast-films was studied with Scanning Electrochemical Microscopy (SECM, Uniscan Instruments SECM 270, 0.005M H_2SO_4 electrolyte, separation - 5μm, raster speed - 5μm s^{-1}). Thermal stability was determined with Thermogravimetry (TGA, Rheometric Scientific STA 1500, N_2 - 50 mL min^{-1}, 25 – 850 °C, 15 °C min^{-1}). Surface oxidized species (metal chemical state) were analyzed using Temperature-Programmed Reduction (TPR, Micromeritics Autochem 2910, 25 mg sample, -80 – 900 °C, 15 °C min^{-1}, H_2/Ar - 50 mL min^{-1}). Electro catalytic activity was compared using Chrono Voltammetry or Cyclic Voltammetry (CV), using the Autolab PGSTAT 30, or BAS 100 electro-analytical systems). Rheology of inks was determined using an Anton Paar Physica MCR 300 system. Hall mobility and resistivity was measured using a Lakeshore 775 HMS Matrix Hall measurement system. Further details of experimental set-ups will be specified where applicable in each chapter.

Operating parameters utilized during the characterization of materials prepared in this study were as follows: The X-ray diffraction spectra were obtained using a Phillips X-ray diffractometer fitted with a copper tube of Kα radiation of wavelength λ = 1.54 Å. Operating parameters of the XRD were: Scanning range 4-47 °2θ; Step size 0.1 °2θ; Time constant 1 s; Preset 1000 counts s^{-1}; Voltage 40 kV; Current 25mA; Anti-scatter slit 1°.

CHAPTER 3

Scanning calorimmetry, namely specific heat capacity, phase transitions and heat of reaction (endothermic and exothermic) as well as thermo gravimmetry including thermal decomposition and volatile content was performed using a thermal analyser (STA thermal analyzer TGA/DTA/STA (gravimetric/calorimetric) by Rheometrix). Approximately 50 mg of as-synthesised, washed and dried sample was equilibrated at 40 °C for one hour in flowing N_2 (30 mL min^{-1}) in the thermal analyser. Thereafter it was heated to the specified temperature at 10 °C min^{-1} in flowing N_2 (30 mL min^{-1}) and held at this temperature for the required time.

The composition and % metal loading was determined using EDS. The 40 kV Hitachi X650 SEM that was used for obtaining micrographs, was equipped with a Phillips EDAX Energy Dispersive System utilizing a detector with a super ultra thin window offering a resolution of 139 eV. Another instrument, the LEO S440 Analytical SEM, fitted with a KEVEX detector was used to confirm analysis. This instrument was fitted with a berylium window and the operational conditions were an accelerating voltage of 20 kV, and a working distance of 25 mm. Analysis was performed upon carbon coated samples mounted upon aluminium stubs using colloidal glue mixed with conductive carbon.

Scanning electron micrographs (SEM's) were obtained using a 40 kV Hitachi X650 SEM capable of a 10 nm resolution. This instrument was used to determine the approximate particle size, morphology and elemental composition (using energy dispersive spectroscopy (EDS)) of the zeolite crystals. The samples were mounted on aluminium stubs, that had been covered with a mixture of water based glue and colloidal carbon. Thereafter, the samples were coated with a thin layer of Au (carbon samples OMC and CNT were not coated). Operating parameters of the SEM were: Accelerating Voltage 15 keV; Aperture 30; Tilt Angle 30°; Resolution 9; Working Distance 10 to 20 mm. High-Resolution Scanning Electron Microscopy (HRSEM) was performed using the Zeiss Ultra 55 Field Emission with In-lens detection, at 30 kV and 80 μA.

The Transmission electron microscope (TEM) was used to determine the structure, size or morphology of materials. All prepared samples were viewed and photographed at 200 kV in a Joel 200CX microscope, after immobilization in resin followed by microtomy to prepared ultra thin sections that were mounted upon copper grids. High resolution transmission electron micrographs (HRTEM) were taken using a Tecnai G2 F20 X-Twin (FEI company, Eindhoven, the Netherlands).

Fourier Transform Infrared spectroscopy (FTIR) has been extensively used to characterise zeolites before and after post synthesis modifications. This method of characterization is very useful for identifying the different functional groups as well as to characterize acid sites. The spectral analysis from FTIR spectroscopy can be used to identify specific molecular groups that occur within the solid or crystal that has being formed e.g. Si-O bond stretching are found to be in the range 700 to 1100 cm^{-1}. Mid-IR spectra of zeolites in the range 1400-200 cm^{-1} are generally used for the investigation of the framework properties of zeolites. Dried zeolite samples were prepared for scanning by mixing about 0.08 g of dried sample with KBr in a ratio of 1:100. This mixture was finely ground, dried at 100 °C and then pressed into a disc.

Nitrogen porosimetry using a Micromeritics ASAP2000, was used to determine pore size distribution and surface area of selected samples. Approximately 0.5 g sample was dried at 120 -200 °C until a vacuum of 5mm mercury could be obtained. Thereafter the nitrogen adsorption experiment was commenced. The amount of nitrogen adsorbed at LN_2 temperatures, saturation pressure of N_2 (local atmospheric pressure), the partial pressure of N_2 over the sample (30% local atmosphere) and sample weight were used to calculate total surface area, by the Brunauer, Emmett, and Teller (BET) method. The mesopore surface areas were determined from the BJH desorption curves and represent the intracrystalline mesopores between 20-500 Å.

The TPR analysis was performed by flowing an analysis gas (hydrogen in an inert carrier gas such as nitrogen or argon) through ~0.5 g sample, at ambient temperature. While the gas is flowing, the temperature of the sample was increased linearly with

time and the consumption of hydrogen by adsorption/reaction was monitored. Changes in the concentration of the gas mixture downstream from the reaction cell were determined. This information yielded the volume of hydrogen uptake.

3.4 RESULTS AND DISCUSSION

3.4.1 Characteristics of zeolite FAU

The micropore structure and pore size of commercial zeolite FAU (CBV400) was confirmed with HRTEM as shown in Figure 3.2 and 3.3.

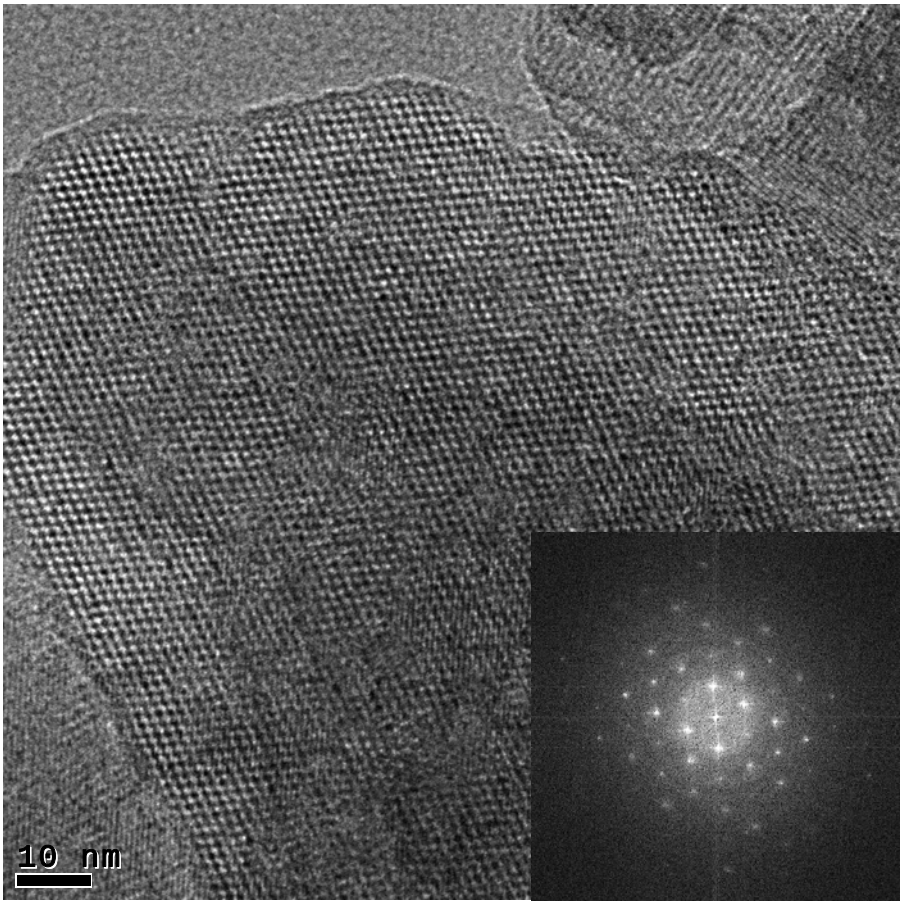

Figure 3.2 HRTEM of zeolite FAU and general crystal structure (Inset SAED)

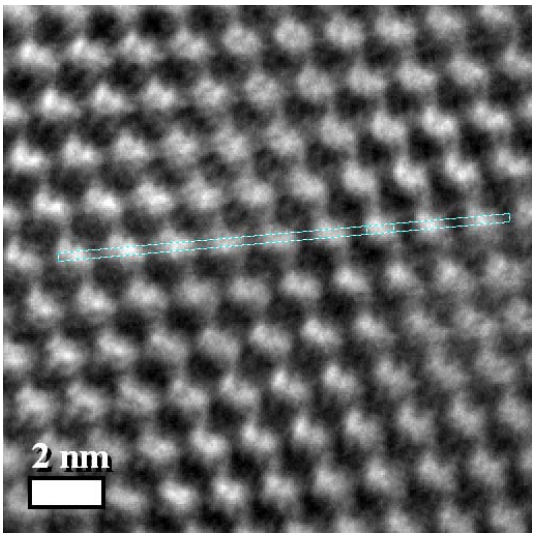

Figure 3.3 HRTEM image of FAU with pore orientation

The best crystal orientation observed in the HRTEM images is [110], where the pores are lying in line (Figure 3.3). Analysis of the grey scale of the marked area in Figure 3.3 along one axis is presented in Figure 3.4, which shows the intensity of the grayscale tone on the y-axis. The dimension of this intensity fluctuation gives another means of probing the pore size which is analyzed to be 0.77 nm.

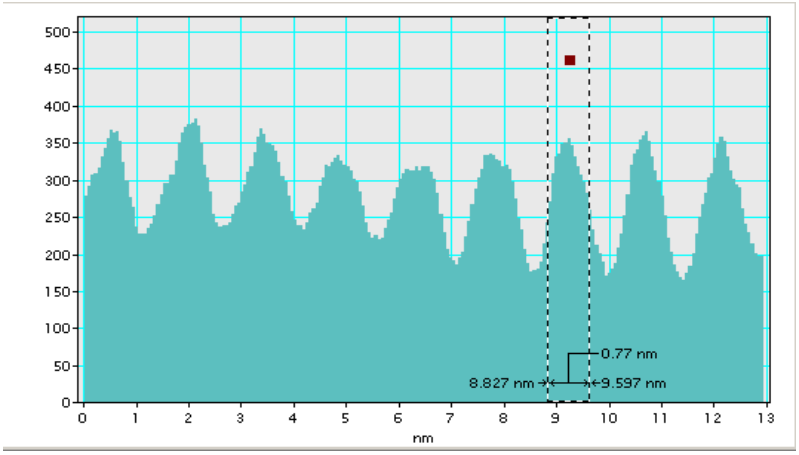

Figure 3.4 Analysis of pore size of zeolite FAU

The HRTEM of zeolite FAU (Figure 3.2) showing the regular angstrom sized pore array and ordered crystalline structure, highlights the potential to use the three dimensional surface area as a substrate to disperse and stabilize the metal electrocatalyst. The measurement of the enlarged image (Figure 3.3) confirms the

pore size is roughly 0.77 nm which is further substantiated by the analysis of the pore size (Figure 3.4). X-ray analysis by EDS (Figure 3.5) shows the composition of FAU is Si, O, Al, with high Si/Al ratio (this sample was dealuminated). The trace of carbon possibly comes from the supporting film underneath.

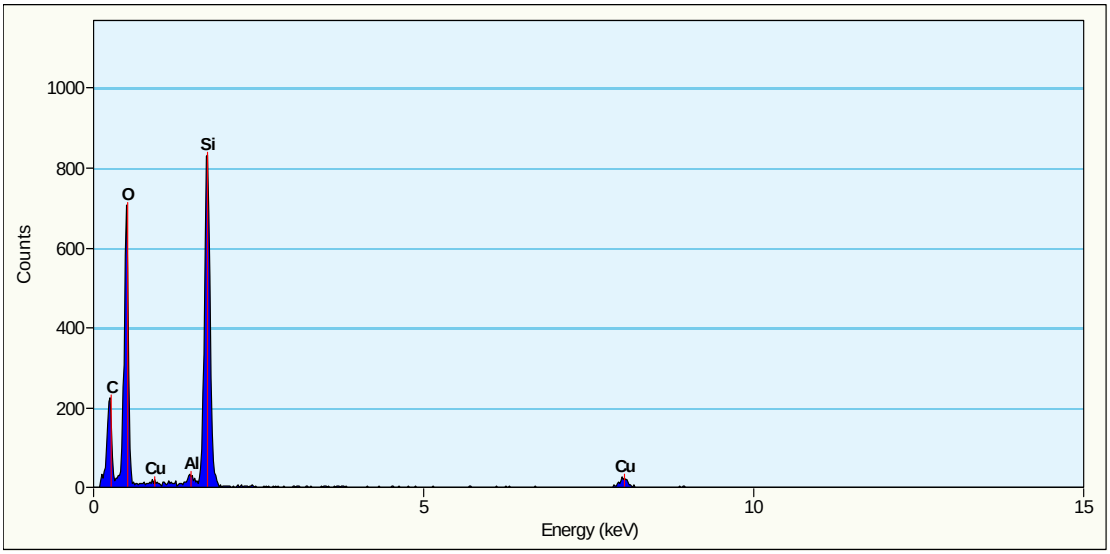

Figure 3.5 X-Ray analysis (EDS) of composition of zeolite FAU

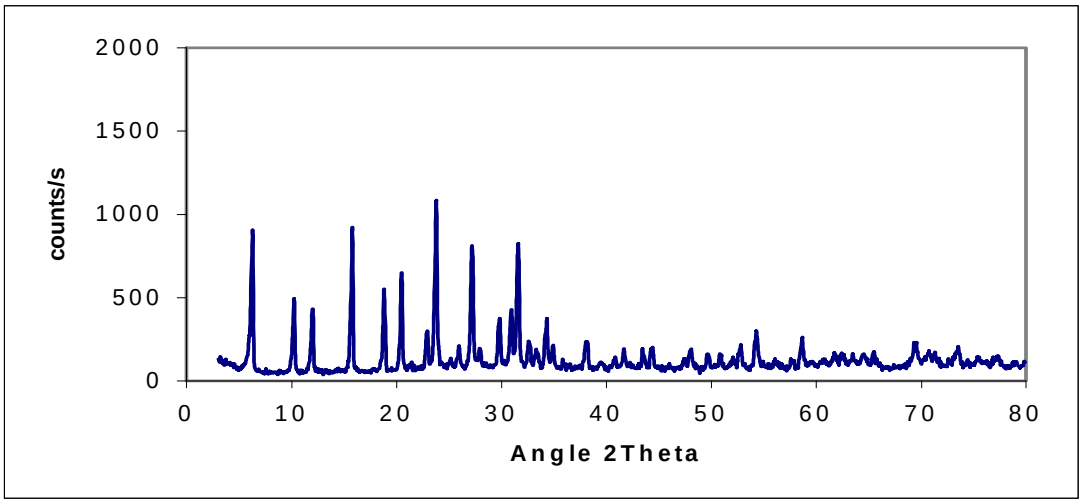

Figure 3.6 XRD of commercial FAU (CBV400)

The XRD of the commercial zeolite FAU shows the typical peak at a low angle of 6 °2θ that defines the pore width of 7.7 Å as was confirmed by the HRTEM images and measurements. Other peaks define the complex geometry of the unit cell lattice

framework as was graphically shown in Figure 3.1 and confirmed by Eva software (JCPDS library supplied with instrument).

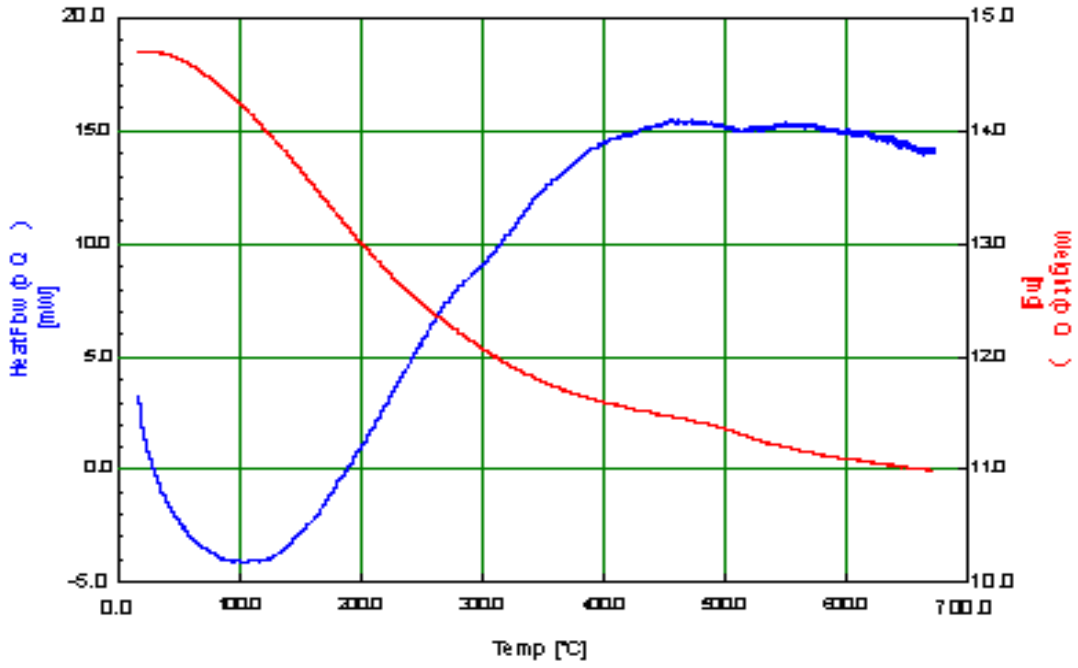

Figure 3.7 Thermal analysis of zeolite FAU

Thermal analysis (Figure 3.7) shows the thermal stability of the zeolite framework and the high capability of the zeolite to adsorb moisture, with about 26 % mass loss up to 600 ºC due to the high moisture content of this hydrophilic zeolite type. The high adsorption capacity for moisture as was observed from thermal analysis as well as the regular porosity visible in the HRTEM images show the high void space in the host zeolite pores, which space is available for the incorporation of metal species.

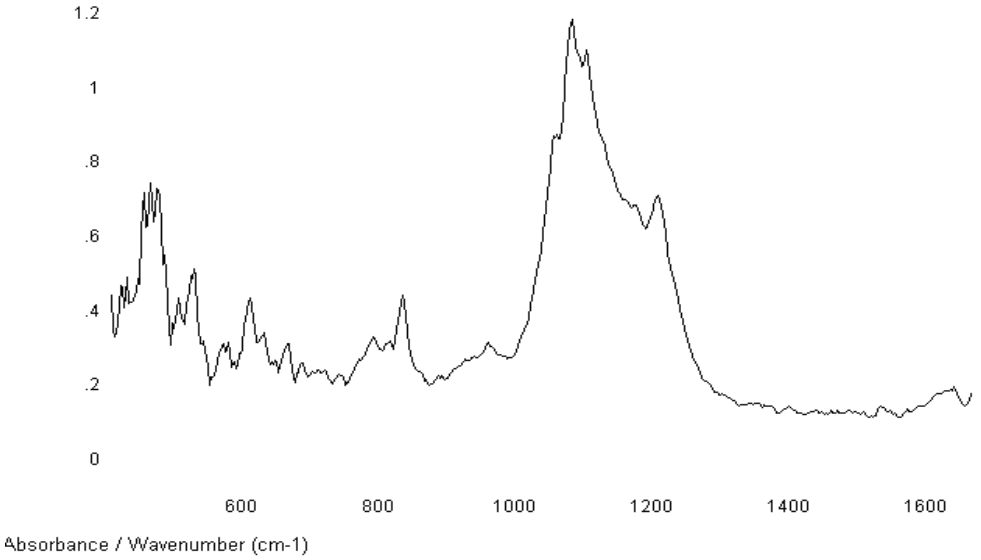

Figure 3.8 FTIR spectrum of FAU

The FTIR spectrum (Figure 3.8) shows the framework structural bands typical of FAU in the region below 600 cm^{-1} as well as the silicate ring structures typical of zeolites between 1000 and 1200 cm^{-1}. Mid-IR spectra of zeolites in the range 1400-200 cm^{-1} are generally used for the investigation of the framework properties of zeolites. The vibrational frequencies of zeolite framework are mostly found to be between 300 cm^{-1} and 1200 cm^{-1} for the crystalline zeolite structure. Various bands visible in the spectrum can be assigned to the following species according to Bass and Turner (1997)

Table 3.1 FTIR spectra for Silicate assignment (after Bass and Turner, 1997)

Wavenumber (cm^{-1})	Assignment
900-850	monomeric silicate species
885	small SiO^{-}
985	(Monomer +trimer,dimer and tetramer) = Q^1
950-910	Monomer dimer.
1000-1010	Mainly linear molecules
1050-1020	SiO^{-1} cyclic anions
1070-1030	Q^2 (3R) rings
1120-1050	Q^3 (3R) , Q^2 (4R) and linear Q^2
1300-1100	Polymer
975,920,850	Monomer alkaline silicates
900-650	Water band

Zeolites are well known as ion-exchange materials (Somerset et al., 2005) and acid catalysts (Petrik et al., 1995) and their acid sites promote the stabilization of metals. It has also been demonstrated that zeolites can be hydrothermally grown directly onto carbon substrates (Smith et al., 1995; Petrik, 2003) which would facilitate their incorporation onto a conductive substrate such as a carbon fibre gas diffusion electrode. Therefore these zeolite materials may be suitable high surface area, three dimensional substrates for preparing dispersed Pt electrocatalysts as is further described in Chapters 4 and 5.

3.4.2 Characteristics of mesoporous substrates

3.4.2.1 Ordered mesoporous silica and carbon

Carbonization of the parent silica substrate, HMS by pyrolysis with LPG using a CVD technique was performed (Petrik et al., 2008). The CVD technique was applied to infiltrate the mesoporous pores with carbon and thus use HMS as sacrificial matrix for preparing a mesoporous carbon. Figure 3.9 shows the STEM/ESB micrographs of parent HMS silica template before (Figure 3.9 (a)) and after carbon infiltration using CVD (Figure 3.9 (b)), and the new ordered mesoporous carbon (OMC) material (Figure 3.9 (c)) obtained after removal of the silica based template with NaOH etching. It was first established that the Si matrix can readily be dissolved by use of 1M NaOH. The sample after LPG carbonization contained between 78 % and 89 % carbon by EDS analysis for carbonization times ranging from 15 min to 90 mins respectively, thus the pores were readily filled with carbon as can be seen in Figure 3.9 (b) showing a HMS sample carbonized for 90 minutes. The structural matrix of the HMS with pores occluded by carbon in-filling, is visible in the micrograph. Although LPG infiltrated the template HMS and began to decompose to carbon species at 600 ºC and 700 ºC there was no formation of the graphitic OMC at these temperatures, whereas a temperature of 800 °C and 90 minutes exposure to the LPG flow was successful to produce OMC. Shorter times allowed carbonization of the

substrate surfaces. The ordered mesoporous carbon (OMC) obtained after dissolution of the Si matrix (Figure 3.9 (c)) had a significantly smaller particle size than the parent HMS as the carbon deposited by CVD occupied the pore voids of the HMS. The ordered wormhole porous nature of the OMC analogous to HMS is visible in the HRTEM image presented in Figure 3.9(d).

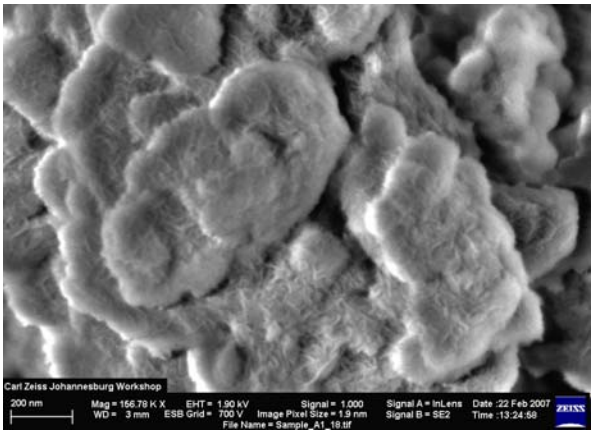

(a) HMS silica template

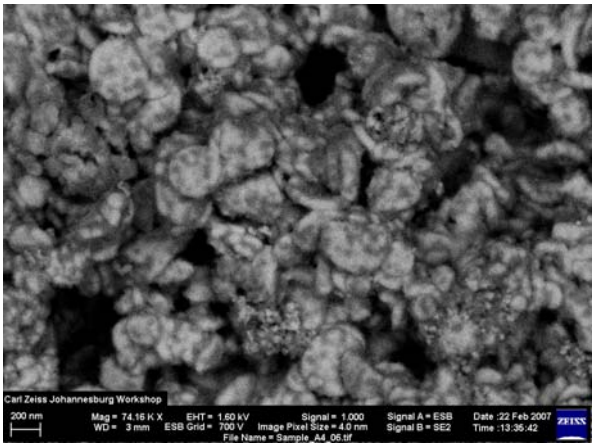

(b) HMS infiltrated with carbon

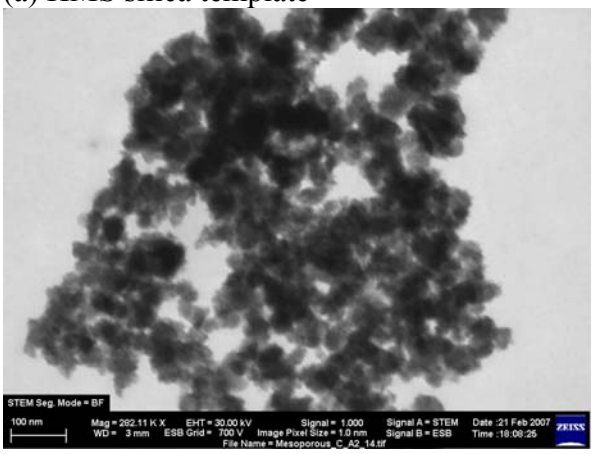

(c) OMC analogue after removal of silica template

(d) HRTEM of OMC showing wormhole pore structures analogous to HMS

Figure 3.9 STEM/ESB and HRTEM images of mesoporous substrates

XRD spectra of the sacrificial template HMS, the carbon infiltrated HMS, and the OMC analogue recovered after removal of silica template are shown in Figure 3.10.

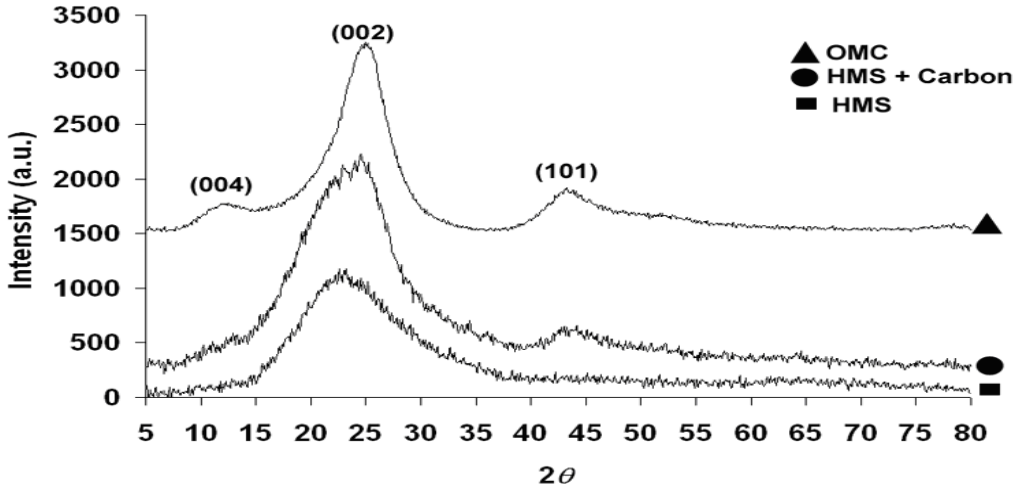

Figure 3.10 XRD of HMS, HMS in-filled with carbon and OMC analogue

The XRD of the HMS template is devoid of any characteristic sharp peaks at relatively high angles, which is typical for this material (Figure 3.10) (Pauli and Pinnavaia, 2001). The OMC had well defined peaks at 2 θ values of 7.39°, 25.3° and 43.5°. The 2 θ values of peaks appearing at 25.3° and 43.5° are ascribed to the (002) and (101) diffraction peaks of graphitic carbon in the OMC pore walls. The d002 spacing obtained from the (002) peak is 3.38 Å, which is very close to the d spacing of ideal graphite (with d002 = 3.35 Å). The peak at 12.64° has not been observed previously for the periodic structures of OMC's. This peak is attributed to C(004). This peak at an angle of 12.64° is a further indication of an ordered graphitic carbon framework appearing at periodic intervals.

Figure 3.11 shows the low angle XRD between 0 and 8 º2θ of the OMC analogue after removal of silica template with an inset of the SAED of the OMC, showing its graphitic crystalline nature. Peaks between 0º - 5º 2 θ were observed during low angle XRD scans (Figure 3.11) done between 2θ values of 0.50° and 9.9° 2 θ at a step size of 0.0330° for both HMS and OMC. These peaks are indicative of regular mesoperiodicity which is a feature of mesoporous materials with pores in the nanometer region. The low angle XRD peak (Figure 3.11), for the silica HMS template was at 2.4 ° 2 θ with a d-space centred at 3.6Å and that of the OMC at 1.83° 2 θ with a d-space at 4.8Å. The XRD pattern of the OMC thus shows the typical low

angle XRD peak indicative of the average pore–pore correlation distance for a mesoporous material.

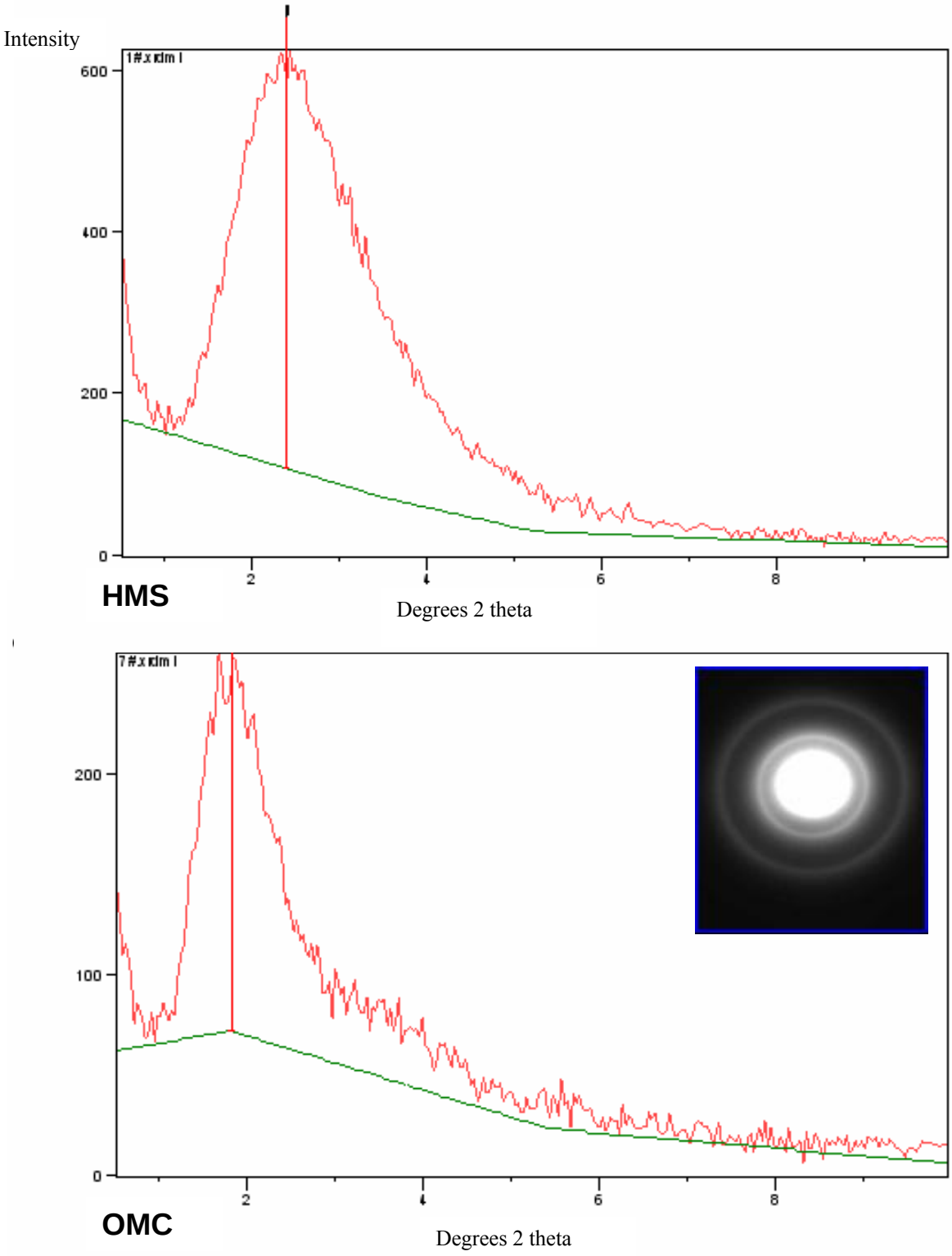

Figure 3.11 Low angle XRD of HMS and OMC analogue (inset SAED of OMC)

Hence, this OMC material has XRD definable periodic pores and pore walls containing graphitic carbon. The XRD peaks indicate that the OMC pore wall formed by carbon deposition in the pores of the parent Si template during infiltration of LPG in the CVD treatment at 800 °C. The infiltrated carbon was successfully converted thermally to graphitic carbon. The presence of graphitic peaks was also observed in the XRD pattern upon infiltration of HMS by carbon (Figure 3.10). The low angle XRD peaks (Figure 3.11), for the silica template and the OMC, confirm the existence of pores in the nanometer region. The OMC pore organization is suggested to be an inverse analogue of HMS which has a wormhole structure with average framework pore sizes in the range 2.9 to 4.1 nm with a porewall thickness of 1 nm (Pauli and Pinnavaia, 2001). Because the pore walls of OMC were created by carbon deposition in the pores of HMS, the pore-pore distances reflect similar dimensions as the HMS template pore wall. The graphitic structure of the OMC was confirmed by Selective Area Diffraction (see inset Figure 3.11 (b)). Clear and sharp rings that indicate a crystalline material were observed in the SAED micrographs obtained on the OMC. The XRD and SAED illustrate that the LPG infiltrated the HMS template during CVD, and was thermally decomposed to a crystalline, graphitic form of carbon, which formed an independent and structurally robust mesoporous material after removal of the silica template.

The porosity of the OMC and parent HMS as well as MCM-41 was further confirmed by N_2 adsorption/desorption at -196 ºC using an Accelerated Surface Area and Porosity apparatus (ASAP 2010, Micromeritics). N_2-adsorption-desorption isotherms of zeolites, MCM-41, and HMS are typically of the type IV isotherm. Thus an increase in N_2 adsorption (within the P/P0 range between 0.2 to 0.4) corresponds to capillary condensation within uniform pores. The sharpness and the height of this step reflects the uniformity of the pore size and the pore volume respectively (Grün et al., 1999). Prior to analysis, 0.2 g of powder was degassed at 200 ºC and 200 mmHg for 12 h. The adsorption isotherms of nitrogen were collected at -196 ºC using approximately 20 values of relative pressure ranging from 0.05 to 0.99. (Figure 3.12).

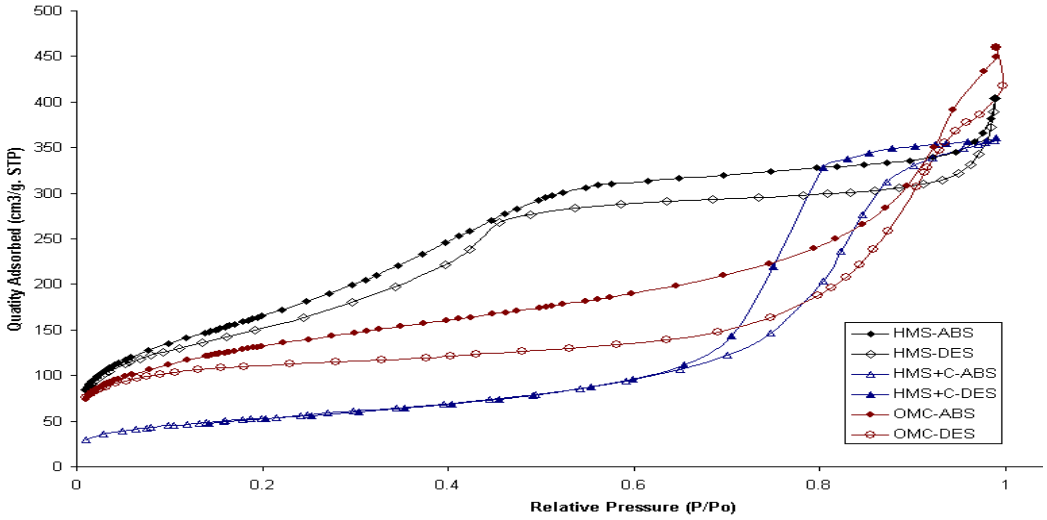

Figure 3.12 The N_2 adsorption/desorption at -196 ºC of the HMS, HMS in-filled with carbon and the OMC

The N_2 adsorption/desorption at -196 ºC showing the sorption isotherm plots of the HMS, HMS in-filled with carbon and the OMC are shown in Figure 3.12. Since the surface area of HMS infilled with carbon is still quite substantial, the degree of infiltration of LPG into the pores may have been limited, because a measureable pore size exists in the carbon in-filled template HMS. After removal of the silica template to produce the OMC the increase in surface area, to values similar to that of the parent mesoporous material is unambiguous proof that the HMS Si template was mainly removed and an ordered mesoporous carbon structure analogous to HMS was produced.

EDS analysis on the HMS silica template before and after carbon infiltration using CVD, and after removal of the silica template, showed a progressive decrease in the Si and O peaks, and an increase in the carbon peak. EDS characterization verified the successful removal of the silica template; however, the final OMC did contain traces of silica thus the removal of the silica template was not 100% complete and the porosity of the OMC was lower than the HMS. This is probably due to a degree of silica occlusion within small areas that are inaccessible during the NaOH dissolution denoting some structural collapse of the OMC or amorphous regions present in the parent HMS material.

The use of a silica based mesoporous template HMS in the CVD system thus resulted in the successful penetration of the precursor LPG into the HMS template. Thermal decomposition of the precursor LPG produced a structurally stable and well ordered mesoporous carbon in a single step. An additional advantage to this method is that the OMC produced is mainly graphitic, thus there is no need for any additional graphitization steps.

The silica based MCM-41 mesoporous material was also characterized by nitrogen adsorption at -196 ºC. Figure 3.13 shows the N_2 adsorption–desorption isotherms at -196 ºC of the MCM-41 which exhibits type IV isotherms with narrow hysteresis loops, which is characteristic of mesoporous materials with pore diameter in the range 2.0–4.0 nm. There is no sharp rise in N_2 uptake as the pressure reaches saturation (P/P0 is near1), which indicates that no macroporosity exist in the material.

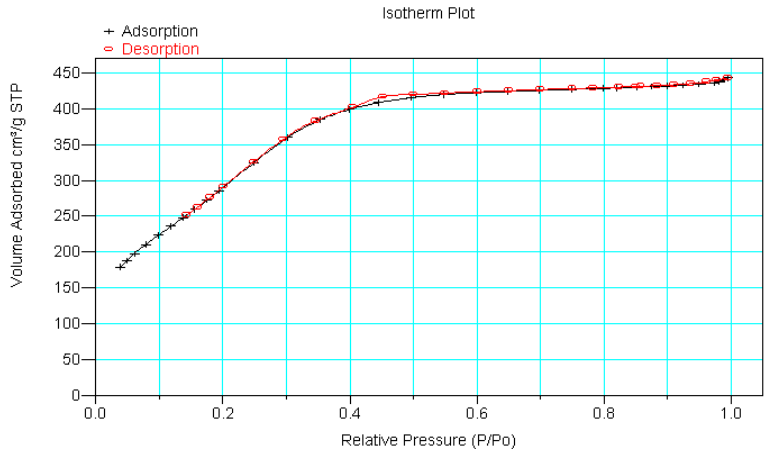

Figure 3.13 Nitrogen adsorption-desorption isotherm of MCM-41

The BET surface area of MCM-41 was 1108.9 m^2g^{-1}. The material has a narrow mesoporous distribution (Figure 3.14). The pore distribution is in the range of 1~4 nm, centred at 1.5 nm.

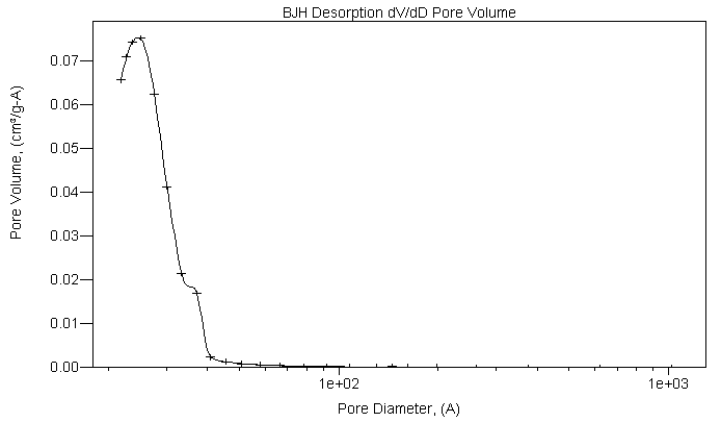

Figure 3.14 Pore distribution of MCM-41 (From incremental BJH desorption data)

The new graphitic mesoporous OMC material as well as HMS and MCM-41 can thus be considered as suitable high surface area, three dimensional, substrates for stabilizing the nanophase Pt electrocatalysts. The OMC material has the advantage of being conductive and this material was further characterized and applied to support Pt and tested as electrocatalyst as is specified in Godongwana (2006) and Petrik et al. (2008). HMS and MCM-41 were applied as supports for nanophase Pt and Au to form composite nanophase electrodes by sequential deposition, as is further detailed in Chapter 5.

3.4.2.2 Characteristics of Carbon nanotubes

The aim of preparing the CNTs and treating them by acid washing was to investigate the feasibility of using carbon nanotubes as supports for platinum as electrocatalyst in electrochemical processes. Chapter 4 details a method for dispersing metals such as platinum upon the CNT. Two samples of CNTs synthesized under the same conditions by the nebulised spray pyrolysis of a solution of ferrocene in toluene or benzene were used. Sample 1 was obtained from the ferrocene-toluene mixture while sample 2 was obtained by using a ferrocene-benzene solution.

Both samples were characterized by TGA and XRD. The XRD results (Figure 3.15) showed the possible presence of small quantities of amorphous carbon (indicated by a

broad low intensity peak at 15 º2θ) in the case of CNT Sample 1 while CNT Sample 2 showed no such peak, thus the use of benzene as carbon source in the synthesis of CNTs may have resulted in a more fully crystalline material.

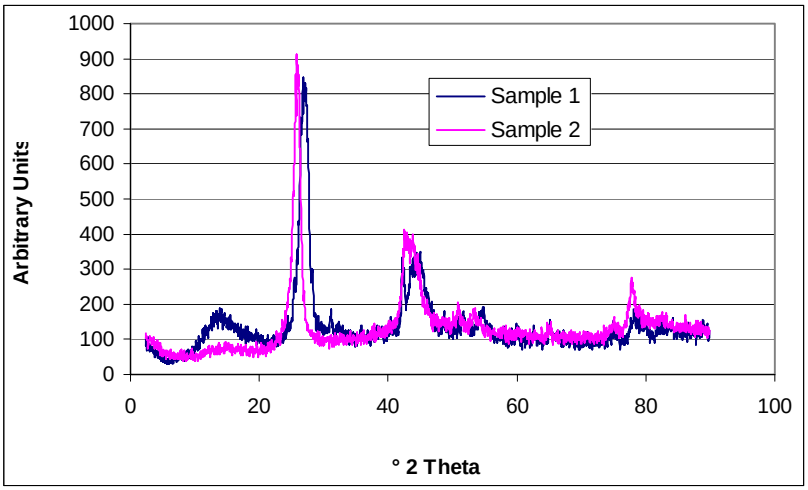

Figure 3.15 XRD spectra of CNT samples prepared using toluene or benzene

XRD shows typical and highly crystalline graphitic carbon peaks at values of 25.6 º2θ (d-spacing of 0.336 nm) and 43.7 °2θ with miller indices (002) and (101) respectively, indicating the presence of a significant graphitic phase (Figure 3.15). These peaks are much more intense than the similar peaks observed for the mesoporous carbon analogues. The slight shift in peak positions of the one sample relative to the other could be due to an artifact caused by sample holder packing since it was difficult to press the CNT flat. The peak centred at 14.5 °2θ visible in CNT Sample 1 could also be indicative of structural ordering at planar spacings at around 3-5 Å that may relate to the internal pore diameter or pore wall thickness for CNT Sample 1 whereas CNT Sample 2 did not have a distinct peak in this area and may thus not have an internal pore. Based upon this premise, CNT Sample 1 (prepared with toluene) was further characterized and used as support. Other peaks visible above 50 °2θ may be due to the ferrocene catalysts used to prepare the CNT.

TEM micrographs (not shown) of un-treated carbon nanotubes, and acid treated carbon nanotubes indicated that the CNTs prepared by spray pyrolysis were not uniform in dimensionality. However, this should not be a problem in the application

of these materials as catalyst support, since uniformity of the support is not a critical requirement. The HR TEM images (Figure 3.16) show that the CNTs prepared by nebulized spray pyrolysis using ferrocene-toluene were multi-walled CNTs. The acid treatment was sufficient to remove the metal ferrocene catalyst to a significant degree but not completely.

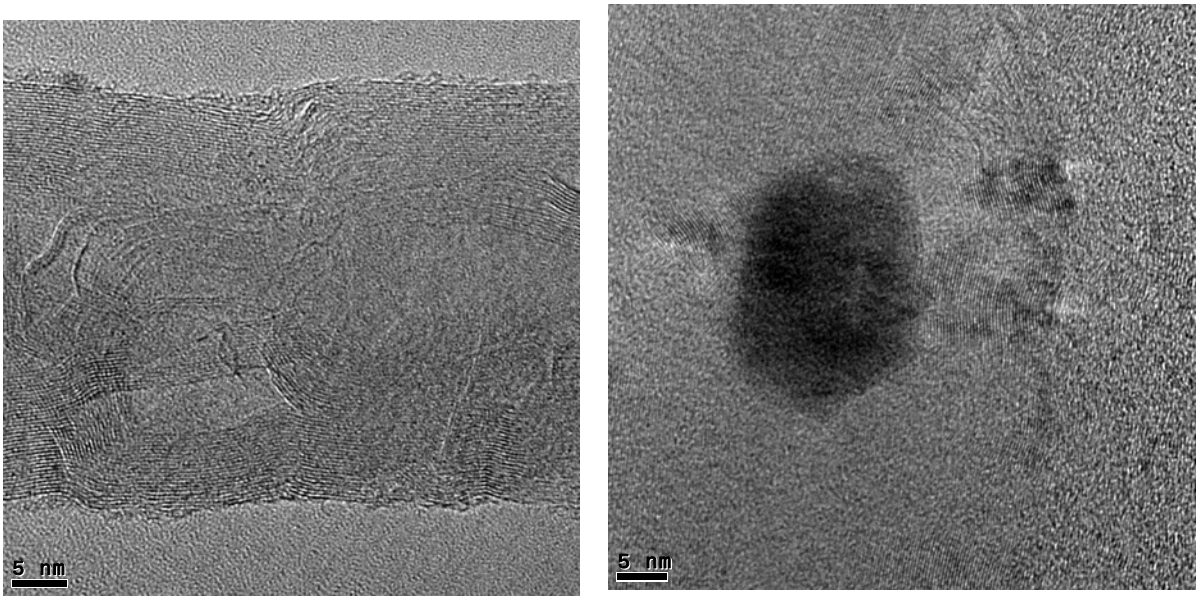

a) Multiwalled CNT with imperfect pore walls

b) Fe impurity in CNT

Figure 3.16 HRTEM images of acid washed CNT prepared by ferrocene-toluene method

The acid washing may have damaged the CNT pore wall to a degree as can be seen in the HR TEM images Figure 3.16(a). HR TEM (Figure 3.16 (b)) and EDS X-ray analysis (Figure 3.17) showed that traces of Fe catalyst remained in the ferrocene-toluene CNT, hence the acid washing technique used was not sufficient to remove all the metal catalyst impurity.

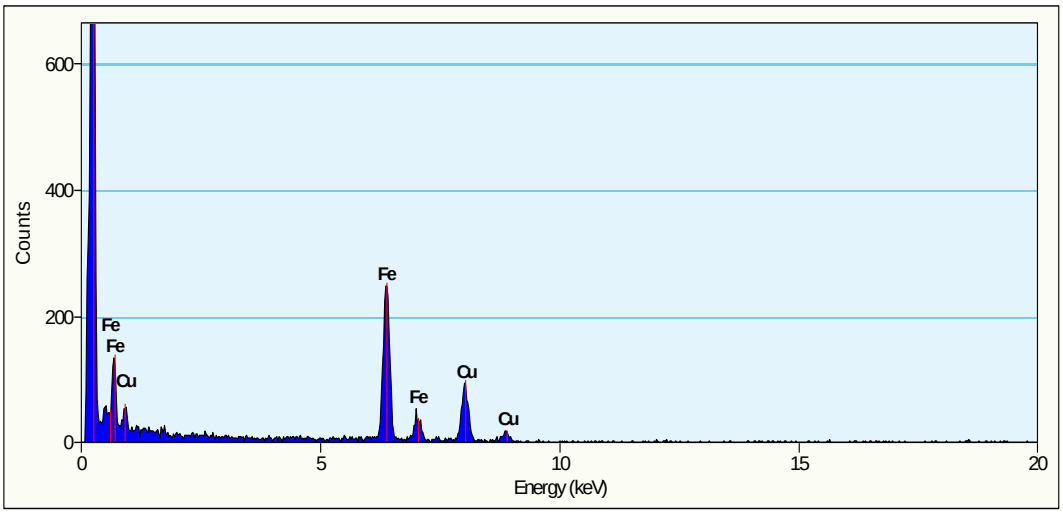

Figure 3.17 X-ray analysis (EDS) of CNT

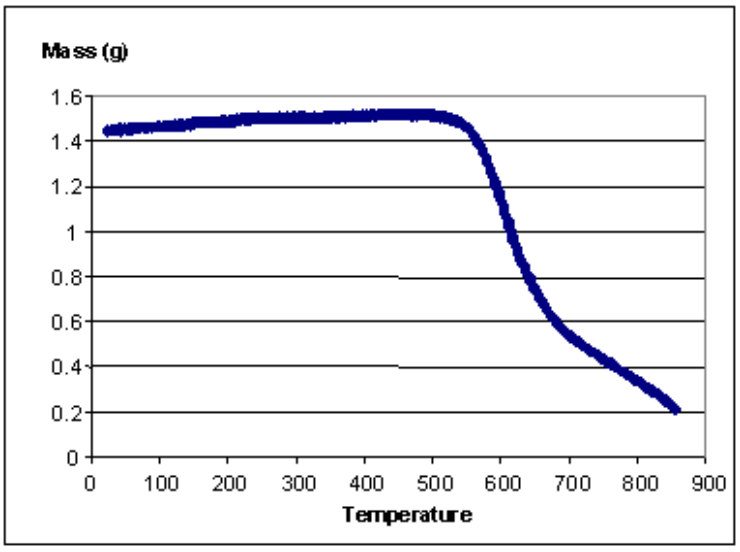

Figure 3.18 Thermal analysis of CNT

The TGA of the CNT sample (Figure 3.18) shows the typical thermal degradation of graphitic carbon above 500°C. No mass loss was observed below this temperature indicating that this material was pure and had no amorphous carbon intermixed with the graphitic CNT. The CNT were processed into a mat or felt as is shown in Figure 3.19 by means of filtering the CNT in solution (Section 3.3.4), which material is termed "CNT paper" in the rest of the study.

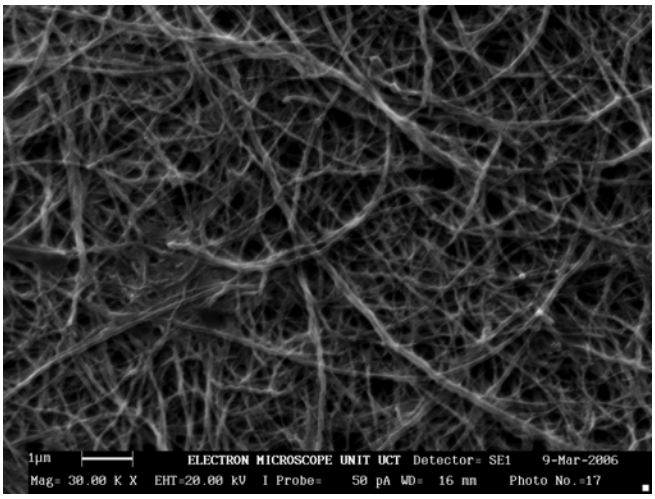

Figure 3.19 SEM of CNT processed into a CNT paper

The SEM of CNT processed into CNT paper (Figure 3.19) shows that the void spaces or "pores" between the matted CNT fibres are in the order of microns, which void spaces thus form macropores, through which pores gas diffusion could take place. The CNTs in turn have an internal mesopore structure which was evident in the HRTEM (Figure 3.16). Hence this processed CNT material contains mesoporosity but is simultaneously a suitable macroporous conductive support once it is converted into a CNT paper. The electrical conductivity as well as the resistance of the carbon nanotube sample processed into the form of CNT paper was initially investigated by a 4 point resistivity technique using a Hall measurement system (Ecopia HMS 3000, Korea).

Table 3.2 Resistance measurements of CNT paper

	Buckey Paper					
Current (mA)	V1(mV)	V2(mV)	V3(mV)	R1(Ω)	R2(Ω)	R3(Ω)
1.000	0.03	0.033	0.033	0.0300	0.0330	0.0330
2.000	0.06	0.066	0.066	0.0300	0.0330	0.0330
3.000	0.089	0.099	0.099	0.0297	0.0330	0.0330
4.000	0.118	0.132	0.132	0.0295	0.0330	0.0330
5.000	0.15	0.164	0.164	0.0300	0.0328	0.0328
6.000	0.197	0.197	0.197	0.0328	0.0328	0.0328

The CNT paper had a low resistivity of approximately 0.033 Ω which was not as low as the typical graphite resistivity that ranges from 9 to 40 µΩm, thus these CNT may

not be fully graphitic. The potentials ranged between and 0.03 and 0.197 mV at an applied current between 1 and 6 mA respectively showing the high conductivity of the paper prepared from CNTs. This CNT paper material was used to stabilize Pt nanophases and bimetallic nanophases as is described in Chapter 4 and CNT paper as well as CNT paper with Pt incorporated is further characterized using the Hall system as is described in Chapter 6.

3.5 CONCLUSIONS

Zeolite FAU obtained from a commercial source was characterized by HRTEM, FTIR, XRD, and TGA and shown to have high porosity on the Angstrom scale, with pore sizes in the region of 7 Å, and high crystallinity and thus should be a suitable substrate for the high dispersion of the active Pt metal phase to prepare nanophase electrocatalysts.

LPG was used as a carbon source in the successful pyrolytic synthesis of nanostructured ordered mesoporous carbon materials with graphitic character. The use of a CVD system resulted in the successful penetration of the carbon precursor into the silica based template and subsequent thermal decomposition of the carbon led to a well ordered carbon mesoporous structure that was recovered after dissolution of the silica template. An advantage to this method is that the carbon produced was graphitic, thus there is no need for any additional graphitization steps. The low angle XRD peak, observed for the HMS silica precursor and also the resulting OMC analogue of HMS, is a typical feature of mesoporous materials with pores in the region of 2-3 nm, and the porosity of the OMC was confirmed by N_2 adsorption. Selected area diffraction established that a crystalline graphitic material was formed in agreement with XRD results. Thus the LPG infiltrated the pores of the HMS silica template, and thermally decomposed mainly to a crystalline form of carbon, which, as a result of the MHS porous template morphology, formed an independent and structurally robust ordered mesoporous carbon material analogous to HMS upon

removal of the silica template. The ordered mesoporous carbon analogue of HMS could thus be suitable as an electro-conductive, high surface area substrate for deposition and stabilization of metal nano-particles of electro-catalysts.

The CNT produced by use of a ferrocene-toluene combination were utilized to prepare a felt or CNT paper with micron sized macropores which could be a suitable high porosity conductive electrode material to be used as a gas diffusion layer in a membrane electrode assembly or as a macroporous catalyst support.

These 3 dimensional substrate materials were applied to support Pt and the resulting electrocatalysts were worked up into composite thin film electrode materials as is further specified in Chapters 4, 5 and 6.

CHAPTER 4

4 PREPARATION AND CHARACTERIZATION OF ELECTROCATALYSTS SUPPORTED ON CNT

This chapter, Chapter 4, focuses mainly on improvement of the catalyst / support interaction by high dispersion of the catalyst on the carbon nanotube (CNT) supports described in Chapter 3. Characterization of the benchmark commercial Johnson Matthey Pt_{40}/C catalyst is also presented in Chapter 4.

For water electrolysis, more conductive and more durable gas diffusion layers are required with a higher surface area and a finer fibre size that will form smaller macropores. The usual carbon cloth gas diffusion layers can possibly be substituted by use of CNT. The CNT fibres are much finer than the typical carbon cloth fibre and if processed into a mat or paper of interwoven fibres could be utilized as a macroporous support substrate for direct deposition of Pt nanoparticles, thus eliminating one intermediate step in processing. In other words, instead of supporting Pt on carbon black which must then be supported on carbon cloth using binders (as is detailed in Chapter 5), in this chapter it is detailed on the one hand how to support Pt on CNT and on the other to utilize a galvanic displacement reaction as deposition technique to deposit Pt directly on CNT which have already been processed into a paper that is suitable as a gas diffusion support substrate and characterize the new material.

4.1 OVERVIEW OF CATALYST PREPARATION CONDITIONS

Platinum Group Metal (PGM) nanophase catalysts play vital roles in fuel cell and electrolyzer technologies. To enhance catalytic performance and reduce operational costs of fuel cell PGM electrocatalysts particle sizes are decreased to the nanometre scale to increase the overall active surface area. As a result, physical and chemical

properties of the electro catalytic materials are altered compared to the original properties of the associated bulk materials. As particle sizes approach the atomic or Angstrom (Å) domain deviations in behaviour arise as the number of surface atoms becomes comparable to that of the interior of the particle. With decreasing particle size larger numbers of surface atoms can be found. The increase in the surface-to-volume ratio is associated with an increase in the interfacial region and thus characteristics are different from interior atoms due to higher instability and reactivity of surface atoms that dictate the surface energy and the chemical behaviour of nanomaterials. Nanophase catalysts are applied in surface-sensitive reactions, where catalytic reactivity is a function of the exposed surface of the catalyst and the interface between the reactant and the catalyst. With the shift of PGM catalyst particle size into the nanometre domain the characteristics of altered electro catalytic properties (e.g. surface reactivity) gains significance because most nanophase PGM catalysts have a functionality based on their structural physico-chemistry (Marković et al, 2003). In electro catalysis, the greater the surface area of the material the greater is the decrease in the activation energy threshold and the greater is the catalytic activity. Geometry and electronic structure are strongly affected by decreasing the particle size. Other changes in properties induced by size reduction to the nanoscale may include electrical resistance/conductivity, specific heat capacity, thermal expansion, magnetism, and lower thermal conductivity. Physical properties that may change upon reducing the particle size to the nanoscale include melting point, hardness, and tensile strength due to a change in the atomic environment of the material.

Carbon supports are used to stabilize electrocatalysts that may be applied in PEM systems because the surface area of the catalyst is increased, and because it allows highly uniform and dispersed catalyst even at high loadings (<30 %) and provides sufficient electronic conductivity and chemical stability (Vielstich et al, 2003). Increase of catalyst stability to prevent agglomeration of small particles. For good catalyst stability it is necessary to achieve high utilization of precious metal by deposition of nanosized particles with high surface area to bulk ratio. Metals need to

adhere to surface of support for long lifetimes and the method of production should be economical and reproducible. The specific surface chemistry of the carbon support affects the chemistry of the metal ion/ atom fixation upon the surface of carbon black and the surface area of Pt can be increased with an increased surface area of the carbon support. Precipitation of the metal catalyst upon a support via a chemical route is common using aqueous solution of precious metals where the metal ions are precipitated by hydrolyzing and transformed to the metallic state using chemical reducing agents. Metal salts are common precursors. The Pt catalyst can be prepared from the chloride solution onto the conductive support at pH 7-9 using a strong reducing agent like formaldehyde. Other routes could be used such as metal sulphite oxidation with H_2O_2 to precipitate chloride free catalysts in a pH range of 8 or above. Powder catalyst materials should be designed specifically for the membrane electrode assembly process, which requires nano particle sizes that are well dispersed in inks, for adhesion, and tailoring of hydrophilic/hydrophobic properties, as well as cost reduction (M. Hampden et al., in Vielstich 2003). Standards are necessary for mass manufacturing, including scalability, reproducibility and quality.

The size of nanophase PGM electrocatalysts raises significant challenges in stabilization. Transition and noble metals typically have high surface free energies, and therefore, small particles or crystallites tend to agglomerate to reduce their surface area. Stabilization of nanosize metal particles therefore requires deposition on the surface of supports providing favorable metal-support interactions. The smaller the particle the more its physical properties and morphology can be affected by these interactions (Allen et al., 2001). Therefore, the nature of the support material for a given metal also critically influences the catalytic properties of the metal particle. Supported metals are in a non-equilibrium state and therefore still tend to agglomerate at sufficiently high temperatures in reducing atmospheres. Solid supported catalysts are complex assemblies, the preparation of which is a challenging task. It is necessary to develop a fine conductive support matrix for nanoparticles deposition. The requirements of a support for an active electrocatalyst are rigorous. It

must provide structural, conductive, and durable support for the active metal particles.

The nanoparticles should be well dispersed over a conductive and high surface area support. Metal nanoparticles are thermodynamically unstable and readily agglomerate through the attachment of particles at crystal edges or corners which promotes mass-conservation and which increases the particle size distribution, decreasing the particle surface area available for chemical reaction. Aggregation is a result of van der Waals attractions existing between particles of similar composition. Aggregation alters the volume, particle size, particle size distribution, porosity and surface area of materials. Changes in surface area and volume by agglomeration or aggregation may influence the chemical reactivity of nanophase electrocatalysts (Simonov et al., 2003). Metal particle size is influenced by the preparation method and nature of the support material. High metal dispersion on the support material and decreased metal particle size generally result in increased catalytic activity whereas a broad metal particle size distribution may lead to inefficient metal utilization. Metal particle size distribution is largely influenced by the metal-support interaction and electrical charging of the particles has a significant effect on the predicted agglomeration rates (Allen et al., 2001).

By far the most common support materials used in PEM fuel cells are carbon blacks. As can be expected, increasing the surface area of the carbon leads to greater Pt dispersion at a given loading. Uchida et al. (1996) showed that Pt crystallite size decreased from 3.7 to 1.0 nm when the carbon surface area increased from 58 to 1500 $m^2\ g^{-1}$ for a series of 23 to 24 wt% Pt catalysts. Similarly, Tokumisu et al. (1999) reported that increasing the carbon surface from 60 $m^2\ g^{-1}$ to over 1300 $m^2\ g^{-1}$ resulted in the reduction of Pt particle size from 2.5 to 1.5 nm for 10 wt% catalyst. Various literature sources state that carbon black with particle sizes of 30-75 nm corresponded to a surface area of 250-300 $m^2\ g^{-1}$ (Li et al, 2004; Prabhuram et al, 2004; Jordan et al, 2000). However, despite the increase in Pt surface area achieved by higher-area carbon support, the cited studies showed little effect of carbon support on catalytic

activity. It was suggested that both the Pt particle size effect and the interaction of the ionomer with the carbon support played important roles in determining activity.

Carbon nanotubes are composed of cylinders in a helical hexagonal arrangement, closed at both ends by hemispherical endcaps. The continuous sp^2 hybridization structure provides unique electronic characteristics. The structure of these cylinders can produce a special interplay between support and metal and could promote the activity of the electrocatalyst (Vogel, 1977). The unique electro-structure of CNTs has a better electronic conductivity than Vulcan XC-72. The electronic conductivity of Vulcan XC-72 on its own is 4.0 S cm^{-1} while that for CNT is 1250 S cm^{-1} (Li et al, 2003).

Commercially, carbon black is typically used as a support for Pt nanoparticles (Pozio et al, 2002). In the case of water electrolysis or fuel cells, after Pt is deposited on the carbon black, this composite Pt/C electrocatalyst still has to be deposited upon a substrate used as gas diffusion layer (GDL) that is typically made of carbon cloth. The GDL support should allow ingress of the reactant, water and egress of the product, air or H_2 (Vielstich et al, 2003). The carbon cloth was found to be problematic as support (as is further described in Chapter 7) as it showed poor durability and disintegrated over time during the flow of water through the electrolysis cell, hence more durable GDL are necessary.

Nanostructured carbon materials with graphitic structure, such as carbon nanotubes (CNTs) and carbon fibers were utilized as catalyst supports and platinum–ruthenium (Pt–Ru) nanoparticles were successfully deposited on the surface of SnO_2 nanowires grown directly on E-TEK carbon paper (Pt–Ru/SnO_2 NWs/carbon paper) by a potentiostatic electrodeposition method and applied for electrocatalytic oxidation of methanol (Saha et al., 2007).

Qu and Dai (2005) reported a substrate enhanced electroless deposition (SEED) procedure of metal nanoparticles on carbon nanotubes. This procedure is a simple

galvanic displacement reaction and could facilitate the large scale production of nanoparticle coated carbon nanotubes. In the electroless deposition procedure only metal ions that have a reduction potential higher than the carbon nanotube can be reduced onto the carbon nanotube. According to Choi et al (2002) a single wall nanotube has a reduction potential of +0.5 V vs SHE (standard hydrogen electrode) and these authors were able to successfully deposit Pt (+0.775 V vs SHE) as nanoparticles through spontaneous reduction of the metal ions by the nanotubes. In the SEED procedure of Qu and Dai (2005) it is shown that metal ions even with a lower reduction potential than that of a conducting carbon nanotube can be reduced onto the support (Figure 4.1) without an additional reducing agent. In this reaction the nanotube acts as cathode for reducing the metal ion in solution whereas a chosen metal substrate (Cu) acts as anode where the metal substrate's atoms are oxidized and displaced into solution (Wen and Yang, 2002).

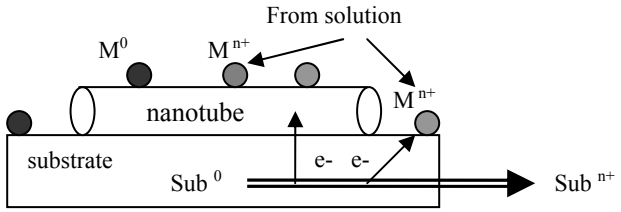

Figure 4.1 Schematic illustration of metal nanoparticle deposition on carbon nanotubes via the SEED process (after Qu and Dai, 2005)

4.2 CHARACTERIZATION OF ELECTROCATALYSTS

The size of nanophase PGM electrocatalysts raises significant challenges in determining the physico-chemical properties of these electrocatalysts. The analytical techniques (Section 3.3.5) that can be used to characterize the minimum set of physico-chemical properties of nanophases facilitates comparison between different electrocatalysts (Williams et al, 2008).

Because it is not always feasible or practical to perform an exhaustive analysis of the materials, it is important to identify the minimum set of properties which have an influence on the catalytic behaviour of nanophase electrocatalysts. The most important information regarding nanophase electrocatalysts is gathered in an electrochemical characterization study incorporating voltammetry. Nanophase PGM electrocatalyst producers, such as Johnson Matthey, rely on measurements of XRD particle size, lattice parameters, and metal surface area as a minimum set of properties required for characterization (Johnson Matthey, 2008).

Scanning Electrochemical Microscopy (SECM) feedback mode and substrate generation-tip collection mode coupled with a chronoamperometric approach could be used to investigate H_2 oxidation and hydrogen evolution reaction (HER) at a polyaniline coated highly oriented pyrolytic graphite (HOPG) electrode. Using the former mode, the heterogeneous electron transfer kinetics for H_2 oxidation could be studied, while the latter mode allowed mapping of the distribution of local [H_2] at the nanoparticulate/aqueous interface, followed by monitoring of the transients at the tip. These studies demonstrated that SECM was useful in evaluating the activity of nanophase electrocatalysts. The resolution of this technique is limited by the diameter of the scanning tip. If nanometer-sized tips or hydrodynamic microjet electrodes were employed where the mass transfer rate was high, it should be possible to investigate the ET kinetics more accurately (Ahmed et al., 2004). However, Williams et al., (2008) found that this technique was merely qualitative and did not allow comparisons to be made between the activities of different electrocatalysts.

4.3 ELECTROCHEMISTRY BACKGROUND

Cyclic voltammetry (CV) can be used to investigate the electro catalytic activity of fabricated electrocatalysts and plays an integral role in a comprehensive characterization of nanophase electrocatalysts (Steigerwalt et al, 2001; Jarvi et al, 1998). Cyclic voltammetry is used for studying the reversibility of electrode

processes and for kinetic observations, and sometimes for analytical purposes. It gives information on the redox behaviour of electrochemically active species and on the kinetics of the electrode reactions as well as offering the possibility of identifying reactive intermediates. It is based on recording the current during a linear change of a voltage at a stationary working electrode. The working electrode serves as the surface where the electron transfer of redox reaction occurs. The redox reaction occurs within the potential range defined by two chosen potential values and the potentials at which reduction or oxidation takes place provide qualitative information about the analyte of interest. The application of an electrical applied potential to the working electrode makes the surface electrochemically act to oxidize or reduce, depending on the applied potential. As the applied potential becomes more negative, the electrode becomes a better reducing agent. As the applied potential becomes more positive, the electrode becomes a better oxidising agent (Williams et al, 2008).

Generally the heterogeneous reaction rate taking place at the electrodes surface is described in units of mol per unit area per second by equation (4.1)

$$Rate\left[\frac{mol}{s.cm^2}\right] = \frac{i}{nFA} = \frac{J}{nF} \qquad (4.1)$$

Where:

i: current (amperes, A); F: Faradays constant, 96485.3 C; A : electrode surface area (cm^2); n : number of electron transfer; j : current density (A cm^{-2})

CV can be used in the determination of the electrochemically-active surface area of carbon-supported nanophase Pt electrocatalysts. The method requires the hydrogen underpotential deposition (H_{upd}) region in the electrolysis of dilute acid on Pt. The H_{upd} region corresponds to Pt-hydride monolayer formation and removal near the reversible H_2 potential (0.0 V_{SHE}). The H_{upd} region consists of cathodic hydride adsorption and anodic hydride desorption surface reactions, which can generally be given as follows:

Hydride Adsorption: $Pt + H^+ + \bar{e} \rightarrow Pt\text{-}H_{ad}$

Hydride Desorption: $Pt\text{-}H_{ad} + H_2O \rightarrow Pt + H_3O^+(aq) + \bar{e}$

The hydride desorption peaks can be integrated to yield a charge (Q_{H^+}), which is used to calculate the electrochemically-active surface area (Nart et al., 2003). This approach is based on the assumption that a complete monolayer corresponds to a surface charge of 210 μC cm^{-2}. Voltammetric charge density, q* (mC cm^{-2}) can also be determined by the mechanical integration of voltammograms (Hrussanova et al., 2004). Therefore, voltammetric charge, q*, is the mean charge between the anodic and the cathodic branches. The charge measures the amount of protons exchanged by the oxide surface with the solution during the potential scan thus q* can be regarded as proportional to the active surface area of a catalyst.

Several authors have compared electrochemical active surface area Pt/C catalysts by cyclic voltammetry. A review is given by Pozio et al., (2002). These authors note that the active surface areas (EAS) determined by cyclic voltammetric for the same commercial Pt/C catalyst in various studies were not similar. Various EAS values were obtained depending upon changes in the Pt loading (mg cm^{-2}). The variation observed was also ascribed to the method of preparation of the catalyst layer in the gas diffusion electrode, where the binder Nafion or PTFE may occlude the catalyst; or to different catalyst loadings that may be obtained; or to variations in the Pt/C to Nafion ratios applied. The coulombic charge for hydrogen desorption was used by these authors to calculate the active Pt surface of the electrode. It was also observed that if the catalytic layer in the electrode became too thick the Pt utilization was limited as an increasing fraction of the Pt surface was occluded by the binder and carbon. Pt loading on the powder catalyst was determined from the Pt/C wt%. Amongst the recommendations made by these authors was that the catalysts should be tested preferentially without binders that could decrease the catalyst utilization values, that careful control of the Pt loading should be observed, and that a simple half cell, three electrode configuration using a geometric 1cm^2 working electrode be used instead of a full cell configuration with a membrane electrode assembly. It is

time consuming and expensive to evaluate electrocatalysts applied in gas diffusion electrodes in working fuel cells or PEM electrolyzers and as Chapter 7 highlights it is not possible to decouple the activity of the electrocatalyst from numerous other parameters that influence the current density obtained. Pozio et al. (2002) noted that the presence of the inert gas flowing on the back of the electrode in a full cell configuration affected the hydrogen adsorption/desorption process during the CV measurements.

Voltammetry can be used to determine thermodynamics and kinetic parameters of electron transfer across the electrode/film interface (Rusling et al., 2003). Using a sufficiently slow scan rate the polymer film can be exhaustively oxidized and the depletion layer extends to the film/solution interface where finite diffusion becomes important. In the ideal case the dynamics of heterogeneous electron transfer across the electrode/film interface are fast enough not to influence the observed response. For surface confined species the peaks are Gaussian at slow scan rates and the separation of the oxidation and reduction peaks is ideally zero. The formal potential $E^{0/}$ shows how readily the redox centres are oxidized within the polymer film. However it is important to distinguish between specific ion effects and changes in $E^{0/}$ brought about by changing the electrolyte concentration. It is of importance to determine the rate of charge transport through the layer that affects the degree of oxidation or reduction of the metal centres (Rusling et al., 2003).

Mass transfer is related to the movement of ions in solutions and in the quiescent electrolytes used in cyclic voltammetric experiments, is due to diffusion. Diffusion describes the mass transfer due to the random motion of ions and results from a gradient in the electrochemical potential (Bard and Faulkner, 2001). The diffusion coefficient can be described as a proportionality constant which relates the flux of ions to a concentration gradient and can be related to the availability of a reagent species to the surface reaction (International Union of Pure and Applied Chemistry, 1997).

The Randles-Sevçik equation (Bard and Faulkner, 2001) may be used to determine the effective diffusion coefficient (D_{CT}) corresponding to diffusion of electrons at relatively high scan rates.

$$Ip=(2.69 \text{ X } 10^5)n^{3/2}AD_{CT}{}^{1/2}\,Cv^{1/2} \qquad (4.2)$$

Where C is the concentration of electro active sites in the film; v is the scan rate; n is the number of electrons transferred.

The Randles-Sevcik equation can be used in determining the diffusion coefficient (D) of an analyte on an electrode surface and predicts that measured peak currents are proportional to the square root of the sweep rate applied. The peak currents from a series of voltammograms are usually recorded at increasing sweep rates. A plot of peak current versus the square root of the sweep rate is then prepared and a linear least squares analysis of the data performed to determine the slope. The slope and the Randles-Sevçik equation are then used to estimate the diffusion coefficient.

The integrated charge required to form or remove the film can be measured using the potential interval ΔE, which is the difference between anodic and cathodic peak voltage,

$$Q = \int_{\Delta E} i dt \qquad (4.3)$$

Where Q is the charge (C); *i* is the current (A), and t is time (s). This gives the determination of the coverage of a film or determination of a true surface area of a roughened electrode (Plambeck, 1982; Riley and Thompson 1987)

In some cases, where the oxidizing scan is switched before reduced sites at the films outer boundary are oxidized the voltammetric wave can show tailing characteristics that indicate semi-infinite linear diffusion (Rusling et al., 2003).

Formal potentials ($E^{0'}$) of catalysts are related to the potentials of electrochemical cell reactions and are simply the average between the anodic (E_{PA}) and cathodic peak

potentials (E_{PC}). The equation for the calculation of formal potentials is given as (IUPAC, 1997; 2005):

$$E^{0'} = (E_{PA} + E_{PC})/2 \qquad (4.4)$$

Iwuoha et al., (2006) showed that the electrochemical behaviour of polymer composites could be evaluated at high potential scan rates. Electrode transfer reactions at the electrode and accompanying physical or chemical processes that have rate constants comparable to the scan rates employed are discernible in the voltammograms. These authors identified quasi reversible electrochemistry as well as electron transfer reactions at the electrode coupled to a diffusion process where the anodic currents were higher than the cathodic currents and $E^{0/}$ values shifted anodically with scan rate. Diffusion processes that may have been detected were charge transfer within the polymer or intra molecular charge transfer along the polymer backbone. Conductance is given by $C=\Delta I\nu/\Delta E\nu$ where $\Delta I\nu$ is $I_{p(\text{highest scan rate mVs}^{-1})} - I_{p(\text{lowest scan rate mV s}^{-1})}$ and $\Delta E\nu = E_{p(\text{highest scan ratemVs}^{-1})} - E_{p(\text{lowest scan rate mV s}^{-1})}$ according to these authors. The average value for all the redox states is the conductance of the material.

In this chapter, Pt/C (commercial) was characterized and compared to several different home made Pt catalysts supported on CNT prepared by a galvanic displacement reaction. These electrocatalysts were evaluated for electrocatalytic activity using cyclic voltammetry after a minimum set of properties were established by HRTEM or SEM and in selected cases by some of the abovementioned methods.

4.4 EXPERIMENTAL

4.4.1. Materials

4.4.1.1 Benchmark catalyst

The benchmark commercial catalyst used in this study was Pt catalyst HiSpec™ 4000, 40% on carbon black with 39.74% Pt, 1.33% moisture, 3.54nm crystalline size, supplied by Alfa Aesar, a Johnson Matthey Company. (Stock #42204; Lot # J26P18 or F01Q12). This catalyst will be referred to as JM Pt_{40}/C. Commercial carbon-supported platinum (JM Pt_{40}/C) fuel cell electrocatalysts containing 40% Pt served as a standardized, well-characterized model material of known properties. Its structural and chemical properties served as benchmark against which fabricated materials could be compared. Home made Pt/CNT catalysts were prepared as is further specified.

4.4.1.2Carbon nanotubes (CNT)

Carbon nanotubes (CNT) were prepared by nebulised spray pyrolysis as is described in Section 3.3.4. After acid washing a portion of the CNT were processed into a dense felt or "CNT paper" by vacuum filtration of a CNT suspension in deionized water onto a 45 μm cellulose acetate filter and in situ drying upon the filter in an adaptation of the method described by Vohrer et al., (2004). CNT and CNT paper were used as substrates where specified, to support Pt upon the exterior of the CNT.

4.4.1.3 CNT-supported Pt electrocatalysts

The CNT-supported Pt electrocatalyst was prepared, using as substrate the CNT made by nebulized spray pyrolysis, which was then treated to Pt impregnation-reduction (Li et al, 2004; Zhou, 2003) by two different routes.

In the first case, the pre-treated CNT were suspended in 1-propanol, $H_2PtCl_6.6H_2O$, and treated with H_2SO_4. Pt was reduced by formaldehyde (Ying, 2005). Typically 20.0 mL distilled water was added to 80 mL 1-propanol and made up to 100 mL in a volumetric flask as solvent. The volumetric ratio of distilled H_2O: 1-propanol was 1:4. Thereafter, 600 mg of pre-treated carbon nanotubes were placed in a 50 mL beaker to which 50 mL prepared 1-propanol solution was added and stirred magnetically for 0.5 h and ultrasonically for a further 15 min. 0.30g $H_2PtCl_6 \cdot 6H_2O$

was weighed out separately and dissolved in a portion of the prepared 1-propanol solvent solution. After the solute was efficiently dissolved, the Pt containing solution was transferred to a 50 mL flask and made up to the mark. The concentration of the solution was 20 mg mL^{-1}. The 50 mL carbon nanotube containing flux was gradually dropped into the flask using a dropper. After mixing thoroughly, the solution was stirred for a further 12 h. The stirred $H_2PtCl_6 \cdot 6H_2O$ solution was titrated with 1M NaOH, until the pH reached 12, and stirred for 1 h. An excess of 40 % formaldehyde (10 mL) was added to the solution in the flask and the flask was kept at 80 ºC for 0.5 h to optimize the reduction reaction. Thereafter, the pH of the solution was readjusted to 2.5 using 1.5 M H_2SO_4. Throughout these steps the solution was protected with inert N_2 gas while stirring continuously. Finally the solution was left at room temperature for 1 h before being filtered. The solid residue recovered after filtration was washed with distilled water and dried under vacuum at 70 ºC for 10 h. The solid Pt/CNT (propanol) sample was ground into a powder using a mortar and pestle. These CNT-supported nanophase Pt electrocatalysts (denoted Pt/CNT(propanol) were compared to JM Pt_{40}/C and to a new series of Pt CNT electrocatalysts prepared using a galvanic displacement technique (Table 4.1).

In the second case a series of nanophase Pt electrocatalysts were made using a modified galvanic displacement technique based upon the approach described by Qu and Dai (2005). This approach aims to rapidly and very simply deposit the Pt electrocatalyst directly onto the gas diffusion layer (GDL) substrate CNT paper fabricated from the CNT prepared by nebulized spray pyrolysis. The method to directly deposit Pt onto preformed CNT buckey paper as GDL eliminated many steps in the processing of the electrocatalysts into composite form.

The galvanic displacement series of catalysts (Table 4.1) were prepared in the following way.

CHAPTER 4

Table 4.1 Details of galvanic displacement samples prepared using CNT and different foils as specified

Foil type	Sample No.	CNT (g)	Foil (g)	Pt soln (mL)	time	CNT final (g)	Foil final (g)	CNT Mass increase (g)	CNT mass % increase	Foil mass decrease of foil (g)	foil Mass % decrease
Al	1	0.0072	0.2	5	10	0.008	0.156	0.0008	11.11	0.0002	0.128
Al	2	0.0076	0.1	5	10	0.0081	0.1433	0.0005	6.58	0.0002	0.139
Pb	3	0.0087	0.6	5	10	0.0102	0.5438	0.0015	17.24	0.0165	2.945
Pb	4	0.0065	0.5	5	10	0.0073	0.5572	0.0008	12.31	-0.0107	-1.958
Fe	5	0.0094	0	5	10	0.0093	0.0103	-0.0001	-1.06	0.0003	2.830
Fe	6	0.0064	0	5	10	0.0063	0.0109	-0.0001	-1.56	-1E-04	-0.926
Al	7	0.0089	0	5	10	0.0093	0.1628	0.0004	4.49	-0.1539	-1729.21
Al	8	0.0066	0.1	5	20	0.0082	0.1475	0.0016	24.24	0.0003	0.203
Al	9	0.0095	0.1	5	20	0.0106	0.1435	0.0011	11.58	0.0003	0.209
Pb	10	0.0096	0.6	5	20	0.0113	0.5486	0.0017	17.71	0.0051	0.921
Pb	11	0.0081	0.6	5	20	0.0097	0.5745	0.0016	19.75	0.0059	1.017
Fe	12	0.0062	0	5	20	0.0072	0.0108	0.001	16.13	-0.0002	-1.887
Fe	13	0.0068	0	5	20	0.007	0.0109	0.0002	2.94	-0.0007	-6.863

A specific size and weight of foil (Lead, Iron and Aluminium foil respectively) as specified in Table 4.1 was clipped tightly with a plastic covered paper clip to a pre-weighed piece of CNT paper. The CNT paper was suspended into a chloroplatinic solution with specific molar concentration of 0.01 M (0.5216 g in 100 mL), for either 10 or 20 min. All samples were made in replicate. Different times of deposition were followed for each foil so that there were two variables that were altered for each system- time of deposition and type of metal foil. The foils were selected on the basis of their reducing ability based upon the respective E ø (volts):

Al: $E^{ø} = -1.66$ (highest)
Fe: $E^{ø} = -0.44$ (intermediate)
Pb: $E^{ø} = -0.13$ (lowest)

The progress of Pt deposition could not be followed electrochemically in a two electrode configuration as it was not possible to configure the system so as to acquire a current whilst not applying a potential.

4.4.2. Characterization

The analytical techniques applied for characterization included various of the following techniques. Crystal/atomic structure and metal particle size was determined by X-ray Diffractometry (XRD, Bruker AXS D8 Advance, Cu Kα (λ = 1.5418), 0.05 º2θ min^{-1}). Crystallite size determination could be performed by measuring the broadening of a particular peak in a diffraction pattern associated with a particular planar reflection from within the crystal unit cell. Particle size is inversely related to the half-width at half maximum of an individual peak and the narrower the peak, the larger the crystallite size. This is due to the periodicity of the individual crystallite domains, in phase, reinforcing the diffraction of the X-Ray beam, resulting in a tall narrow peak. The breadth of the diffraction peak is related to the size of the crystals by the Scherrer equation as given below:

$$d = 0.9\ \lambda_k / (B \cos\theta_{max}) \quad (4.5)$$

where λ_k: wavelength (Cu-Kα, $\lambda = 1.5406$ Å); θ_{max}: half the angle of diffraction (2θ); B: radians. Typically the half-width at half-height of the diffraction peak is used for B which can be estimated as half the peak width on the diffraction spectrum. The size of a crystallite, d, giving rise to diffraction is inversely proportional to the width of the peak (Roe, 2000). Furthermore, the lattice parameter (α) can be calculated by the equation (4.6):

$$\alpha_{fcc} = 2^{1/2}\ \lambda_k / \sin\theta_{max} \quad (4.6)$$

In addition, the metal Pt dispersion (D) (Jordan et al, 2003) was calculated from

$$d = 1.08 / D\ (nm) \quad (4.7)$$

Where, d: average Pt particle size obtained from XRD results.

Surface micro- and macrostructure, and degree of agglomeration were determined by High-Resolution Scanning Electron Microscopy (HRSEM, Zeiss Ultra 55 Field Emission – In-lens detection, 30 kV, 80 μA). Metal particle size, particle size distribution, metal surface area, and metal dispersion/agglomeration were established by Transmission Electron Microscopy (TEM, Hitachi H-800 EM, 200 kV, 20 μA) and total surface area and porosity by N_2-physisorption (Micromeritics ASAP 2010, 20 mg sample).

Electro catalytic activity was compared using Cyclic Voltammetry (CV, Autolab PGSTAT 30, working - glassy carbon (0.07 cm^2), reference – saturated calomel, counter – platinum wire basket. This method was used to initially characterize JM Pt_{40}/C. Preparing thin cast films of Pt/CNT catalysts upon glassy carbon was not possible because of the difficulty of dispersion of CNT based materials for electrochemical testing. Therefore a testing technique using a paste electrode was developed. Comparisons of the commercial catalyst with the CNT-supported

nanophase Pt electrocatalyst (denoted Pt/CNT(propanol)) and the catalysts prepared using the galvanic displacement method were performed using the BAZ 100 electrochemical workstation in a three electrode sytem using a Ag/AgCl reference electrode and a Pt wire as counter electrode with an argon purged $ClLiO_4$ electrolyte with conditions as set out hereunder and at each CV in the result section. The series of Pt/CNT-BP catalysts were compared to the Pt/CNT (propanol) and the JM Pt_{40}/C catalysts using this method.

An impure synthetic graphite powder (Sigma Aldrich;1-2 μm; # 282863) or Ultrapure graphite powder (Alpha Aesar; -200 mesh; 99.9995% pure, synthetic conducting grade Stock #40797; Lot J02R042) were used to prepare paste electrodes. Ultrapure graphite was used in the series of CNT paper supported Pt/CNT catalysts.

Table 4.2 Composition of paste electrodes

	Graphite (g)	**Mineral oil (g)**
GRmix	0.0438	0.0040
Sample	**GR mix (g)**	**Pt catalyst (g)**
JM Pt_{40}/C	0.0280	0.0030
Pt/CNT(propanol)	0.0357	0.0025
Pt/CNT-BP Sample 2 GR02 series	0.0245	0.0020
Pt/CNT-BP Sample 3 GR03 series	0.0143	0.0014
Pt/CNT-BP Sample 5 GR05 series	0.0173	0.0016
Pt/CNT-BP Sample 8 GR8 series	0.0106	0.0017
Pt/CNT-BP Sample 10 GR10 series	0.0438	0.004
Pt/CNT-BP Sample 12 GR12 series	0.0124	0.0011

A stock mixture (denoted GRmix) of ultra pure graphite and mineral oil was blended to a paste in a ratio of 10:1 in an agate mortar and pestle. There after the CNT supported catalyst was added to an aliquot of the paste in a 1:10 ratio, and thoroughly blended together by grinding in an agate mortar and pestle. The paste electrode void was loaded with the catalyst/paste blend. The paste electrode surface was polished to

a smooth finish. A three electrode system was used in 5 mL of a 0.1 M Lithium Perchlorate ($ClLiO_4$) solution. The working electrode was the paste electrode, the counter electrode was a platinum wire, with a Ag/AgCl reference electrode. The system was purged with argon for 15 min prior to commencement of cyclic voltammetry and square wave voltammetry and the electrolyte surface was purged with argon subsequent to the start of experiments.

4.5 RESULTS

4.5.1 Characterization of electrocatalysts

4.5.1.1 CNT paper

Characterization of CNT was presented in Chapter 3. After purification and surface chemical modification by acid treatment, the impurities in CNTs were removed and little remaining Fe from the ferrocene catalyst could be detected by energy dispersive analysis (EDS). XRD analysis of pre-treated CNT showed that after acid washing the XRD pattern for CNT contained the four characteristic diffraction peaks for crystalline graphite, which are at 26.5, 42.4, 54.7 and 77.4° 2 theta, namely of (220), (100), (004) and (110) respectively. The acid washed CNT had a N_2 BET surface area of 49 $m^2 g^{-1}$ of which only 4 $m^2 g^{-1}$ reported to the microporous internal area of the CNT's as the surface area of CNTs are made up of inter-tubular pores and intra-tube pores. These acid washed CNT were processed into CNT paper (Figure 4.2).

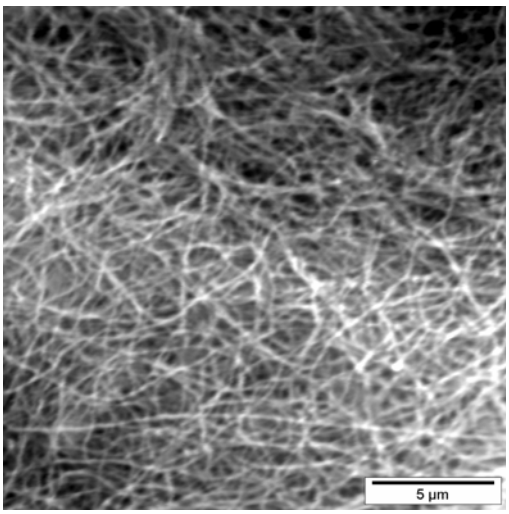

Figure 4.2 SEM micrograph of CNT paper gas diffusion layer made from acid washed CNT

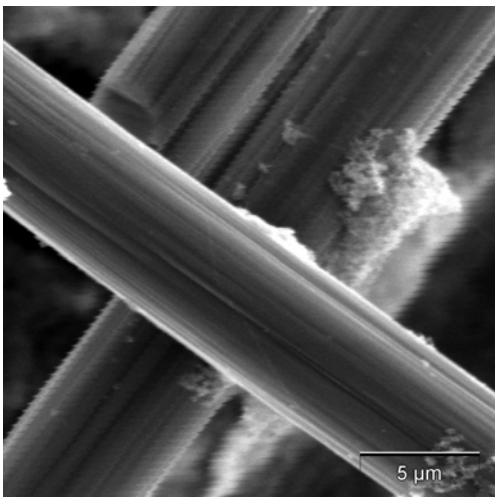

Figure 4.3 SEM micrograph of Carbon cloth gas diffusion layer

From SEM micrographs (Figure 4.2) it is visible that in the case of the prepared CNT paper the overall macroporosity of the gas diffusion layer is very significantly reduced and the external surface area of the gas diffusion layer is significantly increased because the CNT fibres are an order of magnitude finer than the carbon cloth (Figure 4.3) and the voids in between fibres much smaller. The use of the CNT paper as support substrate for Pt should promote an increase of the dispersion of the Pt electrocatalyst because of the much higher effective surface area that is available to support the catalyst. Moreover the contacts between phases necessary to develop the three phase boundary should be highly improved.

4.5.1.2 Characterization of Pt electrocatalysts

A comparison of the XRD spectra of Carbon black (Vulcan XC-72) with JM Pt_{40}/C is shown in Figure 4.4.

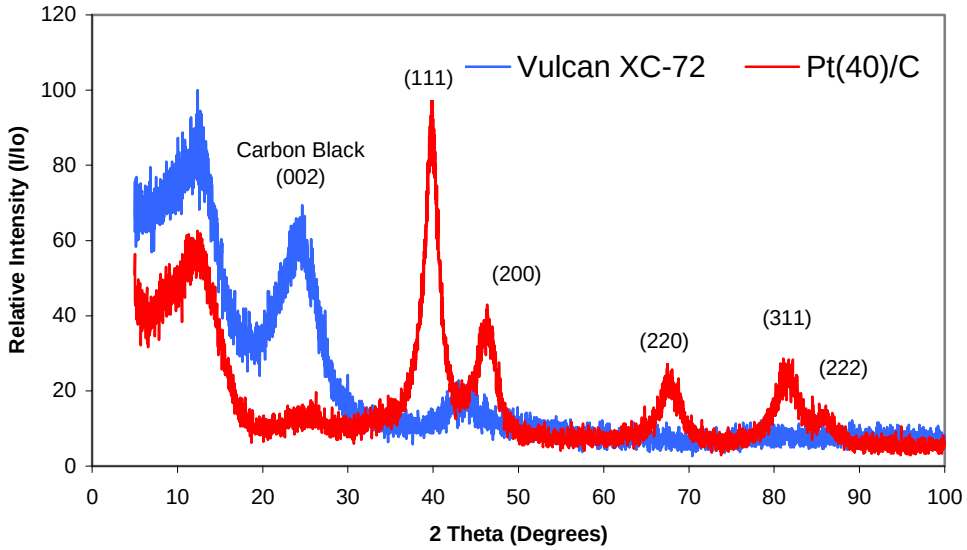

Figure 4.4 Comparison of XRD spectra of Carbon black (Vulcan XC-72) with JM Pt_{40}/C

The XRD spectrum of carbon black (Vulcan XC-72) shows the typical peaks of graphitic carbon with major peak at 26.5° 2 theta, and less prominent peaks at 42.4, 54.7 and 77.4 ° 2 theta, namely of (220), (100), (004) and (110) of face characteristic centred crystalline graphite. The broad peaks below 20 °2θ are due to an instrumental artifact and should be ignored. The XRD spectrum of JM Pt_{40}/C shows remnants of the carbon peaks as well as peaks visible at 39, 46, 68, 82° 2 θ, namely Pt (111), (200), (220) and (311), indicating that the Pt structure was face-centred cubic (FCC) with interplanar spacing (Å) of 2.40 (111), 2.14 (200), 1.66 (220). From XRD the Bravais Lattice is face-centered cubic. According to literature the atomic radii (Å) of Pt is 1.38, the space-filling efficiency is 74 % (CCP), and the particle shape is a Cubo-octahedron with number of atoms 2300 – 2700 (Williams et al., 2008).

After Pt deposition upon the CNT via the propanol/formaldehyde route, thermal analysis showed that Pt/CNT (propanol) had high thermal stability with the only weight loss between 400 °C and 520 °C corresponding to the oxidation of carbon nanotubes. It was calculated by difference from TGA that the Pt deposited upon the

catalyst was 28.3 wt%. Apart from the graphitic peaks that were visible in the XRD spectrum of Pt/CNT (propanol) (Figure 4.5) at 26.5, 42.4, 54.7 and 77.4 °2θ, namely of (220), (100), (004) and (110) indicating face characteristic centred crystalline graphite, the characteristic but broadened Pt diffraction peaks were visible at 39, 46, 68, 82 °2θ, namely Pt (111), (200), (220) and (311), indicating that the Pt structure was face-centred cubic (FCC) (Q.Ying, 2005). The XRD results can be compared with that of JM Pt_{40}/C (Figure 4.4). Generally, the broad Pt diffraction peaks observed from the diffractogram was due to the presence of nano particles of Pt dispersed upon the CNT.

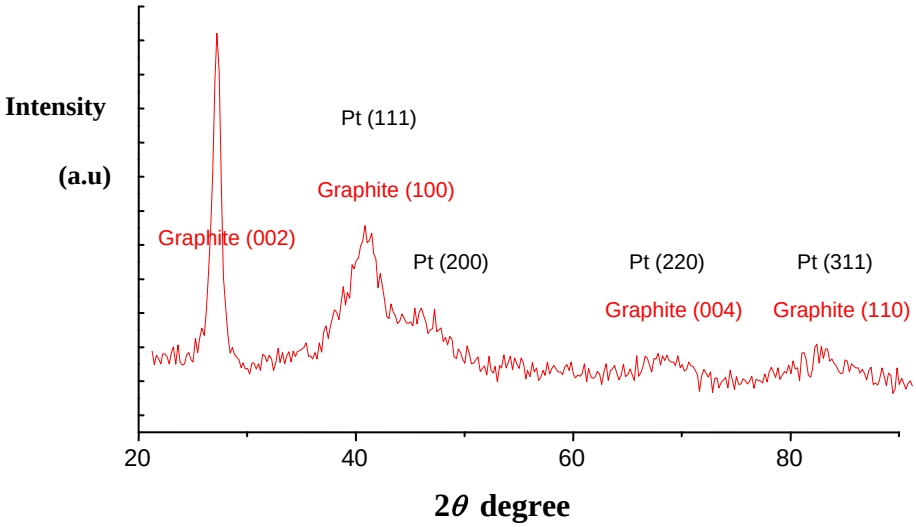

Figure 4.5 XRD spectra of Pt/CNT (propanol)

Through calculation using the Scherrer equation, the XRD Pt particle sizes of the Pt/CNT (propanol) catalyst were found to be on average 2.6nm compared to 4.23 nm for JM Pt_{40}/C. The values obtained for JM Pt_{40}/C compared well to the manufacturers specification of 4.5 nm. Slight inconsistencies in particle sizing data was due to the Scherrer equation being developed for spherical particles, whereas many metal nanoparticles are cubo-octahedral in shape. XRD was thus used to obtain information regarding crystallinity, and particle size, and perform accurate analyses in the

nanometre size domain. However, since XRD is a bulk technique it does not does not provide information on agglomeration of individual Pt nanocrystallites. Therefore, the morphology of Pt electrocatalysts on CNT was further determined by electron microscopy.

TEM (Figure 4.6) was utilized in the direct examination of metal nanoparticle size; nanoparticle size distribution; homogeneity of dispersion; and agglomeration of the metal phase in of JM Pt_{40}/C supported nanophase electrocatalysts.

(a) 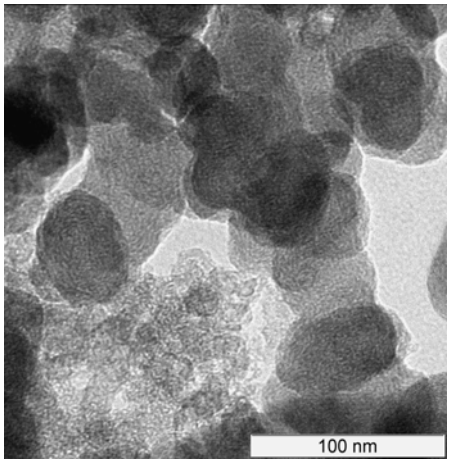

(b) 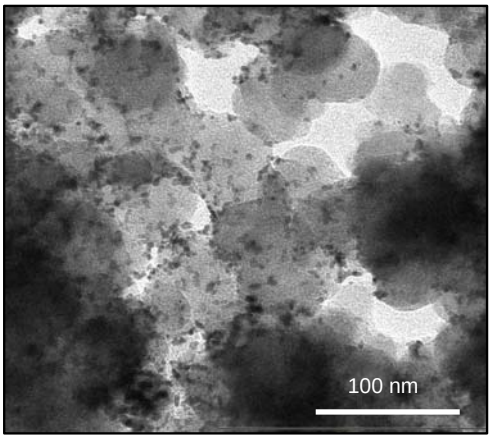

Figure 4.6. Transmission electron micrographs of (a) carbon black (Vulcan XC-72) and (b)JM Pt_{40}/C

The TEM of carbon black (Vulcan XC-72) shows the average carbon particle size to be about 60nm (Figure 4.6 (a)). By TEM, Pt nanoparticles in JM Pt_{40}/C appeared well-dispersed on the carbon support (Figure 4.6 (b)). However, large Pt agglomerates were also observed in certain portions of the sample (Figure 4.7). Pt nanoparticles generally ranged between 2-7 nm in size and were dispersed on carbon particles which were generally 50-60 nm in size. The average Pt particle size was 4.2 nm, representing a metal surface area of 66.7 $m^2\ g^{-1}$ (Prabhuram et al, 2004). Experimental values corresponded with the values determined by the manufacturer - 4.5 nm and 62.3 $m^2\ g^{-1}$ (Johnson Matthey, 2008). The particle sizes also agreed well with those determined in literature (Zhang, 2004; Guo et al, 2005; Cabot, 2008).

CHAPTER 4

Commercial Johnson Matthey JM Pt_{40}/C and the home made Pt/CNT (propanol) sample were further characterized using the VEECO ZEISS Ultra 55 Gemini FE SEM with Energy Selective Backscattered detectors (ESB). Conventional SEM could not clearly resolve metal nanoparticles from the carbon nanotube support materials. The ESB allows clear compositional contrast and high resolution BSE imaging revealed previously unseen image details. Morphological characteristics of the CNT-supported nanophase Pt electrocatalyst (denoted Pt/CNT(propanol)) were compared with the JM Pt_{40}/C commercial electrocatalyst. The ESB image of the commercial JM Pt_{40}/C, which is the benchmark electrocatalyst and the industry standard, showed significant agglomeration of Pt clusters (bright areas) upon carbon support (grey areas) in Figure 4.7.

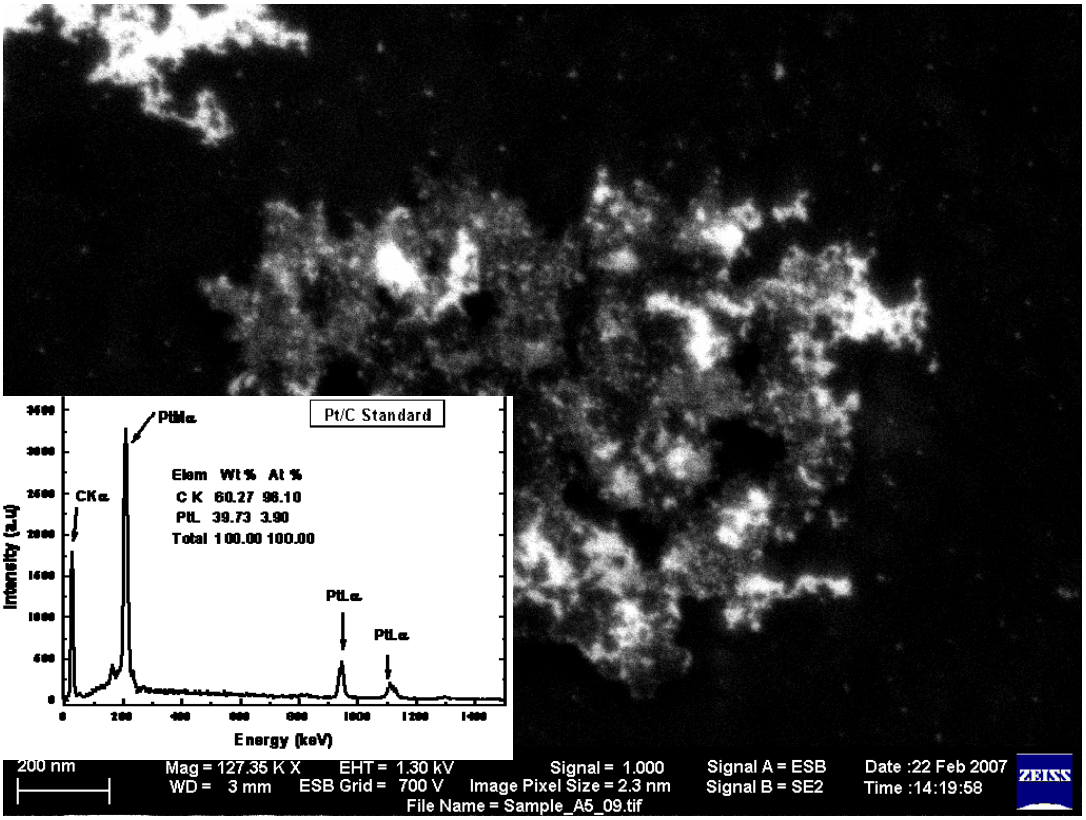

Figure 4.7 ESB image of JM Pt_{40}/C with EDS analysis (inset)

The degree of agglomeration (Figure 4.7) was not apparent from the XRD analysis or from the TEM images. The image also showed the high loading of Pt but uneven

dispersion of Pt particles. The Pt loading was determined by energy dispersive spectroscopy (EDS) and showed the loading of Pt to be 39.7 % (Inset in Figure 4.7), which corresponds to the manufacturer's specifications.

Using ultrahigh-vacuum HRSEM, and high resolution BSE, the Pt particles were visible on the carbon nanotube support materials denoted Pt/CNT (propanol), and can be quantitatively sized at ~8 nm (Figure 4.8). The ESB image (Figure 4.9) of Pt/CNT(propanol) shows some agglomeration and variation in particle size of Pt but high dispersion and much reduced cluster formation compared to the commercial sample. The multi walled nature of the CNT is also evident in the STEM image which revealed CNT structure and uneven dispersion of ultrafine particles of Pt supported on CNT, for sample Pt/CNT (propanol), but agglomeration was less than on the commercial catalyst.

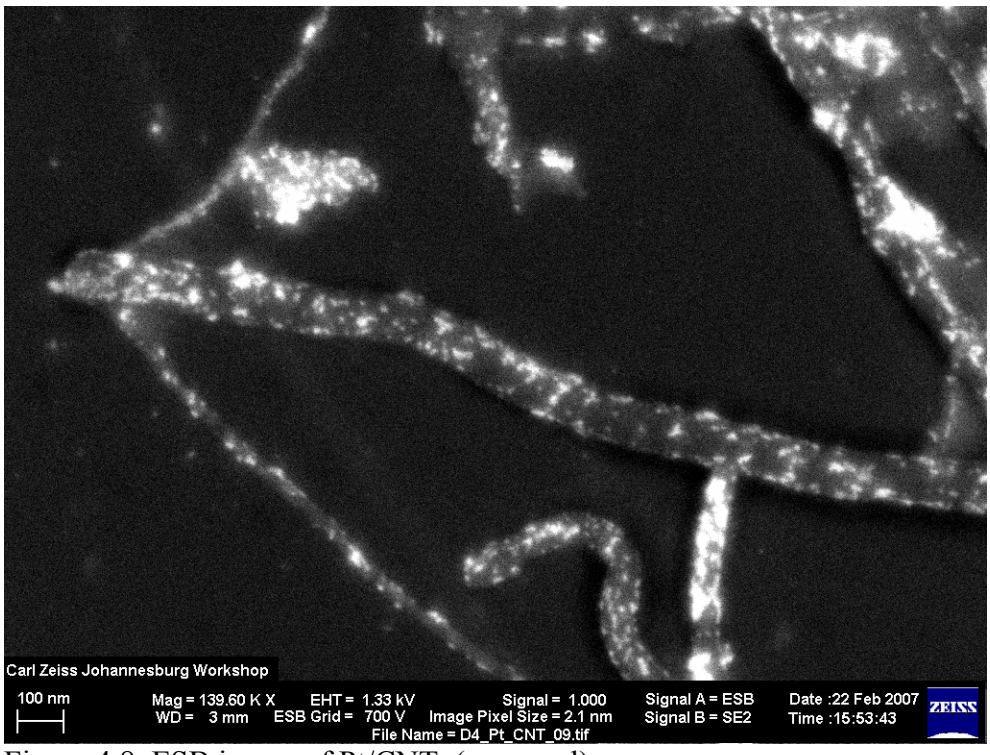

Figure 4.8. ESB image of Pt/CNT (propanol)

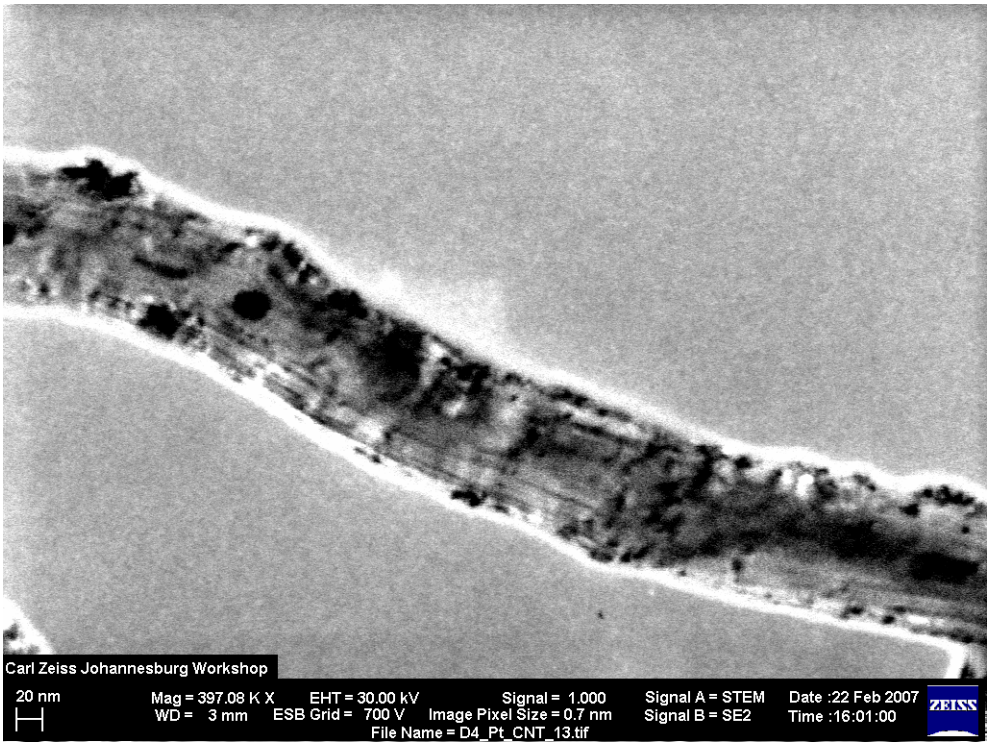

Figure 4.9. STEM imaging of Pt/CNT (propanol)

The HRSEM was thus able to successfully resolve and quantify Pt particle sizes in the nanometer domain upon CNT.

4.5.1.3 Characteristics of electrocatalysts: galvanic displacement technique

The method for deposition of Pt used to prepare the series of Pt/CNT catalysts was adapted from Qu and Dai (2005). In the initial adaptation, a piece of CNT paper (approximate dimensions 0.5 cm x 0.5 cm) was attached to a piece of stainless steel wire mesh using a stainless steel paper clip. The entire assembly was then placed in a 1.0 mM H_2PtCl_6 solution (+0.1 M HCl) for over 8.0 h. There after the assembly was removed from the solution and taken apart, and the nanotube paper was rinsed with copious amounts of water, then acetone, over filter paper on a standard vacuum filtration setup. An SEM micrograph of the resulting Pt plated CNT is shown in Figure 4.10.

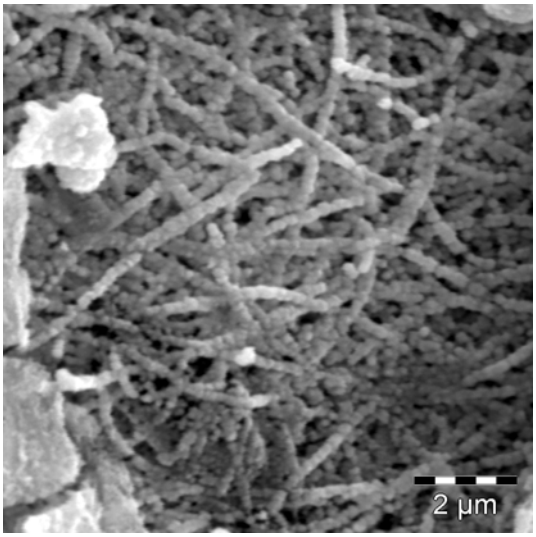

Figure 4.10 Galvanic displacement deposition of Pt (8 h) using stainless steel

Excessive deposition of Pt upon the carbon nanotube paper was observed (Figure 4.10) because of the length of time (8 h) initially used during the galvanic displacement reaction. Moreover significant co-deposition of various components derived from the stainless steel used as sacrificial anode was detected by EDS. Because of the impurities observed when using stainless steel mesh as sacrificial electrode, the use of ultra pure foils was implemented thereafter to promote the galvanic displacements, in order to produce pure bimetallic catalyst systems (as described in Section 4.4.1.2). Much shorter times were applied to minimize the degree of wastage of Pt in the bulk, and directly form nano sized metal deposits on the CNT paper.

After Pt deposition, using the rapid and simple galvanic displacement technique with 99.99% pure Al, Pb or Fe foils respectively, the CNT paper GDL increased in mass (Figure 4.11 and Table 4.1). The replication was poor mainly due to incomplete recovery of the CNT paper from the solution in some cases. However, the mass increase did not follow the trend of $E^{ø}$ (volts) of the Al (-1.66), Fe (-0.44) or Pb (-0.13) foils. Generally the shorter time caused less metal to deposit in the case of Al and Fe foils as was expected. The mass % increase in the case of Al doubled as the time was doubled. In the case of Fe no measureable increase in mass of the CNT

substrate occurred during the first 10min deposition time, possibly indicating a slow galvanic displacement reaction for this system, which is consistent with the low E ø value for this metal. However, this was not true of the Pb foil where both times applied allowed a similar increase in mass of the CNT substrate.

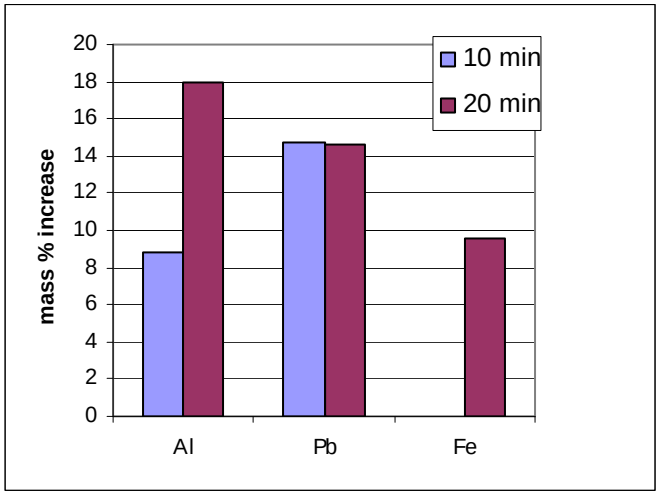

Figure 4.11: Mass % increase of CNT paper after Pt deposition over 10 and 20 min

It was not certain that the mass % increase observed was due only to Pt deposition. EDS was performed after SEM images were obtained to determine the atom % Pt and establish whether any other metal had been co-deposited during the galvanic displacement reaction. The atom % Pt deposited on CNT paper for various foil types used in the galvanic displacement is shown in Figure 4.12.

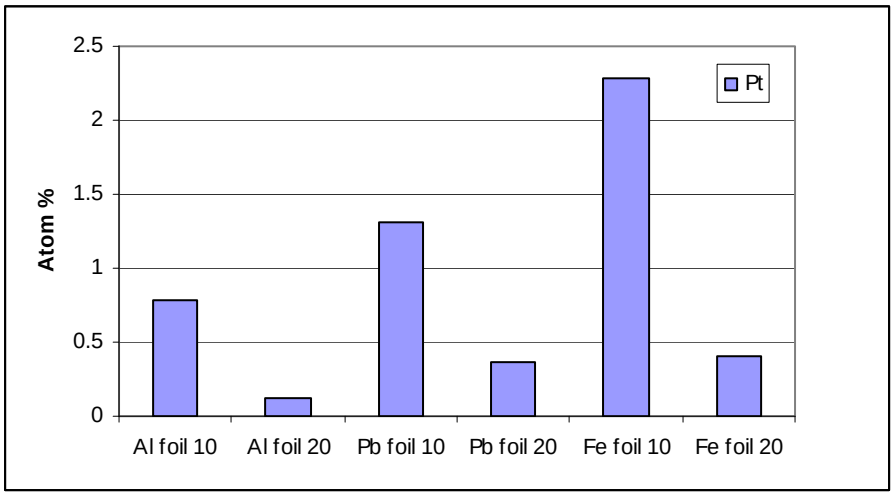

Figure 4.12: Pt Atom % increase of CNT paper after Pt deposition over 10 and 20 min for different foils

Between 0.75 and 2.3 atom % Pt could be rapidly deposited within 10 min using the galvanic displacement technique, depending upon the metal foil of choice (Figure 4.12). The atom % deposition of Pt at 10 min did not follow the trend of $E^{ø}$ (volts) of the Al (-1.66), Fe (-0.44) or Pb (-0.13) foils. The highest Pt loading on the CNT paper was observed in the case of the Fe foil after 10 min. More Pt was deposited on the CNT paper in the first 10 min in the case of the Al, Pb and Fe foils, whereas less Pt was deposited during the longer deposition time of 20 min. However, a large variability was found in the amount of Pt deposited on different areas of the CNT paper in most cases. As there was significant inhomogeneity in the Pt dispersion on the CNT as can be observed by SEM (Figure 4.14 (a to f)), the EDS values of the elemental composition of samples are mainly qualitative.

A significant % of the metal deriving from the foil used in the displacement reaction was co-deposited, thus leading to bimetallic deposits particularly after the longer deposition period in the case of Al foil and in the case of Pb within the first 10 min as shown in Figure 4.13. As the metals differed greatly in MW it is difficult to see trends in the mass % therefore the atom % is presented.

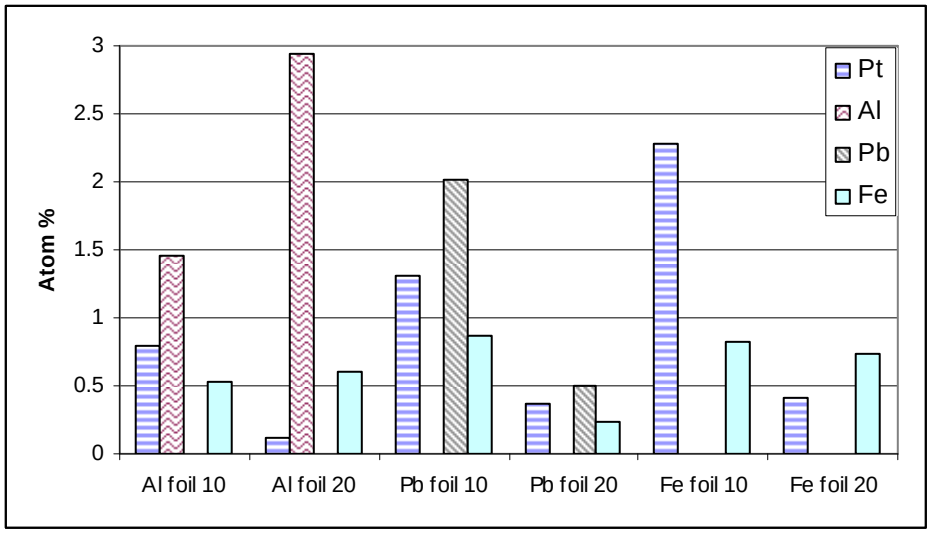

Figure 4.13 Atom % of bimetallic deposits on CNT

Morphological characterization was performed using SEM and a selection of the micrographs are presented in Figure 4.14 (a to f).

Al foil and 10 min deposition (Sample 1)

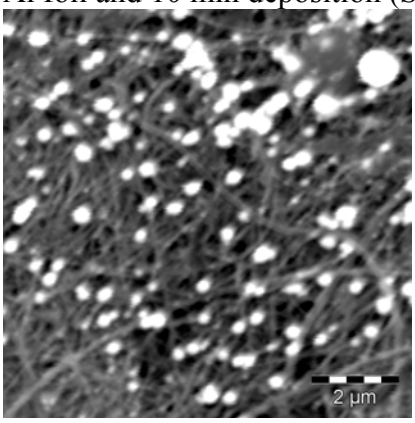

(a)

Al foil 20 min deposition (Sample 8)

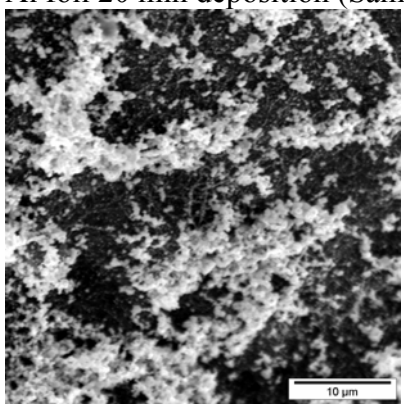

(b)

Pb foil 10 min deposition (Sample 3)

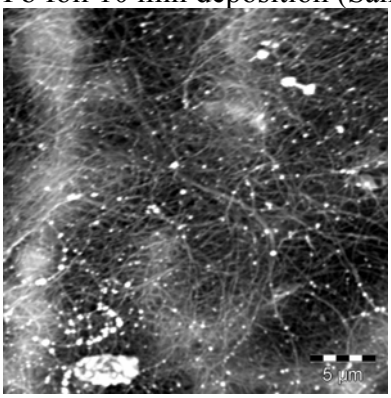

(c)

Pb foil and 20 min deposition (Sample 10)

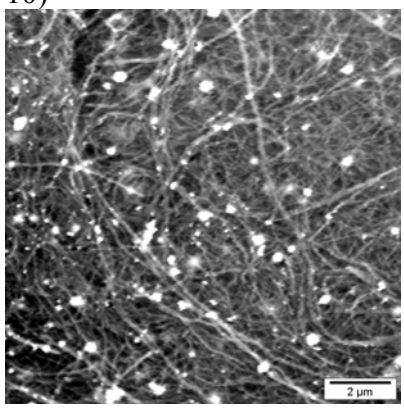

(d)

Fe foil 10 min deposition (Sample 5)

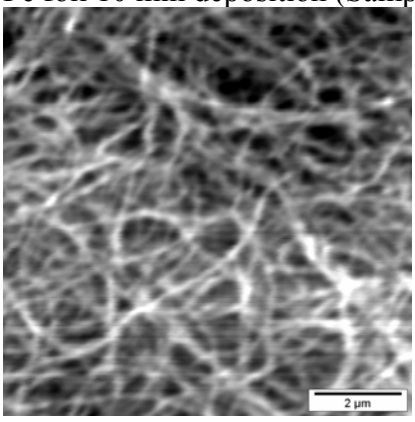

(e)

Fe foil 20 min deposition (Sample 12)

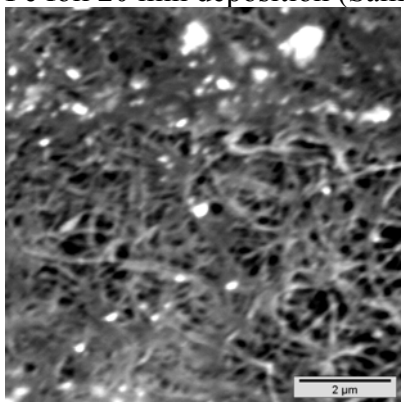

(f)

Figure 4.14. SEM micrographs of CNT paper with Pt deposition using (a,b) Al, (c,d) Fe and (e,f) Pb foils

From the EDS results (Figure 4.13) of the elemental composition of the samples prepared using Al foil the degree of co-deposition of Al ranged from 1.5 to nearly 3 atom % depending on the deposition time of 10 and 20 min respectively and a small

Fe contaminant of between 0.24 to 0.86 atom % was also observed which was unexpected as the metal foils used as sacrificial electrodes were 99.99% pure. The Fe content observed in the various samples may be due to the residual Fe catalyst remaining in the CNT after acid washing and CNT paper formation as was shown in Chapter 3.

In the case of the Fe foil, about 0.8 atom % Fe was co-deposited with the Pt. In the case of Pb foil 2 atom % of Pb was co-deposited with the Pt and more was apparently co-deposited at the shorter deposition time of 10 min than at the longer time of 20 min. This variability in elemental composition determined by EDS may be due to the inhomogeneity of the metal deposition upon the CNT that was observed by SEM (Figure 4.14) and these results should be treated with caution as they are based upon the analysis of very small areas. These are general trends only as there was a large variability in EDS results since this method probes only a very small portion of the sample. From the SEM results it appears that during the galvanic displacement reaction in a Pt solution the use of the Pb foil resulted in relatively consistent and homogeneous Pt deposition and few large Pb containing Pt clusters were formed. In the case of the Pb foil it was also apparent that the deposition time used did not make a large difference in the results obtained and the deposition was also more evenly dispersed. These results highlight that the compositional analysis by EDS is merely qualitative.

In the galvanic displacement the substrate metal acts as a sacrificial anode and donates an electron to the CNT and in the process is oxidized and displaced into solution (Qu and Dai, 2005). However, from the results presented in this chapter it can be seen that the displaced metal ions then compete with the Pt ions in solution, being reduced by the CNT as well, and thus are co-deposited upon the CNT with the Pt after a period of time when sufficient metal ion has been displaced into solution. This is obviously a result of the increasing concentration of the metal ions in solution over time. It appears from the data that the longer the contact time, the more the subsidiary metal predominates in the co-reduction and deposition reaction,

particularly in the case of Al ($E^{ø}$ -1.66), whereas for the metals with lower $E^{ø}$ such as Fe (-0.44) or Pb (-0.13) this trend was not so significant in the time of the reaction.

These results show that it is in principle possible to directly deposit Pt and a second metal on CNT to form a bimetallic electrocatalyst that is directly incorporated into the CNT paper GDL. This procedure would thus eliminate a large amount of processing and illustrates a route to easily form a series of nanophase Pt containing electrocatalysts by use of the galvanic displacement deposition technique. This approach aims to rapidly and very simply deposit the Pt electrocatalyst directly onto the gas diffusion layer (GDL) substrate, CNT paper. This method to directly deposit Pt onto preformed CNT paper as GDL would eliminate many steps in the processing of the electrocatalysts into composite form. This was a proof of concept study and would require optimization to establish the precise conditions for homogeneous deposition of Pt containing bimetallic particles upon CNT paper.

4.5.1.4 Catalytic activity of prepared and commercial materials

Cyclic voltammetry (CV) was used to investigate the electroactivity of the electrocatalysts which were compared to the commercial JM Pt_{40}/C. A typical cyclic voltammogram for JM Pt_{40}/C is presented in Figure 4.15. The electrodes were formed by mixing 0.1073 g of catalyst; 0.25 cm^3 H_2O and 1.25 g of Nafion and depositing this ink on a glassy carbon electrode. The electrode performance was measured in a electrochemical cell equipped with the glassy carbon working electrode, a platinum wire counter electrode and a Mercury Sulphate Electrode (MSE) as the reference electrode. The geometric surface area of the working electrode was 0.08 cm^2. The electrolyte used in the cell was 0.50 M H_2SO_4 and no redox active species were introduced in the electrolyte. The temperature of the electrolyte as kept at 29 ºC.

Since a MSE was used as a reference electrode for this experiment, the following parameters were applied in the potentiostat: Start potential (V):-0.7; First Vertex potential (V):0.8; Second Vertex potential (V):-0.8; Step potential (V):0.00518; Scan

rate (V s^{-1}): 0.05. The reference potential of $HgSO_4$ was approximately 0.68 V hence the redox couple showing electrochemistry in the voltammogram obtained was lower in potential by 0.68 V compared to those of the literature where the reference electrode typically is a reversible hydrogen electrode (RHE) with 0.00 V potential.

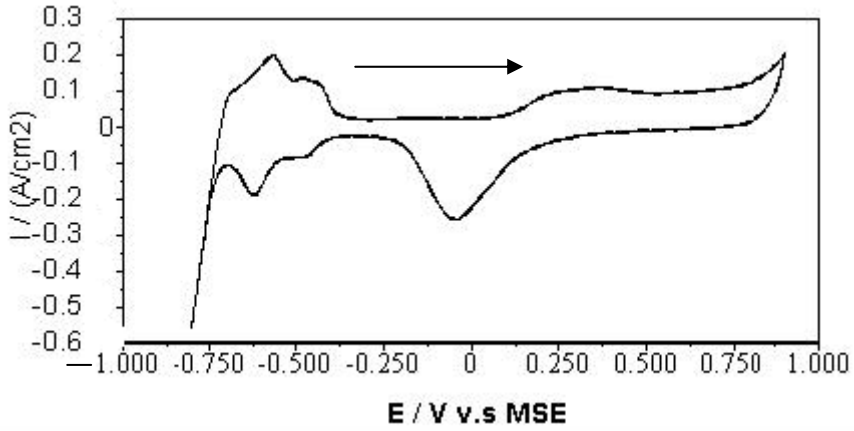

Figure 4.15 Cyclic voltammogram of commercial JM Pt/C 40 catalyst

For the catalyst JM Pt40/C the only current that flows between -0.25 V and 0.125 V is that required to charge the electrolytic double layer. Above 0.125 V oxide chemisorption begins with the process

$Pt + OH^- \rightarrow Pt—OH + e^-$

And above 0.8 V,

$Pt—OH + OH^- \rightarrow Pt—O + H_2O + e^-$

As the potential scan is reversed cathodically, oxygen gas present in the neighbourhood of the electrode is reduced together with the chemisorbed oxide layer. At lower potentials there is a small double-layer region followed by the deposition of hydride as

$Pt + H_2O + e^- \rightarrow Pt—H + OH^-$

Finally close to the thermodynamic potential for the $HgSO_4$ electrode (MSE) i.e. -0.68 V, there is strong evolution of hydrogen (hydrogen evolution reaction), where after the Pt can be re-oxidised once the potential direction is again reversed (Bradley et al., 1989).

In all the subsequent CV experiments the electrolyte system was changed to a $ClLiO_4$ solution and the reference electrode was a Ag/AgCl electrode as set out in Section 4.4.2. The best voltammetric curves were obtained with the following set-up conditions: Start potential (V):-1.1; First Vertex potential (V):1.1; Second Vertex potential (V):-1.1; sensitivity of 100 µA V^{-1}. The scan rate (V s^{-1}) was varied. The reference potential of Ag/AgCl is approximately 0.205 V hence redox couples showing electrochemistry in the voltammograms obtained were higher in potential by 0.205 V compared to those of the literature where the reference electrode typically is a reversible hydrogen electrode (RHE) with 0.00 V potential.

Initial cyclic voltammetry (CV) of the paste made from the ultrapure graphite diluent and mineral oil was performed only to ascertain its relative contribution to the HER. The CV of the ultrapure graphite diluent is presented in Figure 4.16.

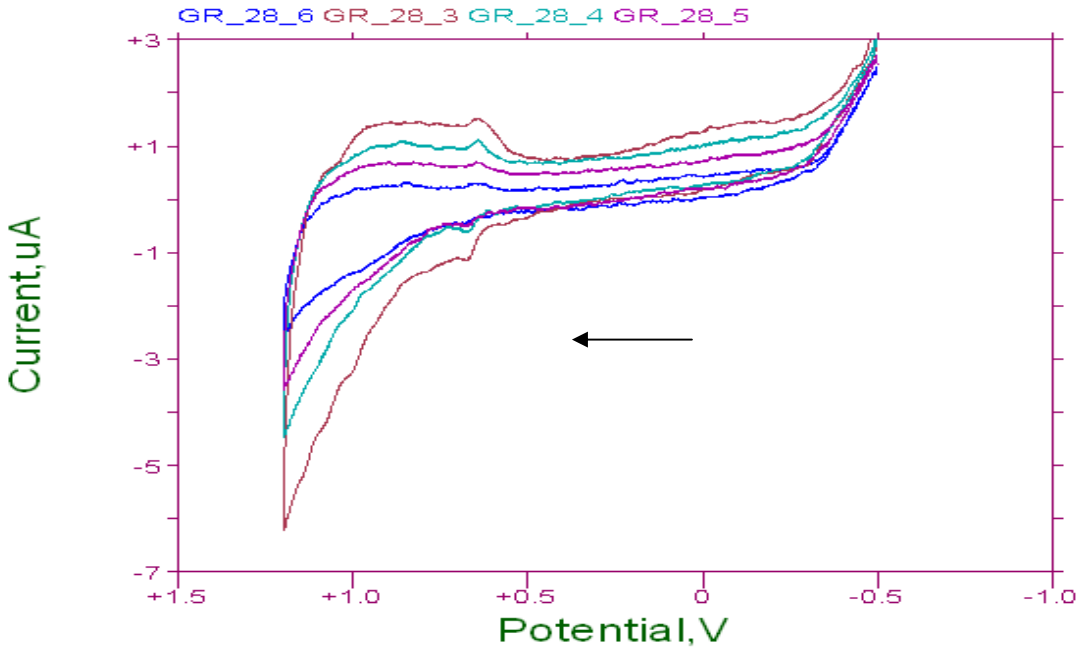

Figure 4.16 CV of ultrapure graphite diluent (scan rate between 10-50 mV s^{-1} between -500 to 1200 V; sensitivity of 100 µA V^{-1})

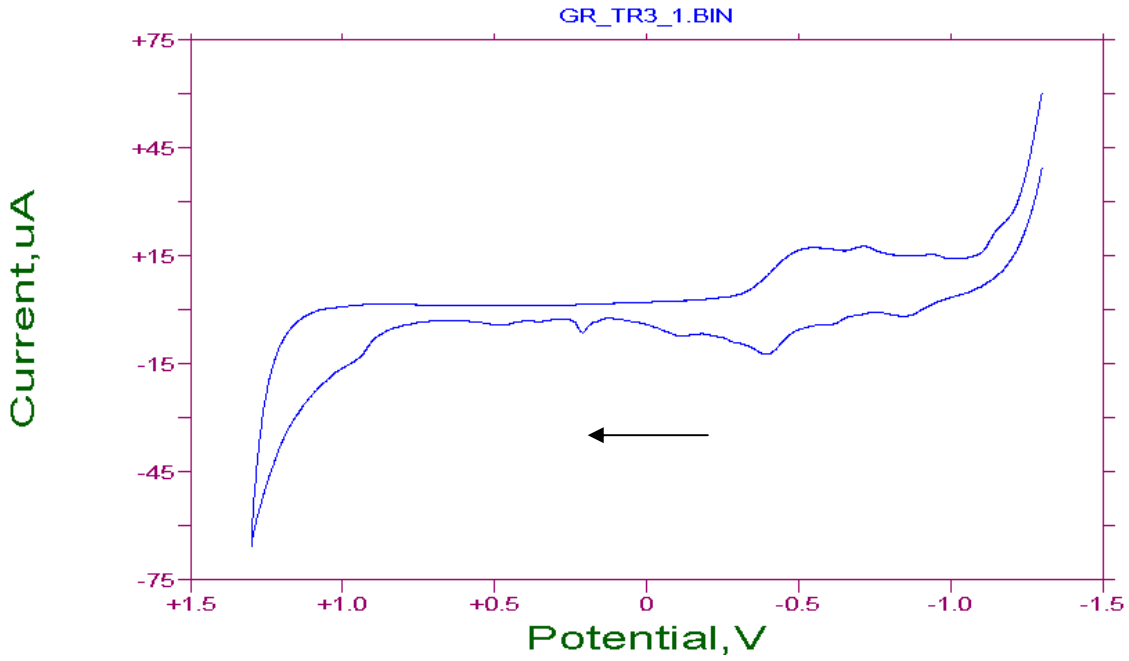

Figure 4.17 CV of impure graphite diluent (scan rate 10 mV s^{-1} between -1.500 to 1.300 V; sensitivity of 100 µA V^{-1})

Cyclic voltammetry of the ultrapure graphite diluent (99.9995% pure) between -500 to 1200 V and at a scan rate between 10-50 mV s^{-1} and sensitivity of 100 µA V^{-1} (Figure 4.16) shows low activity and few peaks for the hydrogen evolution reaction (HER), a low current output signal in the µAmp region, a low current at the peak potential and little noise. On the other hand a less pure graphite diluent (graphite powder; 1-2 µm synthetic (Sigma Aldrich) that was initially used as diluent showed more significant electro activity (Figure 4.17) for HER most likely due to metal impurities. Therefore the mainly electrochemically inactive ultrapure graphite was used as diluent during the preparation of paste electrodes, except in the electrochemical comparison presented in Figure 4.21 where the impure graphite was used as blank diluent to compare the relative contribution of the diluents' electroactivity.

Cyclic voltammetry of JM Pt_{40}/C is presented in Figure 4.18 and Figure 4.19 at scan ranges from 5-50 V and 50-300 V respectively in a $ClLiO_4$ solution and the reference electrode was Ag/AgCl.

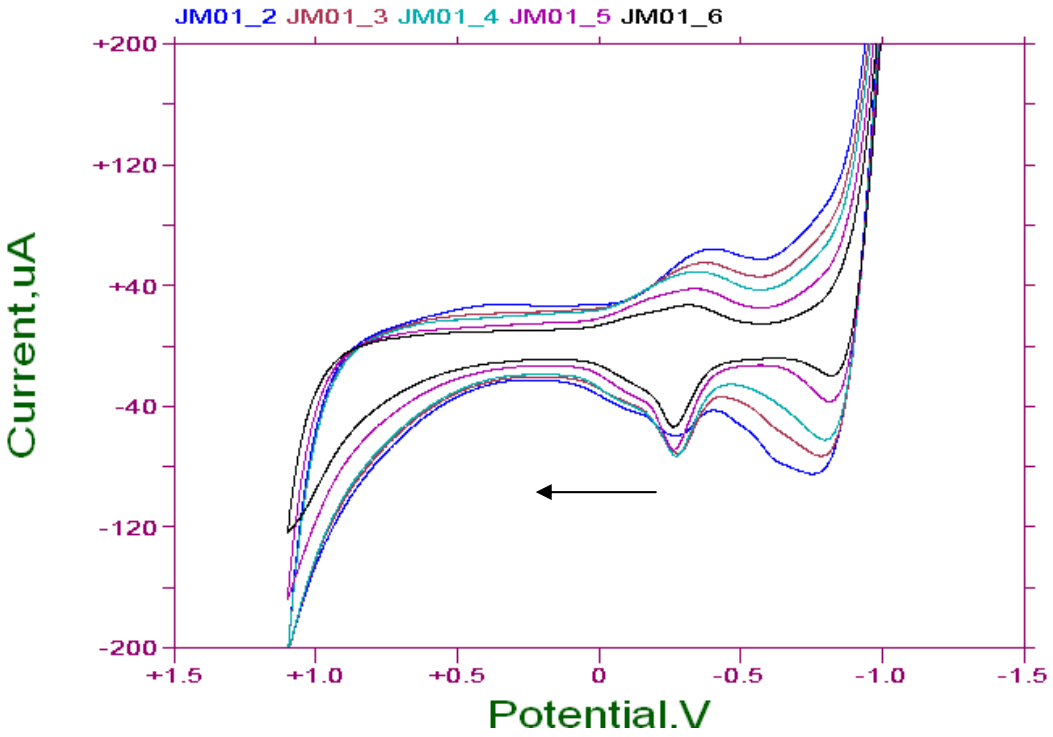

Figure 4.18 JM Pt_{40}/C scanned between 50 and 5 mV s^{-1}; 100 µA V^{-1} sensitivity and scan range between -1100-1000 V (JM01-2=50 mV s^{-1}; JM01-6=5 mV s^{-1})

It can be observed in Figure 4.18 that, in contrast to the H_2SO_4 (SCE) system presented in Figure 4.16 for the commercial standard JM Pt_{40}/C catalyst, in the case of the $ClLiO_4$ (Ag/AgCl) system shown in Figure 4.17, the hydrogen evolution reaction (HER) occurs on the anodic sweep at approximately -0.77 V at 50 mV s^{-1} (and not at -0.68 V as in the H_2SO_4(SCE) system) (Bradley et al., 1989). The slower the scan rate the more negative the voltage of HER peaks observed. At 5 mV s^{-1} it occurred at -0.84 V. In the anodic scan (Figure 4.18) from negative to positive, after the onset of H_2 evolution the hydride deposition occurs at about -0.27 V at 50 mV s^{-1}. In the cathodic scan from positive to negative, the oxide chemisorption occurs at about -0.41 V and PtO forms at about 0.35 V at 50 mV s^{-1}. The one electron transfer is shown by the approximately 0.5 V difference between the hydride formation and the hydrogen evolution.

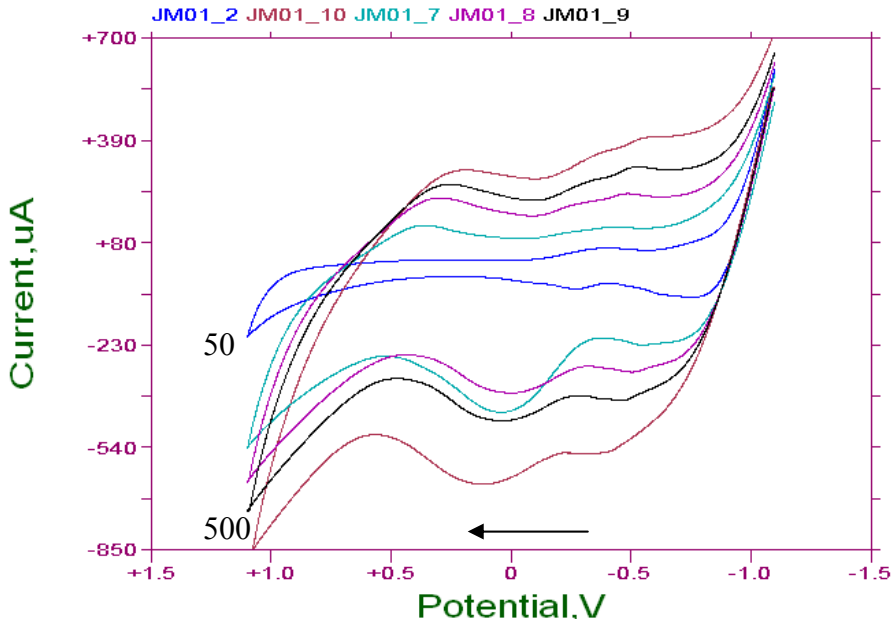

Figure 4.19 CV of JM Pt_{40}/C scanned between 50 (JM01-2) and 500 mV s^{-1} (JM01-10); 100 µA V^{-1} sensitivity and scan range -1100-1100 V

Figure 4.19 shows that as the scan speed is increased in the case of JM Pt_{40}/C scanned in the $ClLiO_4$ (Ag/AgCl) system between 50 (JM01-2) and 500 mV s^{-1} (JM01-10) at 100 µA V^{-1} sensitivity and a scan range between -1100-1100 V, the hydride peak becomes more prominent and the onset of hydrogen evolution occurs at lower overpotentials. As the scan rate was increased to 500 mV s^{-1} the offset of overpotential for the HER decreased to -0.31 V ($ClLiO_4$ (Ag/AgCl) system). Therefore all further samples were compared for cyclic voltammetry at identical scan rate.

Figure 4.20 shows the forward square wave voltammetry of JM Pt_{40}/C commercial catalyst scanned between 5-50 Hz in the $ClLiO_4$ (Ag/AgCl) system at 100 µA V^{-1} sensitivity and a scan range between -1100-1100 V. Square wave voltammetry was performed at different frequencies in the case of the commercial electrocatalyst to discern the different rates of the various reactions.

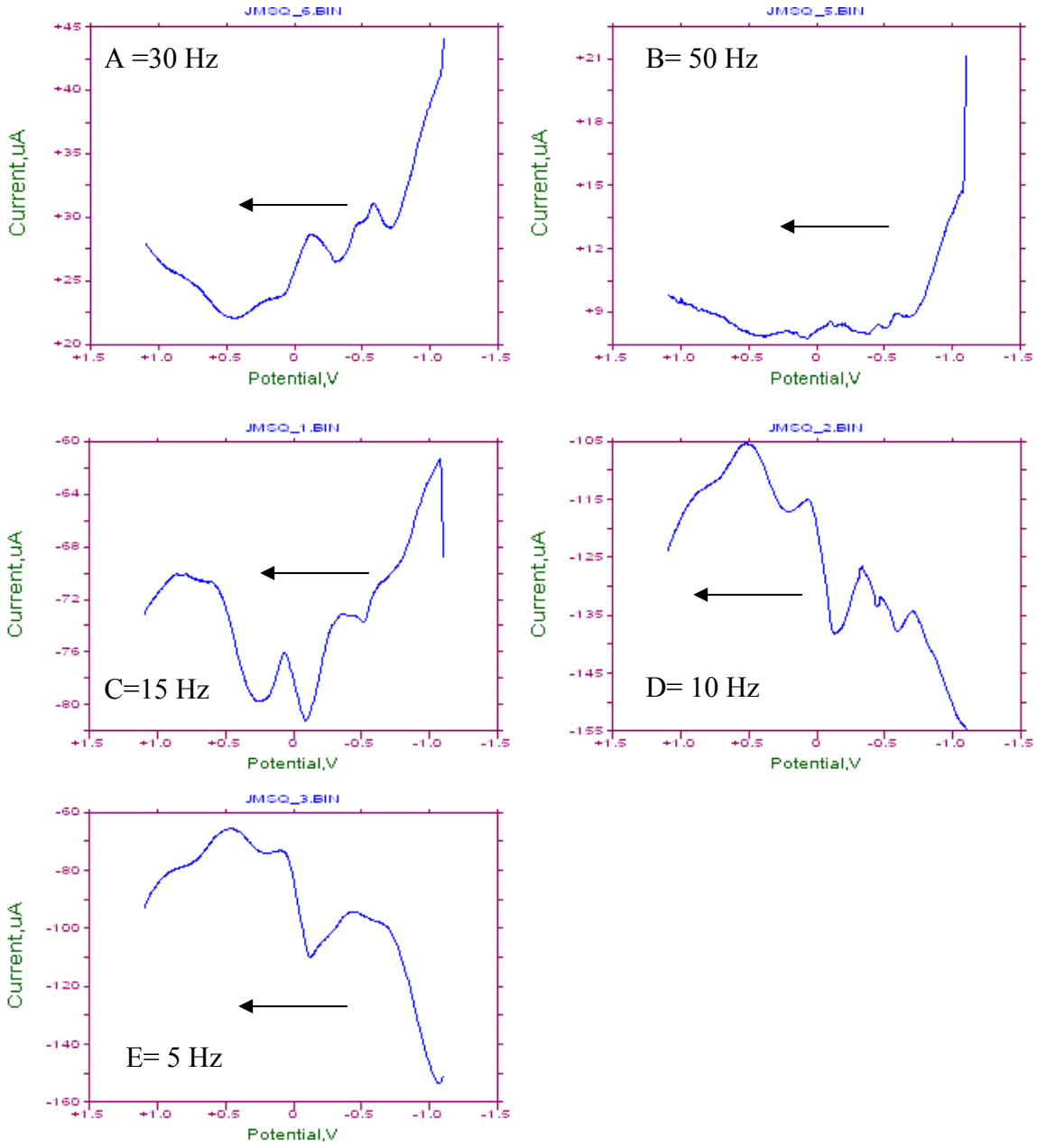

Figure 4.20 Square wave voltammetry of JM Pt_{40}/C commercial catalyst

Figure 4.20 (A-E) shows that the evolution of H_2 at -0.77 V is a fast process detected mainly at frequencies of 30 and 50 Hz. On the other hand H^- formation (-27 V) is an intermediate rate process observed clearly at 15 Hz and at 10Hz. PtO formation and chemisorption is also an intermediate process occurring at +0.341 V.

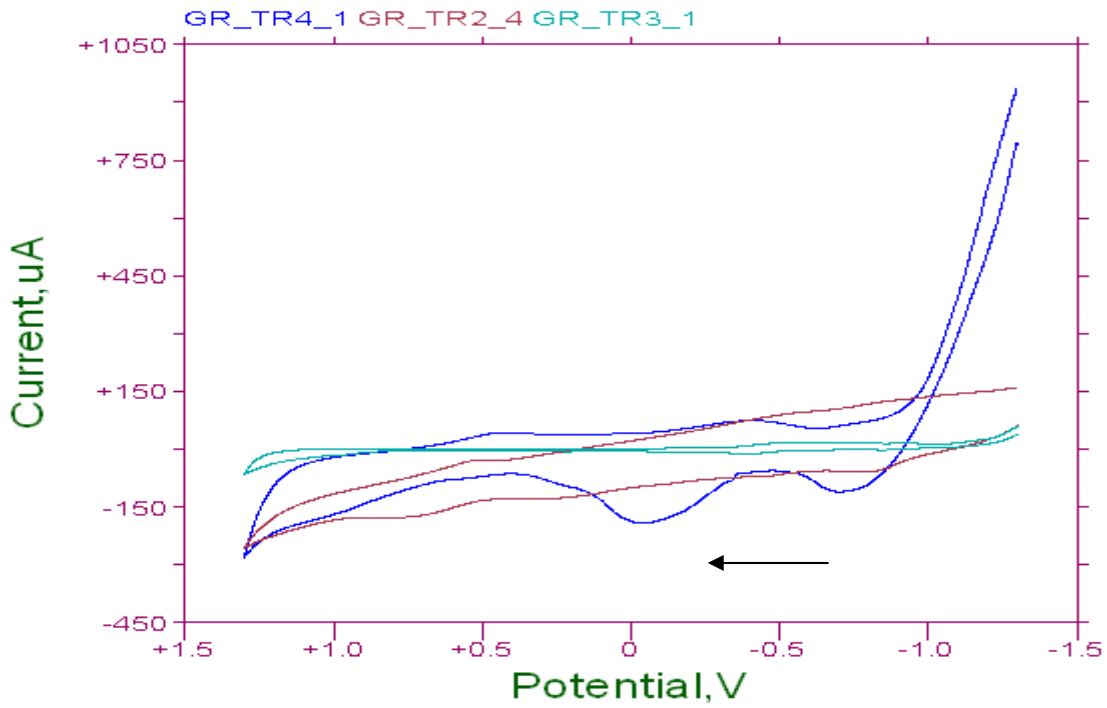

Figure 4.21 Comparison between Graphite diluent (green) vs Graphite/CNT blend (brown) vs Graphite Pt/CNT (propanol) blend (blue) at 10 mV s^{-1}, 100 µA V^{-1} sensitivity and scan range -1300-1300 V

Figure 4.21 shows a voltammetric comparison of activity for the HER in the $ClLiO_4$ (Ag/AgCl) system made between paste electrodes prepared with the graphite diluent (green) by itself; graphite that was blended with as made bare CNT (brown) prior to Pt deposition; and graphite that was blended with the electrocatalyst Pt/CNT (propanol) (blue). Scans were taken at 10 mV s-1, and 100µA V^{-1} sensitivity, with a scan range from-1300 to 1300. Neither of the graphite diluents used in the preparation of the paste electrodes showed distinct peaks indicating activity for HER under the conditions applied (also compare Figures 4.16 and 4.17). In Figure 4.21 two distinct reduction peaks relating to H_2 evolution and hydride deposition are observed on the anodic sweep below zero (10 mV s^{-1}, 100 µA V^{-1} sensitivity) in the case of the Pt CNT (propanol) sample, which peaks were somewhat reversible. Such peaks are orders of magnitude less intense or absent in the case of the blank sweeps of graphite as well as the graphite CNT blend that had no Pt catalyst content. Thus it was possible to clearly discern the different electro activity for HER of the graphite

diluents or the CNT support or the Pt containing electrocatalysts. The following results for cyclic voltammetry were thus obtained by use of paste electrodes comprising the ultrapure graphite diluent, and various CNT supported Pt electrocatalysts in the $ClLiO_4$ (Ag/AgCl) system. Comparison of the voltammetric scans of JM Pt_{40}/C and Pt /CNT propanol at 50 mV s^{-1} between -1100 and 1100 and sensitivity of 100 µA V^{-1} using paste electrodes (Table 4.2) in $ClLiO_4$ (Ag/AgCl) are shown in Figure 4.22.

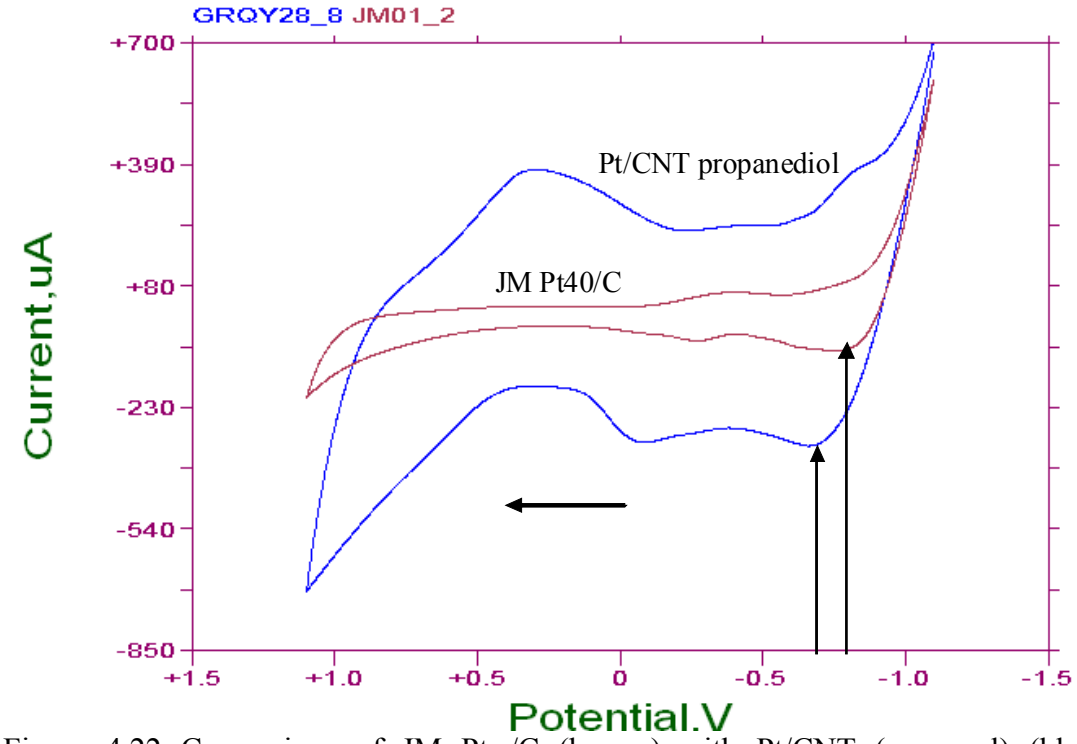

Figure 4.22 Comparison of JM Pt_{40}/C (brown) with Pt/CNT (propanol) (blue) electrocatalysts at 50 mV s^{-1} between -1100 and 1100; sensitivity of 100 µA V^{-1}.

The onset of hydrogen evolution during cyclic voltammetry (Figure 4.22) of a paste electrode containing the Pt electrocatalyst prepared with the impregnation-reduction method (Pt/CNT (propanol)), as was detailed in Section 4.4.1.3, occurred at a lower overpotential (-0.66V) than the commercial JM Pt_{40}/C catalyst (-0.77 V) under the same conditions in the $ClLiO_4$ (Ag/AgCl) system.

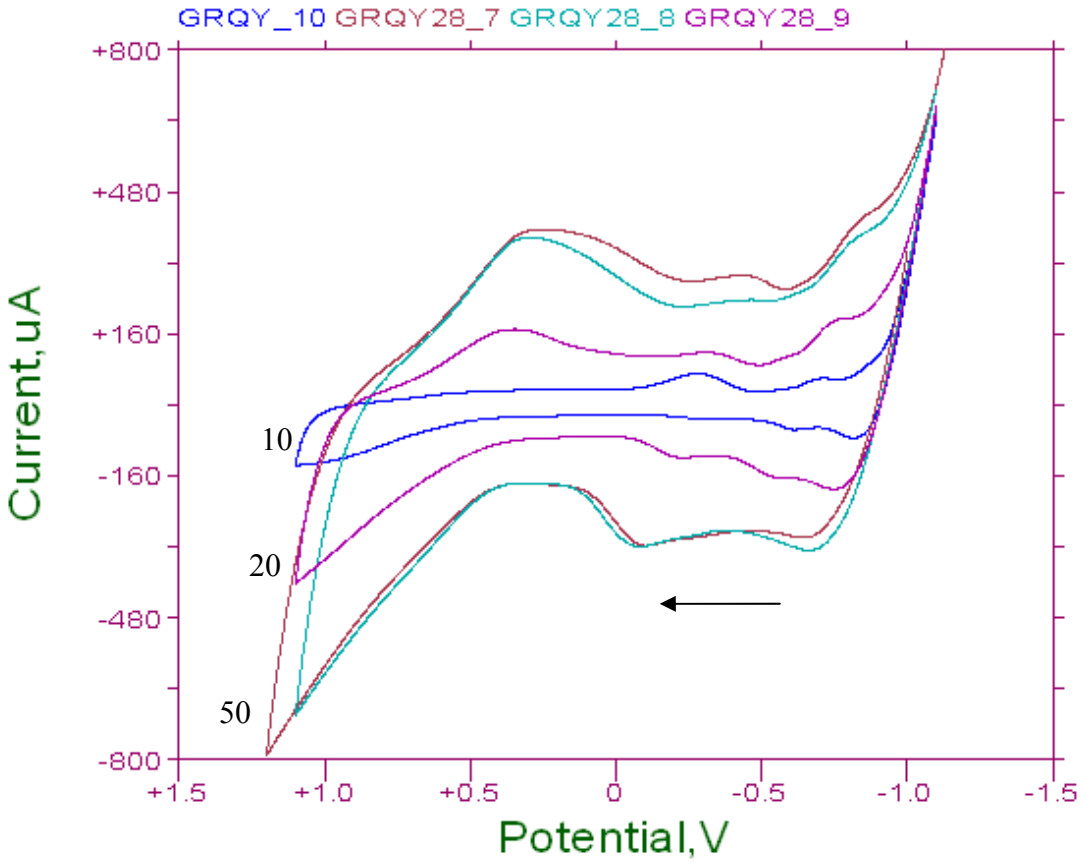

Figure 4.23 Cyclic voltametry of Pt/CNT (propanol) between -1100 - 1100V and scan rate varied between 10 - 50 mV s^{-1} at a sensitivity of 100 µA V^{-1}

Figure 4.23 shows the electro activity of the Pt/CNT (propanol) sample in the $ClLiO_4$ (Ag/AgCl) system scanned at different rates between 10 and 50 mV s^{-1}. This Pt/CNT (propanol) catalyst comprising carbon nanotubes and supported Pt was used as the benchmark CNT supported catalyst for comparison with the electrochemistry of the galvanic displacement sample series prepared as described in Table 4.1 and 4.2 which samples will be denoted Pt/CNT_BP hereafter.

The samples prepared via the galvanic displacement technique (Pt/CNT_BP series) were prepared as paste electrodes (Table 4.2) using the ultrapure graphite as diluent. Cyclic voltammetry was performed in an argon purged $ClLiO_4$ (Ag/AgCl) system between -1100 and 1100 at 50 mV s^{-1} and a sensitivity of 100 µA V^{-1} for Pt/CNT (propanol) and the Pt/CNT _BP samples prepared using the galvanic displacement

technique with Al, Pb or Fe foils and a deposition time of 10 and 20 min respectively are shown in Figures 4.24 to 4.26. The overpotentials for HER of the different samples detected during cyclic voltammetry are listed in Table 4.3. The HER and hydride peaks observed on the anodic sweep are tabulated, however peaks on the cathodic sweep could not definitely be assigned to the specific reactions due to irreversible reactions, distortions in the scans and poor resolution of the peaks. Where no data is shown, no peak for oxide chemisorption or PtO formation was discerned at the applied scan rate and scan range.

Table 4.3. Comparison of hydrogen evolution over different electrocatalysts

	H_2 evolution E_{pa} (V)	Hydride deposition /desorption E_{pa} (V)	Oxide chemisorption E_{pc} (V)	PtO formation E_{pc} (V)	Charging the electrolytic double layer (V)
***$JMPt_{40}$/C catalyst** (SCE system at 0.05 Vs^{-1})					
*Literature ref. (Bradley, 1989)	-0.68 V	~ -0.05	0.125V	above 0.8	~0.25 to 0.125
At 50 mVs^{-1} ($ClLiO_4$ (Ag/AgCl) system between -1100-1000 V; sensitivity 100µA)					
$JMPt_{40}$/C	-0.77	-0.27	0.341	-	”
Pt/CNT (propanol)	-0.66	-0.086	0.296	-	“
Pt/CNT_BP series					
Al 10 min	**	0.0	**	***	“
Pb 10min	-0.0.83	0.107	**	***	“
Fe 10 min	-0.88	-0.104	**	***	“
Al 20 min	-0.667	-0.165	**	***	“
Pb 20min	-0.680	0.107	**	***	“
Fe 20 min	-	0.208	**	***	“

Not well resolved; * In most cases above 1.0V.

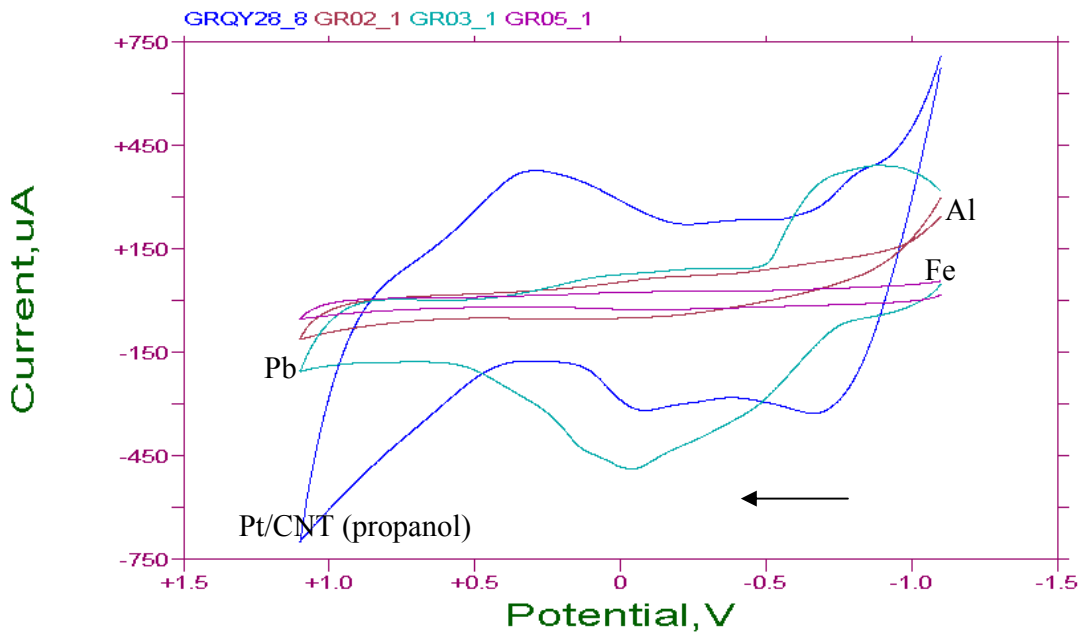

Figure 4.24 CV of Pt/CNT_BP samples prepared for 10 min using Al, Pb or Fe foils compared with Pt/CNT (propanol) in $ClLiO_4$ (Ag/AgCl) between -1100 and 1100 at 50mV s^{-1}; sensitivity of 100µA V^{-1}

CV of the Pt/CNT_BP sample prepared with the galvanic displacement method using Pb as foil and 10 min deposition time, shows quite distinct peaks on both the anodic and cathodic sweeps with a large hydride deposition peak at -0.29 V and a minimal peak for H_2 evolution at a scan rate of 50 mV whereas the Al and Fe foils samples reacted for 10 min did not show a significant electro activity for hydrogen evolution under the conditions tested. The Pt/CNT_BP sample prepared with Fe foil had the highest Pt content of the galvanic displacement samples (Figure 4.12) yet showed dissimilar and low HER activity compared to the Pt/CNT(propanol) sample, showing the effect of the preparation conditions used for making the CNT based electrocatalyst upon the catalytic activity for HER. The very large hydride adsorption peak observed during the anodic sweep in the case of the Pt/CNT_BP sample prepared with Pb foil for 10 min is of interest and may indicate a high hydride adsorption capacity for this bimetallic sample.

Figure 4.25 shows the CVs of Pt/CNT (propanol), in comparison to Pt/CNT_BP samples prepared via the galvanic displacement reaction for 20 min using Al, Pb or Fe foils.

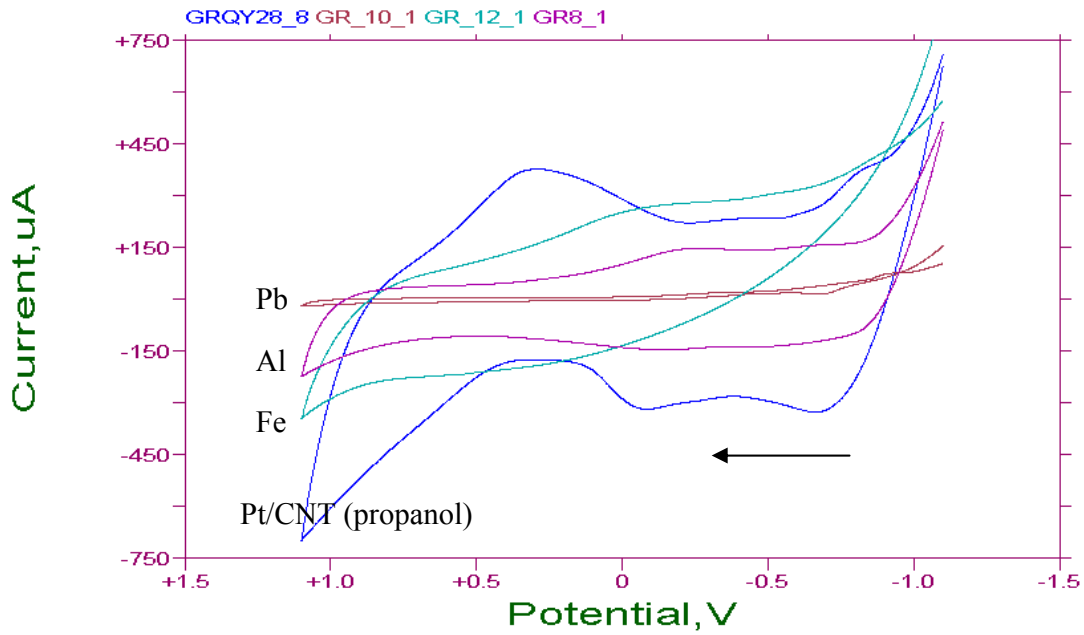

Figure 4.25 CV of Pt/CNT samples prepared for 20 min using Al, Pb or Fe foils compared with Pt/CNT (propanol) scanned in $ClLiO_4$ (Ag/AgCl) between -1100 and 1100 at 50mV s^{-1}; sensitivity of 100µA V^{-1}

In general from Figure 4.24 and 4.25 it was not evident that the electrocatalyst samples prepared using Al, Pb and Fe foils for either 10 min and 20 min using the galvanic displacement reaction had significant electroactivity compared to the commercial $JMPt_{40}$/CNT electrocatalyst (Figure 4.18), during CV scanned at a rate of 50 mV s^{-1} (Table 4.3). The CV scans cycled between -1100 and 1100 V at 50 mV s^{-1} and sensitivity of 100 µA V^{-1} of these bimetallic Pt/CNT_BP series of electrocatalysts are shown individually in Figure 4.26 (a-f). The CVs show that 10 min samples were also significantly different in electroactivity characteristics to 20 min samples, which may be due to the varying ratios of different metals in the bimetallic system observed for the different deposition times. Moreover, the hydrogen evolution peak was only observed clearly on the anodic sweep in the case of the Pt/CNT_BP sample prepared with Pb foil for 20 min (Figure 4.26d), but with very little current flow.

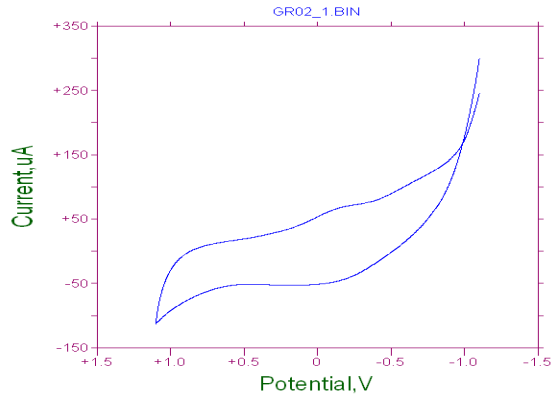

(a) Al 10 min

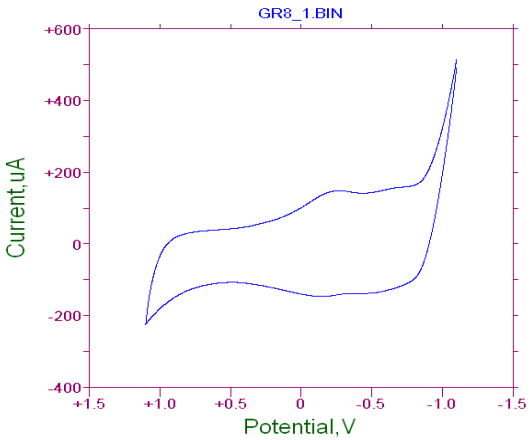

(b) Al 20 min

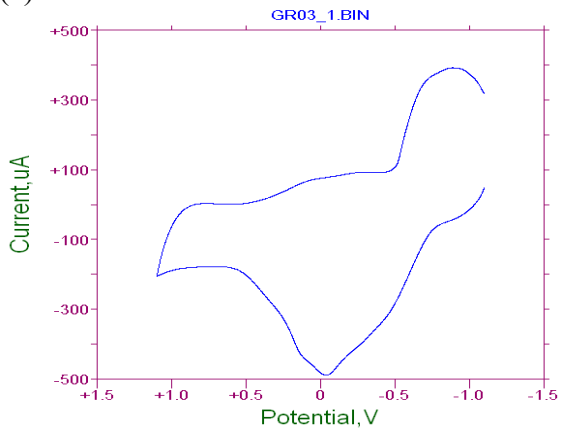

(c) Pb 10 min

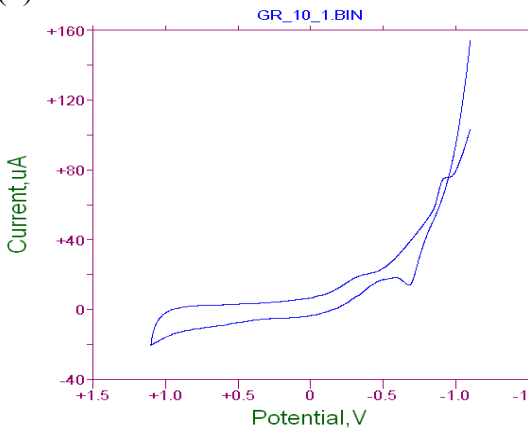

(d) Pb 20 min

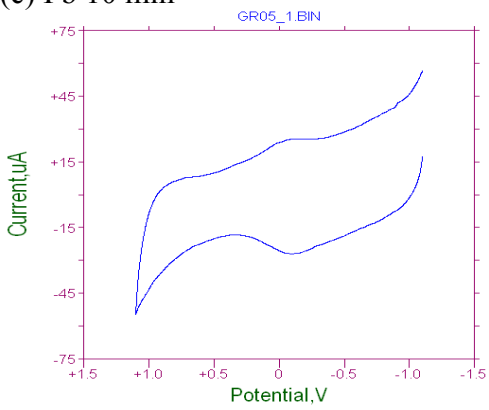

(e) Fe 10 min

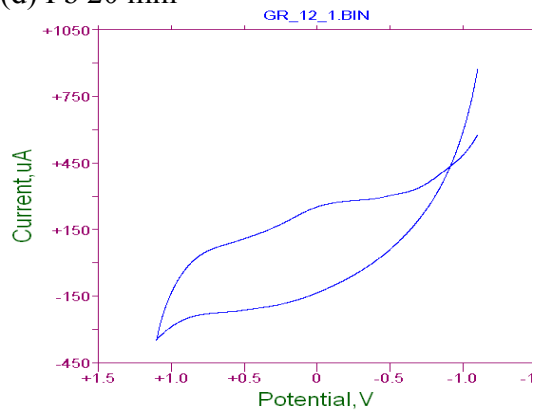

(f) Fe 20 min

Figure 4.26 Cyclic voltammetry of Pt/CNT_BP series of electrocatalysts

Hence, the bimetallic nature of the Pt deposition achieved by galvanic displacement altered the electrochemical characteristics of the Pt metal significantly. The nature of these materials is novel thus their application in the hydrogen evolution or other

reactions would require further investigation to establish whether these CNT supported materials could be beneficially applied. However, in the case of the Pb foil (20 min) sample it is interesting to note (Table 4.3) that the overpotential of hydrogen evolution (-0.68) is lower than the commercial JM Pt_{40}/C sample (-0.77 V) and similar to the case observed in the Pt/CNT (propanol) sample (-0.66).

As the HER peaks of interest were not observed in all cases in the new series of electrocatalysts prepared with the galvanic displacement technique (see Table 4.3) at a sweep rate of 50 mV s^{-1}, therefore different sweep rates were examined for each separate sample. Very large distortions of the voltammetric curves were observed in some cases. This may arise as a consequence of large uncompensated ohmic drops (Gaudet et al., 2005) thus the electro catalytic activity of the various catalysts may be best compared by following the current density at constant electrode potential. Because the determination of the voltammetric charge is complicated by the presence of distorted voltammetric curves, the electrochemical properties of the bimetallic catalysts were not considered further.

4.6 CONCLUSIONS

Methods for preparing active nanophase Pt electrocatalysts on CNT substrates were explored. The CNT made according to a ferrocene-toluene spray pyrolysis synthesis procedure were utilized as a suitable conductive substrate for the preparation of an active Pt electrocatalyst Pt/CNT (propanol). A CNT paper substrate was used as substrate to deposit Pt via a galvanic displacement technique and prepare a nanophase Pt-containing gas diffusion electrode in one simple step, to eliminate the extensive processing that is required for stabilization of nanophases in porous matrixes or in thin film format with binders on support substrates to prepare composite electrodes. Deposition of Pt on CNT paper by a simple galvanic displacement technique formed a new, active Pt containing gas diffusion electrode.

CHAPTER 4

The new electrocatalysts were compared to an industry standard commercial Pt catalyst stabilized on Vulcan carbon black for electro activity. The use of CNT as support substrate and the Pt deposition techniques applied are shown to result in electrocatalysts that could reduce the energy requirements of the hydrogen evolution reaction, particularly in the case of Pt electrocatalyst Pt/CNT (propanol). In the case of the electrocatalyst sample Pt/CNT_BP (Pb foil (20 min)) the overpotential of the anodic hydrogen evolution peak (-0.68 V) is similar to the case observed in the Pt/CNT (propanol) sample (-0.66 V) and both occur at lower overpotentials than the commercial JM Pt_{40}/C sample (-0.77 V) when cycled between -1100 and 1100 V at 50 mV s^{-1} at sensitivity of 100 μA V^{-1} in a $ClLiO_4$ (Ag/AgCl) system.

Because of limitations in processing CNT, due to agglomeration of CNT, which need to be overcome and which fell outside the scope of this study, the Pt/CNT (propanol) materials were not further integrated into composite electrode format. Initial electronic characteristics of the Pt/CNT_BP supported on CNT paper are presented in Chapter 6.

In Chapter 5 the development of Si based micro and mesoporous substrates as supports for Pt electrocatalysts will be presented as well as their incorporation into composite electrode format and activity testing for water electrolysis.

CHAPTER 5

5 NANOPHASE COMPOSITE ELECTRODES

5.1 INTRODUCTION

The topic of this chapter is the development and optimization of composite nanophase containing electrodes, utilizing nanophase electrocatalysts. Preparation of nanophase composite electrode materials for potential application in alkaline or solid polymer electrolyte electrolyzers is challenging and requires consideration of the many factors involved in their formation. In the preparation of composite electrodes, the type and ratio of catalyst, of binder and/or proton conductor, the additional electroconductive phase, and solvent type and amount should be optimized in order to achieve maximum activity, stability and durability whilst maintaining access for gas or liquid, and pathways for electrons and protons. It is necessary to achieve the optimum balance between macropores and micropores required for gas access or removal, for liquid access, and pathways for electron and proton conduction at the nanophase electrocatalyst in the composite material. The gas / liquid / solid boundary is known as the three phase boundary and bringing all these three phases into close contact reproducibly poses a particular challenge for fabrication of composite electrodes. Components of the electrodes must be selected to ensure stability in the presence of a corrosive electrolyte as well as gaseous and liquid reactants.

For cost efficient operation of electro catalytic installations for hydrogen production the development of highly active, selective and stable working nanophase catalysts incorporated in electrodes may offer benefit. Large surface area electrodes may be achieved by the application of supported metal clusters of nanosized catalysts supported in three dimensional substrates. These materials must then be attached to the electrode surfaces. Because of their large active surface areas these nanophase containing electrodes could significantly reduce the overpotential of the electrolyzer cell.

CHAPTER 5

Generally, a bulk metal such as Ni is used as the active electrode component in alkaline electrolyzers, because of cost considerations (Imariso et al., 1980). Use of nanosized electrocatalysts would allow highly active but costly precious metals such as Pt to be applied most economically and could minimize their wastage and maximize their active catalytic surface area. Formation of composite nanophase electrodes by sequential deposition has been identified in the thesis as being a possible method for simple fabrication of electrodes. The first step in the process of sequential deposition is the preparation of the catalyst support (see Chapter 3 and Chapter 4) and the subsequent stabilization of the active nanophase electrocatalysts on the support to prevent agglomeration of the nanophase metal centres (also see Chapter 4). The preparation of supports was detailed in Chapter 3 and routes to stabilize Pt nanophase electrocatalysts upon CNT supports was detailed in Chapter 4.

The sequential stabilization of heterogeneous nanophase materials upon a variety of Si based porous substrates, followed by stabilizing these materials on electro conductive supports to prepare composite electrodes and then applying the electrodes in high electrolyte environments for water electrolysis forms the focus of this chapter.

The type of nanophase electrocatalyst, and ratio of catalyst to binder, was investigated in different combinations with various porous and non porous conductive and non-conductive substrates. In most cases the same proton and electro-conductive phase was added, but in varying amounts. The stability, activity and durability of nanophase composite electrodes prepared by sequential deposition was also examined by a rapid testing protocol as specified in this chapter. This protocol was applied for screening composite nanophase electrode materials using hydrogen production at relatively high applied potentials in a high electrolyte environment. Hydrogen production in the alkaline electrolyte was used as a simple and relatively rapid qualitative measure of the electro catalytic activity of the nanophase electrocatalyst in this composite format. Poor catalytic performance for hydrogen production was taken as a simple measure of the occlusion of catalytic sites by binders and / or gaseous

layers or the lack of adequate conductive pathways and was used as rapid indicator for optimization of formulations of micro-emulsions or inks. The expected high gas evolution under the applied conditions was used as an accelerated aging test of the stability and durability of the composite electrode components. Delamination of the catalytic component during high gas evolution was used as a simple measure of inadequate stabilization of the electrocatalyst containing film upon the substrate.

Composite electrodes prepared by sequential deposition in this study are composed of a electrocatalyst containing film comprised of stable and catalytically active particulate or heterogenous nanophase material, stabilized with a binder, that is supported upon a conductive substrate. By their nature these composite electrodes are mainly gas diffusion electrodes (GDE) that can be used in fuel cells, gas sensors, some types of batteries and electrolyzers. In this chapter the focus is on hydrogen production by water electrolysis as a simple reaction used as measure to optimize and understand the nature of the electrodes.

5.2 BACKGROUND

Water electrolysis is the process of dissociation of water (H_2O) under the influence of an electrical current. Electrolysis of H_2O leads to formation of H_2, O_2, H^+ and OH^-. Only H_2 and O_2 involve a change of oxidation state. Hydrogen in H_2 has a lower oxidation state (0) than hydrogen in H_2O (+1), whereas oxygen in O_2 has a higher oxidation state (0) than oxygen in H_2O (-2). Therefore water can be reduced to H_2 or oxidized to O_2.

Solutions to increasing catalytic and current efficiency, obtaining high current densities, minimizing power consumption and lowering the cost of hydrogen production by water electrolysis are constantly sought. Because of the high cost of electrical power it is desirable to reduce the voltage at which a solution is electrolyzed to as low a value as possible. In the electrolysis of water there is considerable scope for achieving a reduction in electrolyzing voltage by reducing the

hydrogen overpotential at the cathode. There have been many attempts to achieve a reduction in hydrogen overpotential. For example, it is well known that the hydrogen overpotential at a cathode may be reduced by increasing the surface roughness and thus the surface area of the cathode. Other methods of producing low hydrogen overpotential cathodes which have been described involve coating the surface of a cathode with an electrocatalytically active material (Wood, 1986).

Physical and chemical variables that can have an impact on energy loss in these systems include the supporting electrolyte type and concentration, temperature, pressure, gas to liquid ratio, distance between working electrodes, cell geometry, flow velocity, gas evolution and product separation from the electrolyte (Imariso et al., 1983).

Two different diffusion processes take place in GDE electrodes namely, gas diffusion and the liquid or vapour diffusion. During the phase transition of gas/liquid in an electrochemical reaction, diffusion limitation may occur because of the difference in density and mobility, and thus the time scale. Material characteristics that are important for the liquid transport include the wetting angle of the catalyst, and the respective catalyst support. The wettability affects the electrolyte uptake and the osmotic flow. Liquid transport can change from a diffusion to an osmotic mode depending upon the characteristics of the composite (Kinoshita,1988).

The process of hydrogen generation during water electrolysis is often impeded by the formation of a “locking” gas layer on the cathode surface. As a result, the potential drop between two electrodes rises sharply and both process efficiency and economics suffer. The specific resistance of the electrolyte between the two opposite electrodes during alkaline water electrolysis will be increased by the presence of gas bubbles, decreasing the energy efficiency of the electrolysis process (Sillen et al., 1980). These authors investigated the role of bubble density, average bubble radius, and the gas volume fraction at the electrode surface at various current densities, flow velocities, electrolyte concentrations and temperatures. Ohmic potential drop occurs in the

electrolyte space between the electrodes and the separating diaphragm which is filled by the gas produced (Appleby and Crepy, 1978).

Although introduction of porous electrode structures and net or mesh configurations lower the negative effect of the surface gas layer, more drastic changes to catalyst morphology is needed in order to bring about potential drop values close to economically justifiable values. The formation of electrocatalytic structures on the surface of mesh or porous electrodes has been reported as electrode materials in liquid phase alkaline electrolyzers (Divisek and Schmitz, 1984).

Not only the electrochemical reactions, but also adsorption-desorption processes at the electrode surface as well as transport processes such as the molecular transport of hydrogen and the thermal behavior of gas diffusion electrodes need to be considered. Sunde (2000) reviewed approaches to models and computer simulations of conductivity, polarization resistance, and impedance of composite electrodes that could be used to model the highly disordered structure of composite electrodes typically used in solid oxide fuel cells (SOFC). Approaches included a thin film model, Monte Carlo calculations, or a macroscopic porous-electrode model. The macroscopic porous-electrode theory was modified to include non-linear kinetics and gas-phase diffusion. Sunde found that most of the electrochemical reaction occurred in a region closer than 10 μm to the bulk electrolyte. The current-collector potential at a given current was found to be nearly independent of thickness above 10 μm. These authors report that the rate balance was controlled by porosity, volume fraction of catalyst and particle size, which could be varied within the limitations relating to the requirement of percolation in the gas phase and the conductive networks.

Kaisheva (2004) studied the activity and the transport hindrances in air gas-diffusion electrodes. The structure of the electrode in their study was a double-layer electrode comprising a porous hydrophobic gas diffusion layer, and a catalytic layer where the electrochemical reduction of oxygen took place. They found that the air gas-diffusion electrode had a complicated porous structure in which several electrochemical and

transport processes were occurring simultaneously and performance was influenced not only by the activity of the catalyst, but also by all transport processes occurring in its porous structure. In addition the transport hindrances in the electrode were also a function of the pore structure and the surface properties of the catalyst. The hindrances in the transport of molecular oxygen were higher in the electrodes with thicker gas layers. It was theoretically predicted and experimentally proven that the existence of a network of hydrophobic pores in the carbon-catalyst grains played an important role for the effective operation and stability of the electrodes.

In bi-polar electrolyzer units the application of a cell potential of 1.8 to 2 volts (V) resulted in a relatively low current density of 200 to 300 mA cm^{-2}. The efficiency of such cells was therefore poor, calculated on the reaction enthalpy. For achievement of a 100 % yield at economically feasible current densities the total cell potential should be of the order of 1.5 V (Divisek and Schmitz, 1984).

These earlier studies highlight the various aspects that can affect the performance of the electrodes and more recent studies show attempts to address the challenges inherent in the alkaline electrolyzer system, based on obtaining an understanding and optimization of the physical structure of the electrode.

The current density (j) and cell voltage (I-V) relationship is the most important characteristic of any electrochemical cell. Because the I-V relationship changes with different loads and operating conditions it can be used to determine the performance of the system. Electrochemical reactions differ from other heterogeneous reactions as their rate constants depend on the potential difference, (V) at the metal-solution interface (Ebbing, 1993). During the water electrolysis process electrical current flows through the electrolyte when the external voltage is applied, thus the flow of current depends on the applied potential. Current density is described as a measure of the rate of electron transfer at equilibrium, for example if the potential is increased, current density also increases and hydrogen bubbles are produced rapidly. Therefore the current of an electrochemical cell will depend on the kinetics of the electrode

reactions as well as the energy required for the electrode to provide a given amount of current (Shukla et al., 2002).

5.3 COMPOSITE ELECTRODE FABRICATION METHODS

Nanophase composite gas diffusion electrodes (GDE) as defined in this study comprise an assembly of (1) a supported or unsupported nanophase electrocatalyst, that is dispersed upon (2) a suitable porous conductive substrate in the form of (3) a catalyst containing film in which the three phase boundary between gas, liquid and solid is achieved. The film is prepared by use of a micro emulsion or ink constituted with the catalyst, a suitable binder, a solvent, and a proton- and electro-conducting phase.

Gas diffusion electrodes (GDEs) typically are constructed of high-surface area supports for metal catalysts, as well as solid inert materials with high gas permeability. Typical composite GDEs consist of carbon black and a binder such as polytetrafluoroethylene (PTFE) in close contact with a porous current collector through which the gas can pass. The hydrophobic PTFE inhibits aqueous solutions from completely penetrating the porous structure but the carbon black support is capable of being wetted by the electrolyte. The solution layer may act as a thin meniscus that can support high gas flux rates. Limitations caused by lack of gas solubility in the electrolyte is offset by the very thin diffusion layer formed with the wetted electrode surface. The additional three-dimensional surface area incorporating a gas-liquid-solid interface into the electrode element that is inherent in most GDEs can significantly amplify the current compared to that obtained on an equivalent simple two dimensional geometric area (De Castro, 1996).

Many thin film deposition methods have been developed and commercialized. Thin films are usually considered to be less than 10 μm thick. Schuegraf (1988) reviews thin-film deposition techniques. Of these technologies, chemical vapour deposition, spray deposition and thermal spraying deposition are the techniques most relevant,

and are encompassed in the overall methodic of the sequential deposition technique developed in this chapter, Chapter 5.

Ahn et al. (1997) reported the fabrication of fibre composite gas diffusion electrode (GDE) structures and their performance for oxygen reduction in an alkaline electrolyte. The electrode structure was formed with 2 μm diameter activated carbon fibres interlocked within a network of 2 μm sinter-bonded metal fibres to form the composite which was stable, highly conductive and had a void fraction exceeding 95 %.

Franco et al. (1998) studied the electric properties of polymer electrolyte / carbon black composites, but these materials were not based on thin films. These authors prepared composites based on the solvent casting technique. The polymer complexes, appropriate solvent and the required amount of highly conductive carbon black or polymer electrolyte were blended. The concentration of conductive carbon black particles used was close to the percolation threshold value, which was found in their case to be in the range of 15 to 20 wt % of carbon black. After removal of the solvent the electrode samples were prepared by pressing the ground components at 4 ton cm^{-2} followed by thermal treatment (80 ºC, 24 h) to homogenize the material.

In a study by Legagneur et al. (1999), composite electrodes were prepared and deposited as a thick film or pressed against a Pt disk using 10 % by mass of carbon black with addition of the catalytic component (85 % by mass) and 5 % of an organic binder.

Low cost electrode fabrication techniques were investigated by Pham et al. (1999) including methods such as dip coating, spin coating, slurry painting, and electrophoretic deposition. Films were required to be 10 μm or less and repeated processing was applied to achieve thicker films for stable long term operation of electrodes. These electrodes were suitable for application in a SOFC fuel cell operating at 1000 °C. Delamination was prevented by spraying a colloidal solution on

a heated substrate to remove the solvent during deposition. The authors found that the abrupt interface between components of the electrode was suppressed.

Furuya (2001) reported the production of a gas diffusion electrode where electrode materials were dispersed in aqueous solution with a surfactant. The dispersion was flocculated, filtered, dried and subjected to a sheeting process to form the electrode sheet, the surfactant was removed, and it was hot-pressed at 380 °C and 4.9 MPa for 1 min with copper mesh that was integrated in the gas-supply layer and used as a current collector. The gas diffusion electrode was made using a dispersion with PTFE, carbon blacks and a catalyst. The loading of catalyst was 0.3 – 0.001 mg cm^{-2}. The potential of the gas diffusion electrode was measured in 32 wt% sodium hydroxide solution at 80 °C for applied current densities.

The patent literature has many descriptions of ways to prepare gas diffusion electrodes. Some of the most relevant patents are briefly summarized here. United States Patent (USP) 6838408 (Bulan et al., 2005) describes a method for producing gas diffusion electrodes, for use in electrolysis cells, by preparing a sheet-like structure by rolling a powder mixture containing a catalyst or a catalyst mixture and a binder, and then the sheet-like structure is connected to an electrically conductive catalyst support by rolling. USP 6881511 by Tosco et al., (2005) describes gas diffusion electrodes containing modified carbon products with attached organic groups that were used as part of the active layer and/or the blocking layer to extend the service life of electrodes. USP 6361666 (Lipinski and Leuschner, 2002) describes the preparation of thin, flat, porous gas diffusion electrodes made of carbon, which have a smooth surface with regulated porosity obtained by pyrolysis of a composite of an organic polymer and a reinforcing skeleton formed partially using organic material. USP 5733430 (Ashida et al., 1998) describes a gas diffusion electrode that can be applied as an oxygen cathode for sodium chloride electrolysis, which is formed of a porous layer containing a super-fine particle catalyst and a fluorine-containing material on a substrate that is connected to a gas-liquid permeable collector. USP 5618392 (Furuya, 1997) describes a gas diffusion electrode

comprising a reaction layer and a gas diffusion layer attached to each other. The electrode has apertures through the electrode to facilitate the flowing of an electrolyte and a gas even though the interelectrode distance is small.

Cox et al. (2005) in United States Patent 6911411 describe catalyst agglomerates for membrane electrode assemblies. This patent indicates the different formulations of ink required on either the anode or the cathode and recommends that the amount of polymer solution added as binder should contain a weight of polymer from 6 to 15 % of the catalyst for the anode side electrode and 7.5 to 15 % of the catalyst for the cathode side electrode. The optimum level of polymers depended on the type of polymers, the operating conditions including aspects such as temperature, gas humidification level, and passive or active transport of reactants to the electrode surface. The catalyst composition could be applied onto the polymer membrane by using techniques such as sputtering, painting, electro-deposition, spraying, decal transferring, filtering and filtering transfer, tape casting, and screen printing. The coated layer was either hot or cold pressed or calendered. Another approach given was that the catalyst agglomerates could be applied onto a backing layer to be indirectly transferred to the membrane surface. In this patent a dilute Nafion® ionomer solution was prepared by mixing 3.584 g of 5 % ionomer, 1.792 g of water, and 1.792 g of isopropanol (isopropanol:water=1:1) using a sonication bath for 10 min or by mixing 8.823 g of 5 % Nafion® ionomer and 26.47 g of water (3 times the amount of 5 % ionomer).

As these various studies and patents show, various aspects need to be considered in the preparation of composite electrodes. The support substrate type as well as the components and the composition of the micro emulsion or ink used to form the electrocatalyst containing film upon the support requires optimization. The variables that can be explored include different support substrates, different binders, different supported or unsupported nano scale electrocatalyst, and various solvents. The relative amounts of each component of the ink should be considered in terms of the

final concentration of electrocatalyst desired per unit area in the thin film deposited on the substrate.

Pt containing gas diffusion electrodes are described by various authors. Pt is considered to be the best metal for the reduction of hydrogen ions. The rate of hydrogen evolution from different metal surfaces can vary greatly (Tafel, 1905). The value for the exchange current density of hydrogen evolution on platinum is approximately 10^{-2} A cm^{-2} whereas on Ni it is 10^{-7} A cm^{-2}, which is five orders of magnitude lower than Pt for the rate of hydrogen evolution. The exchange current density is defined as the rate of oxidation or reduction of the metal electrode at equilibrium expressed in terms of current and represents the rates of oxidation and reduction of a given single electrode at equilibrium, when no loss or gain is experience by the electrode material. The magnitude of exchange current density is a function of metal composition, surface roughness, concentration of both the reactants and products involved in the reaction, and surface impurities (Corrosion Source, 2008). This source reveals that a higher exchange current density exists for the H^+/H_2 system equilibrium on platinized platinum (10^{-2} A cm^{-2}) with a high surface area compared to bright platinum (10^{-3} A cm^{-2}), but is markedly reduced in the same system by the presence of trace impurities such as sulfur. The approximate exchange current density for the reduction of hydrogen ions on a range of materials is shown in Table 5.1.

Table 5.1 Approximate exchange current density (j^0) for the hydrogen oxidation reaction on different metals at 25 ºC (Corrosion Doctors, 2008).

Metal	$Log_{10}\, j^0$ (A cm^{-2})
Pb	-13
Zn	-11
Sn	-10
Ni	-7
Fe	-6
Pd	-4
Pt	-2

It requires an overvoltage of about 0.2 V to liberate hydrogen gas from a polished platinum surface and the factors that determine the overvoltage of an electrode at any

one pressure is the size of the gaseous nuclei that can cling to it, the surface tension, and the pressure (Macinnes and Adler, 1919; Macinnes and Contieri, 1919). The potential windows of Pt, Ni and carbon electrodes differ in aqueous solution and it is necessary to consider the electrode's hydrogen overvoltage, oxygen overvoltage and dissolution as well as the electrolyte pH. For instance, Pt has a potential window between about -1.1 and 1.2 V at pH 14 whereas the window changes to between -0.9 and 0.9 V at pH 7 and about -0.3 and 1.25 V at pH 0, and Ni metal dissolves in acidic solution.

Nørskov et al. (2005) studied the bond energies of various transition and noble metals to understand the trends in the exchange current for the hydrogen evolution reaction (HER) and they found a relationship between the exchange currents and the calculated hydrogen adsorption energies. Calvo and Balbuena (2007) on the other hand studied the oxygen reduction reaction (ORR) over Pt and Pt-Pd alloys and found that none of the alloys tested provided better sites than those of pure Pt both for O_2 dissociation and for the reduction of oxygen and OH to water. The kinetics of the HER in 6 M KOH electrolyte have been studied (Elumalai et al., 2002) on electrodes made from the pressed powders of submicron size Co, Ni and Co–Ni alloy powders.

Morimoto et al. (2000) describe gas diffusion electrodes made of electroconductive porous PTFE sheets supporting Pt catalysts that were used as the oxygen reduction cathodes for chlor-alkali electrolysis. These authors found that the activity of the cathode deteriorated because of loss of Pt catalyst due to the oxidative corrosion of the carbon substrate.

Hayashi and Furuya (2004) describe the preparation of gas diffusion electrodes by precipitates deposited from carbon-polytetrafluoroethylene dispersions using an electrophoretic deposition technique. These electrodes were applied in a fuel cell using Pt as a catalyst in alkaline solution to promote oxygen reduction and the ability of the gas diffusion electrode for hydrogen oxidation was reportedly high.

CHAPTER 5

A bifunctional electrode structure for a unitized proton exchange membrane regenerative fuel cell was developed by Shao et al. (1999). The electrode comprised a thin catalyst layer with a loading of 0.4 mg cm^{-2}, which minimized mass transport and ohmic limitations. In that study platinum black was used as bifunctional hydrogen catalyst, and platinum black and iridium oxide was used as the bifunctional oxygen catalyst. The combination of 50 wt% Pt and 50 wt% IrO_2 was reported to be a good bifunctional catalyst for the oxygen electrode. The electrode support layer used was a sheet of carbon paper that was soaked in a PTFE emulsion and the support thus contained about 30 wt% PTFE. The thin film fabrication approach is most similar to that described in this chapter.

Some studies use alloys of metals and various combinations of base metals for electrode formation which may be useful for the HER. The purpose of using mixed oxides is to modify the electrochemical properties of the active metal by modifying its composition. In United States Patent 4586998 (Wood, 1986) cathodes were produced by electro-depositing an outer layer of Pt group metal on a nickel or nickel alloy substrate. In United States Patent 4273624 (Laitinen and Thornton, 1981) a thin platinum film was electrodeposited on a conductive tin oxide surface. This patent indicated that tin oxide electrodes are less active compared with platinum because of high overpotentials, which result in very high power losses in commercial processes. Pure tin oxide (SnO_2) has a relatively high electrical resistance in comparison to other metals and observed current densities were about 10^{-4} A cm^{-2} for a polished tin oxide substrate. The electrical stability and conductivity may be improved through the introduction of a dopant, such as antimony. Electrodes, such as Ti/SnO_2 electrodes possess relatively high oxygen evolution reaction (OER) potential to produce a high concentration of OH radicals and are typically used for the oxidation of organic pollutants (Ding et al., 2007). SnO_2 particles as Pt support have been used for PEMFCs and DMFCs, and have revealed high catalytic activities toward methanol oxidation (Jiang et al., 2005). Three dimensional Ti/Co/SnO_2-Sb_2O_5 electrodes combined with activated carbon are described by Wang et al. (2007) for the electrochemical treatment of wastewater. Mixed-oxide electrode coatings based on

IrO_2, RuO_2 and SnO_2, for the oxygen evolution reaction (OER) were prepared using a thermal decomposition method (Vazquez-Gomez et al., 2006). SnO_2-RuO_2 oxides were prepared by mechanical alloying using high-energy ball milling of various proportions of pure SnO_2 and RuO_2 powders (Gaudet et al., 2005). The electrodes were made with slurries containing the oxide material, water, and 10 wt. % Teflon which was then painted on both sides of pretreated Ti platelets.

Giz et al. (2003) describe Ni-Cu-Fe electrodes obtained with an acetate bath for the electrochemical codeposition of Ni-Cu-Fe at low pH. These electrodes showed low overpotentials for the HER, around 0.150 V at 80ºC, in brine solution (160 g L^{-1} NaCl and 150 g L^{-1} NaOH), and good stability under continuous long-term operation for 260 h was reported. The overpotential under the same conditions for the Ni-Cu-Fe electrode was 249 mV lower than that of mild steel (404 mV), used in commercial unipolar electrolyzers. Poor intrinsic catalytic activity of the Ni-Cu-Fe electrodes was compensated by an improvement due to the larger electrode surface area obtained by this technique of preparation.

This route of enhancement of surface areas of non-noble metals as electrode materials is one route to overcoming the low activity of these materials, and was the approach followed in this chapter where certain of these non-noble metals (SnO_2, Ni) were applied as stabilized nano particles.

5.4 APPROACH IN FORMATION OF COMPOSITE ELECTRODES

This chapter further explores the effect of varying components upon the activity of the composite electrodes. The type of catalyst and ratio of catalyst to Nafion®, as binder and proton conductor and any additional electroconductive phase, as well as the necessary solvents and dispersant medium may be varied in order to optimize the composition of the catalytic ink. The formation of nanophase containing composite electrodes is described in the following sections.

CHAPTER 5

Composite nanophase electrodes were formed by sequential deposition through firstly preparing the mesoporous and microporous supported catalysts described in section 5.6.1.5 of this chapter where after admixtures of the powder nanophase electrocatalysts were made with a conductive phase (carbon black), and various binder types, or a proton conductive phase (Nafion® LIQUION 1100). Solvents that were used included ultra pure water, acetone, and toluene.

The micro emulsions or inks formed by these admixtures were coated upon a variety of conductive substrates by various deposition techniques (spray coating, dip coating, casting, or hot-pressing with polytetraflouroethylene). The catalytic inks contained various binders or proton conductive phases in ratios of solids that took consideration of the percolation threshold. Different ratios of catalyst to binder and conductive phase were explored. In some cases the electrocatalytic material was substituted with commercial nanomaterials such as nanophase antimony tin oxide.

Various methods were investigated for deposition of the micro emulsion or ink, which included spray coating, dip coating, sponge coating, casting, as well as heat and pressure fusion. Moreover the method for mixing of the ink was evaluated and it was found that ultrasonication of the ink was necessary for good dispersion but that excessive ultrasonication could damage the catalytic particles. Since this method of mixing is established practice, the dispersion by stirring and ultrasonication was not further varied.

5.5 CHARACTERIZATION OF COMPOSITE ELECTRODES

Cyclic voltammetry and chronoamperometry analysis were chosen as the most suitable methods to determine the activity of newly developed electrode materials after controlling the accuracy and reproducibility of the technique under the chosen experimental conditions. In chronoamperometry the current, which is recorded continuously, is measured versus time at a defined potential and variations over time are then integrated numerically. Measurements may be done under galvanostatic

control of the current, or potentiostatic control of the voltage and in this study were obtained potentiostatically using the Autolab galvanostat and potentiostat and General Purpose Electrochemical system software (GPES by Ecochemie, Netherlands). The Autolab galvanostat, potentiostat and GPES provided a computer controlled electrochemical measurement system which can be used for cyclic and linear sweep voltammetry, including techniques such as galvanostatic cyclic voltammetry, and chrono methods.

In voltammetry the current density (mA cm^{-2}) of the materials as a function of the applied potential are taken as a measurement of the activity for water electrolysis under conditions that caused polarization of the working electrode. All variables that may influence concentration polarization and thus the over-potential and therefore the electrode response were kept constant as far as possible. By this means, competing equilibria of dissociation, association and complex formation were avoided as far as possible or at least were present to an equivalent degree. In particular the geometric electrode area and shape in the case of membrane electrodes were carefully controlled. Moreover, in high electrolyte studies, an excess of inactive supporting electrolyte was used and electrolyte concentration, temperature and stirring rate were also identical in all cases to maintain similar conditions of species diffusion, migration and convection. Samples were purged with a flow of nitrogen to minimize residual currents due to small amounts of dissolved oxygen.

Cyclic voltammetry and chrono amperometric experiments were performed over electrodes that had not been exposed to an oxidizing cycle. The oxidation and reduction wave, onset of hydrogen evolution and increasing over potentials over a number of cycles were evaluated for some samples in order to optimize the testing conditions. Selected samples were exposed to aging in 40 % KOH and retested for reproducibility. Furthermore, some samples were exposed to extended cycling or high voltages during voltammetry in order to accelerate aging and test composite layer stability.

CHAPTER 5

Initially the relative electro activity of various electrocatalysts was determined qualitatively in liquid alkaline electrolyte systems at low temperatures (0-5 ºC) to reduce the effect of nuisance variables such as temperature changes during testing and in order to screen prospective candidate nanophase electrocatalyst and optimize ink formulations. Selected electrode materials were characterized by optical microscopy and SEM and tested at higher temperatures.

5.6 EXPERIMENTAL: MATERIALS AND METHODS

5.6.1 Materials

5.6.1.1Binders

The different binders or conductive phases that were used in the processing of the composite electrodes, and their designated codes are listed in Table 5.2.

Table 5.2 Types of binder or conductive phase

Code	NAME	SUPPLIER	Stock and Lot no.
A	Polyvinyl acetate	Industrial Analytical (Pty) Ltd.	A12732; D9795C
B	Polystyrene	Industrial Analytical (Pty) Ltd.	A11170; C5600
C	Polytetraflouroethylene	Industrial Analytical (Pty) Ltd.	A12613; B5544C
N	Nafion® LIQUION 1100	Ion Power Co., Glasgow	5 wt% EW solution in water
CB	Hydrophilic carbon black	Source: Cabot Botlek BV	grade: m Vulcan x C72; sample no.: GP3784

Nafion® perfluorinated ion exchange resin solution 5 wt% is presented as a lower aliphatic alcohol and water 85 % ethanol and 15 % methanol mixture, Aldrich catalogue no. 527084. Nafion® polymer solution is a dispersion of perfluorosulfonic

acid and polytetrafluoroethylene copolymer, and is a product of E. I. du Pont de Nemours Company.

5.6.1.2 Supports

The different support substrates that were investigated and their designated codes, used as descriptor in graphics, are specified in Table 5.3.

Table 5.3 Types of support substrates

Code	Support Type
a	Carbon black on carbon cloth (code 6100-200 CB) supplier Lydall
b	Carbon cloth (code: 6100-300) supplier Lydall
c	Activated carbon on carbon cloth (6100-200 AC) supplier Lydall
d	ZrO_2 backed with stainless steel mesh, (Product number: Z240S lot Hy Te 010806/01/05 (17), Ω 0.7, 240 nm pore size) supplier Creavis Gesellschaft für Technologie und Innovation mbH D-45764 Marl
e	Lydall Technical Ceramic paper: Sample: 3000LF
f	Lydall Ceramic paper 40% glass: Grade IP-397-2
g	Teflon (PTFE) sheet
h	Stainless steel mesh

5.6.1.3 Solvents

The following solvents were varied in the preparation of nanophase composite electrodes:

Ultra pure water, acetone, toluene.

5.6.1.4 Commercial Electrode Materials

For comparative purposes, the following commercial Ni foil materials were tested under identical conditions to the nanophase composite electrodes:

i) Flat Ni foil – 0.787 mm thick, 99.5 % metals basis. Alpha Aesar stock # 14193; Lot # J22J09.

ii) Ni Foam manufactured by Recemat International B.V., P.O.B. 88 2920 AB Krimpen A/D IJSSEL.

Type A –. RCM-Ni-4852-01.6

Type B – RCM-Ni-2733.3

Type C – RCM NC-4852.01.6

5.6.1.5 Nanophase Electrocatalysts

In those cases where an electro active nanophase catalyst was included in ink formulations, the following particulate or micro and mesoporous supported nanophase materials were evaluated for electro catalytic activity in a high electrolyte environment.

i. Nanotek Antimony Tin Oxide (designated SbSnO in this study), 99.5 % pure consisting of a ratio of Sb_2O_5 : SnO_2 of 10: 90 obtained from Nanophase Technologies Corporation. (Part #: ATO- 2400-000-025; batch # AT00831 – 05X; product code 2400). Particle size ranging between 11-29 nm; a surface area of 30-80 $m^2 g^{-1}$ (BET) with density of 6.8 g cm^{-3}.

ii. Platinum, nominally 40 % on carbon black (supplied by Alpha Aesar a division Johnson Matthey) denoted JM Pt_{40}/C in this study and characterized in Chapter 4.

iii. Zeolite H-FAU (CBV780 Lot. No 78001N00257; Zeolyst International; dealuminated faujasite with a given analysis of: Si/Al 80; wt% Na 0.03; BET surface area of 780 m^2g^{-1}, was impregnated with 1 mL 0.1545 M H_2PtCl_6 soln, and Pt reduction was achieved with sodium hypophosphite as follows. A solution of 0.48 g of sodium hypophosphite was made in 10 mL H_2O. 2.5 mL of this solution was added to 1.0 g of Pt zeolite samples that had been impregnated by the incipient wetness technique. Samples were shaken in solution and then placed in a hot air oven at 50 °C for 4.5 h. The oven temperature was increased to 100 °C overnight in sealed containers. Thereafter the samples were thoroughly rinsed and dried at 80 °C. Nanosized

particles of Pt were supported upon the zeolite as observed by Transmission Electron Microscopy, with Pt cluster sizes ranging between 5-10 nm.

iv. Ni plated gamma alumina: Pre-dried gamma alumina (Condea) was plated with Ni according to the following Ni electroless plating technique. About 2 g of gamma-Al_2O_3 was contacted with 20 mL 0.01 M $PdCl_2$ for 1 h under stirring, then filtered, rinsed and dried in a vacuum oven overnight. Thereafter the modified alumina was contacted with 10 mL NaH_2PO_2 for 1 h under stirring and subsequently filtered, rinsed and dried in a vacuum oven. The sample was then exposed to 15 mL of a Ni plating solution for 1 min at 80 °C under stirring, where after it was filtered, rinsed thoroughly and dried overnight in a vacuum oven at 80 °C. The plating solution was composed of 31 g L^{-1} $NiSO_4$, 54 g L^{-1} NaH_2PO_2, 50 g L^{-1} lactic acid and 38 g L^{-1} acetic acid, which was adjusted to a pH of 4.5 prior to use.

v. Au HMS: The deposition and reduction method (methanol / formaldehyde reduction method) was as follows. 1.0 mL of 0.3004 M $Na[AuCl_4]$ + 0.60 mL of ultra pure water + 0.80 mL of methanol +1.60 mL formaldehyde were mixed. 1.0061 g of HMS (prepared as specified by Zang et al., 1997) was mixed thoroughly with 1.0 mL of reduction solution and followed by drying the sample in an oven at 100 ºC for 1 h to initiate primary seeding of Au. The sample was allowed to cool down and the rest of the 3.0 mL of the reduction solution was added. It was then kept at room temperature for 24 h. The colour of the sample was yellow at this stage. It was then subjected to heat again at 100 ºC for 2-3 h, but no colour change was observed. Then it was heated at 350 ºC in a furnace for 4 h. The sample turned reddish pink in colour.

vi. Pt HMS carbonized and Pt MCM-41 carbonized: The mesoporous substate was prepared as is specified in Chapter 3. The Pt containing electrocatalyst denoted Pt HMS carbonized and Pt MCM-41 carbonized were prepared by an incipient wetness impregnation procedure as follows: A solution of 0.1545 M H_2PtCl_6 was prepared using 1.00 g H_2PtCl_2/12.5 mL H_2O to give a 0.1545 M solution. 1 mL of this solution was impregnated into 1.0031 g HMS zeolite as well as 1.0054 g MCM-41 zeolite. The slurry formed was stirred at 80 ºC until

dry. Pt reduction was achieved as follows: 1.0081 g of MCM-41 and 1.0005 g of HMS impregnated with the Pt solution were reduced as follows: 0.8 mL methanol and 1.6 mL formaldehyde (37-41 % solution) were mixed. The above masses of the zeolites were submerged in 1.0 mL plating solution each for 1 h to initiate platinum seeding (this was done at room temperature). The samples were then dried at 100 ºC for 1 h. The samples were kept at room temperature for one day and then heated to 100 ºC for 1 h. The samples were then cooled, thoroughly rinsed and then dried at 80 ºC.

5.6.2 METHODS

The materials mentioned above were utilized to make electrodes in the manner explained below. The block diagram (Figure 5.1) schematically shows the sequential deposition procedure for fabricating the composite nanophase electrodes including characterization and the activity testing.

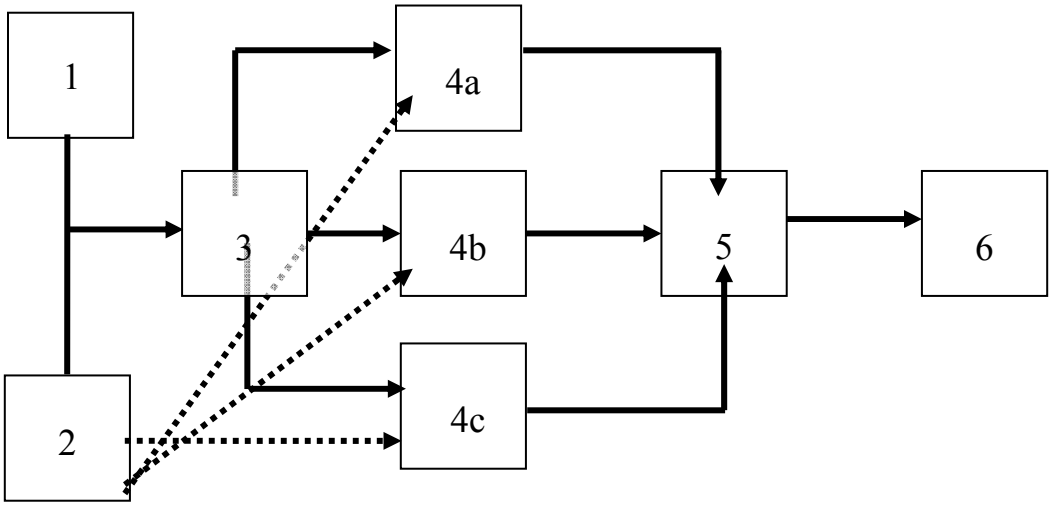

Figure 5.1 Block diagram of the sequential deposition procedure

1. Preparation of nanophase electrocatalyst (supported or unsupported)
2. Support preparation
3. Ink preparation
4. Supporting procedures (a, b, c, etc.)

5. Characterization
6. Electrochemical testing

Each of the steps in the process of sequential deposition for fabricating the composite nanophase electrodes including characterization and the activity testing is described in the results section below.

5.6.2.1 Preparation Of Nanophase Electrocatalysts

Unsupported nanosized $SbSnO_2$ and Pt on carbon based electro commercial catalysts as listed in Section 5.6.1.5 were purchased. Supported Au, Pt and Ni-Pd nano particles were prepared as specified in section 5.6.1.5. A summarized supporting procedure was generally: The metal solutions of interest (e.g. Au, Pt) were impregnated into various micro or mesoporous zeolitic supports (FAU, HMS, MCM-41) and reduction was performed by thermal reduction, methanol formaldehyde or by a sodium hypophosphite method (Petrik, 2003). These materials were not extensively characterized, except by TEM. In some cases, where specified, the supported nanophase catalyst was thereafter carbonized by carbon sputtercoating or by CVD using LPG (Petrik et al, 2008) in order to ensure good conductivity and connectivity between the Si matrix and the carbon black used as conductive phase in the ink formulations (Section 5.6.2.3).

5.6.2.2 Support Preparation

Different electrode substrates (Table 5.2) were used as the electrocatalyst containing film support, and cut into appropriate size before use. The weights of these substrates were recorded before and after deposition of the ink. The substrate by itself or the formed composite electrode was connected to the power source via electrical leads and clips and tested electrochemically.

5.6.2.3 Ink Preparation

The ink was typically prepared by mixing Nafion® ionomer solution, carbon black and the nanophase catalyst in a solvent or solvent/water to make an ink. The mixture

was placed in an ultra sonic bath for 5 min - 1 h and then magnetically stirred overnight. The ink formulations were optimized with reference to catalyst type, catalyst loading, proton and electron conductive phases, binder type, and solvents. All inks with or without catalysts were prepared in the following manner.

The amount of carbon black (conductive phase Carbon black Cabot Botlek BV; grade: n Vulcan x C72; sample no.: GP3784) usually 40 % of the total mass without catalyst (or 20 % of total mass in the case where a catalyst was added) was weighed out. Thereafter the catalyst (usually 20 % of the mass of solids) was weighed and added to the carbon black and mixed by grinding. The appropriate amount of solvent was added. In many cases this was ultra-pure water. Thereafter the binder solution (usually 60 % of total mass of ink formulation) was added, which was Nafion® (5 % solution) in some cases. Then the mixture was placed in an ultrasonic bath for 30 – 60 min to disperse the particles and form a homogenous ink. The ink was magnetic stirred until use to prevent precipitating of the particles. The compositions of the different micro-emulsions or inks used in this study are presented in various tables in the result section in conjunction with the results for electro activity testing.

5.6.3 Supporting Procedure

The different supporting procedures that were used to prepare composite electrodes, namely casting, dip and sponge coating, hotpressing, and spray coating, are described in this section. Nanoparticles of Sb/SnO were used, as an example of processing non-supported nanophase particulates in electrocatalyst containing film format. Pt-FAU, Au –HMS, Pt- HMS and Pt MCM-41 were applied as examples of processing supported nanophase materials in electrocatalyst containing film format.

5.6.3.1 Casting method

A casting procedure was investigated using the following ink mixtures:

i) Polyvinylacetate was dissolved in acetone with carbon black

ii) Polystyrene was dissolved in toluene with carbon black and Sb/SnO

iii) Nafion® and carbon black

i) *Casting method using Polyvinylacetate and acetone with carbon black*

1 g of Polyvinylacetate was dissolved in 25 mL of acetone. 0.5 g of carbon black conductive phase (Source: Cabot Botlek BV; grade: m Vulcan x C72; sample no. GP3784) was mixed into 10 mL of this solution. The mixture was placed in the ultra sonic bath for 30 min, and then magnetically stirred until used.

ii) *Casting method using Polystyrene and toluene with Carbon black and Sb/SnO*

Carbon black:

1 g Polystyrene was mixed into 20 mL toluene [$C_6H_5CH_3$: FW 92.14] and stirred for 1 h to dissolve. 0.5 g Sb/SnO and 0.5 g Carbon black (Source: Cabot Botlek BV; grade: m Vulcan x C72; sample no.: GP3784) were mixed into 10 mL of this solution and placed in an ultrasonic bath for 30 min and the mixture was then stirred magnetically until used.

Carbon black and Sb/SnO

0.5003 g of commercial antimony tin oxide (Sb/SnO) and 0.5007g of Carbon black were weighed and mixed with 20 mL of polystyrene solution (20 mL of toluene and 1.0141 g of polystyrene). The mixture was placed in an ultra sonic bath for 30 min, and then magnetically stirred for 3 h.

iii) *Casting method using 50% of Nafion® and 50% Carbon black*

0.5464 g of Nafion® (Liquion 1100 5wt % Nafion® 1100 EW solution), and 0.5071 g of hydrophilic carbon black (Source: Cabot Botlek BV; grade: m Vulcan x C72; sample no.: GP3784) was weighed respectively and mixed with 10 mL of ultra-pure water. The mixture was placed in the ultrasonic bath for 30 min, and then magnetically stirred until used.

The following casting procedure was used with the prepared ink mixtures. A stainless steel template was manufactured that had exactly sized wells into which exactly sized (2 cm^2) portions of the different support substrates were placed. A precision standard

weighing balance was used to weigh the same amount of ink onto all of the substrates, about 0.55 g of ink was cast onto all of the substrates by using a pasteur pipette. The electrodes were placed in the oven for 30 min at 100 °C to cure the electrode and remove solvents or water.

5.6.3.2 Dip coating and sponge coating

The six different substrates (*a-f*) listed in Table 5.2 were dip coated with the appropriate ink mixture or the ink was sponged upon each respective substrate. The following procedure was followed for the preparation of ink for dip coating or sponging on various substrates. 2.1126 g of Carbon black (Company: Cabot Botlek;Grade: Vulcan xc 72, Sample No: GP 3789 [http://wl.cabot-corp.com/index.jsp]), 5.9460 g of 15 % Nafion® (15 wt% ; 1100 EW solution) and 10.2398 g of water were mixed together. The above mixture was put in an ultrasonic bath for 40 min and then stirred magnetically overnight. The mixture was then divided in two; to one half 2.1375 g Sb/SnO catalyst was added to the mass of the carbon black (denoted N/CB/SnO). (The other half portion without catalyst was denoted N/CB). A further 30 g of water was added to each of the mixtures as the ink initially formed too viscous a slurry. The various substrates were dipped into the appropriate mixture or the inks were sponged upon each respective substrate then dried at room temperature and further dried in an oven at 80 °C overnight. The electrodes were then weighed to determine the increase in mass.

5.6.3.3 Hot pressing preparation technique

Polytetrafluoroethylene (PTFE) was used as binder in the hot pressing technique as PTFE is chemically resistant, incombustible and insoluble in all known solvents, being attacked only by molten alkali metals and by fluorine at high temperatures. PTFE may be used up to 260 ºC. It may be shaped by compression and sintering where its chemical stability and non-wettability make it suitable for use in extreme circumstances. Therefore PTFE particles were used as a binder by mixing them with carbon black and grinding the mixture to its finest state, applying the finely ground mixture onto the substrate and then hotpressing using an Adendorff pneumatic press

with built in heating stage. Various combinations of conductive phase, binder and catalyst were hot pressed onto two different support types (*e* and *g*). In particular, 50 % PTFE binder (C) was pressed in an area of 1 cm^2 with 50 % Carbon Black as conductive phase and in some cases with additional Sb/SnO catalyst. Conditions of hot pressing that were investigated, varied between 150-160 °C, for 2-10 min at 0-20 bars upon a ceramic based support (*e*). Upon support *g* (a Teflon membrane), conditions were varied between 130 and 180 °C for 2 to 3 min at 20 to 41 bar pressure with and without Sb/SnO nanophase catalyst.

5.6.3.4 Spray Coating

Spray coating (with Badger air-brush 150TM) was used to coat the chosen substrates with the catalytic ink. In order to spray the same amount of ink upon all the substrates, a pipette was used to measure the amount of ink to be sprayed upon each of the substrates (about 1 mL of ink) into the well of the airbrush. The electrodes were dried at room temperature or with a jet of hot air and weighed to determine the increase in mass.

In general, a polymeric resin binder was mixed with either 10 mL of toluene or in the case of Nafion®, water, and stirred until dissolved. Thereafter, a portion of this solution was added to a mixture of hydrophilic carbon black (Source: Cabot Botlek BV; grade: m Vulcan x C72; sample no.: GP3784) and a nanophase particulate or supported catalyst (when used). A slurry was thus formed, which was mixed to uniformity in an ultrasonic bath for 10 to 30 min. The slurry was spray coated onto various support substrates chosen from Table 5.2 above using an airbrush with N_2 as carrier. The spray coated samples were dried at 90 °C for 4 hr and the thus formed composite electrodes were then applied in electrochemical tests. The different inks prepared and sprayed included:

i. 60 % Nafion® and 40 % Carbon black
ii. 60 % Nafion®, 20 % Carbon black and 20 % Antimony tin oxide (Sb SnO)
iii. 60 % Nafion®, 20 % Carbon black and 20 % Pt zeolite
iv. 60 % Nafion®, 20 % Carbon black and 20 % Ni-gamma alumina

v. 10 % Polystyrene + 90 % Carbon black mixed in 10 mL of toluene.

vi. 50 % Polystyrene, 25 % Carbon black and 25 % Pt zeolite

Details of different preparation conditions of composites prepared by sequential deposition are summarized below and listed in Tables 5.4 to 5.8

i) Ink preparation using a mixture of 60 % Nafion® and 40 % Carbon black

0.6473 g of Nafion® solution and 0.4040 g of hydrophilic carbon black (Source: Cabot Botlek BV; grade: m Vulcan x C72; sample no.: GP3784) were weighed and mixed in 10 mL of ultra-pure water to prepare the ink. The mixture was placed in the ultrasonic bath for 1 h and then magnetically stirred overnight. Spray coating with an airbrush was used to coat the substrates. In order to spray the same amount of ink upon all of the substrates, a pipette was used to measure the amount of ink to be sprayed upon each of the substrates (about 1 mL of ink). A electrocatalyst containing layer of ink was sprayed, air dried and weighed. This was repeated until the required mass increase was obtained. The electrodes were dried at a room temperature overnight. Thereafter the electrodes were tested for hydrogen production.

ii) Ink preparation of 60 % Nafion®, 20 % Carbon black and 20 % Antimony tin oxide (Sb/SnO)

0.6270 g Nafion® solution, 0.2163 g carbon black and 0.2158 g of Sb/SnO were mixed with 10 mL of ultra-pure water. The ink preparation and spraycoating procedures were the same as in the case of 60 % Nafion® and 40 % carbon black.

iii) Ink preparation for 60 % Nafion®, 20 % Carbon black and 20 % Pt zeolite

0.6048 g Nafion®, 0.2164 g carbon black and 0.2031 g of Pt zeolite were mixed with 10 mL of ultra-pure water. The ink preparation procedure was the same as the above for 60 % Nafion®, 20 % carbon black and 20 % SnO. The procedure of preparing the ink with nickel supported on gamma alumina was the same as that used with the platinum zeolite and Nafion®. The mass of Nafion® used was 0.6133 g, the mass of Ni gamma alumina was 0.2059 g, and the mass of Carbon black was 0.2029 g.

iv) 10 % Polystyrene + 90 % Carbon black mixed in 10 ml of toluene - as in (i).

v) Ink preparation for 50 % Polystyrene solution, 25 % Carbon black and 25 % Pt zeolite

0.5051 g of polystyrene was mixed with 20 mL of toluene to make a solution. Typically 0.25 g of carbon black and 0.25 g of Pt zeolite (or other catalyst) were added into the polystyrene solution to make the ink, which was used for coating the substrates. The ink was placed in an ultrasonic bath for 1 h and then magnetically stirred overnight. Spray coating was used to coat the substrate. About 1 mL of ink was used to spray each of the substrates to make electrodes. A layer of ink was sprayed, air dried and weighed. This was repeated until the required mass increase was obtained. The electrodes were dried at room temperature overnight. Thereafter the electrodes were tested for hydrogen generation.

5.6.3.5 Characterization

Micro and mesoporous electrocatalysts presented in this chapter were characterized mainly by TEM as these materials were prepared using techniques that are well known in gas phase catalysis to result in monodispersed or nanoparticles of Pt or Au. Their application as electrocatalysts is novel. Physical-chemical and structural studies of gas diffusion electrode materials were performed in selected cases using techniques such as optical microscopy, PIXE, and SECM as is described in Chapters 3, 6 and 7. This chapter mainly focuses on characterization of the electrode electrochemical characteristics tested in water electrolysis.

5.6.4. Electrochemical Testing

The electrolysis reaction in an alkaline environment is schematically shown in Figure 5.2 (a) and a schematic of two electrode cell setup for hydrogen production is shown in Figure 5.2 (b).

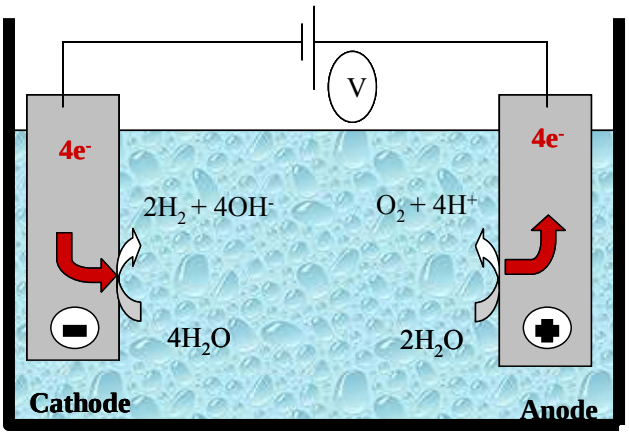

(a) electrolysis reaction in an alkaline environment

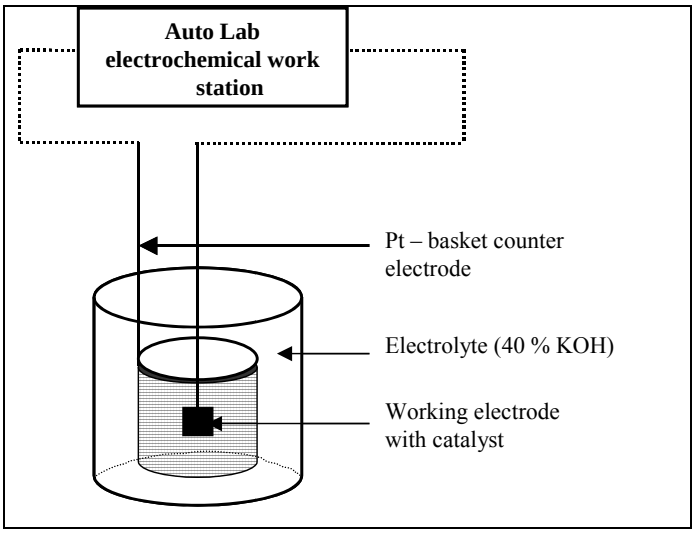

(b) schematic of two electrode cell setup for hydrogen production

Figure 5.2 Water electrolysis in a high electrolyte environment

The activity of the electrodes was tested using a two electrode electrolytic system. Each substrate or composite electrode prepared in the manner specified above, was cut into an approximately 2 cm^2-sized electrode. Stainless steel, corrosive free electrode clips were attached to the electrode and the electrode was masked with vinyl adhesive tape in order to limit the geometric surface area tested to an exactly sized 1 cm^2 of high surface area composite electrode for comparative purposes. The electrode was suspended in 40 % potassium hydroxide (KOH). This working electrode was then clamped with the high surface area of the electrode 1 cm away from and facing toward the counter electrode. A large surface area circular basket Pt

counter electrode was used. All the experiments were performed at 0 to 5 ^{o}C while stirring magnetically after purging with N_2. The temperature was controlled by placing the cell in an ice bath and controlling the temperature with a thermometer. In order to determine the prepared electrode's activity for hydrogen production by water electrolysis, electrochemical analyses was performed on each sample by use of chrono amperometry. Each high surface area sample was subjected to an applied potential in steps from -1 to -6 V over 60 s in which the potential was increased in preset steps at the end of each time interval, at which time the average current was sampled in order to determine the response of the electrodes over time. A qualitative comparison of activity for water electrolysis was made between the electrodes. Figure 5.3 shows a schematic of the two electrode cell setup for hydrogen production. The setup is connected to the Auto lab electro chemical station.

5.7 RESULTS AND DISCUSSION

Composite electrode preparation procedures were used and details of the outcomes of sequential deposition and the results of characterization of electrocatalysts, electrodes and electro-activity testing are presented in this section.

SEM micrographs of the electrocatalysts applied in this Chapter are shown in Figure 5.6 (a to e).

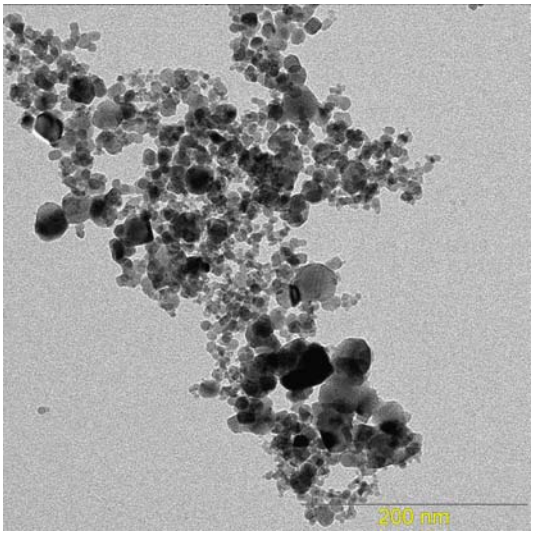

Figure 5.3 TEM micrograph of Sb/SnO commercial nanoparticles

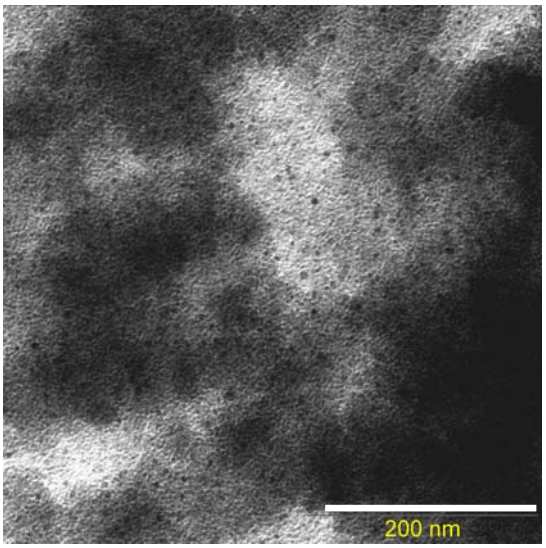

Figure 5.4 TEM micrograph of Pt HMS LPG carbonized

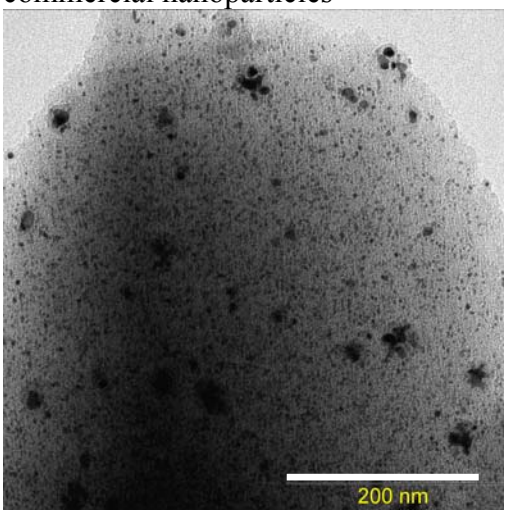

Figure 5.5 TEM micrograph of Pt MCM-41 LPG carbonized

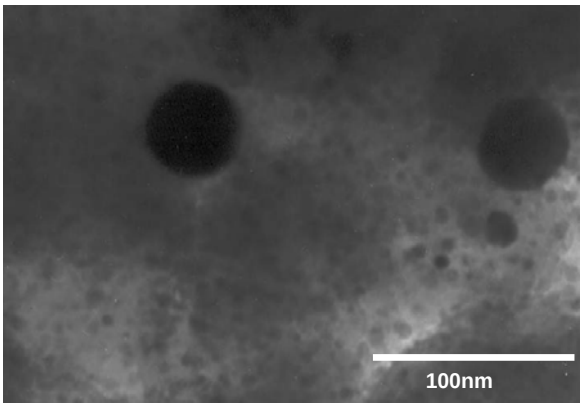

Figure 5.6 TEM micrograph of Au HMS

Nanoparticles of Sb/SnO were used in preparation of films, as an example of processing non-supported nanophase particulates in film format. Pt FAU, Au HMS, Pt HMS and Pt MCM-41 were applied as examples of processing supported 3-dimensional nanophase materials, with high surface areas and high porosity, into electrocatalyst containing films. In the case of commercial Sb/SnO nanoparticles (Figure 5.6 (a)) an average particle size of 27 nm was observed by TEM. For Pt HMS (Figure 5.6 (b)) very small and well dispersed sub- nanometer Pt particles were obtained. Well dispersed Pt nanoparticles were also obtained in the case of Pt-MCM-41 (Figure 5.6 (c)), however, some cluster formation was visible. The difference

observed could be due to the pore structure of the mesoporous matrix which differs. HMS has a wormhole structure with pore sizes in the 2-3 nm range (Zhang, 1997) whereas MCM-41 has a pore size between 2 and 5 nm (Grün et al., 1999; Mastalir et al., 2008). The agglomeration of supported nanophase was more pronounced in the case of AuHMS reduced thermaly that resulted in bimodal distribution of gold nano particles of sizes about 5 nm (well dispersed) and 50-100 nm (large agglomerated particles) in Figure 5.6(d). This agglomeration may be caused due to the reduction temperature used. Average particle sizes for the Pt in Pt HMS and Pt MCM-41 were calculated by XRD line broadening using the Scherrer equation and found to range from 3.5 to 3.7 nm respectively.

5.7.1 Electro activity of composite electrodes: Baseline studies

The electro activity results obtained in this section represent a comparison of the electrochemical response of the composite materials that was determined by the current density (A cm^{-2}) obtained at each applied potential (V) in water electrolysis for hydrogen production, mainly in 40 % KOH electrolyte, at 0 ºC unless stated otherwise.

Because of the three dimensional nature of the prepared composite electrodes, it is necessary to remember that activity data presented in the results section have not been normalized for active surface area, but are based on a geometric 1 cm^2 of composite electrode unless otherwise stated, therefore the results of rapid screening in the high electrolyte environment are qualitative.

It is again emphasized that hydrogen production by water electrolysis in an alkaline electrolyte environment was used as a simple and relatively rapid qualitative measure of the electro catalytic activity of the nanophase electrocatalysts in this composite format. Poor catalytic performance for hydrogen production was taken as a measure of the possible occlusion of catalytic sites by binders or the lack of adequate conductive pathways and was used as rapid indicator for optimization of formulations

of micro-emulsions or inks. The expected high gas evolution under the applied conditions was used as an accelerated aging test of the stability and durability of the composite electrode components. Delamination of the catalytic component during high gas evolution at the high applied potential was used as a measure of inadequate stabilization of the electrocatalyst containing film upon the substrate.

In baseline studies, the commercial JM Pt_{40}/C, as well as the different substrates listed in Table 5.3 and various Ni materials were tested in the high electrolyte environment. In the case of the commercial JM Pt_{40}/C, ink formulations were prepared as specified in Table 5.4.

Table 5.4 Ink formulations using JM Pt_{40}/C catalyst

Sample name	Carbon black	Nafion (5%)	JM Pt_{40}/C
Sample H		0.1012	0.0305
Sample H1		0.0945	0.0346
Sample I		0.0578	0.0330
Sample I1		0.059	0.0349
Sample J	0.0135	0.0906	0.0331

In these formulations prepared in duplicate, the ink firstly consisted of only JM Pt_{40}/C and Nafion® (5 % ionomer soln) at different concentrations (Samples I, I1 and H, H1 respectively). In the second case Nafion® (5 % ionomer soln) and JM Pt_{40}/C were mixed with carbon black (sample J).

These mixtures were spraycoated on a carbon cloth substrate (*b*) as specified in Table 5.3 and dried. Excessive catalyst loading in a film may have the effect of lowering of the conductive particle volume fraction below the percolatory threshold. However, as the commercial Pt catalyst is supported on carbon it is unlikely that this would be the case. Nevertheless, the carbon black was added in the ink applied in Sample J to verify if it would make a contribution to the electro activity of the electrocatalyst containing film.

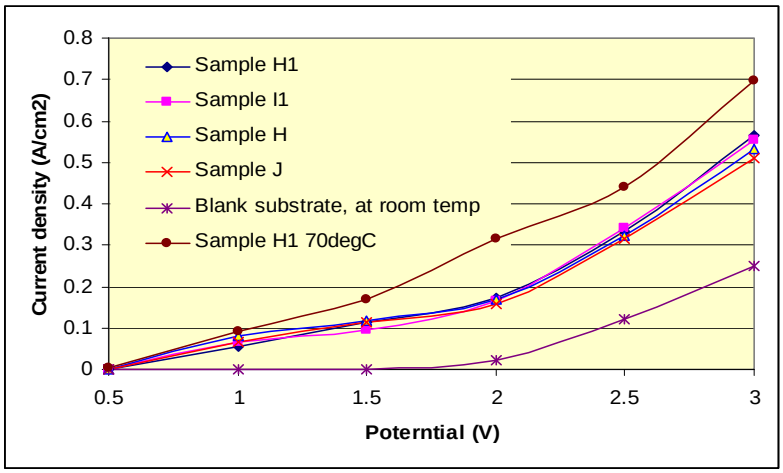

Figure 5.7 Baseline study of composite electrodes prepared with commercial JM Pt_{40}/C catalyst*
*40% KOH electrolyte environment at RT or 70ºC and applied potential between -1 and -3V

PLEASE NOTE that although negative potentials were applied, the results are presented on a positive axis for ease of reference in most figures presented in this chapter.

Fairly good and reproducible current densities of over 0.5 A cm^{-2} were obtained at -3 V at room temperature with the electrocatalyst containing film composite electrodes prepared with the commercial catalyst, compared to the blank substrate (Figure 5.7). Activation was observed below an applied potential of -2 V. Increasing the temperature (70 ºC) gave a higher current density as expected for composite sample H1 to 0.7 A cm^{-1} at -3 V. The electronic conduction may have been assisted by the other components in the composite electrode such as the carbon support, but the effect of the Nafion® binder and carbon black conductive additive was apparently minimal, even though the binder content was nearly halved in the formulation used for samples I and I1, and a significant amount of carbon black was added to the formulation used in Sample J.

Prior to deposition of electrocatalyst containing films of ink composed of binder, conductive phase and electrocatalyst, the various substrates (Table 5.3) that were used as gas diffusion electrode support substrates were tested for their

electrochemical response during chronovoltammetry of an applied voltage between -1 and -6 V for water electrolysis in a 40 % KOH high electrolyte environment at 0 ºC (Figures 5.8). The lower temperature was applied in the following experiments because of the high outputs anticipated and because of the limitation of the electrochemical workstation of 1 A output, as well as to avoid any fluctuations in room temperature that could affect results and because of the difficulty of maintaining the electrolyte concentration at raised temperatures. Results at the lower temperature of 0 ºC are thus expected to be lower than in the baseline study with commercial $JMPt_{40}/C$ which was obtained at room temperature or 70 ºC. The baseline testing was performed to understand the suitability of various commercial substrates. It was taken into account that electrochemically active substrates could cause delamination of the catalytic ink in film form, because of gas evolution on the underlying substrate, hence high electrochemical response was an indicator of potential unsuitability of that substrate as film support.

Commercial Ni metal foil and several commercial Ni foam samples were also tested under identical conditions as the selected substrates between an applied potential of -1 and -6 V in order to provide a comparison of activity of commercial substrates with the selected support substrates and composite electrode materials to be tested. Comparison of electrochemical activity of various types of Ni materials used is shown in Figure 5.9.

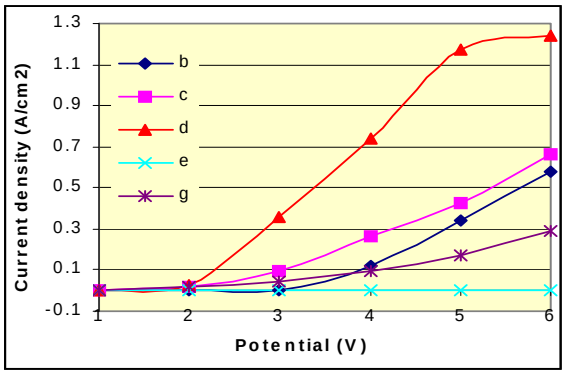

Figure 5.8 Electrochemical activity of blank supports b-g *

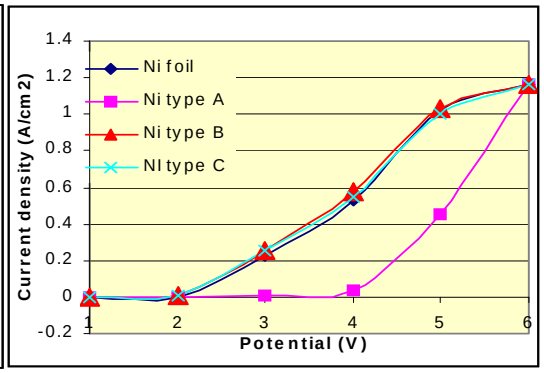

Figure 5.9 Electrochemical activity of various types of Ni metal foam*

*40% KOH electrolyte environment at 0ºC and applied potential between -1 and -6 V

The results determined above a current density of 1 A are inaccurate due to limitations of the electrochemical workstation. None of the substrates that were tested showed activation below an applied potential of -2 V (Figure 5.8). The slight electrochemical response observed for non-conductive substrates *e* and *g*, ceramic paper and Teflon (PTFE) respectively, gives an approximate measure of the electrical contribution of electrode contacts and metallic clips for lead attachments in contact with the electrolyte. Since this was a negligible amount even at high current densities this contribution was not further taken into account. Substrate *d* (Creavis; ZrO_2 on stainless steel mesh) showed a strong electrochemical response (Figure 5.8) above an applied potential of -2 V, increasing to a current density of more than 1A cm^{-2} at -5 V, similar to Ni foil and two of the three Ni foams (Racemat) that were tested (Figure 5.9), and was thus likely to be unsuitable as substrate for supporting a stable thin film because of its intrinsic high activity for the hydrogen evolution reaction (HER) at higher applied potential.

The substrates (Figure 5.8) and different Ni metal samples (Figure 5.9) themselves showed no activation below an applied potential of -2 V but some of the Ni metal foam samples were generally capable of high current densities at an applied potential of -5 to -6 V. Although Ni foam samples have highly enhanced surface areas, the surface integrity of the metal foam bubbles prevented access of the electrolyte to the interior surfaces of the foam structure, thus these materials proved not to be much more active than Ni foil by itself under the applied conditions.

The rate at which hydrogen ions are transformed into hydrogen gas is a function of the rate of electron transfer from a metal to hydrogen ions and as there is a wide variability in this transfer rate of electrons by various metals, the rate of hydrogen evolution from different metal surfaces can vary greatly (Tafel, 1905). In the case of the Ni electrodes, it should be considered that the exchange current density (j_0) of Ni is orders of magnitude higher than that of Pt. As there was no reference electrode

used relative to the NHE in this rapid screening system, it is thus not possible to directly compare the activity towards HER of different metals and substrate types.

Studies by Kuch et al. (1993) showed that water adsorbs without dissociation upon a pure Ni single crystal surface whereas when oxygen is present above about 0.33 monolayers, NiO islands are formed which grow laterally into a closed epitaxial NiO-layer. When the oxygen coverage is large enough for NiO islands to be formed, a part of the water adsorbs dissociatively (OH+H). With the growth of NiO-islands, the amount of dissociated water increases (Kuch et al. 1993; 1994). The differences observed in the activity of the Ni substrates could thus be due to differences in the oxide coverage on the Ni Type A substrate surface compared to the other Ni electrode samples affecting the rate of dissociation of water.

5.7.2 Electro activity of composite electrodes: Effect of Supporting Procedures

5.7.2.1 Dip coating and sponge coating

The six different substrates (*a-f*) were dip coated with the ink mixture or the ink was sponged upon each respective substrate. The samples were then weighed to obtain the total mass % increase as is shown in Table 5.5.

Table 5.5. Mass % increase of dip coated and sponge coated substrates

Support type	Dip coated (N/ CB)	Sponge coated (N/CB)	Dip coated (N/CB/SnO)	Sponge coated (N/CB/SnO)
a	42.0 %	35.99 %	69.23 %	60.60 %
b	28.26 %	14.36 %	54 %	59.4 %
c	33.55 %	34.55 %	67.52 %	70.33 %
d	2.55 %	1.66 %	6.64 %	7.22 %
e	2.75 %	0.3 %	6.43 %	5.79 %
f	13.43 %	9.06 %	30.08 %	22.88 %

As the variable mass % increase results tabulated above show, neither dip coating nor sponge coating allowed for reproducible preparation of uniform composites, although the effect of the support surface interaction with the ink is apparent in the % loading obtained. Support *e* (Ceramic paper: Lydall Technical Papers: Sample: 3000LF) was least prone to accept deposition of an electrocatalyst containing film whereas the different carbon cloths (*a, b* and *c*) allowed relatively high loadings of ink to be obtained. The substrate *f* (Ceramic paper 40 % glass) showed an intermediate uptake. Significantly higher loadings were obtained in all cases where the particulate nanophase Sb/SnO was added, showing the significant effect of the viscosity of the ink, due to a higher percentage of solid particulates, on the degree of loading obtainable by these two methods.

The different electrodes made using various substrates were tested for activity for hydrogen production and results for dip coating and sponge coating are shown in Figures 5.10 and 5.11 respectively.

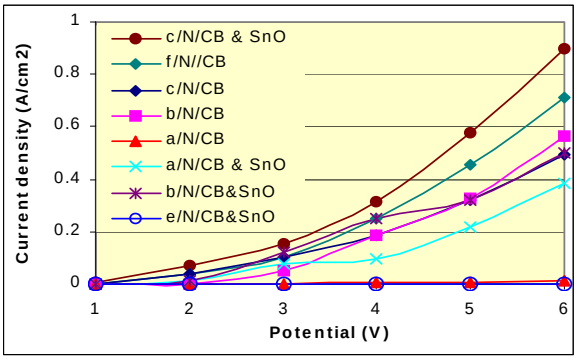

Figure 5.10. Composite electrodes prepared by dipcoating various substrates in Nafion®/CB or Nafion®/CB/SbSnO mixtures*.

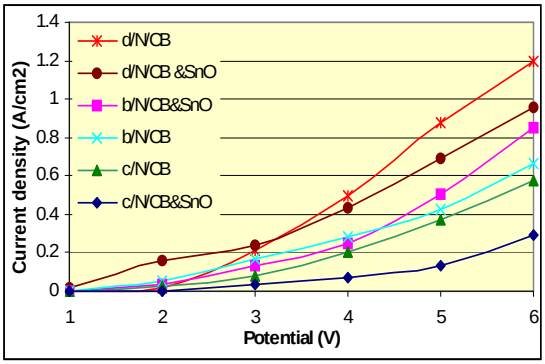

Figure 5.11. Composite electrodes prepared by sponge coating various substrates in Nafion®/CB or Nafion®/CB/SbSnO mixtures*.

*40% KOH electrolyte environment at 0ºC and applied potential between -1 and -6 V

Almost all these combinations showed some activation below -2 V. Relatively high current densities were obtained for several combinations of support, binder, catalyst and conductive phase using dip coating and sponge coating as ink deposition method, and a current density of <0.2 mA cm^{-2} was also observed below -2 V for most of these combinations, unlike in the case of the Ni foils and substrates, where no current

output was observed below -2 V. In some cases the additional electrocatalyst containing film reduced the activity of the substrate itself at high potentials (e.g. substrate *d*). Results for electrochemical activity were combination specific and showed that addition of the commercial nanophase Sb/SnO may have enhanced the observed activity in some combinations (c/N/CB&SnO and a/N/CB & SnO) or increased the current density at lower voltages (d/N/CB &SnO). Moreover, the conductive substrates (*b*, *c* and *d*) used as supports had a considerable effect upon the activity observed. Although low loadings were deposited by spongecoating on substrate *d*, combination d/N/CB & SnO showed the highest current density at -2 V.

It was interesting that activity could be enhanced in several cases by merely enhancing the substrate surface area with the application of conductive carbon suspended in a binder even in the case where the substrate was non-conductive (f/N/CB). The fact that electrodes were able to withstand the very high degree of gas evolution at the applied potential of -6 V showed that even under these aggressively accelerated testing conditions the inks made with Nafion® as binder were stable and relatively durable. Neither dip coating nor sponge coating was pursued as suitable ink deposition method because of the lack of reproducibility. Although these results are merely qualitative, they indicated that the observed activity for water electrolysis of such composites electrodes could be affected by the presence of the additional conductive phase such as carbon, the additional nanophase, the degree of loading and by the substrate used.

5.7.2.2 Casting method

A casting procedure was used. The materials are tabulated in Tables 5.6 and 5.7 and a summarized outcome of the integrity of the composite made by each preparation method is added as a comment where necessary, in tabular form.

Table 5.6. Casting method using ink with 10 % Polystyrene binder (B) + 90 % Carbon black in 10 mL of toluene as solvent on various supports.

Sample no.	Support type	Support mass	Binder B mass (g)	Carbon Black (g)	Comments
a/B/CB	a	0.0226	0.1064	0.9084	Composite samples were completely cracked when dried thus were not tested.
b/B/CB	b	0.0333	0.1064	0.9084	
c/B/CB	c	0.0212	0.1064	0.9084	
d/B/CB	d	0.1005	0.1064	0.9084	
e/B/CB	e	0.1038	0.1064	0.9084	
f/B/CB	f	0.0857	0.1064	0.9084	

Table 5.7 Casting method using ink with 50% Polystyrene binder (B) + 25% Carbon Black + 25% SbSnO with solvent toluene (20 mL) on various supports.

Sample no.	Support type	Support mass	Binder B (g)	Carbon Black (g)	Sb/SnO (g)	Comments
a/B/CB &SnO	a	0.0234	1.0141	0.5007	0.5003	Ink deposited smoothly
b/B/CB &SnO	b	0.0359	1.0141	0.5007	0.5003	Ink deposited smoothly
c/B/CB &SnO	c	0.0207	1.0141	0.5007	0.5003	Ink deposited smoothly
d/B/CB &SnO	d	0.0965	1.0141	0.5007	0.5003	Ink cracked when dry
e/B/CB &SnO	e	0.1081	1.0141	0.5007	0.5003	Ink deposited smoothly
f/B/CB &SnO	f	0.0887	1.0141	0.5007	0.5003	Ink cracked when dry

Electrodes prepared by the casting technique were evaluated for electrochemical activity in water electrolysis in the two electrode set up at 0-5 ºC in 40% KOH and results of the current densities achieved at the applied voltages between -1 and -6 V are shown in Figures 5.12 and 5.13.

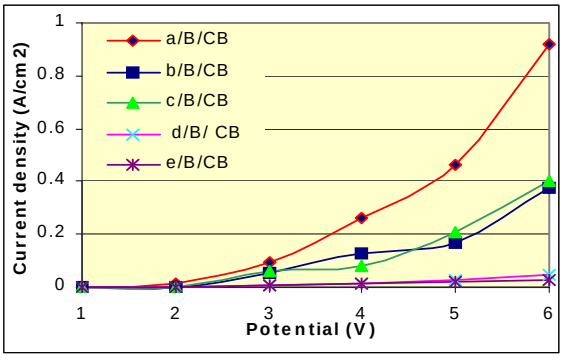

Figure 5.12 Composites cast with 50 % Polystyrene binder, 50 % carbon black in toluene upon different support types*

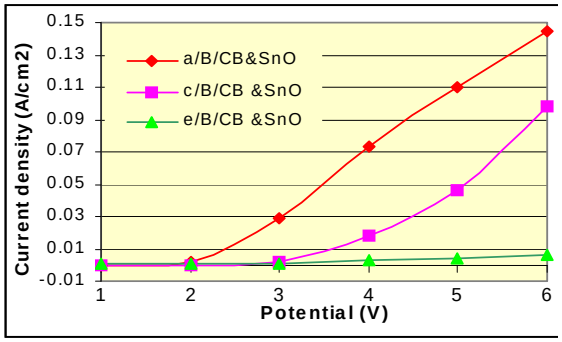

Figure 5.13 Composites cast with 50 % Polystyrene binder, 25 % Sb/SnO 25 % carbon black in toluene: supports a,c&e*

*40% KOH electrolyte environment at 0ºC and applied potential between -1 and -6 V

Composites cast with 50 % Polyvinylacetate binder and 50 % carbon black in acetone on three support types were also prepared (results not shown) and showed

intermediate activity compared to that of the polystyrene binder and carbon black combination. The effect of the conductive substrate could be distinguished in the activity observed at higher applied voltages. None of these electrodes showed activation below -2 V. Higher current densities were observed at high applied potential particularly for cast electrodes prepared using substrate *a*, (Carbon black on carbon cloth (code 6100-200 CB) supplier Lydall) with polystyrene as binder and carbon black as conductive phase without additional catalyst. Low current density was observed for cast electrodes prepared with inks, in cases where additional Sb/SnO catalyst was added, indicating high resistance with excessive loading of the particulate oxide and the probable lowering of the conductive particle volume fraction below the percolatory threshold. The layers deposited upon the electrodes by casting were stable at high applied potentials. Crack formation was observed when the electrodes prepared by casting were completely dry. It was concluded that crack formation could be caused by the different coefficients of expansion between the layers of the catalyst/binder and support resulting because too thick a film was deposited upon the substrate and excessive shrinkage occurred during drying when using the casting method, therefore hot pressing and spray coating methods were investigated.

5.7.2.3 Hot pressing preparation technique

A hot pressing method was used to hot press various combinations of conductive phase, binder and catalyst onto two different support types (*e* and *g*). Details of preparation procedures and outcomes are tabulated in Tables 5.8, 5.9 and 5.10.

Table 5.8 Hot pressing method with 50 % PTFE binder (C) + 50 % Carbon Black as conductive phase upon a ceramic based (e) support.

Substrate	Temp (°C)	Pressure (bars)	Time (min)	Carbon black	Binder C	Comments
(*e*)	150-160	5	5	50 %	50 %	Mixture adhered/support broke
	150-160	0	6	50 %	50 %	Mixture adhered/support broke
	150-160	0	10	50 %	50 %	Mixture adhered/support broke
	150-160	20	2	50 %	50 %	Support broke completely
	150-160	10	2	50 %	50 %	Support broke completely
	150-160	5	2	50 %	50 %	Mixture adhered/support broke

Table 5.9 Hot pressing method with 50 % PTFE (C) binder + 50 % Carbon Black as conductive phase upon a Teflon based (g) support

Substrate	Temp (°C)	Pressure (bars)	Time (min)	Carbon black	Binder C	Comments
Teflon (*g*)	130	10	2	100 %	-	Carbon black adhered to support
	130	10	2	50 %	50 %	Mixture adhered to support
	150	12.5	2	100 %	-	Carbon black adhered to support
	150	12.5	2	50 %	50 %	Mixture adhered to support

Table 5.10 Hot pressing at elevated temperature with 50 % PTFE (C) + 50% Carbon Black as conductive phase upon a Teflon support (g)

Substrate	Temp °C	Pressure (bars)	Time (mins)	Carbon black	Binder C	Comments
Teflon (*g*)	165-170	20	2	50 %	50 %	Mixture adhered to the support in all cases
	175-180	21	2	50 %	50 %	
	175-180	30	2	50 %	50 %	
	175-180	40	3	50 %	50 %	

Table 5.11 Hot pressing at elevated temperature with 50 % PTFE, 25 % C/ black and 25 % Sb/SnO nanophase catalyst on a Teflon support (g).

Substrate	Temp (°C)	Pressure (bars)	Time	Conductive phase	Binder	Catalyst	Comments
Teflon (*g*)	170-180	40	3	Carbon Black	PTFE	Sb/SnO	Mixture adhered to the support in all cases
	180-185	41	3	Carbon Black	PTFE	Sb/SnO	

The current density obtained in water electrolysis for these composite materials hotpressed with PTFE is shown in Figure 5.14.

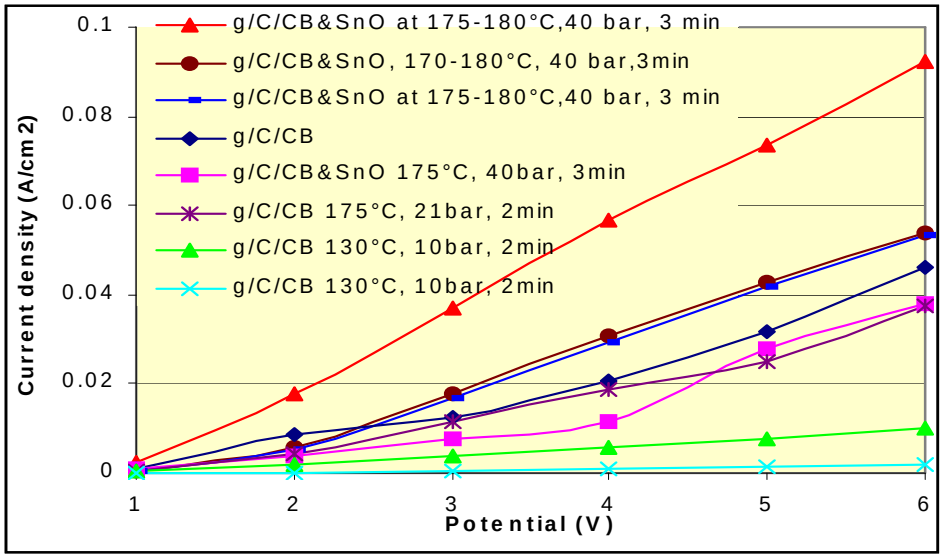

Figure 5.14 Comparison of electrochemical activity by hot pressing PTFE, carbon black and Sb/SnO on support (*g*)*

*40% KOH electrolyte environment at 0ºC and applied potential between -1 and -6 V

Adhesion of powdered PTFE to support *e* was poor, probably due to mutual repulsion between the materials used. Adhesion of admixtures containing PTFE on support *g* (Teflon sheet) was successful by the hot pressing technique. Current densities of materials prepared by the hot pressing technique were very low (mainly due to the non-conducting nature of the Teflon support and PTFE binder). However, the effect of various pressing techniques and different combinations of composite ingredients could be discerned (Figure 5.14). Moreover, activation below -2 V became apparent for combinations containing Sb/SnO nanoparticles. Problems such as insulating interphases, and suppression of interphase reactivity may have arisen, as each new material introduced into a composite may introduce its own set of interface problems. Hot pressing was not a suitable technique for application on the other supports (*a-c* and *f*) investigated as these materials lost their integrity during hot pressing. Further development of the hot pressing technique upon more appropriate supports with optimized pressures and temperatures may yet prove to result in highly stable, easily prepared composite electrodes.

5.7.2.4 Spraycoating method

A spraycoating method with Nafion® (5 % in water) used as binder with conductive phase of carbon black was spraycoated on various supports (Table 5.12).

Table 5.12 Spraycoating method with 60 % Nafion® (5 % in water) binder (N)+ 40 % Carbon Black on various supports.

Sample no.	Support	Binder N	Carbon black	Mass of support (g) (before)	Mass after spraying (g)	Mass % increase	Loading (g cm^{-2})
J-26	a	60 %	40 %	0.0236	0.0371	36.4	0.0135
J-27	b	60 %	40 %	0.0347	0.0455	23.7	0.0108
J-28	c	60 %	40 %	0.0213	0.0331	35.6	0.0118
J-29	d	60 %	40 %	0.1015	0.1054	3.7	0.0039
J-30	e	60 %	40 %	0.0631	0.0690	8.5	0.0059
J-31	f	60 %	40 %	0.0856	0.0943	8.4	0.0087

A noticeable difference in loading was obtained between the electrodes prepared using Lydall carbon cloth substrates (*a-c*) and the other substrates tested, with the lowest loading obtained on substrate *d*, which also resulted in the most active composite electrodes (Figure 5.15). In all cases it was however difficult to get exactly similar, reproducible loadings.

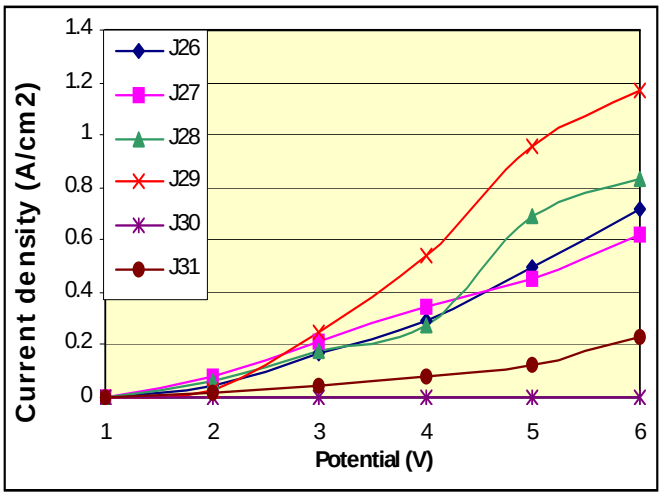

Figure 5.15 Electrochemical activity of composites formed with Nafion® binder and carbon black spraycoated on supports *a-f*, without additional catalyst

*40% KOH electrolyte environment at 0ºC and applied potential between -1 and -6 V

The composite electrodes formed with Nafion® binder and carbon black spraycoated on supports *a-f*, without additional catalyst showed relatively high current densities for the applied potential and the activity observed was highly substrate dependant. It was noticeable that sample J-29 made using substrate *d,* the ZrO_2 backed with stainless steel substrate from Creavis was highly active and even so maintained the integrity of the film containing carbon black well during high applied potentials. The size of the evolving H_2 gas bubbles was significantly different between the different substrate samples, with the finest bubbles being observed on this substrate (*d*). The effective discharge of such minute gas bubbles from the ZrO_2 coated electrode surfaces probably resulted from lower surface adhesion/tension between electrode surfaces and the smallest bubbles. This may have also contributed significantly to the observed high activity of this substrate and the electrodes made with it. The ceramic paper based composite electrodes (*e* and *f*) performed very poorly overall, whereas the samples prepared on carbon cloth substrates (J-26, J-27 and J-28) showed an intermediate performance slightly better than the substrates only (Figure 5.8).

Various electrodes were then prepared by spraycoating inks containing different components, namely: (i) 60 % Nafion® (5 % in water) binder with 20 % Carbon Black and 20 % SbSnO (ii) 60 % Nafion® (5 % in water) binder with 20 % Carbon Black and 20 % Pt –FAU zeolite, and (iii) 60 % Nafion® (5 % in water) binder with 20 % Carbon Black and 20 % Ni-gamma – alumina on various supports (Table 5.13, 5.14 and 5.15).

Table 5.13 Spraycoating with 60 % Nafion® (5 % in water) binder (N) + 20 % Carbon Black + 20 % SbSnO on various supports.

Sample no.	Support	Binder N	Carbon black	Active catalyst Sb/SnO	Mass of support (g)	Mass after spraying (g)	Mass % increase	Loading (g cm^{-2})
J-32	a	60 %	20 %	20 %	0.0241	0.0445	45.8	0.0204
J-33	b	60 %	20 %	20 %	0.0336	0.0462	27.3	0.0126
J-34	c	60 %	20 %	20 %	0.0218	0.0357	38.9	0.0139
J-35	d	60 %	20 %	20 %	0.0976	0.1016	3.9	0.0040
J-36	e	60 %	20 %	20 %	0.0633	0.0689	8.13	0.0056
J-37	f	60 %	20 %	20 %	0.0841	0.0901	6.66	0.0060

Table 5.14 Spraycoating with 60 % Nafion® (5 % in water) binder (N) + 20 % Carbon Black + 20 % Pt –FAU zeolite on various supports.

Sample no.	Support	Binder N	Carbon black	Active catalyst Pt –FAU zeolite	Mass of support (g)	Mass after spraying (g)	Mass % increase	Loading (g cm^{-2})
J-38	a	60 %	20 %	20 %	0.0234	0.0452	48.2	0.0218
J-39	b	60 %	20 %	20 %	0.0338	0.0633	46.6	0.0295
J-40	c	60 %	20 %	20 %	0.0214	0.0397	46.1	0.0183
J-41	d	60 %	20 %	20 %	0.1005	0.1050	4.3	0.0045
J-42	e	60 %	20 %	20 %	0.0637	0.0704	9.5	0.0067
J-43	f	60 %	20 %	20 %	0.0859	0.1026	16.3	0.0167

Table 5.15. Spraycoating method with 60 % Nafion® (5 % in water) binder (N) + 20 % Carbon Black + 20 % Ni-gamma – alumina on various supports.

Sample no.	Support	Binder N	Carbon black	Active catalyst Ni -alumina	Mass of support (g)	Mass after spraying (g)	Mass % increase	Loading (g cm^{-2})
JA-50	a	60 %	20 %	20 %	0.0235	0.0379	38	0.0144
JA-51	b	60 %	20 %	20 %	0.0351	0.0518	32.2	0.0167
JA-52	c	60 %	20 %	20 %	0.0203	0.0406	50	0.0203
JA-53	d	60 %	20 %	20 %	0.0981	0.1003	2.2	0.0022
JA-54	e	60 %	20 %	20 %	0.1089	0.1160	6.12	0.0071
JA-55	f	60 %	20 %	20 %	0.0849	0.1010	15.9	0.0161

It was once again noticeable that variable and non-reproducible loadings were obtained that were related to the substrate type used, with substrate *d* always taking up the least, and the carbon cloths the most catalytic ink. The current densities obtained in electrochemical activity for water electrolysis in the case of the various electrodes prepared by the spray coating technique using combinations tabulated in Tables 5.13, 5.14 and 5.15 are shown in the following figures (Figures 5.16-5.21), where electrodes prepared using the same substrate but with different ink compositions containing various supported or particulate electrocatalyst, namely Pt FAU, Ni-Alumina or SbSnO, are compared with the composites composed of substrate, carbon black and binder only, as detailed in Table 5.12 above. Once again the current density obtained was highly substrate dependent with support *d* composites being most active at high applied potentials.

The films were mostly stable at the applied potentials and high H_2 evolution conditions, thus Nafion® solution acts as a suitable binder. Samples supported on carbon cloth substrates showed activation at <-2 V. Of these composite electrodes, the highest current density of over 1 A at a potential of -5 V was obtained in the case of an electrode sample (J-41) prepared with nanophase Pt-FAU spraycoated with Nafion® and carbon black upon support type *d* (Figure 5.19). The electrocatalyst containing film samples containing Pt-FAU or nanophase SbSnO generally performed better than the Ni-alumina containing samples. In several cases, relatively high current densities were obtained with enhanced surface area electrodes prepared by spraycoating with only binder and carbon black conductive phase on various substrates as was previously noted.

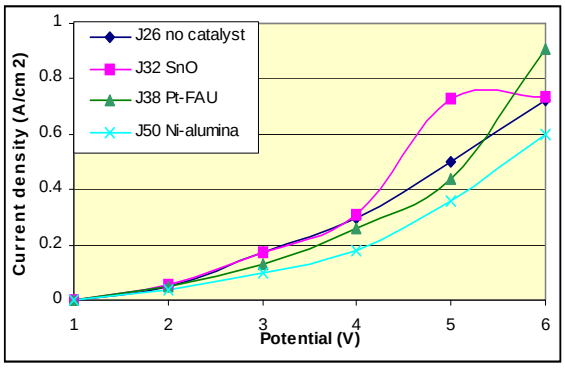

Figure 5.16 Composite electrodes spraycoated with Nafion® binder, carbon black and either nanophase Sb/SnO, Ni-alumina or Pt-FAU upon on carbon based support (*a*).

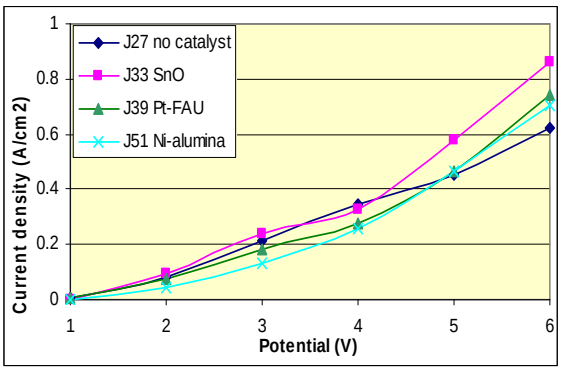

Figure 5.17 Composite electrodes spraycoated with Nafion® binder, carbon black, and either Nanophase Sb/SnO, Ni-alumina or Pt-FAU on carbon cloth support (*b*).

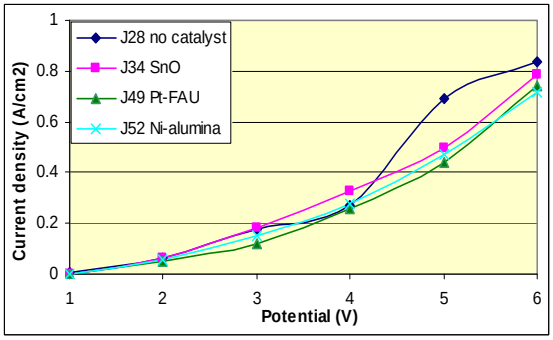

Figure 5.18 Composite electrodes spraycoated with Nafion® binder, carbon black, and Nanophase Sb/SnO, Ni-alumina or Pt-FAU on carbon cloth support (*c*).

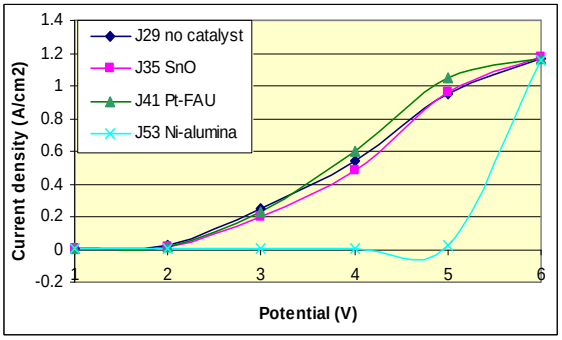

Figure 5.19 Composite electrodes spraycoated with Nafion® binder, carbon black, and Nanophase Sb/SnO, Ni-alumina or Pt-FAU on ZrO2/SS support (*d*).

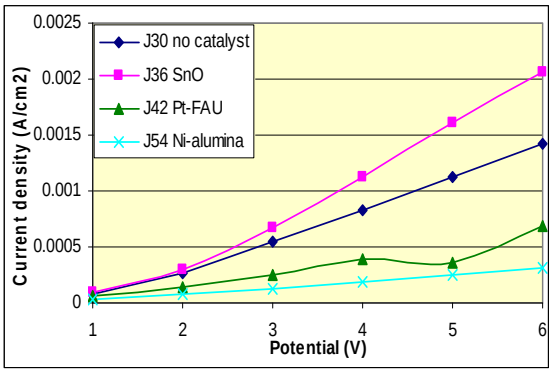

Figure 5.20 Comparison of activity of nanophase composites spraycoated with Nafion® binder and carbon black and Sb/SnO, Ni-alumina or Pt-FAU upon on ceramic support (*e*).

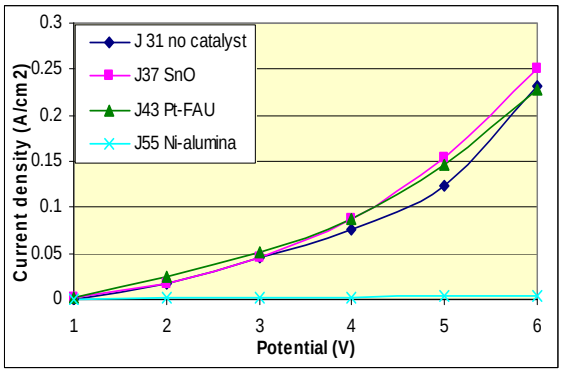

Figure 5.21 Comparison of activity of nanophase composites spraycoated with Nafion® binder and carbon black and Sb/SnO, Ni-alumina or Pt-FAU upon on ceramic support (*f*).

*40% KOH electrolyte environment at 0ºC and applied potential between -1 and -6 V

Delamination of some electrodes was observed as can be seen in the case of sample JA 32 in Figure 5.16 that was supported on substrate *a*. However, most electrodes were stable at the very high potential applied in these accelerated aging tests performed at 0 ºC in 40 % KOH. The electrochemical workstation used had a current maximum of 1.2 Amp thus the curve flattening observed is an artifact of the measuring system.

It was not possible to accurately characterize the film containing the electrocatalyst by itself in this system because of the extraneous variables that complicated the accurate measurements of the activity of the electrocatalyst containing film and distinct trends for the different electrocatalyst were not clearly discernable, except that Sb/SnO containing films performed generally better than Ni-alumina containing composites regardless of substrate type in this series. A system to accurately characterize only the electrocatalyst containing films is required and this will form the topic of Chapter 6.

Composite electrodes were also prepared by spraycoating various substrates with an ink formulation containing 50 % Polystyrene binder, 25 % Carbon Black and 25 % Pt-FAU in toluene as solvent (Table 5.16).

Table 5.16. Spraycoating with 50 % Polystyrene binder (B) + 25 % Carbon Black and 25 % Pt-FAU in toluene on various supports.

Sample no.	Support	Binder B	Carbon black	Active catalyst Pt – FAU zeolite	Mass of support(g)	Mass after spraying (g)	Mass % increase	Loading (g cm^{-2})
JA-44	a	50 %	25 %	25 %	0.0223	0.1390	84	0.1167
JA-45	b	50 %	25 %	25 %	0.0331	0.1052	68.5	0.0721
JA-46	c	50 %	25 %	25 %	0.0222	0.0848	73.8	0.0626
JA-47	d	50 %	25 %	25 %	0.1034	0.1321	21.7	0.0287
JA-48	e	50 %	25 %	25 %	0.0711	0.1548	54	0.0837
JA-49	f	50 %	25 %	25 %	0.0934	0.1442	35.2	0.0508

The current density obtained for composite electrodes using Polystyrene as binder in toluene with Carbon Black and Pt-FAU on various supports is shown in Figure 5.22.

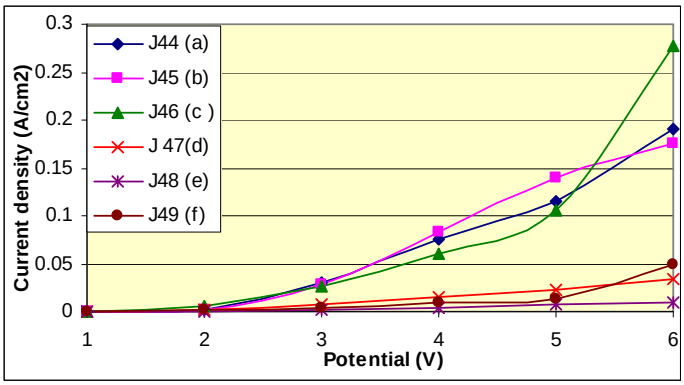

Figure 5.22 Composites spraycoated with 50 % Polystyrene binder, 25 % Pt FAU and 25 % carbon black in toluene on different supports
*40% KOH electrolyte environment at 0ºC and applied potential between -1 and -6 V

Use of the polystyrene binder reduced the electro activity of composite electrodes significantly and these results show the effect of an insulating binder replacing the proton conducting Nafion® binder. Nevertheless, the carbon cloth based composite electrodes performed overall better than the other substrates when polystyrene was used as binder. The substrate *d* was remarkably deactivated by the polystyrene containing film deposited. The effect could be due to excessive passivation of the catalytic components on the electrode surface by too high a ratio of the binder phase used.

5.7.2.5 Pt and Au supported on mesoporous HMS and MCM 41 materials

Finally a comparison was made of the activity of various nanophase catalysts supported on mesoporous substrates (HMS and MCM 41). The nanophase catalyst was supported on Carbon cloth, (Thickness: 500mm, 6100-300 (support b)). Conditions were the same as for previous chronovoltametric tests at 0 ºC in 40 % KOH and each sample was subjected to potential steps between -1.0 to -6.0 V over 60 s. The ink formulations (approx. 60% Nafion, 20 % Carbon black & 20 % nanophase catalyst) for preparation of films containing electrocatalyst (Pt and Au supported on mesoporous HMS and MCM 41 materials) on Carbon cloth, Thickness: 500mm, 6100-300 (support b) are presented in Table 5.17 and results of electrochemical testing in Figure 5.23.

Table 5.17 Ink formulation for preparation of films containing electrocatalyst (Pt and Au supported on mesoporous HMS and MCM 41 materials)

Sample no.	Nafion 5 % (g)	Carbon black (g)	Catalyst (g)
Nafion and carbon black	0.6473	0.4040	nil
Pt HMS carbonized	0.1127	0.0309	0.0306
Pt MCM carbonized	0.1110	0.0306	0.0301
Au HMS	0.1224	0.0325	0.0351

Figure 5.23 shows the electro activity of composite electrodes spraycoated with Nafion® binder, carbon black, and either Au-HMS, Pt MCM or Pt HMS supported nanophases on carbon cloth support (b).

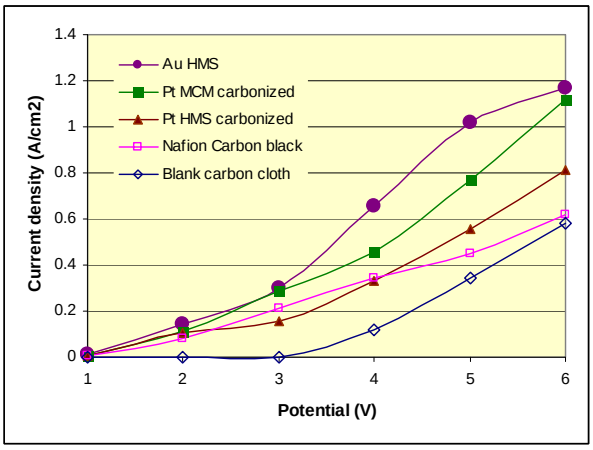

Figure 5.23 Composite electrodes spraycoated with Nafion® binder, carbon black, and either Au-HMS, Pt MCM or Pt HMS supported nanophases on carbon cloth support (b)*

*40% KOH electrolyte environment at 0ºC and applied potential between -1 and -6 V

The composite electrode prepared with HMS Au containing gold nanoparticles as catalyst showed a high current density of nearly 1.2 A at -6 V (and >0.3 A at -3 V) at 0 ºC and generally the nanophase electrocatalyst enhanced the current density compared to the combinations tested without catalyst under the same conditions.

These results at 0 ºC show the positive effect that addition of a nanophase metal had upon the electrochemical activity of the composite electrode even when the electroactive metal was supported on an insulating Si mesoporous matrix. Since these composite electrodes were tested at 0 ºC they are thus considerably more active than the composites prepared using the commercial JM Pt_{40}/C presented in the baseline study, which were tested at room temperature (25 ºC).

A higher temperature (60 ºC) was finally applied in the high electrolyte environment for water electrolysis and the inks containing the best performing particulate nanophases (Sb/SnO) or nanophases supported on mesoporous materials (Pt HMS) were applied directly to a fine stainless steel mesh as substrate and tested for their electro activity at low applied potentials as are shown in Figures 5.24 and 5.25. In this case the actual negative axis is presented in the figures.

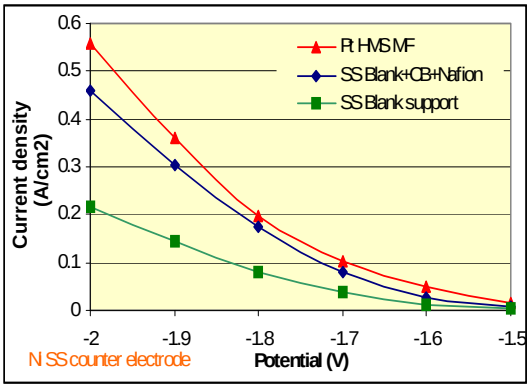

Figure 5.24 Electroactivity of Pt on HMS (Conditions: 60 °C; 40 % KOH)

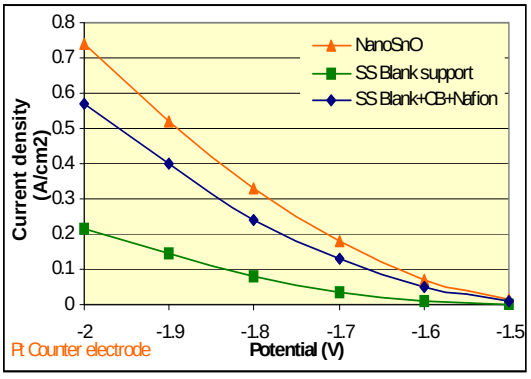

Figure 5.25 Electroactivity of Nanophase Sb/SnO_2 (Conditions: 60 °C; 40 % KOH)

Under the applied conditions of 60 °C, the composite nanophase coated electrodes were stable and gave a high current density of between 550 and 750 mA at -2 V, whereas the JM Pt_{40}/C produced only 320 mA at -2 V and 70 ºC. The films

containing the Pt HMS nanophase or Sb/SnO particulates significantly enhanced the current density and thus the hydrogen production rate.

This result was further confirmed using several differently reduced (methanol formaldehyde, or sodium hypophosphite) and carbonized Pt HMS electrocatalyst samples as is shown in Figure 5.25. The results are compared with the output achieved in the baseline study with the commercial HiSpec JM Pt_{40}/C catalyst at -2 V and 70 ºC in 40 % KOH.

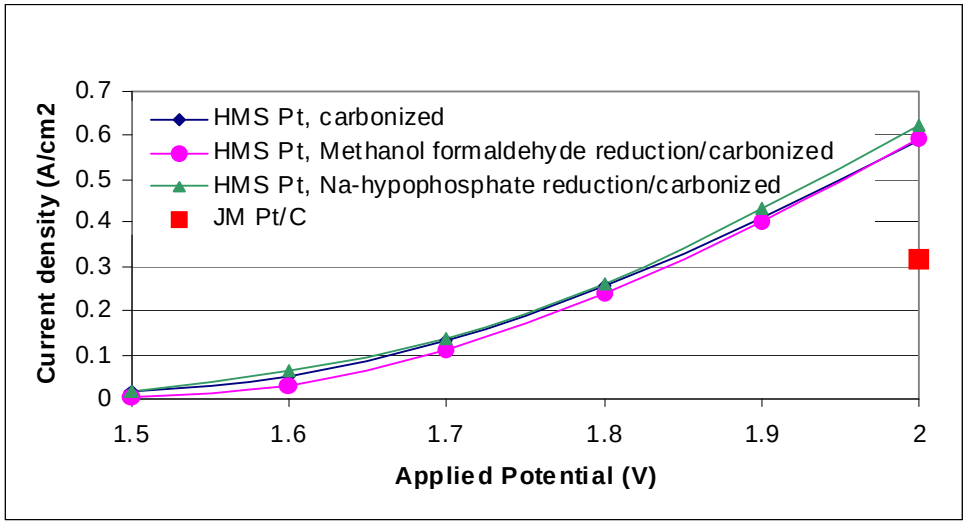

Figure 5.26 Replication study of Pt HMS containing composite electrodes

Nanophase electro active metals (Pt, Au) supported upon mesoporous supports HMS and MCM-41 generally showed higher electro activity for H_2 production than when supported upon microporous Si support zeolite FAU (see also Petrik, 2003). Use of different zeolite types to immobilize and support monodisperse Pt or nanoparticulate Pt clusters is well known prior "art". The nature of the zeolite, namely its framework structure, shape selectivity resulting from size exclusion, acidity and pore size has been previously shown (Petrik, 2003) to affect the electro activity of supported Pt clusters in zeolites, with pores in the Ångstrom dimensions (FAU has pores of 7.5 Å). The more open pore of the mesoporous materials HMS and MCM-41 with pores between 2-4 nm, thus could have promoted the ingress of the reactant water and the product H_2 leading to the enhancement of electrocatalytic activity observed in this

study. However, the nature of the composite electrodes and the contribution from binders and conductive phases make it difficult to exactly characterize the contribution of the electrocatalyst itself and these supported nanophase electro catalytic materials should be further investigated for their electro activity under more controlled conditions.

5.8 CONCLUSIONS

This study has identified commercially viable methods for preparing highly active nanophase Pt, and Au electrocatalyst supported upon mesoporous HMS and MCM-41, and also methods for preparing nanophase composite electrode materials stable in high electrolyte environments for hydrogen production, that are active, cheap to prepare and easy to upscale. Far less of the PGM was utilized than in bulk electrodes.

Sequential deposition was found to be an effective method to stabilize nanophase electrocatalyst on mesoporous support matrices and thereafter to incorporate them into composite membrane electrode format. Different combinations of nanophase electrocatalyst and various binders, supports, and conductive phases were evaluated in this study. This method to form nanophase containing composite membrane electrodes was found to be a promising low cost method for preparing larger scale composite membrane electrodes that could be applied for H_2 production by water electrolysis in high electrolyte media and could be useful as electrodes for other electro-driven reactions.

The electrochemical response of nanophase composite membrane electrodes formed by sequential deposition was combination specific and high current densities were obtained by nanophase composite electrodes in water electrolysis in a high electrolyte environment. In general it could be stated that addition of particulate nanophase Sb/SnO and supported Pt in the form of Pt FAU, Pt HMS or Pt MCM-41 increased the catalytic activity of composite materials prepared by several techniques with

Nafion® or Polystyrene as binder, especially on a zirconium based support (type *d)*, which is also a highly electro-active substrate without additional deposited layers. Polystyrene was prone to inertize composite surfaces when used in spray coating, but proved effective as binder in the casting method where only carbon black was used on support *a*. Hot pressed composites prepared with PTFE were stable but had low activity. The various Ni foils that were used for comparison purposes were active but less active than some of the composites prepared by sequential deposition or support *d* by itself. The nanophase catalysts investigated showed an ability to enhance electro catalytic activity of electrode surfaces.

Au and Pt nanoparticles supported on mesoporous MCM-41 or HMS were more active than Ni on Alumina or Pt nanoparticles supported on microporous FAU. Electro activity of supported electrocatalysts (Pt, Au) was found to be a complex function of metal concentration, metal type, host matrix, zeolite typology, porosity, and acidity as well as supported metal nanocluster size. The isolating nature of the inorganic porous zeolite framework matrix did not inhibit the activity of nanophase electrocatalyst, but in fact promoted water electrolysis. The optimum supported nanoscale metal cluster size resulting in significant electro activity was about 5 nm.

Relatively high activity was also observed for commercial Sb/SnO nanoparticles processed into electrodes, which was comparable to the Pt containing electrode samples. The nanophase metal type, and reduction procedures, as well as pore size of inorganic matrix support are shown to play a role in the electro activity of electrocatalysts processed in composite membrane electrode form. Regardless of the reduction technique (methanol formaldehyde, sodium hypophosphite), the Pt and Au electrocatalysts supported upon mesopore materials (HMS, MCM-41) showed the best activity. Thus pore size of host matrix support is a significant parameter in preparing zeolite supported electrocatalysts.

Sequential deposition was found to be an effective method to firstly stabilize nanophase electrocatalysts on mesoporous support matrices and thereafter to

incorporate them into composite membrane electrode format upon conductive substrates by application in the form of catalytic inks. The electrocatalyst containing film composite nanophase gas diffusion electrodes were formed by deposition of catalytic inks on supports that could act as gas diffusion layers. This method to form nanophase composite gas diffusion electrodes was found to be a promising low cost method for preparing larger scale electrodes that could be applied for H_2 production by water electrolysis in high electrolyte environments. Cost could be reduced through minimizing the PGM utilized.

Homogeneous distribution and loadings of nanophases was dependent upon deposition method, substrate type as well as ink formulation. Reproducible production of standard electrode materials containing nanophase electrocatalyst would require careful control of the processing techniques, which could not be achieved by hand. Incorporating supported nanophase electrocatalysts in composite gas diffusion electrodes resulted in production of electrodes capable of current densities of between 550 and 750 mA cm^{-2} at 60 °C at an applied potential of -2 V. The fact that the electrodes were able to withstand the very high degree of H_2 gas evolution at an applied potential of -6 V showed that even under these aggressively accelerated testing conditions the nanophase containing inks were stable and durable. Nanophase electro catalytic materials could thus successfully be incorporated into composite gas diffusion electrodes and resulted in significant catalytic activity for hydrogen production.

Aspects that require attention were identified; these were quantification of the amount of electrocatalyst per unit area of electrode sample and quantitative catalytic activity. Although the electroactivity for water electrolysis was used as semi quantitative method to characterize the composite electrodes, the substrate used as support for the catalytic layer on the electrode influenced the results obtained significantly therefore it was not possible to accurately determine the I/V characteristics of the electrocatalyst containing film deposited.

Some of these aspects are addressed in Chapter 6 which will focus on screenprinting as a processing method to deposit uniform and reproducible catalytic films of known structure and characterize such films. The means to obtain specific and well dispersed metals loading in the electrocatalyst containing film over the surface of the electrode is also addressed. Chapter 6 also presents a new technique to characterize the electronic properties of the catalyst layer supported on the substrate using the Hall measurement system.

CHAPTER 6

6. DEVELOPMENT OF GAS DIFFUSION ELECTRODES BY SCREEN PRINTING OF CATALYTIC INKS

6.1 INTRODUCTION

Development of suitable high activity electrocatalysts (as described in Chapter 4) needs to be coupled with the methodology to incorporate such catalytically active materials into composite gas diffusion electrodes (GDE) for various applications, including water electrolysis or fuel cells. Prerequisites for such systems are complex. It is not suitable to utilize these particulate materials in powder form in electro driven reactions, therefore the composite electrocatalyst would need to be stabilized upon a suitable conductive substrate in film format using binders in order to prepare a stable and durable composite gas diffusion electrode whilst retaining sufficient electro activity.

Preparation of a film containing active metal components upon a suitable conductive substrate is complex. The emulsions used as catalytic ink typically contain the electro active component, and electro conductive phases as well as a proton conducting phase which may or may not act as a binder, and if necessary, dispersants or solvents. The most immediate problem in the preparation of an emulsion or ink of the correct formulation is to prevent aggregation of the nanophase particles, which should be highly dispersed. Moreover, the film should be highly proton conductive. Furthermore, an electro conductive phase should be present in the film formulation that takes into account the percolation threshold, which can be significantly improved by the application of nanophases. Each active catalytic site should have sufficient access to the three phase boundary (gas, liquid, solid). Thereafter a further challenge arises in that the relative electron and proton conductivity of the system should be maintained whilst still allowing ingress of reactant and egress of gaseous product, requiring either hydrophilic surfaces in the case of water electrolysis or hydrophobic

surfaces in the case of, for instance, direct methanol fuel cells. In addition, the application of a film upon a suitable conductive substrate requires that suitable binders are utilized that will neither hinder proton conductivity, nor cause the occlusion of catalytically active sites by the binder. Thereafter, the application of the ink to form the film upon a substrate requires selection of the most suitable substrate for the application and a methodology of deposition, which can be achieved by, for instance, spray coating or by various printing procedures (Vielstich et al., 2003).

Once all these requirements are optimized, it is still necessary to tailor the surface and interfacial tension of the liquid phase and surface free energy of the solid phase to ensure that highly homogeneous and un-agglomerated films will form upon removal of the solvent in the ink during the drying process. Support substrates and films being deposited should have the same coefficient of expansion so that adhesion is good and crack formation is minimized in order to prepare a stable and durable composite gas diffusion electrode (Wang et al., 1998; Chen and Tsao, 2006). Composite gas diffusion electrode surfaces containing catalytic nano phases should result in high activity because of optimized geometry, electro and proton conductivity, high surface area, and enhanced porosity and transport of reagents and products.

Typical preparations of a PEM electrode for a fuel cell are well described in the literature and the membrane electrode assembly (MEA) structure and components are reviewed in Chapter 7 (see also Figure 7.1 and 7.2). This chapter describes efforts to address some of the above challenges in understanding the role of variables affecting the successful preparation of gas diffusion electrodes suitable for polymer electrolyte membrane (PEM) electrolyzer systems. Of the methods that are suited to processing particulate catalytic materials into films on suitable substrates, screenprinting was selected and is described in this chapter. The goal was to prepare a stable, well dispersed and homogeneous film containing active metal components upon a suitable substrate by use of emulsions containing an electro active component, and electro as well as a proton conducting phase, binder, and solvents and understand some of the

properties of the film in isolation from the other components of the electrolyzer system.

6.2 OVERVIEW

Intensive development of fuel cells, especially based on proton exchange membranes (PEM), has stimulated the development of PEM electrolyzers to produce hydrogen, as fuel for application in hydrogen energy and technology. Hydrogen production technology for water electrolysis by the solid polymer electrolyte membrane (PEM) method, has advantages in terms of high efficiency and low cost compared to conventional hydrogen production methods (Grigoriev et al., 2006).

The electrode in electrolyzer system functions as a support for the catalyst, an electron and proton pathway, as well as needing to distribute the liquid reactant and remove the gaseous products. The performance of membrane electrode assemblies (MEAs) in fuel cells or electrolyzers is substantially affected by the structure of the electrodes and satisfactory and uniform spatial characteristics are required. Hence, the key technical issues for polymer electrolyte membrane (PEM) based systems such as fuel cells and electrolyzers are porous structure, incorporation of catalytic materials, membrane stability, adequate flow distribution, and system design. Electrochemical reactions, heat transfer, and mass transport occur in the three-phase interface among gaseous phase (hydrogen, air or water vapour), liquid phase (proton hydrate, hydroxyl ion, peroxide ion, and water), and solid phase (porous gas diffusion layer, catalyst composite, Nafion® electrolyte) (Zhu et al., 2007). The components needed for each reaction determine the structure of the composite MEA and ultimately the stability, degradation and lifetime of the MEA.

There are different approaches to preparing the system required for electrolysis using a PEM system. In an early study, high-purity hydrogen was prepared by bringing a hydrogen containing gas in contact with a hydrated solid polymer electrolyte cell

comprised of a catalytic anode, perfluorocarbon sulfonate ion exchange membrane and a catalytic cathode. Direct current energy was supplied between the electrodes to overcome the internal resistance of the cell, dissociate the hydrogen in the impure gas to protons, and drive the protons through the cation membrane for recovery at the opposite electrode (Sedlak et al., 1981).

Takenaka et al., (1982) showed that electrocatalysts can be directly plated upon perfluorosulfonic acid polymer membranes and applied for solid polymer electrolyzers (SPE). Noble metals and their alloys were directly attached to both sides of the membrane without a binder by metal plating methods, utilizing reactions of a metal salt solution with a reducing agent on the membrane surface, which made it possible to increase the adhesive strength of electrocatalysts to the membrane and also to reduce the resistance of the electrocatalyst/SPE interface. Millet et al. (1990) prepared electrocatalyst composites for water electrolysis, consisting of microparticles of noble metal electrocatalyst, that were precipitated simultaneously on both sides of a perfluorinated ion-exchange membrane by chemical reduction of cationic precursor salts. Anodic overvoltage, cathodic overvoltage, ohmic drop within the SPE and roughness factor of the electrodes were measured and low noble metal loadings (< 1 mg cm^{-2}), low cell voltage (-1.75 V at 1 A cm^{-2} and 80 °C) and long term stability (over 15,000 h of continuous electrolysis) was achieved.

However, these various plating methods mainly produce a bulk two dimensional metal film upon the membrane and the active catalytic surface area is relatively low. Therefore there is an interest in the use of nanoparticulate electrocatalysts, but stabilizing these materials is complex.

Various electrode fabrication techniques have been reported in literature such as rolling, screen-printing, and spraying techniques, each with its own merits and problems. Low operating and low capital cost, with high through-put and increased turnaround times are necessary when fabricating components for electronic devices such as PEM electrolyzers. This can be achieved by depositing catalytic materials in

particulate form using spraycoating, screen-printing or by digital inkjet printing for printing on fragile, dimensionally unstable and expensive substrates. Other methods for preparing the electrode may include gravure coating, offset coating, comma coating, die coating, slit coating, spray coating, plating, sol-gel processes, film processes, chemical vapour deposition (CVD), vapour deposition, sputtering, and ion plating (Okada et al., 2007). Not all of these methods are suited to processing particulate catalytic materials.

6.2.1 Approaches To Preparing Gas Diffusion Electrodes

The gas diffusion electrodes (GDE) incorporating the catalyst in fuel cells and electrolyzers are currently typically prepared by rolling, spraying, and recently by screen printing methods (Tanaka et al, 2005) and the proton conductive phase, normally a Nafion® solution, can be impregnated into the gas diffusion layer (GDL) using for instance, spraying and brushing methods.

Direct-printing of an outer and an inner catalyst layer on the PEM in a layered anode structure for a fuel cell is reported to improve the CO-tolerance ability and utilization efficiency of the catalyst (Wan and Zhuang, 2006a; 2006b). The MEAs consisted of a Nafion® 117 membrane and a commercial electrocatalyst (20% Pt/C from E-TEK) on the cathode side. The inner catalyst layer providing the hydrogen oxidation reaction was a pure Pt layer (0.07 mg cm^{-2}) that was prepared by directly printing on PEM. This example highlights the difference in the requirements between an electrolyzer and a fuel cell, since in the electrolyzer water splitting replaces hydrogen oxidation. The combination of catalyst deposition and screen-printing could allow the mass production of materials possessing catalyst activity for hydrogen evolution.

The differences and complexity of each system affect the electrochemical reactivity (Wang et al., 1998). Existing ink deposition methods such as spray painting are not well suited for low (<0.5 mg Pt cm^{-2}) catalyst loadings because of lack of reproducibility and slow throughput. Moreover, the solution properties should also be

compatible with the printing method, and catalyst utilization should be optimized (Tanaka et al, 2005).

Recently, inkjet printing (IJP) has been developed (Murthy et al., 2000) and was used to deposit water based catalyst ink solutions containing catalysts supported on different carbon black sources onto gas diffusion layers (GDL) that were made into membrane electrode assemblies (MEAs) for the polymer electrolyte fuel cell (PEMFC). Ink jet printed MEAs with catalyst loadings as low as 0.020 mg Pt cm^{-2} showed Pt utilizations in excess of 16,000 mW mg^{-1} Pt which is higher than traditional printed MEAs (800 mW mg^{-1} Pt). A graded distribution of Pt/C catalyst structure using standard Johnson Matthey (JM) catalyst, showed enhanced performance (Taylor et al., 2007).

A hybrid technique for fabricating low platinum loading electrodes was claimed to be more successful than spraying and screen-printing techniques for the preparation of PEMFC electrodes (Abaoud et al., 2005). Towne et al., (2007), used commercial desktop inkjet printers to deposit the active catalyst electrode layer directly from print cartridges onto Nafion® polymer membranes in the hydrogen form. Good adhesion was achieved without any post-deposition hot press step and the layers were subjected to tape peel, bending and abrasion tests. The elimination of the hot pressing step indicated that inkjet-based fabrication or similar processing technologies may provide a route to less expensive large-scale fabrication of MEAs, but these authors concluded that it remained to be determined whether such routes for MEA production offer performance advantages or lead to more efficient utilization of expensive catalyst materials.

In the case of proton exchange membrane fuel cells the interfacial contact of the catalyst with the membrane has been studied in a MEA fabrication method where perfluorosulfonyl fluoride copolymer powder was pressed into a sheet at 230°C by hot pressing. The Pt/C catalyst was screen-printed onto either side of the sheet, followed by hot pressing which embedded the coated catalyst layer into the

membrane. The resultant MEA was converted into perfluorosulfonate polymer by hydrolysis using a NaOH solution (Kim et al., 1998).

U.S. Patent 5,783,325 (1998), UK Patent 2,316,802 (1999) and U.S. Patent 6,103,414 (2000) by Cabasso describe a polymer solution made of thermoplastic film former, e.g., polysulfone and polyvinylidene fluoride, mixed with carbon and a common solvent (DMF and NMP) that was cast on glass in the form of asymmetric flat sheet electrodes to control of the gas-diffusion pores, and the electrode-catalyst-membrane interface. A substantial reduction of the catalyst in the MEA was claimed, and less than 0.1 mg cm^{-2} was shown to produce a high performance MEA.

The direct fabrication of Au and Pt nanoparticles by an electro deposition process on screen-printed carbon strips was possible (Chikae et al., 2006). This is one approach to the incorporation of nanophases into the screen printed carbon film. In another approach a platinum loading of 0.38 mg cm^{-2} on a Nafion® membrane electrode was achieved for the PEMFC by the simultaneous deposition and reduction of platinum through an impregnation/reduction method. The current density reported was between 500 and 1000 mA cm^{-2} at 0.6 to 0.7 V (Rajalakshmi et al., 2004; 2007).

Most recently, studies have shown that optimization of the electrode structure is still desirable. Zhang et al., (2007), describe a process for preparing a catalyst coated membrane (CCM) to fabricate the MEA for solid polymer electrolyte (SPE) water electrolysis. Spray coated Nafion® layers are shown to be effective for increasing the reaction interface between SPE and the electrode catalyst layer. Their study of the SPE electrolyzer with a new MEA structure could achieve about 0.1 V lower voltage at atmospheric pressure and 2 A cm^{-2}. Reshetenko et al., (2007), optimized the cathode structure for an air-breathing direct methanol fuel cell (DMFC) by application of pore-forming agents such as ammonium carbonate and ammonium hydrocarbonate that form additional macro and mesoporosity increasing the electrochemical active area and catalyst utilization. Improved performance of the MEA was also attributed to the porosity of the cathode electrode by Chen and Tsao

(2006), because a network of macro fissures and sub-micro fissures allowed air to penetrate the electrode in the case of the fuel cell MEA. The relationship between the total porosity of the electrodes and the MEA performance was demonstrated and the specific power density nearly doubled when the total porosity was increased from 57% to 76%.

These efforts show that there is considerable opportunity to increase efficiencies by improving the manner in which the electrode or MEA is structured for each application.

6.2.2 Differences Between Fuel Cells And Electrolyzers

From the literature it is evident that most efforts have focused upon the optimization of printing methods to prepare MEAs for the fuel cell and less effort has been aimed at optimization of electrodes for SPE electrolyzer systems. The electrocatalyst configuration and type used for hydrogen production is somewhat different to that applicable in fuel cells. Electrodes for the electrolyzer systems are reversed compared to the fuel cell system. In electrolyzer systems, water splitting is achieved on the anode accompanied by evolution of O_2 and hydrogen being produced on the cathode; whereas in a fuel cell the oxidant (O_2) and fuel (H_2 or hydrocarbon) fed to the cathode are recombined to form water on the anode. Thus accumulation of evolving gas on the electrodes can occlude the electrode surface in electrolyzer systems whereas water flooding is typically a problem of electrodes in PEM fuel cells (Tanaka et al, 2005). Hence, a different approach is required to preparing electrodes for each specific system.

Hydrophobicity is required in a fuel cell to prevent flooding of the electrode, unlike in the case of a SPE electrolyzer, where hydrophilic catalyst layers, coatings or gas diffusion layers are required, in order to optimize the ingress of the reactant, water. The diffusion layer in a PEMFC generally consists of a thin layer of carbon black mixed with hydrophobic polytetrafluoroethylene (PTFE) that is coated onto a sheet of

macro-porous carbon backing cloth or other substrates (Tanaka et al, 2005). Yu et al., (2006) showed that the catalyst microstructure and water transport is one of the key components of PEMFCs because the electrochemical reaction occurs at the three-phase interface of the catalyst layer. They found that it was necessary to optimize the hydrophobic and/or hydrophilic properties of catalyst layers, which have a large impact on the water transport and on the performance of the PEMFC.

The requirement for the anode also differs from that of the cathode. Jung et al., (2006) showed that different hydrophobic/hydrophilic conditions apply to the cathode compared to the anode for fuel cells because of the difference conditions required at the respective electrodes. According to these authors, wettability of the fuel cell cathode caused flooding whereas increased wettability of the anode catalyst layer caused by SiO_2 addition allowed beneficial water adsorption from back diffusion. Choi et al., (1996) demonstrated that in PTFE-bonded carbon electrodes, when the hydrophobicity of the electrocatalyst layer increased, the hydrogen chemisorbed Pt fraction and utilization of Pt decreased.

Because of the different reactions occurring in PEM electrolyzers compared to PEM fuel cells it is not possible to directly apply the advances made in one system to that of the other, and specific optimization of each electrode in each system is required. Hence it is of importance to understand the parameters that may influence the performance of these different gas diffusion electrodes.

6.2.3 Requirements Of Gas Diffusion Electrodes

It is well known that in electrochemical systems that the nature of the redox processes that occur at the electrode/electrolyte interface and their rates can be partially controlled by the applied potential, which may be influenced by the speed of interfacial electron transfer. This is a function of the electrode structure which, in the case of gas diffusion electrodes for electrolyzers and fuel cells, is composed of redox centres (on the metal catalyst), an electron conductive phase (carbon) and a polymer

binder (Nafion®) that also functions as a proton conductor/solid electrolyte. The rate of charge transport in response to a change in the redox reaction on the metal centre depends strongly upon the polymer electrolyte. The overall performance of these electrodes is thus a function of the electron transfer at the electrode film interface, charge transport through the layer, and mass transport of the reactant and products within the layer (Rusling and Forster, 2003).

The performance of the PEM fuel cell or PEM electrolyzer electrodes is dependent upon the proton network, electronic network and the interface between the electrolyte and the electrocatalysts as well as the interfacial resistance (Rajalakshmi et al., 2007).

A two phase flow within the gas diffusion layer is caused by the reactant (liquid) supply to the active layer and the removal of product (gaseous). In PEM electrodes, an effective mass transport of reactants to, as well as of products from the reaction zone is required to achieve high reaction rates and reduce efficiency losses. Therefore electrodes in PEM electrolyzers or fuel cells include a porous GDL between the flow field of the bipolar plate and the reaction zone of the electrode's active layer, to ensure a homogeneous and efficient mass transport over the whole active area of the cell. Typically, the GDL is one to two orders of magnitude thicker than the active layer where the reactions take place. The structure of the porous gas diffusion layer, including its porosity and tortuosity, affects the two-phase mass transport in the electrodes. The effects of different fabrication methods, thicknesses of gas diffusion layer and the impregnation method of Nafion® solution, upon porosity and on fuel cell performance have been explained in terms of reduced charge transfer resistance and extension of the three-phase region (Lee et al., 2004).

Films of catalyst and ionomer in the micrometer range do not have the mechanical integrity to be freestanding, therefore a composite is required in which a thin catalytic substrate zone is located within a highly porous conductive matrix or upon the polymer membrane itself. Cabasso, et al., in U.S. Patent 5,783,325 (1998) point out that the most common binder and membrane used for composite electrodes is

Nafion®, because of its proton conductive characteristics. The optimum Nafion® content as binder affects both the activity of a catalyst and also the ionic resistance of the electrode, therefore its presence in the catalyst layer is necessary for good performance. These patents give typical Nafion® contents that may range from 30 – 40 dry wt % and loading is calculated as a dry weight (wt%) of ionomer divided by the total dry weight of the catalyst and ionomer and multiplied by 100. Nafion® solution has been used successfully in MEAs, but the mechanical properties of Nafion® change above 90 ºC and under pressure plastic flow occurs and at >120ºC, collapse of the interface occurs and the MEA irreversibly loses its properties. Although many other substitutes for Nafion® have been explored, this problem has not been solved yet.

Other issues such as variable membrane hydration, ternary gas mixtures for reactant streams, phase change of water in the gas diffusion electrodes, and the temperature distribution across the cell are also of importance in MEA performance (Rowe and Li, 2001). Two-phase transport of reactants and products constitutes an important limit in performance of polymer electrolyte systems. For instance, in fuel cells at high current densities or low gas flow rates, product water condenses in the open pores of the cathode gas diffusion layer (GDL) and limits the effective oxygen transport to the active catalyst sites (Pasaogullari and Wang, 2004). Dynamic interactions within a PEM electrolyzer such as water phenomena, electro-osmotic drag and diffusion through the membrane should also be considered (Görgün, 2006).

The overall MEA performance will also be a function of the way in which the catalyst is supported and the microstructure of the catalyst support as well as that of the catalyst. For instance, carbon aerogel supported Pt catalysts with different pore size distributions and Pt content were synthesized and tested in a PEMFC operation. The microstructure of the support, the perfluorosulfonate-ionomer distribution and the pore size distribution of the aerogel supported Pt catalyst was shown to have an effect on the performance of the PEMFCs. The PEMFC prepared with a low Pt loading (0.1 mg cm^{-2}) of a porous aerogel supported catalyst showed high power

densities up to 0.8 mW cm^{-2} in fuel cell operation conditions in air and at ambient pressure (Smirnova et al, 2005).

MEA performance is highly dependent on catalyst structure, specifically the relative volume fractions of gas pores and polymer membrane contained within the active region as well as the geometry of the individual catalyst agglomerates (Siegel et al., 2003).

These examples show that the performance of a MEA is not only determined by the electrocatalyst activity, but by numerous other parameters relating to the electrode structure. Although many of the above studies relate to the requirements of fuel cell MEAs, the conclusions drawn can be extrapolated with due caution to the case of the SPE electrolyzer MEAs, with consideration of the differences between the systems.

6.2.4 Screenprinting

Because screen printing was the method chosen for preparing electrodes in this chapter, the general procedure was reviewed. It was not the aim of this study to optimize the screen printing method but to adequately characterize the morphology and electrical properties of the screenprinted film. The inks used for screenprinting in this study consisted of finely divided particles in a paste blend.

Although screen and stencil technologies are well developed for manufacturing fuel cell electrodes and membranes (DEK® International, 2007), production methods of active components for fuel cell and electrolyzers must become faster and more highly automated for lower costs and higher production volumes. High-speed, accurate, repeatable, cost-effective screen printing with optimized ink formulations should enhance delivery of high-quality membrane electrode assemblies (MEAs) suitable for application in PEM systems such as SPE electrolyzers.

During the screen printing process a free flowing ink is spread using a squeegee and forced through the apertures of a screen mesh, overlaid with a patterned stencil (Davis, 1999). Screens are made with various thread counts which can be altered depending upon the chosen design. Typical screen materials are nylon, terylene and metal and the film is about 20 μm in thickness. Various kinds of support materials or carriers can be printed, using ultraviolet screen printing inks (Abbott, 2005). The screen pitch, which is the shortest distance between the centres of two adjacent screen apertures or cells, depends on the technology and the geometry used. A typical pitch value for metal screens is 83 μm. The standard lines-per-inch (LPI) of a screen printable design is 65 lpi for automatic process prints.

Problems in printing can be reduced by using a different angle of print with a higher mesh count of 4 to 5 times the LPI (Fresener, 2008). During screen-printing with a grid pattern, printing defects are likely in electrode layers. For instance, moire caused by interference with the mesh of the screen of the printing plate, or breaking and thickening of thin lines, may occur making precise printing difficult (Okada et al, 2007). United States Patent 6505554 issued to Rhein (2003) describes a process of screen printing images on a substrate that utilizes specific screen angles which effectively diminishes the moire effect and other screen printing process distortions. Multiple layering is recommended as a means to avoid these problems. Other problems that may arise during printing (Technigraphics, 2002) include smearing, streaking, reduction, bleeding, haze, flow marks, pin holes, voids, and inconsistency.

Screen printing presents advantages as a high-throughput, automated solution for creating fuel cell components. As example, the Hydrogen Institute of Applied Technologies (H.I.A.T. gGmbH) advertise that proprietary screen-printing techniques are a rapid, low-cost and repeatable way to prepare bifunctional catalytic electrodes in a homogeneous layer of uniform thickness for polymer electrolyte membrane fuel cells. Screen printing is possible on most polymers (e.g. different types of Nafion®) as well as on gas diffusion layers (e.g. Toray paper). Homogeneous

current distribution as well as optimized orientation of microstructure in the electrode has been claimed.

Replicable, stable cell currents and voltages were obtained by screenprinted electrodes (Pettersson, 2006). Various approaches have been taken to improve ink formulations in screen printing for electrode performance. Eggins (2002) reports that various modifying components can easily be incorporated into a carbon paste ink suited for screen-printing thick film graphite powder based sensors. The electrochemical behavior of thick film carbon sensors fabricated with four different commercial carbon inks was compared for redox systems and different background currents showed that the choice of the ink would depend upon the specific technique being used (Wang et al., 1998).

Glycol-based solvent and iron oxide inks have been studied, to improve viscosity and achieve a good level of screen printing performance by slurry control during screen-printing. Optimum parameters of the screen such as aperture diameter (70 mesh) and emulsion thickness (over 30 mm) were established (WE-NET, 1998). Screen-printing of PEM fuel cell electrodes has been reported in the open literature (Park, 2002; Tanaka et al, 2005). Tanaka and co-authors imply that the success of screen printing is a complex interplay of the format of the screen printer device, the type of dispersant used in the ink, the viscosity of the ink, as well as the ratios of the different components in the inks. These variables have an effect upon the shear rate and thixotrophy index of the ink. The complexity in preparing carbon based electrodes and incorporating nanophases into electrodes result in many differences in the composition of commercial and proprietary carbon inks used for fabricating screen-printed electrodes.

Screen printing is not always the best approach to preparing electrodes for a specific application as can be seen in the case of electrodes for solid oxide fuel cells (SOFC). Good bonding and mechanical stability of screen printed electrodes for solid oxide fuel cells requires high firing temperatures, which could cause formation of resistive

reaction products detrimental to the electrode performance (Labrincha et al., 1993). Cathodes could be deposited by screenprinting or by firing. Tape casting and co-firing were methods used to prepare reduced temperature solid oxide fuel cell (SOFC) anodes where thin film 8YSZ electrolytes were deposited on Ni–YSZ anode support plates. (Van Herle et al., 2001).

Many electrochemical properties change when the electrodes in cells are layered (Majima, 1997a and b; Majima, 1999; Majima, 2001; Kitoh, 1996). The different zones of the screenprinted electrodes as well as the electrical contacts should be studied in order to optimize both the composition and distribution of the layers deposited on the support for the construction of a homogeneous and reproducible layer of the catalyst on the substrate.

6.2.5 Other Applications Of Screenprinted Electrodes

Screen printing as an approach for the preparation of electrodes is widely utilized for various other applications and a few examples are given. Screen-printing technology is used for the mass-production of disposable electrochemical sensors. Multilayer films containing multiwall carbon nanotubes and redox polymer were successfully fabricated on a screen-printed carbon electrode using a layer-by-layer assembled method for electro catalysis of ascorbic acid (Sha et al., 2006). Different strategies, including palladium electro deposition, Pd sputtering and Nafion®-solubilized carbon nanotube casting, were used to modify screen-printed carbon electrodes for the fabrication of amperometric enzyme biosensors (Lee et al., 2007). In another earlier example, semiconductor TiO_2 thick film electrodes were prepared by screen printing for sunlight photo electrolysis of water (Ahmed, 1986).

6.2.6 Ink Formulations

From various references it could be seen that much of the information on ink formulations is proprietary or patented. In U.S. Patent 7316475, issued to Cornell et al. (2008), and 6158843 issued to Murthy et al. (2000) thermal inkjet printing of aqueous inks heavily loaded with silver nanoparticles, typically the mole fraction of water in the ink should be greater than 0.9 with respect to only the liquid components of the ink and the ink viscosity be less than 3 Pa-s at 22 ºC, for inks containing metal nanoparticles. According to Cornell et al., (2008) US patent 2003/0185971 by Saka claims conductive ink formulations with low viscosity for ink jet printing, which are limited to 10 % solids. The particle size should be less than 50 nanometers (nm) for the best resolution and minimal settling. An upper limit to prevent excess particle settling is about 132 nm (Cornell et al., 2008). Polymeric dispersants such as ionic hydrophilic methacrylic acid and nonionic hydrophilic polyethylene glycol are used in aqueous inkjet inks as dispersants, as well as ingredients such as humectants to reduce evaporation, and such inks resulted in a sheet resistance of 0.16 Ohm (Guan et al., 2006). According to Cornell et al., (2008) no theoretical basis exists for the viscosity of liquid mixtures. This patent states that the mole fraction of water in the ink should be greater than 0.9 computed with respect to only the liquid components.

An important requirement of a commercial ink formulation is to make a stable aqueous based colloid dispersion. There are many ways to prevent the metal colloid to agglomerate and precipitate. USPTO Application 20060044382 discloses stabilizers such as surfactants, polyelectrolytes, gelatin, polyphosphates, amino grafted polymer, or oligomer, dendrimer, crown ethers and amphiphilic polymers such as carboxymethyl cellulose sodium salt. However, these stabilizers could cause problems such as increasing the viscosity of the dispersion or not being compatible with the components of the system or may introduce unwanted salts into the system, and may create problems to remove the excess salt or stabilizer after printing.

CHAPTER 6

Differences in conductive ink formulations can have a pronounced effect upon electrode performance. If nanoparticles form part of an ink formulation, it is necessary to optimize the conductive inks and tailor the ink to provide high conductivity and low resistance at low curing temperatures, to ensure good adhesion on flexible substrates such as Nafion®, reduce interfacial problems and to provide additional functionalities, such as diffusional properties. Moreover, different printing technologies can introduce flaws such as severe moire patterns, horizontal print banding frequencies and also result in ink bleeding due to too much ink printed locally (Shu et al., 1997).

In many cases heat curing of the printed layer is desirable as at 66°C water begins to leave the ink and at 94°C the binder may reach its lowest viscosity and maximum surface contact is made with the substrate. At 105°C water should leave the ink rapidly and at 133°C approximately fifty percent of the water is gone and the binder and particles start to cure. By 150°C most of the water is gone and the binder-particulate combination is partially cured. Maintaining this temperature for 30 s to 1 min should allow the binder and particulate to cure (NEHOC, 2008). However, when using Nafion® PEM membranes as a substrate for printing, high heat curing is not possible as the membrane is heat sensitive.

Tanaka et al (2005) used either dibutyl phthalate or isopropanol as dispersion media or solvent during the development of an ink paste suited for screen-printing catalytic electrodes for micro electromechanical system (MEMs) based fuel cells. Dibutylphthalate was found to have the appropriate viscosity whereas isopropanol had an undesirable decrease in viscosity at high shear rate causing unwanted and excess flow during screen-prinitng. These authors also found that the viscosity of the ink at a low shear rate should not be too high if uniformity of the screen-printed layer was to be achieved. A degree of flow due to surface tension was required for uniformity. The thixotrophy index should thus be small for screen printed inks.

Based upon the limited information available on screen printing conductive nanoparticle containing inks, this chapter focused on investigating the effect of some variables such as dispersant type and ratio, overall ink composition, and substrate type upon the electronic characteristics of the film formed on the substrate which was either a gas diffusion layer or the ionomer membrane.

6.2.7 Surface Tension, Viscosity and Rheology

Surface tension is the energy required to stretch a unit change of the surface area due to the unbalanced force experience by molecules at the surface of a liquid. As a result of surface tension, a drop of liquid tends to form a sphere, which shape offers the smallest area for a definite volume. Different liquids have different surface tensions. The surface tension of water is 72.8 dynes cm^{-1} and the surface tension of propylene glycol is 40.1 dynes cm^{-1} at 25 °C. Substances with low surface tension have a tendency to form films. The intermolecular attraction between like molecules is called cohesion, and adhesion is the attraction between unlike molecules. Liquids with high surface tensions have strong cohesion forces, and are poor wetting liquids due to low adhesion forces. A wetting agent increases the adhesion force between two different materials. Molecules of wetting agents usually have a polar and a non-polar portion. When added, the wetting agent increases the wetting action of water with the non-polar material. For propylene glycol solutions in water the surface tension decreases with increasing mass fraction (Horibe et al., 1997). Propylene glycol has an amphiphilic nature, and hydrogen-bonding with strong solvation interactions with water thus different molar fractions in water may allow tailoring of the hydrophilic/hydrophobic balance. The interactions with water arise from the hydrogen bond donor and acceptor properties of the hydroxyl function (---OH) and the direct interactions between the alcohol groups and water are sufficiently high to prevent phase separation at higher temperatures (Bauduin et al., 2004).

Viscosity is a measure of the resistance of a fluid which is being deformed by either shear stress or extensional stress. Viscosity describes the internal resistance to flow of

a fluid. Water has a viscosity of 1 centipoise at 20 °C and the viscosity of ethylene glycol is 16.1 centipoise at 25 °C (Lide, 1992). Fluids such as the inks formulated in this study do not have a constant viscosity, thus are Non-Newtonian fluids. Such fluids exhibit a variety of different correlations between shear stress and shear rate.

Rheological characterization of ink is of relevance in printing technologies (Tanaka et al. 2005). Modelling the rheological properties of solutions has received attention. One of the more general models (Chhabra & Richardson, 1999) which has been used consistently in the literature to describe the time independent viscous characteristics of slurries such as the inks, is the Yield Pseudoplastic or Herschel-Bulkley model. This model is also able to describe Power-law or pseudoplastic behaviour and Bingham plastic behaviour. The general forms of these models are shown in Figures 6.1 to 6.3 (Chhabra & Richardson, 1999). The Newtonian model would appear as a horizontal line in Figure 6.2. Referring to Figure 6.3, it can be seen that all three models illustrate shear thinning behaviour, as viscosity decreases with an increase in shear rate.

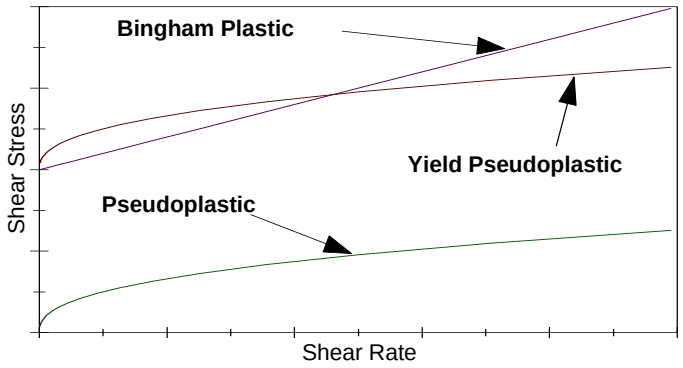

Figure 6.1 General form of the flow curve (or rheogram) - linear axes.

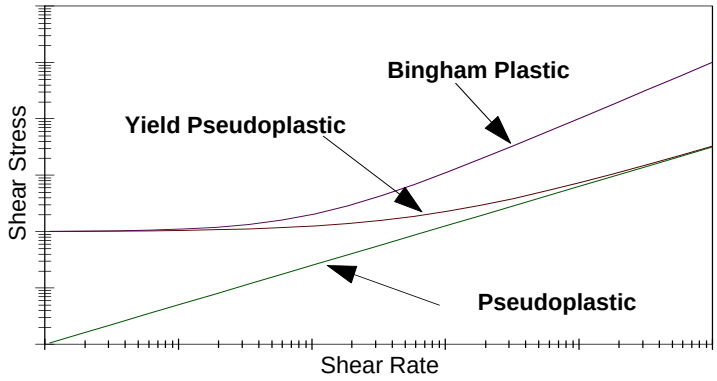

Figure 6.2 General form of the flow curve (or rheogram) - logarithmic axes.

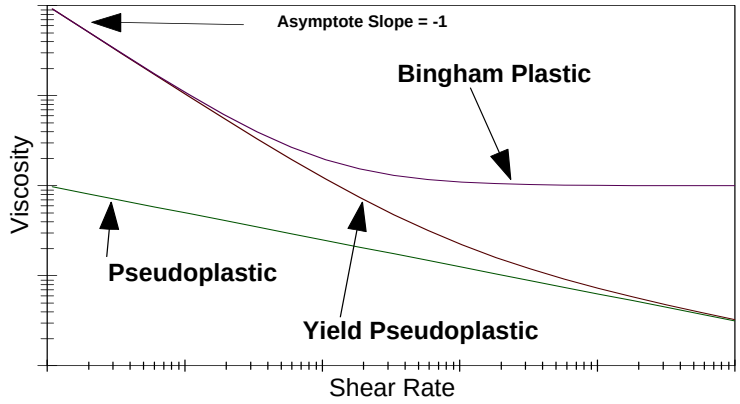

Figure 6.3 General form of the viscosity diagram for the rheological models on logarithmic axes.

Solids concentration is perhaps the most important parameter affecting slurry rheology and slurry rheology can be correlated with solids concentration. It is important that empirical methods are used in order to relate rheology to concentration for the most meaningful and comparable results to be obtained (Chhabra & Richardson, 1999).

Besides solids concentration, a related factor influencing the rheology of the slurry is maximum packing density which in turn is influenced by the particle size distribution. Very little work has been done in attempting to relate these and other particle properties to the rheology (Dabak & Yucel, 1987). Unfortunately there is no correlation proposed for the flow behaviour index (n). Despite this, the rheological constants can be correlated against concentration using simplified versions of the correlations proposed by Landel et al. (1963) for the fluid consistency index (K) and Dabak & Yucel (1987) for the yield stress (τ_y). In order to determine the rheological parameters, a flow curve is needed, measuring the shear stress over a range of shear rates. For any suspension, there may be time dependant behaviour. This is important when constructing the flow curve, because if there are significant changes with time, the flow curve should be constructed using viscosities measured at a time where it is constant. This phenomenon can be investigated by measuring the change of viscosity with time. The slurry viscosity may be stable with time for the first time period, after which it may start to decrease as the solid particles began to settle out. At higher shear rates, the particles may be kept in suspension with no significant decrease in the viscosity (Chhabra & Richardson, 1999).

6.2.8 Characterization: Hall Measurements

Characterization of the activity of gas diffusion electrodes is typically confined to cyclic voltammetry or stack testing. However, as Chapter 7 will specify, this can introduce extraneous interferences which make it difficult to examine the quality of the film containing the nanophase electrocatalyst. Various approaches have been described for measuring the homogeneity of a gas diffusion electrode in a working cell or stack (Stephan et al., 2006; Ghosh et al., 2006; Brett et al., 2007; Sauer et al., 2008). Characterization of the homogeneity and current density of the electrode layer prior to incorporation in the MEA is of importance, as inhomogeneity will directly impact on its performance in a stack.

Typically in this study (see Chapter 7) the MEA for H_2 production was prepared as follows: the cathode was prepared by spray painting or coating the carbon-supported Pt electrocatalyst (1 to 6 mg cm^{-2}) and ionomer onto the GDL. The anode was prepared by spraying about 6mg cm^2 IrO_2 or carbon supported Pt onto pretreated titanium fibre as GDL. The MEA was pressed by sandwiching the ionomer membrane (typically Nafion® 117) between the cathode and anode electrodes and hot-pressing at 130ºC and 40 bar for 5min. However, this procedure resulted in many extraneous variables influencing the performance of the MEA, as is further described in Chapter 7. Thus it was not possible to accurately characterize the films containing the electrocatalysts separately once formed into a MEA.

Therefore the film was separately characterized using the Hall measurement system by printing the film on a non-conductive substrate such as paper or on the PEM itself and comparing the printed layers on these substrates with the substrate typically used as gas diffusion layer in MEAs, namely carbon cloth.

Utilization of a magnetic field for characterization of the distribution of current densities in proton exchange membrane fuel cells (PEMFC) to enable optimisation of fuel cell performance has recently been described (Candusso et al., 2004). Hall measurements were shown for IrO_2 films (Patil et al., 2003). The Hall effect measurements were carried out at room temperature and the values of Hall resistivity (ρH) and carrier concentration (NH) were deduced showing their variation with film thickness. These authors demonstrated that as film thickness increased, ρH decreased. The decrement in ρH was ascribed to the increase in carrier concentration, which stemmed from ionization of defect and change in mobility of charge carriers of IrO_2 films. The surface properties or large defect concentration can dominate the transport properties of such dioxides.

Current distribution mapping, increasing the homogeneity of the current density distribution and achieving a uniform utilisation of the active area is of significant importance in fuel cell and electrolyzer MEA developments (Eckl et al., 2006). The

structure and current carrying capability of the catalyst containing film on the electrode is the prime aspect in this chapter that was investigated. An intrinsic material property such as resistivity (or conductivity) is required to quantify the current-carrying capability of the material for comparisons between different samples. Resistivity is not a fundamental material parameter, because different materials can have the same resistivity. Different sample geometries also give different resistance values. Thus it is necessary to consider carrier density n and mobility μ in the electrical characterization of a material. In order to determine both the mobility μ and the sheet density n_s, a combination of a resistivity measurement and a Hall measurement is required.

6.2.9 Resistivity And Hall Effects

The resistance (R) and conductance (G) of a material are measurable physical quantities obtainable from two-terminal current (I) and voltage (V) measurements. The resistance alone, however, does not adequately discriminate between materials as different sample shapes give different resistance values. Resistivity on the other hand allows the quantification of the current-carrying capability of a material for relevant comparisons between different samples (EEEL-NIST, 2008).

The Hall effect is the potential difference (Hall voltage) on the opposite sides of an electrical conductor created by a magnetic field applied perpendicular to a current flow (EEEL-NIST, 2008). The Hall effect discriminates between positive charges or holes moving in one direction and negative charges moving in the opposite.

Because resistivity by itself does not fully characterize the electrical transport of a material, and carrier density n and mobility μ need to be considered it is necessary to apply a magnetic force normal to the direction of the electron flow (Figure 6.4).

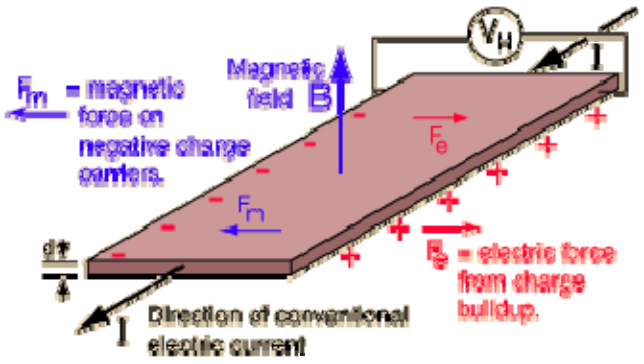

Figure 6.4 Hall effect in a thin flat conductor (http://hyperphysics.phy-astr.gsu.edu/hbase/magnetic/hall.html)

The force that arises as a result of the simultaneous current and magnetic flux is called the Lorentz force, which influences the electrons to move sideways with a drift velocity away from the line of electron flow, resulting in an excess surface electrical charge accumulating on one side of the sample. This charge results in the Hall voltage, a difference of potential between the two sides of the sample (Putley, 1960).

Various problems may arise in the measurements because of offset voltage caused by nonsymmetric contact placement, sample shape, or non-uniform temperature (Chwang et al., 1974), but modern instrumentation and careful sample preparation can minimize these effects. The magnitude of the Hall voltage V_H is equal to

$$V_H = IB/qnd \qquad 6.1$$

where I is the current, B is the magnetic field, n is electron bulk density, d is the sample thickness, and q (1.602 x 10-19 C) is the elementary charge. Layer or sheet density ($n_s = nd$) can be substituted instead of bulk density, thus:

$$n_s = IB/q|V_H| \qquad 6.2$$

The values of I, B, and q are known and the Hall voltage V_H can be measured, thus the sheet density n_s of charge carriers can be determined.

The Hall mobility μ is calculated as follows:

$$\mu = 1/qn_sR_S \text{ (in units of } cm^2V^{-1}s^{-1}) \qquad 6.3$$

from the sheet carrier density n_s and the sheet resistance R_S. The sheet resistance R_S is determined by use of the van der Pauw resistivity measurement technique (Van der Pauw, 1958; Putley, 1960). A resistivity and a Hall measurement are needed to determine the mobility μ and the sheet density n_s (ASTM method F76, 2000). The Hall measurement, carried out in the presence of a magnetic field, yields the sheet carrier density n_s and the bulk carrier density n if the conducting layer thickness of the sample is known. The carriers can be a positive or negative carrier type. Conventionally in a dry semi-conducting material the positive carriers are "holes" and the negative carriers, electrons. In electrolytes both carriers can be ions.

6.3 MATERIALS AND METHODS

6.3.1 Ink Preparation

The electrocatalyst used in the optimization of the ink formulation for screen printing was a commercial electrocatalyst (Alpha Aesar 40% Pt on Carbon Black; Hispec 4000 (Stock 42204 ; Lot F01Q12)) in most cases. Sample series LP06 was made with Alpha Aesar 40% Pt on Carbon Black (Hispec 4000: Lot J26P18). This commercial catalyst was chosen as it is well characterized by the vendor and gives satisfactory performance as the catalytic electrode of conventional PEM fuel cells and is the benchmark in the thesis.

Solvents that were used included ultra pure water, isopropanol or alternatively 1,2-propanediol (Propylene Glycol) 99% (Sigma Aldrich, Cat. No. 13436B; Lot S39776-337). Propylene Glycol specifications are: Boiling Point, °C : 187.3 ; Density, 20/20 °C : 1.0381; Surface Tension, dynes cm^{-1}, 25 °C : 40.1; Viscosity, cP, 20 °C : 0.581 ;Vapour pressure, mm Hg, 20 °C : 0.07 ; Solubility in water : Completely soluble.

Where any additional conductive phase was added to the catalytic ink a product sold as "Fullerenes" by Aldrich (37946-2.56 03702HE 99.5% FW 720.67) was used. Table 6.1 gives the exact composition of each ink. The catalyst was weighed and the water added prior to addition of the solvent to prevent combustion of the catalyst upon addition of the solvent. Each component was weighed sequentially into a vial which was sealed until use. Inks were generally sonicated for 5 min prior to use.

Table 6.1 Ink compositions

Series	Catalyst JM Pt_{40}/C (g)	Water	Nafion® 5% (g)	Isopropanol (g)	1,2 Propanediol (g)	Fullerenes (g)
LP00	0.0532	100 μL	0.0877	nil	nil	nil
LP01	0.526	0.0984 g	0.0652	0.5432	nil	nil
LP02	0.1125	0.0999 g	0.0783	nil	0.5218	nil
LP03	0.1009	0.1002 g	0.0788	nil	0.7481	nil
LP04	0.1017	0.2173 g	0.0795	nil	0.6217	nil
LP05	0.0983	0.2978 g	0.0793	nil	0.3191	nil
LP06	0.0989	0.2952 g	0.0977	nil	0.2993	0.0353
LP07	0.1008	0.3324 g	0.0768	nil	0.3031	nil

Table 6.2 shows the molar ratio of the dispersants H_20 and 1,2 propanediol, normalized to H_2O for ease of reference. The water and solvent accompanying the Nafion® should also be considered but, as the value was kept fairly constant apart from series LP06, this value was neglected for the purposes of calculating the molar fractions of the dispersants H_20 and 1,2 Propanediol.

Table 6.2 Molar ratio of dispersants H_20: 1,2 Propanediol

	H_2O M	1,2 Propanediol M
LP02	1	1.24
LP03	1	1.77
LP04	1	0.68
LP05	1	0.25
LP06	1	0.24

6.3.2 Screen Printing Experimental

Films of nanophase containing catalytic ink were screen printed onto selected substrates using a Presco screen printer (Model MSP-645 Affiliated Manufacturers Incorporated (AMI)) operated at air pressure maximum of 80 psi. The speed of the squeegee was factory preset, and the angle of attack, from the geometry of the squeegee settings, is about 45 degree. The screen used for printing was a polyester screen with 35 μm thread thickness and number of threads per cm is 120 lines cm^{-2} with an aperture pore size of about 50 μm. The screen print design was manufactured by a photo resist technique to produce four exactly 1 cm^2 sized electrodes per print run on each substrate. Therefore each print run produced four distinct 1 cm^2 sized electrodes. Exact registry of print layers was determined by careful sizing and exact placement of the substrate prior to screening.

Screen printing of catalytic inks into films to form the composite electrode format was done onto two different substrates for Hall measurements namely, bond paper (Mondi Rotatrim 80 g m^{-2} uncoated paper) and Nafion® sheets (N117 1100 EW produced by Ion Power). Bond paper is generally used in ink jet printers. These papers may have coatings to receive ink or fillers to achieve a specific mass per unit size. Nafion® sheets are used as the PEM electrolyte in electrolyzers and fuel cells. Nafion® sheets were prepared as is specified in Chapter 7 prior to use. Upon removal from storage in ultra-pure water, each Nafion® sheet was air-dried for 30 min and then pressed between leaves of paper for approximately 2 h to ensure flatness prior to screen printing.

Each substrate was carefully weighed before and then after deposition and drying of the separate layers with a hand held blow drier, and the mass calculated for each print area of 4 cm^2 in size, comprising four 1 cm^2 electrodes. After the solvent evaporated, the film that was deposited consisted primarily of electrocatalyst with only a small amount of incorporated Nafion® ionomer as binder. No other components were added to the ink formulations to minimize interferences.

Optical microscopy of printed electrode layers was performed to evaluate the printed layer homogeneity and catalyst particle dispersion or agglomeration. Images were taken with an Olympus SZX12 optical microscope at 20x magnification.

6.3.3 Hall Measurement Experimental

6.3.3.1. Sample preparation

After screen printing, electrode samples were prepared for resistivity and Hall effect characterization. The 1 cm^2 screen printed electrode was carefully trimmed and mounted on thin cardboard to ensure flatness and thereafter mounted onto the Lakeshore Sample Holder (part number 750SC10-50) with "solvent and acid free water soluble glue" (Henkel Pritt). The electrical contact was made by placing four small ohmic contacts on the four corners of the supported film (Figure 6.5 (a and b)) using silver conductive ink (screen printed or hand painted using DuPont Silver paint 5000).

Thereafter contacts were hand painted between each corner of the 1 cm^2 electrode and silver contact points 1, 2, 3 and 4 on the Lakeshore Sample Holders. Mounted samples were cured at 70 °C in a hot air oven for 30 min to ensure contact dryness. This treatment was not suitable for Nafion® based samples as the Nafion® degraded, thus samples on Nafion® substrates were air-dried.

The printed sample could be connected to the Lakeshore Sample Holders (part number 750SC10-50) using silver wire and Indium solder for electrical contact, because the low temperature melting of indium allowed soldering of silver contacts with indium foil onto paper backed samples and did not damage the sample as paper can withstand 250 °C. Indium welded silver contacts were used in cases where the catalytic ink was overprinted upon silver printed contacts as can be seen in Figure 6.5(b). It was found that hand painting the silver contacts onto the 1 cm^2 screen printed electrodes was more suitable for Hall measurements of these samples and this was the mounting procedure used for characterization of screen printed sample electrodes.

(a) Indium contacts for samples overprinted onto silver printed contacts on Lakeshore Sample Holders 750SC10-50

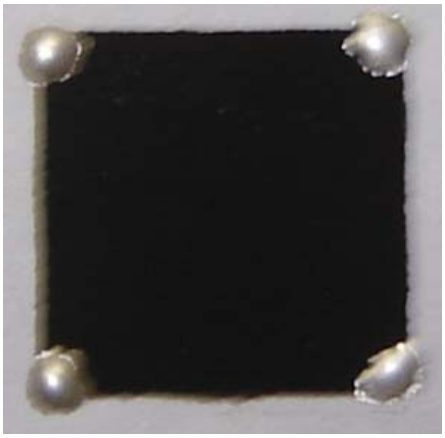

(b) Silver contact hand painted on screen printed samples

Figure 6.5 Electrode preparation for sample mounting

6.3.3.2 Instrumental set up conditions

The Hall measurements were obtained using a Lakeshore 7704 system with HMS Matrix 775 control instrument sample Module Model 75013SCSM (max 100 V) and a Sample Module Model 75013SCSM (Figure 6.6) to apply the magnetic field (with a maximum of 10.8 Gauss).

Figure 6.6 Lakeshore 7704 HMS Matrix Hall measurement system

Hall effects were determined at ambient temperature but without equilibration of moisture content by placing mounted samples in a light proof sampling chamber (Figure 6.6). The Lakeshore system was used to determine the film resistance R_S via the van der Pauw technique (Putley, 1960). The film carrier density n_s was measured by the Hall voltage V_H .

Manual resistance measurements were firstly obtained to check the integrity of contacts according to the van der Pauw geometry which is geometry independent (van der Pauw, 1958). Terminals were painted on the corners of each electrode (Figure 6.5 (b)). Connections were made according to the (R12,12; R23,23; R34,34; R41,41) configuration for each prepared electrode after mounting in a Lakeshore sample holder and a voltage applied between each terminal successively.

The Van der Pauw geometry (Van der Pauw, 1958; Putley, 1960) was used for IV curve measurement starting at -1.0 mA to 1.0 mA with a step size of I=100 mA and a dwell time of 5s. Thereafter a Variable Field measurement was obtained for each sample between 10 kG and 1 kG at a step size of 1 kG and dwell time of 10 s at a current of 1 mA. The mode chosen was linear sweep with field reversal and geometry A+B to minimize any lack of symmetry.

6.3.4 Experimental: Rheology of inks

Ink samples were prepared for rheological measurements using different solvents, liquid to solids and solvent to water ratios as given in Table 6.3.

Table 6.3 Liquid to solid ratio and solvent to water ratios of ink formulations

Sample Name	LPO 1	LPO 10	LPO 4	LPO 5	LPO 11
Liquid:Solid ratio	14	14	8	6	14
Solvent: water ratio	5:1	5:1	3:1	1:1	1:1
Solvent type	Iso-propanol	Propanediol	Propanediol	Propanediol	Propanediol

After weighing and mixing the ingredients of each ink for 30 min using a magnetic stirrer, inks were ultrasounded for 5 min before viscosity measurements were taken. Rheological measurements were conducted using the Anton Paar Physica MCR 300 system. Viscosity measurements were obtained at 25ºC using CP50-4 measuring system and TEK 150 PA-C measurement cell with 0.5 mm cone/plate gap, between 1 and 1000 reciprocal seconds.

6.4 SCREEN PRINTING RESULTS

A series of electrodes were printed as specified with either a single print or one or two overprints as is listed herewith:

LP02: Run 1 = one layer; Run 2=one overprint, replicated 3 times

LP04: Run 1= 1 layer; Run 2=one overprint (2 layers); Run 3=two overprints (3 layers)

LP05: Run 1= 1 layer; Run 2=one overprint (2 layers); Run 3=two overprints (3 layers)

LP06: Run 1 =1 layer; Run 3= two overprints (3 layers)

Ink formulations printed on Nafion® sheet 117 as substrates, are denoted with the suffix “nafion” in the text. These substrates could not be weighed accurately due to

slow moisture loss from the moisturized Nafion® substrate over time. Nafion sheets were printed at STP and were equilibrating during printing as the drying time of 30 min prior to printing was chosen to reduce deformation of the sheet and maintain some hydration for characterization.

The mass % increase determined for the series of electrodes printed on bond paper as substrate using the respective isopropanol or 1,2 propanediol based ink formulations given in Table 6.1 are presented in Table 6.4.

Table 6.4 Mass % increase of substrate before and after printing (area of print = 4 cm^2).

	LP02	LP04	LP05	LP06
Run 1 before (g)	0.7014	0.7039	0.6544	0.6509
Run 1 after (g)	0.7017	0.7081	0.6589	0.6554
Mass % increase	0.0428	0.5931	0.6829	0.6866
Run 2 before (g)	0.6595	0.6523	0.6825	
Run 2 after (g)	0.6661	0.6603	0.6898	
Mass % increase	0.9908	1.2116	1.05828	
Run 2 before (g)	0.6527			
Run 2 after (g)	0.6588			
Mass % increase	0.9259			
Run 2 before (g)	0.6922			
Run 2 after (g)	0.6992			
Mass % increase	1.00114			
Run 3 before (g)		0.648	0.6441	0.6783
Run 3 after (g)		0.6602	0.6554	0.6873
Mass % increase		1.84793	1.7242	1.3095

Each print run using the respective formulations listed in Table 6.1 produced four distinct 1 cm^2 sized printed electrodes upon the selected substrate. The general design of the screen, with 4 separate 1cm^2 electrodes, thus gave two circular and two square shaped electrodes for each print run. The shape of the electrode (round versus square) was varied to establish what effect this would have on print quality and take-off effects.

The mass increase of the film deposited on the substrate (paper), after each 4 cm^{-2} layer of ink was deposited by screen printing was fairly reproducible (Figure 6.7)

using different the ink formulations detailed in Table 6.1. Series LP03 was not weighed accurately thus this mass is not reported.

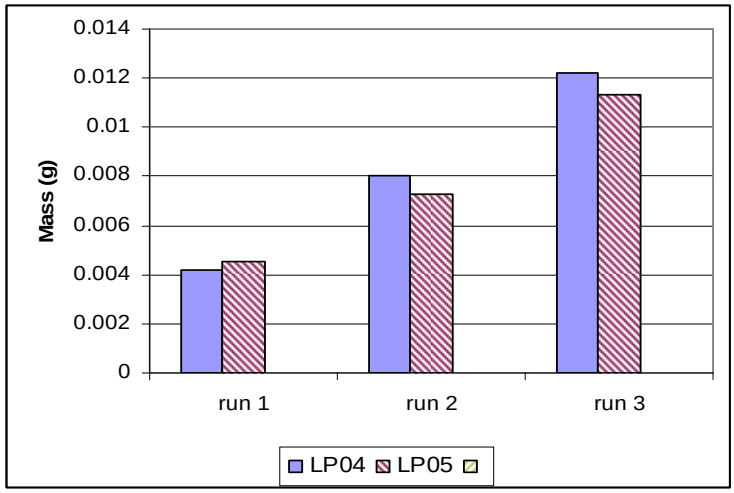

Figure 6.7 Mass (g) increase of the substrate after each successive overlayer for print series LP04 and LP05.

The mass (g) of the substrate approximately doubled upon deposition of each successive layer superimposed upon the previous layer, increasing the substrate mass by approximately 0.004 g / 4 cm $^{-2}$ each time (Figure 6.8). Thus each separate electrode of 1 cm^2 increased by approximately 0.001 g with each successive overprinted layer.

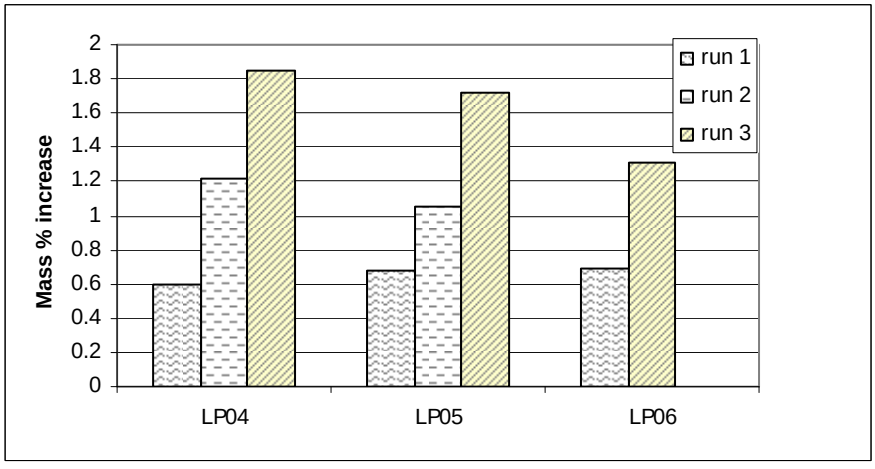

Figure 6.8 Mass % increase of electrodes for electrodes after each successive deposition over 4 cm $^{-2}$

It was thus possible to accurately deposit a chosen mass of active component per unit area using the screen printing method, which depended upon the ink viscosity and the

mass % increase was consistent between print runs and series (Figure 6.8). Ink viscosity was a function of the amount of particulate matter (electrocatalyst) in the formulation as well as the amount of Nafion® ionomer used as binder and the type and relative amounts of each dispersant / solvent chosen. The amount of ionomer and electrocatalyst was kept more or less constant, thus in this study the dispersant / solvent type and ratio played the major role in ink viscosity.

6.4.1.1 LP01 series

Figure 6.9 shows the results of printing with series LP01 ink where an ink based upon isopropanol as dispersant/solvent was used.

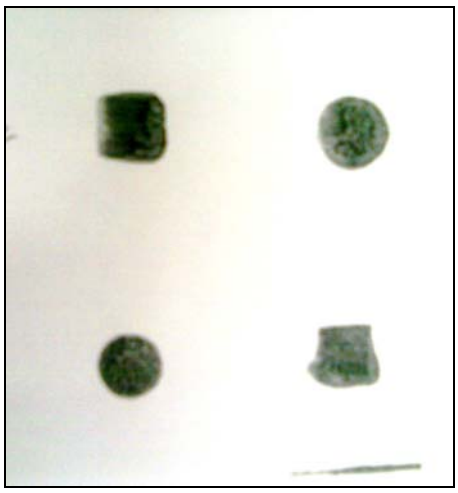

Figure 6.9 Series LP01 print run-1

LP01 series were printed using a typical spraycoating ink formulation used in preparing fuel cell MEAs (Chapter 6), containing isopropanol (and not 1,2 propanediol) as is given in Table 6.1. Optical microscopy images (backlit) of the films printed on bond paper are shown in Figure 6.10 (a-d).

LP01 series print runs 1-3 comprised of single print runs. LP01-4 comprised of one overprint (2 runs). This formulation containing isopropanol and water was found to be an inappropriate dispersant for screen printing, resulting in significant bleeding of ink around the edges of the defined 1cm ^{2} print areas, and marked inhomogeneity of printed layers, with smearing, flow marks and streaking visible on each printed

electrode, and low density or opacity of the layer after printing. Similar problems are reported by Tanaka et al., (2005) for this dispersant.

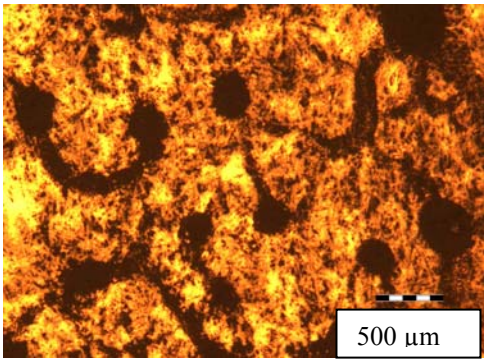

a. LP01-1

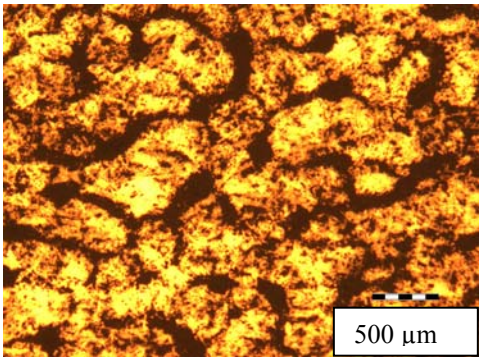

b. LP01-2

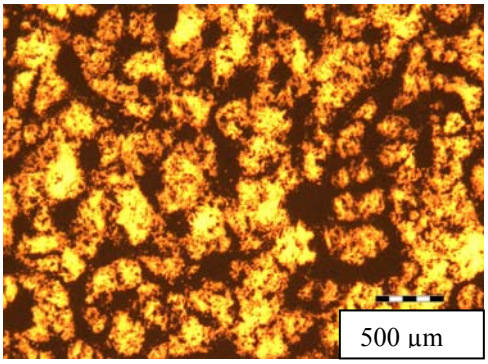

c. LP01-3

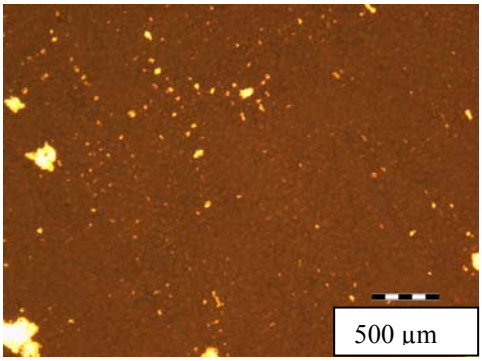

d. LP01-4 (2 runs)

Figure 6.10 Optical microscopy of LP01 series

The ink formulation used in the LP01 series was too thin/liquid and caused agglomerated and very poorly connected islands of the electrocatalyst particles which were poorly distributed upon the substrate showing significant lift-off characteristics and uneven deposition. This formulation that is usually used for spray coating was also unsuitable for use in screen printing as the ink spread outside the printing area because of its low viscosity. The formulation used had 5.5 parts of isopropanol to 1 part of water as solvent (neglecting the isopropanol in the Nafion® solution that was kept approximately constant throughout (Table 6.3)).

A single overprint gave more homogeneous results (LP01-4). However, the ink had dried considerably between the time taken (<5 min) between the first print and the

overprint because the dispersant evaporation (isopropanol) was too rapid, therefore print surface coverage was incomplete and irregular.

Thus isopropanol as dispersant was unsuitable as it evaporated too quickly to achieve good surface coverage during screenprinting. The volatility of the dispersant determined the ease with which the screen printing could be repeatedly overprinted with the same ink. As Tanaka et al., (2005) found, the screen-printability of inks degraded progressively over time, particularly in the case of the isopropanol-based inks. These authors also found that isopropanol had a lowered viscosity under increased shear rate, which caused the ink to flow from the openings on the screen and spread around the printed area as was observed in LP01 series.

6.4.1.2 LP02 series

LP02 series were printed using a formulation where isopropanol was substituted with 1,2 propanediol (99% Sigma Aldrich Lot S39776-337; Cat No. 13436B) in order to increase the drying time of the ink and improve the viscosity. The amount of catalyst was doubled with respect to the solvents for all the subsequent samples to further increase the ink viscosity compared to LP01 series. This formulation had approximately 1 part of water to 5 parts of 1,2 propanediol mass to mass as dispersant (molar fraction 1:1.24 of H_20:1,2 propanediol).

LP02-1 was printed once (run 1) without overprinting, showing a low ink deposition rate. Ink deposition was much improved for this formulation by thereafter overprinting the electrode once. Samples LP02-2 to 4 were each separately overprinted once (2 runs). Figure 6.11 shows the replicability in mass increase of overprinting of the electrode.

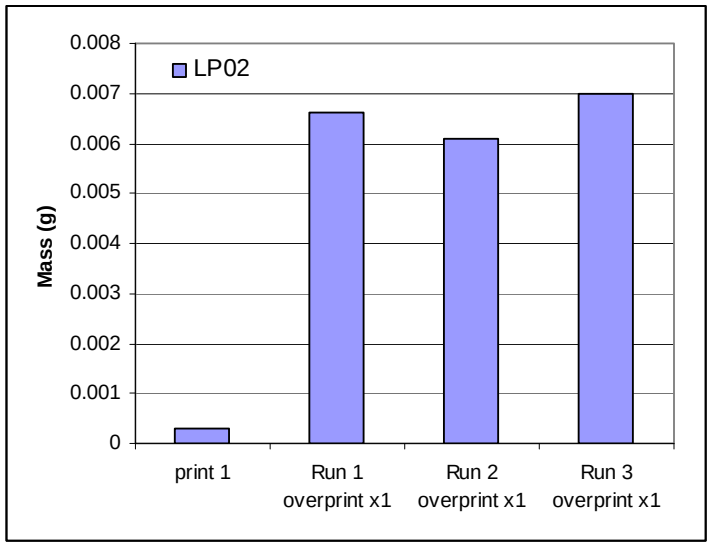

Figure 6.11 Replicability of overprinting

The degree of replicability in the mass deposition observed for the overprinted samples indicates that it was possible to accurately deposit between 0.006-0.007 g over 4 cm^2 of substrate. LP02-4 (one overprint (Run 3)) gave a somewhat denser film indicating that the dispersant had started evaporating from the ink solution before the overprint print could be done, hence it may be necessary to add a humectant to this formulation when used in bulk.

For the ink formulation containing 1,2 Propanediol that was used in the LP02 formulation very little catalyst was deposited in the first run (LP02-1). Merely 0.0003 g was deposited. The ink formulation used in the LP02 series was visibly drying during the time between print and overprint (approximately 5 min) yet this did not significantly change the amount of ink deposited during overprinting, which was replicable (compare Run 1 (LP02-2), Run 2 (LP02-3) and Run 3 (LP02-4)). The difference in the deposited mass measured for 4 cm^2 between Print 1 (LP02-1) and one overprint (LP02-2) was 0.0063 g; between Print 1 (LP02-1) and replicate overprint LP02-2 was 0.0057 g and between Print 1 (LP02-1) replicate overprint LP02-3 was 0.0058 g. The mass % difference between replicate overprinting runs (LP02-2, LP02-3 and LP02-4) was within 1% of each other showing good reproducibility of the overprinting. The difference in mass between replicated

overprinted layers (LP02-4) was an order of magnitude less than the difference observed between the first print and the subsequent overprinted layer. The first print run (LP02-1) deposited 20 times less catalyst than the subsequent overprinting run. The difference in mass observed between the first print and the overprinted layer cannot be ascribed to a change in the ink viscosity during the time taken to deposit Print 1 and overprint one time. Hence, the inconsistent increase in mass between the first print and the subsequent overprinting run indicates that the surface tension of the substrate, paper, played a role in the degree of uptake of the ink upon the substrate. The first layer merely served to prime the substrate for the subsequent printed overlayer.

Optical microscopy with backlighting of series LP02 is presented in Figure 6.12.

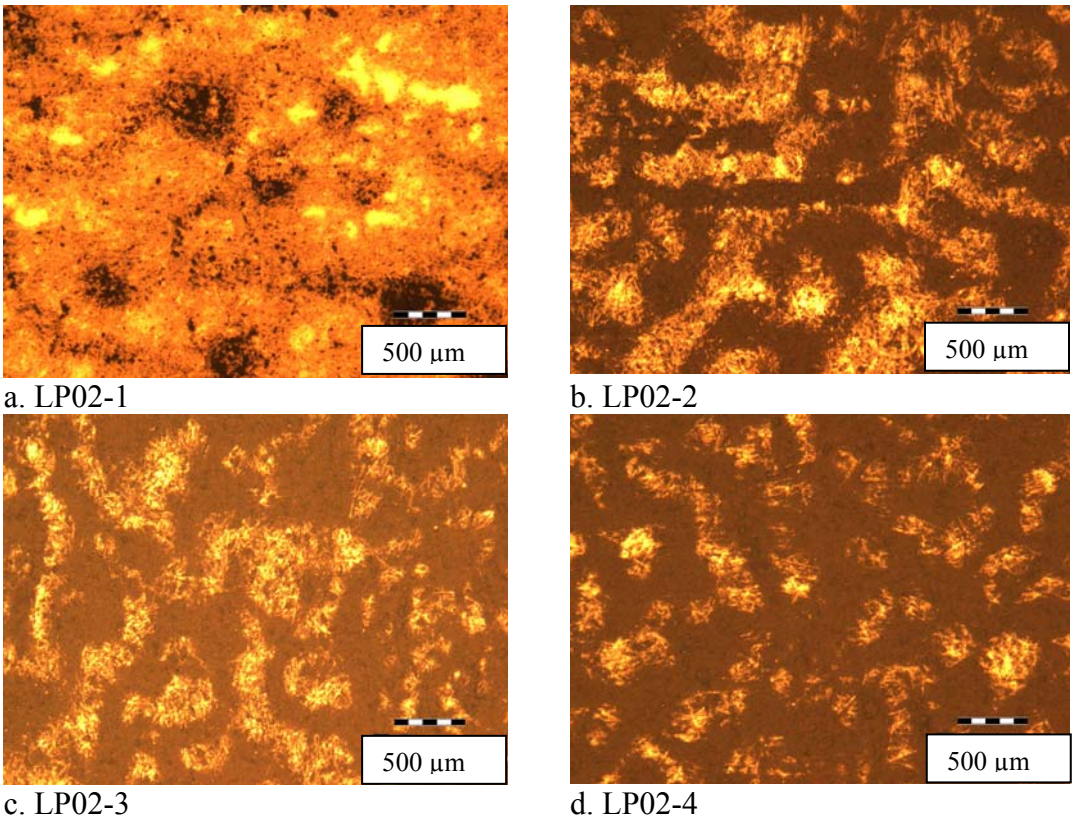

a. LP02-1 b. LP02-2

c. LP02-3 d. LP02-4

Figure 6.12 Optical microscopy of series LP02

The smearing and bleeding observed with the isopropanol formulation (LP01 series) is not visible in the overprinted samples of series LP02, which ink formulation contained the dispersant 1,2 propanediol, showing that the substitution of isopropanol

and the increase of the solid fraction (doubled) in this ink formulation resulted in a significant improvement in the printing quality (SGIA, 2008). Mottling with voids and substrate show through effects are still visible in samples LP02-4 which may be reduced by overprinting to improve the density (opacity) of the film. Registry of the overprinting was exact and no offset, bleeding or jagged edges were observed.

6.4.1.3 LP03 Series

Figure 6.13 shows optical microscopy images of LP03 series.

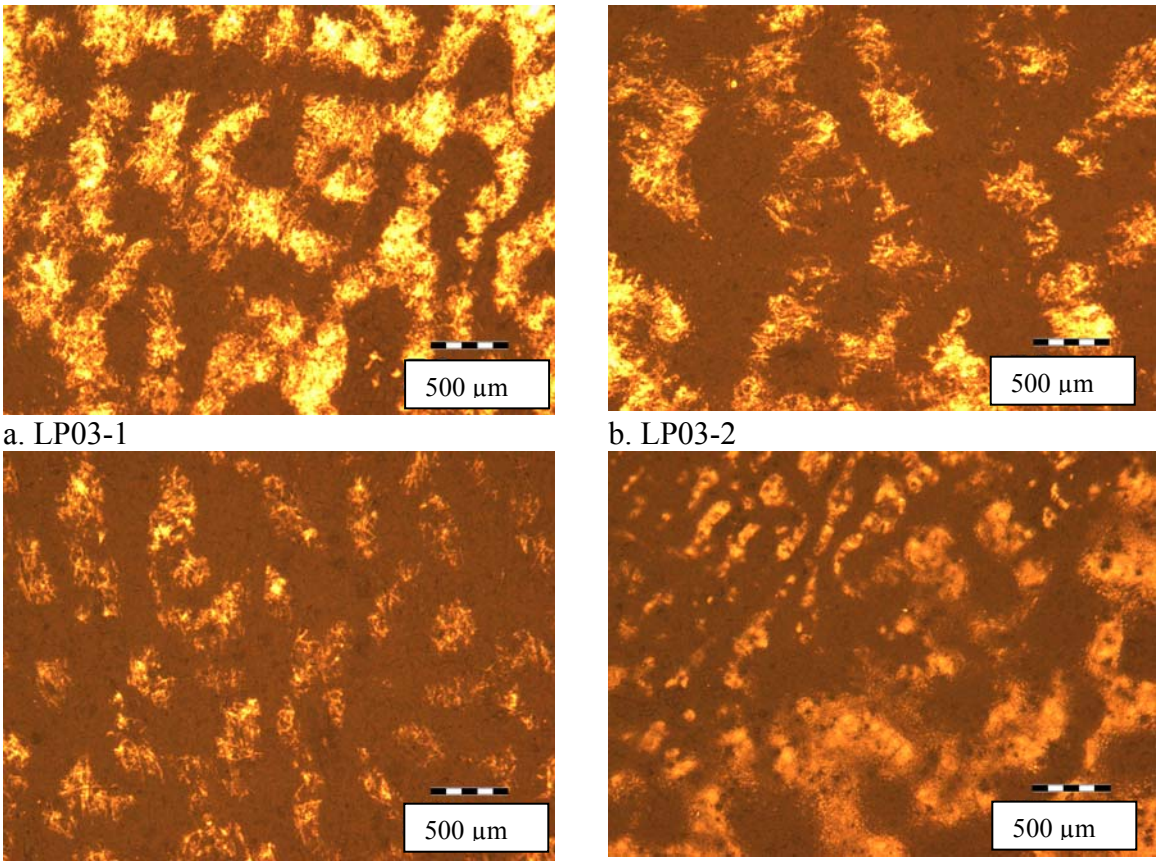

a. LP03-1 b. LP03-2

c. LP03-3 d. LP03- Nafion

Figure 6.13 Optical microscopy images of LP03 series

LP03 series were printed using a formulation similar to that used in LP02 series with slightly more 1,2 propanediol to adjust ink viscosity slightly to improve screening of the ink during overprinting. This formulation had 1 part of water to 7.5 parts of 1,2 propanediol on a mass to mass basis of dispersant (molar fraction 1:1.77 of H_20:1,2 propanediol). Some smearing of the layer was observed during screening LP03-1 but

better deposition of the electrocatalyst was achieved in the first print run than was the case for sample LP02-1. LP03-2 comprised of two overprints (3 runs) and LP03-3 comprised of one overprint (2 runs) as at this stage the ink became thicker due to its volatility and print quality was better.

The inconsistency found in the deposition indicated that this formulation was still too volatile over the duration of the overprinting therefore the ratio of water to 1,2 propanediol was adjusted further. The LP03 formulation was used for printing on the treated Nafion® substrate as a trial run (Figure 6.13 (d)) and it was observed that the particulates in the first printed layer on Nafion® showed similar patterns of mottling, voids and agglomeration visible on the paper, which were still visible after overprinting twice (3 runs). On the Nafion® flow patterning and lift-off smearing of the print was also visible.

6.4.1.4 LP04 series

LP04 series were printed using a formulation where the mass of water was increased and that of 1,2 propanediol was decreased in order to improve the wetting of the Nafion® sheet during printing and try to minimize the mottling and agglomeration observed in series LP03. This formulation had 1 part of water to 2.9 parts of 1,2 propanediol mass to mass as dispersant (molar fraction 1:0.68 of H_20:1,2 propanediol).

Figure 6.14 shows optical microscopy images with backlighting of series LP04.

LP04-1 (Figure 6.14(a)) comprised of one print run and showed good coverage but slight bleeding was observed around the edges of the print. LP04-2 (Figure 6.14 (b)) comprised of two layers (one overprint) and LP04-3 comprised of three layers (two overprints) and achieved better coverage and opacity on the paper than was achieved in previous series, showing that the higher water content relative to 1,2 propanediol (1: 2.9 mass by mass ratio) improved the ink formulation for printing on paper.

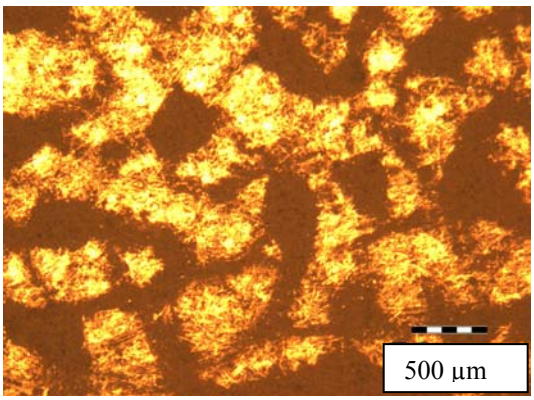

a. LP04-1

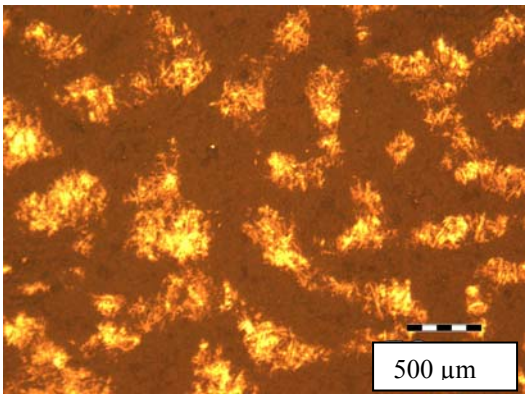

b. LP04-2

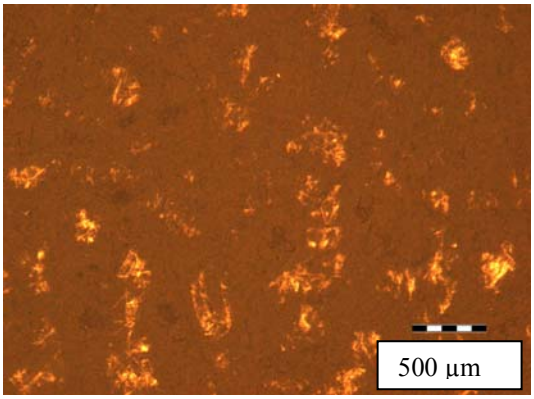

c. LP04-3

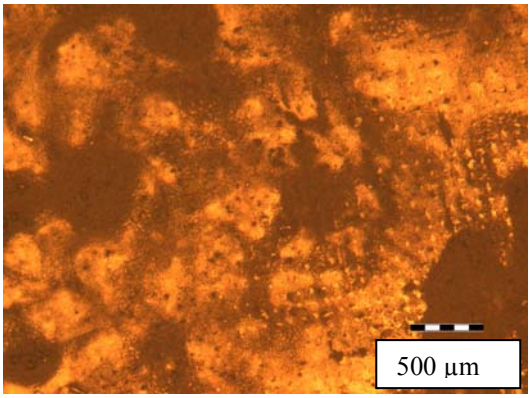

d. LP04-Nafion three runs

Figure 6.14 Optical microscopy images of LP04 series

However, this formulation was still not entirely satisfactory when Nafion® was used as substrate (LP04-Nafion – Figure 6.14(d)). On the first Nafion® print run significant take off effects were observed especially on circular designs of electrodes whereas the quality of square design electrode prints were better. The first overprinted layer on Nafion®, showed improvement of the printing for square designs, whereas the circular electrode designs still showed problematic lift off effects. During the second overprint on the Nafion® substrate fairly good surface coverage was obtained.

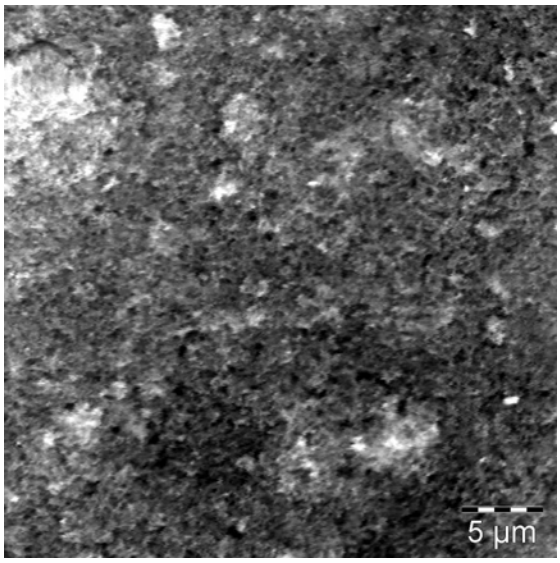

In order to view the structure of the printed layers Scanning Electron micrographs were obtained and the image for LP04-3 is shown in Figure 6.15. The particulate nature of the electrocatalyst can be seen as well as the porous nature of the deposited film. There is considerable surface roughness and in some areas small cracks could be observed.

Figure 6.15 LP04-3 SEM image at 3K

6.4.1.5 LP05 series

LP05 series were printed using a formulation where the mass of water was further increased and that of 1,2 propanediol was decreased with respect to only the liquid components of the ink without changing the overall amount of liquid, to improve the wetting of the Nafion® sheet during printing. This formulation had 1 part of water to 1.07 part of 1,2 propanediol as dispersant on a mass to mass ratio (molar fraction 1:0.25 of H_20:1,2 propanediol)), whereas the formulation for LP04 contained 1:0.68 molar ratio of water to 1,2 propanediol. Optical microscopy images of Series LP05 with backlighting are shown in Figure 6.16.

LP05-1 (Figure 6.16(a)) comprised of a single layer that was of a much better quality than observed in any of the previous screen printed series. In this sample the screen structure is visible with some pin hole defects but the electrode prints showed very few lift-off effects. LP05 -2 (Figure 6.16(b)) comprised of 2 layers (one overprint) and LP05 -3 (Figure 6.16(c)) comprised of 3 layers (overprinted twice), all samples of which were significantly improved with respect to the surface coverage obtained as well as a great improvement in the degree of bleeding and very little mottling or agglomeration was noticeable on the paper compared with all other formulations.

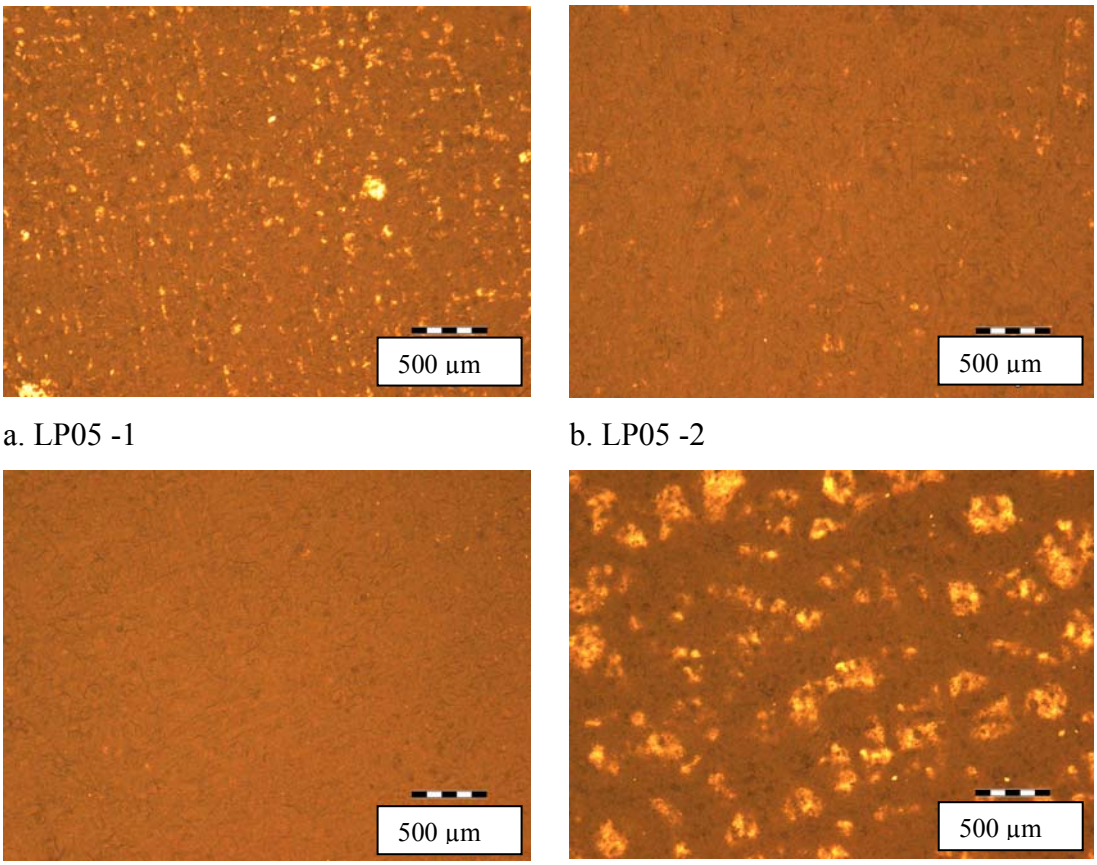

a. LP05 -1

b. LP05 -2

c. LP05 -3

d. LP05-Nafion – three runs

Figure 6.16 Optical microscopy images of Series LP05

LP05-Nafion (Figure 6.17(d)) comprised of three layers (two overprints). Although the sample comprising of three layers is of better quality than the previous samples printed on Nafion®, there is still a degree of mottling and agglomeration visible. The lift-off on the circular electrode design was still apparent whereas the square electrode design resulted in a relatively good quality print after three layers were deposited.

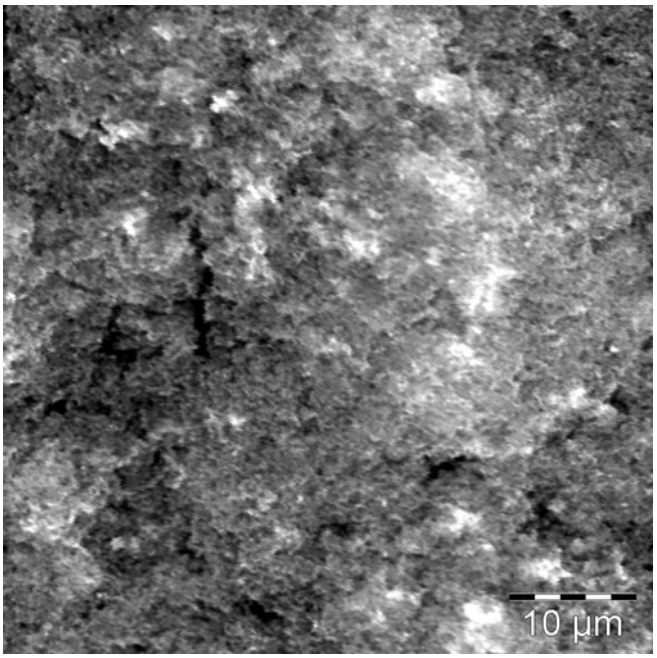

Figure 6.17 LP05-3: SEM image at 2K of Series LP05

In order to view the structure of the printed layer Scanning Electron micrographs were obtained and the image for LP05-3 is shown in Figure 6.17. Similar to LP04 series the particulate nature of the electrocatalyst can be resolved as well as the porous nature of the deposited film. Once again there is considerable surface roughness and in some areas small cracks could be observed.

6.4.1.6 LP06 Series

LP06 series were printed using a formulation where the dispersant ratio was similar to LP05 with 1: 1.01 H_20:1,2 propanediol on a mass to mass basis (molar fraction 1:0.24 of H_20:1,2 propanediol) but about 30 mass % fullerenes relative to the electrocatalyst mass were added to the formulation in order to determine the effect, if any, on resistivity and electronic characteristics. It was expected that the fullerenes would dominate the electronic characteristics of the electrodes. LP06-1 comprised of one layer (1 run) and LP06-2 comprised of 3 runs (overprinted twice).

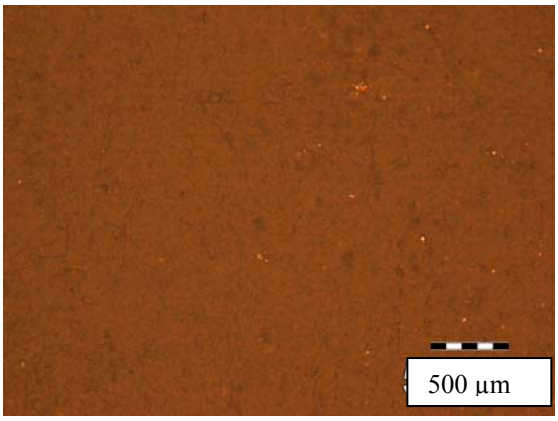

(a)LP06 1

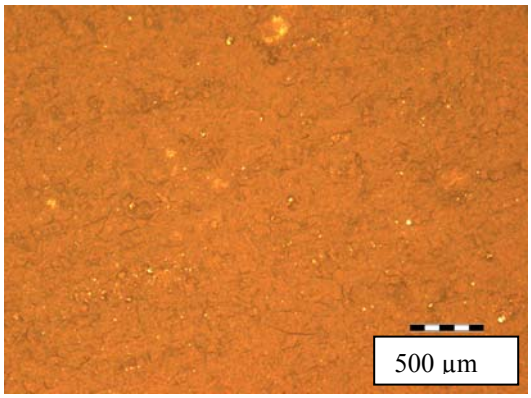

(b)LP06-2 3 runs

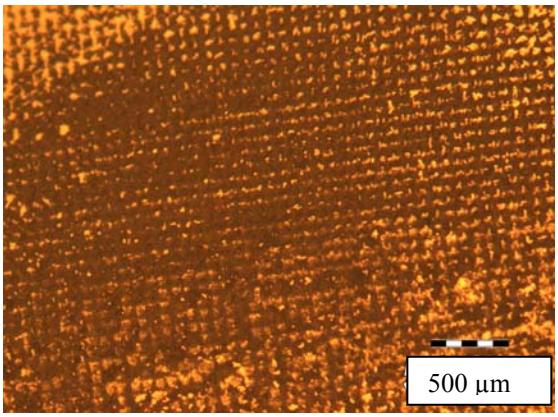

(c) LP06 –Nafion one run

Figure 6.18 Optical microscopy images of Series LP06

In the LP06 series the printing of only one layer already gave a homogeneous and dense layer of the particulate electrocatalyst on paper (Figure 6.18(a)). Overprinting this layer twice created a thick film on the paper substrate (Figure 6.18 (b). The ink was however, too paste-like and viscous because of the additional solid phase to allow the ink to flow readily upon the Nafion® substrate (sample LP06-nafion) and the screen pitch or thread line widths are clearly visible due to lack of gain.

The SEM image of LP06-2 (Figure 6.19) again shows the particulate nature of the electrocatalyst as well as the porous nature of the deposited film. Yet again there is visible surface roughness but cracking was reduced compared to other formulations.

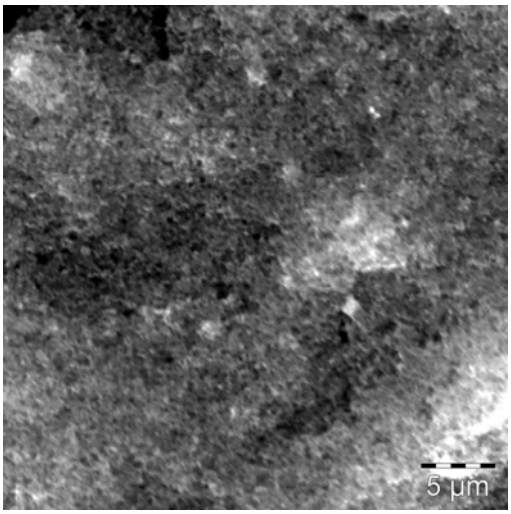

Figure 6.19 LP06-2 SEM image at 3K

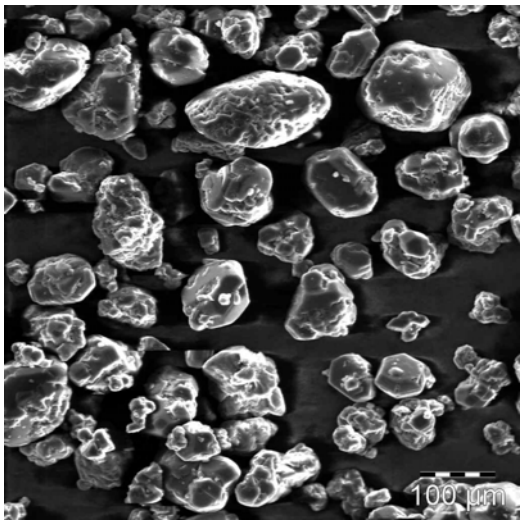

Figure 6.20 "Fullerenes" as supplied by Aldrich

The fullerenes supplied by Aldrich did not appear to have a fullerene crystal morphology and the material was significantly agglomerated into large particles (Figure 6.20). However, EDS analysis showed that this material was mainly composed of carbon. The addition of the fullerenes to the ink increased the solids fraction of the ink and appeared to improve the film structure when investigated by optical microscopy and SEM.

6.4.1.7 LP07 series

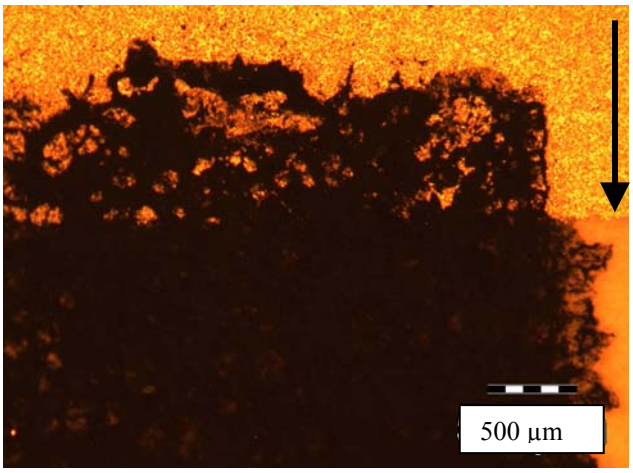

Figure 6.21 LP07-1 Electrode screen printed on silver contact

Figure 6.21 shows the optical microscopy image of the electrode LP07-1 screen printed on to a silver contact preprinted upon paper. The arrow indicates the boundary of the preprinted silver contact.

Three overprints of ink LP07 were screen printed onto prepared paper that already had nanoparticulate silver contact strips screen printed for Hall measurements, as can be seen in Figure 6.21. However, print registry between overprints was inexact and the catalytic ink did not adhere at all well to the screen printed silver ink contacts. The Hall effects were therefore not determined by using silver screen printed contacts, but by handpainting silver contacts.

Figure 6.21 shows jagged edges and voids in the electrocatalyst printed layer overlaying the silver contact. This result highlights the problem of unsuitable surface energy of the substrate or any underlying printed contact. Thus ink formulations would need to be significantly adapted to print directly onto printed conductive silver contacts, which fell outside the scope of this study.

6.5 ELECTRONIC CHARACTERISTICS OF FILMS

6.5.1 Results and Discussion: Resistivity characteristics

Resistivity and Hall effects were obtained of each printed sample using the method specified in Section 6.3.3 to characterize the electronic properties of the films containing the particulate nano structured electrocatalyst. IV curve measurements gave the following resistance readings (Table 6.5) between each contact pair probed.

For comparison, the resistances of Lydall carbon cloth (6100-300) and a spraycoated electrode made with Lydall 6100-300 and JM Pt_{40}/C (used in MEA65 as described in Chapter 7) are shown in Table 6.5. Furthermore, the results obtained for CNT paper (as described in Chapter 3) and CNT paper coated with Pt nanoparticles using the galvanic displacement technique (described in Chapter 4) are also included.

Table 6.5 Resistance of screenprinted samples (Units in K Ω unless specified)

Sample	R12,12	R23,23	R34,34	R41,41
Blank paper (G Ω)	6.8	12.8	7.5	10.0
Blank Nafion® (M Ω)	72.3	253.3	214.9	188.3
LP02-1 (G Ω)	5.573	5.017	3.611	4.148
LP02-2	17.654	74.88M Ω	2.347M Ω	769.18
LP02-4	11.185	16.338	14.235	8.608
LP02-Nafion	17.71	8.56 M Ω	9.169M Ω	449.59
LP03-1	40.118	5.177 M Ω	467.82 M Ω	39.243
LP03-2	4.724	6.37	7.748	7.567
LP03-3	4.724	6.37	7.748	7.567
LP03-Nafion	17.317	58.231	65.973	18.11
LP04-1 (G Ω)	2.388	2.838	7.473	7.95
LP04-2	6.443	11.803	11.976	8.515
LP04-3	4.398	4.007	3.085	3.251
LP04-Nafion	5.780	5.502	5.341	6.183
LP05-1	8.377	7.481	5.835	6.437
LP05-2	3.045	3.018	3.341	3.217
LP05-3	1.498	1.379	1.593	1.625
LP05-Nafion	4.45	6.733	7.814	5.837
LP06-2	1.715	1.628	1.691	1.692
LP06-Nafion	19.54	14.143	13.59	111.41
Lydall 6100300 blank (Ω)	51.5	50.84	51.03	50.75
Lydall 6100300 S4 (Ω)	50.78	51.52	51.19	50.41
CNT paper (Ω)	49.57	49.65	49.39	49.30
CNT paper + Pt (Ω)	60.61	102.23	102.58	61.54

The variability of resistance between contact pairs was not significant for series LP04, LP05 and LP06 except for LP06 Nafion where one contact was of poor quality. The variation seen in LP01, LP02 and LP03 series in most cases, was attributed to poor film quality and not to poor contacts as the contacts were inspected and their

quality was acceptable. The resistance of the Nafion® blank (Table 6.5) was somewhat lower than the paper sample showing the less insulating nature of this substrate. Figure 6.22 shows the resistance of each film sample in each series graphically.

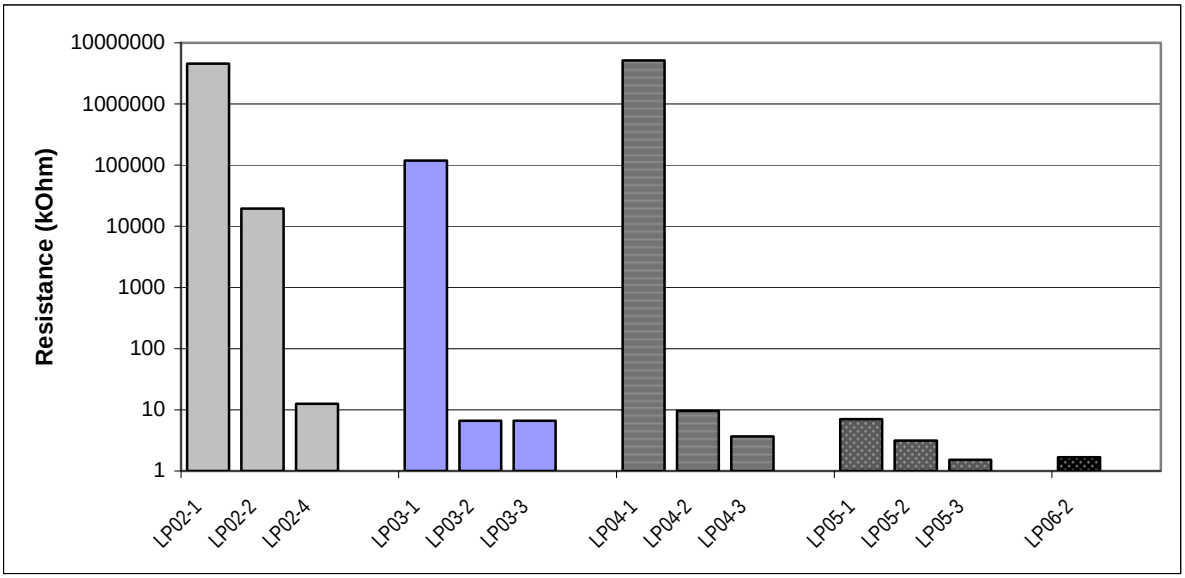

Figure 6.22 Averaged resistance as a function of number of layers of ink for each series printed on paper

Samples LP02-1 and 2 on paper substrates showed excessive resistivity (Figure 6.22) which in the case of LP02-1was nearly equivalent to the blank paper sample, thus these samples were not characterized further. LP02-2 had a similar mass loading to LP02-4, but the resistivity was much higher. This shows the difficulty of achieving reproducible electrical characteristics of films. Catalyst loading is not the only variable of significance, the structure of the film contributes significantly to the electronic properties of the film. Visual inspection and optical images of the printed layers showed that the film obtained in the case of sample LP02-4 was more coherent, with fewer void spaces and less mottling than was the case in sample LP02-2. Hence basing electrode quality on mass loading measurements only is not sound.

In the case of series LP03, the first layer was poorly dispersed and thus highly resistive whereas subsequent layers resulted in a significant decrease in resistance, showing the importance of film thickness in reducing resistance.

All the series showed a lowered resistance trend for each additional printed overlayer (Figure 6.22). This reduction in resistance correlated inversely to the mass of electrocatalyst loaded upon the substrate as can be seen in Figure 6.23. The correlation between resistance and grams loaded for LP05 series is shown in Figure 6.23.

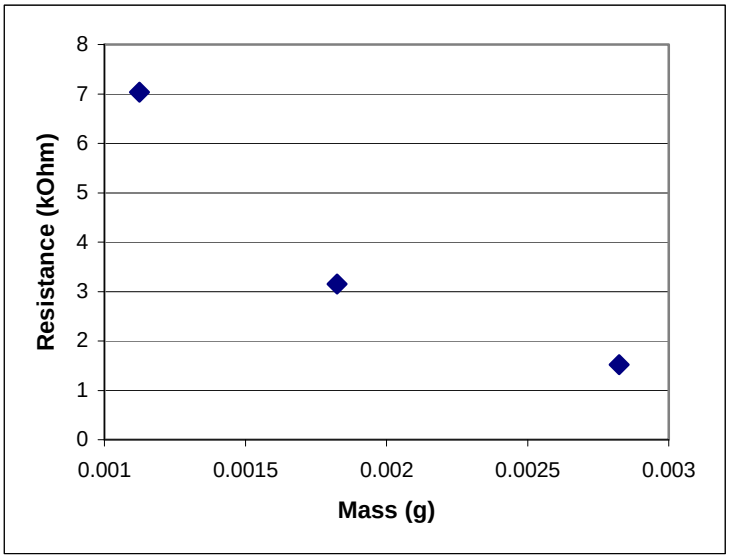

Figure 6.23 Correlation between resistance and grams loaded for LP05 series

Table 6.6 Resistance as a function of loading of electrocatalyst upon substrates

	Mass (g) cm^{-2}	Ave. Resistance (k Ω)
LP04-1	0.00111	5162250
LP04-2	0.0020	9.68425
LP04-3	0.00305	3.68525
LP05-1	0.00113	7.0325
LP05-2	0.00183	3.15525
LP05-3	0.00283	1.52375

Figure 6.23 and Table 6.6 demonstrate that the amount of conductive electrocatalyst in the film directly impacted upon the conductivity of the film, since the only electro conductive component in the film (and substrate) was the commercial electrocatalyst,

composed of Pt on carbon. However, the LP04 series had roughly similar amounts of electrocatalyst deposited per unit area for each layer compared to LP05 (Table 6.6) yet showed generally much higher resistance, because of poorer print quality. The resistivity results for sample LP04-1 were in Gohm (Table 6.5) as this single layer was not homogenous or continuous due to poor dispersion and agglomeration of the ink upon the substrate as can be seen in Figure 6.14 (a). The resistivity of the electrode was significantly lowered by overprinting two successive ink layers there after (Table 6.6, samples LP04-2 and LP04-3).

The difference in resistance observed between these two series cannot be ascribed to catalyst loading only but also to the print quality and the conductive pathway created by adjoining clusters of printed electrocatalyst, which was affected strongly by the ink formulation. Hence, no matter how active the electrocatalyst, if the deposition of the film on the substrate is substandard, electro activity will be low.

In series LP05, even the first printed layer on non-conductive paper (Table 6.5) had a relatively low resistance (below 10 k Ω compared to 100,000 k Ω for other single printed layers) showing the benefit of this water rich formulation to form a cohesive film. Significantly less mottling and agglomeration was observed because of the higher water content and resulted in better catalyst/binder dispersions upon the substrate paper even for the first layer printed. The affinity of the water enriched formulation for the surface of the substrate was thus improved, showing the impact of the interaction of the ink with the substrate.

It is postulated that this effect is due to improved matching of the surface free energy of the liquid with that of the substrate. The surface energy of a solid cannot directly be measured (Kruss, 2008) but can be determined by contact angle measurement of the liquid in contact with the surface considering surface interaction, surface reactivity and surface solubility and will be specific to the liquid. The surface tension of 1,2 propanediol increases as the concentration of the water in the mixture increases (Horibe et al., 1997).

As the change in the dispersant ratio in the formulation relates mainly to modifying the polarity and surface tension of the mixture incrementally, with an increased water content rendering the solution more polar, it is likely that molecular interactions have improved between the ink formulation used in this case and the paper substrate surface because of liquid/solid surface interactions increasing.

The formulation used for LP06 series showed low resistances for the sample prepared on paper and overprinting resulted in an electrode with similar resistances compared to LP05, despite the addition of a high proportion of “fullerenes”. The additional “fullerenes” appeared to have no significant effect upon the resistance of the electrode.

The samples that were printed on paper showed a good correlation between each successive overprinted layer thickness and lowered resistance. The first printed layer is typically high in resistance, the next overprinted layer reduced the resistance of the electrode by orders of magnitude and the third overprinted layer caused the electrode resistance to reduce even further. Addition of fullerenes did not apparently affect the resistance significantly as the resistance of LP06-2 which contained fullerenes (three successive overprinted layers) is similar to the resistance obtained with three layers of the ink without fullerenes (LP05-3).

Comparison of the average resistance of samples prepared on the Nafion® substrate (Figure 6.24) shows the large effect of the ink formulation upon the resistance of the film.

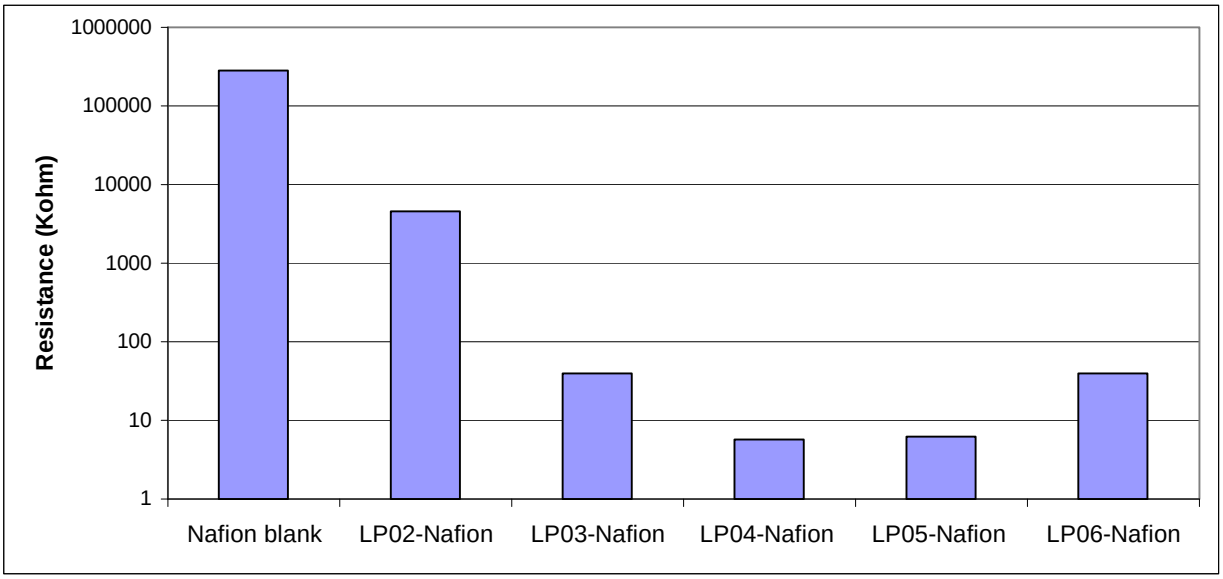

Figure 6.24 Average resistance of samples prepared with Nafion® as substrate

For the samples screen printed upon Nafion® substrates it appeared that the more water in the formulation, the better the adhesion and integrity of the film printed upon the Nafion® substrate, up to an optimum low resistance achieved in the formulation used for series LP04 that used a molar ratio of 1: 0.68 water to 1,2 propanediol. The ink formulations and specifically the dispersant type, content and ratios are thus shown to have a significant impact upon the electronic properties of the deposited film.

The optimum resistance for the paper substrates was achieved with LP05 formulation containing a molar ratio of 1:0.25 water to 1,2 propanediol, whereas the optimum resistance for the Nafion® substrate was achieved in sample LP04 nafion, with a molar ratio of 1: 0.68 of water to 1,2 propanediol, showing how differences in the composition of the ink formulation could impact upon the electronic nature of the film, depending upon the substrate used.

The films printed on Nafion® did not generally have the lowest resistance compared to those printed on the paper substrate, mainly because the films screen printed upon Nafion® substrates were generally neither homogenous nor very well dispersed, due to the interaction of the ink with the substrate. This shows the significant impact that

the interaction of the surface of the substrate with the ink has upon the electrical characteristics of the film. The effect is postulated to relate to adhesion energy and interfacial tension. Sample LP06 Nafion showed high resistance for points R41,41 that was anomalous and could indicate poor contact or damage of the film on the electrode between these points, hence this result is merely shown for comparative purposes. This sample had been cured at 80º C unlike other Nafion® printed samples and the Nafion® had also been heat damaged. Curing would not be possible when printing on Nafion® polymer electrolyte membrane because of its heat sensitivity, thus formulations that do not require heat curing should be developed.

Spraycoated electrode samples on carbon cloth (as described in Chapter 7) and carbon nanotube paper samples were tested for comparative purposes. The resistance of samples 6100300 (Lydall carbon cloth 6100-300) and 6100300 S4 (Lydall carbon cloth 6100-300 with spraycoated layers of JM Pt_{40}/C namely MEA 65 as is described further in Chapter 7) were measured using the Hall measurement system. Both these samples showed an order of magnitude lower resistance than the samples prepared on paper showing the effect of using a conductive support upon the resistance of the composite electrode material. The difference in resistance due to the additional spraycoated ink layer cannot easily be discriminated by resistance measurements alone when using carbon cloth as substrate. The CNT paper itself had the lowest resistance of all the substrates tested (49 Ω). Once the Pt was deposited upon the CNT paper using the galvanic displacement technique the resistance increased to an average resistance of 81 Ω.

These results show that the film characteristics depended upon the dispersant / water ratio in the ink mixture and the type of dispersant used, the film layer thickness and morphology as well as the nature of the substrate. Such large changes in the resistance of the printed film as was observed in these experiments would have a very significant impact on the ohmic drop experienced in a working cell, thus all these factors should be taken into account when formulating a screen printing ink and

depositing it. Resistance measurements showed some of the electronic properties of the films.

6.5.2 Results and Discussion: IV Curve Measurement

Since resistance alone does not fully characterize a material, IV measurements and Hall measurements were taken for the above samples. In this section the IV results of samples screenprinted on paper and Nafion® as substrate are presented. For comparative purposes the Lydall carbon cloth blank (6100-300) and the MEA 65 cathode electrode (6100300 S4) prepared by spraycoating layers of ink upon substrate 6100-300 (as is described in Chapter 7) was tested with the Hall measurement system and results are shown as well where relevant. Furthermore, the results obtained for CNT paper (as described in Chapter 3) and CNT paper coated with Pt nanoparticles using the galvanic displacement technique (described in Chapter 4) are also included. The galvanic displacement technique was used as an alternative and rapid route to depositing Pt upon the GDL substrate without the need for binders, inks or printing.

A comparison of the IV curve measurements for each sample prepared on paper substrates are shown in Figures 6.25- 6.30 which depict the voltage obtained under a variable applied current from -1.0mA to 1 mA in steps of 100 μA.

6.5.2.1 Series LP02

The IV curves of series LP02 are shown in Figure 6.25. Samples LP02-1 and 2 are not presented due to excessive resistance. At an applied current of -0.001mA a voltage of >10 was obtained for both LP02-3 and LP02-nafion electrodes and the film on the Nafion® substrate required a significant higher voltage (-17.7V) to achieve a current flow of -0.001mA, showing the poor current carrying capacity obtained even for overprinted films prepared with this ink formulation on the Nafion® substrate.

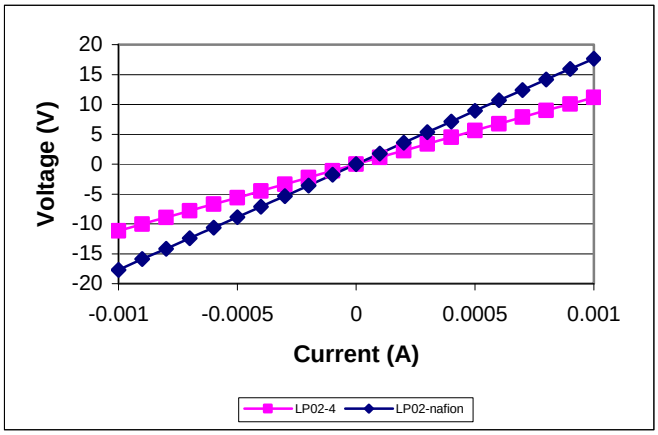

Figure 6.25 IV curves of series LP02

Although the mass of catalyst deposited upon this series of films prepared on bond paper using isopropanol as solvent/dispersant was replicable, the films were not homogeneous or continuous and this can be seen in the high resistance and the high voltage required, between -18 and -11 V at -1 mA showing low current carrying capacity.

6.5.2.2 Series LP03

The IV curves of series LP03 are shown in Figure 6.26.

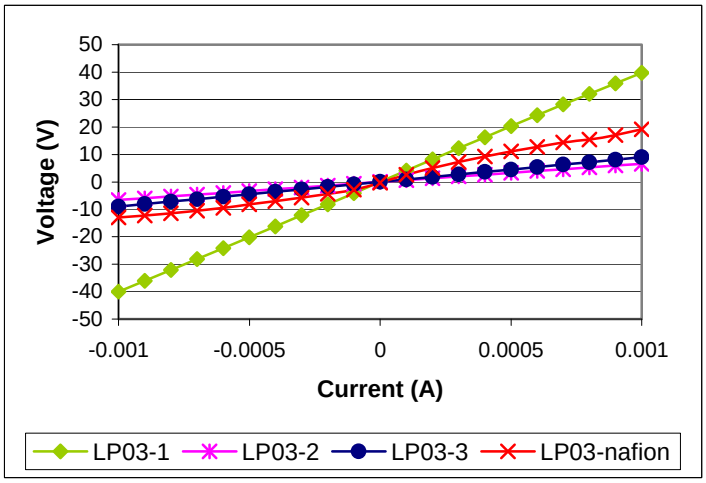

Figure 6.26 IV curves of series LP03

A high voltage requirement was necessary for LP03-1 because of the poor integrity of the first layer of film deposited which resulted in the poor performance observed during the linear IV sweep (Figure 6.26). Similar and lower voltage requirements (<

10 V at applied current of -1 mA) were obtained for both samples LP03-2 and LP03-3 during the linear IV sweep. Better film integrity was obtained both on the bond paper with this formulation containing 1,2 propanediol than the previous formulation. This resulted in less agglomeration during screen printing. The Nafion® based sample LP03-nafion showed a non–linear IV curve with an increasing voltage requirement as the sweep progressed from negative values to positive values. This is atypical of an IV curve of a conducting material, and could relate to the poor structure of the film prepared on this sample.

6.5.2.3 Series LP04

The IV curves for series LP04 are shown in Figure 6.27

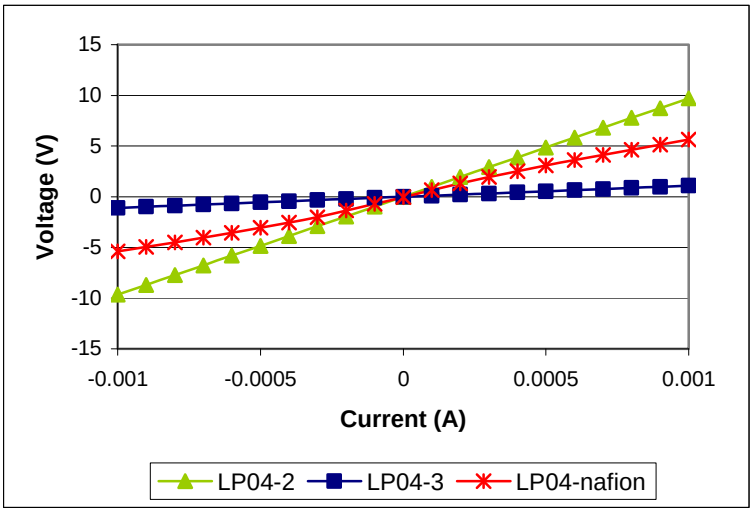

Figure 6.27 IV curves for series LP04

The curve for sample LP04-1 is not shown as this sample showed high resistance. The curves for LP04-2 and LP04-3 show the impact of the second overprinted layer on the electrical properties of the film. A denser film with fewer voids was obtained after overprinting (3 runs) in the case of LP04-3 which significantly improved the performance of the film (<-2 V at -1 mA). The Nafion® sample was also overprinted (3 runs) yet showed an intermediate performance (-5 V at -1 mA), as this ink formulation did not disperse as well on the Nafion® substrate as on the paper.

6.5.2.4 Series LP05

The IV curves for series LP05 are shown in Figure 6.28.

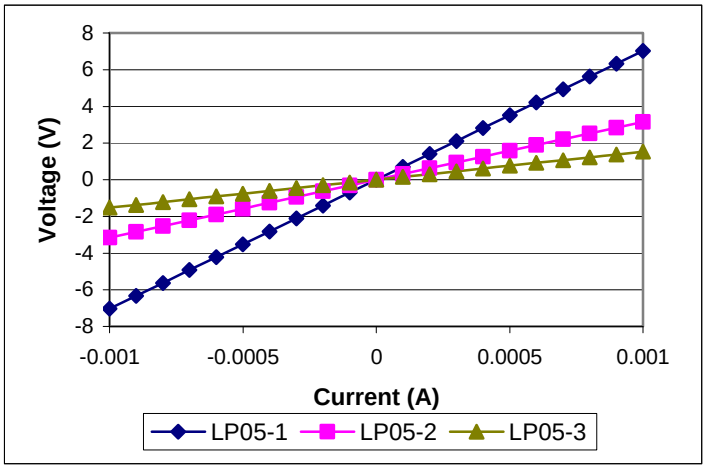

Figure 6.28 IV curves for series LP05 printed on paper

Overprinting in the case of the LP05 series incrementally improved the electrode performance and LP05-3 showed about -1.5 V at -1 mA, the best performance in the series of electrodes prepared on a paper substrate.

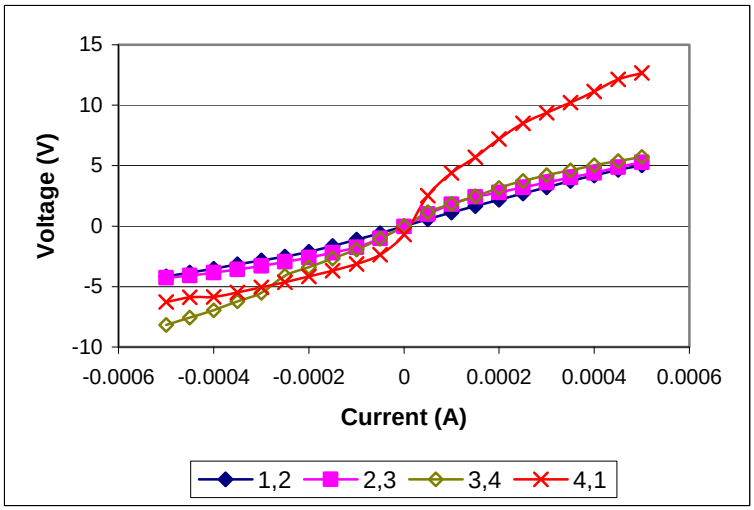

Figure 6.29 IV curves for LP05-Nafion

The linear IV sweep (Figure 6.29) of each contact set (1,2; 2,3; 3,4; 4,1) in the van der Pauw configuration of sample LP05-Nafion showed a sigmoidal IV curve particularly for the contact set 4,1. This film sample printed on Nafion® did not show perfect surface coverage being non-uniform between contact pair (3,4) and (4,1) thus causing high resistance for these contact points, yet this sample gave the best

performance of the Nafion® series of samples. Nonlinearity can be attributed to defects in contact point number 4.

6.5.2.5 Series LP06

The IV curves for LP06 series are shown in Figure 6.30.

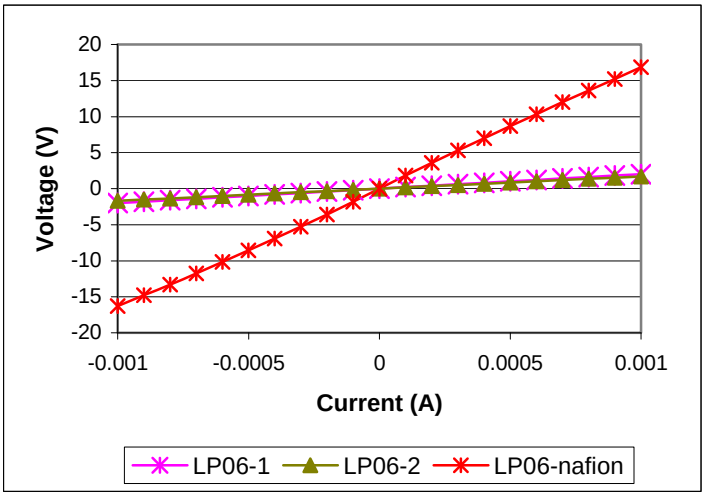

Figure 6.30 IV curves for LP06 series

A comparison of the IV curve measurements (Figure 6.30) for LP06-1 and LP06-2 show that the performance was similar, with similar voltage (<-2 V at -1 mA) obtained as was the case for LP05-3, whereas the performance of the LP06 nafion sample was poor, due to poor film integrity as observed by microscopy. Thus there was no particular benefit apparent in the IV performance by adding an additional fullerene phase to the ink formulation.

Comparison of IV curves for film samples prepared upon paper substrate is made in Figure 6.31.

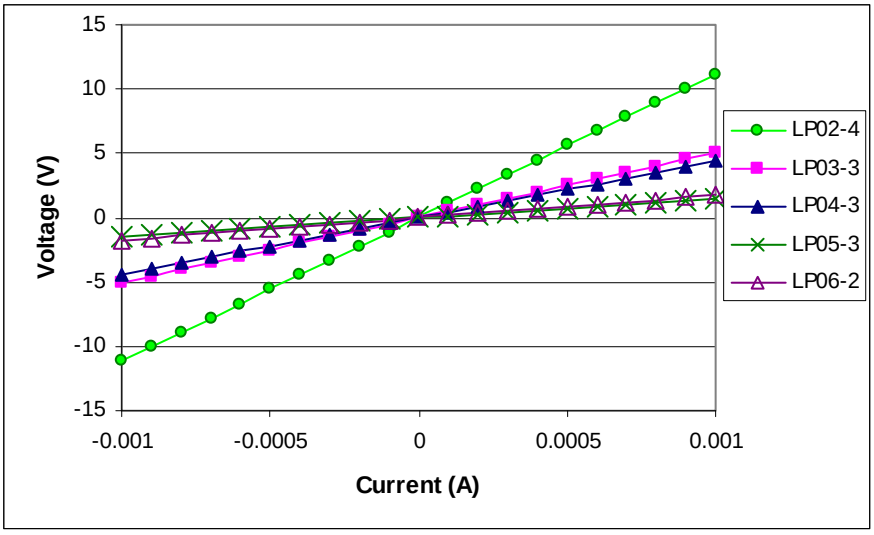

Figure 6.31 Comparison of IV curves for film samples prepared upon paper substrate.

Linear IV curves were obtained for films on a paper substrate, with LP02-4 showing the highest overvoltage whereas samples LP05-3 and LP06-2 show similarly low overvoltage. These two samples also had the lowest resistance. Samples LP03-3 and LP04-3 show an intermediate overvoltage. These results show that the best films were obtained on paper with the formulations used for LP05 series and LP06 series and specifically after 3 overprints. These two samples would require the lowest energy input for a current to flow and there was a linear relationship between current and voltage for all samples on the paper substrate.

The IV curve measurements for samples prepared on a Nafion® substrate are compared in Figure 6.32 which depicts the voltage under a variable applied current from -1.0mA to 1 mA in steps of 100 µA.

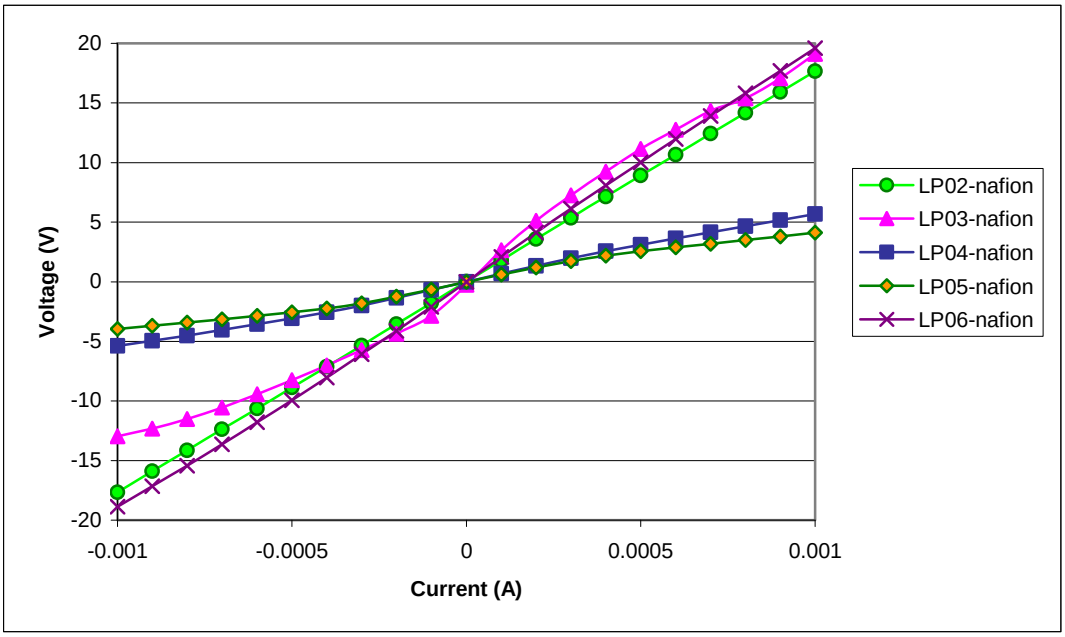

Figure 6.32 IV curves for samples prepared on a Nafion substrate

The Nafion® substrate samples cluster into two groups, namely the group of LP04-nafion and LP05-nafion that show a lower overvoltage and thus low potential requirement for each applied current and the group (LP02-nafion; LP03-nafion; LP06-nafion) that resulted in significantly higher overvoltage and thus high potential requirement for the same current input. These three samples also had significant higher resistances (above 10 kOhm) than the other samples. Interestingly the samples prepared on the Nafion® substrate in some cases showed a sigmoidal curve during the IV measurement which indicates that an energy barrier should be overcome before the current can flow. This was particularly noticeable for sample LP03-nafion and in this case there was significant agglomeration of the particulates in the ink (see Figure 6.13) which could indicate non continuous conductive pathways that impede the flow of current, forcing the current to flow through the Nafion® film.

For comparative purposes the IV curves of Lydall carbon cloth blank (6100-300) and the MEA 65 cathode electrode prepared by spraycoating layers of catalyst containing ink upon substrate 6100-300 (6100300 S4) are shown in Figure 6.33. Furthermore, the IV curves obtained for CNT paper (as described in Chapter 3) and CNT paper

coated with Pt nanoparticles using the galvanic displacement technique (described in Chapter 4) are also included.

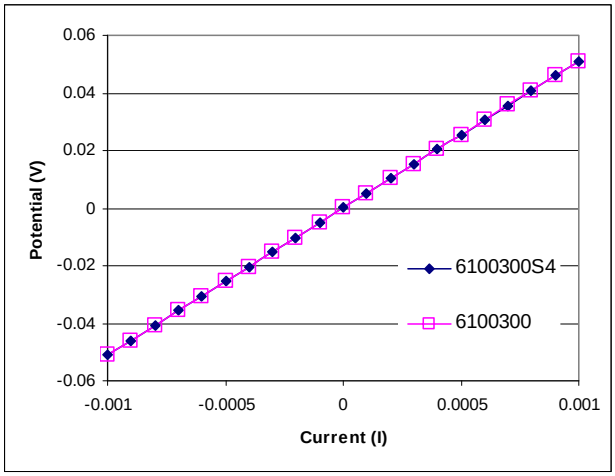

Figure 6.33 IV curves for samples prepared by spraycoating on a carbon cloth substrate

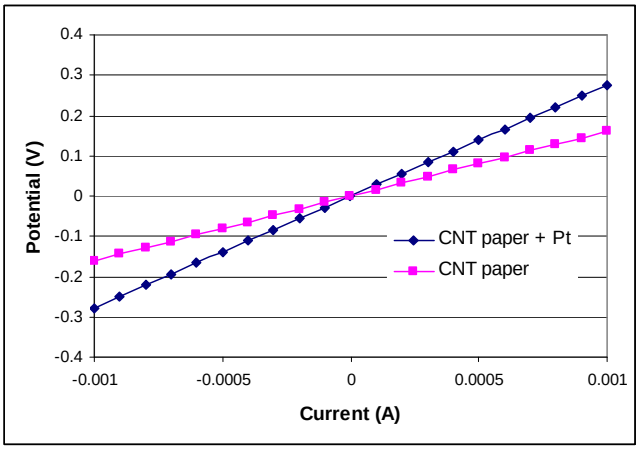

Figure 6.34 IV curves for the CNT paper and CNT paper + Pt

The IV curve (Figure 6.33) of the electrode sample MEA65 (denoted 6100300 S4) prepared with spraycoating using Nafion® binder and JM Pt_{40}/C is very similar to that of the carbon cloth substrate (Lydall 6100300) without ink. The resistance measurements of the two samples did not allow the discrimination of the characteristics of the film itself separately from the substrate, and neither did the IV curve, even though much lower overvoltages (Figure 6.33) were recorded for this electrode compared to those prepared on the paper substrate or on Nafion® as substrate. The carbon cloth substrate's conductivity dominated the IV curve. The performance of CNT paper (-0.1604 V at 1 mA) and CNT paper + Pt (-0.1604 V at 1

mA) also showed very low potential at the applied currents (Figure 6.34). The carbon cloth used is slightly more conductive than the CNT paper due to the cross sectional area of the carbon cloth fibres and the thickness of the carbon cloth.

Based upon the structure of the electrodes, where R1 represents the catalyst containing film and R2 the substrate upon which the film is printed the equivalent circuit of an electrode with a film is shown in Figure 6.35

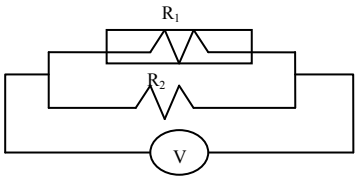

Figure 6.35 Equivalent circuit of printed electrode

It should be considered that $1/R_{eq} = 1/R_1 + 1/R_2$ and thus $R_{eq} = R_1R_2/R_1+R_2$.
When $R_1 << R_2$
R_1 becomes negligible and can be neglected in the term R_1+R_2

Thus $R_{eq} = R_1R_2/R_1+R_2$ can be rewritten as $R_{eq} = R_1R_2/ R_2$ and since R_2 cancels, the equation can be written as $R_{eq} = R_1$. In the cases where bond paper, with a far greater resistance than the catalyst containing film, is used as substrate to support the film, this case exists. Hence the use of the paper substrate for deposition of the film allowed the detailed electronic characterization of the structure of the screenprinted film by itself. Whereas in the case where the substrate is of equivalent resistance to the film the equation $R_{eq} = R_1R_2/R_1+R_2$ can be rewritten as $R_{eq} = R^2/2R$ or $R_{eq} = R/2$. Thus it becomes difficult to describe the film by itself when a conductive substrate is used to support the film. Hence the substrate chosen as support for the electro catalytic film is shown to have a very significant effect on the overall performance of the electrode and upon its characterization. From these results it can be concluded that the ink formulation, as well as the ink film thickness and the substrate type significantly affect the IV relationship and the current density of electrodes prepared with either screenprinted or spraycoated films containing the electrocatalyst.

6.5.3 Results and Discussion: Variable Field Measurements

6.5.3.1 Sheet resistivity

Sheet resistivity measurements as a function of applied variable magnetic field for the different series of screen printed electrodes are presented in Figures 6.36- 6.43.

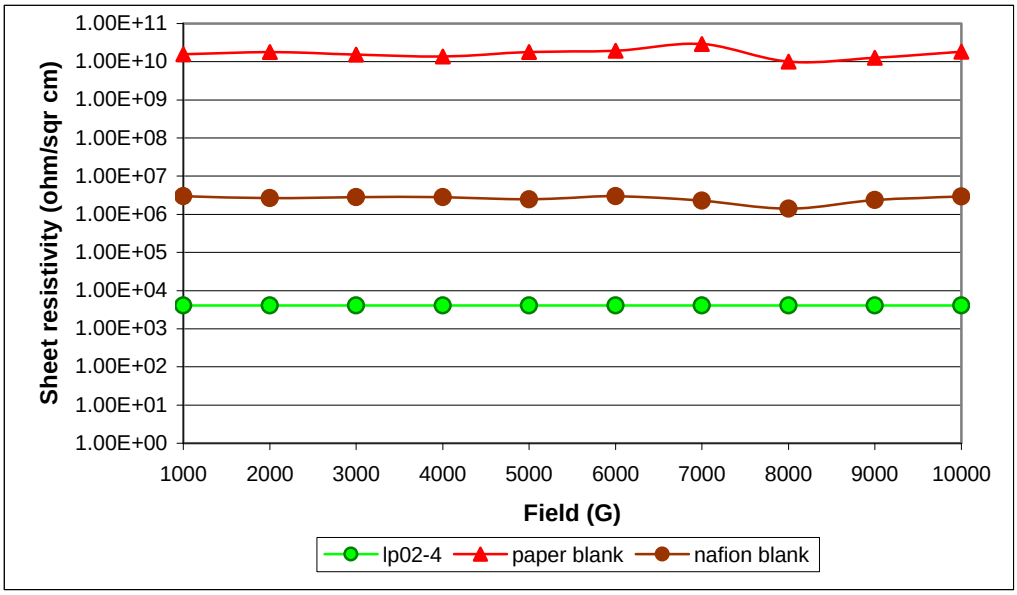

Figure 6.36 Sheet resistivity of LP02-4 (3 runs) compared to blank substrates

As expected the blank substrates, Nafion® and bond paper, had high sheet resistances which were reduced significantly by the deposition of a catalytic film by screenprinting (LP02-4) upon the paper substrate (Figure 6.36). The sheet resistivity was orders of magnitudes higher on both of the blank substrate types than on the samples printed with a film of catalytic ink, showing the significant electronic pathway provided by the film of catalytic ink, even in the first printing layer (Figure 6.37), which in this sample (LP03-1) was also not very homogeneous.

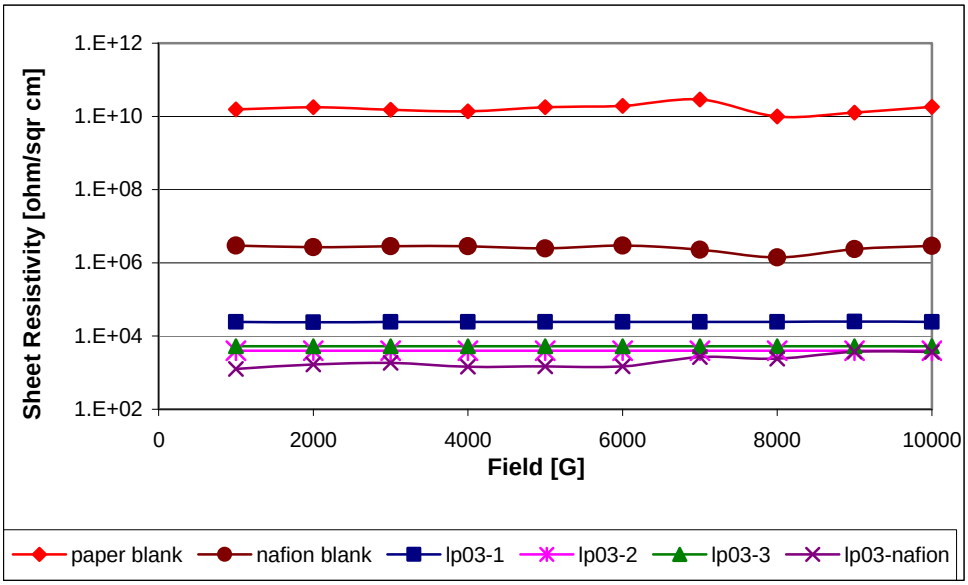

Figure 6.37 Sheet Resistivity of series LP03

The sheet resistivity of series LP03 (Figure 6.37) decreased for subsequent layers once the first layer was overprinted (from 24593 to 3941 Ω cm^{-2}). The lowest resistivity for this series was observed in the case of the sample prepared using Nafion® as substrate (2158 Ω cm^{-2}). Similar trends are observed in the case of series LP04 (Figure 6.38). However in series LP04 the first layer (LP04-1) did not give positive values and is thus not presented.

The ink formulation used for LP05 series (Figure 6.39) showed generally lower sheet resistivity (584 -2670Ω cm^{-2}) than the formulation applied in LP03 (3941-24593 Ω cm^{-2}) and LP04 series (1257-4360 Ω cm^{-2}).

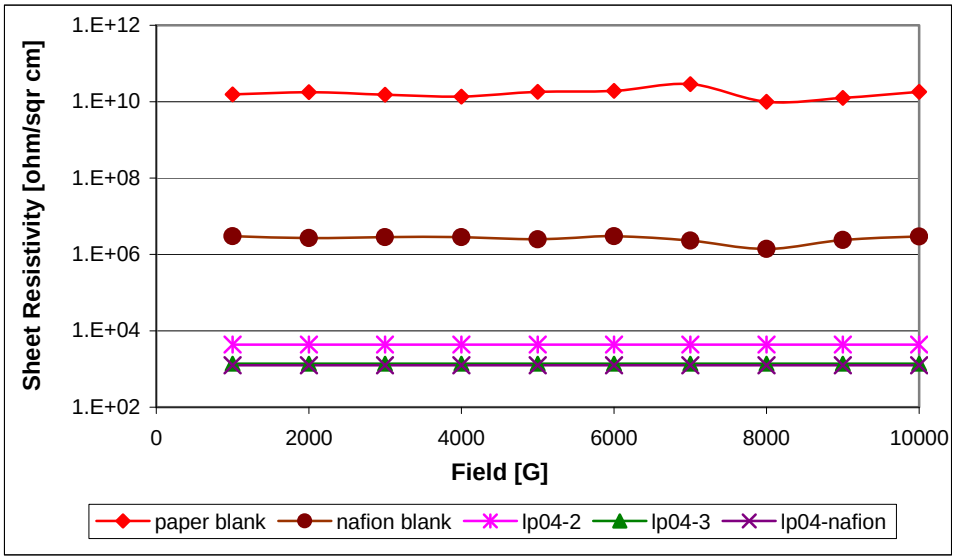

Figure 6.38 Sheet Resistivity of series LP04

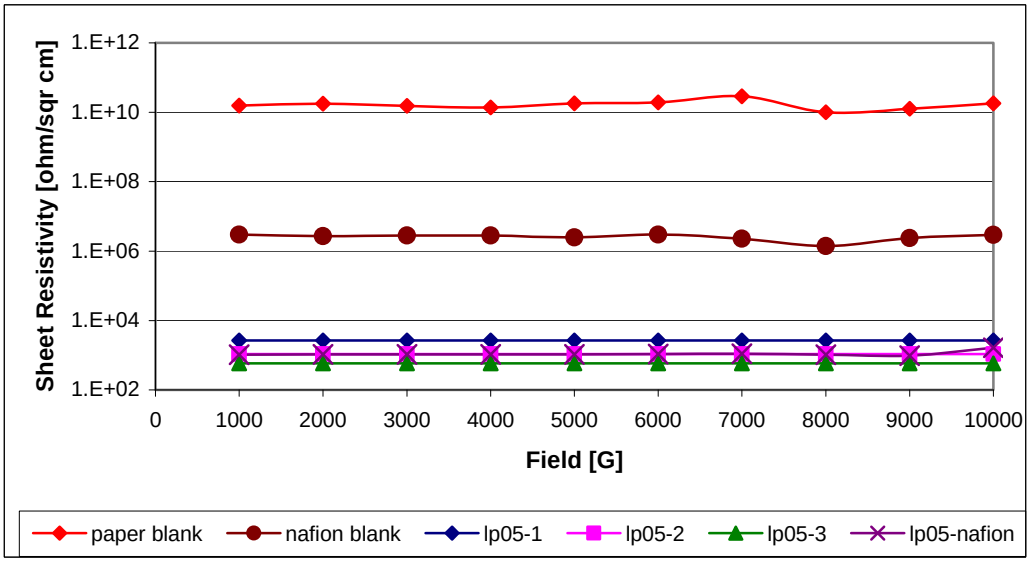

Figure 6.39 Sheet resistivity of series LP05

Each successive overprinting showed a decreasing tendency of the sheet resistivity which ties in with the degree of electrode surface coverage obtained with this formulation for each successive overprint layer. It is interesting that the Nafion® substrate LP05-nafion showed an intermediate sheet resistivity (1101 Ω cm^{-2}) which relates to the relatively less favourable surface coverage obtained on this substrate with this ink formulation. Addition of fullerenes (LP06 series) to this formulation further lowered the sheet resistivity (Figure 6.40), hence the fullerenes are shown to have a positive impact on sheet resistivity and thus film characteristics.

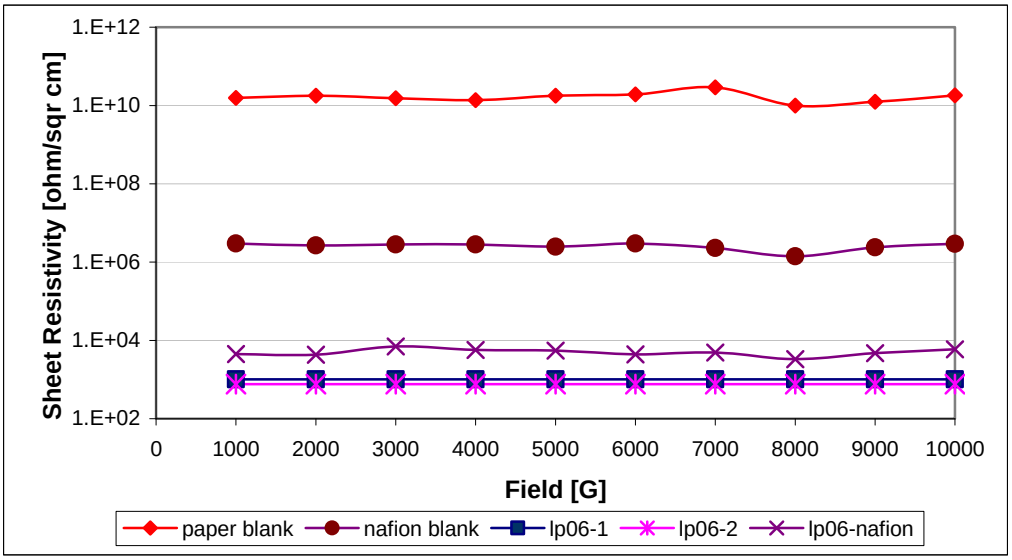

Figure 6.40 Sheet resistivity of series LP06

The sheet resistivity of LP06-1 and LP06-2 was about 300 Ω cm^{-2} and that of the Nafion® supported sample LP06 nafion about 370 Ω cm^{-2}.

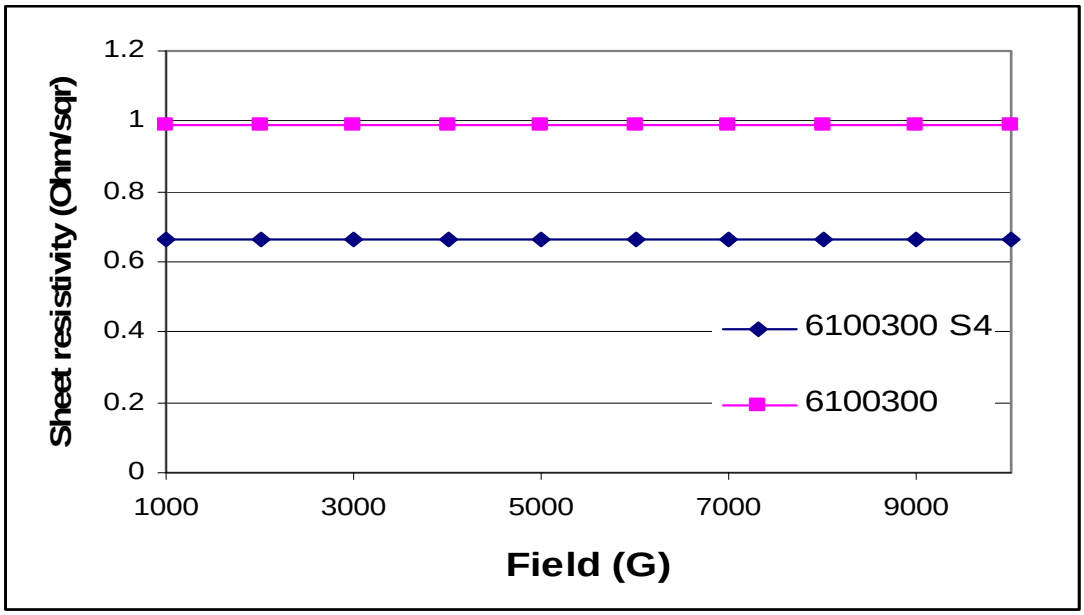

Figure 6.41 Sheet resistivity of sample prepared on carbon cloth (Lydall 6100-300)

The sheet resistivity (Figure 6.41) of the electrode sample (6100300 S4; MEA65) prepared by spraycoating the typical isopropanol ink formulation upon the Lydall carbon cloth substrate (6100 300) was much lower than samples prepared on Nafion® or paper substrates and lower than the carbon cloth substrate by itself (0.67

vs 0.99 Ω cm^{-2}). This result illustrates that the Hall sheet resistivity measurement is able to discriminate the change in sheet resistivity due to the film of electrocatalyst deposited upon the carbon cloth during spraycoating, whereas neither resistance measurement or IV measurements could distinguish the difference. The sheet resistivity of CNT paper compared to the Pt containing CNT paper prepared by galvanic displacement is shown in Figure 6.42.

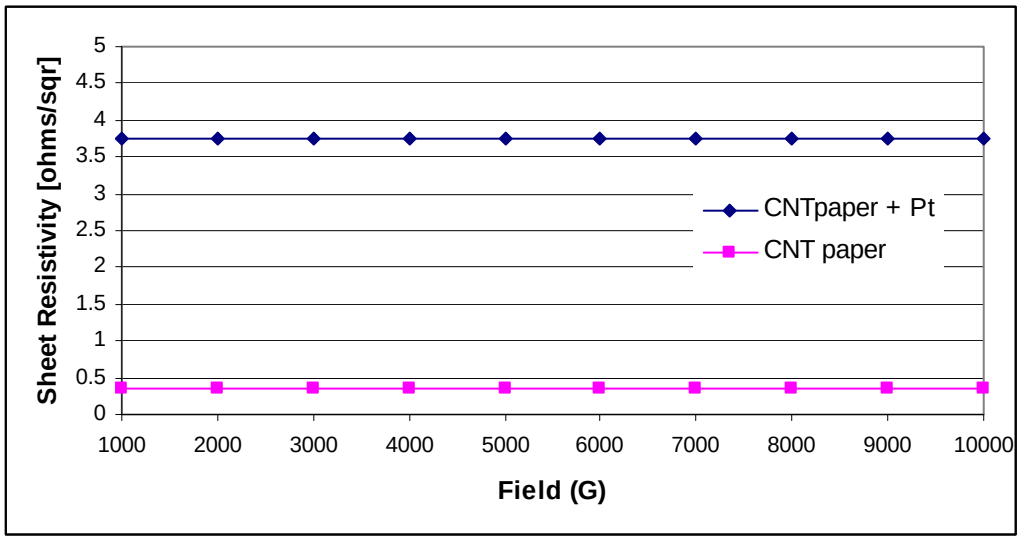

Figure 6.42 Sheet resistivity of CNT paper compared to CNT paper + Pt

The sheet resistivity of CNT paper was 0.35 Ω cm^{-1} compared to CNT paper + Pt which was 3.75 Ω cm^{-1} thus a small increase in sheet resistivity was observed when the Pt was incorporated in the CNT paper. The use of a highly electroconductive substrate thus had a significant effect upon lowering the overall sheet resistivity. The applied magnetic field did not cause significant fluctuations in the sheet resistivity for any samples, but the carbon cloth and CNT substrates showed the lowest fluctuations in overall sheet resistivity under the applied field overall.

6.5.3.2 Sheet carrier density

Sheet carrier density as a function of magnetic flux for each series of screen printed electrodes is presented in Figures 6.43- 6.50.

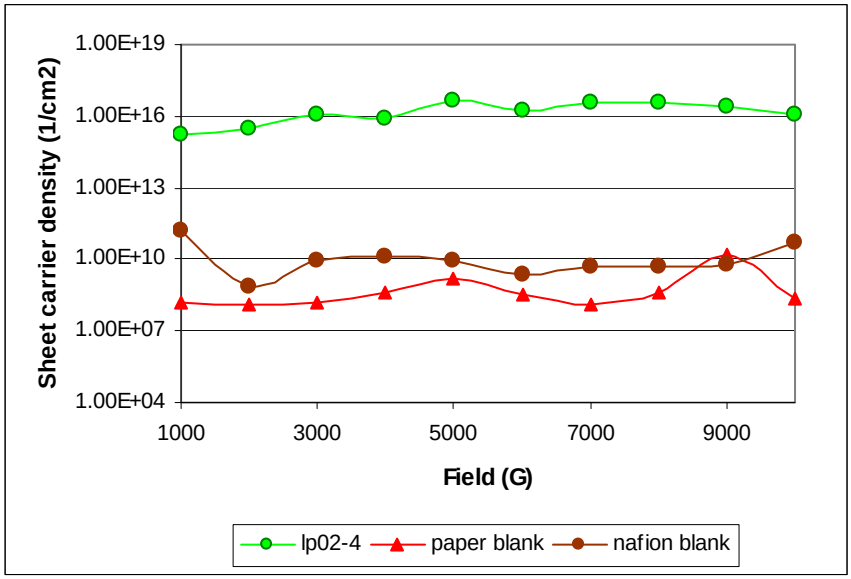

Figure 6.43 Sheet carrier density of LP02-4 (3 runs)

The sheet carrier density for the blank bond paper and Nafion® substrates are low and were significantly improved by even the poorest film (LP02-4) screenprinted upon the paper.

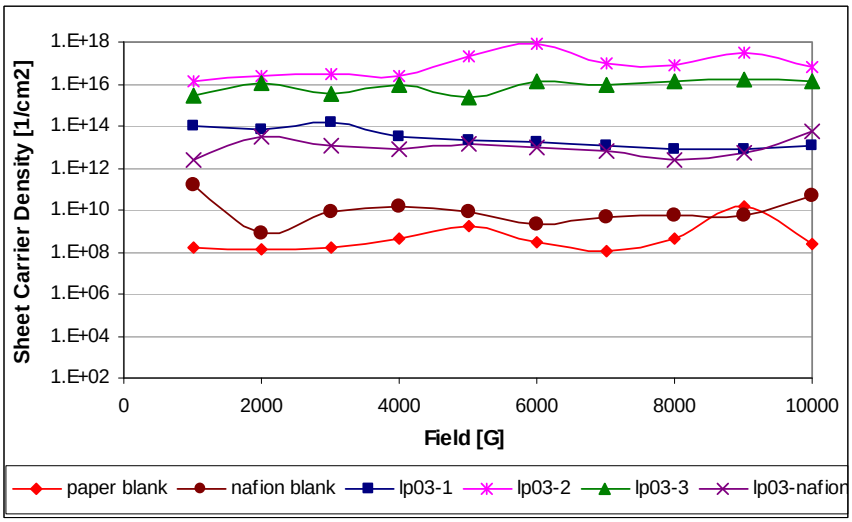

Figure 6.44 Sheet Carrier Density of Series LP03

The sheet carrier density was significantly improved by the films of catalytic ink applied in series LP03. The first printed layer was inhomogeneous and its carrier density is lower than the samples that were overprinted (LP03-2 and LP03-3). The poor surface coverage obtained in the case of the sample backed with Nafion® substrate is visible by the lower sheet carrier density obtained in this case.

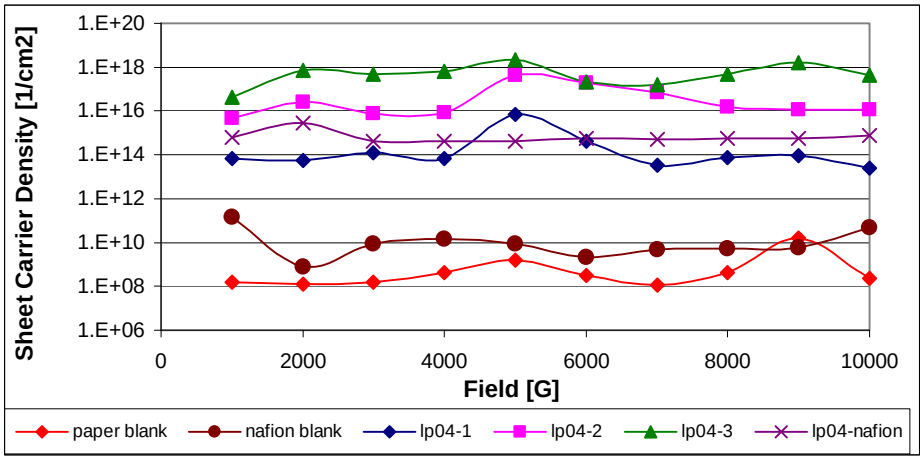

Figure 6.45 Sheet Carrier Density of Series LP04

Sheet carrier density of electrodes improved with each successive overprint on samples with a paper substrate in series LP04. The formulation of ink used to print series LP04 resulted in a higher carrier density than was the case in the LP03 series. Once again the sample prepared with a Nafion® substrate showed an intermediate sheet carrier density. This can be explained by the relative inhomogeneity of the Nafion® printed films.

The sheet carrier density of all paper backed electrode samples prepared in Series LP05 (Figure 6.46) showed an improved sheet carrier density compared to the previous series once again showing the effect of the ink formulation upon the dispersion and homogeneity of the film on this substrate. However, this formulation did not result in an exceptional sheet carrier density for the electrode prepared using Nafion substrate, and results showed that the formulation for Nafion® substrates may require further optimization.

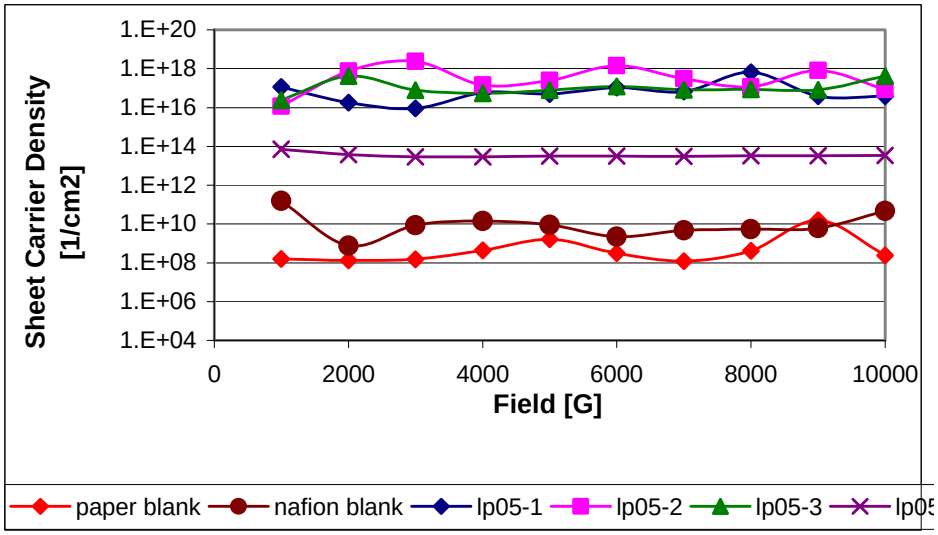

Figure 6.46 Sheet Carrier Density of Series LP05

Lower results were observed when fullerenes were added to this formulation printed on Nafion® thus the addition of an additional conductive phase to the ink did not improve the sheet carrier density (Figure 6.47).

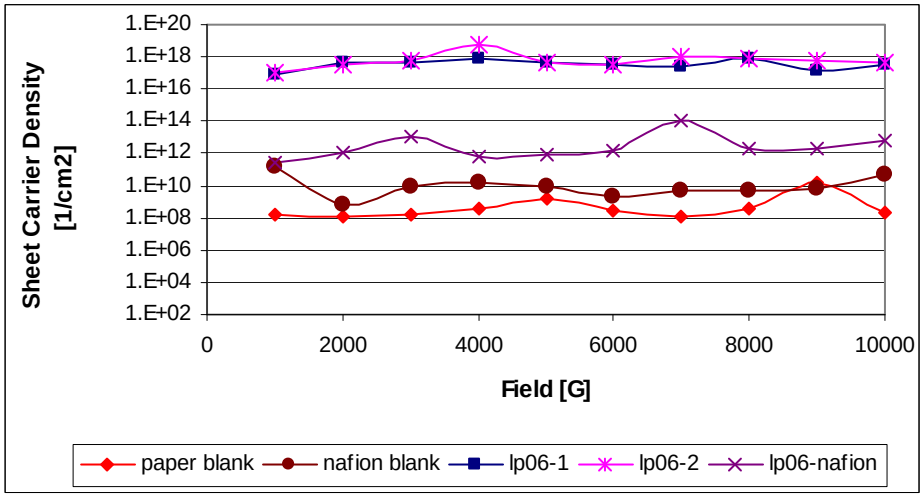

Figure 6.47 Sheet Carrier Density for Series LP06

The sheet carrier density was relatively independent of the applied magnetic field as no significant deviation was observed, for samples prepared on paper and on Nafion® substrates. However this was not the case where carbon cloth was used as substrate (Figure 6.48), where a significant fluctuation can be observed above 6000 G.

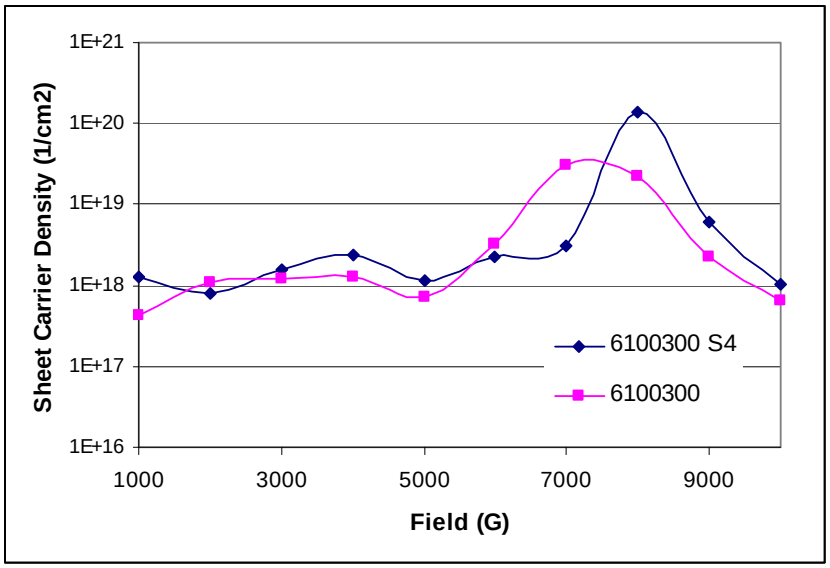

Figure 6.48 Sheet carrier density of sample prepared using carbon cloth as substrate

The sheet carrier density of the electrode sample (6100300 S4; MEA 65) prepared by spraycoating a film of electrocatalyst on Lydall carbon cloth (6100 300) was in the same order of magnitude as samples of film prepared by screenprinting on paper. This measurement did not discriminate the separate contribution of the film as opposed to the substrate itself in the case of the conductive carbon substrate which was also the case in the CNT paper and CNT + Pt samples (Figure 6.49).

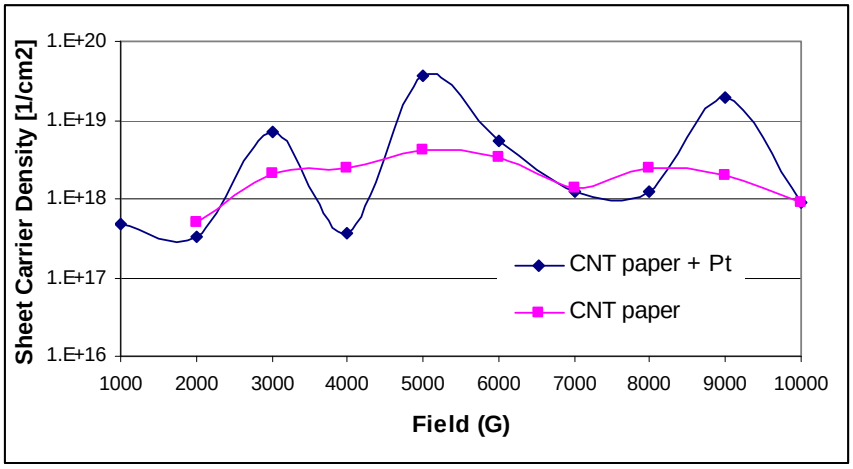

Figure 6.49 Sheet carrier density for CNT paper and CNT paper + Pt

In the case of the CNT paper and Pt containing CNT paper shown in Figure 6.49, the sheet carrier density was generally similar and of the same order of magnitude as the carbon cloth samples and paper samples thus neither of the conductive substrates

made a significant difference to the sheet carrier density characteristics overall. An anomalous fluctuation was observed in the case of the CNT+Pt sample during the application of the magnetic field and this may be due to instability caused by mechanical movement or displacement of the Pt particles relative to the CNT under the applied magnetic field. The galvanic displacement method deposited not only Pt but other metals from the sacrificial anode, the presence of which metals may have caused a magnetic interaction. These results show that the hall measurement system accurately determined sheet carrier density for the films supported on paper, and that the film consisting of the Pt electrocatalyst and Nafion®, by itself functioned as main carrier, whereas when carbon cloth or CNT was used as substrate the substrate also acted as carrier.

6.5.3.3 Sheet Hall Coefficients

The average Sheet Hall Coefficients of the film samples are tabulated in Table 6.7 and the dominant carrier is shown for each case. As the Sheet Hall Coefficient is reduced and values approach zero or become negative the sheet becomes more electro-conductive.

Table 6.7 Average Sheet Hall Coefficient ($cm^2\ C^{-1}$)

Sample	Average Sheet Hall Coeficient [$cm^2\ C^{-1}$]	Dominant carrier
Bond paper blank	2.76E+09	p
Nafion blank	2.50E+08	p
LP03-1	326000	P
LP03-2	52.1	P
LP03-3	1020	P
LP04-1	72400	P
LP04-2	157	P
LP04-3	5.7	P
LP04-nafion	11200	P
LP05-1	66.5	P
LP05-2	-66.9	N
LP05-3	-84.5	N
LP05-nafion	724000	P
LP06-1	-14	N
LP06-2	8.22	P
LP06-nafion	-5370000	N
6100300	-3.24	N
6100300 S4	-3.29	N
CNT paper	-1.383	N
CNT paper + Pt	1.372	P

Table 6.7 shows that generally as film characteristics improved on the paper substrates the positive Sheet Hall Coefficient was lower and conductivity became dominated by n-type carriers (electrons) whereas when film integrity was not good, p-type carriers (holes or positive ions) dominated the conductivity. It appears that p type carriers dominate when the main connection is the Nafion® binder soaking the paper between catalyst agglomerates, whereas the n –type dominate where good connectivity between catalyst particles was found.

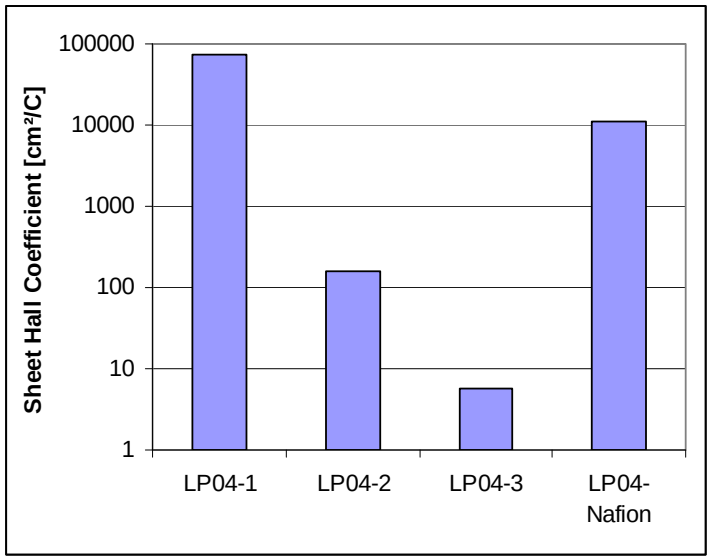

Figure 6.50 The decreasing trend in p-type carriers for LP04 series

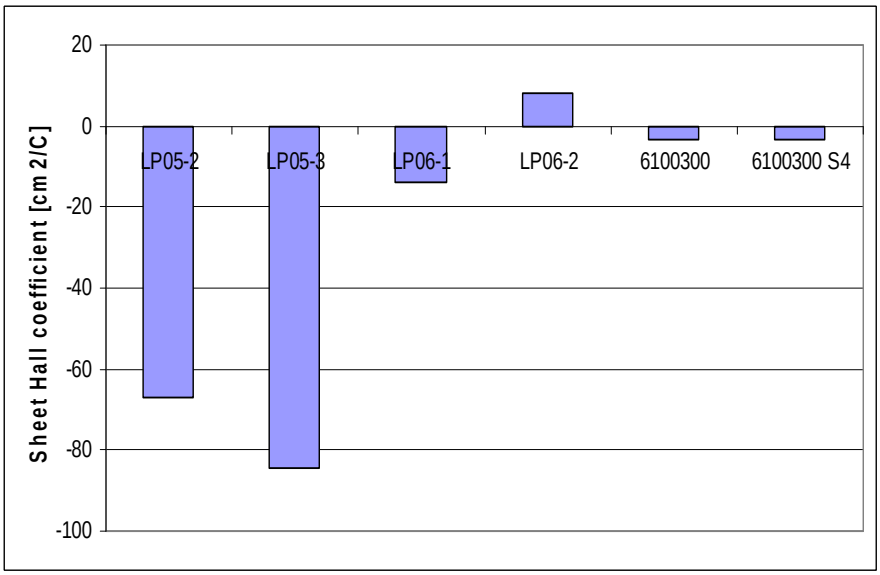

Figure 6.51 The Sheet Hall Coefficients of samples with n-type carriers

Improving the characteristics of the film layers containing the electrocatalyst, reduced the positive Sheet Hall Coefficient significantly and promoted n- type carriers. This is demonstrated in the case of the LP04 series shown in Figure 6.50. The LP04 series (Figure 6.50) showed a consistent decreasing trend (several orders of magnitude) in positive Sheet Hall Coefficients with improvement of film characteristics. High positive Sheet Hall Coefficient values could indicate entrapment of the carriers in the unconnected or poorly connected agglomerates of the films observed in the case of

LP04-1 and -2 respectively. The paper supported samples (LP05 and LP06) with the best film characteristics upon visual inspection in terms of good dispersion and homogeneity as well as in terms of IV, sheet resistance etc, were predominantly n-type carriers as is shown in Figure 6.51. Some samples switched from p- type carriers to n – type carriers with improving film characteristics, notably series LP05. It is not clear why this switch should be observed in series LP06 as these films, containing fullerenes were well connected and homogeneous overall.

The CNT paper sample switched from n- to p-type carrier upon deposition of the Pt, indicating that electron conduction changed to hole conduction upon deposition of the Pt. This is a unique result and should be further investigated. It is possible that Pt becomes a site for carrier recombination, thus the Pt may capture the charge carriers and build up a charge as it can easily take up the charge but cannot transfer it further via a chemical reaction due to the lack of reactant in the experimental system. This may be indicative of quantum confinement of carriers in the nanoparticles of Pt dispersed upon the CNT (Oncel et al., 2005).

The carrier densities of Nafion® based samples should not be compared directly to that of the best samples prepared on the paper substrate which generally were dominated by n-type (electron) carriers because of the different characteristics of the proton conducting substrate. It is not clear whether the physical carrier is a positive charge in the case of Nafion® substrate samples thus the carriers may be holes or protons. The carrier types for the Nafion® substrate based samples (Table 6.7) were p-type carriers except in the case of LP06-nafion which was dominated by n-type carriers. This difference may be due to the addition of the conductive phase of fullerenes that was added to this sample and should be further investigated. The addition of a conductive phase to films printed upon the Nafion® substrate may thus enhance the electron charge transfer. The Nafion® samples' sheet carrier density (Section 6.5.3.2) appears lower than the paper substrate samples because they mostly had p-type carriers, which are less mobile than electrons.

N-type carriers , which are normally found in metallic conductors, allow the transfer and flow of electrons. In the cases where p-type carriers dominated it may be that the electron flows were impeded due to lack of connectivity between catalyst particles. Adequate connectivity between catalyst particles or agglomerates would be required for a percolation pathway threshold. An optimum distribution and density is required for continuous electronic contact.

6.5.3.4 Hall Mobility

Hall mobility as a function of magnetic flux for each series of screen printed electrodes is presented in Figures 6.52- 6.57.

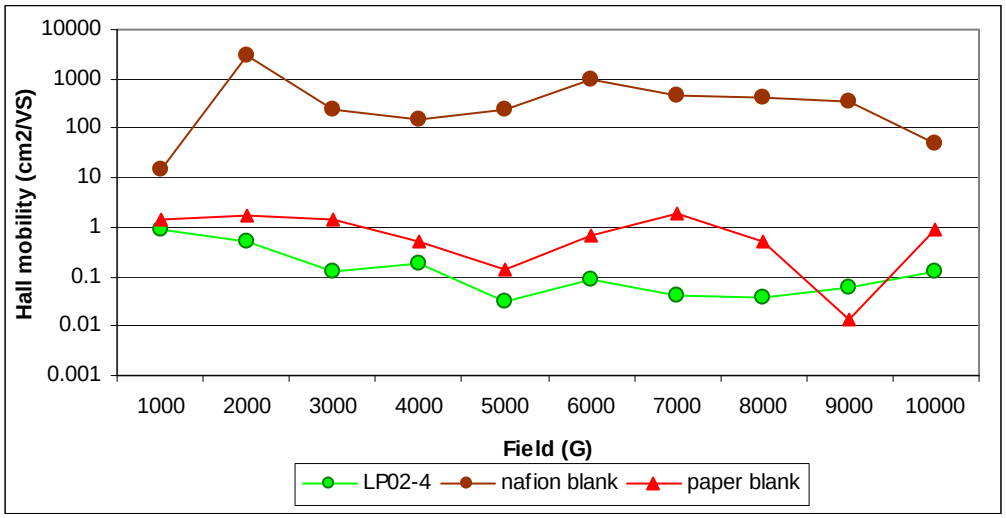

Figure 6.52 Hall mobility of LP02-4 (3 runs)

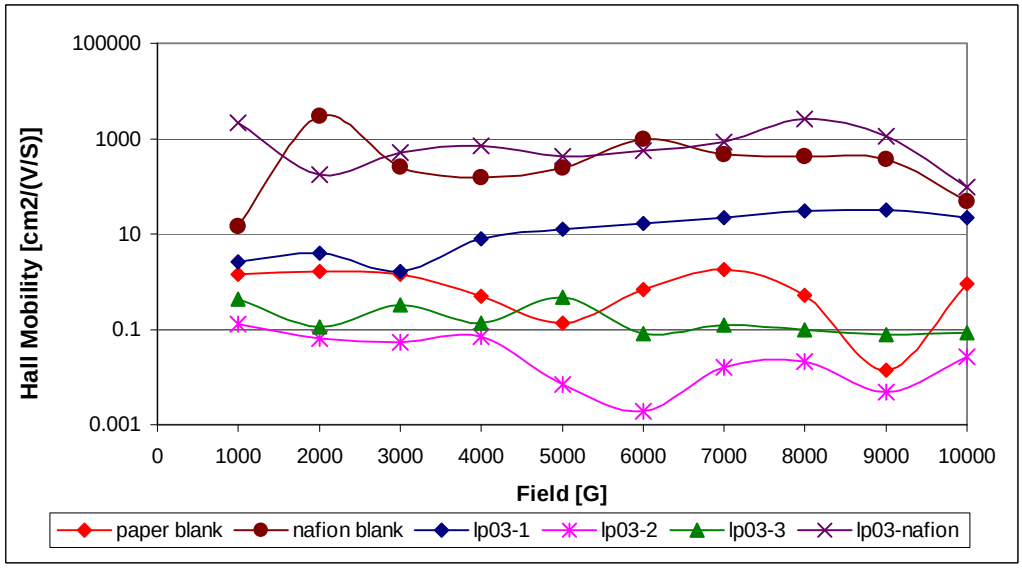

Figure 6.53 Hall Mobility of Series LP03

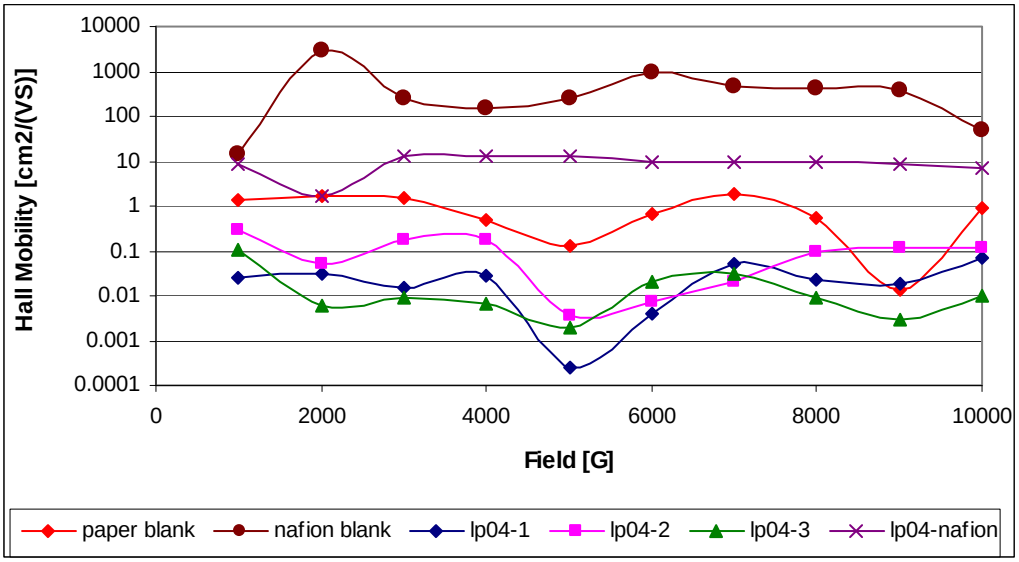

Figure 6.54 Hall Mobility of Series LP04

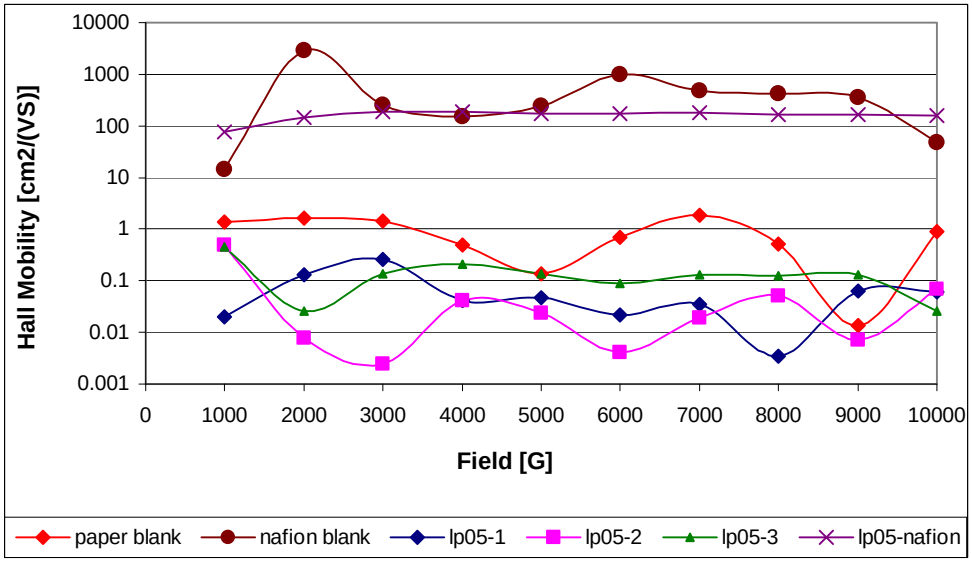

Figure 6.55 Hall Mobility of Series LP05

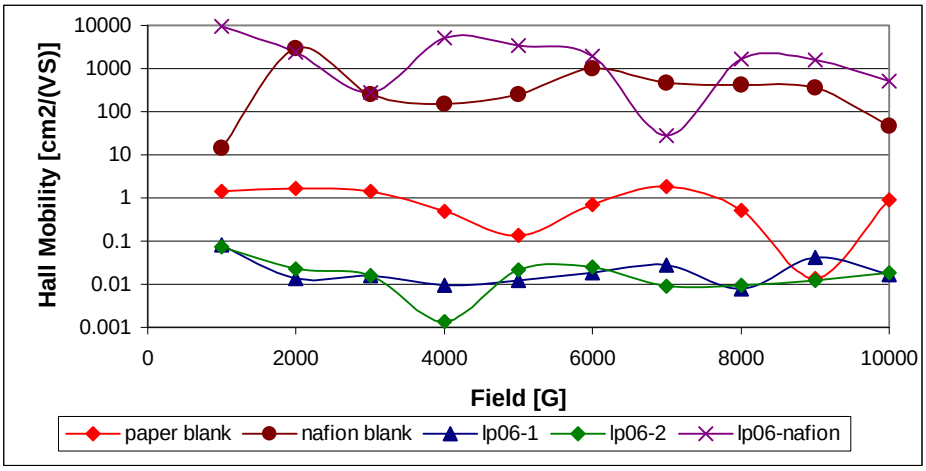

Figure 6.56 Hall Mobility of Series LP06

Hall mobility indicates the possible pathways for the charge carriers to move and gives an indication of the length of the carrier pathway before recombination in the case of holes. The hall mobility (Figures 6.52- 6.57) was significantly affected by the substrate type and Nafion® as substrate caused significant hall mobility whereas the hall mobility was orders of magnitude lower for paper and paper based electrodes. The lowest hall mobility was observed in the case of the LP06 series which had the fullerenes added as additional component to the ink formulation. The hall mobility did not correlate well with film thickness and overprinting did not result in a significant difference in hall mobility. In fact the blank substrates showed the greatest hall mobility compared to the respective printed electrodes, which indicates that the hall mobility is a function of the substrate characteristics, which dominated the effect. Fluctuations in the hall mobility were observed under the applied magnetic field but this was variable and did not correlate directly or inversely to the applied field. The mobility of carriers was independent of film thickness.

6.5.3.5 The effect of Nafion substrate

The hall mobility, sheet resistivity and sheet carrier density for electrodes on Nafion® substrate are presented in Figures 6.57- 6.59.

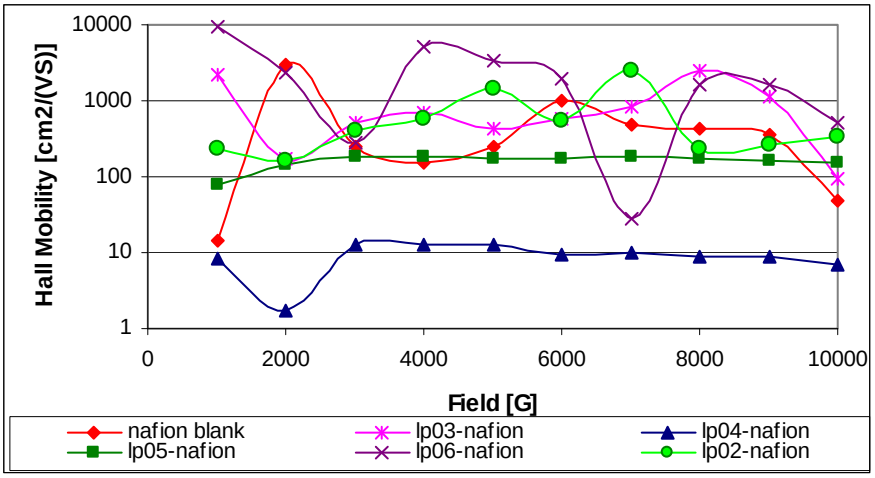

Figure 6.57 Comparison of Hall mobility of samples screenprinted on Nafion® substrate

The Hall mobility of samples was independent of film layer thickness but was dominated by the substrate in the case of Nafion® supported electrodes, except in the case of the LP04-nafion that showed low hall mobility. This sample was also the Nafion® – based sample with the highest sheet carrier density and lowest sheet resistivity.

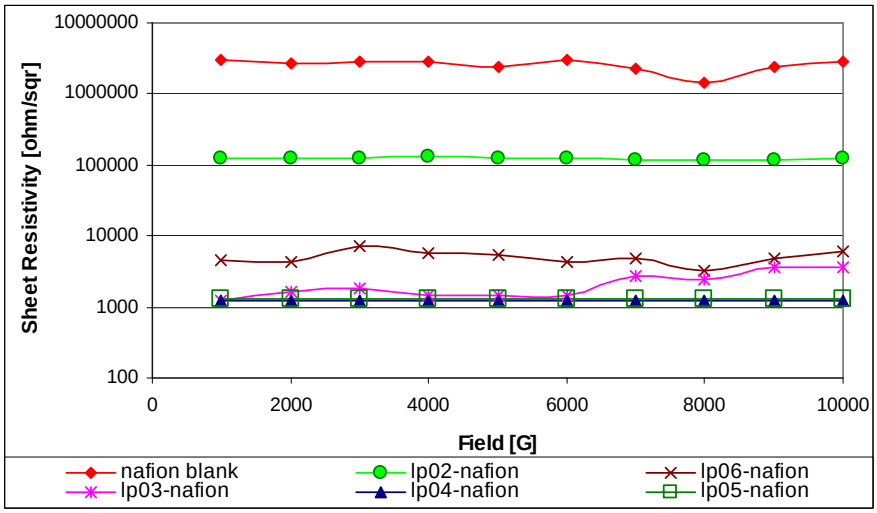

Figure 6.58 Comparison of sheet resistivity of samples screenprinted on Nafion® substrate

The Nafion® supported electrodes generally had similar sheet resistivity (Figure 6.58) despite the different ink formulations that were applied, except in the case of

LP02-nafion and the ink formulation which had fullerenes added, in which case the sheet resistivity was increased significantly.

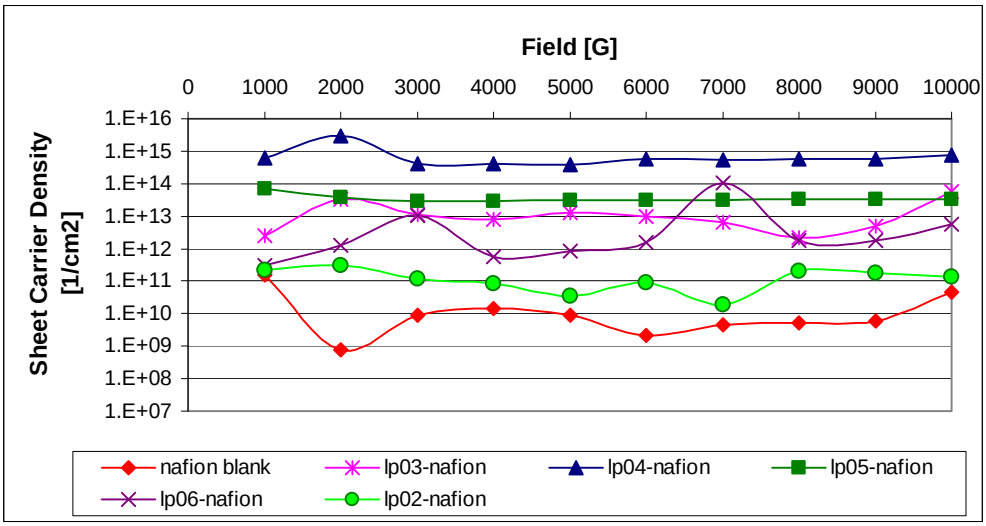

Figure 6.59 Sheet carrier density of samples screenprinted on Nafion® substrate compared

Differences were observed in sheet carrier density of samples screenprinted on Nafion® (Figure 6.59). The sheet carrier density of the ink formulation used in series LP04, when printed on Nafion® substrate, resulted in the highest sheet carrier density, followed by that of the formulation used in series LP05, whereas the sheet carrier density for the formulation used for LP02-nafion was the lowest. These results indicate that the composition of the ink formulation and thus the relative ratio of the solvents used, had a discernible impact upon the functionality of the resultant Nafion® supported electrode, because of the film morphology.

6.5.3.6 The Hall mobility of conductive substrates

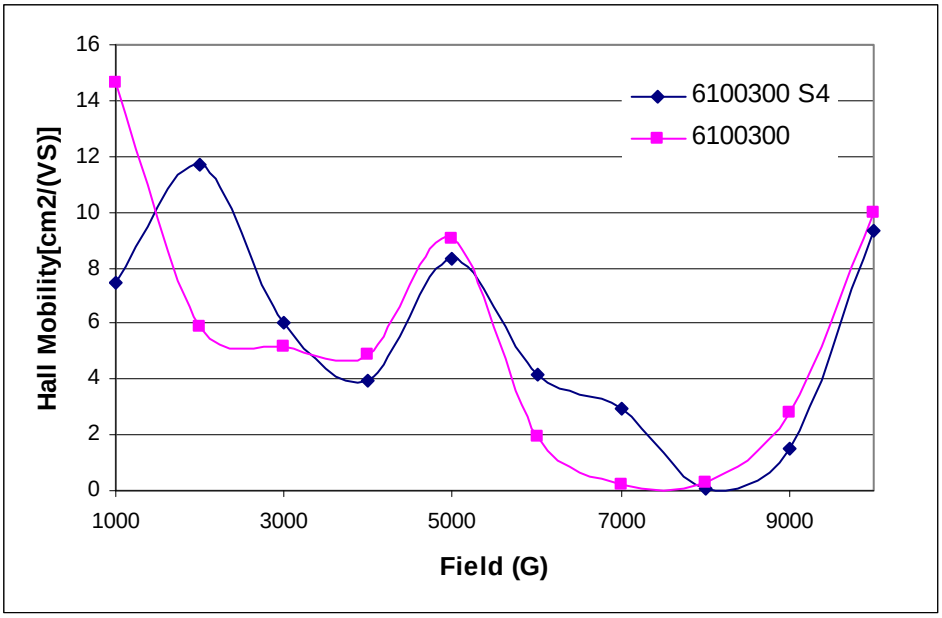

Figure 6.60 Hall mobility of Carbon cloth based samples

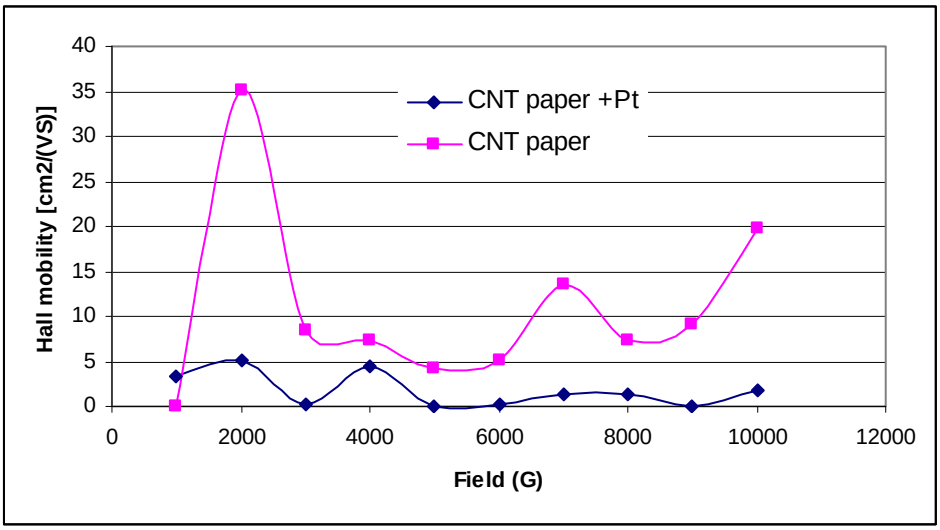

Figure 6.61 Hall mobility of CNT based samples

The Hall mobility of the CNT based electrode samples (Figure 6.61) were in the same order of magnitude as those of the carbon cloth samples (Figure 6.60) and the Hall mobility of both these series was between one and two orders of magnitude higher than the films supported on the paper substrates, but generally lower than those samples prepared on the Nafion® substrate. It is interesting to observe that deposition of Pt upon CNT reduced the overall hall mobility, which once again may indicate the role of Pt as a recombination site and supports the possibility of quantum confinement of charge carriers by Pt nanoparticles (Oncel et al., 2005).

CHAPTER 6

6.6 RHEOLOGICAL CHARACTERISTICS OF INKS

Screen printing of inks used in this study was performed at high shear rate of about 2000 reciprocal seconds, with a short contact period between ink and substrate. To correlate rheology with the application it is interesting to measure viscosity at high shear rates. On the other hand, the yield stress related to final printing quality is measured at very low shear rates.

Viscosity of a liquid is a measure of its resistance to flow, and this is measured in N s m^{-2} (SI Units) or poise (P) or centipoise (cP). The viscosity of water depends on temperature. At 20 °C the viscosity of water is 1.002 cP (1 P = 0.1 N s m^{-2} ; 1 cP = 0.001 N s m^{-2}). Its viscosity decreases as the temperature increases. The viscosity of Propylene glycol (1,2 propanediol) is 0.581 cP at 20 °C, (Cyberspace Chemistry, 2008).

In Newtonian fluids, the stress is linearly proportional to the strain rate. Non-Newtonian fluids have a non-linear response to the strain rate and the relationship between stress and strain depends on time, thus their viscosity is not constant but dependant on shear rate. Their effective stiffness depends on the rate of application of the load. Viscoelastic substances lose energy when a load is applied, then removed. Viscoelastic materials have an elastic component and a viscous component and viscoelasticity is due to a molecular rearrangement (Viscoelasticity, 2008). In the case of viscoelastic material hysteresis is seen in the stress-strain curve and stress relaxation occurs.

The viscosity in the printing stage should not be too low but at the same time it should not be too high. Too low a viscosity can cause penetration of ink into the substrate giving a 'blurred' impression. Too high a viscosity causes flow instabilities during printing, which can result in uneven printing as well as bad coverage. The effects of solvent type and solids loading on yield stress and viscosity was determined

for the ink formulations used in screen printing catalytic particles upon various substrates. The following results show the effect of different formulations on the rheological behaviour of the ink. From the shear stress versus shear rate curve, the yield stress can be obtained which determines the processability and storage stability of the ink sample.

Samples LP0 1 and LP0 10 were compared at the same liquid to solid (L:S) ratio with different solvents (isopropanol vs 1,2 propanediol respectively) to understand the effect of changing the solvent on the rheology of the ink. Ink sample LP0 5 was compared with LP0 11 to understand the effect of changing the L:S ratio (6:1 vs 14:1). LP0 10 and LP0 11 were compared to understand the effect of the solvent to water ratio (5:1 vs 1:1 respectively). These two samples were prepared for the rheological experiments but were not used during screenprinting. A standard Pt printing ink (Pt ink for ceramic substrates; stock# 43653; supplied by Alpha Aesar) was compared for reference. The viscosity of the inks was compared (Figure 6.62).

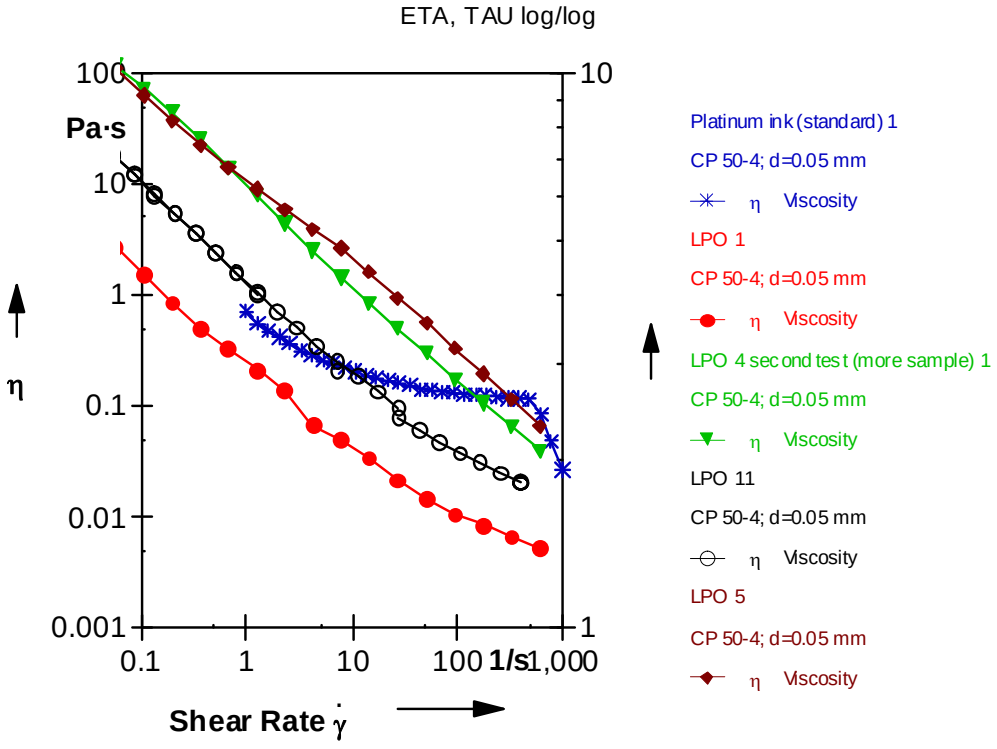

Figure 6.62 Viscosity of screenprinting formulations compared to a standard Pt ink

In Figure 6.62 a comparison of the shear stress (τ) vs shear rate (γ) curves of ink samples is presented.

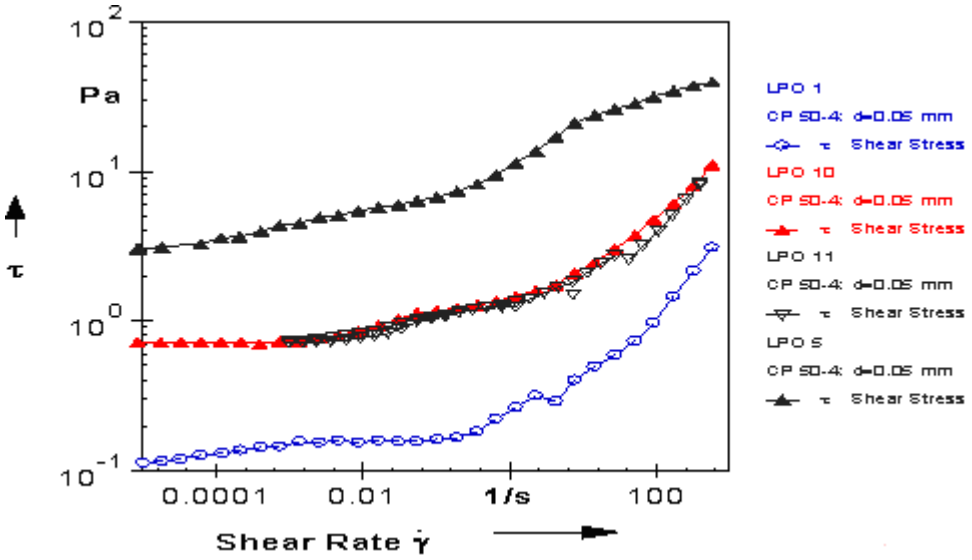

Figure 6.63 Comparison of the shear stress (τ) vs shear rate (γ) curves of ink samples

A very low viscosity (Figure 6.62) was observed in the case of LP0 1, containing the solvent isopropanol. Replacing the solvent isopropanol (LP0 1) with 1,2-propanediol (LP0 10) increased both the viscosity and the apparent yield stress of the ink at the same solids loading, improving the structure of the ink. Changing the solvent to water ratio for the same solvent (1,2 propanediol) had no effect on the viscosity (LP0 10 compared with LP0 11 in Figure 6.3). Increasing the solids loading (LP0 5 compared with LP0 11) increased the viscosity (Table 6.8 and Figure 6.2) and the yield stress (Figure 6.3) of the ink indicating an improvement in the structural strength of the ink compared to the formulation containing isopropanol. This was also confirmed by the higher values obtained for the elastic modulus (Figure 6.64) which shows the viscoelastic behaviour of these two inks with the elastic modulus (G') as a function of shear stress (τ).

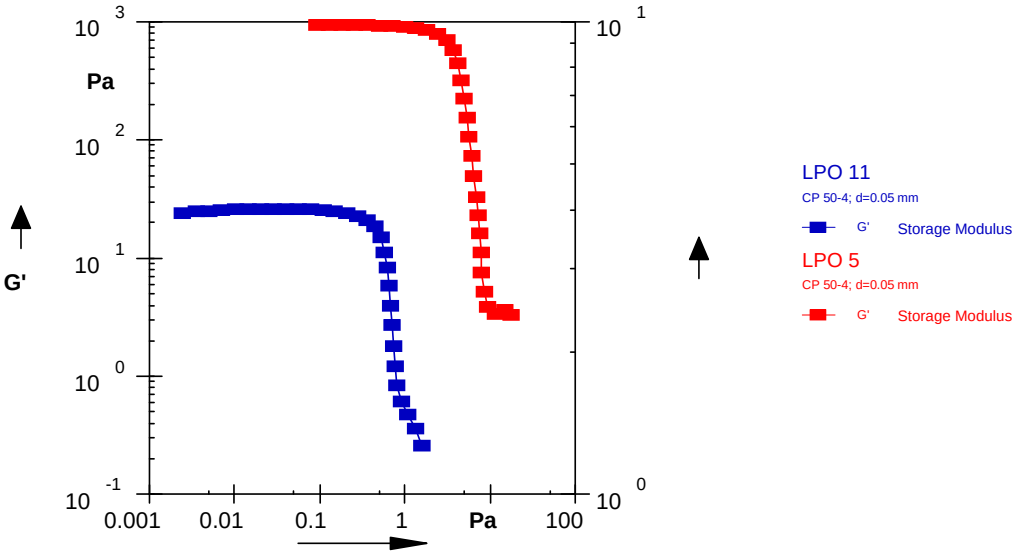

Figure 6.64 Viscoelastic behaviour of inks: elastic modulus (G') as a function of shear stress (τ)

The longer linear viscoelastic region for LP0 5 extends to higher shear stresses (2 Pa) than LP0 11 (0.3 Pa), indicating a more homogeneous structure. LP0 5 with a higher solid loading but the same solvent had a higher level of structure than LP0 11, indicated by the higher values obtained for the elastic modulus (Figure 6.64). A more finely dispersed system resulted in a longer linear viscoelastic region which was observed in the case of LP0 11.

A higher degree of viscoelasticity will produce a better printing quality. Greater interaction between the particles gives a higher viscosity and viscoelasticity. Indications of these interactions could be observed at low frequencies, by monitoring the elastic modulus. The level of structure is directly proportional to the elastic modulus, G' (Chhabra & Richardson, 1999). For non-agglomerated ink samples, the elastic modulus would be lower indicating less strength in the interactions but when a higher value of the critical strain is observed, this would show that the ink sample was more homogeneous and therefore more stable. Agglomeration is indicated by an increase in elastic modulus, G', and a decrease in the critical strain. High agglomeration leads to bad printing quality. Therefore, for non-agglomerated samples, the elastic modulus would be lower indicating less strength in the

interactions but when a higher value of the critical strain is observed, it shows that the sample is more homogeneous and therefore more stable. LP05 had a higher degree of viscoelasticity as well as a higher value of critical strain showing this formulation's homogeneity as well as stability.

Plotting the elastic (or storage) modulus (G') as a function of shear stress (Pa) (Figure 6.65) showed that for the samples made with the same L:S ratio but different type of solvents (LP0 1 and LP0 11), G' is the same, but G" (loss modulus) is quite different. In Figure 6.65 the storage modulus (G') is plotted vs strain (x-axis) and G" (secondary y axis) for ink samples LP0 1 and LP0 11 in which the solvent : water ratio varied between 5:1 and 1:1 respectively at a L:S ratio of 14. LP0 4 and LP05 are included for comparison as these inks gave the best print quality.

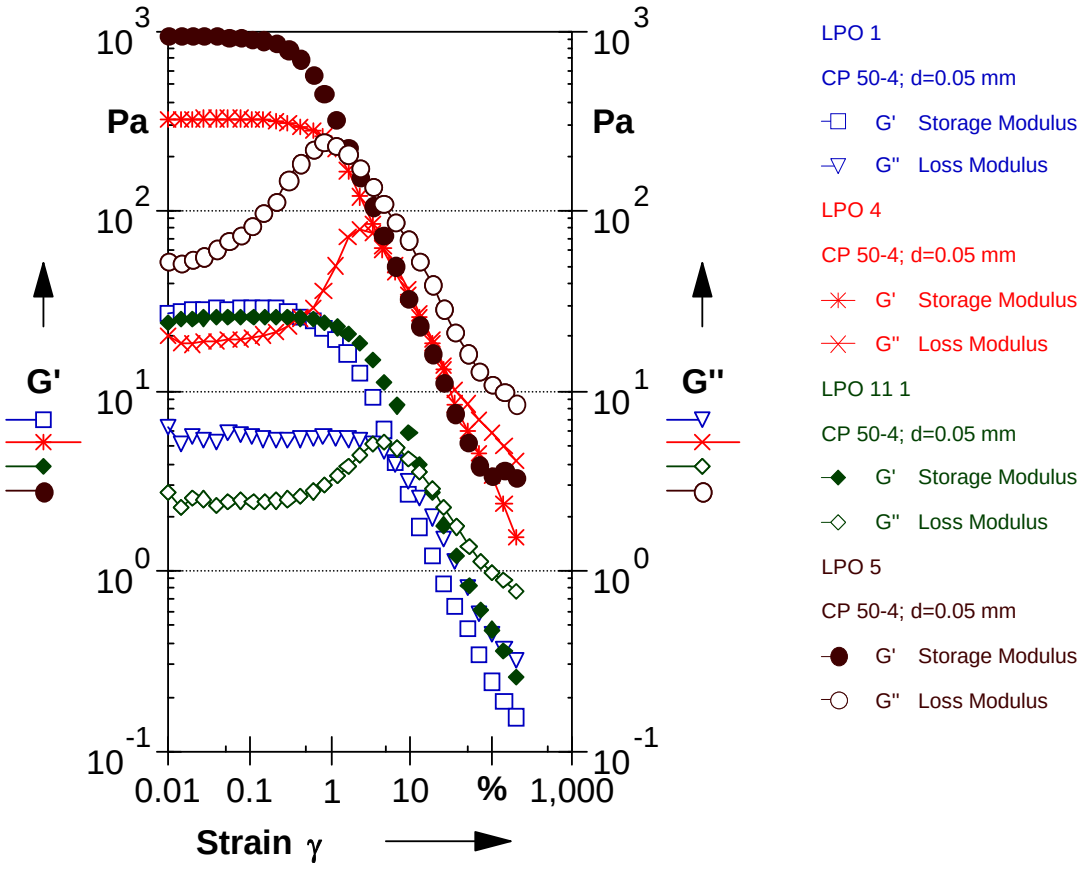

Figure 6.65 Storage modulus (G') plotted vs strain for ink samples LP0 1 and LP0 11

The loss modulus G" is plotted on the secondary y axis. As G' was higher than G" in all cases, the elastic behaviour dominated the viscous behaviour. The crossover points between G' and G" for each of the different formulations are shown in Table 6.8 and the viscosity in Table 6.8 and Figure 6.65.

Table 6.8 Viscoelastic crossover points (G' vs G") and viscosity of ink formulatons

Ink formulation	G' (y-axis)	Strain (x-axis)	Viscosity (η at 0.1γ)	Viscosity (η at 100γ)
LP0 1	3.9	6.4	1.2	0.01
LP0 4	84.7	3.2	100	0.13
LP0 5	224	1.6	100	0.15
LP0 11	3.9	13.0	10	0.08
Standard reference Pt ink			~10 (by extrapolation	0.12

The storage modulus (G') for LP0 4 and LP0 5 was 84.7 and 224 respectively (Figure 6.65) whereas that of the isopropanol based ink LP0 1 had a storage modulus of only 3.9. Energy losing materials display irreversible behaviour. LP0 1 had the lowest overall viscosity and a low G'. This may be why, after this ink was sheared during screen printing, it flowed outside the printed area. On the other hand the inks containing 1,2 propanediol (LP0 4, LP0 5 and LP0 11) showed higher viscosity and shear dependant and reversible storage behaviour visible by the reversible inflections in G" curves and thus were quite elastic, indicating a breaking of the agglomerated structure under shear and then a reagglomeration of the particles when the shear is removed. G" is a function of the deformation energy used up in the sample during the shearing process. This energy is either lost to the sample afterwards by changing the structure of the sample permanently or is dissipated as heat (Mezger in Zorll, 2002). The storage modulus is also a measure of the energy stored in the shearing process and when the shear force is removed this energy is available as a driving force causing re-agglomeration of particles.

Hence structural decomposition after shearing (thixotrophy) was observed for the ink prepared using isopropanol (LP0 1) whereas structural regeneration (rheopexy) was observed for the ink formulations containing 1,2 propanediol (LP0 4, LP0 5 and LP0

11). It is also noteworthy that a difference in G' exists between the formulation used for LP0 4 and LP0 5. LP0 4 formulation was more suitable for printing on Nafion® whereas LP0 5 formulation gave the best coverage on paper substrates.

A high yield stress as well as viscoelasticity which is correlated with high solids content in sample LP05 is preferable for inks, as the higher solids content creates a more structured material which will result in precise, quality printing. The higher solids content provides higher structural strength and therefore the plateau of the amplitude sweep dependence continues to higher stresses for this sample.

The difference in the G" values (at the same G' value) can be understood if one bears in mind that G' is related to the solid phase and G" to viscosity of a liquid phase. Therefore by changing the solvent the G" values could be controlled. For practical application, viscosity (and G") should be low enough for high fluidity of inks but still high enough for the printed layer to be stable on a substrate (higher yield stress that correlated with G').

The optimum ink formulation had a ratio of between 3 - 1 : 1 of 1,2 propanediol:water, a liquid: solid ratio of between 6-8:1 and a storage modulus (G') of between 84 and 224. Reversible viscoelastic behaviour of inks correlated with good print quality. Rheological determination of ink formulations is thus demonstrated to give good predictive information of the printability of an ink upon paper, but formulations would require further optimization depending upon the surface energy of the substrate type chosen.

6.7 CONCLUSIONS

Screen printing a nanophase containing catalytic ink is shown to be reproducible. Each electrode of $1cm^2$ increased by approximately 0.001 -0.0015 g with each successive overprinted layer using the screenprinting technique as a means to directly

and rapidly deposit a catalytic ink upon a substrate. Accurately depositing a specified amount of electrocatalyst per unit area of substrate in a uniform, homogeneous and well dispersed manner required optimization of the ink formulation. Homogeneity was dependent upon the substrate type as well as the ink formulation. Significant take off effects were observed especially on circular designs of electrodes whereas the square design electrode prints were of more consistent quality.

Different ink formulations were suitable for printing upon specific substrates but ink formulations suited for spray coating were not suitable for screen printing. The volatility of the solvent determined the ease with which the ink could be repeatedly overprinted. Low viscosity of isopropanol based inks during screenprinting causing bleeding and agglomeration and also caused too rapid drying of ink in between successive print runs. In this study variation of the solvent played the major role in ink viscosity. Substitution of isopropanol with 1,2 propanediol resulted in an improvement of viscosity, which was tailored by increasing the amount of water and solids in the formulation. The surface tension of the substrate played a role in the degree of uptake of the ink upon the substrate.

The optimum ink formulation had a ratio of between 2.9 -1.0 : 1 of 1,2 propanediol to water as solvent. These ink formulations were more appropriate for printing on Nafion® substrates and less agglomeration was observed because of the higher water content and resulted in better catalyst/binder dispersions even for the first layer printed, as well as better deposition on the Nafion® substrate. The samples that were printed on paper showed a good correlation between each successive overprinted layer thickness and lowered resistance. The first printed layer was typically high in resistance, the next overprinted layer reduced the resistance of the electrode and the third overprinted layer caused the electrode resistance to reduce even further. Addition of fullerenes did not apparently affect the resistance significantly.

As the change in the dispersant ratio in the formulation relates mainly to modifying the polarity and surface tension of the mixture incrementally, with an increased water

content rendering the solution more polar, it is likely that molecular interactions were improved between the ink formulation used and the paper substrate surface because of liquid/solid surface interactions increasing.

Variable Field Hall measurement showed that the film characteristics depended upon the solvent used as well as the printed layer thickness and the nature of the substrate. The sheet resistivity was orders of magnitudes higher on both of the blank substrate types than on the samples printed with a film of catalytic ink, showing the significant carrier pathway provided by the film of catalytic ink, even in the first printing layer, even though that was generally not very homogeneous. Each successive overprinting showed a decreasing tendency of the sheet resistivity which correlated with the degree of electrode surface coverage. The use of an electro-conductive substrate had a significant effect upon lowering the sheet resistivity. The substrate chosen as support for the electrocatalytic film was shown to have a very significant effect on the overall performance of the electrode. The difference in resistance observed could not be ascribed to catalyst loading only but also to the print quality and the conductive pathway created by adjoining clusters of printed electrocatalyst, which was affected strongly by the ink formulation. Hence, no matter how active the electrocatalyst, if the deposition of the film on the substrate is substandard, electro activity will be low. Films screen printed upon Nafion® substrates were generally neither homogenous nor very well dispersed, due to the interaction of the ink with the substrate. This shows the significant impact that the interaction of the surface of the substrate with the ink has upon the electrical characteristics of the film. The effect is postulated to relate to adhesion energy and interfacial tension (Hartland, 2004; Pourdeyhimi et al., 2007; Britton et al, 2007).

The hall mobility did not correlate well with film thickness and overprinting did not result in a significant difference in hall mobility. In fact the blank substrates showed the greatest hall mobility compared to the respective printed electrodes, which indicates that the hall mobility is a function of the substrate sheet resistivity, which dominated the hall mobility. The ink formulation used in series LP04, when printed

on Nafion® substrate, resulted in the highest sheet carrier density, followed by that of the formulation used in series LP05. The addition of a conductive phase to films printed upon the Nafion® substrate may enhance the electron charge transfer significantly. These results indicated that the composition of the ink formulation and the relative ratio of the solvents used, had a discernible impact upon the functionality of the resultant Nafion® supported electrode, because of the film morphology.

Generally, as film characteristics improved on the paper substrates, the Sheet Hall Coefficient was lower and conductivity became dominated by n-type carriers (electrons) whereas when film integrity was not good, p-type carriers (holes) dominated. Improving the characteristics of the film layers containing the electrocatalyst, reduced the positive Sheet Hall Coefficient significantly and promoted n-type carriers.

Rheological determination of ink formulations gave good predictive information of the printability of an ink upon paper. Increasing the solids loading and changing the solvent increased the viscosity, and the storage modulus (G') of between 84 and 224 and viscoelastic behaviour of inks correlated with good print quality. Formulations would require further optimization depending upon the surface energy of the substrate type chosen.

This study demonstrated that the film characteristics depended upon the dispersant / water ratio in the ink mixture and the type of dispersant used, the film layer thickness and morphology of the film formed as well as the nature of the substrate. Such large changes in the characteristics of the printed film as was observed in this study would have a very significant impact on the ohmic drop experienced in a working cell, thus all these factors should be taken into account when formulating and optimizing a screen printing ink and depositing it upon a substrate.

CHAPTER 7

7. MEMBRANE ELECTRODE ASSEMBLIES FOR SPE ELECTROLYZERS

In this chapter the technological optimization of a solid polymer electrolyzer is studied using commercial materials.

7.1 INTRODUCTION

In about 1929 Bacon built a demonstration fuel cell consisting of porous nickel electrodes and is credited with creating a stable three phase reaction zone of electrode, gas, and electrolyte. In 1957 Grubb reported that the liquid electrolyte in a gas diffusion electrode (GDE) could be replaced by a solid, ionically conductive polymer to form electrode-electrolyte assemblies consisting of porous electrodes and ionically conductive polymers. These electrode assemblies that incorporate a gas-liquid-solid interface into the electrode element using a solid polymer electrolyte thus eliminate the liquid electrolyte and can be applied in various electrochemical processes. The electrolytic production of pure hydrogen and oxygen is possible through a solid polymer electrolyte assembly where an ion-exchange membrane such as DuPont's Nafion® is the electrolyte. These assemblies are called either membrane electrode assemblies (MEA), or solid-polymer electrolyte (SPE), or proton exchange membrane (PEM) which terms refer to the use of an ionically conducting membrane as an integral element in a device (De Castro, 1996).

Water electrolysis in a SPE cell possesses certain advantages compared with the classical alkaline process such as increased energy efficiency and specific production capacity and a simple system with a solid electrolyte operating at a low temperature. The cell resistance of the SPE system including the MEA can be as low as 0.075 Ohm in ultra pure water. On the other hand the relatively high resistance (about 0.2 Ohm) for alkaline systems limits the output of alkaline cells to about 1A cm^{-2}, since

above this current density the ohmic drop becomes high. The specific energy consumption of the SPE electrolyzer has been reported as 4.1 kWh Nm^{-3} - H_2 at 1 x 10^4 Am^{-2} which is better than the typical specific energy consumption of 5 kWh Nm^{-3} -H_2 for an alkaline electrolyzer (Kondoh et al., 2000). A commercial system analysed by Ivy et al., (2004) had a system efficiency of 73%.

This study is limited to the optimization of the SPE electrolyzer MEA using commercial benchmark electrocatalysts. Requirements were investigated for membrane electrode assemblies for SPE systems and prototype SPE electrolyzer operation including the selection of components and optimizing the system. In this chapter the choice of components, as well as the working conditions of the MEA were explored. Choices were made of substrates and supports that could be used as gas diffusion layers for the anode and the cathode. Furthermore, different anode and cathode catalysts were investigated which were processed in the form of micro-emulsions using the most suitable binders and applied to the gas diffusion layers or alternatively to the polymer electrolyte membranes. Conditions were evaluated to assemble the MEA and form the composite electrodes. The operational issues of a working module such as temperature, flow rate, moisturization, gas evolution, and insulation were also examined. Impediments for durability and stability and issues of reproducibility were addressed for scaleability and modularization.

7.2 OVERVIEW OF SPE ELECTROLYZER SYSTEMS

General Electric Co. developed the first electrolyzers using polymer membranes as electrolyte in 1966 for space applications (Davenport et al., 1991). Extensive research and development on solid polymer electrolyte (SPE) or otherwise named polymer electrolyte membrane (PEM) electrolyzers has been performed over the last several decades. The company ABB developed the commercial Membrel electrolyzer in the period 1976/1989 (Stucki and Scherer, 1998). Two units of 100 kW were tested over the longer term with an average voltage 1.75 V at 1 A cm^{-2} and 80 °C. Within the Japanese WE-NET program a cell voltage of 1.68 V at 1 A cm^{-2} was

obtained on a single cell of 50 cm^2 at 80 °C. The goal of the WE-NET programme is to construct a worldwide energy network for effective supply, transportation and utilization of renewable energy using hydrogen (Mitsugi et al., 1998).

A schematic of a typical membrane electrode assembly for an electrolyzer is shown in Figure 7.1.

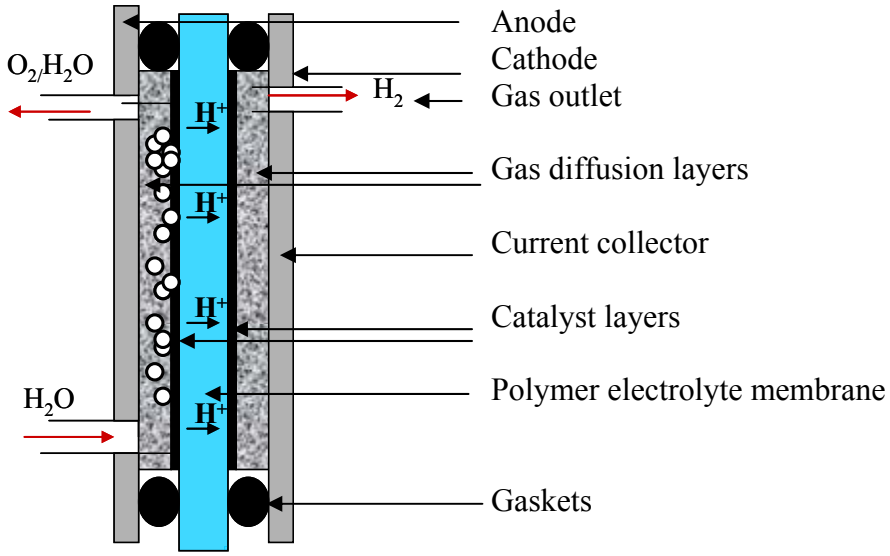

Figure 7.1 Schematic of membrane electrode assembly for the SPE electrolyzer

The main working components of the membrane electrode assembly (MEA) are (i) the gas diffusion layers, and (ii) the catalytic layers, which are layered on both sides of the (iii) polymer electrolyte membrane. This assembly is clamped and sealed between the current collectors serving as anode and cathode that are connected to an external circuit, across which a working potential is applied to polarize the electrodes. Ultra pure water is typically fed only to the anode side as reactant and also serves to remove the O_2 evolving during electrolysis. Water can be fed on the cathodic side to keep the MEA evenly moisturized and to act as a medium to remove the H_2 gas that evolves during electrolysis and prevent its build-up. A schematic comparison of the fuel cell and the electrolyzer functionality is presented in Figure 7.2.

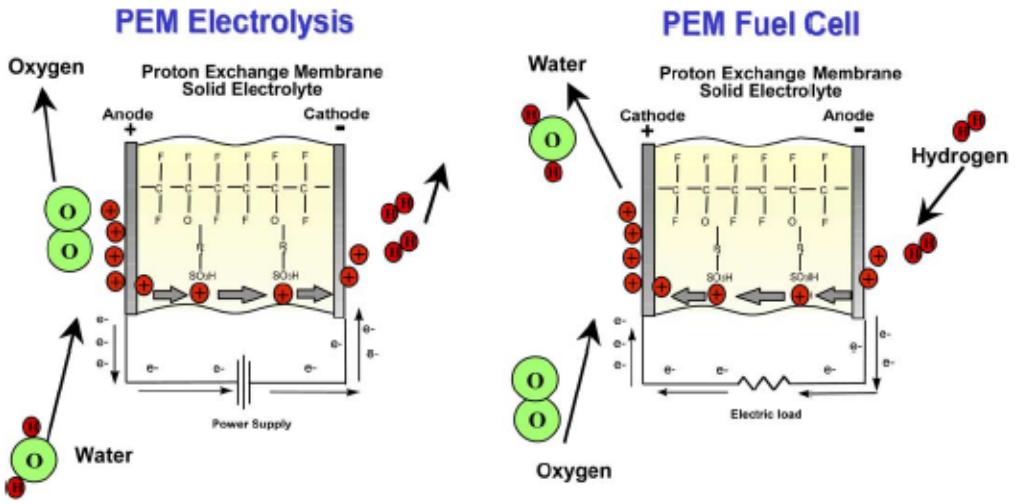

Figure 7.2 Schematic representation of PEM water electrolyzer and a fuel cell (Barbir, 2005)

It is possible to reverse the direction of the electrolyzer and allow it to operate in fuel cell mode periodically, utilizing the H_2 prepared during electrolysis as fuel. Such systems are termed unitized regenerative fuel cells (URFC). However the efficiency of both processes is reduced in regenerative systems because of the different optimized requirements for the fuel cell reactions versus those of the electrolyzer. Liu et al., (2004) describe a composite electrode assembly incorporating the proton exchange membrane for unitized regenerative fuel cells (URFCs) with an improved cycle life. In this system the cell works in electrolysis mode for one cycle and then by reversing the polarity, operates in fuel cell mode in the next cycle. The cycle life and polarization curves for both fuel cell and electrolysis modes of URFC operation were investigated with a new electrode with a composite structure and performance was found to be constant over 25 cycles, demonstrating that this dual system has potential.

7.2.1 Electrocatalysts

In the assembly of the SPE (or PEM) system it is firstly required that the correct choice of catalyst is made for the reaction occurring on the anode versus the reaction that takes place on the cathode. The electrocatalyst must be an electrical conductor in

addition to being an active catalyst. This restricts the choice of catalysts mainly to metals. The catalyst may be distributed in the bulk of substrate grains or at their external surface (Chirkov and Rostokin, 2005). An extensive review of scientific knowledge on this topic is reported by Wiesener et al., (1990). The catalysts can be used as bulk powders, or as admixtures, to which graphite powders are added in order to increase the transversal electric conductivity within the layer and decrease the amount of catalyst used. Catalysts may also be supported on a conductive material free of catalytic activity, e.g. carbons optionally graphitised in part, like those commercialised by Cabot Corporation under the trademark Vulcan XC-72 or Shawinigan Acetylene Black. Vulcan XC-72 is reported to have a surface area of $250 m^2 g^{-1}$ (Vielstich et al., 2003). Typically the catalysts sold by various commercial suppliers such as Johnson Matthey may contain 10 to 50 % of the precious metal catalyst dispersed on the conductive support. Such materials are disclosed, with the relevant fabrication methods, in the patent literature, e.g. in United States Patents 4,614,575 (Juda et al., 1986) and 5,584,976 (Nishiki et al., 1996). Carbon nanotubes have been used to stabilize high Pt dispersions, and increase the electronic conductivity of the electrodes and also improve the gas transport rate through the electrodes reactive layers. Scodelaro et al., (2005) demonstrated that high loadings (20-30 wt %) of Pt with high dispersions (Pt nanoparticle sizes as low as 1-2 nm) could be obtained upon CNTs. Commercial catalysts are sold with even higher loadings of Pt.

Platinum based, bimetallic and ternary electrocatalysts have been well described in the literature. Pt is used because of its stability and because it is a hydrogen absorbing metal which is capable of electro-chemically absorbing and desorbing hydrogen. Platinum is well known to be the best catalyst for water electrolysis due to its moderate strength of adsorption of the reaction intermediates. It has the lowest over-voltage of all metals. Ultra-fine Pt particles can either be deposited on the electrode support i.e. the gas diffusion layer, or directly onto the polymer electrolyte membrane (Millet et al., 1988).

CHAPTER 7

The oxygen electrode (anode) is the main source of overpotential in the water electrolysis process using the SPE system. The low activation loss on the cathode electrode where hydrogen is produced is usually neglected. There are few electrode materials that resist both dissolution and the formation of obstructive films when anodically polarised. For example, in contact with the acidic Nafion® membrane non-noble catalytic metals like Ni and Co will corrode and Pt will be covered by a low conducting oxide film. Henry B. Beer obtained a patent on dimensionally stable anodes (DSA) in 1965, and oxides of Ir and Ru have typically been used as anode catalysts on titanium substrates in DSA (Rasten et al., 2003). Various attempts to change the catalyst type have been made. For instance, Andolfatto et al., (1994) found that the performance and long-term stability of a water electrolysis pilot plant could be enhanced when IrO_2/Ti electrodes were hot-pressed on both sides of a Nafion® membrane in comparison with Pt electrodes, and they obtained lower anodic overvoltages and a better long-term stability of the cell voltage due to a lower sensitivity to poisoning.

The theory of the process mechanisms at the oxygen evolution electrode is less well understood than for hydrogen evolution reactions because of the difficulties introduced by the participation of the anode material itself in the electrode process. The most probably discharge step involves the formation of oxygen atoms lightly adsorbed on a metal already covered with strongly bound oxygen atoms:

$$MO + OH \xrightarrow{\text{Discharge}} MO - O + H^+ + 2e \qquad (7.1)$$

Where MO – O represents an oxygen atom lightly adsorbed on an oxidized surface of the metal M. The discharge of hydrogen ions is believed to occur in two possible desorption steps that lead to the formation of the molecular product, in this case, oxygen. The first step is

$$2MO - O \xrightarrow{\text{Combination}} 2MO + O_2 \qquad (7.2)$$

This is followed by a secondary step with the secondary discharge of a hydroxyl ion and the desorption of a lightly adsorbed oxygen atom (Potter (1970).

$$2MO - O + OH^- \xrightarrow{2^o \text{ discharge}} 2MO + O_2 + H^+ + 2e^- \qquad (7.3)$$

Generally the heterogeneous reaction rate taking place at the electrodes surface is described in units of mol per unit area by equation 4.1 (Chapter 4).

The rate of the electrode reaction $O + ne^- \leftrightarrow R$ depends on various surface effects in addition to the usual kinetics variables. The reaction is thus composed of various steps to convert the dissolved oxidized species to the reduced form (Yaritsa, 2004). The electron transfer has to proceed at a reasonable rate and produce an efficient quantity of product, thus if an anodic catalyst's activity is poor a significant amount of applied voltage would be required. Minimizing the activation overpotential requires maximizing the catalyst area available for the reaction. The chemical processes that contribute to the activation loss involve the adsorption of reactant species, transfer of electrons across the double layer of an electrolyzer, desorption of a product species, and the nature of the electrode surface (Bard and Faulkner, 2001).

Yim et al., (2005) prepared bifunctional electrocatalysts for the oxygen electrode that were tested on the URFC performance including both fuel cell and water electrolysis in a single cell URFC system. The Pt black catalyst performance in fuel cell mode was higher than bi or trimetallic catalysts whereas in water electrolysis mode the performance of PtIr was better than Pt black. Overall the PtIr combination catalyst showed the best URFC performance. As the Ir or IrO_2 content in the anode catalyst was increased the fuel cell performance decreased while the water electrolysis performance was significantly improved. The catalyst content was optimized at 1.0 mg cm^{-2} of Pt black as hydrogen electrode and 2.0 mg cm^{-2} of PtIr (99:1) as oxygen electrode. In binary mixtures such as IrO_2 +SnO_2, the activity during oxygen evolution was enhanced as the proportion of IrO_2 increased in the mixture (Kawar et

al., 2003). IrO_2 is known for its high chemical stability, high mechanical strength, superior oxidation resistance and high electrical conductivity, however it is a somewhat less active electrocatalyst than RuO_2 for oxygen evolution although it is less susceptible to corrosion than RuO_2. The metal oxides of IrO_2 or RuO_2 are normally mixed with inert components like Ta_2O_5, TiO_2 or SnO_2. The metal oxides are preferred to the metal only because the metal catalysts are unstable (Musiani et al., 1999).

Such studies highlighted the performance of Pt as multifunctional catalyst for the URFC system and the benefits of Ir catalysts for the anode in electrolyzer systems (Ioroi et al., 2000; 2002). Chen et al., (2001) looked at combinations of the following elements (Pt, Ru, Os, Ir, and Rh) and found that the ternary catalyst comprised of PtRuIr, with atomic ratios of 4.5:4:0.5 respectively, was the best performing oxygen reduction catalyst for URFC. The addition of Ru to the Pt/Ir electrode helped to increase the reaction rate because it stabilized surface atom/oxygen bonds. Anode catalysts based on platinum-ruthenium and platinum-molybdenum alloys have been developed by Johnson Matthey (Platinum Metals Review - Volume 46 Number 3 (July 2002)). The use of IrO_2 still permits electron conduction to take place. Trassati et al., (1991; 2000) suggested that the oxide layer resistivity is related to the intergrain region and that conductivity takes place by hopping mechanisms from grain to grain.

Transition metal oxides, like IrO_2 constitute an interesting class of materials because of various properties they exhibit. Their characteristics have been found to depend strongly on the kind of preparation techniques and conditions (Mousty et al., 1999). In studies of its electroactivity by cyclic voltammetry (da Silva et al., 1997; Mousty et al., 1999), the main feature of Ir was the presence of the reversible peaks (at about 0.9V) which are generally attributed to the redox process Ir(III) to Ir(IV), corresponding to the formation of $IrO(OH)_2$. Ir(IV) may be further oxidised at higher potential to a final oxidation state of Ir(VI). This final redox state was achieved (at

about 1.3V), and it has been proposed to correspond to Ir(IV)/Ir(VI). During the anodic sweep equation 7.4 takes place:

$$IrO_3 + 2e^- + 2H^+ \leftrightarrow IrO(OH)_2 \quad (7.4)$$

This reaction becomes competitive to the oxygen evolution reaction:

$$IrO_3 + H_2O \rightarrow IrO(OH)_2 + 1/2O_2 \quad (7.5)$$

Andolfatto et al., (1994) did durability studies for membrane electrode assembly (MEA) with IrO_2 catalysts supported on titanium fibre in both electrodes. The durability was found to be nearly 6000 h at standard conditions, 2.2 V cell voltage and with a current density output of 500 mA cm^{-2}. The relatively low performance reported may be due to the low catalyst loading used, which was 2.4 - 3 mg cm^{-2}. Based on the stability obtained by Andofaltto et al., IrO_2 can be an interesting catalyst for both anode and cathode for further research.

The effects of catalyst preparation and dispersion on activity are among the major issues that still need to be addressed for improving cell performance and so that an optimum compromise is achieved between performance and cost. A significant ohmic, activation and transport loss is attributable to the dispersion of the metal oxide catalyst on a conductive support. Good contact between the electrocatalyst and the support is essential in order to minimize the ohmic losses and contact between the electrocatalyst and electrolyte is a necessity for proton transport to the electrocatalyst particles. The electrolyte, which is in contact with the active layer of the supported electrocatalyst upon the GDL of the electrode, also has to be continuous up to the interface of the active layer with the polymer electrolyte membrane layer to minimise ohmic loss. The overall catalytic performance is affected by the catalyst layer and therefore it is important to achieve the optimum catalyst loading on the GDL in contact with the polymer, which should provide ionic pathways for protons and low resistance to proton transport. Only catalysts in contact with the polymer electrolyte as well as the reactant are electrochemically active. The catalyst particles should also be electrochemically connected to the external circuit.

Thus catalysts in the electrode structure should not be buried in the bulk of the support (Lee et al., 1998; Wang et al., 2001).

Moreover, the electrode kinetics, electrolyte mass transfer, ionic and electronic conductivity also determine the electric potential and current distribution in the three-dimensional electrode structure and ultimately affect the catalytic activity.

7.2.2 Choice of gas diffusion layers

A gas diffusion electrode (GDE) is constructed by forming an asymmetric electrode from a porous substrate layer called a gas diffusion layer (GDL) that contains or supports a super-fine particle catalyst layer. The GDL connects the current collector via its gas-liquid permeable layer to the electrode substrate. Various configurations of GDL are, for instance, foams with open cells, matted felts consisting in entangled fibres, or planar meshes formed by layers of crossed and overlaid or interwoven fibres. The challenge in preparing the gas diffusion electrode is to have a durable and high surface area gas- liquid permeable layer, that is simultaneously electro conducting and of the right texture to support the catalyst layer. The mass transport characteristics of a GDL are defined by the morphology and characteristics of the material, such as its pore size distribution, interconnectivity and hydrophilicity (Kramer et al., 2008). Many patents have been granted for the development of GDE that are applicable to electrolyzers or fuel cells (e.g. United States Patent 5618392 (Furuya, 1997); United States Patent 6444602 (DeMarinis et al., 2002); United States Patent 5733430 (Ashida et al., 1998); United States Patent 6361666 (Lipinski and Leuschner, 2002)). According to the patent literature, improving gas, liquid and vapour transport through the electrode can be achieved by regulating the porosity of the GDL, reformulating the applied ink containing the electrocatalyst, and creating a film coating structure of the ink on a conductive matrix.

In some studies hydrophobic PTFE is applied to inhibit aqueous solutions from penetrating the electrode structure whereas the typically used carbon black catalyst support can be wetted by the electrolyte (De Castro, 1996). Direct electrochemistry on a gaseous species is limited by the gas-liquid solubility, but the solution layer acts as a thin meniscus which is able to achieve high gas flux rates. The high surface area that is inherent in most GDEs forming part of the MEA may allow an order of magnitude amplification of current compared to what may be achieved on an equivalent geometric area.

Hayashi and Furuya (2004) describe the preparation of gas diffusion electrodes by electrophoretic deposition of precipitates deposited from carbon-polytetrafluoroethylene dispersions. Pt was then incorporated as catalyst and in alkaline solution the gas diffusion electrode promoted oxygen reduction and hydrogen oxidation in an H_2-O_2 fuel cell. Morimoto et al., (2000) describe gas diffusion electrodes made of electro conductive porous polytetrafluoroethylene (PTFE) sheets supporting Pt catalysts that were applied as the oxygen reduction cathodes for chlor-alkali electrolysis. These authors also report the oxidative corrosion of the carbon carrier.

GDEs using ionically conductive polymer electrolytes require improved electrode structures, and the void volume percentage, average pore diameter size, and electrode thickness should be taken into account. Good wettability of GDL surfaces may promote complete occupation of the void spaces in the electrodes by the liquid reactant water which is desired in electrolyzers but not beneficial to fuel cell systems. The release of the gas bubbles from the reaction liquid in which they are formed, gives rise to difficulties such as anodic and cathodic pressure variations that may be harmful for the ion-exchange membranes, or partial blocking of the electrodes under the action of the adhering bubbles causing increased ohmic drop, as the electric conductivity is decreased by the presence of gas. The gaseous product normally causes a gas film layer at the electrode surface that constitutes a resistance to flow. This can be minimized by rapidly removal of the electrode gases by either employing

a thinner gas diffusion layer (GDL), a special type of flow field plate or changing water flow rate (Reiger, 1994; Bockris, 1973; Koryta et al., 1993; Hamman et al., 1998; Crow, 1994). Furthermore, combining these changes with an optimized coating methodology may allow the production of GDEs in an automated way.

7.2.3 Ionomer content in electrodes

Proton conductive polymers play varied roles within the MEA as they must create a durable and robust binder or structure for catalyst retention that must adhere well to the membrane-electrolyte or GDL, and enhance ion exchange or proton conduction capacity of the electrode. The polymer ionomer content in the electrodes simultaneously affects the activity of a catalyst and also the ionic resistance, therefore the optimum ionomer content in the catalyst layer is necessary for good performance. Normally ionomer loading as wt % is calculated as a dry weight of ionomer divided by the total dry weight of a catalyst and ionomer and multiplied by 100. Many studies have reported the effect of ionomer content, with differing optimum contents recommended by different researchers. Lee et al., (1998) showed that the Nafion loading correlated with the activation polarization characteristics which showed increased activity up to a loading of 1.3 mg cm^{-2} followed by a more gradual change with maxima at 1.9 mg cm^{-2} which trend was found to correlate well with the decrease in charge transfer resistance and increase in the electrochemically active surface area. Ioroi et al., (2002) reported that the amount of Nafion added as binder to the catalyst layer and proton conductor should be in the range of 7-9 % by weight. Other studies confirmed that the catalyst is more active at an ionomer content ranging from 30 – 40 dry wt %. In porous gas diffusion systems with polymer electrolytes the electrode is often coated with a solution of the solid electrolyte and aliphatic alcohol to increase the catalytically active area in contact with the ionomer and to achieve penetration of the polymer electrolyte into the electrode (Wöhr et al., 1996; Ioroi et al., 2003).

7.2.4 Choice of solid polymer electrolyte membrane

In polymer electrolyte membrane (PEM) form, the polymer should be impermeable to gas whilst being simultaneously able to take up and retain moisture and enable ion conductance in order to be a suitable separator of the anodic and cathodic compartments of a working SPE cell. The behaviour of the membrane is closely linked to its structure. The fixed anions in the pores of the ionomer, which are filled with water, exert an electrostatic influence on the ions of the electrolyte so that a diffuse double layer is formed in the pores. The ion-exchange properties proceed under the flow of electric current across the membrane. The membrane must remain hydrated in order to be proton conductive. The requirement to keep the membrane hydrated restricts the operation of the cell to temperatures under the boiling point of water (Robbins, 1972).

Intense studies have been carried out in recent years on the synthesis of new proton conducting membranes, which may play the role of a solid electrolyte in SPE systems such as electrolyzers and fuel cells. The classical methods include the synthesis of polyelectrolytes comprising SO_3H groups (e.g. poly perfluorosulfonated acids and sulfonated polysulfines). In these membrane there is a hydrophobic region containing the fluorocarbon backbone and a hydrophilic region containing the sulphonate sites, the protons and the water of hydration. The solid polymer electrolyte typically consists of a chemically altered solid fluoropolymer containing sulphonic acid groups, SO_3H, which release their hydrogen as positively-charged protons:

$SO_3H \rightarrow SO^{3-} + H^+$

These charged forms promote water penetration into the membrane structure but exclude the product gases, molecular hydrogen and oxygen. The resulting hydrated proton, H_3O^+, is free to move whereas the sulphonate ion is part of the backbone of fluorocarbon comprising the repeating structural unit of the ionomer. Proton conduction through the membrane proceeds via the protons from the anode entering the membrane, becoming solvated by water molecules and thus giving rise to H_3O^+

ions which move through the hydrated regions to the cathode. The phenomenon of the proton transport via the water molecules is called 'Electro-osmosis' (Koryta, 1986; Okada et al., 1998). Formation of a Zundel cation, $H_5O_2^+$ from combination of the 'proton hole', H_2O and a nearby hydronium ion, H_3O^+ has also been reported (Eikerling et al., 2003). In water electrolysis the hydrated protons are attracted to the negatively-charged electrode (cathode) when an electric field is applied across the membrane and thus the membrane acts as a proton conductor (Greenwinds, 2002).

A typical example of this material is the perfluorinated sulfonic acid polymers such as Nafion® that can be obtained from the E. I. Dupont De Nemours and Company. It is available as thin pre-formed membranes in thicknesses of about 100 μm, or as a 5 % solution which may be deposited and evaporated to leave a polymer layer. Nafion® has some limitations due to high cost and lack of thermal stability in high temperature applications and is problematic in fuel cell assemblies because of methanol crossover (Liao et al., 2002a; 2004), which was not a problem in the electrolysis system being investigated.

The proton conductivity of Nafion® membrane materials is complex, being favoured by a high level of hydration and dependent on the pre-treatment, operating temperature and operational conditions. The structure of the Nafion® membrane is shown in Figure 7.3. The values of *n*, *x* and *m* can be varied to produce the material of equivalent weight (EW), where EW is the number of grams of the polymer per mole of fixed sulphonate sites.

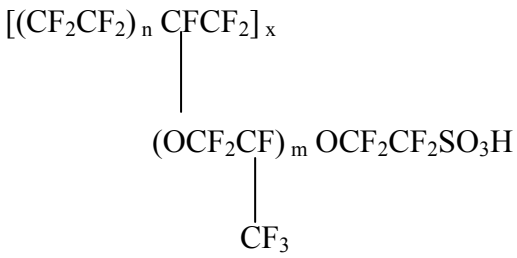

Figure 7.3 General structure of a Nafion® membrane

According to Sone et al., (1996) the membrane conductivity without heat-treatment was ca. 7.8×10^{-2} S cm^{-1} at ambient temperature and 100 % relative humidity and varied strongly with the humidity and heat-treatment of the membrane. Slade et al., (2002) demonstrated that Nafion® 112 exhibited the best performance compared to other available Nafion® membranes such as 117, 115 and 113. These membranes all have the same equivalent weight (EW), 1100, but their proton conductivity is different as well as the film diameter thickness of 175, 125, 87, and 50 μm respectively for the different Nafion® membranes 117,115,113, and 112.

Many attempts have been made to improve the PEM. For instance, Gore-Textile Associates developed Gore-Select™ composites by impregnating Nafion® solution in highly porous polytetrafluoroethylene (PTFE) films (Bahar et al., 1997). Zhang et al., (2006) found that doped sulfonated poly(phthalazinone ether ketone) (SPPEK) membrane showed higher water uptake and proton conductivity than pure SPPEK membranes. Thus composite membranes can be an alternative solution, in which inorganic acids are immobilized in polymeric matrices characterized by strong basic properties (e.g. H_3PO_4 / polybenzimidazole system). Suitable proton conductive polymers include those in U.S. Patent 7052805 (Narang et al., 2006), describing a polymer with acidic subunits, another polymer with basic subunits, and an elastomeric polymer with elastomeric subunits. U.S. Patent 5,783,325 (1998), UK Patent 2,316,802 (1999) and U.S. Patent 6,103,414 (2000) by Cabasso describe a polymer solution made of thermoplastic film former, e.g., polysulfone and polyvinylidene fluoride, mixed with carbon and a common solvent (DMF and NMP) and cast as asymmetric flat sheet electrodes on glass to control the gas-diffusion pores, and the electrode-catalyst-membrane interface. A substantial reduction of the catalyst in the MEA was claimed, and less than 0.1 mg cm^{-2} was shown to produce high performance MEA.

There are many efforts reported in the literature to enhance or replace the Nafion based membrane (Linkov et al., 2002; Liao et al., 2002 b; Vaivars et al., 2004;

Alonso and Turrillas, 2005). However, since developing the polymer electrolyte membrane was not the focus of this study such efforts are not further reviewed. This study mainly considered the effect of different film thicknesses of Nafion® or commercial substitutes for this material, and assembly conditions, upon overall cell performance.

7.2.5 Assembly of the Membrane Electrode Assembly

The various components specified above were used to assemble the membrane electrode assembly (MEA). Chinese GEFC®- MEA made by Golden Energy Fuel Cell Co., Ltd. (Beijing) is an example of a commercially available ready to use MEA for the reversible H_2 PEM cell and is also used as the proton exchange membrane (PEM) in the direct methanol fuel cell (DMFC). It is a catalyst coated membrane MEA along with two separate high efficiency gas diffusion layers trademarked as GEFC®-GDL. According to the suppliers' technical notes it consists of proprietary GEFC®-11N (N=1~20 mil) perfluorinated PEM coated with a bi-network electrode on either side of the PEM, where the bi-network electrode is interconnectively composed of the catalyst network coated with thin perfluorinated proton exchange film and electrolyte network coated with thick perfluorinated proton exchange film. The technical index given by the supplier states that the reversible H_2 MEA is configured as a Pt-PEM-Pt MEA with 2.5 mg Pt cm^{-2} and 2.5 mg Pt cm^{-2} on the anode and cathode side respectively and is specified to have a maximum power density of between 0.3 and 0.6 W cm^{-2} (at 30 °C, 0.0 MPa dry H_2/Air & O_2 respectively). This technical description gives the characteristics of typical assembly conditions for the MEA.

There are various approaches to preparing and assembling the components of the MEA used in a SPE electrolyzer. After a choice is made of the specific components for the anode or the cathode side of the MEA, the components have to be assembled together. Firstly the chosen catalyst has to be deposited on the polymer electrolyte or

onto the GDL using an appropriate binder and deposition technique for the anode and cathode respectively. Typically an ink is prepared containing the catalyst. A basic method for preparation of a catalyst ink composed of the ion conducting copolymer (usually 5% polymer by weight) dispersed in a diluent, the catalyst particles, and additives to ease processing is described by Shin et al., (2002). The catalyst can be incorporated into the MEA using various techniques including: i) coating of catalyst ink on the GDL, ii) coating of the catalyst ink directly upon the proton-exchange membrane and iii) using transfer decals to apply catalyst ink over the membrane by hotpressing.

Thereafter the asymmetric cathode and anode electrodes have to be bonded to the solid polymer electrolyte membrane. Yamaguchi et al., (1995) describe a hot-press method in which a catalyst film is adhered to the polymer membrane by means of hot pressing to create the three-dimensional electrode membrane interface. In their study the catalyst was introduced into a PTFE solution and a film containing the catalyst was formed and dried where after the catalyst film was heat treated and then laminated on the ion-exchange membrane followed by the hot-pressing stage.

The Handbook of Fuel cells (Vielstich et al., 2003) describes various approaches for the preparation of the MEA. For instance, the catalytic paste could be prepared by ball milling a solution of the ionomer used as binder and proton conductor with the electrocatalyst in an alcoholic solution until the carbon showed a uniform size distribution (Tada in Vielstich et al., 2003). The paste was then printed onto a prepared gas diffusion layer (GDL) and was dried at 100 °C for 3 h and then hot pressed at 130 °C for 1 min at 20 kg cm^{-2}. The process could be repeated until the required catalyst loading was obtained. It was observed that the higher the ionomer content of the ink paste, the lower the pore volume of the carbon black support. The ionomer was used in the ink paste to obtain sufficient proton conductivity and catalyst utilization in the catalyst layer, as well as binder to ensure durability of the electrode. The oxygen diffusion was inhibited through the catalyst layer when the pore volume was decreased because of the addition of ionomer. The amount of

ionomer per gram of carbon black depended on the pore volume of the support and amounts of 0.2 - 0.4 g of ionomer per gram of carbon black was recommended by these authors.

The amount of catalyst and Nafion in the ink deposited on the GDL plays a major role in the activity of the MEA. Ioroi et al., (2002) showed that the Nafion content in the electrode affected the water electrolysis performance and 7–9 wt.% Nafion showed good performance. A typical Pt loading on electrodes was 0.25 mg cm^{-2}, which was dependent on the cell voltage applied. These authors found that the utilization of the anode catalysts was effective only in a thin segment of the catalyst layer because of a gradient of electrochemical potential caused by limited electronic conductance of the catalyst layer. It has also been demonstrated that higher catalyst loading and thinner layers gave better overall results (Vielstich et al., 2003).

Millet et al., (1990; 1993) describe a procedure for the preparation of the SPE electrocatalyst in which noble metal cationic species were chemically reduced directly on both surfaces of a perfluorinated ion-exchange membrane by chemical reduction of cationic precursor salts. They found that the metallic particles were not homogeneously distributed across the SPE thickness but predominated near its surfaces. The electrodes were then bonded onto the SPE. Low noble metal loadings (< 1 mg cm^{-2}) and a low cell voltage of 1.75 V at 1 A cm^{-2} at 80 degree ºC and long time stability (over 15,000 h of continuous electrolysis) were reported.

7.2.5 Challenges in the enhancement of MEA output

It is not a simple process to optimize a MEA because of the multitude of variables that play a role in the overall output of the electrolyzer cell. It is difficult to compare the overpotentials of electrodes that are disclosed in various patents and articles mentioned in this review because each system uses different electrolytes and different temperatures and not all procedures are specified for SPE electrolyzers but

are designed for MEA systems used in fuel cells of various configurations. Diverse approaches have been taken to establish the contribution of the various components and operational parameters in the working cell by various authors. However, based on estimations, all SPE electrolyzers typically work between 1.6-1.8 V and 300-1000 mA at 80-100 °C. Isolating the effect of any one variable is a complex and challenging process and was not the main focus of this study.

The overpotential for the production of hydrogen using Pt electrodes is 0.6 V of which 0.5 V is required for oxygen evolution and 0.1 V for hydrogen (Atkins, 1989). Appreciable product formation is only obtained if the applied potential is greater than the cell potential. Solid polymer membrane electrolyzers should maintain a reasonably current density i.e 1 A cm^{-2} or more and an energy efficiency of more than 90 % (Hijikata, 2002). Energy conversion efficiency (η_{ε}) and cell effiency (η_{cell}) are given by Equation (7.5) and Equation (7.6) respectively:

$$\eta\varepsilon = \frac{Ecell}{V} X100 \tag{7.5}$$

$$\eta cell = \frac{Ecell}{E} X100 \tag{7.6}$$

where V and E are the theoretical values of enthalpy voltage and electrolysis voltage respectively. The standard potential of the water electrolysis cell is 1.23 V at 25 °C. The positive voltage indicates the Gibbs Free Energy for electrolysis of water is greater than zero for these reactions. This can be found using the Nernst Equation at equilibrium. The reaction cannot occur without adding necessary energy. At a normal operating current density (~1A cm^{-2}) of a commercial electrolyzer, the voltage ranges between 1.8 V to 2.0 V and thus an electrolyzer that is operating at 1.9 V gives a cell efficiency of 65 % (1.23/1.9). To increase energy efficiency it is necessary to operate at a lower voltage thus highly active catalysts are required or a decrease in the current density will result in a decrease in the rate of hydrogen and oxygen production (Khaselev et al., 2001).

The surface properties as well as the energetics at the electrode/electrolyte interface contribute to the complexity of the working catalyst and affect the electrochemical reaction steps, the adsorption-desorption processes at the electrode surface as well as the transport processes and thermal behaviour of gas diffusion electrodes (M. Wöhr et al., 1996).

In the membrane electrode assembly used in SPE electrolyzers there are two different diffusion processes, the gas diffusion and the liquid or vapour diffusion. During the phase transition of gas/liquid occurring in the electrochemical reaction (water to oxygen and hydrogen) it is possible to hamper the reactions by diffusion limitations that may occur because of the significant difference in density and mobility, and the different time scales of both diffusion processes (Wang et al., 1999). For liquid transport the material characteristics are important, especially the wetting angle of the catalyst, and the characteristics of the respective catalyst support. The liquid transport can be changed from a diffusion mode to an osmotic mode by varying the composition of the electrode.

The interface of the electrode and electrolyte is a solid-solid transition that may consist of a high number of single contact points. This interface can therefore produce high ohmic losses on charge transition (Wöhr et al., 1996). Properties such as the anodic overvoltages, cathodic overvoltage, ohmic drop within the SPE and roughness factor of electrodes have been measured (Millet et al., 1989; 1990). The ohmic overpotential is due to the total resistances in the electrolyzer. These resistances can be found in practically all cell components: ionic resistance in the membrane, ionic and electronic resistance in the electrode and electronic resistance in the gas diffusion layer, flow field plate and terminal connections (Roshandel et al., 2005). But the largest source of ohmic loss in the cell arises from the electrolyte membrane.

Grigor'ev et al., (2004) developed a mathematical model for analyzing spatial distributions of the transport and the concentration of reactants and current density

over a fuel cell with a solid polymer electrolyte. The effect of the catalytic layer activity, reactant speed, bipolar-plate geometry, thickness and porosity of current collector and gas-diffusion layer, and the reaction mixture composition on the fuel cell efficiency was modelled and the relative contribution of each component highlighted. That study highlights the complexity of the SPE system.

Chirkov and Rostokin (2005) showed that the magnitude of currents of electrodes in hydrogen-oxygen fuel cells of all types is determined by values of the effective coefficient of gas diffusion, the effective coefficient of ionic conduction, and the characteristic bulk current density.

7.2.6 The working cell

Industrial electrolyzers are made of a multiplicity of elementary cells in hydraulic and electrical connection, pressed one against the other to form a modular arrangement. The electrical connection may be of a monopolar or bipolar type and the cell constitutes one of a repeating element in a modular electrolyzer. An intimate contact between membrane, electrode and current distributor should be mechanically ensured and the elements comprising the cell should have sufficient elasticity to undergo a deflection when the various constitutive elements are tightened in the modular arrangement. A fully operational electrolyzer system is described for instance, in United States Patent 6569298 (Merida-Donis, 2003) where the deionization of water and hydrogen fuel production in a fuel generation mode, and electricity production in a power generation mode are integrated. A capacitive deionization device receives water and electrical energy to produce deionized water that is transferred to the PEM electrolyzer to produce hydrogen fuel. A storage system receives the hydrogen which is then transferred to the PEMFC device that produces electrical energy.

In this study only a single element of a modular array was optimized. Full integration with the peripheral systems was not considered as this fell outside the scope of the study. The objectives of this part of the study were to gain an understanding of the factors that have an effect upon the operation and current density of a working module, to decouple the effect of the catalyst and influence of different components from operational issues. Effect of variables such as ink composition, type of gas diffusion layer, loading variability, stability and durability, catalyst type for anode and temperature were investigated.

7.3 EXPERIMENTAL: MEMBRANE ELECTRODE ASSEMBLIES FOR SPE SYSTEMS

This section lists the chemicals, components and methods used to assemble the MEAs that were then tested in the electrolyzer cell module.

7.3.1 Chemicals

i) De-ionized water

ii) Iso-propanol 99 %, liquid, m.p-89.50 and b.p-82.40 from Aldrich

iii) Nafion® solutions in water

Ion Power, Inc supplied LIQUION™ solutions which are dissolved NAFION® resins in a mixture of water and alcohols. The NAFION® is Perfluorosulfonic Acid/TFE Copolymer. The solutions are available in solid concentrations of 5 or 15 weight %. The solutions can be dried to form films and coatings of NAFION® or mixed with other solids to form electrodes.

7.3.2 Components

7.3.2.1 Polymer Electrolyte Membranes

Available commercial proton conductive polymers membranes used to separate the anode and cathode compartments of the water electrolyzer included:

Perfluorinated sulfonic acid polymer membrane Nafion® from the E. I. Dupont De Nemours and Company, which is supplied by Electro chem. Inc. 400 West Cummings Park, Woburn MA 01801 USA and available in sheet form as Nafion membranes "EC – NM – 117" , "EC – NM – 115", and "EC – NM – 112" which specifies the thickness of the PEM films. For instance Nafion 112 has a thickness of 50 μm; Water uptake of about 25% ; Proton conductivity(S cm^{-1}) about 1.0×10^{-2}.

A Chinese equivalent GEFC®-11N perfluorinated proton exchange membrane was also used. The technical indices of this material were: Nominal Thickness: N mil (N=1~20); Acid Capacity 0.97 mmol g^{-1}; Conductivity 0.1 S cm^{-1} (25 °C); Water Uptake 50 % (at 100 °C, 1 h); Linear Expansion 1% (at 23 °C, from 50 % RH to water soaked); Tensile Strength 37 MPa (at 50 % RH, 23 °C, Isotropy); Melting Point 219 °C.

7.3.2.2 Gas diffusion layers

Lydall Carbon cloth called Technimat, which is a carbon paper used as pyrolysed diffusion layer with no PTFE content, with controlled porosity. Technimat exists in a number of basis weights (from 6.8 to 102 g m^{-2}). Various grades were considered and a typical specification given by the suppliers of the 6100-200 grade was: Grade-Basis Weight 41.7; Lbs/3000 ft²-Caliper @ 4psf 56.6; mils-Caliper @ 8 psi 25.8; mils-Tensile MD 3800; gms/inch-Tensile CD 5400; gms/inch-MD/CD Ratio1.07.

Etek LT-1400W GDL with electrical resistance of 500 mΩ cm^{-1}; air permeability 500 mL min^{-1}; mean pore size 7 μm (further specifications available from Etek, 2008).

Titanium fibre Bekinit KK, supplied by Bekaert (Japan) stock number ST/Ti/20/200/56, with specifications of t=0.1 mm; or Bekinit ST/Ti/20/400/76, with specifications t = 0.35 mm (Bekaert BFT, 2008). Both types have fibre diameter of 20 μm; weight : 300 to 200 g m^{-2}; porosity : 52 to 56 %; thickness : 0.14 to 0.1 mm.

7.3.2.3 Binders

5 wt % LIQUION™ composition is: NAFION® 4.95-5.05 wt% in a solvent comprising Water: 20 wt%; Isopropanol :75 wt% ; Density: 0.86 g cm^{-3}

15 wt% LIQUION™ composition is: NAFION® 14.9-15.1 wt% in a solvent comprising Water: 45 wt%; Isopropanol :40 wt% ; Density: 1.0 g cm^{-3}; Electrical properties: 880 Ω cm^{-1} DC, 330 Ω cm^{-1} AC

7.3.3 Methods

7.3.3.1 Pretreatment of titanium fibre GDL.

20 g of Oxalic acid was dissolved in 200 mL water (10 % w/w solution). The solution was heated to boiling and then the required size of the fibre was placed in the boiling solution, treated for 6-7 min, rinsed with de-ionized water and then dried.

7.3.3.2 Preparation of Proton conducting membrane

Chinese Proton Exchange Membrane GEFC®-11N was soaked in 5% H_2O_2, H_2O, 0.5 M H_2SO_4 and H_2O respectively at 80 °C for 1 h, and rinsed thoroughly with pure water. The treated membranes may be stored in pure water or allowed to dry.

Perfluorinated Proton Exchange Membrane Nafion® sheets were cleaned and activated as follows: The Nafion® sheet was cut into appropriate sizes and boiled in 9 M HNO_3 for 1 h, rinsed with deionized water, and then placed in H_2O_2 solution for 1 h at 60 °C. (The H_2O_2 solution is made with 51 mL in 1 L distilled water). The Nafion® sheet was rinsed in distilled water for 30 min while heating. Thereafter the Nafion® sheet was boiled in H_2SO_4 for 1 h (the H_2SO_4 solution was prepared from

54.3 mL in 1 L distilled water). Finally the Nafion® sheet was washed in distilled water for 30 min while heating.

7.3.3.3 Catalysts

Commercial anode and cathode catalysts obtained from Alpha Aesar, a division of Johnson Matthey, were applied in the MEA assembly unless otherwise specified.

Premion Iridium (IV) oxide, 99.99 % (metals basis) Ir 84.5 % minimum, total impurities <100 ppm supplied by Alfa Aesar, a Johnson Matthey Company (Stock # 43396; Lot # E27P20). This catalyst will be referred to as JM IrO_2.

Pt catalyst HiSpec™ 4000, 40 % on carbon black with 39.74 % Pt, 1.33 % moisture, 3.54 nm crystalline size supplied by Alfa Aesar, a Johnson Matthey Company (Stock #42204; Lot # J26P18 or F01Q12). This catalyst will be referred to as JM Pt_{40}/C.

Homemade IrO_2 Catalyst preparation method.

In the synthesis of Iridium oxides, Iridium chloride (H_2IrCl_6 or $IrCl_3$) precursors were oxidised within a melt of sodium nitrate according to the Adam's fusion method. To evenly disperse the precursor throughout the $NaNO_3$, 0.4 g of $IrCl_3.x$ H_2O and 20 g of $NaNO_3$ were dissolved in 100 mL of deionised water. The solution was stirred for more than 6 h using a magnetic stirrer. The solution was dried in an oven at 80 °C. The dried mixture was then introduced into a pre-heated ceramic furnace at 350 - 450 °C and kept in these conditions for 30 min until a dark brown nitrous gas evolved. The fused salt melt was cooled to room temperature and then leached by repetitive washing with deionised water to leach out all the excess salt. The oxidised iridium solids remaining were then separated by the use of a centrifuge and the wet IrO_2 particles were dried at 80 °C. Further heat treatment was performed in a preheated furnace at 450 – 580 °C to anneal the catalyst. This catalyst will be referred to as IrO_2 HM.

7.3.3.4 Ink formulations

Specific ink formulations that were used are specified with each particular experimental result in the following sections. The inks were prepared according to the following basic formulation as is given in Table 7.1 which was varied. The Nafion® solution should always be added after the water because the catalyst can ignite the solvent. The ink mixture was ultra sounded for 5 min then stirred until use.

Table 7.1 Ink formulations

	Anode	Cathode
Catalyst	0.1275 or 0.05 g	0.1275 or 0.05 g
Water	0.25 cm^3	0.25 cm^3
Nafion solution	1.275 or 0.06 g	1.275 or 0.06 g
Iso-propanol	0.5 cm^3	0.5 cm^3

7.3.3.5 Drying/curing procedure

After deposition of the ink on the chosen GDL, the solvent should be removed by heating the electrode at 50 °C for 30 min, followed by a curing step at 80-120 °C for 15 min.

7.3.3.6 Ink deposition

The ink was deposited on a specifically sized inert GDL substrate (either of 5 cm^2, 4 cm^2 or 1 cm^2) and cured to form the GDE. The catalytic ink was alternatively spraycoated or brushcoated onto the GDL. Spraycoating was achieved by use of an artist's airbrush or airgun No. 100 fine 0.1755CG, Badger USA by loading the ink into the reservoir and propelling the ink with a pure N_2 stream. In Chapter 6 screen printing as ink deposition was assessed after developing new ink formulations suitable for screenprinting.

The inks were applied directly onto different types of GDL comprising carbon cloths (Lydall, 6100-200AC or 6100-300) or titanium fibre (Bekinit, thickness 0.1mm; Bekinit St Ti 20 200 56 or Bekinit St Ti 20 300 66) for cathode and anode respectively. ETEK ready to press with ionomer was also compared as GDL for the MEA. Various mass % loadings were achieved and compared to find an optimum loading.

The catalyst containing ink was deposited on one side of a GDL, for instance, the JM Pt_{40}/C ink was deposited upon the hydrophilic carbon cloth (6300-100) and the JM IrO_2 ink was deposited upon the Titanium fibre (Bekinit, thickness 0.1 mm) at specific loadings. The Bekinit titanium fibre was firstly pretreated as specified. The specific different combinations that were assessed will be specified with the MEA activity results.

The electrodes so formed were asymmetric with the catalyst layer dispersed on one side of the chosen GDL only. Once the ink was dried and cured in a film upon the substrate, the electrode was formed which, depending upon the combination of GDL substrate and catalyst, was either applied as an anode or a cathode. Cyclic voltammetry of the catalysts and chronoamperometry of electrode materials was performed as is specified in Chapters 4 and 5.

7.3.3.7 Hotpressing the MEA

The Nafion® membrane was treated first in order to remove all the impurities and include the sulphonic groups as specified previously. After pre-treatment and air drying, the membrane was ready to be assembled with the electrodes into a MEA. When the electrodes were dry they were hot pressed together with the pretreated ionomer membrane using a hydraulic press. The respective cathode and anode electrodes were hot-pressed on either sides of the ionomer membrane (typically Nafion® 117) with the catalyst layer in direct contact with the ionomer membrane. In some cases an additional thin layer of ionomer solution was spraycoated onto the catalyst layer to ensure complete integration of the catalyst layer and ionomer membrane. Recommended hotpressing conditions specified by commercial vendors ETEK are given in Table 7.2.

Table 7.2 Recommended commercial hotpressing conditions

Pressing conditions	
Pressure	30 bars
Temperature	125-130 ºC
Time	5-7 min

The specific components and hotpressing conditions that were applied in this study varied between about 3-7 min, 120-130 ^{0}C and 20-140 bars, and are specified separately in the appropriate sections.

7.3.3.8 SPE Electrolyzer Cell Assembly

The MEA was assembled in the SPE test module as is schematically shown in Figure 7.4.

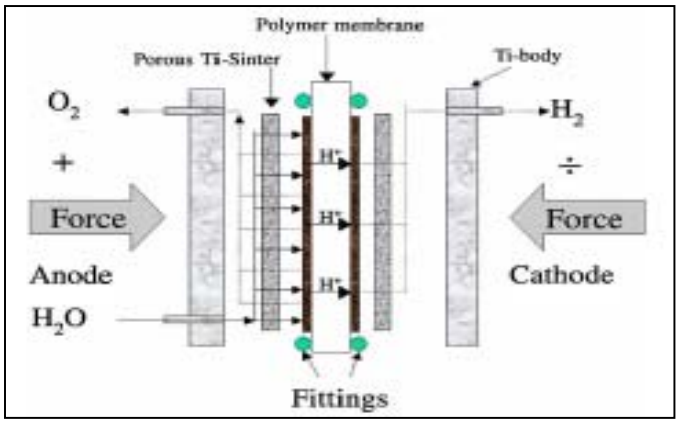

Figure 7.4 Schematic assembly of the SPE electrolyzer

A current collector with serpentine channels for water flow was clamped on each side of the MEA with suitable seals. A porous titanium frit was interspersed on each side between the current collector and the MEA to support the MEA and to ensure even water distribution and gas removal. The current collector was suitably insulated from the clamps and peripherals on each side of the cell. Electric leads were connected to each side of the cell. The piping from the cell to the water reservoir was attached as shown in Figure 7.5. Each MEA was moisturized for a specific time as specified prior to the start of the experiment.

7.3.3.9 SPE Electrolyzer operation

Setting up the prototype bench scale module of a SPE electrolyzer included modular cell design and peripheral selection. The SPE electrolyzer setup is shown in Figure 7.5.

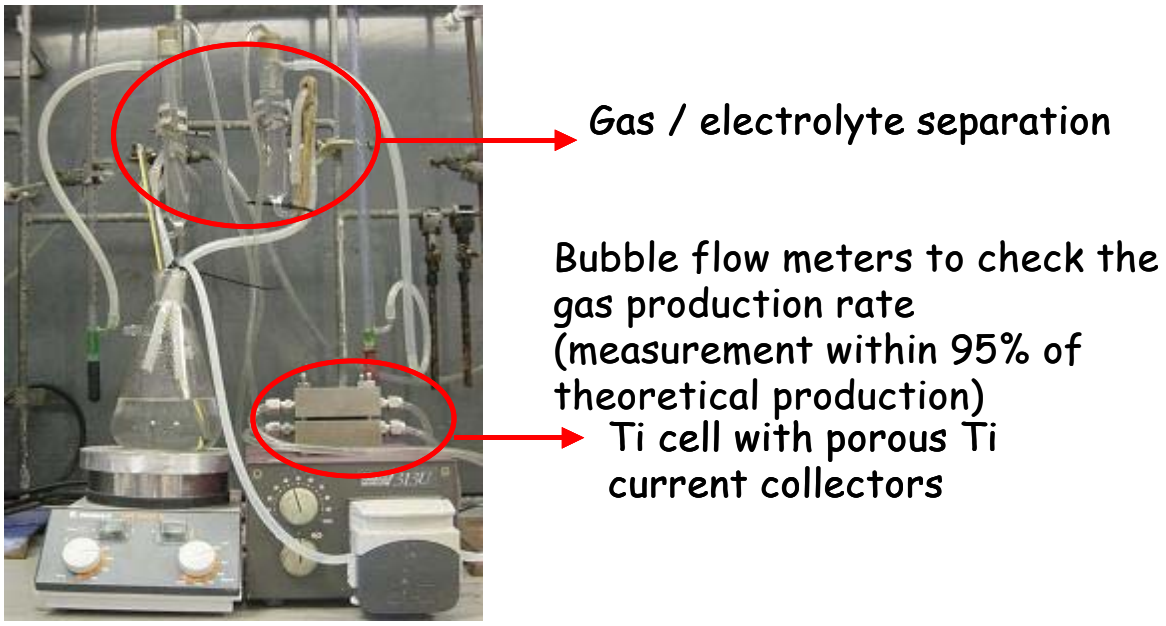

Figure 7.5 Laboratory scale set up and SPE testing module

The following peripheral equipment was required to operate the SPE testing module: Magnetic heater and stirrer; Gas separation system including fittings, glassware and tubing for feed and product streams; 2 X Soap bubble meters; Electrolyzer module; Watson-Marlow 323 U/D peristaltic pump; Watson-Marlow 313X Extension Pumphead; Hoiki 3560 AC milli Ohm Hi Tester for testing cell resistance; Autolab PGSTAT 30 (Eco Chemie BV, Netherlands) as power source. A power source Powerflex TT CPX Dual PSU with maximum output of 35 V and 10Amp was used as potentiometer in some cases.

A process flow diagram is presented schematically in Figure 7.6 for assembling and testing the MEA.

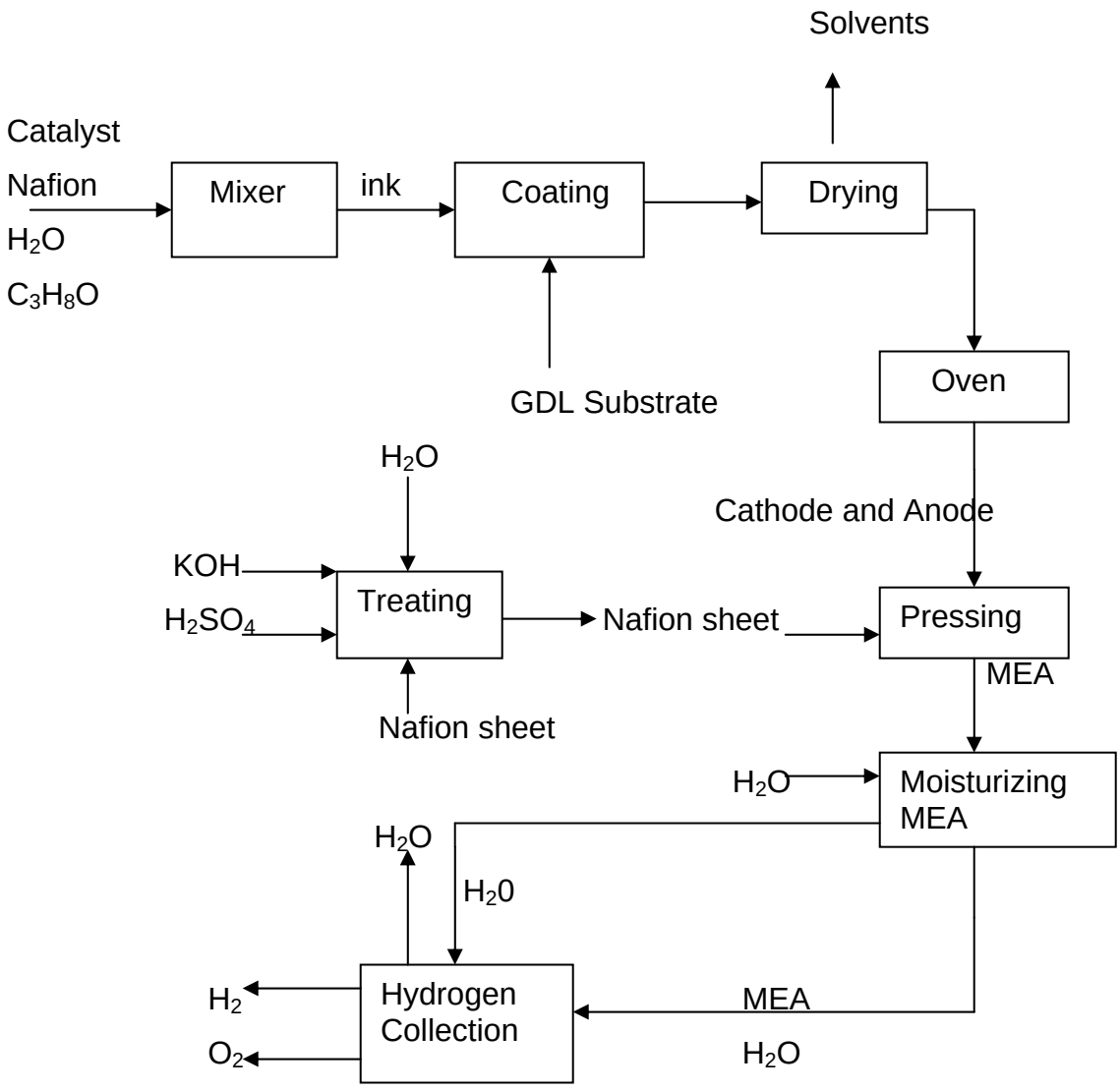

Figure 7.6 Schematic process flow diagram for assembling and testing the MEA

The power source provided the electrical potential across the cell. The ultrapure water feed was pumped at a set rate using the pump, from the reservoir to the electrolyzer module, where the water was split into hydrogen and oxygen, which gases were then respectively collected in the gas phase separators. Gas flow rate was measured using the soap bubble meters. The operational parameters that were optimized as well as the activity of the catalyst were identified by the current density that was registered on the Auto lab.

The MEA was thus prepared and tested according to the following summarized steps:

i. Separately weigh appropriate amount of electrocatalyst for anode and cathode.
ii. Mix the cathode and anode catalyst separately with appropriate amount of ultra pure water.
iii. Weigh appropriate amount of Nafion solution (5 % w/w) and add drop wise to each catalyst, while stirring.
iv. Add isopropanol drop wise to each catalyst with stirring.
v. Ultrasound ink for 5 min and continue with magnetic stirring overnight.
vi. Cut and weigh the appropriate GDL substrate for cathode and anode respectively.
vii. Deposit respective anode and cathode inks upon appropriate substrates using appropriate deposition technique, drying and weighing in between. Repeat until appropriate layer thickness /loading achieved. The calculated catalyst (e.g. platinum or iridium metal loading) should be about 1-6 mg cm^{-2} both for anode and cathode.
viii. After the respective coating, dry and cure gas diffusion electrodes (GDE).
ix. Pretreat the appropriately sized Nafion® membrane sheet.
x. Place treated Nafion membrane sheet between the anode and cathode GDE, and hotpress using suitable hotpressing conditions.
xi. Test current density after suitable moisturization times of MEA

7.4 RESULTS AND DISCUSSIONS

7.4.1 Characterization of components

7.4.1.1 Catalysts for anode and cathode of SPE electrolyzer

Characteristics of the commercial electrocatalysts that were applied in this study are given in the specifications from the suppliers. Micrographs and other characteristics of JM Pt_{40}/C are given in Chapter 4. SEM micrographs of (a) Ir Black and (b) IrO_2 (HM) prepared according to Section 7.3.3.3 that was also tested as anode catalyst are presented in Figure 7.7.

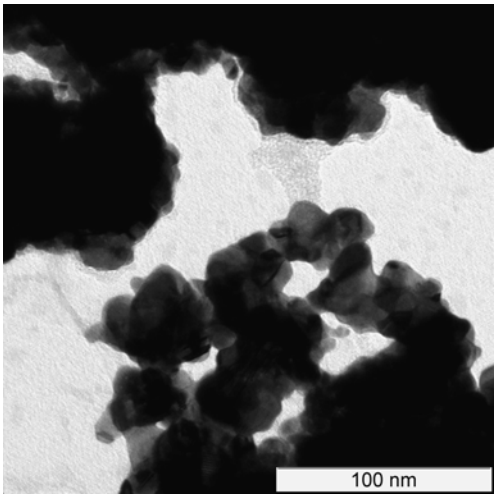

(a) Johnson Matthey Ir Black with particles size range 30-50nm

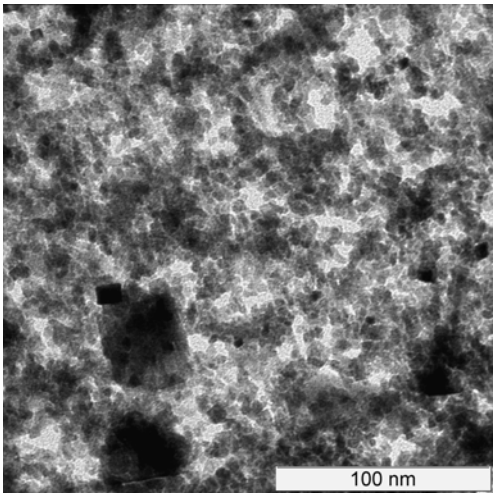

(b) Annealed HM IrO_2 with particle sizes average 5-10nm

Figure 7.7 SEM micrographs of Iridium catalysts

The XRD spectra of the benchmark commercial JM IrO_2 and HM IrO_2 pyrolysed at 450 ºC and annealed at 550 ºC are presented in Figure 7.8.

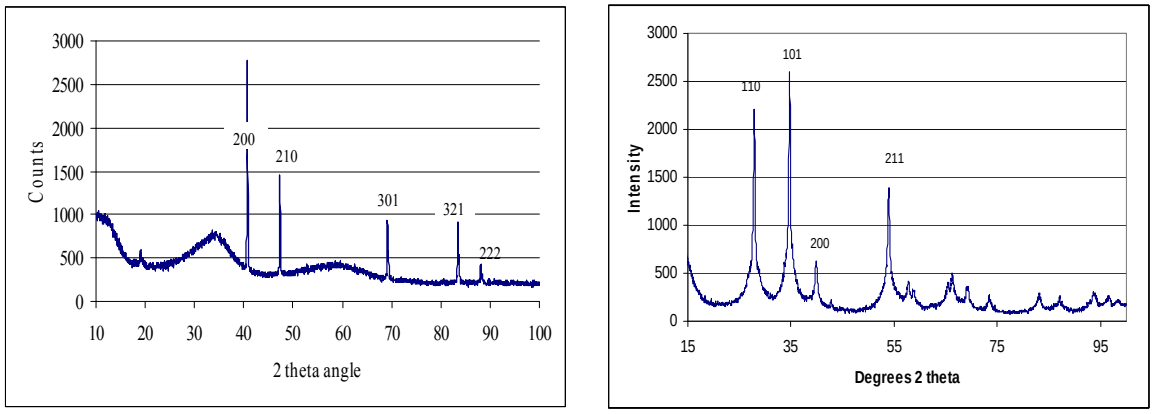

(a) (b)

Figure 7.8 XRD spectrum of (a) commercial JM IrO_2 (b) HM IrO_2 pyrolysed at 450 ºC and annealed at 550 ºC

The observed *d* values of the major XRD reflections were compared with standard *d* values as given in the JCPDS data file. Typical reflections for IrO_2 can be observed at 28.05 º2θ, (110), 34.95 º2θ (101), 55.34 º2θ (211) and 39.75 º2θ (200), with standard *d* values respectively of: 3.1780 (110); 2.582 (101); 2.2488 (200); 1.696 (211) (Osaka et al., 1994). The commercial sample consisted of four major peaks that are associated with 200, 210, 301, 321 faces, whereas XRD peaks for homemade samples were associated with 101, 110, 211, 112 faces with good agreement between the observed and standard *d* values. The annealed IrO_2 particles sizes were between 8-10 nm as calculated by the Scherrer equation from XRD data and by visual inspection of TEM images and most of these particles were agglomerations of smaller particles showing the sintering effect of the high annealing temperature used. An annealing temperature of 550 ºC was applied. It is well known that the material properties of IrO_2 are susceptible both to the deposition technique and preparative parameters (Patil et al., 2003).

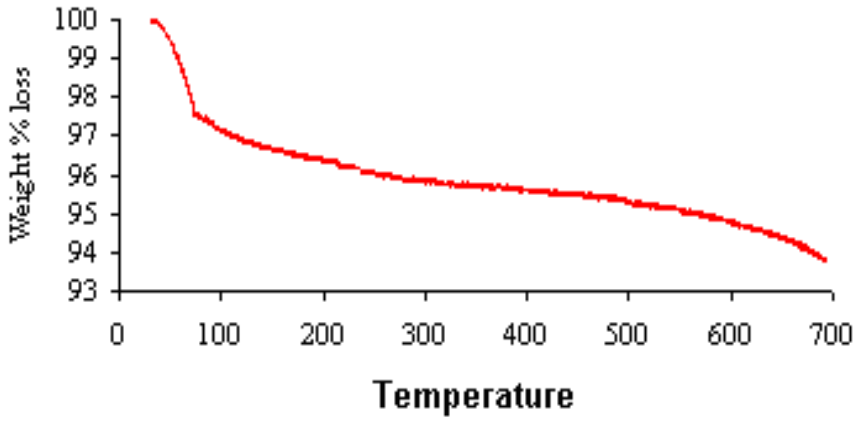

Figure 7.9 TGA of HM IrO_2

The thermal analysis (Figure 7.9) showed that the prepared IrO_2 nanoparticles were not stable. Mass loss was observed between 50-100 ºC and again between 100-700 ºC. The first mass loss of about 3 % was attributed to the removal of moisture and a portion of the second mass loss (between 100-300 ºC) could be attributed to the possible removal of the remainder of NO_2 formed during the Adams fusion method. Thereafter a slow but steady mass loss was observed. This mass loss is ascribed to the fact that the chemical stoichiometry of the oxide nanoparticles is not maintained as the temperature increases. It is only under high annealing temperatures that the surfaces of metal oxides are terminated with metal cations (al-Abadleh Hind et al., 2003). These authors found that under non-annealing temperatures, metal oxide nanoparticles are oxygen terminated and metal cations fully coordinated in the bulk. High concentration of negative oxide ions on the surface causes oxide ion bond lengths to relax and react with ambient gases, such as water, forming hydroxyl groups, of which residual groups persist on the surface of nanoparticles even after relatively high thermal treatment. Annealing of the IrO_2 caused sintering of the nanoparticles and crystal growth, as is apparent from the observed high intensity XRD peaks, which may have improved electronic pathways by creating gooseneck boundaries between crystals. Hackwood et al. (1982) showed that exothermic transitions exist at 300 °C and at 700 °C, the higher of which is due to amorphous-to-crystalline transition where after IrO_2 loses its electro catalytic properties that are associated with the fast-ion mobility in the amorphous state.

7.4.2 Characteristics of macroporous conductive supports

Micrographs of the various carbon based support substrates used as GDL are shown in Figure 7.10 (a to c).

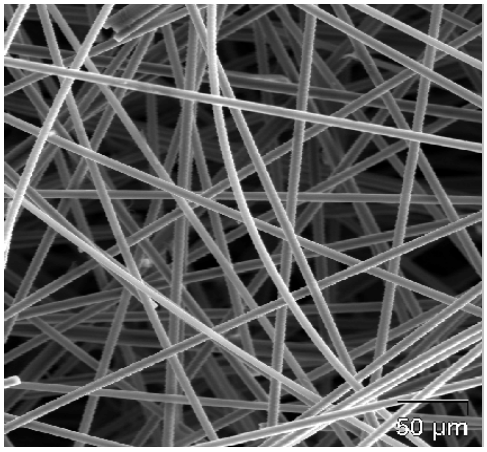

(a) Hydrophilic carbon cloth (Lydall 6100-200AC)

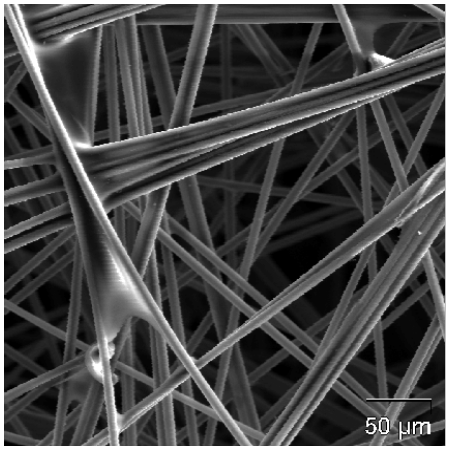

(b) Hydrophilic carbon cloth (Lydall 6100-300)

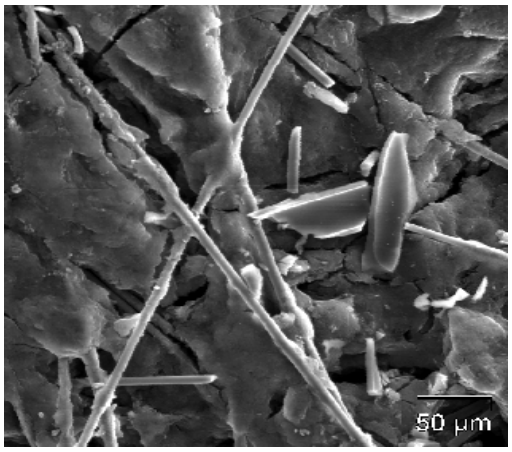

(c) Hydrophobic carbon cloth (Lydall 484C)

Figure 7.10 Types of carbon cloth support taken at 300 magnifications, by Scanning Electron Microscope (SEM)

The micrographs in Figure 7.10 (a-c) show the typical macroporosity of these GDL substrates with large, 50-100 µm sized void spaces and the matted fibrous structure of the carbon matrix. The commercial hydrophobic cloth (Figure 7.9(c)) is typically impregnated with PTFE to repel water ingress into the GDL layer and thus the gas diffusion pathways are partially obstructed. In GDL with various PTFE loadings of

the hydrogen electrode (Ioroi et al., 2001; 2002; 2003), both the fuel cell and water electrolysis performances were not affected by the amount of PTFE loading and 5–7 wt % was found appropriate. These authors found that the efficiency of the URFC decreased with increasing cycles when the PTFE loading on the oxygen side GDL was too low. Hence the PTFE treated hydrophobic GDL would be of importance as anodic substrate should the SPE cell be operated in both electrolyzer and fuel cell mode. Micrographs of other commercial GDL materials are presented in Figures 7.11 (a to d).

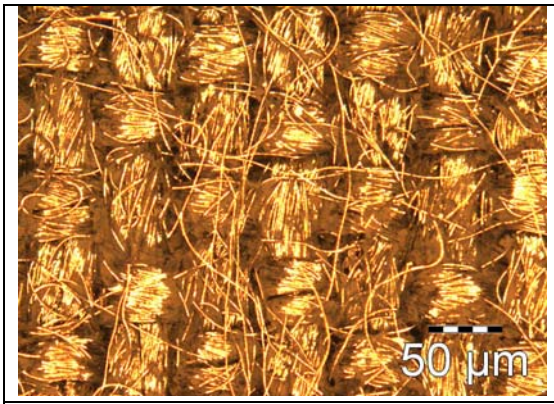

a) ETEK ready to press with ionomer – GDL side woven matrix

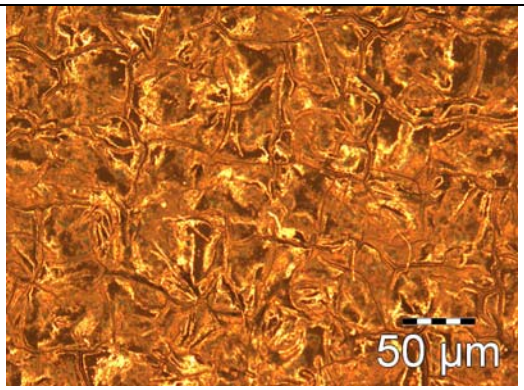

b) ETEK ready to press with ionomer – ionomer side

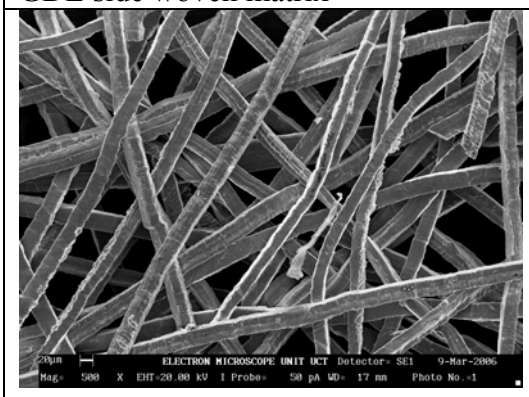

(c) Bekinit St Ti 20 200 56

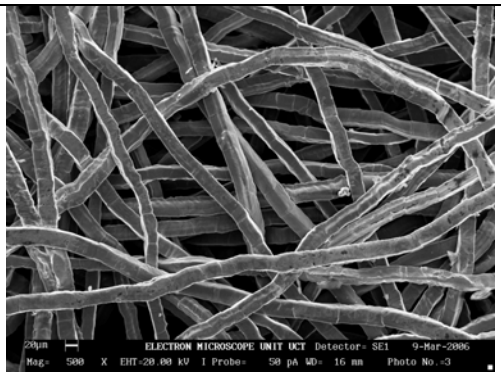

(d) Bekinit St Ti 20 300 66

Figure 7.11 SEM micrographs of GDL substrates

ETEK ready to press GDL with ionomer is shown in Figure 7.11 (a) on the GDL side exposing the woven matrix and (b) on the ionomer coated side, which shows the much denser woven fibrous texture of this commercial GDL material, with gas diffusion pores in the region of 5-10 µm. The Titanium meshes supplied by Bekaert (Bekinit type) are presented in Figure 7.11 (c and d).These micrographs show the

matted metallic mesh diameter (50 μm) and the large void spaces representing the gas diffusion pathways or porosity between the individual strands of Ti. The difference between these two Ti materials is the thickness.

7.4.3 Characteristics of ink formulations

The characteristics of the ink formulations are described in Chapter 6 in which the viscosity and rheology of the different formulations used in screen printing are investigated. In this section the inks were mainly used directly after composing them due to the volatility of the isopropanol solvent used in spraycoating and brushcoating. It was evident that particles were agglomerating and thus the JM Pt_{40}/C ink formulation was checked for particle distribution using a non-invasive backscatter spectroscopy (NIBS) technique.

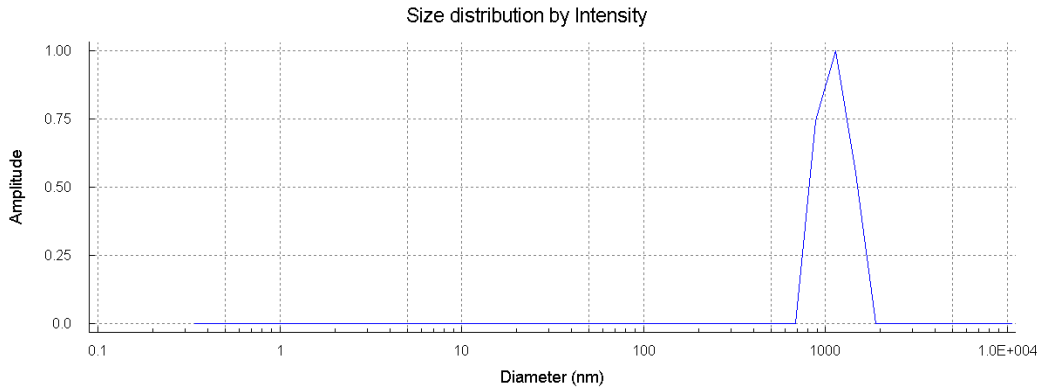

Figure 7.12 Particle size distribution for the typical JM Pt_{40}/C ink formulation

Particle size distribution (Figure 7.12) determined by NIBS for the JM Pt_{40}/C ink formulation, revealed no bimodal distribution for the catalyst containing sample and the diameter of the particles was close to 1000 nm, showing that the catalyst particles supported on carbon black were prone to agglomeration in the formulations used. SEM micrographs (Chapter 4) showed that the Vulcan carbon black upon which the nanoparticles of Pt are supported in the case of the JM Pt_{40}/C catalyst was typically between 2-5 μm in particle size. Hence inter particular attraction played a role in causing particle agglomeration, which resulted in uneven particle deposition. To prevent this from occurring many patented ink formulations add various or

undisclosed dispersants. In this study these additives were not added to the ink formulations used in order to eliminate extraneous variables during electrode testing.

7.4.4 Characteristics of electrodes

There are many different ink formulations, and types of GDL substrates as well as various ways of depositing the ink on the GDL reported in the literature and each preparation technique as well as the different choices of components may have an effect on the overall activity of the electrolyzer cell. In this section the electrodes are characterized after the deposition and curing of the ionomer containing catalyst layer. The purpose of the characterization was to establish whether good dispersion of Pt catalyst and homogeneous electrode structures had been prepared. Homogeneity or high dispersion versus agglomeration and poor dispersion was initially determined by optical or scanning microscopy.

The ink solution for JM Pt_{40}/C on carbon cloth as well as for Pt HMS (carbonized) on Bekinit titanium support was typically prepared as follows: 0.25 g of catalyst was mixed with 1.00 g H_20, 0.67 of 5 % Nafion solution and 1.00 cm^3 of isopropanol. This formulation was varied as is further specified. Selected examples of SEM micrographs, alternatively optical microscopy of typical Ir and Pt containing composite electrodes prepared as anodes and cathodes using carbon cloth GDL are presented in Figure 7.13 and Figure 7.14 after ink deposition with anodic and cathodic inks upon carbon cloth substrates, showing ink adhesion on carbon fibres.

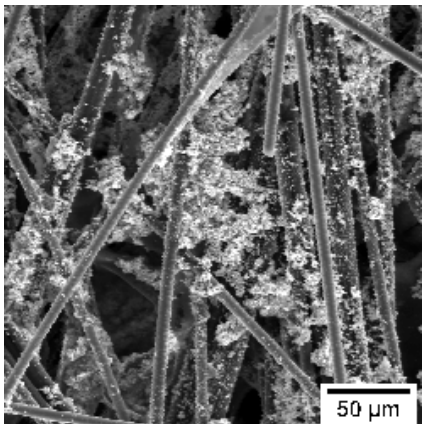

Figure 7.13 SEM of Ir Black on carbon cloth anode

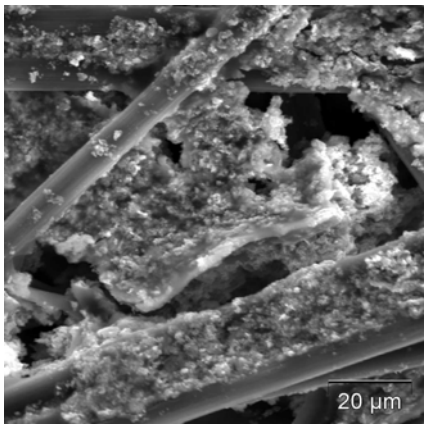

Figure 7.14 SEM of IrO_2 on carbon cloth anode

The SEM micrographs of the Ir containing catalytic ink dispersed upon the gas diffusion layer (Figure 7.13 and 7.14) shows that there is much potential for improvement that can be achieved by using a finer and possibly more dense carbon backing layer as GDL. It is highly unlikely that more than a very insignificant portion of the catalyst could be in intimate contact with the Nafion membrane or with the carbon cloth due to the large voids and catalyst interpenetration between fibres of the GDL. Possibly, direct electrochemical deposition of Ir upon carbon may result in more uniform and stable coatings, where after the material may be impregnated with Nafion.

Figure 7.15 Optical microscopy of typical composite electrode JM Pt_{40}/C on carbon cloth

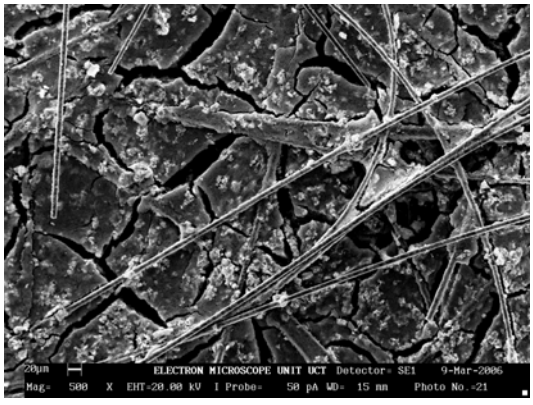

Figure 7.16 Ink coated by brushing Pt ink on cathode (MEA 59) on GDL Lydall Carbon Cloth 6100-300

Optical microscopy and SEM micrographs of typical JM Pt_{40}/C on carbon cloth GDL forming a composite electrode are shown in Figures 7.15 and 7.16, before hot-pressing the electrodes into a MEA. SEM micrographs of anodes prepared using Titianium mesh (Bekinit) are shown in Figures 7.17 and 7.18 and in Figures 7.19 and 7.20 spraycoated cathodes are shown.

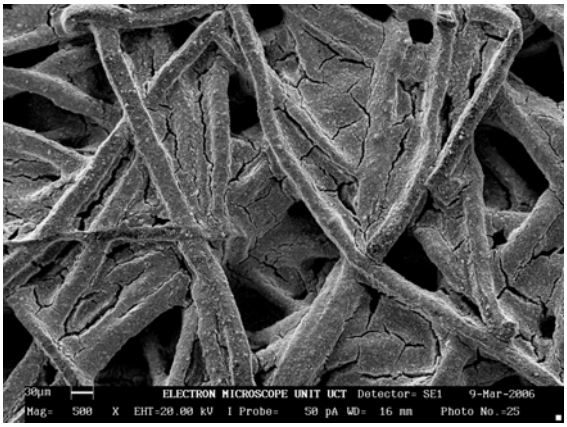

Figure 7.17 Anode based upon Bekinit St Ti 20 300 66; ink brush coated (IrO_2 MEA 59)

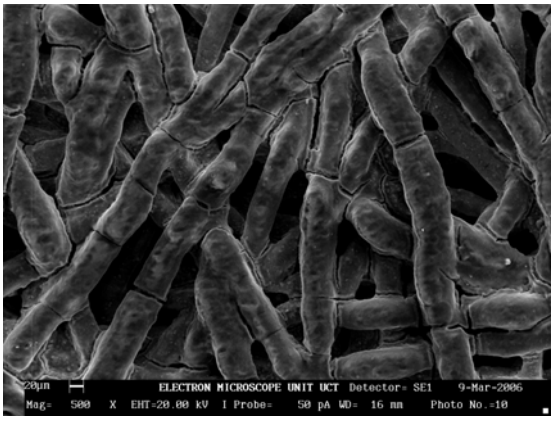

Figure 7.18 Anode based upon Bekinit St Ti 20 300 66; ink spraycoated (with 6 mg IrO_2)

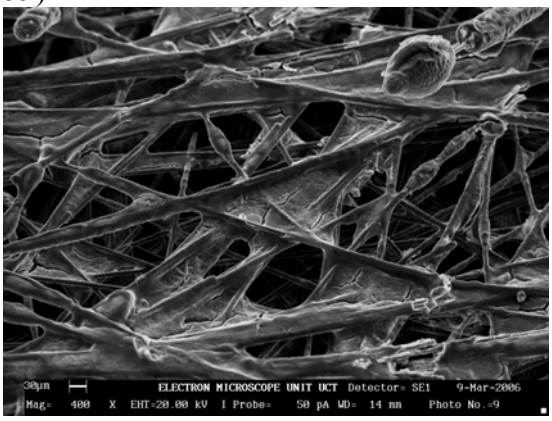

Figure 7.19 Pt cathode based on GDL Lydall Carbon Cloth 6100-300; ink spray coated

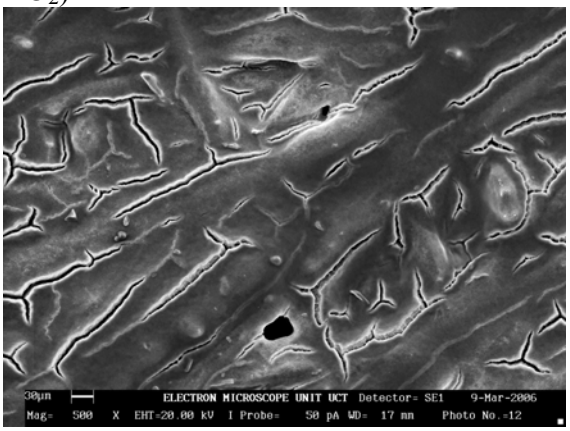

Figure 7.20 Pt cathode on GDL Lydall Carbon Cloth 6100-300; ink spray coated with higher loading of catalyst

SEM and optical microscopy showed that typically after ink deposition and curing a catalyst layer was formed that interpenetrated the fibres of the GDL and adhered to the fibre surfaces. As the resolution of optical microscopy was sufficient to inspect electrodes, this method was generally used as quality control measure during MEA preparation.

Ink adhesion upon the GDL was generally good, and the correct catalyst loading could be achieved by careful weighing in between deposition of layers and weighing the product after ink deposition. As the micrographs show, the integrity of the film layers was higher when spraycoating was used instead of brushcoating, but this depended upon the loading achieved as well as the substrate type. Brush coating was found to result in lack of reproducibility in catalyst loading, and a greater degree of crack formation. Spray coating was more reproducible but it was found to be laborious and care was required to ensure that all areas of the electrode were coated evenly and that equivalent loadings were achieved from one MEA to the next. Both techniques were wasteful of the expensive catalysts due to losses occurring during preparation. The layers of cured ink containing the electrocatalyst and the ionomer were prone to a high degree of crack formation upon drying and curing, most likely due to the different coefficient of expansions or thermal shocks during heat curing of the ink layer and the underlaying GDL (Patil et al., 2003) or the lack of elasticity and heat sensitivity of the ionomer Nafion® that was used as binder, which may contract or degrade during heat curing. Samples exhibit a characteristic "cracked-mud" appearance. Transition metal dioxide layers very often exhibit such features. Such features are, in principle, favourable for some applications such as O_2 or H_2 evolution because it gives rise to higher macroscopic surface area (Hine et al., 1979; Pizzini et al., 1972; Savinell et al., 1990). However, the micrographs gave no indication of the dispersion of Pt over the electrode surface. Determining the electrical conductive characteristics of the electrodes would require different means of characterization which are set out in Chapter 6.

7.4.5 Characterization of homogeneity and reproducibility of electrodes

Characterization of the spatial distribution of Pt or Ir nanoparticles upon modified electrodes prior to hot pressing was necessary in order to develop well defined deposition technology. The characteristics of representative electrodes were

determined in terms of Pt or Ir loading per geometric surface area, as measured by photon induced X-Ray emission (PIXE) spectroscopy using a dynamic mapping technique (Ryan et al., 1995). This was characterized by elemental mapping of micro-regions in the micrometer scale of active elements dispersed upon conductive (i.e. carbon based and titanium based) support matrixes (Figures 7.21 and 7.22).

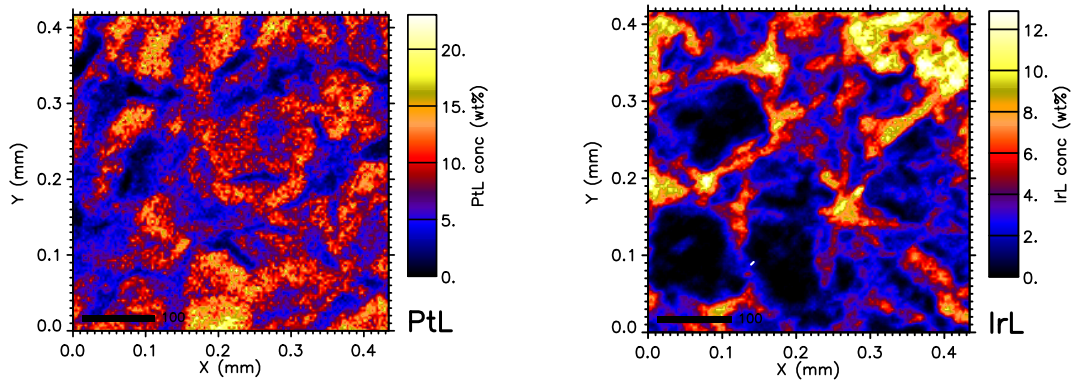

A B

Figure 7.21 Elemental distribution map of Pt (A) and Ir (B) on carbon cloth electrodes calculated by Dynamic Analysis method of mapping from micro-PIXE data

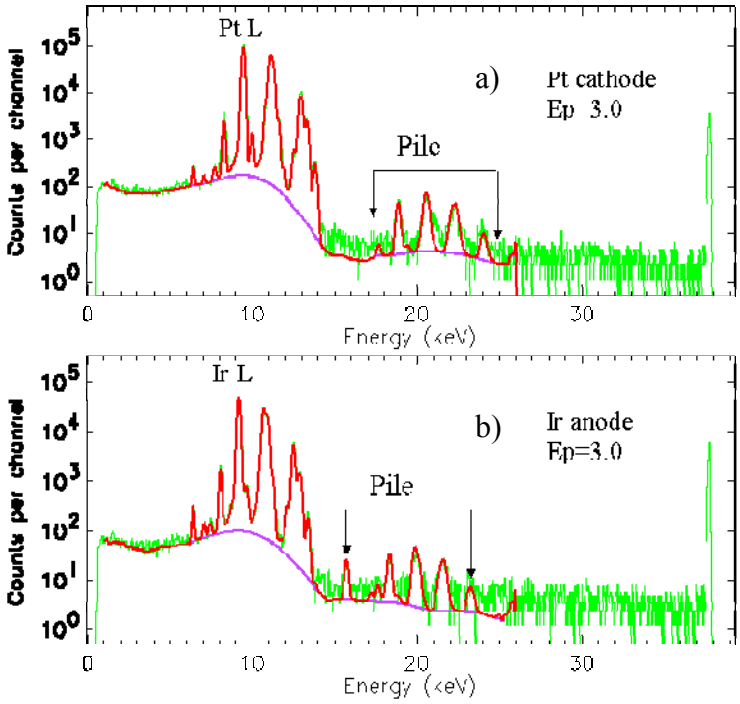

Figure 7.22 PIXE spectra of (a) Pt cathode and (b) Ir anode

PIXE spectra shown in Figure 7.21 from a Pt cathode (a) and an Iridium oxide anode (b) were obtained from irradiation with 3.0 MeV protons at the nuclear microprobe

facility, Materials Research Group, iThemba LABS. All X-ray lines correspond to the L-shell X-ray excitation from both Pt and Ir. The smaller lines on the right of each spectrum are artefacts related to pile-up in the Si(Li) X-ray detector. Calculation of Pt and Ir concentrations were done using the Ļ lines marked in Figure 7.22.

PIXE analysis and SEM micrographs showed that the uneven dispersion as well as agglomeration and cracking of deposited catalytic ink layers that occurred after drying and curing, particularly in the case of brush coated electrode preparation techniques, resulted in inhomogeneity of catalytic nanoparticles in the deposited layers. In Figure 7.21 (a) the layer of Pt ink presents localised areas of agglomeration (with maximum Pt concentration levels at 25 %) separated by regions where the Pt concentration was depleted (~2 %). In the case of the IrO_2 the PIXE map shows restricted regions of high (10 %) and low (0-2 %) concentrations of Iridium Oxide. The Pt particles are more dispersed than the IrO_2 particles over the whole micro-region, which indicated that the formulations of inks would need to be optimized considerably to prevent the significant agglomeration and poor dispersion observed. This aspect was addressed in Chapter 6.

The agglomeration that was observed could be caused by inter particular attraction due to electrostatic forces or by surface energy of the substrate, or by polarity of the solvent used in the ink. The ink formulations were further optimized as is described in Chapter 6 and the interplay between these forces is explored therein.

SECM imaging of activity of the composite JM Pt_{40}/C catalyst deposited on highly orientated pyrolytic graphite (HOPG) as conductive substrate towards the hydrogen evolution reaction (HER) in 5 mM H_2SO_4 electrolyte solution is shown in Figure 7.23.

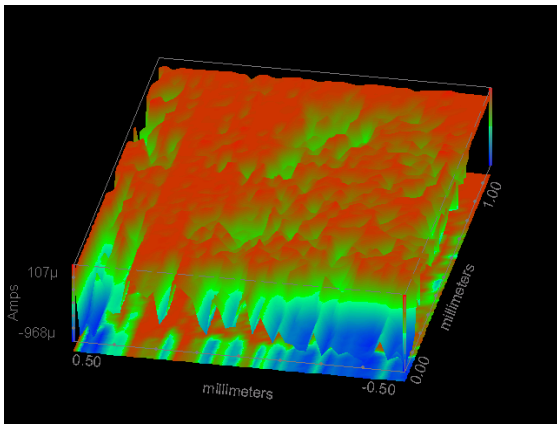

Figure 7.23 SECM Imaging of activity of Pt_{40}/C electrode towards HER in 5 mM H_2SO_4 electrolyte solution

The SECM imaging (Figure 7.23) indicated a similar trend to that observed in the PIXE elemental maps, of relative inhomogeneity of the active surface area of the active electrocatalyst dispersed in the composite electrode. Better uniformity of the electrodes was achieved by changing the substrate type and the type of catalyst support combination (Figures 7.24 and 7.25).

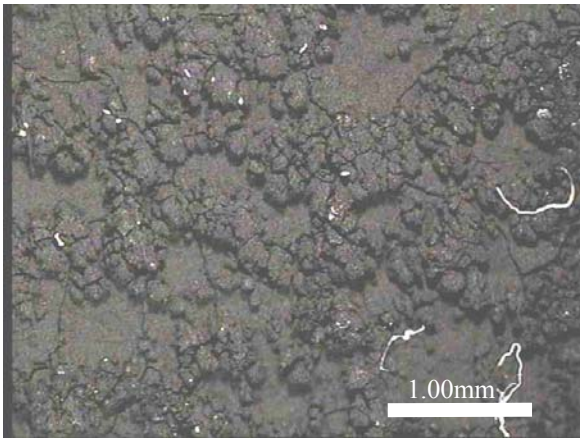

Figure 7.24 JM Pt_{40}/C on carbon cloth

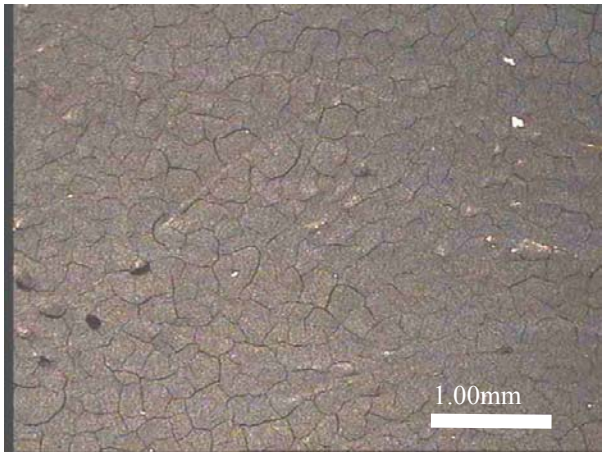

Figure 7.25 Pt HMS (carbonized) on Bekinit substrate

Optical micrographs of comparable scale of a micro-region selected at random on a cathode with JM Pt_{40}/C spraycoated on carbon cloth (Figure 7.24) or Pt HMS (carbonized) catalyst spraycoated on the Bekinit titanium substrate as cathode is shown in Figure 7.25. The preparation of Pt HMS (carbonized) catalyst was described in Chapter 4. The optical micrograph of the electrode is compared with elemental maps for Pt and Ti calculated by Dynamic Analysis method from micro-

PIXE data obtained on the JM Pt_{40}/C spraycoated on carbon cloth and Pt HMS (carbonized) on Ti support as cathode samples, that are shown in Figure 7.26 (a) and (b) respectively.

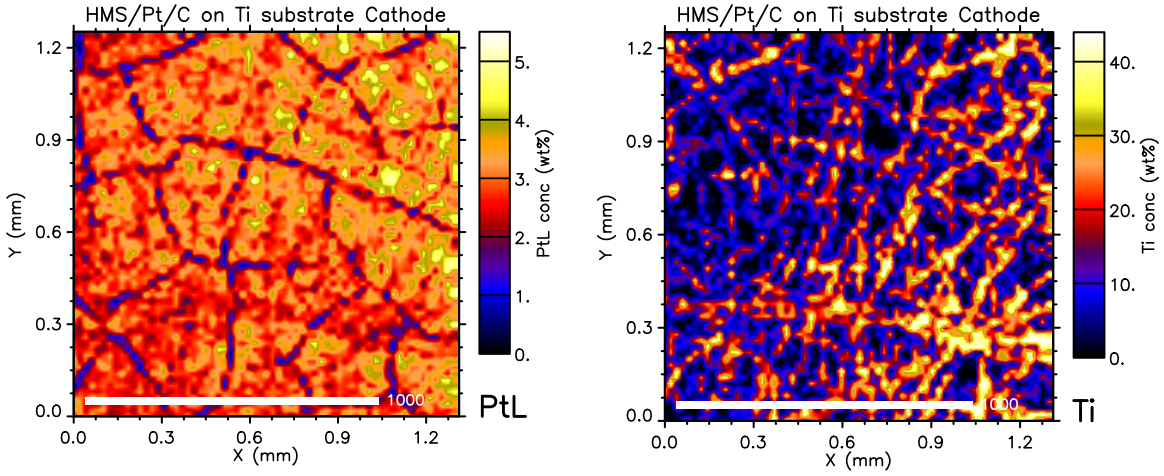

(a) Pt elemental map of Pt HMS (carbonized) catalyst deposited on Ti Bekinit substrate

(b) Ti elemental map of Pt HMS (carbonized) catalyst deposited on the Ti Bekinit substrate

Figure 7.26 Elemental distribution map of Pt (a) and Ti (b) in titanium substrate GDL electrodes containing a film of supported Pt HMS (carbonized) catalyst

The elemental distribution map (Figure 7.26) of Pt (a) and Ti (b) of an electrode prepared with Pt HMS (carbonized) catalyst on titanium Bekinit substrate was calculated by the Dynamic Analysis method of mapping from micro-PIXE data. PIXE spectra were obtained from irradiation with 3.0 MeV protons. X-ray lines correspond to the L-shell X-ray excitation from Pt and K-shell excitation from the rest of the elements (Ti, Cr, Fe, Cu, Zn and Ru). The map for Pt (Figure 7.26(a)) shows regions of homogeneous and well dispersed concentration distribution levels of Pt (Pt~3 %) even though some crack formation is apparent. These regions are undergirded by the Ti substrate fibres (Figure 7.27(b)) where Pt conc. is lower (Pt~1 %). The Ti is distributed according to the network of Ti fibres in the GDL support with levels of 10-40 % by mass. A Fe signal was also detected in the Ti substrate as can be seen in the PIXE spectrum shown in Figure 7.27.

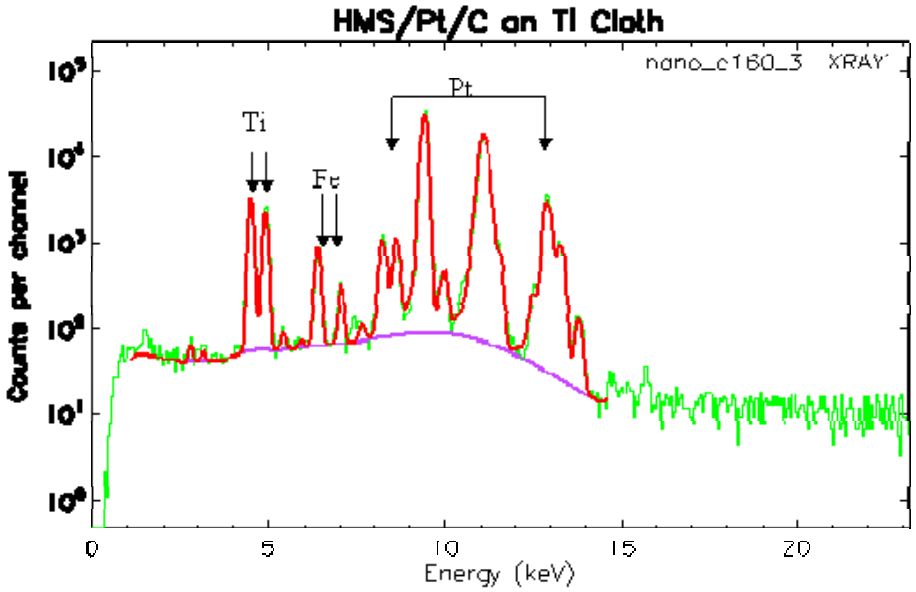

Figure 7.27 PIXE spectra of HMS/Pt/LPG catalyst on titanium substrate

The substrate/ film interaction was significantly improved and much more uniform distribution with less agglomeration of the electrocatalyst was achieved for the Pt HMS (carbonized) catalyst on titanium GDL substrate electrode combination, most likely due to the inter particular repulsion between the HMS Si substrate supported Pt nanoparticles causing less agglomeration. The HMS is an isolating Si based support matrix and relatively hydrophobic because of its siliceous nature. Inter particular repulsion is thus likely. This interesting result offers scope for further investigation. PIXE is thus shown to be a powerful technique to determine the distribution and homogeneity of the electrocatalyst in the composite electrode.

7.4.6 Conclusions on characterization of electrodes

There are many different combinations of catalysts and gas diffusion layers and also various ways of depositing the ink on the GDL and each has an effect on the characteristics of the electrode. The deposition methods characterized in this section were brush coating and spray coating. The brush coating method was a relatively simple way of depositing the ink upon the electrode but non-uniformity and high crack formation was apparent. The spray coating technique allowed better control of

the deposition process and the layer by layer deposition allowed careful measurement of the degree of coating and the amount deposited. It was however a considerably more tedious method to prepare the electrode and electrodes were ultimately also prone to crack formation unless deposited layers were kept very thin or great care was taken not to exceed the thermal degradation point of the ionomer added to the ink during curing of the electrode. The Lydell 6100-300 carbon cloth and the Bekinit titanium mesh GDL were both found to be suitable GDL. The carbon cloth did not have a high physical integrity and was inclined to shed fibres during processing whereas the thin titanium mesh was stronger yet sufficiently flexible to process into MEA.

It was found that supporting the electrocatalysts upon these gas diffusion layers was successful but that composite electrodes were not easily prepared in reproducible and homogeneous fashion, thus this aspect of the study required further attention, and different supports should be explored that may be more durable and that have a finer porous texture. This aspect was partially addressed in Chapter 5 and in Chapter 6. There is still much potential for improvement that can be achieved by using a finer GDL and different types of electrocatalysts. Possibly, direct deposition of the catalyst upon carbon fibres may result in more uniform and stable coatings, where after the material may be impregnated with Nafion. This deposition approach was investigated in Chapter 4.

PIXE was found to be a relatively accurate way to establish the spatial distribution and % loading of catalyst per geometric area and determine whether adequate spatial distribution was achieved on the cathode and anode. Catalytic activity could further be confirmed by SECM analysis, however this was not quantitative.

7.5 OPTIMIZATION OF SPE ELECTROLYZER

7.5.1 Components, design and configuration

The various MEA tested in the SPE electrolyzer were prepared according to Section 7.2.5. Various combinations of components were tested (Table 7.3).

Table 7.3 Summary of different membrane electrode assembly (MEA) components

No	Conditions for MEA assembly	Anode GDL	Anode catalyst	ionomer	Cathode catalyst	Cathode GDL
2	120ºC at 40 bars for 2min:Flow 2mL s^{-1}	Toray 0% PTFE	JM Pt_{40}/C	Nafion® 117	JM Pt_{40}/C	Toray 0% PTFE
3	120ºC at 40 bars for 2min	Toray 0% PTFE	JM Pt_{40}/C	Nafion® 117	JM Pt_{40}/C	Toray 10% PTFE
4	120ºC at 40 bars for 2min;Flow 2mL s^{-1}	Toray 6% PTFE	JM Pt_{40}/C	Nafion® 117	JM Pt_{40}/C	Toray 10% PTFE
6	130ºC at 80 bars for 2min;Flow 2mL s^{-1}	Lydall 6100-200	JM Pt_{40}/C 0.0507g / 5cm^2	Nafion® 117	JM Pt_{40}/C 0.0644g/ 5cm^2	Lydall 6100-200
7	130ºC at 80 bars for 2min;Flow 2mL s^{-1}	Lydall 6100-200	JM Pt_{40}/C 0.0560g/ 5cm^2	Nafion® 117	JM Pt_{40}/C 0.0626g / 5cm^2	Lydall 6100-200
8	130^{0}C at 80bars for 2min; Flow 2mL s^{-1}	Lydall 6100-200	JM Pt_{40}/C 0.0268g/5cm^2	Nafion® 117	JM Pt_{40}/C 0.032g/ 5cm^2	Lydall 6100-200
9	135ºC and 40bars for 2min; Flow 2mL s^{-1}	Toray 10% PTFE	JM IrO_2 0.0285g /5cm^2	Nafion® 117	JM Pt_{40}/C 0.054g/ 5cm^2	Toray 0% PTFE
10	130^{0}C at 40bars for 2min; Flow 2mL s^{-1}	Lydall 6100-200	JM Pt_{40}/C 0.0137g OR 0.00915 per 5cm^2	Nafion® 117	JM Pt_{40}/C 0.0195g OR 0.023 per 5cm^2	Lydall 6100-200
11	130^{0}C at 40bars for 2min;Flow 2mL s^{-1}	Lydall 6100-200	JM Pt_{40}/C 0.0381g per5cm^2	Nafion® 117	JM Pt_{40}/C 0.0367g /5cm^2	Lydall 6100-200
13	135ºC at 40bars for 2 min;Flow 2mL s^{-1}	Lydall 6100-300	JM Pt_{40}/C ~0.06g / 5cm^2	Nafion® 117	JM Pt_{40}/C ~0.06g / 5cm^2	Lydall 6100-300
14	135ºC at 40bars for 2 min;Flow 2mL s^{-1}	Lydall 6100-300	JM Pt_{40}/C ~0.06g / 5cm^2	Nafion® 117	JM Pt_{40}/C ~0.06g / 5cm^2	Lydall 6100-300
15	135ºC at 40bars for 2 min;Flow 2mL s^{-1}	Lydall 6100-300	JM Pt_{40}/C ~0.06g per 5cm^2	Nafion® 117	JM Pt_{40}/C ~0.06g per 5cm^2	Lydall 6100-300
16	135ºC at 40bars for 2 min; Flow 2mL s^{-1}	Lydall 6100-300	JM Pt_{40}/C ~0.06g per 5cm^2	Nafion® 117	JM Pt_{40}/C ~0.06g per 5cm^2	Lydall 6100-300
17	135ºC at 40bars for 2 min; Flow 2mL s^{-1}	Lydall 6100-300	JM Pt_{40}/C ~0.06g per 5cm^2	Nafion® 117	JM Pt_{40}/C ~0.06g per 5cm^2	Lydall 6100-300
25	135ºC at 40bars for 3 min; Flow 2 mL s^{-1}	Lydall 6100-200	Iridium black 0.0027g cm^{-2}	Nafion® 117	JM Pt_{40}/C 0.0049g cm^{-2}	Lydall 6100-200
26	135 °C at 60 bars for 3min;Flow 4.34 mL s^{-1}	Lydall 6100-200	JM Pt_{40}/C 0.0068g cm^{-2}	Nafion® 117	JM Pt_{40}/C 0.007g cm^{-2}	Lydall 6100-200
28	130ºC at 40bars for 5min; Flow 4.34 mL s^{-1}	Lydall 6100-300	Iridium black 0.0045g cm^{-2}	Nafion® 117	JM Pt_{40}/C 0.0048g cm^{-2}	Lydall 6100-300
29	130ºC at 40bars for	Lydall 6100-	Iridium black	Nafion®	JM Pt_{40}/C	Lydall 6100-

	5min;Flow 4.34mL s^{-1}	300	0.0022g cm^{-2}	117	0.0035g cm^{-2}	300
31	130 ºC 30bar 5min Flow 4.34mL s^{-1}	Etek LT 1400-W	JM IrO_2 0.0025 g cm^{-2}	Nafion® 117	0.00305g cm^{-2}	GDL Etek LT 1400-W
32	150 ºC 30bar 5min Flow 4.34ml s^{-1}	Etek LT 1400-W	JM IrO_2 0.0028 g cm^{-2}	Nafion® 117	Pt incorporated	Etek Ready-to-Press
33	150 ºC 30bar 5min; Flow 3.34mL s^{-1}	Etek LT 1400-W	JM IrO_2 0.0031g cm^{-2}	Nafion® 117	Pt incorporated	Etek Ready-to-Press
38	130ºC at 30bars for 5min Flow 3.34mL s^{-1}	Lydall 6100-300	0.0092 g	GEFC-112	JM Pt_{40}/C 0.0085 g cm^{-2}	Lydall 6100-300
42	130 °C at140bars for 6 min Flow 3.34mLs^{-1}	Bekinit Ti GDL	JM IrO_2	GEFC 117	JM Pt_{40}/C	Bekinit Ti GDL
51	130ºC at140bars for 6min;Flow 3.34mL s^{-1}	Bekinit Ti GDL	HM IrO_2 0.0078 g cm^{-2}	Nafion® 117	JM Pt_{40}/C 0.0083 g cm^{-2}	Bekinit Ti GDL
55	130ºC at 140bar for 6min;Flow 3.34mL s^{-1}	Bekinit Ti GDL	JM Ir Black 0.0025g cm^{-}	Nafion® 117	JM Pt_{40}/C 0.0056g cm^{-2}	Lydall 6100-300
63	130ºC at 400 bar and 5 min;Flow 4.2mLs^{-1}.	Bekinit Ti GDL	JM IrO_2 0.006g cm^{-2}	Nafion® 117	JM Pt_{40}/C 0.001g cm^{-2}	Lydall 6100-300
64 / 65	130ºC at 400 bar and 5 min; Conditioned 6 days Flow 4.2mLs^{-1}.	Bekinit Ti GDL	JM IrO_2 0.006g cm^{-2}	Nafion® 115	JM Pt_{40}/C 0.001g cm^{-2}	Lydall 6100-300

Numbering of the MEA combinations is not consecutive (Table 7.3) as some combinations were unsuccessful. The configuration and process conditions of the SPE system were iteratively optimized. The following section will describe the effect of different components, configurations and process conditions.

Chrono amperometry of the MEA was performed using a power source. The potential was stepped up in 0.5-1.0 V steps after a dwell time of 300 s at each applied potential in most cases to check for MEA activity for the hydrogen evolution reaction (HER) and electrode stability, as is shown by example in Figure 7.28.

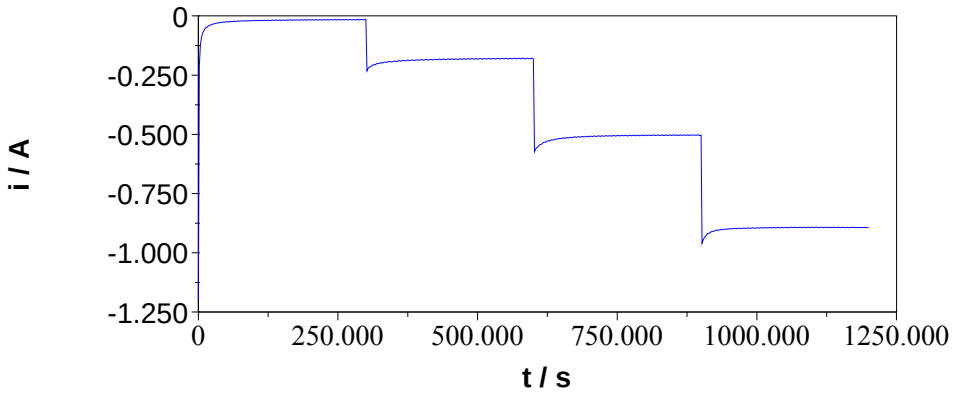

Figure 7.28 Chrono amperometry cycle used to test MEA activity for H_2 production

The average current density obtained at atmospheric pressure, per geometric area (A_g) over time for each applied potential and each MEA combination was plotted as a function of the current – voltage (I-V) relationship. In each case the activity for the HER of the various MEA tested is given as a function of current density per A_g specified. The hydrogen was collected initially and the amount produced at each temperature was recorded at the applied voltage for a specific period of time to ensure that the cell did not leak and no crossover or permeation occurred through the ionomer membrane.

The influence of various parameters will be described according to incremental improvements obtained in cell output for different applied potential. Where components were altered these will be specified prior to the obtained results. Data for the initial experiments are presented for A_g of 5 cm^2 because of the low current densities obtained, and once better outputs were achieved the data is normalized to A_g of 1 cm^2.

PLEASE NOTE: For simplicity all potentials are represented in the positive direction on the x–axis in the figures presented in this Chapter whereas the actual applied potential was negative, between -1.3 V and -2 V.

7.5.1.1 The effect of hydrophobicity of the GDL

MEA series (2,3,4 and 5) were prepared using Toray carbon paper with various degrees of Poly-tetra-floro-ethylene (PTFE) incorporated to understand whether hydrophobic elements in the GDL would be beneficial to the MEA assembly and cell output. A further MEA series (MEA 6 and 7) were prepared on hydrophilic carbon cloth (Lydall 6100-200). The ink formulations used are specified in Tables 7.4 and 7.5.

Table 7.4 Ink formulation for MEA series 2,3 and 4

Material used	Cathode	Anode
JM Pt_{40}/C (g)	0.2101	0.2133
Nafion (5%) (g)	0.6774	0.6763
De-ionized water (g)	1.0180	1.0259
Isopropanol (g)	1.0166	1.0017

Table 7.5 Ink formulation for MEA series 5 and 6

Component	Anode	Cathode
JM 40% Pt/C	0.2114 g	0.2101 g
Nafion (5%)	0.8007 g	0.8086 g
H_2O	1.0123 g	1.0210 g
Iso-propanol	1.0180 g	1.0206 g

The ink was spray coated for MEA2 upon Toray carbon paper with 0 % PTFE that was used as GDL on both the cathode and anode side. In the case of MEA3 a GDL with 10 % PTFE (hydrophobic) was used for the cathode and for the anode a GDL with 0% PTFE (hydrophilic) was used and spraycoated with the same ink formulation. In MEA4 a GDL containing 10 % (hydrophobic) PTFE was used as cathode and for the anode a GDL containing 6 % PTFE was used. After the ink had been deposited and dried each electrode was coated with a thin layer of Nafion before hot pressing. The electrodes were combined with the Nafion membrane by hot pressing at 120 ºC at 40 bars for 2 min.

MEA series (MEA 6 and 7) were prepared on hydrophilic carbon cloth (Lydall 6100-200) The Nafion solution in the ink formulation was increased to about 0.8 g as the step of coating a thin film of the Nafion on the carbon cloth before pressing was eliminated because the Nafion film caused the carbon cloth to adhere to the polytetrafloroethylene (PTFE) liner of the hot press during lamination of the MEA.

The ink mixture was brushcoated over A_g 5 cm^2 pieces of carbon cloth. After each coat of ink the electrodes were put into an oven for 2 min at 100 ºC. The MEA was hot pressed at 130 ºC at 80 bars for 2min with Nafion 117 ionomer membrane to improved lamination of the MEA. Care was taken to improve the reproducibility of catalyst loading and the loading achieved is detailed in Table 7.6. The A_g of these MEA electrodes was 5 cm^2.

Table 7.6 Catalyst loading on 5cm^2 for MEA 6, 7 and 8

Mass loading on 5cm^2	Anode (g)	Cathode (g)
MEA6	0.0507	0.0644
MEA7	0.0560	0.0626
MEA8	0.0268	0.032

NOTE: In the masses given as loadings there is always the small amount of Nafion used as binder in the ink formulation which remains after curing the electrode and which has not been corrected for in the given catalyst loading.

After assembly of the MEA in the cell, the MEA was moisturized for 30 to 60 min before applying a voltage across the cell at 25 ºC. The water flow rate was 23.5 mL min^{-1}. The overall cell resistance was 0.3 Ω for MEA2, 0.15 Ω for MEA3 and 0.072 Ω for MEA4. This MEA combination was not stable therefore the hot pressing conditions were changed using a higher temperature and longer time. The cell resistance for MEA 6 was 0.081 Ω and for MEA 8 was 0.079 Ω.

Chrono amperometry was performed using a power source between an applied potential of -1.3 and -2 V. The potential was stepped up after a dwell time of 300 s at each potential to check for MEA activity and stability. The average current density over 5 cm^{-2} for each potential step and each MEA combination was plotted in Figure 7.29.

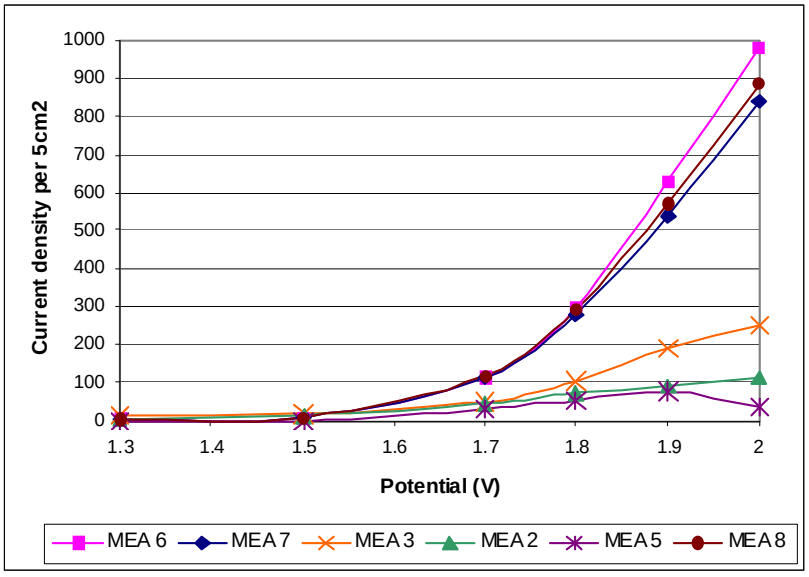

Figure 7.29 MEA output using Toray PTFE or Lydall 6100-200 carbon paper at 25 ºC over 5 cm $^{-2}$

The average current density output for MEA over 5 cm $^{-2}$ using Toray paper at 25 ºC was low but improved stepwise according to the applied potential between -1.3 and -2.0 V as expected, for MEA 3. The low output observed for MEA 2 and 4 combinations was ascribed to the PTFE content of the GDL. It was also possible that the temperature of hot pressing was inadequate, because MEA 4 became unstable at an applied voltage of -1.9 V. Ioroi et al., (2002; 2003) found that cell performance was not affected by the PTFE loadings on the GDL in the cathode side of electrolyzer cells whereas the PTFE loadings on the oxygen electrode GDL affected cell output considerably. However, in their study the cell was operated in both electrolysis mode and fuel cell mode in sequential cycles and it was largely the fuel cell mode that was affected. They found however, that the Nafion content in the electrode affected both the fuel cell and water electrolysis performance; their electrodes containing 7–9 wt % Nafion showed good performance. They also demonstrated that lower catalyst loadings could be applied without detrimental effect and that a small % of Ir added to the anode would improve the fuel cell cycle without impeding the electrolytic cycle. Because this study was restricted to optimizing the SPE electrolyzer mode, and because the results of MEA formed with PTFE content in the GDL were low overall the Toray hydrophobic GDL were not tested further.

The results of MEA series 6 and 7 and an additional replicate (MEA 8) were reasonably reproducible, with MEA 6 giving slightly higher output (980 mA per 5cm^2 at -2 V) compared to MEA 7 and 8 (841 and 844 mA respectively per 5cm^2 at -2 V). All MEAs that were assembled using the hydrophilic Lydall 6100-200 GDL were significantly more active than those prepared using PTFE coated Toray paper. The increase of the cell temperature in the case of MEA 8 significantly improved the cell output to above 1 A per 5 cm^2 at -2.0 V. The moisturization time of the MEA had a significant effect upon overall cell resistance with moisturization time inversely correlating with resistance as is shown in Figure 7.30.

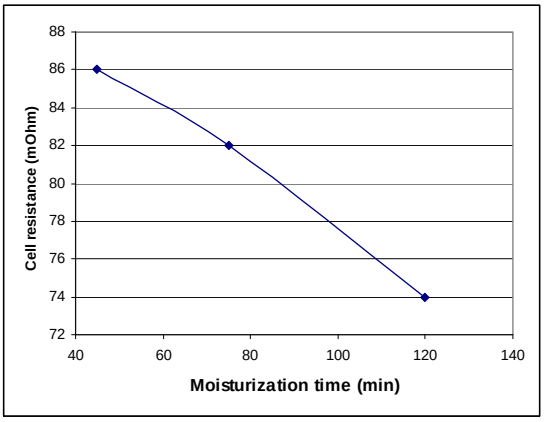

Figure 7.30 Effect of MEA moisturization time upon overall cell resistance

The change in cell resistance due to moisturization time is a function of the water uptake into the Nafion® membrane, and it can be expected that the thickness of the Nafion® film as well as the amount of Nafion® ionomer incorporated as binder in the ink formulation would have an effect on the time required before the MEA is fully moisturized. It was therefore necessary to test all MEA at the same time after commencement of moisturizing to eliminate this extraneous variable and this moisturization time was set at 30 min for initial tests. Thus it is evident that preliminary testing was not fully optimized as the tests were performed before the water content of the ionomer was properly equilibrated and thus an incomplete level of proton conduction may have added to cell resistance.

7.5.1.2 The effect of catalyst loading

The effect of catalyst loading was assessed in MEA 10 and MEA 11 using the Lydall 6100-200 GDL and hot pressing conditions of 130 ºC at 40 bars for 2 min. In these combinations the JM Pt_{40}/C catalyst loading on MEA 10 was 0.0137 g on the anode and 0.0195 g per 5 cm^2 on the cathode, whereas in MEA 11 the loading was 0.0381 g and 0.0367 g per 5 cm^2 respectively, (more or less double the amount) which in both cases was considerably less catalyst than was used in the MEA 6 and 7 series. All other variables were kept as constant as possible (except for temperature which was 20 ºC in this case) and the tests were performed as previously specified. The current density of the two MEAs with different catalyst loading is compared in Figure 7.31 (a).

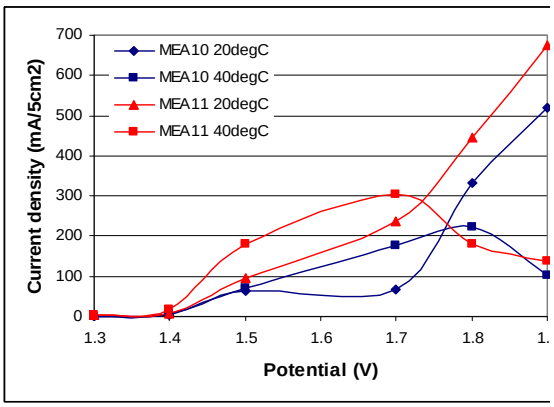

(a) Effect of catalyst loading on current density for JM Pt_{40}/C catalyst at 20ºC

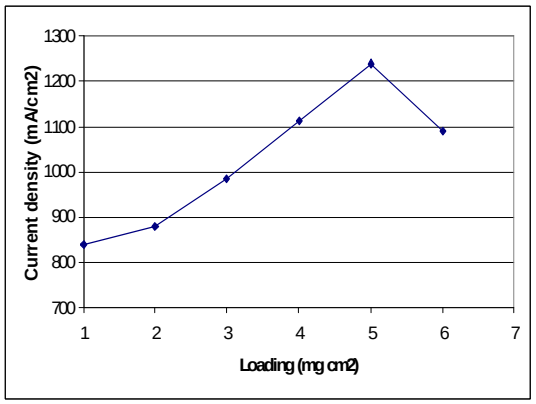

(b) Effect of catalyst loading on current density for IrO_2 at -1.8 V, 80 ºC and water flow rate 3.17 ml s^{-1} ;A_g 1cm^{-2} (Thamahane, 2005)

Figure 7.31 Effect of catalyst loading on current density

The effect of catalyst loading on current density at 20ºC for JM Pt_{40}/C catalyst could be discerned (Figure 7.31(a)). At higher temperatures the MEA both became unstable and output decreased dramatically. Even though MEA 10 and MEA 11 had considerably less catalyst on both anodes and cathodes than the previous series, the current density at 20 ºC was equivalent to the previously tested MEAs in the case of MEA10, which only had 0.0137 g per 5 cm^2 JM Pt_{40}/C on the anode and 0.0195 g per 5 cm^2 of JM Pt_{40}/C on the cathode. MEA 11 showed a better output than the previous series at -1.9 V with a catalyst loading of 0.0381 g JM Pt_{40}/C per 5 cm^2 on

the anode and 0.0367 g JM Pt_{40}/C per 5 cm^2 on the cathode. The series (MEA 6 to 8 and MEA13 to 17) had approx 0.06 g JM Pt_{40}/C per 5 cm^2 on either side of the MEAs. This result highlights the importance of using no more than necessary of the expensive Pt catalyst. The loading of the IrO_2 catalyst on the anode was also shown to require optimization (Thamahane, 2005). In that study an optimum loading of IrO_2 was achieved at 0.005 g cm^{-2} as is shown in Figure 7.31 (b). The decrease in performance observed at the higher temperature Figure 7.31 (a) was ascribed to excess accumulation of gas in the cell and further testing was performed to eliminate this problem. The cell was there after operated in a vertical position with the water outlets on top to allow gas egress due to gravity. The change in cell orientation resulted in a continuous flow of fine bubbles being observed in the water outlet tubes. With the change of position of the cell the improved flow significantly reduced the electrode blinding problems, which showed that the effects of gravity need to be kept in mind.

7.5.1.3 Reproducibility and stability of MEA assembly

Reproducibility and stability of MEA assembly was tested in a series of MEAs, MEA 13 to 17, assembled using similar process conditions and the same components. The ink formulation used for this series is shown in Table 7.7.

Table 7.7 Ink formulation used for MEA 13 to 17

Component	Anode (g)	Cathode (g)
Pt catalyst	0.2131	0.2123
Water	1.0362	1.0399
Nafion (5 %)	0.8086	0.8042
Iso-propanol	1.0089	1.0023

The inks were stirred overnight and then electrodes were prepared. The mass of JM Pt_{40}/C catalyst loaded was typically 0.06 g per 5 cm^2 on the anode as well as on the cathode side respectively. This ink formulation had a somewhat higher Nafion ionomer content than used in previous ink formulations, in order to improve adhesion of layers and limit delamination problems.

Reproducibility was tested in the assembly of MEA 13,14,15,16 and 17 using the Lydall 6100-300 GDL for the cathode as well as the anode and the following hot pressing conditions: 135 ºC at 40 bars for 2 min. The JM Pt_{40}/C catalyst was used on both anode and cathode side and catalyst loadings varied somewhat but was around 0.06 g per 5 cm^2 for both the cathode and the anode.

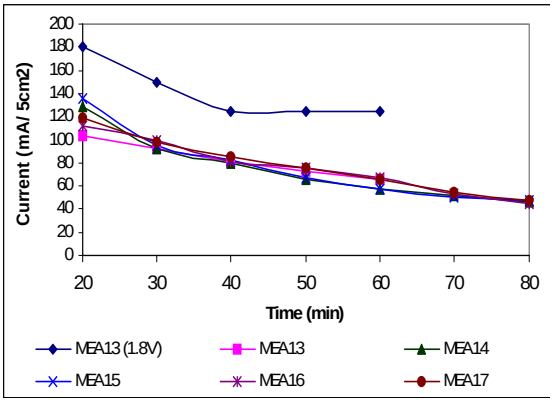

Figure 7.32 Replication study of steady state current density output at -1.7 V of MEA 13 to 17

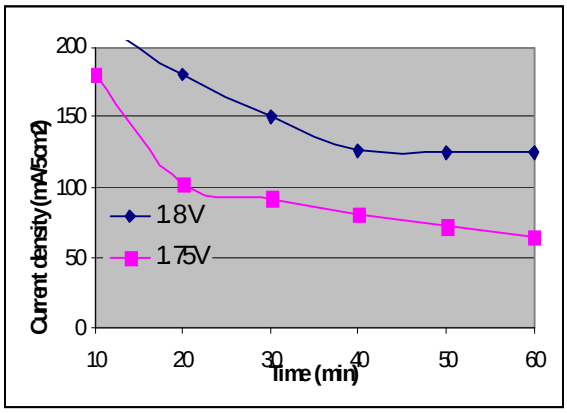

Figure 7.33: Current density trend over time after 24h (-1.8V) and after 48h (-1.75 V) for MEA 13

The current output was obtained at -1.7 V to prevent delamination, as above this potential vigorous evolution of gas was observed. Testing of the MEAs at room temperature (Figure 7.32) and -1.7 V over a period of time showed that even though catalyst loading on the electrodes varied somewhat, a relatively reproducible but low initial current density output of between 100-140 mA over a geometric area of 5 cm^2 at -1.7 V (an average of about 25 mA cm^{-2} at -1.7 V and 25 ºC) was achieved which output was not stable over time, decreasing to below 60 mA over 5 cm^2 at -1.7 V after 80 min. The use of the Lydall 6100-300 GDL apparently did not have any effect upon the performance of the cell as the output at -1.7 V was similar to the output at that potential when Lydall 6100-200 GDL was used previously. The only difference between these two GDL materials from the same supplier was the thickness of the GDL layers. Increasing the applied voltage to -1.8 V (MEA 13) increased the current density as expected, to an output of 180 mA over an A_g of 5 cm^2. The catalyst loading varied in these tests but the lack of sensitivity of the cell output to the degree of catalyst loading indicated that the Pt catalyst was not being applied to good effect and that catalyst loading could be optimized. Furthermore the lack of stability

indicated a degradation of the MEA over time. The MEA 13 tested above was further tested for durability over time at room temperature at a fixed applied voltage by restarting the test after 4 and 24 h at -1.8 V, and thereafter after 48 h at -1.75 V (Figure 7.33). Current density after 24 h and 48 h in Figure 7.33 are aggregate figures from data obtained over 1 h at the time specified. It is interesting to note that the MEA returned to above the initial outputs (obtained at lower potential) when restarted after 24 and after 48 h and slowly lost output over the hour tested. This indicates the occurrence of a reversible process which is eliminated during the resting periods. It was not clear whether the observed deterioration of the performance of the MEA over time was due to some degradation during testing or whether the low output was still due to a gas transport problem with accumulation of gases in the cathode and/or anode compartment or blinding of the electrodes under an applied potential. Since the process was reversible it was more likely to be the latter case. An increase in the water flow rate may further reduce the gas accumulation.

7.5.1.4 The effect of using an iridium oxide catalyst for the anode

In order to assess the effect of the anode catalyst type on current density and improve the MEA stability MEA 9 was assembled with HM IrO_2 catalyst as anode catalyst made as specified in Section 7.3.3.3, using ink formulations specified in Table 7.8.

Table 7.8 Ink formulation used for MEA 9

Component	Anode	Component	Cathode
HM IrO_2	0.2145 g	40% Pt	0.2151 g
H_2O	0.5 cm^3	H_2O	1.041 g
Nafion (5%)	1 cm^3	Nafion (5%)	0.6754 g
Iso-propanol	1.5 cm^3	Iso-propanol	1.0104 g

HM IrO_2 loading on the anode on Toray 10% PTFE GDL was 0.0285 g per 5 cm^2 and JM Pt_{40}/C loading on the cathode Toray 0% PTFE was 0.054 g per 5 cm^2. The MEA was formed by hot pressing at 40 bars and 135 ºC for 2 min and tested under identical conditions as specified above. The cell resistance was 0.33 Ω. The average

current density after a dwell time of 1000 s at each applied potential obtained for the 5 cm^2 MEA for different temperatures is presented in Figure 7.34 and Table 7.9.

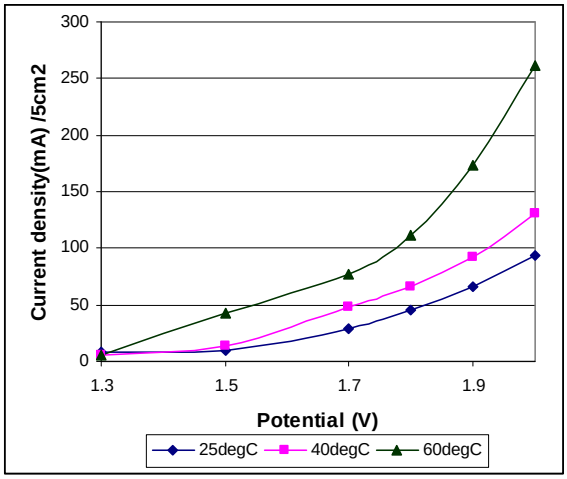

Figure 7.34 Output of MEA 9 with HM IrO_2 anode catalyst at different temperatures

A clear trend of increasing current density output (mA per 5 cm^2) was observed when the temperature was increased step wise after each experiment at a specific temperature and at the specified applied potentials between -1.3 and -2 V. The current output achieved for this MEA in the electrolyzer test at -2.0 V and at 25 ºC was lower (250 mA per 5 cm^2) than that achieved over Pt catalysts (980 mA per 5 cm^2). This poor performance could have been due to the use of the PTFE loaded Toray GDL as this GDL type previously gave poor results most likely because of exclusion of the feed water from the GDL due to its hydrophobicity. This MEA was also tested for durability over 5 days after steady state polarization at -2 V. Table 7.9 specifies the current density obtained on 5 cm^2 over 1000 s at -2 V and at different temperatures for MEA 9.

Table 7.9 Current density over time for MEA 9 with IrO_2 anode at different temperatures

Temperature	Volts	Time	Current
25^0C	-2 V	1000 s	97 mA
40^0C	-2 V	1000 s	187 mA
60^0C	-2 V	1000 s	301 mA

Under steady state polarization the output of MEA 9 with HM IrO_2 anode catalyst was stable for 5 days, whereas previous MEAs prepared with Pt containing anodes degraded after 2 days of steady state polarization. This result showed that the problem of MEA durability could be improved by application of the IrO_2 catalyst on the anode and indicated that catalyst type and stability may have a role in preventing the degradation of the MEA performance over time.

7.5.1.5 The effect of an iridium black catalyst for the anode

In a further experiment MEA 28 and 30 were prepared using the ink formulation specified in Table 7.10. The catalysts used were JM Pt_{40}/C on carbon for the cathode and J.Matthey Iridium black 99.8% (Stock # 12071, Lot # K01M11) for the anode. The electrode size was 4 cm^2 but the data presented in Figures 7.35 and 7.36 have been normalized to 1cm^2. The anode loading was 0.0045 g cm^{-1} and the cathode loading was 0.0048 g cm^{-1} in the case of MEA 28 and in the case of MEA 29 the loading was 0.0022 g and 0.0035 g respectively.

Table 7.10 Ink formulation for MEA 28 and 29

	Anode	**Cathode**
Catalyst	0.1072 g	0.1071 g
Water	0.25 cm^3	0.25 cm^3
Nafion soln (5%)	1.2476 g	1.2477 g
Iso-propanol	0.5 cm^3	0.5 cm^3

The MEAs were assembled using hot pressing conditions of 40 bars at 130 ºC for 5 min with GDL 6100-300 for both cathode and anode and Nafion®117 as ionomer membrane and tested in the cell at a flow rate of 4.12 mL s^{-1}. Cell resistance was 171.187 mΩ. The comparison of the IrO_2 anode catalyst with commercial JM Ir Black as anode catalyst at 40 ºC is presented in Figure 7.35.

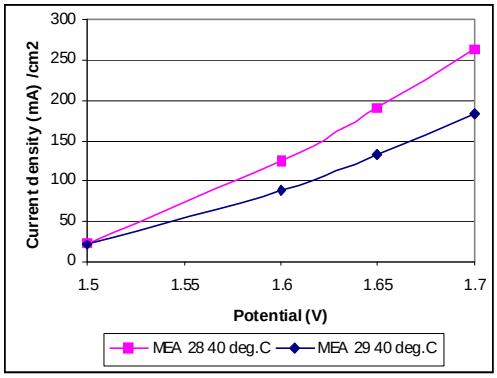

Figure 7.35 Comparison of current density (mA cm^{-2}) of JM IrO_2 with JM Ir Black (MEA28 and MEA 29) at 40ºC

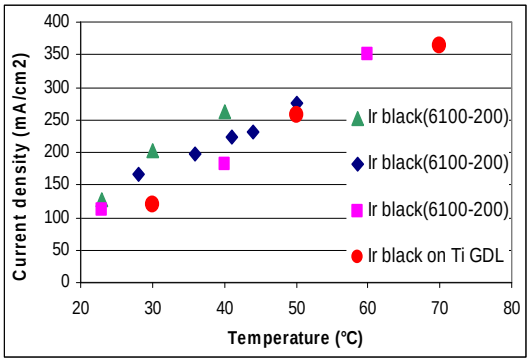

Figure 7.36 Replication study of current density (mA cm^{-2}) using Ir black as anode catalyst at -1.7 V

Figure 7.36 shows that an optimum catalyst loading on the anode or cathode may affect the cell output, since MEA 28 which had the higher anode and cathode catalyst loading performed at more than 250 mA cm^{-2} at -1.7 V and 40ºC whereas MEA29 with significantly lower catalyst loading on the anode gave a lower current density output of under 200 mA cm^{-2}. Figure 7.36 shows the replication studies performed on Ir black anodes assembled into MEAs and tested at fairly similar catalyst loadings under similar conditions. The temperature was increased at a fixed potential of -1.7 V and the results also indicated that increased activity could be expected at higher temperatures once stability of the MEA could be achieved. Figure 7.36 also shows that replacing the GDL 6100-300 with the Bekinit titanium mesh GDL on the anode side (sample Ir Black on Ti GDL) had little overall effect on cell output in this case. The Ti GDL delaminated during testing when hot-pressed under the same conditions as the other MEAs, so the hot-pressing time should be increased in order to improve the contacts between the components.

These results show that applying IrO_2 or Ir black by itself as anodic catalyst is not the only factor requiring attention for improving cell output of the SPE electrolyzer. Various other factors such as ink formulations and deposition conditions (adding different amounts of proton conductive phase as binder, loading different amounts of catalyst), components used (different catalysts or use of hydrophobic vs hydrophobic GDL), operational conditions (changing operating temperature, or moisturization

time), may all affect the output of the cell. The multi-variant complexity of assembly, operation and testing an SPE electrolyzer makes this system a very poor choice as system for testing catalyst activity per se or for assessing the quality of electrodes or the effect of different components.

7.5.1.6 Effect of ionomer membrane type

Replacing the Nafion® membrane in the MEA by using Chinese GEFC-11N type GEFC-112 with conductivity of 0.1 S cm^{-1} (25 °C) was tested in order to establish whether a thinner ionomer membrane could reduce cell resistance and improve output accordingly. New MEAs were prepared using the thin Chinese proton conductor, GEFC-11N type GEFC-112 (Perfluorinated Proton Exchange Membrane) to separate the anode cathode compartment of Proton Exchange Membrane (PEM) water electrolyzer. The MEA 38 was prepared using Lydall carbon cloth 6100-300 and JM Pt_{40}/C catalyst (Lot#D20K28) on both cathode (loading 0.0085 g cm^{-2}) and anode side (loading 0.0092 g cm^{-2}). The cell was tested at a flow rate of 3.34 mL s^{-1} and cell resistance was between 146.91, 112.05, 77.14, and 69.72 mΩ respectively for each temperature tested (23, 30, 50 and 70 °C). The current density (mA cm^{-2}) obtained at various applied voltages and temperatures are shown in Figure 7.37.

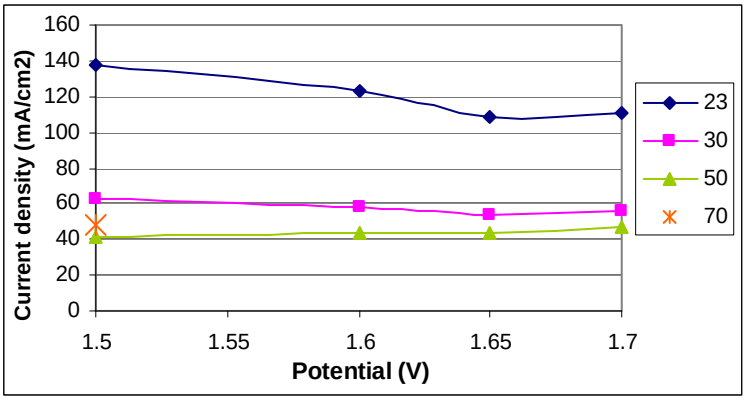

Figure 7.37 Current density (mA cm^{-2}) for MEA 38 prepared with Chinese ionomer membrane GEFC-11N type GEFC-112

No current density increase was observed with an increase in applied voltage. The results shown in Figure 7.37 were not encouraging, as it appeared that the thin ionomer membrane may allow gas diffusion. The overall cell resistance indicated that the MEA did, however, maintain its integrity during testing. Cyclic voltammetry

was performed to understand whether there was a possibility of short circuit by penetration of the MEA during hot pressing. The cyclic voltammogram did not indicate any short circuit caused by perforation of the membrane. The conclusion drawn was that the membrane was too thin and may allow gas diffusion, or otherwise proton conduction degradation occurred during the experiment by instability of the membrane.

The effect of using the thicker Chinese proton conductor, GEFC-11N type GEFC 117 (Perfluorinated Proton Exchange Membrane) was tested in MEA 42. The ink formulation used is shown in Table 7.11.

Table 7.11 Ink formulation for MEA 42.

	Anode	Cathode
Catalyst type	JM IrO_2	JM Pt_{40}/C
Catalyst quantity (g)	0.1072	0.10725
Water (cm^3)	0.25	0.25
Nafion (5%) soln (g)	1.245	1.2459
Iso-propanol (cm^3)	0.5	0.5

The inks were brush coated upon the respective anode and cathode GDL. The catalyst loading on the anode was 0.00457 g cm^{-1} and on the cathode 0.00475 g cm^{-1}. The thin Bekinit titanium GDL was applied on both anode and cathode side and hot pressing conditions used were a pressure of 140 bars and a temperature of 130 °C and a time of 6 min. These more stringent conditions were applied to properly laminate the ionomer and the rigid Ti GDL layers. The cell resistance of MEA 42 was 249 mΩ. The flow rate of water was 3.34 mL s^{-1}. The current density obtained for MEA 42 is shown in Figure 7.38.

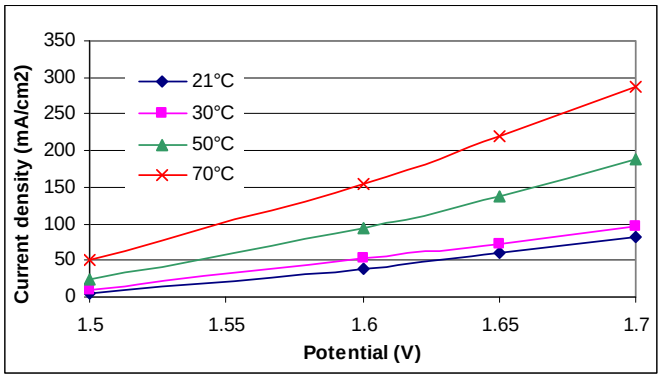

Figure 7.38 The current density (mA cm^{-2}) of MEA 42 using GEFC-11N type GEFC 117 ionomer

The activity of this MEA was quite high with an output of nearly 300 mA at -1.7 V at 70 ºC even though the catalyst loading on the cathode side was low, and the ideal MEA pressing conditions had not yet been established for the relatively rigid Bekinit Ti GDL. Thus the replacement industrial ionomer of similar thickness to the Nafion® ionomer did not negatively affect the cell performance and neither did the application of the Ti GDL and these results show the potential of using alternative cheaper commercial components in MEA assemblies. However various commercially available materials may not all be suitable as components for the SPE electrolyzer as can be seen in the case of the ionomer.

7.5.1.7 Effect of catalyst deposition method

MEA 26 was prepared using a different ink composition and deposition method using the usual hydrophilic carbon gas diffusion layer (6100-200AC). The ink was prepared, with the composition shown in Table 7.12.

Table 7.12 Ink Composition for MEA 26

	Anode	Cathode
Catalyst	0.050 g	0.050 g
Water	0.3999 g	0.4056 g
Nafion (5%)	0.2086 g	0.2002 g
Iso-propanol	nil	nil

This mixture with no additional solvent, apart from water and the solvent inherent in the Nafion solution, was placed in the ultrasound bath for 1 min then magnetically

stirred for 10 min and again put in the ultrasound bath for another 5 min. The catalytic ink was then brush coated onto the carbon gas diffusion layer. The MEA was hot pressed at 60 bars and 135 °C for 3 min. The MEA size was 4 cm^2. The flow applied in this experiment performed using MEA 26 was 4.34 mL s^{-1}. Each data point obtained was stable over 300s during chrono-coulometry with the GPES system. The cell resistance was between 133.62 mΩ over the time of the experiment. However, although this ink formulation allowed a high catalyst loading (0.0068g cm^{-2}) on the GDL, the high catalyst loading did not correlate with high current density (only between 22-38 mV cm^{-2} at 1.8 V at 25 ºC), compared to the results obtained previously.

A further set of experiments was performed in which the aim was to determine the performance of catalyst, using unsupported cathode and anode catalysts deposited directly onto the ionomer membrane. MEAs were prepared according to the procedure described by Ioroi et al (2002). As an anode catalyst, commercial JM IrO_2 was processed into an ink that was dispersed on a 5 cm^2 PTFE sheet used as transfer decal. The same procedure was done for the cathode catalyst using the JMPt_{40}/C. The PTFE sheets were dried at 80 °C, then the electrocatalyst-coated PTFE sheets were placed on both sides of the pre-treated 117 Nafion membrane and finally hot-pressed to form a MEA at 130 °C. After hot-pressing the PTFE sheets were gently removed leaving the catalyst attached onto either side of the Nafion membrane and this composite was placed directly against the Ti frits without any additional GDL. The catalyst loading on PTFE for MEA IrO_2 sample was 0.0013 g cm^{-2} on the anode and 0.0025g cm^{-2} JM Pt_{40}/C on the cathode. The MEA pressing conditions were 140 bars at 120 °C for 3 min. The MEA size was 5 cm^2. However the results that were obtained from this literature referenced method were very poor compared to the results that had been obtained using the carbon hydrophilic gas diffusion layer (6100-300). The maximum current density of 93.6 mA cm^2 at 70 ºC, was far lower than what was obtained previously. This confirms the vital role that adequate gas diffusion has on the outcome of the overall MEA output.

7.5.1.8 Effect of water flow rate, water purity and temperature

The effect of the water flow rate was evaluated with MEA 25. The anode catalyst was Iridium Black (Alpha Aesar Lot#K01M11, Stock#12071) and the cathode catalyst was JM Pt_{40}/C. The MEA size was 4 cm^2 and the anode and cathode GDL was Lydall 6100-200 carbon cloth, with a loading of 0.0107 g catalyst on the anode and 0.0198 g catalyst on the cathode per 4 cm^2. The ink composition is given in Table 7.13.

Table 7.13 Ink Composition for MEA 25

Component	Mass
Catalyst	0.1072 g
Water	0.25 cm^3
Nafion (5%)	1.2487 g
Iso-propanol	0.5 cm^3

MEA assembly conditions applied were a pressure of 40 bars and a temperature of 135 ºC for 3 min. Each data point obtained was stable over 300 s during chrono-coulometry with the GPES system. The results were obtained at 23 ºC. Three different water flow rates were applied namely 2 mL s^{-1}, 3.27 mL s^{-1} and 4.2 mL s^{-1}. The cell resistance was 164 mΩ. The current density obtained when altering the flow rate of water is presented in Figure 7.39. The direct correlation between flow rate and current density is shown in Figure 7.40.

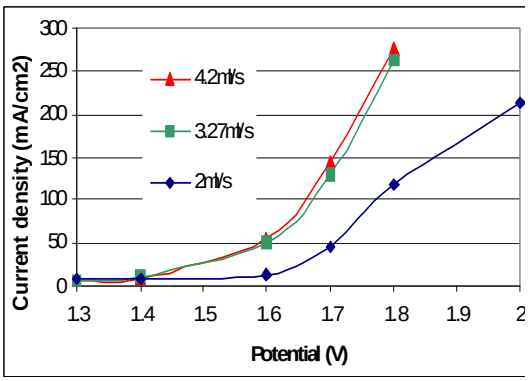

Figure 7.39 The effect of the water flow rate on current density (mA cm^{-2}) at 23 ºC for MEA 25

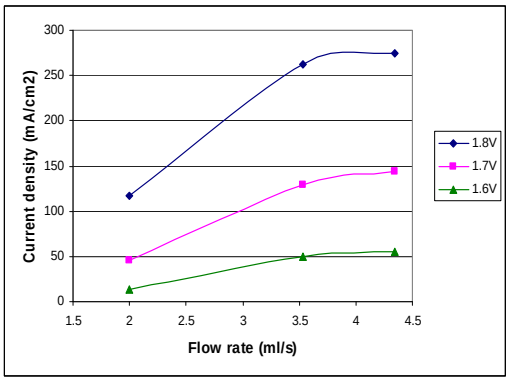

Figure 7.40 Positive correlation between flow rate and current density (mA cm^{-2}) at applied voltages between -1.6 and -1.8 V

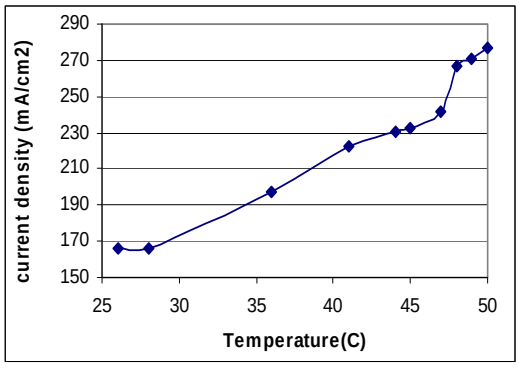

Figure 7.41 The effect of increasing temperature at a potential of -1.7 V on current density (mA cm^{-2}) for MEA 25

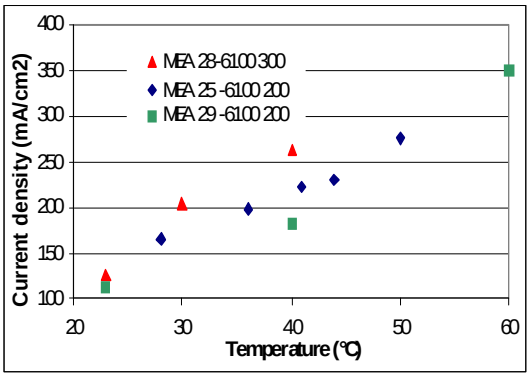

Figure 7.42 Comparison of current density (mA cm^{-2}) of MEA 25 with MEA 28 and 29 at -1.7 V

An increased flow of water from 2 mL s^{-1} to 3.27 mL s^{-1} through the cell improved the cell output considerably from 117 to between 262 and 275 mA cm^{-2} at the specified conditions because of the more efficient removal of generated gas which would otherwise occlude the electrode surfaces and also increase the resistance of the cell (Figure 7.39). Further increasing the flow did not improve the cell output for this MEA therefore it is evident that an optimum flow rate was achieved at 3.27 mL s^{-1} for this laboratory scale electrolysis module testing system. After a flow of 3.27 mL s^{-1} it was deemed that no further accumulation of gases causing blinding and occlusion of catalytic sites would have occurred as the flow rate increase showed no further improvement.

In a separate test, the performance of the cell was severely impacted by the use of tap water instead of ultrapure water as feed and the detrimental effect of an impure feed stream upon cell performance highlighted the necessity of providing consistently high purity water to an SPE electrolyzer if catalyst poisoning or ionomer degradation is to be prevented.

The effect of increasing temperature at a fixed applied potential on current density for MEA 25 is shown in Figure 7.41. When the temperature was incrementally raised over time at the same applied potential (-1.7 V) the current density improved, as was previously observed for MEA 9. It is worth noting that the MEA 25 produced current

densities that were over range for the Autolab at -1.8 V for the geometric surface area tested (4 cm^{-2}, but reported as 1 cm^{-2}) which may have affected the results obtained at the higher ranges.

Several more MEAs were made in the same manner with only slight differences in the GDL components (using Lydall carbon cloth 6100 300 or 6100-200 GDL) used for assembly and compared to MEA 25 as is shown in Figure 7.42. These adjustments in the MEA preparation procedure did not show a significant effect on performance. MEA 28 was prepared using the Lydall GDL 6100 300 compared to the 6100-200 GDL and a higher anode loading of catalyst and performed somewhat better than MEA 25. MEA 29 was made using an ink that was ultra-sounded for 30 min before deposition. The purpose of increasing ultrasound time was to ensure high dispersion of the catalyst particles in the ink, however, this additional processing step did not apparently lead to higher activity. It is also noteworthy that MEA 29 was tested at a high temperature of 70 ºC and this MEA was robust enough to withstand the high degree of gas evolution at this temperature.

7.5.1.9 Comparison with industrial GDL components

The objective of the following experiments was to further assess industrially available GDL materials. Etek carbon cloth GDL and Bekinit Ti GDL materials were assessed. By changing the GDL the assembly conditions of the MEA required optimization for each new type of GDL. Contact between the membrane and the electrode is very important to minimize cell resistance. Moreover, sometimes too much pressure and an overly long hot pressing time or too high temperature may result in ionomer membrane damage. The Etek materials came with manufacturer specified conditions for hot pressing and these were followed. In the case of the Ti GDL optimized conditions were determined (Thamahane, 2005), and applied in this study.

MEA 31 was prepared using GDL Etek LT 1400-W for both the cathode and anode side whereas MEA 32 and MEA 33 were prepared using Etek LT 1400-W as GDL

for the anode with the JM IrO_2 catalyst and Etek Ready-to-Press-to-MEA (ionomer incorporated) for the cathode which is a Pt and Nafion impregnated carbon cloth on the cathode side. In the case of MEA 32 and 33 the catalyst loading was not specified in the case of the commercial Pt containing Etek GDL.

MEA 31, 32 and 33 were prepared using commercial J.Matthey Iridium (IV) oxide 99.99 % ink painted on the anode. The anode catalyst loading for MEA 31, 32 and 33 was 0.0025, 0.0028 and 0.0031 g cm^{-2} respectively. The cathode loading in the case of MEA 31 was 0.00305 g cm^{-2} of JM Pt_{40}/C.

The cell resistance for MEA 31 ranged from 313 to 270 mΩ; for MEA 32 from 244-164 mΩ; and for MEA 33 from 223 to 179 mΩ. The cell resistances started somewhat high at 23 ºC and decreased during testing at higher temperatures (50-70 ºC). Thus the two MEAs prepared with the Etek Ready-to-Press-to-MEA Pt and ionomer incorporated GDL on the cathode had lower cell resistances than that of MEA 31 made with Etek LT 1400-W on both cathode and anode sides.

The recommended Etek GDL LT 1400-W MEA pressing conditions were 30atm at 130 ºC for 5min, which were used. The MEA 31 and 32 were tested under a flow of water of 4.34 mL s^{-1} at 30, 40 and 60 °C respectively and MEA 33 was tested under a flow of 3.34 mL s^{-1}. The results obtained (Figure 7.43) were not as high as the current density (mA cm^{-2}) of MEA 25 and 29 previously obtained at -1.7 V and 30 to 60ºC as can be seen in Figure 7.44. However, the anodic catalyst was also different as the previous MEAs were prepared using JM Ir Black which may account for the differences observed.

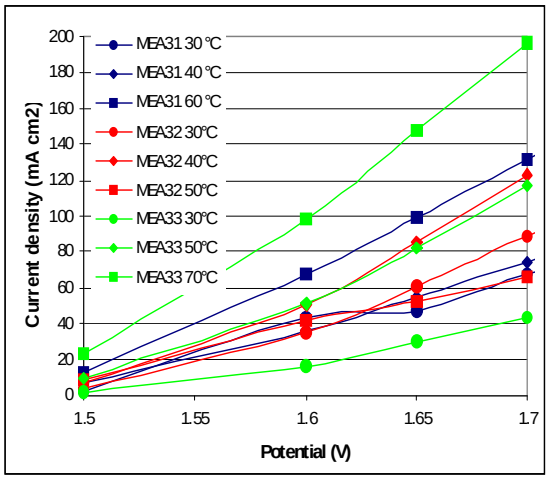

Figure 7.43 Comparison of current densities (mA cm^{-2}) obtained for MEA 31, 32 and 33 using Etek GDL

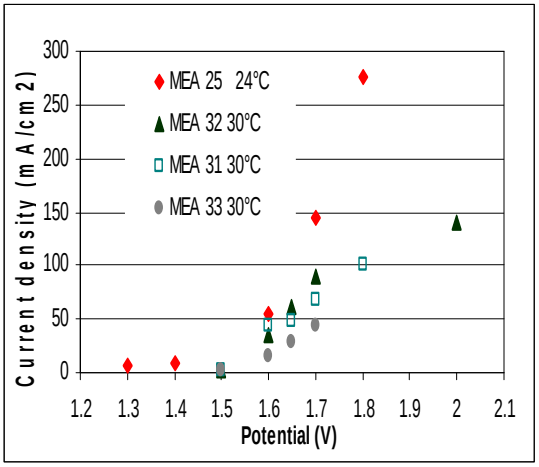

Figure 7.44 Comparison of current densities (mA cm^{-2}) obtained for Etek materials with MEA 25 at low temperatures

Due to the parameters that varied the results obtained for MEA 31, 32 and 33 are not similar and no clear trend could be discerned except the effect of temperature. MEA 32 became unstable at 50 ºC and MEA 33 performed the best at a high temperature with an output of about 200 mA cm^{-2} at -1.7 V and 70 ºC. These results however, indicate that neither the Etek gas diffusion layer nor the Etek catalyst containing GDL are critical parameters for high performance but that Lydall 6100-200AC GDL is probably a better GDL to use. However, the durability of the Lydall materials is not exceptionally good. Therefore the Bekinit Titanium mesh was further evaluated as GDL. A series of MEAs were prepared using the Ti GDL. The ink formulation for MEA 51 is shown in Table 7.14.

Table 7.14 Ink formulation for MEA 51

	Anode	Cathode
Catalyst type	HM IrO_2	JM Pt_{40}/C
Catalyst quantity (g)	0.0504	0.0497
Water (g)	0.25 cm^3	0.25 cm^3
Nafion (5%) soln (g)	0.0622	0.0599
Iso-propanol (g)	0.5 cm^3	0.5 cm^3

A catalyst, HM IrO_2 prepared at 350 ºC and annealed at 450 ºC, was used as anode catalyst for MEA51 and the JM Pt_{40}/C was used as the cathode catalyst and Nafion®

117 as ionomer membrane. The ink was brush coated on the cathode (loading 0.0083 g cm^{-2}) and on the anode (loading 0.0078 g cm^{-2}). Bekinit Ti GDL was used on both the cathode and anode side. Nafion® membrane 117 was used, as previously, for the ionomer membrane. The hot pressing conditions that were applied to form the MEA51 were a pressure of 140 bars, at 130 ºC for 6 min. The flowrate of water was 3.34 mL s^{-1}. The results of chrono amperometry of MEA 51 are presented in Figure 7.45 and compared with replicated results in Figure 7.46 at 80 ºC. The cell resistance of MEA 51 varied with temperature and the inverse correlation is shown in Figure 7.47.

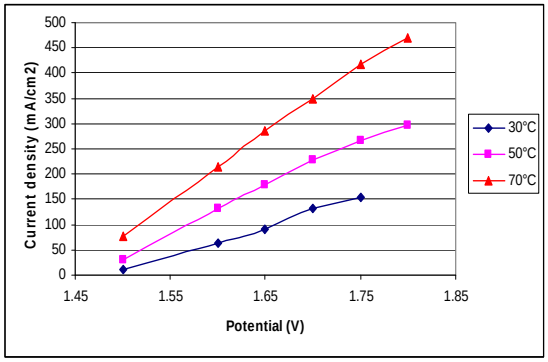

Figure 7.45 Chrono amperometry of MEA51 at different temperatures; flowrate of water 3.34 mL s^{-1}

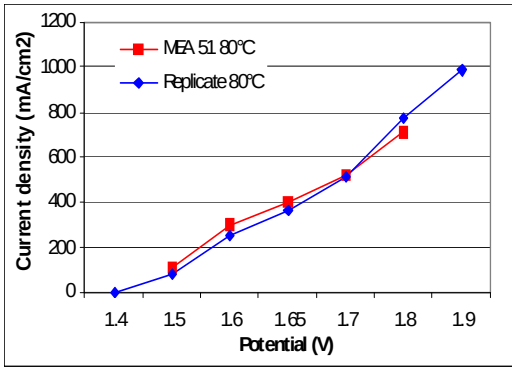

Figure 7.46 Comparison of current density (mA cm^{-2}) of MEA 51 with replicate MEA52 at 80 ºC

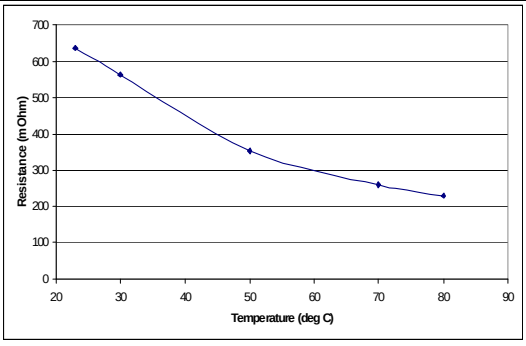

Figure 7.47 Inverse correlation between temperature and cell resistance

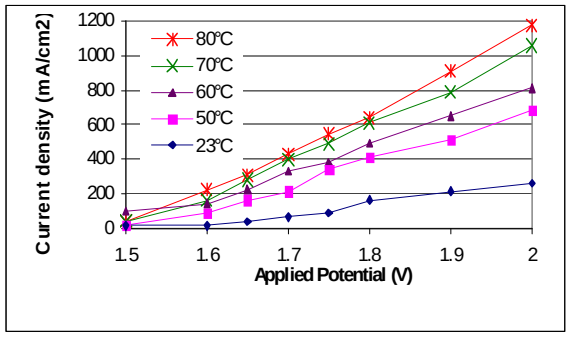

Figure 7.48 Current density (mA cm^{-2}) of MEA 55 with Ti fibre anode and Lydall 6100-300 cathode GDL

Good replication and high outputs were achieved in the range between -1.5 and-1.7 V compared to previous results. A high current density of nearly 500 mA cm^{-2} was

obtained at -1.7 V and at 80 ºC (Figure 7.46), which could be replicated and was similar to that obtained by Thamahane (2005).

A further experiment was performed with MEA55 (Figure 7.48) where the GDL used for the cathode was the Lydall 6100-300 and the anode used was the Ti GDL. The ink formulation used is shown in Table 7.15.

Table 7.15 Ink formulation for MEA55

	Anode	Cathode
Catalyst type	Iridium black	Platinum
Catalyst quantity (g)	0.04	0.05
Water	0.2 cm^3	0.25 cm^3
Nafion (5%) soln (g)	0.048	0.06
Iso-propanol (g)	0.4 cm^3	0.5 cm^3

Catalyst loadings differed in the MEA 55 compared to MEA 51 and 52 prepared previously due to the problem of changes in the viscosity of inks as a result of the volatility of the solvent isopropanol during ink processing. The loading for the MEA55 was 0.0025 g cm^{-2} for the anode and 0.0056 g cm^{-2} for the cathode. The hot pressing conditions were 140 bar at 130 ºC for 6 min. Cell resistance varied from 700 to 300mΩ depending on the temperature applied. The flow rate of water was 3.34 mL s^{-1}. The current density at different temperatures and applied potentials is presented in Figure 7.48. The output of this MEA was slightly lower at -1.7 V than MEA 51. However, when the potential was increased to -2 V at 80ºC an output current density of nearly 1200 mA cm^{-2} was achieved.

The fact that MEA 51 was somewhat more active than MEA 55 may possibly be ascribed to the use of the Bekinit Ti mesh on both anode and cathode side of MEA 51. The anode catalyst loading of MEA55 was also considerably lower (0.0025 g cm^{-1} compared to 0.0078 g cm^{-1} in the case of MEA51) and could have affected the output as well. Too much catalyst on the surface might also have had an effect on the mass transport of water in the case of MEA51 which may have affected the performance. Nevertheless, the current density for MEA 51 of about 550 mA cm^{-2} at

80 ºC and 1.7 V was close to that obtained by Ioroi et al., (2002) for IrO_2/Pt composites. These values were, however, still not equivalent to other values reported in literature (Millet et al., 1989; Khaselev et al., 2001; Hijikata et al., 2002) but it should be considered that the output is given for one geometric cm^2 and can be increased by increasing the geometric area of the cell or increasing the operational temperature.

7.5.1.10 Durability study

A durability study was performed on MEA 55 (prepared as is described in Section 7.5.1.7) at 60 °C and -1.7 V. The electrolyzer operated at atmospheric pressure and at a water flow rate of 3.17 mL s^{-1}. The electrode geometric area was 1 cm^{-2} and results of the durability study are presented in Figure 7.49.

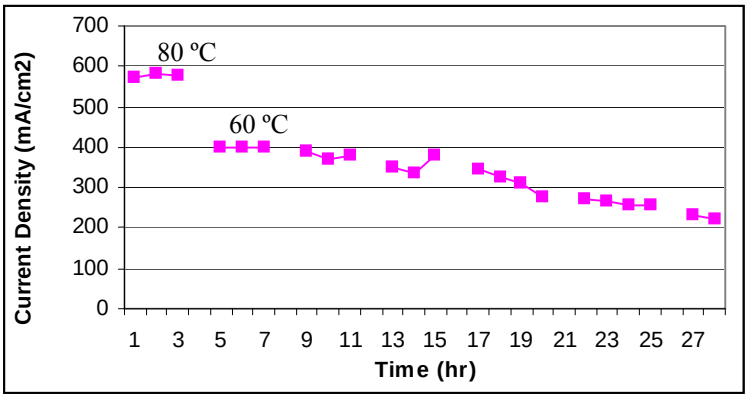

Figure 7.49 Durability study of HM IrO_2 catalyst applied in MEA 55 at -1.7 V

Stability tests were initially performed of the MEA55 at -1.7 V and 80 °C giving a current density of 581 mA cm^{-2} at the beginning in the first cycle (Figure 7.49). Thereafter the temperature was lowered to 60 °C and a stable output of 400 mA cm^{-2} was achieved for 6 h. The MEA testing was stopped overnight after each subsequent 6 h testing period and cooled down, and a lower output was observed upon start up after each shut down cycle period. A continuous testing system should be implemented to prevent this problem. It is not clear why the output was lower in this case after restarting the durability test, whereas previously transient changes were observed that were eliminated by intermittent testing.

Replication of the durability study with continuous testing was performed using JM IrO_2 as anode catalyst and also using a lower loading of the HM IrO_2 catalyst with other variables kept constant. Catalyst loadings differed in the various MEAs prepared due to the problem of viscosity of inks previously mentioned. The loadings on the anodes were 0.0072 g cm^{-2} for the JM IrO_2 MEA (JM) sample that was stable for 900 h, but was 0.0059 g cm^{-2} for the MEA sample marked HM IrO_2 tested for 200 h and 0.0042 mg cm^{-2} for the HM IrO_2 low loading sample, that was stopped after 60 h.

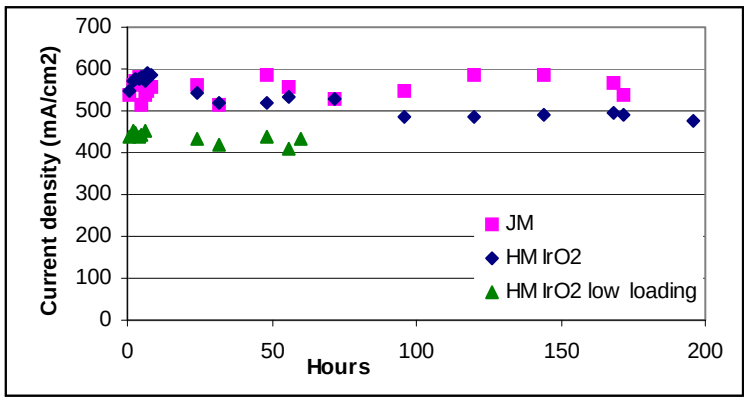

Figure 7.50 Replication study of MEA durability at 60 °C and -1.7 V at atmospheric pressure and water flowrate of 3.17 mL s^{-1}.

The MEA (sample HM IrO_2) was tested for 200 h (Figure 7.50) where after the activity decreased. The cell output under continuous operation was however generally higher (approximately 550-600 mA at -1.7 V) and much more stable than the output seen for MEA55 which decreased from about 580 mA to below 400 mA at -1.7 V after interrupted testing. Hence the problem of decreasing activity observed during the intermittent testing was eliminated by continuous testing. It is surmised that the slow decrease in activity over time could be because of contamination of the ultrapure water which was recycled or to slow degradation of the anode catalyst. If it was due to a reversible problem such as inadequate gas removal the output would have decreased as previously observed prior to optimization of flow rates and cell position. The HM IrO_2 low loading sample underperformed because of the lower catalyst loading on the anode, but still gave a steady output of above 400 mA cm^{-2} for 60 h under the applied conditions.

7.5.1.11 The optimized MEA conditions

In a further series of MEAs the optimization of fabrication of electrodes compared to previous MEA series was achieved. Various parameters were implemented that had been shown to have an effect previously and conditions of preparation were adjusted accordingly. Parameters that were improved and are demonstrated in the case of MEA63 included 3 h ultrasound of the ink formulation and spray coating of the ink using a Badger airbrush. The ink formulation used is shown in Table 7.16

Table 7.16 Ink formulation for MEA 63, 64 and 65

	Anode	Cathode
Catalyst type	JM IrO_2	JM Pt_{40}/C
Catalyst quantity (g)	0.080	0.192
Water (g)	0.160	0.384
Nafion (5%) soln (g)	0.480	1.152
Iso-propanol (g)	1.440	3.456

In the preparation of MEA 63, 64 and 65, electrodes sizes of 12 cm^{-2} were prepared for the cathodes and anodes and divided into 4 cm^2 pieces for each MEA in order to minimize differences in the electrode morphologies and loadings. The ink was spray coated in layers and dried with a blow-drier then weighed in between each layer. The Pt catalyst loading was minimized by depositing 0.001 g cm^{-2} JM Pt_{40}/C on the cathode and using an optimum loading of 0.006 g cm^{-2} JM IrO_2 on the anode. Nafion® 117 was used as ionomer in the case of MEA 63 and Nafion®115 in the case of 64 and 65. Bekinit Ti GDL was used for the anode and Lydall 6100-300 was used as GDL for the cathode. The MEAs were hotpressed at 400 bar at 130 ºC and 5 min, and tested at atmospheric pressure and a flow rate of 4.2 mL s^{-1}. Figure 7.52 shows the current density at different temperatures for MEA 63.

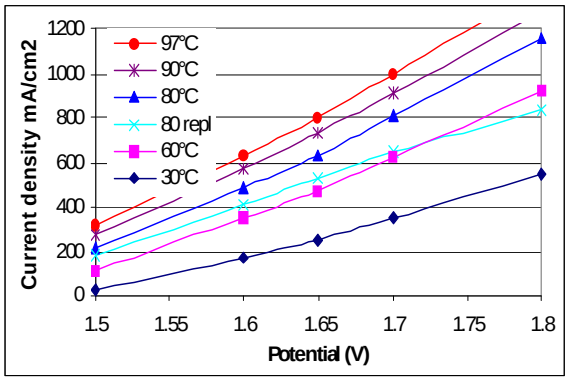

Figure 7.51 Current density (mA cm^{-2}) of MEA 63 at atmospheric pressure; flow rate 4.2 mL s^{-1}

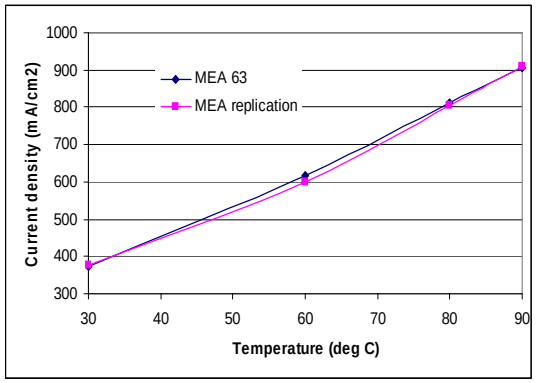

Figure 7.52 Replicate of MEA 63 tested at atmospheric pressure; flow rate 4.2 mL s^{-1}

The current density (mA cm^{-2}) of MEA 63 was obtained at atmospheric pressure at a flow rate of 4.2 mL s^{-1} after 6 days of conditioning (Figure 7.51). Sample (80repl) is a replicate MEA tested under similar conditions after 6 days of conditioning at 1.7 V. MEA63 and its replicate (Figure 7.52) gave an output of above 600 mA cm^{-2} at 60 °C at an applied voltage of -1.7 V and above 800 mA cm^{-2} at 80 °C. At 97 °C a current density of 993 mA cm^{-2} at -1.7 V was achieved thus the output of this optimized MEA was nearly one Amp cm^{-2}. The water bath temperature could not reach 100 °C with the set-up used.

The installation of MEA 63 in the test module was also improved because of better isolation between current collectors and clamps using Teflon washers, and a torque wrench was used to exactly tighten the set-up. Since the performance (electrolysis reaction) depends mainly on the potential applied between the electrodes, the contact between the MEA and the current collector is a crucial junction, which had not previously been controlled adequately. To estimate the magnitude of the effect, the cell was tightened further after the initial readings were taken and the performance of MEA63 was retested. An increase of about twice the performance was noted. At 60 ºC and 1.7 V the current before and after tightening the cell was 756 and 1204 mA cm^{-2} respectively. This highlights the fact that the pressure applied between the current collector blocks of the cell plays a critical part in the reproducibility and the performance of the cell. This also indicates that the pressure applied should be the

maximum to get the best output. Pressure was best controlled using a torque wrench to be kept constant. The tightening of the cell to the correct reading on the torque wrench was extremely important to eliminate problems in replicability. Contact resistance between the GDL and flow field rib in the current collectors, as well as GDL bulk conductivity, is strongly dependent on clamping pressure and represents a substantial amount of the total ohmic drop (Freunberger et al., 2006). Since great care was taken to do this tightening exactly the same in the replicate, the slight difference for the replicate showed that there were other nuisance variables to consider. The output of MEA 63 compared to the replicate showed that the reproducibility of the MEA could be influenced by contact issues. The MEA 63 is assumed to be somewhat better in performance than the replicate, because of better isolation using Teflon washers. The effect of flow rate was previously established up to 4.2 mL s^{-1}. A higher flow rate was evaluated with MEA 63 (Figure 7.53) because of the high degree of gas evolution that was achieved with the spray coated electrodes.

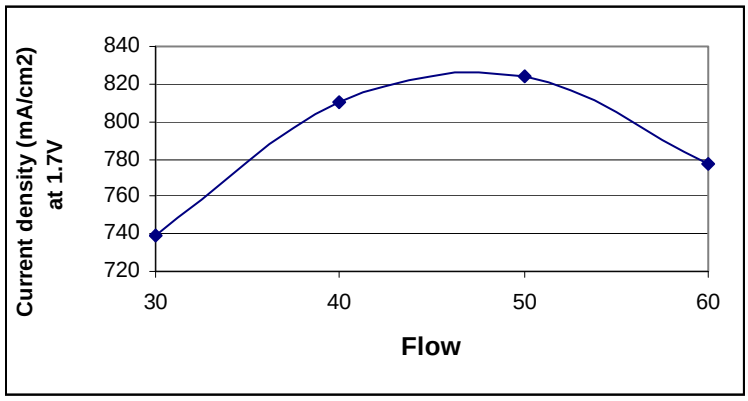

Figure 7.53: Effect of water flow on current density for MEA 63 at 1.7 V and 80 °C

A rapid flow rate (setting 50 on the pump) somewhat above 4.2 mL s^{-1} (setting 40) improved the current density output to above 820 mA cm^{-2} at 1.7 V and 80 °C but too rapid a flow (setting 60) led to a decline in performance to levels slightly above that observed for 3.47 mL s^{-1} (setting 30). In MEA 63 the highest outputs obtained on previously prepared MEAs was considerably exceeded, and this high current density was achieved with less than half the amount of Pt catalyst used previously for the cathode during brush painting.

One of the problems identified with ink deposition using brush coating was that when the catalyst ink was painted on the electrode, while making the anode electrode on Bekinit Ti mesh the ink was found to run through the GDL. Another problem was replicating the loading of the electrodes using brush coating, where reproducing fixed amounts of catalyst was difficult. Changing the ink deposition method to spray coating allowed much greater reproducibility of loading and better distribution across the electrode. Spray coating the electrodes improved these problems as careful control of the mass of each sprayed layer was performed by drying and weighing the electrodes between each layer deposited. However, this was a time consuming procedure when done manually and as was shown in PIXE studies, the ink significantly agglomerated, lowering the catalyst utilization values.

The cell performance increased with time of conditioning, from 1047 mA cm^{-2} on the first day to 1253 mA cm^{-2} after two days and 1277 mA cm^{-2} after six days at 80 ^{o}C and 1.7 V. Moreover it was observed that it took nearly a week of moisturization in the cell for stable readings to be obtained on the MEA63 mainly because of the effect of moisturization time upon resistance (Figure 7.54).

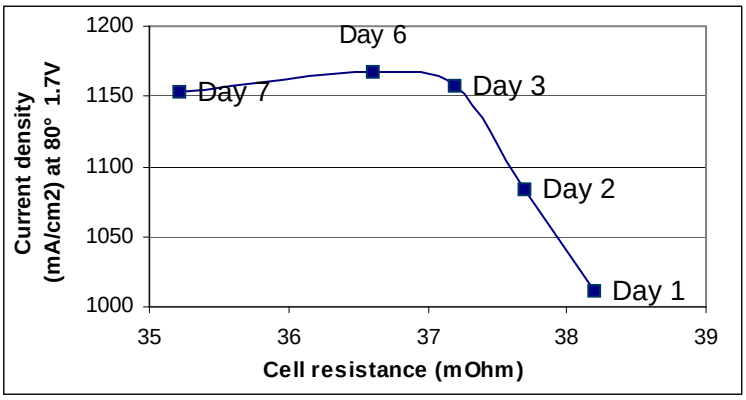

Figure 7.54 Effect of moisturization time on cell resistance at 80 °C and 1.8 V

It is not clear why the output tailed off after 6 days moisturization (Figure 7.54). It may be because the water feed was recycled and may have become contaminated and perhaps have inactivated the catalyst or else the catalyst was slowly leaching out of the MEA during the working cycles.

MEA 64 was assembled with the same materials at that of MEA63 but with Nafion®115 instead of Nafion®117. The results compared to Nafion®117 are tabulated below (Table 7.17) at -1.7 V and a flow rate of 4.2 mL s^{-1}. As expected, Nafion®115 was found to perform better than Nafion 117. The comparison between Nafion®115 and 117 is shown graphically in Figure 7.55 in which comparison of current density (mA cm^{-2}) obtained using Nafion 115 (MEA63) instead of Nafion 117 (MEA 64) at different temperatures is made. Nafion 117 has a thickness of 178 µm and Nafion 115 is 127 µm thick.

Table 7.17 Nafion® 117 compared with Nafion®115 at -1.7 V; Flow 4.2 mLs^{-1}.

Temperature / °C	MEA 63 Nafion 117 / mA cm^{-2}	MEA 64 Nafion 115 / mA cm^{-2}
30	377	404
60	601	685
80	805	899
90	909	986

The cell output was improved by about 10 % merely by using a thinner ionomer membrane and thus reducing the cell resistance as is shown in Figure 7.55 and 7.56.

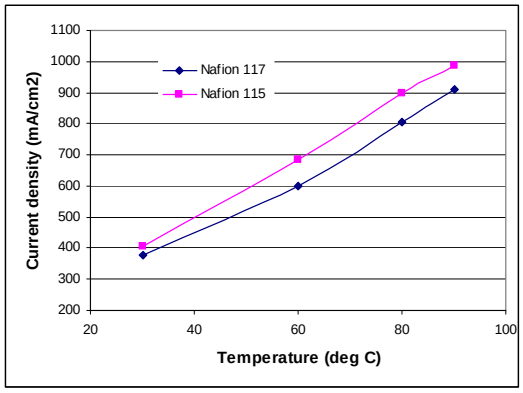

Figure 7.55 Comparison of current density (mA cm^{-2}) obtained using Nafion 115 (MEA63) instead of Nafion 117 (MEA 64) at -1.7V and different temperatures

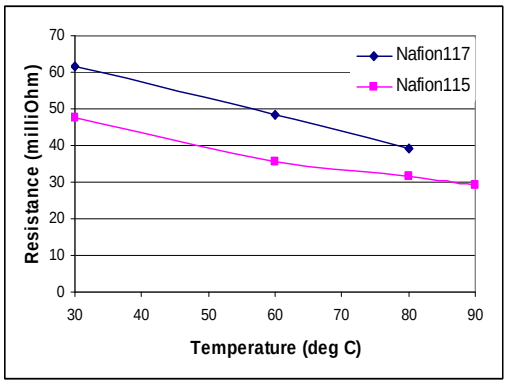

Figure 7.56 Comparison of overall cell resistance (mΩ) at different temperatures using either Nafion 117 or Nafion 115 as ionomer in MEAassembly

Comparison of overall cell resistance (mΩ) prior to applying a potential across the cell, at different temperatures, using either Nafion®117 or Nafion®115 as ionomer in MEA assembly is shown in Figure 7.56. The difference in resistance was more pronounced at lower temperatures and overall cell resistance was reduced between 14 to 8 mΩ by using Nafion®115 instead of the thicker Nafion®117. Another MEA was assembled with Nafion®112 membrane, expecting the performance to be better than that of Nafion®115. However, preliminary tests showed a direct contact between the electrodes (cell resistance of 1.69 mΩ was noted). The reason for this might be due to a puncture of the ionomer membrane causing a short circuit. Hot-pressing the membrane using previous MEA hot pressing conditions might have perforated the membrane. Optimizing the hot pressing conditions for this thin membrane type or other similar types may in future make it possible to reduce the cell resistance even more, without short circuiting the cell.

The electric cables leading to the power source were changed with that of a low resistance copper type cable. The leads were tested for resistance and 1 m of the cable used in previous tests (rated 60 V DC; 16 A) had a resistance of 21.20 mΩ m^{-1} whereas the new cable used as leads had a resistance of 5 mΩ m^{-1}. The change in current density observed when using either high or low resistance cabling as electrical leads between the power source and the cell is shown in Figure 7.57.

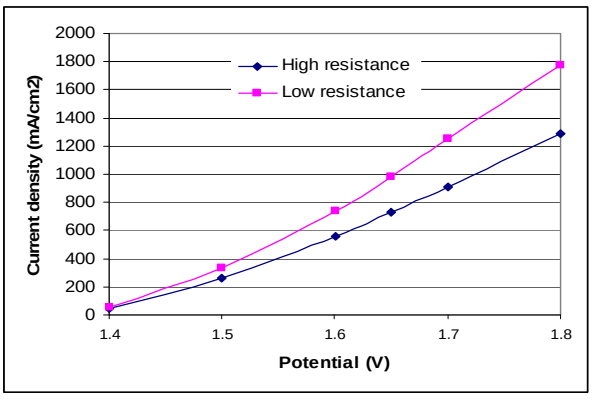

Figure 7.57 Cell performance using MEA 65 made with Nafion 115 and tested with low and high resistance leads

The cell with MEA 65 was tested at 90 °C and at -1.7 V the current density was 909.25 mA cm^{-2} before changing the wires and 1248 mA cm^{-2} after changing the

cables (Figure 7.57). The increase in the current density output is attributed to the minimized resistance of the new cables. These results again emphasize the fact that cell output was incrementally improved step by step not only by optimizing the components used in the assembly but also operational and systemic conditions. This improvement was most noticeable at higher applied potentials. The cell was tested with low resistant cables at 97 ^{o}C and -1.7 V and the current density output was 1329 mA cm^{-2}, an improvement of over 480 mA cm^{-2} (38%). This was the highest output achieved in this study and is also significantly higher than electrolyzer output typically reported in literature.

7.6 CONCLUSIONS

The objective of this study was to fabricate the state of the art of membrane electrode assemblies (MEAs), gaining detailed understanding of electrode structure in order to get maximum catalyst utilization. Issues of reproducibility for scalability as well as durability and stability were addressed. Different types of MEA- preparation methods were carried out in search for conditions that would give better catalyst utilization. Another objective was to study the effect of catalyst loading on the activity of water electrolysis based on the anode electrode where the water oxidation takes place. Finally, it was necessary also to study the effect of operational parameters such as temperature and water flow rate during water electrolysis.

On the development of membrane electrode assemblies (MEA) various components were evaluated for effectiveness as part of a MEA. This was done by using different diffusion layers (GDL) and ionomer membranes and testing the activity at similar catalyst loading and conditions. Ink formulations and deposition methods were varied to improve homogeneity of electrodes and attain even loading. The inks were applied either directly onto the membrane or onto different types carbon cloths (Lydall) or titanium fibre (Bekinit, thickness 0.1 mm) by a brushing method or spray coating method.

The cell performance was increased with temperature due to enhancement of electrode kinetics, proton transport, and also the conductivity of the membrane. The performance was also improved by higher water flow rates due to better removal of gaseous product accumulating in the anode and cathode compartments that caused blinding of electrodes and increased cell resistances. It also became apparent that components provided commercially for fuel cells, such as thin ionomer membranes, are not necessarily usefully applied in a solid polymer electrolyte electrolyzer. Several of the commercially available components were not beneficial to improving cell output and were too heat labile or fragile to withstand the hot pressing conditions applied. Moreover, it was highly problematic to achieve adequate replication, due to the many different variables that had to be accurately controlled both in the assembly and in the operational conditions. Delamination of MEA was a problem which required optimization of laminating conditions during hot pressing and pressure, temperature, as well as hot pressing time were iteratively improved.

Bekinit Titanium fibre substrate was the most promising anodic GDL and catalyst support, compared with GDL such as Lydall carbon cloth (6100-300 and 6100-200), Toray carbon cloth (hydrophobic), or with direct deposition methods onto the membrane. The cathode loading of 1 mg cm^{-2} and anode loading of 6 mg cm^{-2} was found to be the optimum loading that could be used for water electrolysis. The Nafion®115 membrane proved to be the best ionomer membrane applied in this study. High current densities of 1329 mA cm^{-2} at 97 ^{o}C and 1.7 V were achieved when the correct choice of components as well as the optimum catalyst loading for anode and cathode was made but this was only achieved when the system parameters such as high operational temperature, optimum water flow rate, extensive moisturization time, correct current collector clamping pressure, proper insulation and low resistance electrical leads were implemented.

This study demonstrated that applying highly active electrocatalysts in the MEA is not the only factor requiring attention for improving cell output of the SPE electrolyzer. Various other factors such as ink formulations and deposition

conditions (adding different amounts of proton conductive phase as binder, loading different amounts of catalyst), components used (different catalysts or use of hydrophobic vs hydrophobic GDL), operational conditions (changing operating temperature, or moisturization time), as well as systemic components (such as electrical resistivity of leads, proper insulation, adequate water flow paths) may all affect the output of the cell. The multi-variant complexity of assembly, operation and testing an SPE electrolyzer makes this a very poor choice as system for testing catalyst activity per se or for assessing the quality of electrodes and even the most active catalyst will not enhance SPE cell performance unless other parameters are adequately addressed.

CHAPTER 8

8. OVERALL CONCLUSIONS

The summary of findings and the overall conclusions of the thesis are consolidated in this chapter. A summary of the contributions that this dissertation has made as well as recommendations for future research are then presented. A list of the outputs in terms of the peer reviewed publications and other presentations of this study are then provided as a citations list.

8.1 SUMMARY OF FINDINGS

South Africa, the main supplier of PGM metal, stands to benefit from diversification of Pt containing materials and developed capabilities in the emerging hydrogen economy. When hydrogen production cost can be reduced and the output increased, a viable hydrogen economy may be realized. An overview of the literature showed the necessity for improving electrolyzer systems for hydrogen production to facilitate the realization of the hydrogen economy. Diverse authors detail what the problems are that limit the large scale application of hydrogen from water electrolysis systems, which mainly is related to the cost of the components and excessive power consumption of operating electrolyzer systems.

The purpose of this study was the development of nanophase noble metal electrocatalysts based on high surface area supports and their application in composite gas diffusion electrodes, for improving the efficiency of hydrogen generation by water electrolysis through reduction of the overvoltage of electrolyzer systems. The development of a three dimensional array of active sites on electrodes was the main approach as the necessary catalytic activity has to date not yet been achieved on a two dimensional planar electrode element. Incorporation of nanophase components into electrolyzers required consideration of many aspects of assembly for integration into the working system.

Three dimensional macro-, meso- and microporous supports were therefore selected or developed as matrixes to stabilize nanophase electro active noble

metals in high dispersion and low agglomeration. Microporous zeolites such as FAU, mesoporous Si materials such as HMS and MCM-41, newly developed conductive mesoporous carbon (OMC), and carbon nanotubes (CNT) were explored as supports suitable for stabilizing electro catalytic nanoparticles. The characterization of these materials elucidated their porous nature and their stability. A CVD technique using LPG as a carbon source, pyrolized upon a mesoporous Si matrix, HMS, produced nanostructured ordered mesoporous carbon (OMC) with graphitic character after removing the Si matrix. The low angle XRD peak, observed for the HMS silica precursor and also the resulting OMC analogue of HMS, is a typical feature of mesoporous materials with pores in the region of 1-3 nm, and the porosity of the OMC was confirmed by N_2 adsorption and HRTEM. Selected area diffraction established that a crystalline graphitic material was formed in agreement with XRD results. This OMC is useful as a conductive three dimensional porous matrix for support of catalytic nanophase Pt metals.

Processes to incorporate active nanophase Pt metal electrocatalysts into microporous FAU, and mesoporous HMS or MCM-41 were developed. The influence of the nature and porosity of the catalyst support upon activity was demonstrated with Pt FAU< PtHMS=PtMCM-41 showing the beneficial effect of a nanometre sized porous structure compared to an Ångstrom sized porous support. Thus the pore size of the host matrix support is a significant parameter in preparing supported electrocatalysts.

Methods for preparing active nanophase Pt electrocatalysts on CNT or CNT paper substrates were developed. The nano-dimensions of the CNT fibres in the CNT paper that could be utilized as a gas diffusion layer, resulted in a material with macropores an order of magnitude smaller than the typical commercial carbon cloths applied as gas diffusion layers. The CNT paper also showed high conductance. Deposition of Pt on CNT paper by a simple galvanic displacement technique formed a new, highly conductive and active Pt gas diffusion electrode, eliminating the extensive processing required to prepare composite gas diffusion electrodes (GDE). It was found that the reduction potential of the sacrificial anode (Al, Fe, Pb foils) did not correlate with Pt deposition rate but bimetallic

systems were controlled by deposition time. CNT were also applied to prepare a Pt/CNT (propanol) electro catalyst via a wet chemical route using propanol and the analysis of its structure showed well dispersed Pt nanoparticles. The new electrocatalysts were compared to an industry standard commercial Pt catalyst stabilized on Vulcan carbon black for electro activity and in the case of the electro catalyst sample Pt/CNT_BP (Pb foil (20 min)) the anodic peak indicating the overpotential of hydrogen evolution (-0.68 V) was similar to the case observed in the Pt/CNT (propanol) sample (-0.66 V) and both peaks occurred at lower overpotentials than the commercial JM Pt40/C sample (-0.77 V) when cycled between -1100 and 1100 V at 50 mV s^{-1} and sensitivity of 100 µA V^{-1} in a $ClLiO_4$ (Ag/AgCl) system. Thus the use of CNT as support substrate and the Pt deposition techniques applied were shown to result in electrocatalysts that could reduce the energy requirements of the hydrogen evolution reaction.

Pt-FAU, Au–HMS, Pt-HMS and Pt-MCM were applied as examples of processing 3-dimensional supported nanophase materials, with high surface areas and high porosity, into supported films to form composite gas diffusion electrodes (GDE). Nanoparticles of Sb/SnO were used in preparation of such films, as an example of processing non-supported nanophase particulates into composite GDE. It was shown that Pt-FAU, Au–HMS, -HMS and Pt-MCM containing electrodes achieved current densities of ~650 mA cm^{-2} at 60 °C at an applied potential of -2V in an alkaline electrolyzer. It was found that nanophase Sb/SnO, a non noble nano particulate, could also be applied as electro catalyst for hydrogen production. Homogeneous distribution and loadings of nanophases on electrode substrates was dependent upon deposition method, substrate type, binder type as well as ink formulation.

Optimization of the ink formulation and the ink deposition method using screenprinting produced homogeneous and well dispersed layers of 0.001 - 0.0015 g cm^{-2} of electro catalyst per unit area of substrate. Substitution of isopropanol with 1,2 propandiol as solvent in inks resulted in an improvement of viscosity and viscoelasticity which was tailored by increasing the amount of water and solids in the formulation to print quality catalytic films on Nafion® substrates. Rheological determination of ink formulations gave good predictive

information of the printability of an ink upon paper. The optimum ink formulation had a ratio of between 3 - 1 : 1 of 1,2 propandiol : water, a liquid : solid ratio of between 6-8 : 1 and a storage modulus (G') of between 84 and 224. Reversible viscoelastic behaviour of inks correlated with good print quality. The morphology of the film was strongly affected by the ink formulation. Film quality depended upon the polarity and viscosity of the solvent, the printed layer thickness, the nature and the surface energy of the substrate. Hence, no matter how active the electro catalyst, if the deposition of the film on the GDE substrate is substandard, resistance will be high and electro activity low.

A method using of a paper substrate was developed to evaluate the electronic characteristics of films separately from the GDL substrate using Variable Field Hall measurements. Variable Field Hall measurements showed that the electronic characteristics of catalyst containing films could be separately evaluated from the substrate by use of the paper substrate method. The addition of a conductive fullerene nanophase to films printed upon Nafion® substrates may enhance the electron charge transfer. It was found that improving the film characteristics by improved ink formulations and print quality reduced the positive Sheet Hall Coefficient significantly and promoted n-type rather than p-type carriers. The substrate chosen as support for the electrocatalytic film was shown to have a very significant effect on the overall performance of the electrode. The difference in resistance observed could not be ascribed to catalyst loading only but also to the print quality and the conductive pathway created by adjoining clusters of printed electro catalyst, which was affected strongly by the ink formulation. CNT based Pt containing electrodes were studied and it was found that n-type carrier CNT paper with low resistance and high carrier density switched to a p-type carrier upon deposition of Pt by galvanic displacement.

Technological optimization of membrane electrode assemblies applicable in a solid polymer electrolyte electrolyzer resulted in a current density of 1.33A cm^{-2} at 97 ^{o}C and -1.7 V. Several of the commercially available components were not beneficial to improving cell output. Bekinit Titanium fibre substrate was the most promising anodic GDL catalyst support, and hydrophilic Lydall carbon cloth (6100-300 and 6100-200) was suitable as cathode GDL. A cathode loading of 1

mg cm^{-2} Pt/C and anode loading of 6 mg cm^{-2} IrO_2 was found to be the optimum catalyst loading using commercial catalysts. The Nafion®115 membrane proved to be the best ionomer membrane. High output was realized when system parameters such as operational temperature, water flow rate, moisturization time, current collector clamping pressure, insulation and low resistance electrical leads were optimized.

Various factors such as ink formulations and deposition conditions (adding different amounts of proton conductive phase as binder, loading different amounts of catalyst), components used (different catalysts or use of hydrophobic vs hydrophobic GDL), operational conditions (changing operating temperature, or moisturization time), as well as systemic components (such as electrical resistivity of leads, proper insulation, adequate water flow paths) may all affect the output of the SPE electrolyzer cell.

8.2 CONCLUSIONS

High dispersal of nanophase metals in three dimensional substrates enhanced the process of water electrolysis. Composite gas diffusion electrode surfaces containing nanophases resulted in high activity for hydrogen production because of high dispersion, high surface area and enhanced transport of reagents and products. Highly dispersed active nano sized Pt, Au, Ir and SnO components reduced the over voltage of electro catalytic reactions resulting in overall increase in energy efficiency of the processes. Nanophase electro catalytic materials were successfully incorporated into composite gas diffusion electrodes in catalytic films and maintained high catalytic activity for hydrogen production and achieved high electro- and proton conductivity. This study demonstrated that applying highly active electrocatalysts in the MEA is not the only factor requiring attention for improving cell output of the SPE electrolyzer. The multi-variant complexity of assembly, operation and testing an SPE electrolyzer makes this a very poor choice as system for testing catalyst activity per se or for assessing the quality of electrodes and even the most active catalyst will not enhance SPE cell performance unless other parameters are adequately addressed.

CHAPTER 8

8.3 SUMMARY OF CONTRIBUTIONS

In this dissertation the following contributions were made:

CHAPTER 3:
Demonstrated new route to make graphitic ordered mesoporous carbon that can be applied as nanophase metal catalyst support

Developed fabrication route for preparing CNT paper from multiwalled CNT

CHAPTER 4:
Developed routes to prepare nanophase Pt and Au electrocatalysts based on microporous (FAU zeolite) and mesoporous supports (HMS and MCM-41)

Demonstrated preparation and metal reduction procedures for fabricating nanophase electrocatalysts that can be easily upgraded to industrial conditions

Developed CVD route using LPG to deposit a conductive layer of carbon on Si matrix supported electrocatalysts

Demonstrated proof of concept of new route to use CNT paper as nanophase catalyst support by deposition of bimetallic nanophase electrocatalysts using a galvanic displacement technique

Demonstrated preparation procedure to directly incorporate the active nanophase bimetallic Pt containing particle on CNT paper suited as gas diffusion electrode thus eliminating the need for processing of pre-prepared electrocatalysts into films for deposition on substrates to form composite electrodes

Pt on CNT paper by a simple galvanic displacement technique formed a new, highly conductive and active Pt containing gas diffusion electrode

CHAPTER 8

CHAPTER 5:

Developed processing methodology by sequential deposition for incorporating and stabilizing supported or unsupported nanophase electrocatalysts into catalytic films as composite gas diffusion electrode materials for alkaline electrolyzer systems

Prepared new nanophase containing catalytic ink formulations that can be spraycoated for preparation of composite electrodes

Developed nanophase deposition procedures suitable for different substrate types to form composite electrodes containing nanophase electrocatalysts

Achieved techniques of electrode preparation incorporating supported nano materials for hydrogen production in alkaline electrolyzers

Developed rapid screening technique to screen materials for activity and durability in high electrolyte systems

Developed stable and durable nanophase nanophase containing composite gas diffusion electrodes capable of high current densities with high hydrogen production capacity

Demonstrated the suitability of various nanophase materials, proton and electron conductive phases, binders and solvents for composite formation on a variety of conductive substrates

Demonstrated the activity of microporous and mesoporous supported electrocatalytic nanoparticles in composite format for hydrogen production in alkaline electrolyzers

Demonstrated the activity of unsupported SbSnO nanoparticles in composite format for hydrogen production in alkaline electrolyzers

Fabricated electrodes containing nanophase particulates of Sb/SnO or supported electrocatalysts, Pt FAU, Pt MCM-41, Pt HMS or Au HMS composite GDE materials prepared with Nafion® as binder, with capability of current densities of between 600 and 750 mA cm^{-2} at 60 °C at an applied potential of -2 V in an alkaline electrolyzer.

CHAPTER 6:

Demonstrated an approach to achieving homogeneity and high dispersion of active nanophases in composite format by matching substrate and electro catalyst type

Demonstrated method to characterize homogeneity and high dispersion of the active metal component in composite gas diffusion electrodes using micro PIXE

Developed new nanophase containing catalytic ink formulations that are printable by the screenprinting technique

Developed methodology for direct screen printing of nanophase containing catalytic ink upon Nafion or other substrates

Developed screenprinting ink formulations with a ratio of between 3 - 1 : 1 of 1,2 propandiol:water, a liquid: solid ratio of between 6-8:1 and a storage modulus (G') of between 84 and 224.

Demonstrated the application of the Hall measurement technique for characterizing the electronic properties of films containing the nanophase electrocatalysts

Developed a paper substrate methodic that allowed the electronic characteristics of films to be evaluated separately from the substrate using Variable Field Hall measurements

CHAPTER 7:

Developed optimized process conditions for preparation of membrane electrode assemblies that are applicable to SPE electrolyzers and regenerative fuel cells

Developed stable and durable membrane electrode assemblies applicable to SPE electrolyzers

Demonstrated the role of process variables in the output of an SPE electrolyzer and the relative contribution of each variable upon the functionality of the system

Obtained overall increase in energy efficiency of the electrolysis process both in alkaline and SPE electrolysis systems

Developed a membrane electrode assembly fabrication process using Bekinit Titanium fibre anodic GDL catalyst support, and hydrophilic Lydall carbon cloth (6100-300 or 6100-200) cathode GDL with cathode loading of 1mg cm^{-2} Pt/C and anode loading of 6mg cm^{-2} IrO_2 and a Nafion®115 membrane, that produced a current density of 1.33A cm-2 at 97^{o}C and -1.7V

8.4 RECOMMENDATIONS AND FUTURE RESEARCH

Future work in composite preparation by sequential deposition should include the following aspects:

- Investigate other ratios, different loadings and different types of nanophase electrocatalysts should be investigated.
- The lowest required loading of noble metal on supports should be determined.
- The possibility to use nanophase metal oxides such as SnO should be further explored.
- The use of the new mesoporous conductive OMC substrate to support metals should be further evaluated and optimized.
- Binder to conductive phase ratios should be further optimized.

- More resilient supports that are also conductive should be sourced and used as substrates for hotpressing
- Other conductive binders should be investigated in spraycoating techniques as Nafion® is expensive.
- Processing techniques would need to be automated to prepare reproducible materials in a standardized manner.
- Processing techniques would need to be automated to prepare reproducible materials in a standardized manner.
- The benefit of higher activity of the newly developed electrocatalysts and gas diffusion electrodes should be explored in the SPE electrolyzer system.
- The optimum catalyst type for the O_2 evolution anode used in water electrolysis based upon bimetallic nanophase metal oxides should be explored in the form of physical admixtures with conductive binders
- Printing technologies such as screen printing or ink jet printing should be further explored
- Standardized fabrication procedures and high throughput screening techniques to screen materials for activity and durability.

8. 5 CITATIONS

Petrik, L. F.; Z. G. Godongwana; P. Ndungu; V. M. Linkov; and S. Liao. 2008. LPG synthesis of carbon analogue of HMS. In: Hadjiivanov, K.; V. Valtchev; S. Mintova; and G. Vayssilov (eds.). Topics in Chemistry and Material Science, Vol.1: Advanced Micro- and Mesoporous Materials. Sofia: Heron Press

L.F.Petrik, Z.G.Godongwana, E.I. Iwuoha. Platinum Nanophase Composite Gas Diffusion Electrodes. In Press: POWER Ms. Ref. No 10855. J. Power Sources (2008), doi:10.1016/j.jpowsour.2008.06.091

L. F. Petrik, Z. G. Godongwana, P. Ndungu, A. Nechaev, S.Liao, V. Linkov. Synthesis of Carbon Nanostructured Materials Using LPG. In Press: Ms. Ref. No.: MICMAT-D-08-00143. Microporous and Mesoporous Materials (2009), doi:10.1016/j.micromeso.2008.05.030

INTENDED PUBLICATIONS AND JOURNALS

Petrik, L. F., P. Ndungu, E.I. Iwuoha. 2008. Galvanic displacement technique for preparing gas diffusion electrodes based on carbon nanotubes. Submitted to J.Power Sources

Petrik, L.F. V.Fester, E.I. Iwuoha. 2008. Rheological characteristics of screenprinting ink formulations for the preparation of nanophase containing composite electrodes. (In preparation).

Petrik, L.F. M.Härting, D.T. Britton, E.I. Iwuoha. 2008. Electronic characteristics of nanophase containing composite electrodes. (In preparation). To be submitted to the J.Power Sources

REFERENCES

al-Abadleh Hind, A.; and V. H. Grassian. 2003. Oxide surfaces as environmental interfaces. *Surface Science Reports* 52 (3–4): 63–161.

Abaoud, H. A.; M. Ghouse; K. V. Lovell; and G. N. al-Motairy. 2005. A hybrid technique for fabricating PEMFC's low platinum loading electrodes. *International Journal of Hydrogen Energy* 30 (4): 385–91.

Abbott, S.. 2005a. Explaining moiré effects in screen printing. News release from MacDermid Autotype, Wantage, UK. In: Mayor, I. (ed.), *Printingtalk,* 18 February 2005. [*Printingtalk,* free e-mail newsletter.] London: Pro-Talk Ltd / Centaur Media plc. http://www.printingtalk.com/news/aot/aot109.html. [May 2008]

Abbott, S.. 2005b. Screen printing moiré—its main characteristics. News release from MacDermid Autotype, Wantage, UK. In: Mayor, I. (ed.), *Printingtalk*, 30 March 2005. [*Printingtalk,* free e-mail newsletter.] London: Pro-Talk Ltd / Centaur Media plc. http://www.printingtalk.com/news/aot/aot110.html. [May 2008]

Adora, S.; J. P. Simon; Y. Soldo-Olivier; R. Faure; E. Chaînet; and R. Durand. 2004. Electrochemical deposition of platinum nanoparticles on carbon: A study by standard and anomalous x-ray diffraction. *ChemPhysChem* 5 (8): 1178–84.

Ahmed, S. M.. 1986. The Canadian contribution to the I.E.A. [International Energy Agency] work on photoelectrolysis of water. *International Journal of Hydrogen Energy* 11 (10): 627–37.

Ahmed, S.; J. I. Shan; L. Petrik; and V. M. Linkov. 2004. Scanning electrochemical microscopic study of hydrogen oxidation and evolution at electrochemically deposited Pt nanoparticulate electrode incorporated in polyaniline. *Analytical Sciences* 20 (9): 1283–7.

Ahn, S.; and B. J. Tatarchuk. 1997. Fibrous metal–carbon composite structures as gas diffusion electrodes for use in alkaline electrolyte. *Journal of Applied Electrochemistry* 27 (1): 9–17.

Allen, E.; P. Smith; and J. Henshaw. 2001. A review of particle agglomeration. Report no. AEAT/R/PSEG/0398, 25 April 2001. Prepared for US Department of Energy (DOE). Contract no. DE-GI01-00EW-56054. http://www.tanks.org/ttgdoc/AEAT-R-PSEG-0398.doc. [May 2008]

Alonso, J. A.; and X. Turrillas. 2005. Location of H+ sites in the fast proton-conductor $(H_3O)SbTeO_6$ pyrochlore. *Journal of the Chemical Society, Dalton Transactions* 2005: 865–7.

AMIA Labs. 2005. Application note C01, Crystallite size and microstrain analysis of thin films. Leesburg, VA: AMIA Laboratories. http://amialabs.com/AppNoteC01.swf. [May 2008]

Andolfatto, F.; R. Durand; A. Michas; P. Millet; and P. Stevens. 1994. Solid polymer electrolyte water electrolysis: Electrocatalysis and long-term stability. *International Journal of Hydrogen Energy* 19 (5): 421–7.

Appleby, A. J.; and G. Crepy. 1979. Improvements in electrolysis technology in alkaline solutions. In: Veziroglu, T. N.; and W. Seifritz (eds.), *Hydrogen Energy System. Proceedings of the Second World Hydrogen Energy Conference (WHEC), Zurich, Switzerland, 21–24 August 1978 (Vol 1).* Oxford: Pergamon Press, 227–40.

REFERENCES

Ashida, T; T. Shimamune; Y. Nishiki. 1998. Gas diffusion electrode and electrolytic method using it. US Patent 5733430, issued 31/03/1998; Application No. 626924 filed on 04/03/1996; Assignee Permelec Electrode Ltd.

ASTM Standard F76–86. 2002. Standard test methods for measuring resistivity and Hall coefficient and determining Hall mobility in single-crystal semiconductors. *Annual Book of ASTM Standards, Vol. 10.04: Electronics; Declarable Substances in Materials*. West Conshohocken PA: ASTM International. http://www.astm.org/Standards/F76.htm. [May 2008]

Atkins, P. W.. 1989. *General Chemistry*. New York: Scientific American Books, distr. W. H. Freeman and Co., 644.

Bahar, B.; A. R. Hobson; and J. A. Kolde. 1997. Electrode apparatus containing an integral composite membrane. US patent 5635041, issued 1997/06/03. Application no. 567466, filed 1995/12/05. Assignee: W. L. Gore & Associates, Inc..

Bahar, B.; A. R. Hobson; and J. A. Kolde. 1997. Integral composite membrane. US patent 5599614, issued 1997/02/04. Application no. 561514, filed 1995/11/21. Assignee: W. L. Gore & Associates, Inc..

Barbir, F.. 2005. PEM electrolysis for production of hydrogen from renewable energy sources. *Journal of Solar Energy* 78 (5): 661–9.

Bard, A. J.; and L. R. Faulkner. 2001. Ch. 10, Techniques based on concepts of impedance. In: *Electrochemical Methods: Fundamentals and Applications*, 2 ed.. New York: John Wiley & Sons, 368–416.

Bard, A. J.; and L. R. Faulkner. 2001. *Electrochemical Methods: Fundamentals and Applications*, 2 ed.. New York: John Wiley & Sons, 137; 226–49; 376–87.

Barrer, R. M.. 1981. Zeolites and their synthesis. *Zeolites* 1 (3): 130–40.

Barrer, R. M.. 1982. *Hydrothermal Chemistry of Zeolites*. London: Academic Press.

Bass, L. J.; and G. L. Turner. 1997. Anion distributions in sodium silicate solutions. Characterization by ^{29}SI NMR and infrared spectroscopies, and vapor phase osmometry. *Journal of Physical Chemistry B* 101 (50): 10638–44.

Bauduin, P.; L. Wattebled; S. Schrödle; D. Touraud; and W. Kunz. 2004. Temperature dependence of industrial propylene glycol alkyl ether/water mixtures. *Journal of Molecular Liquids* 115 (1): 23–8.

Baughman, R. H.; A. A. Zakhidov; and W. A. de Heer. 2002. Carbon nanotubes—the route toward applications. *Science* 297 (5582): 787–92.

Beer, H. B.. 1969. Improvements in or relating to electrodes for electrolysis. British patent GB1147442, published 1969/04/02. Application no. 20133/65 (GB19650020133), filed 1965/05/12. Assignee: Chemnor Corporation AG (BR). http://www.wikipatents.com/gb/1147442.html. [May 2008]

Bekaert BFT. [nd]. About metal fibres. [What are metal fibres; metal fibre manufacturing – bundle drawing; shaving (Bekinit®); available forms/alloys; unique characteristics.] http://www.bekaert.com/bft/About%20metal%20fibres.htm. [May 2008]

Bekinit K. K. [nd]. Bekinit® sintered titanium fiber—Titanium porous structure. http://www.bekinit.co.jp/downloads/Engtitanium_outlined.PDF. [May 2008]

Bekinit K. K. The Metal Fiber Company. [Development, manufacture using metal fiber products. Joint venture between N.V. Bekaert S.A., Belgium, and Nippon

REFERENCES

Institute of Technology (NIT), Saitama Prefecture, Japan.] http://www.bekinit.co.jp/English/. [May 2008]

Beni, G.; S. Hackwood; and J. L. Jackel. 1982. Continuous electrowetting effect. *Applied Physics Letters* 40: 912.

Beni, G.; and J. L. Shay. 1978. Electrochromism of heat-treated anodic iridium oxide films in acidic, neutral, and alkaline solutions. *Applied Physics Letters* 33: 567.

Benning, P. J.; F. Stepniak; D. M. Poirier; J. L. Martins; J. H. Weaver; L. P. Chibante; and R. E. Smalley. 1993. Electronic properties of K-doped C60(111): Photoemission and electron correlation. *Physical Review B: Condensed Matter* 47 (20): 13843–7.

Benson, J.; G. Gericke; G. Mutemeri; W. Nel; L. Petrik; R. Pickering; R. Rossouw; and D. van Vuuren. 2006. South African fuel cell and hydrogen economy baseline study. CSIR File: Contract 86DB / HT544. Prepared for F. Molebatsi, Department of Science and Technology (DST) in July 2004. Issued in February 2006.

Bentham, J.. 2005. News: Shell opens hydrogen fueling site in DC. *Fuel Cells Bulletin.* 2005 (1) January: 5

Bessel, C. A.; and D. R. Rolison. 1997. Topological redox isomers: Surface chemistry of zeolite-encapsulated Co(salen) and $[Fe(bpy)_3]^{2+}$ complexes. *Journal of Physical Chemistry B* 101 (7): 1148–57.

Blouin M.; and D. Guay. 1997. Activation of ruthenium oxide, iridium oxide, and mixed Ru_xIr_{1-x} oxide electrodes during cathodic polarization and hydrogen evolution. *Journal of the Electrochemical Society* 144 (2): 573–81.

Bockris, J. O'M. (ed.). 1973. *Electrochemistry*. Vol. 6 of *Physical Chemistry Series 1*, ser. ed. A. D. Buckingham. London: Butterworth, 49–105.

Bradley, S. A.; M. J. Gattuso; and R. J. Bertolacini (eds.). 1989. *Characterization and Catalyst Development: An Interactive Approach* (ACS Symposium Series 411). Washington, DC: American Chemical Society, 279–85.

Breck, D. W.. 1973. *Zeolite Molecular Sieves: Structure, Chemistry and Use*. New York: John Wiley & Sons.

Brett, D. J. L.; S. Atkins; N. P. Brandon; N. Vasileiadis; V. Vesovic; and A. R. Kucernak. 2007. Membrane resistance and current distribution measurements under various operating conditions in a polymer electrolyte fuel cell. *Journal of Power Sources* 172 (1): 2–13.

Britton, D.T.; Odo, E.A.; Härting, M.. 2007. Thick Film Semiconducting Inks. WO/2007/072162. International Patent Application No.: PCT/IB2006/003666; Publication Date: 28.06.2007; International Filing Date: 18/12/2006

Bruce, J. Todd. 1996. Rustenburg and Johnson Matthey, An Enduring Relationship. Sixty-five years of continuous committed development. *Platinum Metals Review*. 40 (1) January: 2-7

Bulan, A.; F. Gestermann; H-D Pinter; P. Weuta; W. Klesper. 2005. Method for producing gas diffusion electrodes. US Patent 6838408, issued 04/01/2005. Application No. 10815711 filed on 04/02/2004; Assignee Bayer Material Science AG

Cabasso, I.; and Y. Yuan. 1998a. Gas diffusion electrode based on polyethersulfone carbon blends. Patent CA2213967, published 1998/02/27. Application no. CA19972213967, filed 1997/08/26. Applicant: Research Foundation of State University of New York (SUNY). Also published as JP10092439(A);

GB2316802(A); FR2755542(A1); DE19737389(A1); BR9704215(A); TW4040079B(B). [Canadian Intellectual Property Office (CIPO). Dead application 2003/08/26.] http://www.wikipatents.com/ca/2213967.html. [May 2008]

Cabasso, I.; and Y. Yuan. 1998b. Gas diffusion electrode based on polyethersulfone carbon blends. UK patent GB2316802 (GB9718153.1), published 1998/03/04. Application no. GB19970018153, filed 1997/08/27. Priorities: US08/697583, filed 1996/08/27. Applicant: Research Foundation of State University of New York (SUNY). [UK patents ceased 2002/08/27 (per Patents Office *Patents and Designs Journal* no. 5943, 16 April 2003).] http://www.wikipatents.com/gb/2316802.html. [May 2008]

Cabasso, I.; Y. Yuan; and C. Mittelsteadt. 2000. Blend membranes based on sulfonated poly(phenylene oxide) for enhanced polymer electrochemical cells. US patent 6103414, issued 2000/08/15. Application no. 133228, filed 1998/08/13. Assignee: Research Foundation of State University of New York (SUNY).

Cabasso, I.; Y. Yuan; and X. Xu. 1998. Gas diffusion electrodes based on poly(vinylidene fluoride) carbon blends. US patent 5783325, issued 1998/07/21. Application no. 697582, filed 1996/08/27. Assignee: Research Foundation of State University of New York (SUNY).

Cabot™ Corporation. [nd]. Creating what matters. [Global chemical manufacturer of carbon black, fumed metal oxides, tantalum, inkjet colourants, Nanogel® aerogels, masterbatch, conductive compounds, specialty fluids, micropowders, supermetals.] http://w1.cabot-corp.com/index.jsp. [May 2008]

Calvo, S. R.; and P. B. Balbuena. 2007. Theoretical analysis of reactivity on Pt(111) and Pt-Pd(111) alloys. *Surface Science* 601 (21): 4786–92.

Candusso, D.; J. P. Poirot-Crouvezier; B. Bador; E. Rullière; R. Soulier; and J. Y. Voyant. 2004. Determination of current density distribution in proton exchange membrane fuel cells. *The European Physical Journal Applied Physics (EJP AP)* 25 (1): 67–74.

Chhabra, P. P.; and J. F. Richardson. 1999. Ch. 1, Non-Newtonian fluid behaviour; and ch. 2, Rheometry for non-Newtonian fluids. *Non-Newtonian Flow in the Process Industries. Fundamentals and Engineering Applications.* Oxford: Butterworth-Heinemann, 1–36; 37–70.

Che, G.; B. B. Lakshmi; C. R. Martin; E. R. Fisher; and R. S. Ruoff. 1998. Chemical vapor deposition based synthesis of carbon nanotubes and nanofibers using a template method. *Chemistry of Materials* 10 (1): 260–7.

Chen, C. Y.; and C. S. Tsao. 2006. Characterization of electrode structures and the related performance of direct methanol fuel cells. *International Journal of Hydrogen Energy* 31 (3): 391–8.

Chen, G.; D. A. Delafuente; S. Sarangapani; and T. E. Mallouk. 2001. Combinatorial discovery of bifunctional oxygen reduction—water oxidation catalysts for regenerative fuel cells. *Catalysis Today* 67 (4): 341–55.

Chikae, M.; K. Idegami; K. Kerman; N. Nagatani; M. Ishikawa; Y. Takamura; and E. Tamiya. 2006. Direct fabrication of catalytic metal nanoparticles onto the surface of a screen-printed carbon electrode. *Electrochemistry Communications* 8 (8): 1375–80.

REFERENCES

Chirkov, Y. G.; and V. I. Rostokin. 2005. Calculating a characteristic bulk current density in the cathode of a hydrogen–oxygen fuel cell with a solid polymer electrolyte. *Russian Journal of Electrochemistry* 41 (9): 985–95.

Choi, B.-W.; S.-J. Chung; and D.-R. Shin. 1996. Microstructure of PTFE and acid absorption behavior in PTFE-bonded carbon electrodes. *International Journal of Hydrogen Energy* 21 (7): 541–6.

Choi, H. C.; M. Shim; S. Bangsaruntip; and H. Dai. 2002. Spontaneous reduction of metal ions on the sidewalls of carbon nanotubes. *Journal of the American Chemical Society* 124 (31): 9058–9.

Chwang, R.; B. J. Smith; and C. R. Crowell. 1974. Contact size effects on the Van der Pauw method for resistivity and Hall coefficient measurement. *Solid-State Electronics* 17 (12): 1217–27.

Cornell, R. W.; J. Casteel Holiway; and A. P. Holloway. 2008. Thermal printing of silver ink. US patent 7316475, issued 2008/01/08. Application no. 10985708, filed 2004/11/10. http://www.patentstorm.us/patents/7316475.html. [May 2008]

Corrosion Doctors. [nd]. What is an overpotential? www.corrosion-doctors.org/Corrosion-Kinetics/Overpotential_definition.htm. [May 2008]

Corrosion Source. [nd]. The exchange current. [Definition and variables affecting exchange current density.] www.corrosionsource.com/technicallibrary/corrdoctors/Modules/Kinetics/Exchange.htm. [May 2008]

Cox, P; S.-Y. Cha; G. Hou; N. Tran; and A. Duong. 2005. Catalyst agglomerates for membrane electrode assemblies. US patent 6911411, issued 2005/06/28. Application no. 10301131, filed 2002/11/21. Assignee: Polyfuel, Inc..

Crow, D. R.. 1994. *Principles and Applications of Electrochemistry*, 4 ed.. Glasgow: Blackie Academic and Professional, 129–50.

Cyberspace Chemistry (CaCt). 2008. The Liquid State. [http://www.science.uwaterloo.ca/~cchieh/cact/c123/liquid.html]

Dabak, T.; and O. Yucel. 1987. Modelling of the concentration and particle size distribution effects on the rheology of highly concentrated suspensions. *Powder Technology* 52 (3): 193–206.

Da Silva, L. A.; V. A. Alves; M. A. P. da Silva; S. Trasatti; and J. F. C. Boodts. 1997. Oxygen evolution in acid solution on IrO_2+TiO_2 ceramic films. A study by impedence, voltammetry and SEM. *Electrochimica Acta* 42 (2): 271–81.

Davenport, R. J.; F. H. Schubert; and D. J. Grigger. 1991. Space water electrolysis: Space station through advanced missions. *Journal of Power Sources* 36 (3): 235–50.

Davis, R. 1999. Identifying, understanding, and controlling tertiary moiré. When separation angles clash. *Screenweb*, 15 December 1999. [Companion site for *ScreenPrinting* magazine.] Cincinnati, OH: Screenweb, ST Media Group International. http://www.screenweb.com/index.php/channel/1/id/4/. [May 2008]

De Castro, E. S.. 1996. The electrochemistry of gases: New sensing opportunities. *Watts New* (Quarterly newsletter of Electrosynthesis Co., Inc.) 2 (1): [np]. http://www.electrosynthesis.com/news/w2content.html. [May 2008]

De Jong, K. P.; and J. W. Geus. 2000. Carbon nanofibers: Catalytic synthesis and applications. *Catalysis Reviews—Science and Engineering* 42 (4): 481–510.

REFERENCES

DEK® International. 2007. Fuel cells. [Screen printing processes and technologies for commercial high-volume fuel-cell production – process challenges – manufacturing challenges – screens and stencils – enclosed head printing – fuel cell successes.] http://www.dek.com/web.nsf/dek/fuel_cell. [May 2008]

DeMarinis, M.; E.S. De Castro; R.J. Allen; K. Shaikh. 2002. Structures and methods of manufacture for gas diffusion electrodes and electrode components US Patent 6444602, issued 03/09/2002; Application No. 715458 filed on 14/11/2000

Ding H.; Feng Y.; and Liu J.. 2007. Preparation and properties of Ti/SnO_2-Sb_2O_5 electrodes by electrodeposition. *Materials Letters* 61 (27): 4920–3.

Divisek J.; and H. Schmitz. 1984. Electrolyzer for alkaline water electrolysis. US patent 4445994, issued 1984/05/01. Application no. 06/351408, filed 1982/02/23. Assignee: Kernforschungsanlage Jülich GmbH (DE). http://www.patentstorm.us/patents/4445994.html. [May 2008]

Du, L.; S. Huiyu, Y. Xu, S. Liao, L.F. Petrik. 2008. A novel hollow sphere mesoporous material synthesized by using DADD template and embedding Nd into framework simultaneously. *Microporous and Mesoporous Materials* 113: 261–7

Ebbing, D. D.. 1993. *General Chemistry*, 4 ed.. Boston: Houghton Mifflin Co., 743–819.

Eckl, R.; R. Grinzinger; and W. Lehnert. 2006. Current distribution mapping in polymer electrolyte fuel cells—A finite element analysis of measurement uncertainty imposed by lateral currents. *Journal of Power Sources* 154 (1): 171–9.

EEEL-NIST. 2008. Electronics and Electrical Engineering Laboratory publications. National Institute of Standards and Technology (NIST). http://www.eeel.nist.gov/812 [May 2008]

Eggins, B. R.. 2002. *Chemical Sensors and Biosensors*. New York: John Wiley & Sons.

Eikerling, M.; S. J. Paddison; L. R. Pratt; and T. A. Zawodzinski, Jr. 2003. Defect structure for proton transport in a triflic acid monohydrate solid. *Chemical Physics Letters* 368 (1–2): 108–14. http://nrc.org/publ/ICCN2002/307.pdf. [May 2008]

Elumalai, P.; Vasan, H. N.; Munichandraiah, N.; Shivashankar, S. A.. 2002. Kinetics of hydrogen evolution on submicron size Co, Ni, Pd and Co-Ni alloy powder electrodes by DC polarization and AC impedence studies. *Journal of Applied Electrochemistry* 32 (9): 1005–10.

Ertl, G.; H. Knözinger; and J. Weitkamp (eds.). 1997. *Handbook of Heterogeneous Catalysis*. 5 vols.. Weinheim, Germany: Wiley-VCH.

Erwin A., Minister of Public Enterprises. 24 Feb 2006. The challenges facing South Africa's power-generation sector. [E-mail transcript, circulated by ESKOM.]

Etek, 2008. http://www.etek-inc.com/standard/product_GDL%20LT.php?prodid=56 [May 2008]

Feijen, E. J. P.; J. A. Martens; and P. A. Jacobs. 1997. Hydrothermal zeolite synthesis. In: Ertl, G.; H. Knözinger; and J. Weitkamp (eds.), *Handbook of Heterogeneous Catalysis*. Weinheim, Germany: Wiley-VCH.

Franco, R. W. A.; J. P. Donoso; C. J. Magon; C. B. Rodella; A. O. Florentino; M. J. Saeki; J. M. Pernaut; and A. L. de Oliveira. 1998. Electric and magnetic properties of polymer electrolyte/carbon black composites. *Solid State Ionics* 113–5: 149–60.

REFERENCES

Fresener, S. 2008. Glossary of screenprinting terms. Tempe, AZ: US Screen Print and Inkjet Technology. http://www.screenprinters.net/articles.php?art=33. [May 2008]

Freunberger, S. A.; M. Reum; A. Wokaun; and F. N. Büchi. 2006. Expanding current distribution measurement in PEFCs to sub-millimeter resolution. *Electrochemistry Communications* 8 (9): 1435–8.

Frost and Sullivan Research Service. 2003. D270, Renewable Energy Technologies: Global Developments (Technical Insights). (Published 23 December 2003.) www.frost.com/prod/servlet/report-brochure.pag?id=D270-01-00-00-00.

Frost and Sullivan Research Service. 2004. D318, Hydrogen Storage—Advances in Hydrogen Production and Storage Technologies (Technical Insights). (Published 13 December 2004.) www.frost.com/prod/servlet/report-brochure.pag?id=D318-01-00-00-00.

Fuertes, A. B.; and D. M. Nevskaia. 2003. Control of mesoporous structure of carbons synthesised using a mesostructured silica as template. *Microporous and Mesoporous Materials* 62 (3): 177–90.

Furuya, N.. 2001. Gas diffusion electrode, method for manufacturing the same and fuel cell using it. International patent no. WO/2001/094668, published 2001/12/13. International application no. PCT/JP2001/004693, filed 2001/06/04. (WIPO).

Furuya, N.. 1997. Gas diffusion electrode. US Patent 5618392, issued 08/04/1997; Application No. 421840 filed on 04/13/1995; Assignee Tanaka Kikinzoku Kogyo K.K.Furuya; Nagakazu

Furuya, N.; and H. Aikawa. 2000. Comparative study of oxygen cathodes loaded with Ag and Pt catalysts in chlor-alkali membrane. *Electrochimica Acta* 45 (25–26): 4251–6.

Furuya, N.; and H. Aikawa. 1999. A study of the gas-diffusion electrodes for chlor-alkali membrane cell. In: Burney, H. S.; N. Furuya; F. Hine; and K. Ohta (eds.), *Chlor Alkali and Chlorate Technology: R. B. MacMullin Memorial Symposium, Honolulu, Hawaii, Fall 1999.* Pennington, NJ: Electrochemical Society. PV99-21: 180.

Furuya, N.. 2001. http://www.electrochem.org/dl/ma/206/pdfs/1834.pdf and www.aba-brno.cz/aba2002/abstracts/24.pdf [May 2008]

Gaudet, J.; A. C. Tavares; S. Trasatti; and D. Guay. 2005. Physicochemical characterization of mixed RuO_2-SnO_2 solid solutions. *Chemistry of Materials* 17 (6): 1570–9.

General Electric Company. 1981. Solid polymer electrolyte water electrolysis technology development for large-scale hydrogen production. DE82010876, Final report for the period October 1977–November 1981. [Report no. DOE/ET/26202-1; covers portions of General Electric Electrolyte Bulk Hydrogen Water Electrolysis Development Program sponsored by DOE from October 1997 to November 1981, under contract no. AC02-78ET26202.] Wilmington, MA: General Electric Company; and US DOE.

Ghosh, P. C.; T. Wüster; H. Dohle; N. Kimiaie; J. Mergel; and D. Stolten. 2006. In situ approach for current distribution measurement in fuel cells. *Journal of Power Sources* 154 (1): 184–91.

Ginter, D. M.; C. J. Radke; and A. T. Bell. 1989. Applications of MAS-NMR spectroscopy to the study of faujasite synthesis. In: Jacobs, P. A.; and R. A. van

REFERENCES

Santen (eds.), *Zeolites: Facts, Figures, Future.* Vol. 49A of *Studies in Surface Science and Catalysis*. Amsterdam: Elsevier Science Publishers B.V., 161–8.

Giz, M. J.; M. C. Marengo; E. A. Ticianelli; and E. R. Gonzalez. 2003. Electrochemical and physical characterization of Ni-Cu-Fe alloy for chlor-alkali hydrogen cathodes. *Eclética Química* (São Paulo) 28 (2): 21–8.

Godongwana, Z. G.. 2006. Homogeneity of nanophase electrocatalysts supported on mesoporous materials. Unpublished MSc thesis. Department of Chemistry, University of the Western Cape.

Goldemberg, J. (ed.); and United Nations Development Programme (UNDP). 2000. *World Energy Assessment. Energy and the Challenge of Sustainability*. New York: UNDP, UN-DESA, and World Energy Council, 221. http://www.undp.org/energy/weapub2000.htm. [May 2008]. Download individual chapters or overview *WEA in Brief* [42 pp.]: http://www.undp.org/activities/wea/draft-start.html.

Görgün, H.. 2006. Dynamic modelling of a proton exchange membrane (PEM) electrolyzer. *International Journal of Hydrogen Energy* 31 (1): 29–38.

Govindaraj, A.; S. R. C. Vivekchand; and C. N. R. Rao. 2007. Novel vapor phase reactions for the synthesis and modification of carbon nanotubes and inorganic nanowires. *Journal of Nanoscience and Nanotechnology* 7 (6): 1695–702.

Greenwinds. 2002. Electrolyzers. [Introduction and overview – process details – glossary.] http://www.pege.org/greenwinds/electrolyzer.htm. [May 2008]

Grigor'ev, S. A.; A. A. Kalinnikov; V. I. Porembskii; I. E. Baranov; E. V. Borisova; and V. N. Fateev. 2004. Optimization of mass transfer processes in the zone of the air electrode of a fuel cell with a solid polymer electrolyte. *Russian Journal of Electrochemistry* 40 (11): 1188–92.

Grigoriev, S. A.; V. I. Porembsky; and V. N. Fateev. 2006. Pure hydrogen production by PEM electrolysis for hydrogen energy. *International Journal of Hydrogen Energy* 31 (2): 171–5.

Grubb, W. T.. 1957. Ion-exchange batteries. In: *Proceedings of the 11th Annual Battery Research and Development Conference, Atlantic City, N.J., 22–23 May 1957*. Red Bank, NJ: PSC Publications Committee, 5–8.

Grün, M.; K. K. Unger; A. Matsumoto; and K. Tsutsumi. 1999. Novel pathways for the preparation of mesoporous MCM-41 materials: Control of porosity and morphology. *Microporous and Mesoporous Materials* 27 (2–3): 207–16.

Guan, Y.; J. X. Sun; and M. N. Sun. 2006. Metal colloid dispersions and their aqueous metal inks. USPTO application no. 20060044382, filed 2006/03/02.

Guo, J. W.; T. S. Zhao; J. Prabhuram; R. Chen; and C. W. Wong. 2005. Preparation and characterization of a PtRu/C nanocatalyst for direct methanol fuel cells. *Electrochimica Acta* 51 (4): 754–63.

Hackwood, S.; A. H. Dayem; and G. Beni. 1982. Amorphous-nonmetal to crystalline-metal transition in electrochromic iridium oxide films. *Physical Review B: Condensed Matter* 26 (2): 471–8.

Hamann, C. H.; A. Hamnett; and W. Vielstich. 1998. *Electrochemistry*. Weinheim, Germany: Wiley-VCH Verlag GmbH, 143–50; 216–24.

Hampden Smith, M.; P. Atanassova; O. Atanassov; and T. Kodas. 2003. Ch 40, Manufacture of electrocatalyst powders by a spray-based production platform (polymer electrolyte membrane fuel cells, PEMFC). In: Vielstich, W.; A. Lamm;

REFERENCES

and H. A. Gasteiger (eds.), *Handbook of Fuel Cells: Fundamentals, Technology and Applications.* Vol 3, *Fuel Cell Technology and Applications* (Part 1). West Sussex: John Wiley & Sons, 497–508.

Hartland S.. (ed.). 2004. *Surface and Interfacial Tension: Measurement, Theory, and Applications*, New York, Marcel Dekker, 425 – 81.

Hartmann, M.. 2005. Ordered mesoporous materials for bioadsorption and biocatalysis. *Chemistry of Materials* 17 (18): 4577–93.

Hashimoto, K.; T. Sasaki; S. Meguro; and K. Asami. 2004. Nanocrystalline electrodeposited Ni-Mo-C cathodes for hydrogen production. *Materials Science and Engineering A* 375–7: 942–5.

Hayashi, K.; and N. Furuya. 2004. Preparation of gas diffusion electrodes by electrophoretic deposition. *Journal of the Electrochemical Society* 151 (3): A354–7.

Hijikata, T.. 2002. Research and development of international clean energy network using hydrogen energy (WE-NET). *International Journal of Hydrogen Energy* 27 (2): 115–29.

Hine, F.; M. Yasuda; T. Noda; T. Yoshida; and J. Okuda. 1979. Electrochemical behavior of the oxide-coated metal anodes. *Journal of the Electrochemical Society* 126 (9): 1439–45.

Ho, L.-W.; C.-P. Hwang; J.-F. Lee; I. Wang; and C.-T. Yeh. 1998. Reduction of platinum dispersed on dealuminated beta zeolite. *Journal of Molecular Catalysis A: Chemical* 136 (3): 293–9.

Hoogers, G. (ed.). 2003. *Fuel Cell Technology Handbook*. Boca Raton, FL: CRC Press.

Horibe, A.; S. Fukusako; M. Yamada; and K. Fumoto. 1997. Surface tension of aqueous binary solutions at low temperatures. *International Journal of Thermophysics* 18 (2): 387–96.

Horkans, J.; and M. W. Shafer. 1977. An investigation of the electrochemistry of a series of metal dioxides with rutile-type structure: MoO_2, WO_2, ReO_2,RuO_2, OsO_2, and IrO_2. *Journal of the Electrochemical Society* 124 (8): 1202–7.

Hrussanova, A.; E. Guerrini; and S. Trasatti. 2004. Thermally prepared Ti/RhO_x electrodes IV: O_2 evolution in acid solution. *Journal of Electroanalytical Chemistry* 564 (Special issue): 151–7.

HyWeb Gazette. Online newsletter of Ludwig-Bölkow-Systemtechnik GmbH (LBST) and the German Hydrogen Association (DWV). http://www.hydrogen.org/News/gazette.htm. [May 2008]

IEA Renewable Energy Working Party. 2002. *Renewable Energy into the Mainstream*. Paris: International Energy Agency (IEA). [54 pp.]. www.iea.org/textbase/nppdf/free/2000/Renew_main_2003.pdf. Adapted from: Goldemberg, J. (ed.); and United Nations Development Programme (UNDP). 2000. *World Energy Assessment. Energy and the Challenge of Sustainability*. [500 pp.]. New York: UNDP, UN-DESA, and World Energy Council. [May 2008]

Iijima, S.. 1991. Helical microtubules of graphitic carbon. *Nature* 354: 56–8.

Iijima, S.; and T. Ichihashi. 1993. Single-shell carbon nanotubes of 1-nm diameter. *Nature* 363: 603–5.

REFERENCES

Ikhsan, J.; B. B. Johnson; and J. D. Wells. 1999. A comparative study of the adsorption of transition metals on kaolinite. *Journal of Colloid and Interface Science* 217 (2): 403–10.

Imarisio, G.; and A. S. Strub (eds.); Commission of the European Communities. 1983. *Hydrogen as an Energy Carrier: Proceedings of the 3rd International Seminar, Lyon, 25–27 May 1983*. Dordrecht, Holland: D. Reidel Publishing Co.. [Sold and distributed in the USA and Canada by Kluwer Academic Publishers, Hingham MA, and in all other countries by Kluwer Academic Publishers Group, Dordrecht, Holland.]

International Union of Pure and Applied Chemistry (IUPAC); McNaught, A. D.; and A. Wilkinson (compilers). 1997. *IUPAC Compendium of Chemical Terminology ('The Gold Book')*, 2 ed.. London: Blackie Scientific Publications. PDF version: http://old.iupac.org/publications/compendium/. [May 2008]

International Union of Pure and Applied Chemistry (IUPAC); Nic, M.; J. Jirak; and B. Kosata. 2005. *IUPAC Compendium of Chemical Terminology ('The Gold Book')*. Advanced XML version: http://goldbook.iupac.org/. [May 2008]

IZA_online, 2008. International Zeolite Association 2008. http://www.IZA_online.com [May 2008]

Ioroi, T.; N. Kitazawa; K. Yasuda; Y. Yamamoto; and H. Takenaka. 2001. IrO_2-deposited Pt electrocatalysts for unitized regenerative polymer electrolyte fuel cells. *Journal of Applied Electrochemistry* 31 (11): 1179–83.

Ioroi T.; N. Kitazawa; K. Yasuda; Y. Yamamoto; and H. Takenaka. 2000. Iridium oxide/platinum electrocatalysts for unitized regenerative polymer electrolyte fuel cells. *Journal of the Electrochemical Society* 147 (6): 2018–22.

Ioroi, T.; T. Oku; K. Yasuda; N. Kumagai; and Y. Miyazaki. 2003. Influence of PTFE coating on gas diffusion backing for unitized regenerative polymer electrolyte fuel cells. *Journal of Power Sources* 124 (2): 385–9.

Ioroi, T.; K. Yasuda; Z. Siroma; N. Fujiwara; and Y. Miyazaki. 2002. Thin film electrocatalyst layer for unitized regenerative polymer electrolyte fuel cells. *Journal of Power Sources* 112 (2): 583–7.

Ivy, J.. 2004. *Summary of Electrolytic Hydrogen Production: Milestone Completion Report.* NREL/MP-560-36734 [replaces 560-35948], September 2004. [27 pp.]. DOE Contract no. AC36-99-GO10337. Golden, CO: National Renewable Energy Laboratory (NREL). http://www/nrel.gov/publications. [May 2008]

Iwuoha, E. I.; S. E. Mavundla; V. S. Somerset; L. F. Petrik; M. J. Klink; M. Sekota; and P. Bakers. 2006. Electrochemical and spectroscopic properties of fly ash–polyaniline matrix nanorod composites. *Microchimica Acta* 155 (3–4): 453–8.

Jakšić, M. M.. 1984. Electrocatalysis of hydrogen evolution in the light of the Brewer–Engel theory for bonding in metals and intermetallic phases. *Electrochimica Acta* 29 (11): 1539–50.

Janssen, H.; J. C. Bringmann; B. Emonts; and V. Schroeder. 2004. Safety-related studies on hydrogen production in high-pressure electrolysers. *International Journal of Hydrogen Energy* 29 (7): 759–70.

Jarvi, T. D; and E. M. Stuve. 1998. Fundamental aspects of vacuum and electrocatalytic reactions of methanol and formic acid on platinum surfaces. In: Lipkowski, J; and P. N. Ross, Jr. (eds.), *Electrocatalysis*. New York: Wiley-VCH, 75–153.

REFERENCES

Jiang, L.; G. Sun; Z. Zhou; S. Sun; Q. Wang; S. Yan; H. Li; J. Tian; J. Guo; B. Zhou; and Q. Xin. 2005. Size-controllable synthesis of monodispersed SnO_2 nanoparticles and application in electrocatalysts. *Journal of Physical Chemistry B* 109 (18): 8774–8.

Johnson Matthey™. [nd]. HiSPEC® Catalyst Datasheet. http://www.johnsonmattheyfuelcells.com/HiSPEC_Datasheet.pdf. [May 2008]

Jordan, L. R.; A. K. Shukla; T. Behrsing; N. R. Avery; B. C. Muddle; and M. Forsyth. 2000. Effect of diffusion-layer morphology on the performance of polymer electrolyte fuel cells operating at atmospheric pressure. *Journal of Applied Electrochemistry* 30 (6): 641–6.

Juda, W.; A.B. Ilan. 1986. Polymeric hydrogel-containing gas diffusion electrodes and methods of using the same in electrochemical systems. US Patent 4614575, issued 30/09/1986; Application No. 06/673041 filed on 19/11/1984; Assignee: Prototech Company.

Jung, U. H.; K. T. Park; E. H. Park; and S. H. Kim. 2006. Improvement of low-humidity performance of PEMFC by addition of hydrophilic SiO_2 particles to catalyst layer. *Journal of Power Sources* 159 (1): 529–32.

Kaisheva, A.. 2004. Comparative methods for gas-diffusion electrodes diagnostics. In: Stoynoy, Z.; and D. Vladikova (eds.), *Proceedings of International Workshop 'Advanced Techniques for Energy Sources Investigation and Testing', Sofia, Bulgaria, 4–9 September 2004*. Sofia: Centre of Excellence POEMES Series.

Kato, T.; M. Kubota; N. Kobayashi; and Y. Suzuoki. 2005. Effective utilization of by-product oxygen from electrolysis hydrogen production. (Paper presented at annual meeting of International Energy Workshop (IEW), held at IIASA, Laxenburg, Austria, 24–26 June 2003. www.iiasa.ac.at/Research/ECS/IEW2003/Papers/2003P_kato.pdf.) *Journal of Energy* 30 (14): 2580–95.

Kawar, P. K.; P. S. Chigare; and P. S. Patil. 2003. Substrate temperature dependent structural, optical and electrical properties of spray deposited iridium oxide thin films. *Applied Surface Science* 206 (1–4): 90–101.

Kendall, T. 2006. *Platinum 2006:* Johnson Matthey plc, London: 1-52

Khaselev, O.; A. Bansal; and J. A. Turner. 2001. High-efficiency integrated multijunction photovoltaic/electrolysis systems for hydrogen production. *International Journal of Hydrogen Energy* 26 (2): 127–32.

Kim, C. S.; Y. G. Chun; D. H. Peck; and D. R. Shin. 1998. A novel process to fabricate membrane electrode assemblies for proton exchange membrane fuel cells. *International Journal of Hydrogen Energy* 23 (11): 1045–8.

Kim, T. W.; I. S. Park; and R. Ryoo. 2003. A synthetic route to ordered mesoporous carbon materials with graphitic pore walls. *Angewandte Chemie* (International Edition) 42 (36): 4375–9.

Kinoshita, K. 1988. *Carbon: Electrochemical and Physicochemical Properties*. New York: Wiley, 147.

Kitoh, K., H. Schönfelder; and H. Nemoto. 1997. Nanostructure criteria for lithium intercalation in non-doped and phosphorus-doped hard carbons. (From 8th International Meeting on Lithium Batteries (IMLB-8), Nagoya, Japan, 16 June 1996. Part II, poster presentations.) *Journal of Power Sources* 68 (2): 258–62.

REFERENCES

Kondoh, M.; N. Yokoyama; C. Inazumi; S. Maezawa; N. Fujiwara; Y. Nishimura; K. Oguro; and H. Takenaka. 2000. Development of solid polymer-electrolyte water electrolyser. *Journal of New Materials for Electrochemical Systems* 3 (1): 61–5.

Koryta, J.. 1986. *Ions, Electrodes and Membranes*, 2 ed.. New York: John Wiley & Sons.

Koryta, J.; J. Dvorak; and L. Kavan. 1993. *Principles of Electrochemistry*, 2 ed.. Chichester and New York: John Wiley & Sons, 253–79.

Kramer, D.; S. A. Freunberger; R. Flückiger; I. A. Schneider; A. Wokaun; F. N. Büchi; and G. G. Scherer. 2008. Electrochemical diffusimetry of fuel cell gas diffusion layers. *Journal of Electroanalytical Chemistry* 612 (1): 63–77.

Krätschmer, W.; L. D. Lamb; K. Fostiropoulos; and D. R. Huffman. 1990. Solid C60: A new form of carbon. *Nature* 347: 354–8.

Kresge, C. T.; M. E. Leonowicz; W. J. Roth; J. C. Vartuli; and J. S. Beck. 1992. Ordered mesoporous molecular sieves synthesized by a liquid-crystal template mechanism. *Nature* 359: 710–12.

Kruss, 2008 USA Technical note#306,; http://higheredbcs.wiley.com/legacy/college/cutnell/0471713988/ste/ste.pdf [May 2008]

Kuch, W.; M. Schulze; W. Schnurnberger; K. Bolwin; and B. Bunsenges. 1993. Kinetics of H_2O adsorption and clean potassium precovered nickel (III) surfaces. *Journal of Physical Chemistry* 97 (3): 356–9.

Kudryashov, I. V.; and E. S. Burmistrov. 1970. Kinetics of the cathodic evolution of hydrogen on single crystals of Ni-CO-Fe ternary alloys. *Elektrokhimiya* 6 (8): 1153–5.

Kudryashov, I. V.; E. S. Burmistrov; and V. L. Kirlis. 1970. Kinetics of the cathodic evolution of hydrogen from single-crystal Ni-CO alloys in various media. *Electrokhimiya* 6 (5): 737–41.

Labrincha, J. A.; L.-J. Meng; M. P. dos Santos; F. M. B. Marques; and J. R. Frade. 1993. Evaluation of deposition techniques of cathode materials for solid oxide fuel cells. *Materials Research Bulletin* 28 (2): 101–9.

Laitinen, H. A.; and Thornton, D. C.. 1981. Thin platinum films on tin oxide substrates. US patent 4273624, issued 1981/06/16. Application no. 06/024531, filed 1979/03/28. Assignee: Board of Regents, State of Florida, for the use and benefit of.

Landel, R. F.; B. G. Moser; and A. J. Bauman. 1965. Rheology of concentrated suspensions: Effect of a surfactant. In: Lee, E. H. (ed.), *Proceedings of the Fourth International Congress on Rheology, Brown University, Providence, Rhode Island, 26–30 August 1963* (Parts 1–4), Part 2. New York: Interscience Publishers, 663–92.

Langley, P. J.; and J. Hulliger. 1999. Nanoporous and mesoporous organic structures: New openings for materials research. *Chemical Society Reviews* 28: 279–91.

Lee, C.-H.; S.-C. Wang; C.-J. Yuan; M.-F. Wen; and K.-S. Chang. 2007. Comparison of amperometric biosensors fabricated by palladium sputtering, palladium electrodeposition and Nafion/carbon nanotube casting on screen-printed carbon electrodes. *Biosensors and Bioelectronics* 22 (6): 877–84.

REFERENCES

Lee, H.-K.; J.-H. Park; D.-Y. Kim; and T.-H. Lee. 2004. A study on the characteristics of the diffusion layer thickness and porosity of the PEMFC. *Journal of Power Sources* 131 (1–2): 200–6.

Lee, J.; J. Kim; and T. Hyeon. 2006. Recent progress in the synthesis of porous carbon materials. *Advanced Materials* 18 (16): 2073–94.

Lee, S. J.; S. Mukerjee; J. McBreen; Y. W. Rho; Y. T. Kho; and T. H. Lee. 1998. Effects of Nafion impregnation on performances of PEMFC electrodes. *Electrochimica Acta* 43 (24): 3693–701.

Lee, T. H.; S. Wang; S. E. Dorris; and U. Balachandran. 2004. Hydrogen production by high-temperature water splitting using electron-conducting membranes. US patent 6726893, issued 2004/04/27. Application no. 10245039, filed 2002/09/17. Assignee: University of Chicago.

Li, N.; C. R. Martin; and B. Scrosati. 2000. A high-rate, high-capacity, nanostructured tin oxide electrode. *Electrochemical and Solid-State Letters* 3 (7): 316–8.

Li, N.; C. J. Patrissi; G. Che; and C. R. Martin. 2000. Rate capabilities of nanostructured $LiMn_2O_4$ electrodes in aqueous electrolyte. *Journal of the Electrochemical Society* 147 (6): 2044–9.

Li, W. Z.. 2003. The research of cathode carbon support platinum catalyst for direct methanol fuel cell. Published PhD thesis. Dalian Institute of Chemical Physics (DICP), Chinese Academy of Sciences, Dalian, People's Republic of China.

Li, W.; W. Zhou; H. Li; Z. Zhou; B. Zhou; G. Sun: and Q. Xin. 2004. Nanostructured Pt-Fe/C as cathode catalyst in direct methanol fuel cell. *Electrochimica Acta* 49 (7): 1045–55.

Liao S; V. M. Linkov; and L. F. Petrik. 2004. Anodic oxidation of ethanol on inorganic membrane-based electrodes. *Applied Catalysis A: General* 258 (2):183–8.

Liao S; V. M. Linkov; and L. F. Petrik. 2002a. Electrooxidation of methanol over a membrane-based electrode and effect of tungsten and molybdenum on the activity. *Applied Catalysis A: General* 235 (1–2): 149–55.

Liao S; V. M. Linkov; and L. F. Petrik. 2002b. Preparation and measurement of inorganic proton conductive membrane for fuel cell. *Battery Bimonthly* (Chinese) 32 (3): 159.

Liao, S.; J. Shan; V.M. Linkov; L.F. Petrik. 2003. Preparation and structure characterization of a mesoporous solid superacid catalyst SO_4^{2-}/Zr-HMS Department of Applied Chemistry, South China University of Technology, Canton, Peop. Rep. China. *Gaodeng Xuexiao Huaxue Xuebao* , 24(3), 469-472. CODEN: KTHPDM ISSN: 0251-0790. Journal written in Chinese. CAN 138:227403 AN 2003:247943 CAPLUS (Copyright 2003 ACS)

Lide D.R., Editor-in-Chief, 1992-1993 *CRC Handbook of Chemistry and Physics*, 73rd edition, CRC Press: Boca Raton FL

Linkov, V.; L. Petrik; G. Vaivars; A. Maluleke; and G. Gericke. 2002. Ceramic-based materials for electrochemical applications. In: Sanderson, R. D.; and H. Pasch (eds.), *Polymer Characterization and Materials Science.* Vol. 178 of *Macromolecular Symposia* (Fourth Annual UNESCO School and IUPAC Conference on Macromolecules and Materials Science, Stellenbosch, South Africa, 7–11 April 2001.) Weinheim, Germany: Wiley-VCH, 153–68.

REFERENCES

Lipinski, M.; R. Leuschner. Gas diffusion electron, process for producing an electrode an carbonizable composite. 2002. US Patent 6361666, issued 26/03/2002 Application No. 575006 filed on 05/19/2000; Assignee: Siemens Aktiengesellschaft

Liu, X. Y.; B. C. Huang; and N. J. Coville. 2002. The Fe(CO)(5) catalyzed pyrolysis of pentane: Carbon nanotube and carbon nanoball formation. *Carbon* 40 (15): 2791–9.

Liu J.; S. Liao; G. Jiang; X. Zhang; L.F. Petrik. 2006. Preparation, characterization and catalytic activity of Zr embedded MSU-V with high thermal and hydrothermal stability. *Microporous and Mesoporous Materials* 95, (1-3): 306-11

Liu, H.; B. Yi; M. Hou; J. Wu; Z. Hou; and H. Zhang. 2004. Composite electrode for unitized regenerative proton exchange membrane fuel cell with improved cycle life. *Electrochemical and Solid-State Letters* 7 (3): A56–9.

MacInnes, D. A.; and L. Adler. 1919. Hydrogen overvoltage. *Proceedings of the National Academy of Sciences of the United States of America* 5 (5): 160–3.

MacInnes, D. A.; and A. W. Contieri. 1919. Some applications of the variation of hydrogen overvoltage with the pressure. *Proceedings of the National Academy of Sciences of the United States of America* 5 (8): 321–3.

Majima, M.; K. Hanafusa; Y. Oka; G. Tanaka; H. Yoshida; E. Yagasaki; and T. Tada. 1997. Development of 1kWh (300 Ah) class lithium-ion battery. *Journal of Power Sources* 68 (2): 448–50.

Majima, M.; Y. Oka; K. Miyazaki; H. Yoshida; E. Yagasaki; and T. Tada. 1997. In: Holmes, C. F.; and A. R. Landgrebe (eds.), *Batteries for Portable Applications and Electric Vehicles.* Pennington, NJ: Electrochemical Society. PV97-18: 362. [Out of print.] Referred to in Park, M.; H. Jung; S.-I. Yoo; J. B. Bates: and S.-K. Joo. 2006. Electrochemical properties of layer-built cells. *Journal of Power Sources* 158 (2): 1447–50.

Majima, M.; T. Tada; S. Ujiie; E. Yagasaki; S. Inazawa; and K. Miyazaki. 1999. Design and characteristics of large-scale lithium-ion battery. *Journal of Power Sources* 81–82: 877–81.

Majima, M.; S. Ujiie; E. Yagasaki; K. Koyama; and S. Inazawa. 2001. Development of long-life lithium-ion battery for power storage. *Journal of Power Sources* 101 (1): 53–9.

Manitoba Hydrogen Steering Committee and Working Group. 2003. *The Preliminary Hydrogen Opportunities Report, 16 April 2003.* Winnipeg: Manitoba Energy, Science and Technology; Energy Development Initiative. http://www.gov.mb.ca/stem/energy/hydrogen/report.html. [May 2008]

Marburger J.; J. Bolten. 2007. "Interagency R&D Priorities"; and also "General R&D Program Guidance" and "R&D Investment Criteria." http://www.ostp.gov/html/budget/2007/ostp_omb_guidancememo_FY07.pdf. [May 2007]

Marković, N. M; V. Radmilovic; and P. N. Ross, Jr. 2003. Physical and electrochemical characterization of bimetallic nanoparticle electrocatalysts. In: Wieckowski, A; E. R. Savinova; and C. G. Vayenas (eds.), *Catalysis and Electrocatalysis at Nanoparticle Surfaces*. New York: Marcel Dekker Inc., 311–42.

REFERENCES

Mastalir, Á.; B. Rác; Z. Király; G. Tasi and Á. Molnár. 2008. Preparation of monodispersed Pt nanoparticles in MCM-41, catalytic applications. *Catalysis Communications* 9 (5): 762–8.

Maxwell, I. E.; and W. H. J. Stork. 2001. Hydrocarbon processing with zeolites. In: Van Bekkum, H.; E. M. Flanigen; P. A. Jacobs; and J. C. Jansen (eds.), *Introduction to Zeolite Science and Practice*, 2 ed.. Vol. 137 of *Studies in Surface Science and Catalysis*. Amsterdam: Elsevier Science Publishers B.V., 747–819.

Meier, W. M.. 1968. *Molecular Sieves*. London: Society of Chemical Industry, 10.

Merida-Donis, W. R. 2003. Apparatus for integrated water deionization, electrolytic hydrogen production, and electrochemical power generation. US Patent 6569298 issued 27/05/2003. Application No. 875281 filed on 06/05/2001; Assignee: Walter Roberto Merida-Donis

Mezger, T.G.. 2002. *The Rheology Handbook*. Coatings Compendium Series, edited by Zorll, U.. Hannover, Germany: Vincentz Verlag.

Millennium Cell, Inc. (MCEL). Hydrogen on Demand (HOD™). http://www.millenniumcell.com/fw/main/Technology_FAQ-33.html. [May 2008]

Millet, P.; T. Alleau; and R. Durand. 1993. Characterization of membrane-electrode assemblies for solid polymer electrolyte water electrolysis. *Journal of Applied Electrochemistry* 23 (4): 322–31.

Millet, P.; R. Durand; and M. Pineri. 1990. Preparation of new solid polymer electrolyte composites for water electrolysis. *International Journal of Hydrogen Energy* 15 (4): 245–53.

Millet, P.; M. Pineri; and R. Durand. 1989. New solid polymer electrolyte composites for water electrolysis. *Journal of Applied Electrochemistry* 19 (2): 162–6.

Mitsugi C.; A. Harumi; and F. Kenzo. 1998. WE-NET: Japanese hydrogen program. *International Journal of Hydrogen Energy* 23 (3): 159–65.

Mogensen, M.. 2000. Composite electrodes in solid oxide fuel cells and similar solid state devices. *Journal of Electroceramics* 5 (2): 141–52.

Morimoto, T.; K. Suzuki; T. Matsubara; and N. Yoshida. 2000. Oxygen reduction electrode in brine electrolysis. *Electrochimica Acta* 45 (25): 4257–62.

Moscou, L. 1991. The zeolite scene. In: Van Bekkum, H.; E. M. Flanigen; and J. C. Jansen (eds.), *Introduction to Zeolite Science and Practice*, 1 ed.. Vol. 58 of *Studies in Surface Science and Catalysis*. Amsterdam: Elsevier Science Publishers B.V., 1–12.

Mousty, C.; G. Fóti; C. Comninellis; and V. Reid. 1999. Electrochemical behaviours of DSA type electrodes prepared by induction heating. *Electrochimica Acta* 45 (3): 451–6.

Murthy, A.; S. R. Komplin; R. W. Cornell; J. H. Powers; and B. D. Gibson. 2000. Ink jet printer nozzle plates with ink filtering projections. US patent 6158843, issued 2000/12/12. Application no. 827242, filed 1997/03/28. Assignee: Lexmark International, Inc..

Musiani, M.; F. Furlanetto; and R. Bertoncello. 1999. Electrodeposited PbO_2+RuO_2: A composite anode for oxygen evolution from sulphuric acid solution. *Journal of Electroanalytical Chemistry* 465 (2): 160–7.

Nanotube Site, The. 2007. [Links to nanotube sites; electronic access to bibliographical information and preprints; information about providers of

REFERENCES

nanotubes.] Maintained by D. Tomanek. http://www.pa.msu.edu/cmp/csc/nanotube.html. [May 2008]

Nanotube Synthesis Site, The. [nd]. [Shared database focused on single-wall nanotube synthesis. Reference, links and information for techniques to grow SWNTs.] Maintained by D. Tomanek. http://nanotube.msu.edu/synthesis/. [May 2008]

Narang, S; S.C. Ventura; D.L.Olmeijer. 2006. Polymer electrolyte having acidic, basic and elastomeric subunits. US Patent 7052805, issued 30/05/2006; Application No. 09872770 filed on 06/01/2001; Assignee: SRI International

Nart, F. C; and W. Vielstich. 2003. Normalization of porous active surfaces. In: Vielstich,. W.; A. Lamm; and H. A. Gasteiger (eds.), *Handbook of Fuel Cells: Fundamentals, Technology, and Applications*. 4 vols.. Vol 2, *Electrocatalysis*. Chichester: John Wiley & Sons, 306–7.

NEHOC. [nd]. Information sheet #25, Screen printing technique. [How to screen print with RISO system, including angle of squeegee, pressure and printing actions.] NEHOC Australia (Pty) Ltd. http://www.nehoc.com.au/training/is/25/index.htm. [May 2008]

Nielsen, L. H.; H. Larsen; J. Jensen; and A. H. Petersen. 2004. Hydrogen infrastructure. In: Larsen, H.; R. Feidenhans'l; and L. Sønderberg Petersen (eds.), *Risø Energy Report 3. Hydrogen and its Competitors*. Risø-R-1469(EN), 52–5.

Nishiki, Y; T. Ashida; T. Shimamune; Y. Nakajima. 1996. Gas diffusion electrode. US Patent 5584976, issued on 17/12/1996; Application No. 636185 filed on 22/04/1996; Assignee: Permelec Electrode Ltd.

Nordstrom, R.. 2003. *Energy Independence: Preparing Minnesota for the Coming Hydrogen Economy.* (Minnesota H_2 Initiative Forum, March 2003.) St Paul, MN: Critical Issues Team, Minnesota Planning. www.pca.state.mn.us/oea/p2/forum/030307nordstrom.ppt. [May 2008]

Norman, T.; and E. Schmitt. 2004. Low cost electrolyzer system. Provisional patent application no. 60/27788, filed October 2004. Cited in: Cropley, C.. 2005. *PD23, DOE Hydrogen Program Review, 25 May 2005.* Giner Electrochemical Systems LLC.

Nørskov, J. K.; T. Bligaard; A. Logadottir; J. R. Kitchin; J. G. Chen; S. Pandelov; and U. Stimming. 2005. Trends in the exchange current for hydrogen evolution. *Journal of the Electrochemical Society* 152 (3): J23–6.

Okada, A.; A. Kiyohara; H. Tanaka; T. Honda; M. Ito; J. Kato; N. Toshima; and Y. Nakao. 2007. Electromagnetic wave shielding material and process for producing the same. USPTO 20070212536, published 2007/09/13. Serial no. 11569544, filed 2005/05/19. Assignee: Gunze Limited Fujikura Kasei Co., Ltd.

Okada, T.; S. Møller-Holst; O. Gorseth; and S. Kjelstrup. 1998. Transport and equilibrium properties of Nafion® membranes with H+ and Na+ ions. *Journal of Electroanalytical Chemistry* 442 (1–2): 137–45.

Oncel, N.; A. van Houselt; J. Huijben; A. Hallbäck; O. Gurlu; H. J. W. Zandvliet; B. Poelsema. 2005. Quantum Confinement between Self-Organized Pt Nanowires on Ge(001). *Phys. Rev. Lett*. 95: 116801

Osaka, A.; T. Takatsuna; and Y. Miura. 1994. Iridium oxide films via sol-gel processing. *Journal of Non-Crystalline Solids* 178: 313–9.

Parfit, M.. 2005. Powering the future. *National Geographic Magazine* 208 (2): [np].

REFERENCES

Park, M.; H. Jung; and S.-K. Joo. 2003. The study on the cell performances by the stacking structure of screen-printed cathodes, electrolytes, and anodes. (Abstract #190; Symposium C1, Battery and Energy Technology Joint General Session.) In: *Proceedings of the 203rd Electrochemical Society Meeting*, *Paris, France, 27 April–2 May 2003*. Pennington, NJ: Electrochemical Society. http://www.electrochem.org/dl/ma/203/pdfs/0190.pdf. [May 2008]

Park, M.; J.-H. Park; H. Jung; and S.-K. Joo. 2002. The study of the fabrication of $LiMn_2O_4$ cathode by screen printing, and characteristics of LiAl anode. (Poster #EE6.11; Symposium EE, Solid-State Ionics.) In: *Technical Program of the 2002 Materials Research Society (MRS) Fall Meeting, Boston, MA, 2–5 December 2002*.

Pasaogullari, U.; and C.-Y. Wang. 2004. Two-phase transport and the role of microporous layer in polymer electrolyte fuel cells. *Electrochimica Acta* 49 (25): 4359–69.

Patil, P. S.; P. S. Chigare; S. B. Sadale; T. Seth; D. P. Amalnerkar; and R. K. Kawar. 2003. Thickness-dependent properties of sprayed iridium oxide thin films. *Materials Chemistry and Physics* 80: 667–75.

Pauly, T. R.; and T. J. Pinnavaia. 2001. Pore size modification of mesoporous HMS molecular sieve silicas with wormhole framework structures. *Chemistry of Materials* 13 (3): 987–93.

Petrii, O.; and G. Tsirlina. 1994. Electrocatalytic activity prediction for hydrogen electrode reaction: Intuition, art, science. *Electrochimica Acta* 39 (11–12): 1739–47.

Petrik, L. F.. 2002. Nanophase composite catalysts for electrosynthesis. Unpublished MSc thesis. University of the Western Cape, South Africa.

Petrik, L. F.; Z. G. Godongwana; P. Ndungu; V. M. Linkov; and S. Liao. 2008. LPG synthesis of carbon analogue of HMS. In: Hadjiivanov, K.; V. Valtchev; S. Mintova; and G. Vayssilov (eds.), *Advanced Micro- and Mesoporous Materials*. (Proceedings of Second International Symposium, Advanced Micro and Mesoporous Materials, Varna, Bulgaria, 6–9 September 2007.) Sofia: Heron Press.

Petrik, L. F.; C. T. O'Connor; and S. Schwarz. 1995. The influence of various synthesis parameters on the morphology and crystal size of ZSM-5, and the relationship between morphology and crystal size and propene oligomerization. In: Beyer, H. K.; H. G. Karge; I. Kiricsi; and J. B. Nagy (eds.), *Catalysis by Microporous Materials.* (Proceedings of Zeocat '95, Szombathely, Hungary, 9–13 July 1995.) *Studies in Surface Science and Catalysis,* vol. 94. Amsterdam: Elsevier, 517.

Pettersson, J.; B. Ramsey; and D. J. Harrison. 2006. Fabrication of bifunctional membrane electrode assemblies for unitised regenerative polymer electrolyte fuel cells. *Electronics Letters* 42 (25): 1444–6.

Pham, A-Q.; T. H. Lee; and R. S. Glass. 1999. Colloidal spray deposition technique for the processing of thin film solid oxide fuel cells. (Abstract #1554.) In: Dokiya, M.; and S. C. Singhal (eds.), *Solid Oxide Fuel Cells (SOFC) VI.* (From the 196th Meeting of the Electrochemical Society / Proceedings of the 6th International Symposium on SOFC, Honolulu, Hawaii, 17–22 October 1999.) Pennington, NJ: Electrochemical Society. PV99-19: 172–8.

REFERENCES

Pinault, M.; M. Mayne-L'Hermite; C. Reynaud; V. Pichot; P. Launois; and D. Ballutaud. 2005. Growth of multiwalled carbon nanotubes during the initial stages of aerosol-assisted CCVD. *Carbon* 43 (14): 2968–76.

Pizzini, S.; G. Buzzanca; C. Mari; M. Rossi; and S. Torchio. 1972. Preparation, structure and electrical properties of thick ruthenium dioxide films. *Materials Research Bulletin* 7 (5): 449–62.

Plambeck, J. A.. 1982. *Electroanalytical Chemistry: Basic Principles and Applications*. New York: John Wiley & Sons, 318–26.

Popov, V. N.. 2004. Carbon nanotubes: Properties and application. *Materials Science and Engineering Reports* 43 (3): 61–102.

Pourdeyhimi, B.; E. Grant ; H. T. Nagle. 2007. Printing Electric Circuits onto Nonwoven Conformal Fabrics. *NTC Project*: F04-NS171. National Textile Center Annual Report: November 2007

Potter, E. C.. 1956. *Electrochemistry. Principles and Applications*. London: Cleaver-Hume Press Ltd; and New York: Macmillan Co..

Pozio, A.; M. De Francesco; A. Cemmi; F. Cardellini; and L. Giorgi. 2002. Comparison of high surface Pt/C catalysts by cyclic voltammetry. *Journal of Power Sources* 105 (1): 13–19.

Prabhuram, J; T. S. Zhao; C. W. Wong; and J. W. Guo. 2004. Synthesis and physical/electrochemical characterization of Pt/C nanocatalyst for polymer electrolyte fuel cells. *Journal of Power Sources* 134 (1): 1–6.

Prisyazhyi, V.D.; D. A. Tkalenko; N. A. Chmilenko; and M. D. Tkalenko. 2000. Overvoltage in cathode evolution of hydrogen from aqueous solutions on the rectifying metals. *Dop NAS of Ukraine* 9: 145–7.

Putley, E. H.. 1960. *The Hall Effect and Related Phenomena*. London: Butterworth.

Qu, L.; and L. Dai. 2005. Substrate enhanced electroless deposition of metal nanoparticles on carbon nanotubes. *Journal of the American Chemical Society* 127 (31): 10806–7.

Rajalakshmi, N.; and K. S. Dhathathreyan. 2007. Catalyst layer in PEMFC electrodes: Fabrication, characterisation and analysis. *Chemical Engineering Journal* 129 (1–3): 31–40.

Rajalakshmi, N.; H. Ryu; and K. S. Dhathathreyan. 2004. Platinum catalysed membranes for proton exchange membrane fuel cells—higher performance. *Chemical Engineering Journal* 102 (3): 241–7.

Rasten, E.; G. Hagen; and R. Tunold. 2003. Electrocatalysis in water electrolysis with solid polymer electrolyte. *Electrochimica Acta* 48 (25–26): 3945–52.

Reiger, P. H.. 1994. *Electrochemistry*, 2 ed.. New York: Chapman & Hall, Inc., 315–69.

Reshetenko, T. V.; H.-T. Kim; and H.-J. Kweon. 2007. Cathode structure optimization for air-breathing DMFC by application of pore-forming agents. *Journal of Power Sources* 171 (2): 433–40.

Rhein, R.. 2003. Screen printing process with diminished moiré effect. US patent 6505554, issued 2003/01/14. Application no. 897343, filed 2001/07/03. http://www.patentstorm.us/patents/6505554.html. [May 2008]

Riley, T.; T. Tomlinson (authors); and A. M. James (ed.). 1987. *Principles of Electroanalytical Methods*. New York: John Wiley & Sons [Published on behalf of ACOL, London, by Wiley], 167–80.

REFERENCES

Robbins, J.. 1972. *Ions in Solution.* Vol. 2, *An Introduction to Electrochemistry*. Oxford: Clarendon Press.

Roe, R. J.. 2000. *Methods of X-ray and neutron scattering in polymer science*. New York: Oxford University Press.

Rolison, D. R.; E. A. Hayes; and W. E. Rudzinski. 1989. Electrode-modified zeolites: Electrode microstructures contained in and on a heterogeneous catalyst. *Journal of Physical Chemistry* 93 (14): 5524–31.

Roshandel, R.; B. Farhanieh; E. Saievar-Iranizad. 2005. The effect of variable porosity distribution of gas diffusion layer on PEM fuel cell performance. *Renewable Energy* 30 (10): 1557–72.

Rowe, A.; and X. Li. 2001. Mathematical modeling of proton exchange membrane fuel cells. *Journal of Power Sources* 102 (1–2): 82–96.

Rusling, J. F.; and R. J. Forster. 2003. Electrochemical catalysis with redox polymer and polyion–protein films. *Journal of Colloid and Interface Science* 262 (1): 1–15.

Rusta-Sellehy, A.; and D. Frank. 2004. Chemical hydride hydrogen generation system and an energy system incorporating the same. US patent 6737184, issued 2004/05/18. Application no. 09986638, filed 2001/11/09. Assignee: Hydrogenics Corporation.

Rusta-Sellehy, A.; D. Frank; and R. Rady-Pentek. 2005. Chemical hydride hydrogen generation system and an energy system incorporating the same. US patent 6946104, issued 2005/09/20. Application no. 09900469, filed 2001/07/09. Assignee: Hydrogenics Corporation.

Ryan, C.G.; D. N. Jamieson; C. L. Churms; and J. V. Pilcher. 1995. A new method for on-line true-elemental imaging using PIXE and the proton microprobe. *Nuclear Instruments and Methods in Physics Research B: Beam Interactions with Materials and Atoms* 104 (1–4): 157–65.

Saha, M. S.; R. Li; and X. Sun. 2007. Composite of Pt-Ru supported SnO_2 nanowires grown on carbon paper for electrocatalytic oxidation of methanol. *Electrochemistry Communications* 9 (9): 2229–34.

Sato, S.; and J. M. White. 1981. Photocatalytic reaction of water with carbon over platinized titania. *Journal of Physical Chemistry* 85 (4): 336–41.

Sauer, D. U.; T. Sanders; B. Fricke; T. Baumhöfer; K. Wippermann; A. A. Kulikovsky; H. Schmitz; and J. Mergel. 2008. Measurement of the current distribution in a direct methanol fuel cell. Confirmation of parallel galvanic and electrolytic operation within one cell. *Journal of Power Sources* 176 (2): 477–83.

Savinell, R. F.; R. L. Zeller III; and J. A. Adams. 1990. Electrochemically active surface area. *Journal of the Electrochemical Society.* 137 (2): 489–94.

Schuegraf, K. K. (ed.). 1988. *The Handbook of Thin-Film Deposition Processes and Techniques: Principles, Methods, Equipment and Applications*. Park Ridge, NJ: Noyes Publications.

Scodelaro, F. A.; B. Hoyos; L. Balzano; and D. E. Resasco. 2005. Performance of PEM fuel cell electrodes using single wall carbon nanotubes as catalyst support. *Proceedings of 2005 AIChE Annual Meeting and Fall Showcase, Cincinnati, OH, 30 October–4 November 2005*. American Institute of Chemical Engineers. http://www.aiche.confex.com/aiche/2005/techprogram/P29188.HTM. [May 2008]

Scriba, M.; L. Petrik; D. Britten; A. Botha. 2003. Nanowonders—endless possibilities: Africa's big opportunity in a small-scale technology. A strategy for

the future SA nanoeconomy. [Policy document. Submitted to Government of South Africa Department of Science and Technology (DST) in August 2003. Issued by the DST as *The National Nanotechnology Strategy* in April 2006 (ISBN 0-621-36395-2). http://www.dst.gov.za/publications-policies/strategies-reports.]

Sedlak, J. M.; J. F. Austin; and A. B. LaConti. 1981. Hydrogen recovery and purification using the solid polymer electrolyte electrolysis cell. *International Journal of Hydrogen Energy* 6 (1): 45–51.

Sha, Y.; L. Qian; Y. Ma; H. Bai; and X. Yang. 2006. Multilayer films of carbon nanotubes and redox polymer on screen-printed carbon electrodes for electrocatalysis of ascorbic acid. *Talanta* 70 (3): 556–60.

Shan, J.; S.Liao,; V.M. Linkov; L.F. Petrik. 2002. Preparation and characterization of novel superacid catalyst SO_4^{2}-/Zr-ZSM-5. *Fenzi Cuihua*, 16(5), 379-383. Chemical Engineering College, South China University of Technology, Canton, Peop. Rep. China. CODEN: FECUEN ISSN: 1001-3555. Journal written in English. CAN 137:342492 AN 2002:877740 CAPLUS (Copyright 2003 ACS)

Shao, Z.; Yi B.; and Han M.. 1999. Bifunctional electrodes with a thin catalyst layer for 'unitized' proton exchange membrane regenerative fuel cell. *Journal of Power Sources* 79 (1): 82–5.

Shen, C.; X. Zhang; Y. Zhou; and H. Li. 2003. Preparation and characterization of nanocrysatlline $Li_4Ti_5O_{12}$ by sol-gel method. *Materials Chemistry and Physics* 78 (2): 437–41.

Shin, S.-J.; J.-K. Lee; H.-Y Ha; S.-A. Hong; H.-S. Chun; and I.-H. Oh. 2002. Effect of the catalytic ink preparation method on the performance of polymer electrolyte membrane fuel cells. *Journal of Power Sources* 106 (1–2): 146–52.

Shu, J.; J. Li; and A. Pascovici. 1997. Multiple layer screening for reducing moiré patterning and ink bleeding. In: *Proceedings of the 1997 International Conference on Image Processing (ICIP '97), Washington DC, 26–29 October 1997*. 3 vols.. Washington DC: IEEE Computer Society, 1: 803–6.

Shukla, P. K.; R.. K. Karn; A. K. Singh; and O. N. Srivastava. 2002. Studies on PV assisted PEC solar cells for hydrogen production through photoelectrolysis of water. *International Journal of Hydrogen Energy* 27 (2): 135–41.

Siegel, N. P.; M. W. Ellis; D. J. Nelson; and M. R. von Spakovsky. 2003. Single domain PEMFC model based on agglomerate catalyst geometry. *Journal of Power Sources* 115 (1): 81–9.

Sillen, C. W. M. P.; and S. J. D. van Stralen. 1980. Gas evolution during water electrolysis: Gas bubble behaviour and potential drop measurements. In: Veziroglu, T. N. (ed.). 1980. *Alternative Energy Sources III: Proceedings of the 3rd International Conference on Alternative Energy Sources, Miami Beach Fl., 15 December 1980.* Washington DC: Hemisphere Publishing Corp., 5 (3): 357–69.

Simonov, P. A.; and V. A. Likholobov. 2003. Ch. 12, Physicochemical aspects of preparation of carbon-supported noble metal catalysts. In: Wieckowski, A.; E. R. Savinova; and C. G. Vayenas (eds.), *Catalysis and Electrocatalysis at Nanoparticle Surfaces*. New York: Marcel Dekker, Inc., 409–54.

Sklyarov, A. T.; F. V. Kupovich; and V. Busse-Macukas. 1991. Cathode with low overvoltage of hydrogen evolution. *Electrokhimiya* 27 (12): 1588–94.

REFERENCES

Sklyarov, A. T.; F. V. Kupovich; V. Busse-Macukas; and A. F. Mazanko. 1991. A cathode with low hydrogen overpotential for the membrane-cell process of chlorine and caustic soda production. *Soviet Electrochemistry* 27 (12): 1405–10.

Slade, S.; S. A. Campbell; T. R. Ralph; and F. C. Walsh 2002. Ionic conductivity of an extruded Nafion 1100 EW series of membranes. *Journal of the Electrochemical Society* 149 (12): A1556–64.

Smirnova, A.; X. Dong; H. Hara; A. Vasiliev; and N.. Sammes. 2005. Novel carbon aerogel-supported catalysts for PEM fuel cell application. *International Journal of Hydrogen Energy* 30 (2): 149–58.

Smith, S. P. J.; V. M. Linkov; C. T. O'Connor; L. F. Petrik; R. D. Sanderson; and K. Keiser. 1995. Preparation of hollow-fibre composite carbon-zeolite membranes. *Microporous Materials* 4 (5): 385–90.

SHEC™ Solar Hydrogen Energy Corporation (SHEC). Press release, 2006 A solution to global warming. http://www.solar-h2.com ; and http://www.shec-labs.com. [May 2008]

Somerset, V.; L. F. Petrik; and E. Iwuoha. 2005. Alkaline hydrothermal conversion of fly ash filtrates into zeolites (2): Utilization in wastewater treatment. *Journal of Environmental Science and Health* 40 (8): 1627–36.

Sone, Y.; P. Ekdunge; and D. Simonsson. 1996. Proton conductivity of Nafion 117 as measured by a four-electrode AC impedence method. *Journal of the Electrochemical Society* 143 (4): 1254–9.

Sørensen, B.; A. H. Petersen; C. Juhl; H. Ravn; C. Søndergren; P. Simonsen; K. Jørgensen; L. H. Nielsen; H. V. Larsen; P. E. Morthorst; L. Schleisner; F. Sørensen; and T. E. Pedersen. 2004. Hydrogen as an energy carrier: Scenarios for future use of hydrogen in the Danish energy system. *International Journal of Hydrogen Energy* 29 (1): 23–32.

Spahr, M. E.; P. Stoschitzki-Bitterli; R. Nesper; O. Haas; and P. Novák. 1999. Vanadium oxide nanotubes. A new nanostructured redox-active material for the electrochemical insertion of lithium. *Journal of the Electrochemical Society* 146 (8): 2780–3.

Specialty Graphic Imaging Association (SGIA). 2008. ASPT student screen printing and digital imaging competition. [Judging criteria.] Fairfax, VA: SGIA. http://www.sgia.org/pdf_server.cfm?pdf=/aspt/downloads/ASPT.pdf. [May 2008]

Steigerwalt, E. S.; G. A. Deluga; D. E. Cliffel; and C.M. Lukehart. 2001. A Pt-Ru/graphitic carbon nanofiber nanocomposite exhibiting high relative performance as a direct-methanol fuel cell anode catalyst. *Journal of Physical Chemistry B* 105 (34): 8097–101.

Stoltenberg J., Press statement. 18.04.2008: http://www.regjeringen.no/en/dep/smk/Press-Center/Press-releases/2008/norway-to-cooperate-with-south-africa-on.html?id=508133. [May, 2008]

Strong, K. L.; D. P. Anderson; K. Lafdi; and J. N. Kuhn. 2003. Purification process for single-wall carbon nanotubes. *Carbon* 41 (8): 1477.

Stucki, S.; and G. G. Scherer. 1998. PEM water electrolysers: Evidence for membrane failure in 100kW demonstration plants. *Journal of Applied Electrochemistry* 28 (10): 1041–9.

Sui S.; Gu J.; Li G.; and Sui Z.. [nd]. Development status of oxygen electrodes for proton exchange membrane fuel cells. http://www.hxtb.org/col/2000/c00009.htm

REFERENCES

(Chinese). Referred to in Lykhnytskyi, K. V.; V. Z. Barsukov; and M. Jaskuła. 2007. Promising catalysts for H_2-O_2 fuel cells (Review). In: Veziroglu, T. N. et al (eds.), *Hydrogen Materials Science and Chemistry of Carbon Nanomaterials*. (*NATO Science for Peace and Security Series A: Chemistry and Biology*, vol. 41). Springer, 177–85.

Sunde, S.. 2000. Simulations of composite electrodes in fuel cells. *Journal of Electroceramics* 5 (2): 153–82.

Szostak, R.. 1992. *Handbook of Molecular Sieves*. New York: Van Nostrand Reinhold.

Tafel J.. The Polarization During Cathodic Hydrogen Evolution. *Zeitschrift fur physikalische Chemie.* Vol. 50, pp 641-712, 1905

Takasu, Y.; S. Onoue; K. Kameyama; Y. Murakami; and K. Yahikozawa. 1994. Preparation of ultrafine RuO_2-IrO_2-TiO_2 oxide particles by a sol-gel process. *Electrochimica Acta* 39 (13): 1993–7.

Tamura, H.. 2004. Theorization on ion-exchange equilibria: Activity of species in 2-D phases. *Journal of Colloid and Interface Science* 279 (1): 1–22.

Tanaka, S.; K.-B. Min; N. Kato; H. Oikawa; and M. Esashi. 2005. Application of screen-printed catalytic electrodes to MEMS-based fuel cells. *IEEJ Transactions on Sensors and Micromachines* 125 (10): 413–7.

Tanev, P. T.; and T. J. Pinnavaia. 1995. A neutral templating route to mesoporous molecular sieves. *Science* 267 (5199): 865–7.

Taylor, A. D.; E. Y. Kim; V. P. Humes; J. Kizuka; and L. T. Thompson. 2007. Inkjet printing of carbon-supported platinum 3-D catalyst layers for use in fuel cells. *Journal of Power Sources* 171 (1): 101–6.

Technigraphics. 2002. Technigraphics cosmetic specifications 2/1/93 Rev. A. [7 pp.]. [Cosmetic reference standard, screenprinting judging criteria, guidelines and definitions of terms.] http://www.technigraphics.com/downloads/cosmetic_specs_020193.pdf. [May 2008]

Thamahane, T. C.. 2005. Development of anodic electrocatalyst and optimization of membrane electrode assembly for hydrogen reduction by water electrolysis. Unpublished MSc thesis. Department of Chemistry, University of the Western Cape.

Thomas, C. E.; I. F. Kuhn, Jr; B. D. James; F. D. Lomax, Jr; G. N. Baum. 1998. Affordable hydrogen supply pathways for fuel cell vehicles. *International Journal of Hydrogen Energy* 23 (6) June: 507-16.

Tokumisu, K.; J. S. Wainwright; and R. F. J. Savinell. 1999. *Journal of New Materials for Electrochemical Systems* 2: 171. [Out of print.]

Tomanek, D. (ed.). [nd]. Carbon arc (CA) synthesis of single-wall carbon nanotubes. http://nanotube.msu.edu/synthesis/ca.html. [May 2008]

Tosco, P.; L. Kosbach; Y. Yu; C. Orecchia. 2005. Gas diffusion electrodes containing modified carbon products. US Patent 6881511, issued 19/04/2005; Application No. 10638260 filed on 08/08/2003; Assignee: Cabot Corporation, Edison Termoelettrica, S.p.A.

Towne, S.; V. Viswanathan; J. Holbery; and P. Rieke. 2007. Fabrication of polymer electrolyte membrane fuel cell MEAs utilizing inkjet print technology. *Journal of Power Sources* 171 (2): 575–84.

REFERENCES

Trasatti, S.. 2000. Electrolysis: Understanding the success of DSA®. *Electrochimica Acta* 45 (15–16): 2377–85.

Trasatti, S.. 1991. Physical electrochemistry of ceramic oxides. *Electrochimica Acta* 36 (2): 225–41.

Turner, J.A.. 2004. Sustainable Hydrogen Production. *Science* 305 (5686) 13 August: 972 - 74

Uchida, M.; Y. Fukuoka; Y. Sugawara; N. Eda; and A. Ohta. 1996. Effects of microstructure of carbon support in the catalyst layer on the performance of polymer-electrolyte fuel cells. *Journal of the Electrochemical Society* 143 (7): 2245–52.

US Department of Energy (DOE). 2002a. *National Hydrogen Energy Roadmap. Toward a more secure and cleaner energy future for America. Production – delivery – storage – conversion – applications – public education and outreach.* (November 2002.) Based on results of National Hydrogen Energy Workshop, Washington DC, 2–3 April 2002. US DOE, Office of Energy Efficiency and Renewable Energy. http://www1.eere.energy.gov/hydrogenandfuelcells/pdfs/national_h2_roadmap.pdf . [May 2008]

US Department of Energy (DOE). 2002b. *A National Vision of America's Transition to a Hydrogen Economy—to 2030 and Beyond. Toward a more secure and cleaner energy future for America.* (February 2002.) Based on results of the National Hydrogen Vision Meeting, Washington DC, 15–16 November 2001. US DOE, Office of Energy Efficiency and Renewable Energy. http://www1.eere.energy.gov/hydrogenandfuelcells/pdfs/vision_doc.pdf. [May 2008]

US Department of Energy (DOE). 2002c. *Proceedings of National Hydrogen Energy Roadmap Workshop, Washington DC, 2–3 April 2002*. US DOE, Office of Energy Efficiency and Renewable Energy. http://www1.eere.energy.gov/hydrogenandfuelcells/wkshp_proceedings.html#vision_roadmaps. [May 2008]

US Department of Energy (DOE). 2002d. *Proceedings of National Hydrogen Vision Meeting, Washington DC, 15–16 November 2001*. US DOE, Office of Energy Efficiency and Renewable Energy. http://www1.eere.energy.gov/hydrogenandfuelcells/wkshp_proceedings.html#vision_roadmaps. [May 2008]

Vaivars, G.: N. W. Maxakato; T. Mokrani; L.F. Petrik; J. Klavins; G. Gericke; and V. Linkov. 2004. Zirconium phosphate-based inorganic direct methanol fuel cell. *Materials Science* 10 (2): 162–5.

Van der Pauw L.J., 1958. A method of measuring specific resistivity and Hall effects of discs of arbitrary shape. *Phillips Res.Repts,* 13 (1-9) 20: No 1: 220-4.

Van Herle, J.; R. Ihringer; R. Vasquez Cavieres; L. Constantin; and O. Bucheli. 2001. Anode supported solid oxide fuel cells with screen-printed cathodes. *Journal of the European Ceramic Society* 21 (10–11): 1855–9.

Vazquez-Gomez, L.; S. Ferro; and A. De Battisti. 2006. Preparation and characterization of RuO_2-IrO_2-SnO_2 ternary mixtures for advanced electrochemical technology. *Applied Catalysis B: Environmental* 67 (1–2): 34–40.

REFERENCES

Vielstich, W.. 2003. *Fuel Cell Technology and Applications* (Part 1). Vol 3 of *Handbook of Fuel Cells: Fundamentals, Technology and Applications* (4 vols.), edited by W. Vielstich; A. Lamm; and H. A. Gasteiger. West Sussex, England: John Wiley & Sons.

Vielstich, W.; A. Lamm; and H. A. Gasteiger (eds.). 2003. *Handbook of Fuel Cells: Fundamentals, Technology and Applications*. 4 vols.. Vol 3, *Fuel Cell Technology and Applications* (Part 1). West Sussex, England: John Wiley & Sons.

Viscoelasticity. (From *Wikipedia*, the free encyclopedia.) http://en.wikipedia.org/wiki/Viscoelasticity. [28 May 2008]

Vivekchand, S. R. C; L. M. Cele; F. L. Deepak; A. R. Raju; and A. Govindaraj. 2004. Carbon nanotubes by nebulized spray pyrolysis. *Chemical Physics Letters* 386 (4–6): 313–8.

Vogel, W.M.; and J. M. Baris. 1977. The reduction of oxygen on platinum black in acid electrolytes. *Electrochimica Acta* 22 (11): 1259–63.

Vohrer, U.; Kolaric, I.; Haque, M.H.; Roth, S.; Detlaff-Weglikowska, U. 2004. Carbon nanotube sheets for the use as artificial muscles. *Carbon* 42 1159–64

Wan, C.-H.; and Q.-H. Zhuang. 2007. Novel layer wise anode structure with improved CO-tolerance capability for PEM fuel cell. *Electrochimica Acta* 52 (12): 4111–23.

Wan, C.-H.; Q.-H. Zhuang; C.-H. Lin; M.-T. Lin; and C. Shih. 2006. Novel composite anode with CO 'filter' layers for PEFC. *Journal of Power Sources* 162 (1): 41–50.

Wang, B.; W. Kong; and H. Ma. 2007. Electrochemical treatment of paper mill wastewater using three-dimensional electrodes with Ti/Co/SnO_2-Sb_2O_5 anode. *Journal of Hazardous Materials* 146 (1–2): 295–301.

Wang, J.; B. Tian; V. B. Nascimento; and L. Angnes. 1998. Performance of screen-printed carbon electrodes fabricated from different carbon inks. *Electrochimica Acta* 43 (23): 3459–65.

Wang, Y; X. Xu; Z. Tian; Y. Zong; H. Cheng; and C. Lin. 2006. Selective heterogeneous nucleation and growth of size-controlled metal nanoparticles on carbon nanotubes in solution. *Chemistry—A European Journal* 12 (9): 2542–9.

Wang, X.; I.-M. Hsing; and P. L. Yue. 2001. Electrochemical characterization of binary carbon supported electrode in polymer electrolyte fuel cells. *Journal of Power Sources* 96 (2): 282–7.

Wang C.Y.; Z.H. Wang, Pan Y. 1999. Two-phase transport in proton exchange membrane fuel cells. *Proceedings of the ASME Heat Transfer Division: 1999*, American Society of Mechanical Engineers

Weitkamp, J.. 2000. Zeolites and catalysis. *Solid State Ionics* 131: 175–88.

Wen, X.; and S. Yang. 2002. Cu_2S/Au core/sheath nanowires prepared by a simple redox deposition method. *Nano Letters* 2 (5): 451–4.

WE-NET. 1998. Development of hydrogen production technology. Summary of Annual Reports 1998. [R&D goals – results in FY 1998 – ion exchange membrane technology – hydrogen production technology by electroless plating method – technology for hydrogen production by hot-pressing method – economics of hydrogen production plant – high temperature resistant polymeric electrolyte – literature pertaining to water electrolysis.] New Energy and Industrial Technology

REFERENCES

Development Organisation. http://www.enaa.or.jp/WE-NET/report/1998/english/4_1.htm. [May 2008]

Wiesener, K.; and D. Ohms. 1990. Electrocatalysis of the cathodic oxygen reduction. In: Wendt, H. (ed.), *Electrochemical Hydrogen Technologies. Electrochemical Production and Combustion of Hydrogen*. New York: Elsevier, 63–103.

Williams, M.; L. Khotseng; Q. Ying; L. F. Petrik; A. Nechaev; V. Linkov. 2008. Applicability of analytical protocols for the characterization of carbon-supported platinum group metal electrocatalysts. Submitted to *South African Journal of Science*.

Wöhr, M.; K. Bolwin; W. Schnurnberger; M. Fischer; W. Neubrand; and G. Eigenberger. 1998. Dynamic modelling and simulation of a polymer membrane fuel cell, including mass transport limitation. *International Journal of Hydrogen Energy* 23 (3): 213–8.

Wood, N. S.. 1986. Electrolytic cell with low hydrogen overvoltage cathode. US patent 4586998, issued 1986/05/06. Application no. 06/642166, filed 1984/08/20. Assignee: Imperial Chemical Industries (ICI) PLC (Great Britain).

Wu, Y. H.; P. W. Qiao; T. C. Chong; and Z. X. Shen. 2002. Carbon nanowalls grown by microwave plasma enhanced chemical vapor deposition. *Advanced Materials* 14 (1): 64–7.

Wurster, R.; and J. Schindler. 2003. Ch. 5, Solar and wind energy coupled with electrolysis and fuel cells. In: Vielstich, W.; A. Lamm; and H. A. Gasteiger (eds.), *Handbook of Fuel Cells: Fundamentals, Technology and Application*. 4 vols.. Vol 3, *Fuel Cell Technology and Applications* (Part 1). West Sussex, England: John Wiley & Sons, 62–78.

Xie, F.; H. Meng; and P. K. Shen. 2008. Diffusion study in a novel three-dimensional electrode for direct methanol fuel cells. *Electrochimica Acta* 53 (15): 5039–44.

X-Ray Diffraction Lab. [nd]. Experiment 2, Pinhole/Polaroid Diffractometer. http://www.eng.uc.edu/~gbeaucag/Classes/XRD/Labs/Lab2html/Lab2 Pinhole_PE.html. [May 2008]

Yamaguchi, M.; T. Shinohara; and K. Okisawa. 1995. In: Proceedings of International Hydrogen and Clean Energy Symposium (IHCE '95), Tokyo, Japan, 6–8 February 1995. Asian Technology Information Program (ATIP) Reports, ATIP95-63: 205–8.

Yamanaka K.. 1989. Anodically electrodeposited iridium oxide films (AEIROF) from alkaline solutions for electrochromic display devices. *Japanese Journal of Applied Physics* 28 (1/4): 632–7.

Yaritza, M.. 2004. Characterization of proton exchange membrane and PEM electrolyzer using non-steady state electrochemical techniques. Unpublished MSc thesis, University of Puerto Rico, 1–23.

Yim, S. D.; G. G. Park; Y. J. Sohn; W. Y. Lee; Y. G. Yoon; T. H. Yang; S. Um; S. P. Yu; and C. S. Kim. 2005. Optimization of PtIr electrocatalyst for PEM URFC. *International Journal of Hydrogen Energy* 30 (12): 1345–50.

Ying, Q.. 2005. Preparation and characterization of highly active nano Pt/C electrocatalyst. Unpublished MSc thesis, University of the Western Cape.

Yogi Goswami, D.. 1998. Solar Thermal Power Technology: Present Status and Ideas for the Future. *Energy Sources, Part A: Recovery, Utilization, and Environmental Effects* 20 (2) February: 137 – 45.

REFERENCES

Yu, H. M.; C. Ziegler; M. Oszcipok; M. Zobel; and C. Hebling. 2006. Hydrophilicity and hydrophobicity study of catalyst layers in proton exchange membrane fuel cells. *Electrochimica Acta* 51 (7): 1199–207.

Yumurtaci, Z.; E. Bilgen. 2004. Hydrogen production from excess power in small hydroelectric installations. *International Journal of Hydrogen Energy.* 29 (7) July: 687-93

Yusti, E.; M. Pilkun; V. Shaibe; and A. Vinsel. 1962. Highly active hydrogen diffusive electrode. *Izd. Inostr. Lit.* Moscow, 296.

Zeolyst company webpage. http://www.zeolyst.com [May 2008]

Zhang, H.; B. Zhu; and Y. Xu. 2006. Composite membranes of sulfonated poly (phthalazinone ether ketone) doped with 12-phosphotungstic acid ($H_3PW_{12}O_{40}$) for proton exchange membranes. *Solid State Ionics* 177 (13–14): 1123–8.

Zhang, J.. 2004. Investigation of CO tolerance in proton exchange membrane fuel cells. PhD thesis. Worcester, England: Worcester Polytechnic Institute.

Zhang, W.; T. R. Pauly; and T. J. Pinnavaia. 1997. Tailoring the framework and textural mesopores of HMS molecular sieves through an electrically neutral (SI) assembly pathway. *Chemistry of Materials* 9 (11): 2491–8.

Zhang, Y.; C. Wang; N. Wan; Z. Liu; and Z. Mao. 2007. Study on a novel manufacturing process of membrane electrode assemblies for solid polymer electrolyte water electrolysis. *Electrochemistry Communications* 9 (4): 667–70.

Zhou, W.. 2003. Research on anode catalysts for low temperature direct alcohol fuel cells. Dalian Institute of Chemical Physics (DICP), Chinese Academy of Sciences, Dalian, People's Republic of China.

Zhou, Y.; and H. Li. 2002. Sol-gel template synthesis and structural properties of a highly ordered $LiNi_{0.5}Mn_{0.5}O_2$ nanowire array. *Journal of Materials Chemistry* 12: 681–6.

Zhou, Z.; S. Wang; W. Zhou; G. Wang; L. Jiang; W. Li; S. Song; J. Liu; G. Sun; and Q. Xin. 2003. Novel synthesis of highly active Pt/C cathode electrocatalyst for direct methanol fuel cell. *Chemical Communications* 3: 394–5.

Zhu, W. H.; R. U. Payne; M. Nelms; and B. J. Tatarchuk. 2007. In situ electrical characterization of PEM fuel cells at load. Paper #295e presented at AIChE Annual Meeting, Salt Lake City, UT, 3–9 November 2007. http://aiche.confex.com/aiche/2007/techprogram/meeting.htm. [May 2008]